

KARST GEOMORPHOLOGY OF THE NORTHEASTERN MACKENZIE
MOUNTAINS

KARST GEOMORPHOLOGY AND HYDROGEOLOGY
OF THE NORTHEASTERN MACKENZIE MOUNTAINS,
DISTRICT OF MACKENZIE, N.W.T.

CANADA

By

JAMES PATRICK HAMILTON, B.A., M.Sc.

Department of Geography

A Thesis

Submitted to the School of Graduate Studies

in Partial Fulfilment of the Requirements

for the Degree

Doctor of Philosophy

McMaster University

© James Patrick Hamilton, August 1995

DOCTOR OF PHILOSOPHY (1995)
(Geography)

McMASTER UNIVERSITY
Hamilton, Ontario

TITLE: Karst Geomorphology and Hydrogeology of the Northeastern Mackenzie
Mountains, District of Mackenzie, N.W.T.

AUTHOR: James P. Hamilton, B.A., M.Sc. (University of Western Ontario)

SUPERVISOR: Professor D.C. Ford

NUMBER OF PAGES: xxii, 532

ABSTRACT

This thesis describes the geomorphology and hydrogeology of karst systems in portions of the northeastern Canyon Ranges of the Mackenzie Mountains and the Norman Range of the Franklin Mountains, N.W.T. In the region, mean annual temperatures are -6 to -8°C, total annual precipitation is 325 to 500 mm, and permafrost has a widespread to continuous distribution. The area was glaciated in the Late Wisconsinan by the Laurentide Ice Sheet.

The Canyon Ranges and Norman Range are composed of a sequence of faulted and folded miogeoclinal sedimentary rocks that span the Proterozoic to Eocene. The geology is reviewed with an emphasis on strata that display karst. Included are several dolomite and limestone formations, two of which are interbedded with evaporites in the subsurface. The principal groundwater aquifer is the Lower Devonian Bear Rock Formation. In subcrop, the Bear Rock Formation is dolomite and anhydrite, outcrops are massive calcareous solution breccias. This is the primary karst rock.

The regional distribution and range of karst landforms and drainage systems are described. Detailed mapping is presented from four field sites. These data were collected from aerial photography and ground surveys. The karst has examples of pavement, single and compound dolines, subsidence troughs, polje, sinking streams and lakes, and spring deposits. The main types of depressions are subsidence and collapse dolines. Doline density is highest on the Bear Rock Formation. Surficial karst is absent or less frequent in the zone of continuous permafrost or outside the glacial limit.

At the field sites, water samples were collected at recharge and discharge locations. Samples were analyzed for a full range of ionic constituents and many for natural isotopes. In addition, several springs were monitored continuously for discharge, temperature, and conductivity. Dye tracing established linkages between recharge and discharge at some sites. These data are summarized for each site, as is the role of permafrost in site hydrology.

The relationships between geological structure, topography, and groundwater

systems are described. Conduit aquifers are present in both dolomite and limestone. These systems are characterized by discharge waters of low hardness and dissolved ion content. Aquifers in the Bear Rock Formation have a mixed flow regime and often have highly mineralized discharge. At the principal field site, there was a time lag of 40 to 60 days between infiltration and discharge in this unit. At a second site, flow through times were on the order of years. Variability in these systems is attributed to bedrock properties and boundary conditions.

Preliminary rates of denudation are calculated from the available hydrochemical data. Total solutional denudation at the primary field site is approximately $45 \text{ m}^3 \text{ km}^{-2} \text{ a}^{-1}$ (mm ka^{-1}). The majority is attributed to the subsurface dissolution of halite and anhydrite. The predominance of subsurface dissolution is linked to the high frequency of collapse and subsidence dolines and depressions.

The karst features and drainage systems of the northern Mackenzie Mountains date to the Tertiary. Glaciation has had a stimulative effect on karst development through the subglacial degradation of permafrost and the altering of boundary conditions by canyon incision.

ACKNOWLEDGEMENTS

The author wishes to acknowledge the many individuals and agencies who contributed to this project. Professor Derek Ford has been a driving force in karst research of the Canadian Cordillera. He identified the field area and provided the support required to undertake this work. Throughout my tenure as a graduate student, Professor Ford organized many karst seminars and sponsored field excursions to the Rocky Mountains, Appalachia, and Europe. During the long process of writing this thesis, Professor Ford has been encouraging, and I thank him for his guidance and endurance. Several geography faculty at McMaster also influenced this project and fostered an atmosphere supportive of northern research, notable are Professors Ming-Ko Woo and Brian McCann. Colleagues that piped in their two cents or other sundry advise include: Joyce Lundberg, Kathy Harding, Mary-Lou Byrne, Dave Halliwell, Peter LaFleur, Marcus Buck, Steve Worthington, Jane Mulkewich, Sue Vajoczki, Ron Stenson, Julian Szeicz, Susan Elliott, and Deborah Young. I thank them for their words and deeds. Capable field assistance was provided by Bob Guilietti, Laura Hastings, Rick Meyers, and Kees Sinke.

Funding for this project was provided by NSERC to Ford, and by the University of Lethbridge to Hamilton. Northern Training Grants were awarded to Meyers and Sinke by the Arctic Institute. Assistance in laboratory analyses was provided by: (i) the staff of the Neutron Activation Laboratory, McMaster University, (ii) the staff of the Lethbridge Office, Water Resources Branch, Department of Environment, Province of Alberta, (iii) John Pullen, formerly of Moneco Inc., (iv) Martin Knyf, isotope laboratory, Department of Geology, McMaster University, and (v) Roy Krouse, Department of Physics, University of Calgary. Thanks are extended to support staff at the Department of Geography, McMaster University, and Department of Geography, University of Lethbridge. A blanket thank you is extended to those northerners for logistical support in the form of helicopters, float planes, and radio communication. Discussions with Alejandra Duk-Rodkin and Owen Hughes regarding the Quaternary of the study area were most helpful. Nico Meijer Drees and Don Morrow provided valuable information on the Devonian of the Mackenzie Shelf and the Bear Rock Formation.

Katherine McLeod contributed greatly to this project as a field assistant, typist, illustrator, and support group. My heartfelt thanks are extended to her. Finally I dedicate this work to my mother and father for their unquestioning confidence.

TABLE OF CONTENTS

DESCRIPTIVE NOTE	ii
ABSTRACT	iii
ACKNOWLEDGEMENTS	v
TABLE OF CONTENTS	vi
LIST OF TABLES	xiv
LIST OF FIGURES	xvi
CHAPTER I INTRODUCTION	
1.1 An Introduction to the Study	1
1.2 An Introduction to Geomorphology	2
1.2.1 Systems and Equilibria in Geomorphology	3
1.2.2 Scale in Geomorphology	4
1.2.3 The Karst System	5
1.2.3.1 Morphological Elements	5
1.2.3.2 Thresholds, Equilibrium and Scale	6
1.2.3.3 The Role of Climate	8
1.2.4 Explanation and Method in Geomorphology	9
1.3 Physical Setting of the Study	12
1.4 Thesis Objectives	13
CHAPTER II KARST IN PERMAFROST TERRAIN	
2.1 Introduction	17
2.2 Dissolution of Karst Rocks	17
2.2.1 Deviations from Equilibrium	18
2.2.2 Anhydrite and Gypsum	19
2.2.2.1 Gypsum Saturation Index	21
2.2.3 Calcite and Dolomite	21
2.2.3.1 Carbon Dioxide	22
2.3 Karst Hydrology and Aquifers	24
2.3.1 Hydrological Components of the Karst System	26
2.3.2 Spring Analyses	27
2.4 Permafrost	27
2.4.1 Permafrost Distribution	28
2.5 Hydrology of Permafrost Terrain	31
2.5.1 Basin Hydrology	32
2.6 Groundwater in Permafrost Terrain	32
2.6.1 Suprapermafrost Aquifer	33

2.6.1.1	Surface and Subsurface Flow	34
2.6.1.2	Chemistry and Discharge of Suprapermafrost Groundwater	36
2.6.2	Intrapermafrost Aquifer	36
2.6.2.1	Chemistry and Discharge of Intrapermafrost Groundwater	37
2.6.3	Subpermafrost Aquifer	38
2.6.3.1	Chemistry and Discharge of Subpermafrost Groundwater	39
2.6.4	Spring-fed Regime in Permafrost	39
2.7	Glaciation, Permafrost, and Karst	41
2.7.1	Glacial Thermal Regime	41
2.7.2	Glacial Erosion and Deposition	42
2.7.3	Glacial Hydrology	43
2.7.4	The Influence of Glaciation on Permafrost	44
2.7.5	Glaciation and Karst	45
2.8	Permafrost Karsts	48
2.8.1	Karst of the Continuous Permafrost Zone	48
2.8.2	Karst of the Discontinuous Permafrost Zone	51
2.8.3	The Effect of Permafrost on Karst	53

CHAPTER III STUDY AREA AND METHODS

3.1	Introduction	64
3.2	The Biophysical Characteristics of the Study Area	65
3.2.1	Climate	65
3.2.1.1	Temperature	66
3.2.1.2	Precipitation	66
3.2.1.3	Evaporation	68
3.2.2	Vegetation	69
3.2.3	Soils	70
3.2.4	Permafrost in the Mackenzie Valley and Area	71
3.2.5	Regional Hydrology	74
3.2.6	Clastic and Dissolved Sediments	76
3.2.7	Regional Hydrogeology	78
3.3	Methods: Data Collection and Analyses	79
3.3.1	Hydrometeorological Measures: Discharge and Precipitation	81
3.3.2	Solute Measurements	82
3.3.2.1	Sample Collection	82
3.3.2.2	Sample Analyses	84
3.3.2.3	Treatment and Presentation of the Solute Data	89
3.3.3	Dye Tracing	90
3.3.4	Stable Isotopes	91

CHAPTER IV GEOLOGY OF THE NORTHEASTERN MACKENZIE MOUNTAIN REGION

4.1	Introduction	103
4.2	Previous Work	103
4.3	Regional Geological Setting	104
4.3.1	Physiography	105
4.3.2	Depositional Setting, Stratigraphy, and Structure	106
4.4	Proterozoic	110
4.4.1	Mackenzie Mountain Assemblage	111
4.4.1.1	Map Unit H ₁	111
4.4.1.2	Tsezotene Formation	112
4.4.1.3	Katherine Group	112
4.4.1.4	Little Dal Group	113
4.4.2	Windermere Supergroup	114
4.5	Cambrian	115
4.5.1	Mount Clark and Mount Cap Formations	116
4.5.2	Saline River Formation	117
4.5.3	Franklin Mountain Formation	119
4.6	Ordovician-Silurian	121
4.6.1	Mount Kindle Formation	121
4.7	Upper Silurian and Devonian	122
4.7.1	Delorme Sequence (Group)	123
4.7.1.1	Tsetso Formation	124
4.7.1.2	Camsell Formation	124
4.7.2	Arnica-Bear Rock Sequence	125
4.7.2.1	Arnica and Sombre Formations	126
4.7.2.2	Bear Rock and Fort Norman Formations	127
4.7.2.3	Origin and Development of Bear Rock Breccias	131
4.7.2.4	Landry Formation and Landry Member	135
4.7.3	Hume Sequence (Formation)	136
4.7.4	Fairholme Sequence	137
4.7.4.1	Hare Indian Formation	137
4.7.4.2	Ramparts Formation (Kee Scarp Formation)	138
4.7.4.3	Canol Formation	138
4.7.4.4	Imperial Formation	138
4.8	Upper Jurassic to Paleogene Assemblages	139
4.8.1	Blairmore and Trevor Assemblages	139
4.8.2	Brazeau Assemblage	141
4.9	Tertiary to Quaternary	142

CHAPTER V QUATERNARY OF THE NORTHEASTERN MACKENZIE MOUNTAINS

5.1 Introduction	160
5.2 Regional Glacial Chronologies	161
5.2.1 Yukon Territory	161
5.2.2 Banks Island, Tuktoyaktuk Coast	162
5.2.3 Bonnett Plume Basin, Richardson and Franklin Mountains, Mackenzie Valley	164
5.3 Mackenzie Mountains	167
5.3.1 Southern Mackenzie Mountains	168
5.3.2 Northern Mackenzie Mountains	169
5.3.2.1 Pre-Wisconsinan Events	170
5.3.2.2 Hungry Creek Glaciation	172
5.3.2.3 Katherine Creek Phase	173
5.3.2.4 Tutsieta and Kelly Lake Phases	176
5.3.2.5 Chronological Summary	176
5.3.2.6 Glacial Thermal Conditions	177
5.4 General Geomorphology, Canyon Ranges	178
5.4.1 Pediments and Planation Surfaces	178
5.4.2 The Valleys and Canyons	180

CHAPTER VI KARST LANDFORMS OF THE NORTHEASTERN MACKENZIE FOLDBELT

6.1 Introduction	194
6.2 Karren	194
6.2.1 Karren on the Mount Kindle Formation	195
6.2.2 Karren on the Bear Rock Formation	199
6.2.3 Karren on the Hume Formation	202
6.3 Dolines and Depressions	202
6.3.1 Distribution and Identification of Dolines and Depressions	207
6.3.2 Collapse-Subsidence Dolines and Depressions	209
6.3.2.1 Regional Structural Setting	210
Vermillion Creek	210
Great Bear Karst	210
Imperial Hills	211
Mountain River	212
Ration Creek	213
Carcajou Canyon	214
6.3.3 Depressions on the Bear Rock Formation	214
6.3.3.1 Dolines	215
6.3.3.2 Compound Dolines	217

6.4 Blind Valleys	217
6.5 Subsidence Troughs	219
6.5.1 MacKay Range	219
6.6 Poljes	220
6.7 Caves	221
6.7.1 Slope Caves	221
6.7.2 Solution Caves	223
6.8 Tufa	225
6.9 Pseudokarst Forms	225

CHAPTER VII THE DODO CANYON SITE

7.1 Introduction	241
7.2 Site Description	241
7.3 Geology of the Dodo Canyon Site	244
7.3.1 Hume Formation	245
7.3.2 Bear Rock Formation	246
7.3.2.1 Landry Member	246
7.3.2.2 Brecciated Member	247
7.4 General Hydrology, Hydrochemistry, and Isotopes	248
7.4.1 Catchment Delineation	249
7.4.2 Variations in Recharge and Discharge	252
7.4.2.1 Winter-Spring: Sink (Recharge) Zone	252
7.4.2.2 Winter-Spring: Fluvial Zone	253
7.4.2.3 Winter-Spring: Discharge Zone	253
7.4.2.4 Summer: Sink and Fluvial Zone	255
7.4.2.5 Summer: Discharge Zone	256
7.4.3 Hydrochemical Signatures	258
7.4.3.1 Recharge Waters of the Sink Zone	258
7.4.3.2 Discharge Waters of the Sink and Fluvial Zones	259
7.4.3.3 Discharge Waters of Carcadodo Valley	260
7.4.3.4 Discharge Waters into Carcajou Canyon	263
7.4.3.5 Spillway Spring	264
7.4.3.6 Mount Kindle Samples	265
7.4.3.7 Dodo West Creek, Dodo Creek, and Carcajou River	266
7.4.4 Meteoric Waters	267
7.4.4.1 Local Meteoric Line	268
7.4.4.2 Sample Deviation from the Local Meteoric Line	268
7.4.4.3 Freezing Effect	270
7.4.4.4 Recharge Area	271
7.4.4.5 Temporal Variations in $\delta^{18}\text{O}$	272
7.5 Hydrochemical Mixing in the Main Karst	274

7.5.1	Fluvial Zone	276
7.5.2	Carcadodo Valley	277
7.5.3	Carca-Spring Stream	278
7.5.4	Temperature of Spring Waters	279
7.5.6	Sulphur Isotopes	280
7.5.7	Model of Circulation in the Main Karst	281
7.6	Hydrograph Analyses	283
7.6.1	Hydrograph Recession	283
7.6.1.1	Recession of Red Rock Brook and Fox Spring	285
7.6.2	Discharge Solute Relationships	286
7.6.3	Hydrograph Separation	287
7.6.3.1	Hydrograph Separation: Fox Spring	288
7.6.4	Water Balance	293
7.6.5	Groundwater Velocity	295
7.7	Summary	296

CHAPTER VIII THE BONUS LAKE SITE

8.1	Introduction	339
8.2	Site Description	339
8.2.1	Geology	341
8.2.1.1	Hume Formation	341
8.2.1.2	Bear Rock Formation	342
8.2.2	Geomorphology	343
8.2.2.1	Upland	343
8.2.2.2	Upper Sink Zone	345
8.2.2.3	Grikeland	346
8.2.2.4	Lower Sink Zone	348
8.2.2.5	Caves	349
8.3	Hydrology and Hydrochemistry	349
8.3.1	Recharge	350
8.3.2	Discharge	351
8.3.3	Stable Isotopes	353
8.3.4	Hydrochemical Facies	355
8.3.4.1	Sink Zones and Grikeland	355
8.3.4.2	Canyon Streams	357
8.3.4.3	Bonus Valley	357
8.4	Summary	359

CHAPTER IX THE PYRAMID LAKE SITE

9.1	Introduction	375
9.2	Site Description	375

9.2.1	Geology	376
9.2.1.1	Structure	376
9.2.1.2	Lithology and Distribution	377
9.2.2	Geomorphology	378
9.3	Hydrology and Hydrochemistry	380
9.3.1	Streams in Misery Valley	381
9.3.2	Low Discharge Springs (Little Keele River)	381
9.3.3	Blue Mountain Streams	382
9.3.4	Pyramid Lake Streams	384
9.3.5	Pyramid Lake	385
9.3.6	Horseshoe Spring	386
9.4	Pyramid Lake Aquifer	387
9.5	Summary: Pyramid Lake Site	389

CHAPTER X THE BEAR ROCK SITE

10.1	Introduction	398
10.2	Geology	400
10.2.1	Lithology and Distribution	401
10.2.1.1	Saline River Formation	401
10.2.1.2	Franklin Mountain Formation	402
10.2.1.3	Bear Rock Formation	404
10.2.1.4	Hume Formation	405
10.2.1.5	Other Units	405
10.2.2	Structure	406
10.3	Geomorphology	410
10.3.1	Glacial	410
10.3.2	Karst	413
10.3.2.1	Mapping	413
10.3.2.2	Dolines and Depressions	414
10.4	Hydrology and Hydrochemistry	418
10.4.1	Recharge Zone	419
10.4.1.1	Water Type 1: Draining Ponds and Dolines	419
10.4.1.2	Water Type 2: Perched Lakes and Ponds	421
10.4.1.3	Water Type 3: Springs and Streams	423
10.4.1.4	Recharge Zone Summary	424
10.4.2	Discharge Zone	426
10.4.2.1	Water Type 4: Forest and Blood Streams	426
10.4.2.2	Water Type 5: Streams	428
10.4.2.3	Water Type 6: Bear Rock Spring Area	429
10.4.2.4	Water Type 7: Congo River	434
10.4.2.5	Water Type 8: Other Springs	436

10.4.2.6 Discharge Zone Summary	436
10.5 Groundwater Circulation at Bear Rock	437
10.5.1 South Karst	438
10.5.1.1 Forest and Blood Streams	438
10.5.1.2. Bear Rock Spring Area	439
10.6 Summary: Bear Rock Site	441
CHAPTER XI DISCUSSION AND CONCLUSIONS	
11.1 Introduction	463
11.2 Distribution of Karst Landforms	464
11.2.1 Morphology, Lithology, and Structure	464
11.2.2 Influence of Glaciation and Permafrost	467
11.3 Karst Hydrogeology	474
11.4 Rate and Distribution of Solution	477
11.4.1 Denudation	479
11.4.1.1 Denudation Rates	481
11.5 Development of the Northern Mackenzie Mountain Karst	484
11.6 Future Directions	486
REFERENCES	496
APPENDIX	523

LIST OF TABLES

Table 1.1	Relationship between spatial and temporal scale of karst features.	14
Table 1.2	The dominant geomorphic processes and landscape characteristics of the morpho-climatic regions and their karst equivalents.	14
Table 2.1	Effects of glaciation upon karst systems.	54
Table 3.1	Mean daily temperature, annual rainfall, snowfall, and precipitation for selected stations in the western N.W.T. and eastern Yukon.	93
Table 3.2	Occurrence of frozen ground for surficial materials in NTS map areas 96C, 96E, and 106H.	93
Table 3.3	Occurrence of frozen ground for genetic terrain types in construction spread 1 (km 0 to km 149.5) of the Norman Wells - Zama pipeline.	94
Table 3.4	Discharge characteristics from streams in the study area.	95
Table 3.5	Instantaneous sediment data for the Redstone, Mountain, and Carcajou Rivers, 1987-89.	95
Table 3.6	Water quality data from Keele, Redstone, and Mountain Rivers.	96
Table 4.1	Descriptive classification of breccia fabrics.	144
Table 4.2	Locations of wells in Table 4.3.	144
Table 4.3	Thickness of Mesozoic to Lower Cambrian units from several cores in the Mackenzie Plain area.	145
Table 4.4	Abbreviations used for lithostratigraphic units in Table 4.3.	146
Table 4.5	Well records from the Mackenzie Plain area that display evidence of groundwater solution in Devonian strata, in particular the Fort Norman Formation.	146
Table 5.1	Map reference, lab numbers, and location of radiocarbon dates in the District of Mackenzie.	185
Table 7.1	Grouping of water samples from the Dodo Canyon Site on the basis of their physical characteristics and location within the karst.	298
Table 7.2	Description and classification of water sampling sites at Dodo Canyon Site.	299
Table 7.3	Mean temperature, conductivity, pH, total hardness, ion concentrations, total dissolved ions, Ca ²⁺ /Mg ²⁺ ratio, saturation indices (calcite and dolomite), and <i>p</i> PCO ₂ for water types of Dodo Canyon Site.	300
Table 7.4	Mean temperature, conductivity, pH, total hardness, ion concentrations, total dissolved ions, Ca ²⁺ /Mg ²⁺ ratio, saturation indices (calcite and dolomite), and <i>p</i> PCO ₂ for water samples in Carcadodo Valley.	301
Table 7.5	δ ¹⁸ O and δD data from precipitation in the study region.	302

Table 7.6	$\delta^{18}\text{O}$ from selected sampling locations in the Dodo Canyon Karst.	303
Table 7.7	Discharge and hydrochemistry of shallow, intermediate, and deep flow components in the Dodo Canyon Karst.	304
Table 8.1	Description of water sampling locations at the Bonus Lake Site.	361
Table 8.2	Grouping of water samples from the Bonus Lake Site on the basis of their location.	362
Table 8.3	$\delta^{18}\text{O}$ of water samples from the Bonus Lake Site.	362
Table 8.4	Mean temperature, conductivity, pH, total hardness, ion concentrations, total dissolved ions, $\text{Ca}^{2+}/\text{Mg}^{2+}$ ration, saturation indices (calcite and dolomite), and $p\text{PCO}_2$ for water samples at the Bonus Lake Site.	363
Table 9.1	Description of water sampling locations at the Pyramid Lake Site.	390
Table 9.2	Temperature, conductivity, pH, total hardness, ion concentrations, total dissolved ions, $\text{Ca}^{2+}/\text{Mg}^{2+}$ ratio, saturation indices (calcite and dolomite), and $p\text{PCO}_2$ of water samples at the Pyramid Lake Site.	391
Table 9.3	Temperature, conductivity, total hardness, and total dissolved ions for Pyramid Lake Site sample groups.	392
Table 10.1	Grouping of water samples from the Bear Rock Site on the basis of location in the karst.	442
Table 10.2	Description and classification of water sampling locations at the Bear Rock Site.	443
Table 10.3	Mean temperature, conductivity, pH, total hardness, ion concentrations, total dissolved ions, $\text{Ca}^{2+}/\text{Mg}^{2+}$ ratio, saturation indices (calcite and dolomite), and $p\text{PCO}_2$ for water types of the Bear Rock Site.	444
Table 10.4	Mean temperature, conductivity, pH, total hardness, ion concentrations, total dissolved ions, saturation indices (calcite and dolomite), and ion balance errors for Bear Rock Springs	445
Table 10.5	$\delta^{18}\text{O}$ and δD values in ‰ SMOW from the Bear Rock Spring Area	446
Table 10.6	$\delta^{34}\text{S}$ values in ‰ for aqueous and precipitated sulphates from the Bear Rock Spring Area.	446
Table 11.1	Mean ion concentrations for rivers of the Mackenzie Mountains and selected water types from Dodo Canyon, Bonus Lake, and Bear Rock field sites.	488
Table 11.2	Solutional denudation in Carcajou, Redstone, and Mountain River basins.	488
Table 11.3	Average ion concentrations for Red Rock Brook, Dodo Canyon Site and load, by ion, as tonnes over the hydrological season.	489
Table 11.4	Volume of halite, anhydrite, and dolomite discharged from the Red Rock Brook aquifer, Dodo Canyon Site.	489

LIST OF FIGURES

Figure 1.1	The morphological components of a simple karst system from the humid temperate zone.	15
Figure 1.2	Morphoclimatic regions as proposed by Wilson (1968).	15
Figure 1.3	The branches of geomorphic inquiry.	16
Figure 2.1	Solubility of carbon dioxide as a function of the partial pressure of CO ₂ in the coexisting gas phase.	55
Figure 2.2	Solubility of calcite as a function of carbon dioxide partial pressure.	55
Figure 2.3	Mean growing season soil log PCO ₂ versus mean annual actual evapotranspiration.	56
Figure 2.4	Controls on the development of karst aquifer flow systems.	57
Figure 2.5	(A) A conceptual classification of karst aquifers into diffuse, fissure (mixed), and conduit types. (B) The predominant flow regimes of the aquifer types.	56
Figure 2.6	Hydrological and solute pathways in a karst system.	58
Figure 2.7	Permafrost zones in North America.	59
Figure 2.8	Interactions between climate and ground thermal regime.	59
Figure 2.9	Hydrographs from basins representing the five streamflow regimes.	60
Figure 2.10	Frozen and unfrozen zones in a permafrost environment and their relationships with surface water and groundwater.	61
Figure 2.11	A simple model of glacial superimposition on permafrost.	62
Figure 2.12	Steady state conditions in permafrost and overlying glacial ice solved for three geothermal heat flux conditions.	62
Figure 2.13	A model depicting the relationships between permafrost, groundwater circulation, and karst activity in terrains of low to moderate relief.	63
Figure 2.14	A zonal model of permafrost distribution showing the relationship between permafrost and karst drainage in rugged terrain.	63
Figure 3.1	Topography, drainage, field site locations, and gauging stations in the northeastern Mackenzie Mountains.	97
Figure 3.2	Mean monthly rainfall and snowfall, daily maximum, mean, and minimum temperatures for Norman Wells and Fort Norman.	98
Figure 3.3	Rainfall at Dodo Base Camp vs rainfall at Norman Wells, June and July of 1987 and 1988.	99
Figure 3.4	Mean monthly discharges over the period 1980 - 90 for Mackenzie Mountain Rivers: Redstone, Mountain, Carcajou, Twitya, and Tsichu.	99
Figure 3.5	Hydrograph of Carcajou River, 1988.	100
Figure 3.6	Suspended sediment and dissolved sediment concentrations vs discharge for Redstone, Mountain, and Carcajou Rivers.	100

Figure 3.7	Trilinear diagram of water samples from Keele, Mountain, and Redstone Rivers.	101
Figure 3.8	Mean ion concentrations for summer and winter samples from Mountain, Keele, and Redstone Rivers.	102
Figure 4.1	Major physiographic and tectonic divisions in the western District of Mackenzie and eastern Yukon.	147
Figure 4.2	General geology of the study region, map shows the distribution of tectonic assemblages and major faults.	148
Figure 4.3	Table of formations from Sans Sault Rapids, Carcajou Canyon, Norman Wells, and Fort Norman map areas.	149
Figure 4.4	Distribution of positive and negative tectonic features on the Mackenzie Shelf.	151
Figure 4.5	Stratigraphic relationships in the northeastern Mackenzie Mountains. . .	152
Figure 4.6	Distribution of major faults and anticlines in the Mackenzie Foldbelt. . .	153
Figure 4.7	Approximate configuration of the Saline Rive Formation depositional basin.	154
Figure 4.8	Isopach map of the Evaporite Member of the Saline River Formation. . .	154
Figure 4.9	Distribution of upper Lower to lower Middle Devonian rocks.	155
Figure 4.10	Isopach map of the Fort Norman Formation.	155
Figure 4.11	Exposure of the Mount Kindle and Bear Rock Formations on the north wall of Carcajou Canyon near the Dodo Canyon Site.	156
Figure 4.12	The Brecciated Member of the Bear Rock Formation at the type section near Fort Norman.	156
Figure 4.13	The Landry Member of the Bear Rock Formation on the east wall of Dodo Canyon at the Dodo Canyon Site.	157
Figure 4.14	The Brecciated Member of the Bear Rock Formation at the Bear Rock Site.	157
Figure 4.15	The solution brecciation process as outlined by Stanton (1966).	158
Figure 4.16	Schematic diagram showing the distribution of formations comprising the Cretaceous and Tertiary clastic wedges of the Peel Trough.	159
Figure 5.1	Wisconsinan ice limits in northwestern Canada.	186
Figure 5.2	Regional correlation of glacial deposits and events in northwestern Canada.	187
Figure 5.3	Glacial limits, type areas, and distribution of deposits in northwestern Canada.	188
Figure 5.4	Retreat positions of the Laurentide Ice Sheet in the Late Wisconsinan, and the locations of the type areas for the major stadials.	189
Figure 5.5	Limits of the Hungry Creek Glaciation (all time Laurentide maximum) and Dark Rock Creek II montane glaciation.	190
Figure 5.6	Glacial landforms in the Carcajou Range, Mackenzie Mountains, N.W.T.	191

Figure 5.7	A south to north transect of the abandoned canyon between Little Keele River and Dodo Creek.	192
Figure 5.8	A photo looking northwest through "Dry Canyon" to Katherine Creek.	193
Figure 5.9	Photograph of "Kindle Canyon".	193
Figure 6.1	Distribution of karst in the northern Franklin and Mackenzie Mountains.	227
Figure 6.2	Oblique aerial view of Dodo Pavement.	228
Figure 6.3	Tors on the Plains of Abraham.	228
Figure 6.4	Dense pitting of the Mount Kindle Formation at the Pyramid Lake Site.	229
Figure 6.5	Solution pan (kaminitza) on the Dodo Pavement.	229
Figure 6.6	Rillenkarren on the Landry Member of the Bear Rock Formation.	230
Figure 6.7	Rillenkarren data from Dodo Site: a) rill width vs rill length; b) rill length vs surface slope.	230
Figure 6.8	Model illustrating the occurrence of aerial subsidence-collapse features in cover units above an evaporite subcrop.	231
Figure 6.9	Distribution of dolines, ponors within closed depressions, dolomite pavement, major springs, and areas of internal drainage in the Carcajou Rang, Mackenzie Mountains, N.W.T.	232
Figure 6.10	A vertical walled collapse doline at the Dodo Canyon Site.	233
Figure 6.11	Examples of dolines from the study region.	234
Figure 6.12	The Imperial Hills cross-section.	235
Figure 6.13	The Bell Creek cross-section.	236
Figure 6.14	The Ration Creek cross-section.	237
Figure 6.15	Two types of dolines in the Bear Rock Formation observed at the Dodo Canyon Site.	238
Figure 6.16	Development of a breached or horseshoe doline.	238
Figure 6.17	Plan view of two dolines in a linear trough at the Dodo Canyon Site.	239
Figure 6.18	The Mackay Range cross-section.	240
Figure 6.19	Characteristic morphology of slope caves in the study region illustrated by three examples.	239
Figure 7.1	Vertical aerial photograph of the Dodo Canyon Site.	305
Figure 7.2	The Dodo Canyon Site is divided into the Dodo West, Main, and North Karsts.	306
Figure 7.3	Oblique aerial photograph looking west over Carcajou Canyon to the Main Karst and Dodo Canyon.	307
Figure 7.4	Oblique aerial photograph looking northwestward over the Main Karst.	307
Figure 7.5	A view of Carcadodo Valley looking west to Dodo Canyon.	308
Figure 7.6	The eastern end of Carcadodo Valley.	308

Figure 7.7	General geomorphology of the Dodo Canyon Site.	309
Figure 7.8	Bedrock geology of the Dodo Canyon Site.	310
Figure 7.9	Karst geomorphology of the Dodo Main Karst.	311
Figure 7.10	A view looking east through "Dry Valley", a linear depression in the Sink Zone of the Main Karst.	312
Figure 7.11	A solution-subsidence doline east of Fan Canyon near D14.	312
Figure 7.12	Monthly temperature and precipitation at Norman Wells, August 1986 to 1988.	313
Figure 7.13	A view of the base of Bear Scat Sink looking west along the Scarp.	314
Figure 7.14	Two views of Terminal Sink, the easternmost pond in Carcadodo Valley.	315
Figure 7.15	(a) Average daily discharge of Red Rock Brook in the 1987 field season. (b) Average daily discharges of Red Rock Brook and Fox Spring in the 1988 field season.	316
Figure 7.16	(a) Discharge of Red Rock Brook versus discharge of Fan Stream. (b) Discharge ratio between Fan Stream and Red Rock Brook versus time.	317
Figure 7.17	Trilinear diagram of waters from the Dodo Canyon Site.	318
Figure 7.18	Summary diagram of data presented in the trilinear diagram from the Dodo Canyon Site.	319
Figure 7.19	Mean concentrations of major anion and cation species for water types in the Dodo Canyon Karst.	320
Figure 7.20	Mean concentrations of major anion and cation species for discharge waters of Carcadodo Valley.	321
Figure 7.21	Sketch map of sample locations at the base of Carcajou Canyon.	322
Figure 7.22	Meteoric water lines from Fort Smith and the study area.	323
Figure 7.23	Isotope samples from the Dodo Canyon Site plotted with the local and Fort Smith meteoric water lines.	323
Figure 7.24	$\delta^{18}\text{O}$ of water samples at the Dodo Canyon Site versus time.	324
Figure 7.25	Model depicting the mixing of two flow components of equal magnitude.	325
Figure 7.26	Model of three-way mixing.	326
Figure 7.27	Concentrations of major anions and cations versus total dissolved ions for the samples of the Fluvial Zone.	327
Figure 7.28	Concentrations of major anions and cations versus total dissolved ions for samples of Carcadodo Valley.	328
Figure 7.29	Concentrations of major anions and cations versus total dissolved ions for samples from Salt and Colluvium Springs, and Carca-Spring Stream.	329
Figure 7.30	Temperature versus total dissolved ions for selected springs in the Main Karst.	330

Figure 7.31	Histogram of $\delta^{34}\text{S}$ values for SO_4^{2-} from gypsum and anhydrite samples of the Bear Rock and Saline River Formations and values from water samples of the Dodo Canyon Karst.	330
Figure 7.32	Schematic diagram of ground water circulation in the Dodo Canyon Karst.	331
Figure 7.33	Terms used in karst spring recession.	332
Figure 7.34	Instantaneous discharge of Red Rock Brook and Fox Spring in the field season of 1988.	332
Figure 7.35	Discharge of Red Rock Brook and Fox Spring over portions of the 1988 field season.	333
Figure 7.36	Concentrations of the major anion and cation species in Red Rock Brook, Fox Spring, and Fan Stream Versus time.	334
Figure 7.37	Separation of a karst spring hydrograph.	335
Figure 7.38	Total hardness, conductivity, $\delta^{18}\text{O}$, and discharge of Fox Spring from June 26 to July 17, 1988.	336
Figure 7.39	Hydrograph separation at Fox Spring.	337
Figure 7.40	Separation of Fox Spring hydrograph into three components.	338
Figure 7.41	General model of hydrograph separation in Carcadodo Valley.	338
Figure 8.1	Vertical aerial photograph of the Bonus Lake Site.	364
Figure 8.2	Map of the Bonus Lake Site.	365
Figure 8.3	Geology of the Bonus Lake Site.	366
Figure 8.4	Karst geomorphology of the core area of the Bonus Lake Site.	367
Figure 8.5	View of the Lower Sink Zone southwest of Bonus Lake.	368
Figure 8.6	Natural bridge exposed on the southern wall of Twin Bridges Canyon, the feature is called the Arch.	368
Figure 8.7	View of the northwestern end of Bonus Lake.	369
Figure 8.8	View of the western end of Trout Lake showing three blocks of the upper Hume Formation.	369
Figure 8.9	Isotope samples from the Bonus Lake Site plotted with the local and Fort Smith meteoric water lines.	370
Figure 8.10	Trilinear diagram of waters from the Bonus Lake Site.	371
Figure 8.11	Frequency of magnesium, calcium, and total hardness in samples across the Bonus Lake Site.	372
Figure 8.12	Mean concentrations of major anion and cation species for water types of the Bonus Lake Karst.	373
Figure 8.13	Saturation index of calcite versus $-\log_{10}$ of the partial pressure of CO_2 for water samples at the Bonus Lake Karst.	374
Figure 8.14	Total hardness versus $-\log_{10}$ of the partial pressure of CO_2 for water samples of the Bonus Lake Karst.	374
Figure 9.1	Vertical aerial photograph of the Pyramid Lake Site.	393

Figure 9.2	Map of the Pyramid Lake Site illustrating topography, drainage, and water sampling locations.	394
Figure 9.3	Geology of the Pyramid Lake Site.	395
Figure 9.4	Isotope samples from the Pyramid Lake Site plotted with the local and Fort Smith meteoric water lines.	396
Figure 9.5	Electrical conductivity versus total hardness (a) and total dissolved ions (b) for water samples at the Pyramid Lake Site.	397
Figure 9.6	Total hardness versus $-\log_{10}$ of partial pressure of CO_2 for water samples from the pyramid Lake Site.	397
Figure 10.1	Map of the Bear Rock Site showing topography and drainage.	447
Figure 10.2	Aerial photograph of the North Karst, Bear Rock Site	448
Figure 10.3	Aerial photograph of the South Karst, Bear Rock Site.	449
Figure 10.4	Camp Depression of the North Karst.	450
Figure 10.5	Photograph of the Bear Rock Spring Area.	450
Figure 10.6	Geology of the Bear Rock Site.	451
Figure 10.7	Karst geomorphology of the Bear Rock Site.	452
Figure 10.8	A view of the North Karst looking east from a position west of sampling point R25.	453
Figure 10.9	Small streamlined ridges and crag and tail features developed on the Bear Rock Formation in the area around point R34.	453
Figure 10.10	Trilinear diagram of waters from the Bear Rock Site.	454
Figure 10.11	Mean concentrations of major anion and cation species for water types at the Bear Rock Site.	455
Figure 10.12	$\delta^{18}\text{O}$ of water samples at the Bear Rock Site versus SO_4^{2-} concentration.	456
Figure 10.13	$\delta^{18}\text{O}$ of water samples at the Bear Rock Site versus time.	456
Figure 10.14	Sketch map of the Bear Rock Spring Area showing the positions of the spring points and streams.	457
Figure 10.15	Isotope samples from the Bear Rock Spring Area plotted with the local and Fort Smith meteoric water lines.	458
Figure 10.16	Concentrations of major anions and cations versus total dissolved ions for samples of the Bear Rock Spring Area.	459
Figure 10.17	Stage recorded at Springs S2 (Location S2 Well) and S3 (Location R3) in June, July, and August of 1988.	460
Figure 10.18	Discharge, temperature, conductivity of Congo River.	461
Figure 10.19	Saturation index of calcite versus the negative logarithm of the partial pressure of CO_2 for water samples of the Bear Rock Site.	462
Figure 10.20	Total hardness versus the negative logarithm of the partial pressure of CO_2 for water samples of the Bear Rock Site.	462

Figure 11.1	Bedrock geology, distribution of dolines, ponors within closed depressions, dolomite pavement, major springs, and areas of internal drainage, Carcajou Range, Mackenzie Mountains, N.W.T.	490
Figure 11.2	Influence of permafrost on hydrological pathways in karst of the northern Mackenzie Mountains	491
Figure 11.3	Specific electrical conductivity vs total dissolved ions concentrations for samples from the field sites.	492
Figure 11.4	Specific electrical conductivity vs total hardness for samples from the field sites.	493
Figure 11.5	Frequency distribution of total hardness from the study region.	494
Figure 11.6	Total hardness vs $-\log_{10}$ of PCO_2 for water samples of the study region.	495

CHAPTER I

INTRODUCTION

1.1 An Introduction to the Study

This dissertation is a study of the distribution, characteristics, and processes responsible for the development of karst landforms and drainage systems in a mountainous region of the District of Mackenzie, N.W.T. Karst is most prevalent in temperate and tropical regions established on areas of carbonate bedrock. In many periglacial regions, the predominance of frost as a weathering agent, the brevity of the hydrological season, and the occurrence of permafrost in the near subsurface inhibits the formation of karst. While periglacial and permafrost karsts are not unknown, little of the literature addresses this field and it represents an area of study where basic research is required. This work examines karst in a region where there is a widespread distribution of permafrost and where there is a record of several Quaternary glaciations. The features under study occur on Cambrian to Middle Devonian carbonate and evaporite sequences. In particular, karst features are well developed on a limestone solution breccia, the Lower Devonian Bear Rock Formation. Much of this thesis describes the surface features and hydrogeology of this formation and other bedrock units that support similar phenomena. The karst landforms and groundwater flow systems reflect a complex geology and geomorphic history.

Due to the regional scope of the investigation and the diverse set of questions that are considered, data are presented and discussed in several independent sections of the thesis. Chapter I serves as a brief introduction to karst geomorphology and outlines the thesis objectives. Chapter II functions as a literature review, focussing on materials that are relevant to karst in permafrost areas. Chapter III describes the

biophysical characteristics of the study region and the methods employed in data collection and analyses. Chapters IV and V review the bedrock geology and Quaternary. The distribution and characteristics of karst landforms are discussed in Chapter VI. Chapters VII through X present and discuss the results of detailed mapping, and hydrological and hydrochemical data gathered from individual study sites. Chapter XI provides a summary of the thesis.

1.2 An Introduction to Geomorphology

The organization of geomorphology as a discipline began in the late 19th and early 20th centuries. Many of the concepts that are now central to it developed during that early period. Most important was the recognition of the nature of the interaction between driving forces and the resisting framework. Davis (1899) theorized that landforms are a function of process, structure, and stage. Process refers to landscape modifying mechanisms that are generated by the driving forces of climate, gravity, and internal heat. Structure describes the lithology and geometry of the resisting framework. Stage is the degree of evolution of a landform or landscape within a cyclic model. Davis' approach of classifying landscapes into an evolutionary cycle was ultimately discredited, but his landform equation, with time substituted for stage, still forms the foundation of the subject.

All landscapes are to varying degrees influenced by the three principle driving forces. Climate and gravity are responsible for the exogenic processes of weathering and mass wasting, as well as the erosional and depositional actions of water, wind, and ice. Internal heat drives vulcanism, epeirogenesis, and plate tectonics. How these processes shape a landscape is dependent on: (i) the characteristics of the original resisting framework, particularly lithology and rock unit geometry, and (ii) the nature of the interaction between process and those rock units. Geomorphic studies at the local or regional scale often focus on the association between exogenic processes and the resisting framework. This association was characterized by Gilbert (1877) as a dynamic adjustment, where landforms are seen to be adjusted to the current process

or processes acting on the landscape. The role of endogenic processes has been largely ignored with the notable exceptions of epeirogenesis and volcanic activity. Davis attempted to describe landscapes within the context of cycles related to episodes of rapid uplift and subsequent denudation. While this did account for some endogenic activity, the models did not adequately address causality. The fundamental differences in the approaches of Davis and Gilbert were, in part, responsible for the divergence of geomorphology into two schools. The historical or evolutionary method of Davis dominated the early part of this century but gradually lost favour and was displaced by a functional approach rooted in the work of Gilbert. This was largely the result of a shift in focus from large scale landscape studies, typified by denudation chronology, to quantitative detailed investigations of landforms at small scales.

1.2.1 Systems and Equilibria in Geomorphology

The growth of the functional or process school was accompanied by the adoption of systems theory in geomorphology (Chorley, 1962; Chorley and Kennedy, 1971). A geomorphic system consists of a series of components representing stores of material in a landscape. Energy and mass may be exchanged between a system and its surroundings and between components within a system. The systems approach is best suited for the examination of geomorphic features where important components and linkages are identifiable and the respective fluxes of energy and mass between them measurable.

Alongside the systems orientation came a recognition of the importance of equilibrium. Hack (1960) reintroduced the dynamic equilibrium concept of Gilbert. A causal relationship was theorized to exist between process and form, and landforms were thought to reflect the prevailing balance or equilibrium between process and geology. Changes in either the process set, or the geology it was acting upon, would trigger a landform adjustment. Equilibrium will be established if controls on landform development remain static for a sufficient period of time. The occurrence of relict

features suggests that for landforms of certain scale, equilibrium has not been established. It is apparent that the nature of process-response is related to the spatial and temporal scale of inquiry. The relationship between time and equilibrium was addressed by Schumm and Lichty (1965) and Chorley and Kennedy (1971). It was proposed that geomorphic systems should be viewed over different time intervals and that equilibrium states are related to the duration of the time interval. Schumm and Lichty (1965) introduced *steady*, *graded*, and *cyclic* to describe increasingly long periods of time over which process-form relationships could be considered. Chorley and Kennedy (1971) and Schumm (1977) coupled time intervals with equilibrium.

1.2.2 Scale in Geomorphology

In any analysis of a geomorphic system, scale is a key consideration. Over short time intervals of static or steady time, there may be significant variations in the morphology of small components of the system, such as bedforms in a stream channel. However, it is unlikely that the larger components will change over the same time intervals, these variables are independent or fixed (Schumm and Lichty, 1965; Schumm, 1977). Since adjustment is related to scale, as scale increases the independence of the system is reduced. Across cyclic time only initial relief, geology, climate, and time are considered independent. It is apparent that for a given landform the nature of the equilibrium is related to the spatial scale of the feature. Thus the association between equilibrium and time may be expanded to encompass spatial scale (Table 1.1). In addition, the relative importance of exogenic and endogenic processes is also related to scale. The development of micro-forms across static or steady time is a function of the operation of exogenic processes on the resisting geology. Only at macro- or mega-scales do endogenic processes assume dominance in landscape generation and modification. The scale of the inquiry dictates which process set warrants examination.

1.2.3 The Karst System

Karst landforms develop where bedrock weathering is dominated by the process of solution. Most frequently, increases in secondary porosity are accomplished by the infiltration of aggressive meteoric waters into the subsurface. Most of the dissolution occurs in a zone at and immediately below the soil-bedrock interface, and also along fissures within the bedrock unit. In addition, there are secondary processes that play a subordinate role in landform genesis, these include: corrasion, precipitation, transportation, sedimentation, subsidence, and collapse (Quinlan, 1978). Karstification is defined as the collective action of any of this set of processes that, in conjunction with solution, produces a landscape of karren, closed depressions, dry valleys, and associated features.

The principle controls on the characteristics of a karst are: (i) the bedrock attributes of solubility, primary porosity, and structure, (ii) the style of the weathering processes operating on that bedrock, and (iii) the boundary conditions which govern the intensity of those processes (Ford and Williams, 1989). The expression and extent to which karst features are developed reflect the geology and geomorphic history operating on a particular landscape. There are several recognized karst morphologies, such as doline karst and cone karst. How the above controls produce these characteristic landform assemblages has been the focus of much debate in the literature. There appears to be a broad climatic zonation but structure and other local factors must also be considered.

1.2.3.1 Morphological Elements

A well developed karst system has three morphological components: (i) input landforms, (ii) a subterranean drainage system characterized by cavernous porosity, and (iii) discharge areas (Ford *et al.*, 1988). All input landforms route surface waters underground, they are classified on the basis of their size and morphology. Karren depicts a series of small scale solution forms, including pits, pans, cutters, groves, and runnels. These features develop on bare rock or beneath soil, and have a maximum

dimension of less than 10 m (Ford, 1980). The fundamental intermediate-scale input landform is the closed depression or doline, this is the characteristic landform of temperate karst terrains. They are of variable morphology with a maximum dimension range of 1 to 1000 m. Large scale input forms include dry valleys, gorges, and poljes. These features are commonly greater than 1 km in length.

It has been argued that karst landscapes evolve from an initial fluvial state to one where surface waters are completely diverted into the subsurface (e.g., Cvijic in Sanders, 1921; Roglic, 1965). The latter terrain is termed a holokarst. A fluviokarst or merokarst is an intermediary stage between the initial fluvial and the holokarst state. Smart (1988) differentiates between fluvial, fluviokarst, and holokarst based on the probability of surface overflow. This concept reinforces the linkage between hydrology and geomorphology in karst areas. The solutional enlargement of bedrock pores and fissures and the possible development of a conduit system influences the surface hydrology and therefore alters the landform generating processes on that surface. Cave systems and the topographic landforms which characterize most karst terrains develop contemporaneously (Ford *et al.*, 1988).

Discharge from karst aquifers is accomplished through spring points or spring lines. The chemical and physical characteristics of discharge waters are a reflection of the travel history, in particular the flow velocity, flowpath length, and stratum encountered en route. Often discharge from regional and intermediate flow systems is thermal and highly mineralized, and constructional features composed of tufa and travertine may occur at spring points. Erosional sapping features may also develop at spring locations. Additional morphological features present in the karst system often include a variety of intermediate scale residual features, such as towers, cones, and pinnacles. A typical landform assemblage of a temperate karst is illustrated in Figure 1.1.

1.2.3.2 Thresholds, Equilibrium and Scale

In many geomorphic systems there are critical thresholds which must be exceeded

before work is done. However, the main process in the karst system is not characterised by such a dynamic threshold; solution or precipitation will proceed if water is present (Ford, 1980; Ford and Drake, 1982). There are intrinsic thresholds, or controls, on the distribution and kinetics of solution within a given aquifer. Adjustments to the configuration of the drainage (conduit) network or a change from open to closed conditions are examples of intrinsic thresholds. Controls on solution may also be of an extrinsic origin. Altering the style of recharge to an aquifer or a lowering of base level would constitute external thresholds. There are critical thresholds related to the secondary processes that influence karst, such as collapse and sedimentation, but these processes become less important with increasing scale.

In karst geomorphology, it is important to consider the scale of the phenomena under study. The morphology of micro-scale erosion features, such as scallops, may reflect very minor changes in mineralogy and controls on solution, such as the velocity of flow. These small forms will adjust rapidly to changing conditions. With an increase in scale, minor spatial variations in the rate of solution are homogenized. Within a limestone or dolomite karst, solution will be governed by factors such as: dissolved carbon dioxide content, open or closed conditions, and climate (temperature and precipitation). At the intermediate or meso-scale, forms reflect interaction between an averaged solution rate over a moderately long period of time and variations in lithology at the unit or formation level. The macro-scale involves aggregates of meso-scale features (Drake, 1984). The characteristics of regional aquifers are a function of the relationship between the gross structure of the resisting framework and the regional climate over long time periods.

The spatial scale of a landform also determines the appropriate temporal scale for examination of the process-form relationship. Micro-forms may be in equilibrium over steady time, but regional aquifers respond slower to changes in process and may be in equilibrium over cyclic time. These relationships are presented in Table 1.1. The magnitude of the spatial dimensions and the divisions between them are somewhat arbitrary and vary according to differences in geology and process rate.

1.2.3.3 The Role of Climate

The range and intensity of exogenic processes that influence a particular landscape are essentially controlled by prevailing temperature and precipitation conditions. Climatic geomorphology is based on the premise that climate exercises such a dominant influence on morphology that structure and endogenic factors are of secondary importance across all scales (Budel, 1982; Tricart and Cailleux, 1972). Under a given climatic regime a distinctive set of processes will produce a unique assemblage of landforms. These unique regions are called morphoclimatic or morphogenetic zones. A classification of morphoclimatic zones, based on mean annual temperature and precipitation, is presented in Figure 1.2 and Table 1.2. The periglacial zone is most relevant to this work. It is characterized by frost action, solifluction, and seasonal fluvial activity. This yields a landscape of patterned ground, gentle cryopediments and cyroplanation surfaces, and large incised and asymmetric valleys (Washburn, 1979). Budel (1982) labels this region as the polar zone of excessive valley cutting with the most striking morphological features being the occurrence of broad deep valleys carved by rapid lateral and vertical erosion.

Lehmann (1954) suggested that each morphoclimatic zone displays a specific karst morphology. These ideas were widely accepted by many French and German researchers and a number of climate-based classifications were developed in the 1950's and 60's. In the polar and periglacial zone, karst phenomena were recognized as being poorly developed and largely restricted to: karren mantled by frost shattered debris, gorges, shallow dolines, and slope caves (Corbell, 1957, 1959, 1964; Ciry, 1962; Sweeting, 1972). Under permafrost conditions, conduit systems and their associated surface landforms would not develop because of the lack of groundwater circulation. However, recent research in permafrost areas describes a diverse collection of features (Chapter II).

The climato-karst approach has been challenged on numerous grounds. Rock control is not adequately addressed, nor are causality and the physical processes themselves. Clearly it does not account for the occurrence of "tropical" karst forms

in temperate and periglacial regions (Brook and Ford, 1978). It is evident that climate does govern karst development to some extent but the static representation of climate embodied by morphoclimatic schemes has not been found to be a powerful explanatory tool in karst studies (Ford, 1980).

Nonetheless, climatic geomorphology has made substantial contributions to the discipline, particularly in the realm of climate change. If it is assumed that a climatic regime will yield a certain assemblage of landforms, then a change in climate will initiate the development of a new assemblage of features that are superimposed upon the pre-existing surface. Depending upon the characteristics of the inherited landforms and the new process set, the relict features may persist. The prevalence of glacial landforms in the temperate zone illustrates that past processes have differed from the modern set in rate and type, yet the geomorphology is still dominated by inherited features. Landscapes may then contain features from a number of climatogenetic regimes and the morphology of features may reflect that polygenetic origin.

1.2.4 Explanation and Method in Geomorphology

Many of the principles introduced in the previous sections have inspired considerable debate in the geomorphic community in the last half century. The concepts of equilibrium were largely developed in studies of fluvial landscapes, the portability of these ideas to terrains influenced by other processes has not been thoroughly explored. The very notion of equilibrium is disputed by researchers who note that the attainment of equilibrium forms requires the unlikely constancy of process and structure over time. However, while the equilibrium concept is somewhat abstract, the framework it provides across a variety of temporal and spatial scales is useful as an explanatory tool in geomorphology.

In discussing explanation in geomorphology, it is useful to contrast the functional and historical schools. The functional approach is most suitable for the examination of landscape features at a small scale. It usually involves the formulation and testing of hypotheses by deductive means under controlled laboratory or field

conditions. This approach is very successful in the study of micro-forms or where landforms adjust very rapidly to changing conditions. Under meso-scale conditions the prevailing processes can be monitored, quantified, and then related to the existing morphology by the back extrapolation of contemporary process-responses. However, this may be inappropriate if features are in equilibrium in cyclic or dynamic time. The problem centres on the debate around uniformitarianism: in the past have geomorphological processes operated at contemporary rates? Clearly a strict adherence to the uniformitarian doctrine is inappropriate given the reality of Cenozoic environmental change. While the physical laws which govern processes are time-invariant, the rates of those processes are not due to variability in the driving forces. Thus difficulties may arise when attempting to evaluate landscape changes through the extrapolation of modern process-response relationships.

The historical approach is linked to Davisian and similar evolutionary models and to denudation chronology, and has received little consideration from geomorphologists in the last few decades. Yet when faced with the study of macro- and mega-forms or landforms with long relaxation times, the functional approach alone is inadequate. Accordingly, with a better understanding of the role of endogenic processes, geomorphologists may now use advances in tectonics to discuss large scale landscape developments across long time periods. Alternatively gross landscape characteristics may be interpreted within a climato-genetic framework.

Given the diversity of opinion regarding the roles of structure, climate, process, and time in shaping landform characteristics, it not possible to define a methodology that is universal to geomorphology. The researcher may employ a variety of techniques and approaches in the study of geomorphic phenomena. This demands a flexible methodology. Chorley (1966) in reviewing geomorphic study separates theoretical and observational works, the latter of which may be field, laboratory, or office based. These four define the main branches of geomorphic inquiry (Figure 1.3). Observational studies focus on morphometric and or process measurements, while theoretical works employ modelling.

It is clear from earlier discussions that the approach or method is dictated in part by the scale of the inquiry. It is appropriate to examine micro-scale process-response mechanisms in the field or laboratory where rapid adjustments facilitate deductive hypothesis formulation and testing. How then to study larger scale problems where landform development occurs over longer time periods? In some circumstances, rates of landform genesis may be determined by quantifying and then back extrapolating contemporary process-responses. Alternatively, the researcher may utilize space-time substitution; when process and structure are held constant the role of time in landform development may be examined by sampling in space for time. This technique has received considerable attention but must be applied cautiously. In a similar manner, the worker may isolate the roles of process and structure by space-process and space-structure substitution. Lastly, simulation techniques may be used to examine landform adjustments across a variety of conditions. These include physical scale models and mathematical models. The latter may be based largely on theory, such as with deterministic and stochastic models, or on field, laboratory, and office measurements, as with statistical models. In a particular investigation the researcher may employ any number of the steps illustrated in Figure 1.3.

Drake (1984) identifies three main research trends in karst studies: (i) hydrodynamics and solution dynamics, (ii) erosion/denudation rates, and (iii) landform description and evolution. Drake observes that: (i) most studies that are concerned with process are seldom conducted at the terrain scale, (ii) denudation studies rarely discuss landform development, and (iii) descriptive works do not address process explanation in a quantitative fashion. Landforms are explained in either functional or historical terms. The functional approach most often employs statistical models, and the historical general evolutionary concepts.

If the objectives of a study are to acquire understanding and to provide explanation regarding landform development, then it is not sufficient to simply invoke generalizing models nor to conduct process measurements without confronting terrain scale variables. This thesis will speak to landform development at the meso-scale and

will attempt to approach explanation from a perspective which includes both description and process.

1.3 Physical Setting of the Study

The study region is in the northeastern section of the Mackenzie Foldbelt. It includes the outer ranges of the Mackenzie Mountains and a portion of the Franklin Mountains in the Norman Wells area (Chapter III). Permafrost has a widespread distribution. Mean annual temperatures are in the range -6 to -8°C. Total annual precipitation is 350 to 550 mm. The region was glaciated in the Late Wisconsinan. The hydrogeology of the Mackenzie District has been described by Brandon (1965) and Michel (1977, 1986a). van Everdingen (1981) has mapped the distribution of karst landforms in parts of the Franklin Mountains and the Great Bear Plain. The Lower Devonian Bear Rock Formation and the Cambrian Saline River Formation are the most important of several bedrock formations that support surface karst and function as karst aquifers. In deep subcrop, both of these formations contain thick intervals of evaporite. The subsurface Bear Rock is dolomite with gypsum or anhydrite, the subsurface Saline River is shale or redbeds with gypsum (anhydrite) and halite. In outcrop, the Bear Rock Formation is a limestone and dolomite breccia and the Saline River Formation is a contorted recessive unit of shale and redbeds. These formations extend in subcrop from the Northern Interior Plains to the rugged Franklin and Mackenzie Mountains. Where they outcrop or are in the shallow subsurface, the terrain is often characterized by solution landforms and surface drainage is captured by the groundwater flow system.

In the southern Mackenzie Mountains, Brook (1976) describes karst and conduit aquifers in the massive limestones of the Nahanni Formation. To the north, previous karst mapping has been of a reconnaissance nature and none has been undertaken in the northern Mackenzie Mountains. In addition, there are few water quality data upon which to assess the erosive role of groundwater in this permafrost environment and there are no detailed analyses at the scale of small basins. In total,

very little is known regarding the distribution and development of solution landforms, their characteristics, and groundwater in the northern Mackenzie Mountains.

1.4 Thesis Objectives

The principal objectives of this thesis are to describe the distribution, morphology, and the development of karst landforms and associated drainage systems in the northern Mackenzie Mountains. In short, the thesis seeks to characterize the geomorphic role of groundwater in the study region. Several avenues of inquiry are pursued. At the regional scale, the locations and range of karst depressions are mapped from aerial photography and surveys. In conjunction with data on structure, lithology, glacial history, and the distribution of permafrost these karst data allow several working hypotheses to be evaluated. Specifically: (i) what are the relationships between geologic structure and lithology and the resulting morphology and density of karst depressions, (ii) what has been the impact of glaciation on karst systems in the region, and (iii) what role does permafrost play in inhibiting or accelerating karstification.

These inquiries are complemented by detailed work at the scale of small basins. This work is intended to provide data on the rate and distribution of solution in the region. Four field sites were selected that displayed the basic components of a karst system (Section 1.2.3.1). At the field sites, geomorphic and geologic mapping were done by ground survey. Hydrological, hydrochemical, and isotopic data were collected from recharge and discharge waters of these systems to provide information on karst processes. From these data it is possible: (i) to describe changes in chemistry as waters pass from zones of recharge to discharge, (ii) to identify flow routes and flow-through times between zones of recharge and discharge, (iii) to identify the lithostratigraphic units that function as the main aquifers. Although limited in number, these data can provide estimates of the spatial and temporal distribution of solution, and therefore a measure of denudation. Coupling the regional observations with the process data, the thesis will attempt to describe the development of karst in the northern Mackenzie Mountains.

Table 1.1: Relationship between spatial and temporal scale of karst features (after Ford, 1980; Drake, 1984; Summerfield, 1991).

	SPATIAL SCALE			
	MICRO	MESO		MACRO
Linear Dimension (m)	<10	10-10 ³	10 ³ -10 ⁶	>10 ⁶
Principal Karst Features	Karren	Dolines, Uvalas	Dry Valleys, Poljes, Local Flow Systems	Regional Aquifer Systems
Predominant genetic mechanisms	Exogenic	Primarily exogenic	Exogenic/endogenic	Exogenic/endogenic
Time required for adjustment of form to process	Short	Moderate	Moderate	Long
Equilibrium temporal scale	Steady 10 ³ a	Dynamic 10 ³ a	Dynamic+ >10 ³ a	Cyclic >10 ⁷ a

Table 1.2 The dominant geomorphic processes and landscape characteristics of the morpho-climatic regions illustrated in Figure 1.2 and their karst equivalents (Wilson, 1968; Sweeting, 1972; Jennings, 1985; Ritter, 1988; Ford and Williams, 1989).

Morpho-climatic Region	Dominant Geomorphic Processes	Landscape Characteristics	Karst Morphology
Glacial	Glaciation, Nivation, Aeolian	Glacial Erosional, Depositional and Meltwater Landforms. Loess, Alpine Topography: Scree, Cirques	Glacio/Nival Karst: Smoothed and Striated Pavements, Small Caves, Gorges, Dolines
Periglacial	Frost Action, Solifluction, Seasonal Fluvial	Patterned Ground, Solifluction Features, Cryoplanation Surfaces, Incised or Asymmetric Valleys	Polar/Permafrost Karst: Debris Mantled Pavements, Scree, Gorges, Micro-karren, Slope Caves
Arid	Desiccation, Aeolian, Fluvial	Dunes, Salt Pans, Deflation Basins, Scree, Canyons	Arid/Semi-Arid Karst: Shallow Depressions, Few Collapse Dolines and Caves, Micro-karren
Semiarid	Fluvial, Mechanical Weathering	Pediments, Fans, Scree, Badlands	
Humid Temperate	Fluvial, Chemical Weathering, Creep, Mass Wasting	Smooth Slopes, Broad Valleys, Alluvial Landforms	Temperate Karst: Dolines, Karren, Large Cave Systems, Polje
Selva Tropical	Chemical Weathering, Mass Wasting, Fluvial	Steep Slopes, Sharp Ridges, Deep Soils, Cavernous Weathering	Tropical Karst: Cones and Cockpits, Towers and Pinnacles, Large Cave Systems

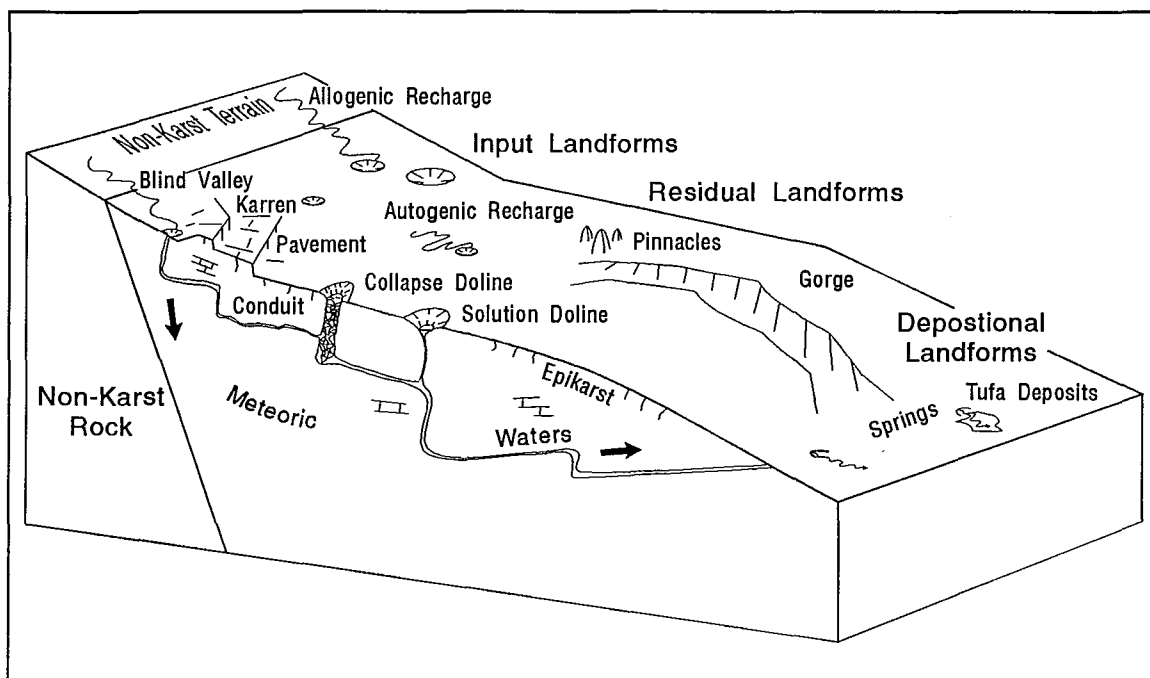


Figure 1.1: The morphological components of a simple karst system from the humid temperate zone.

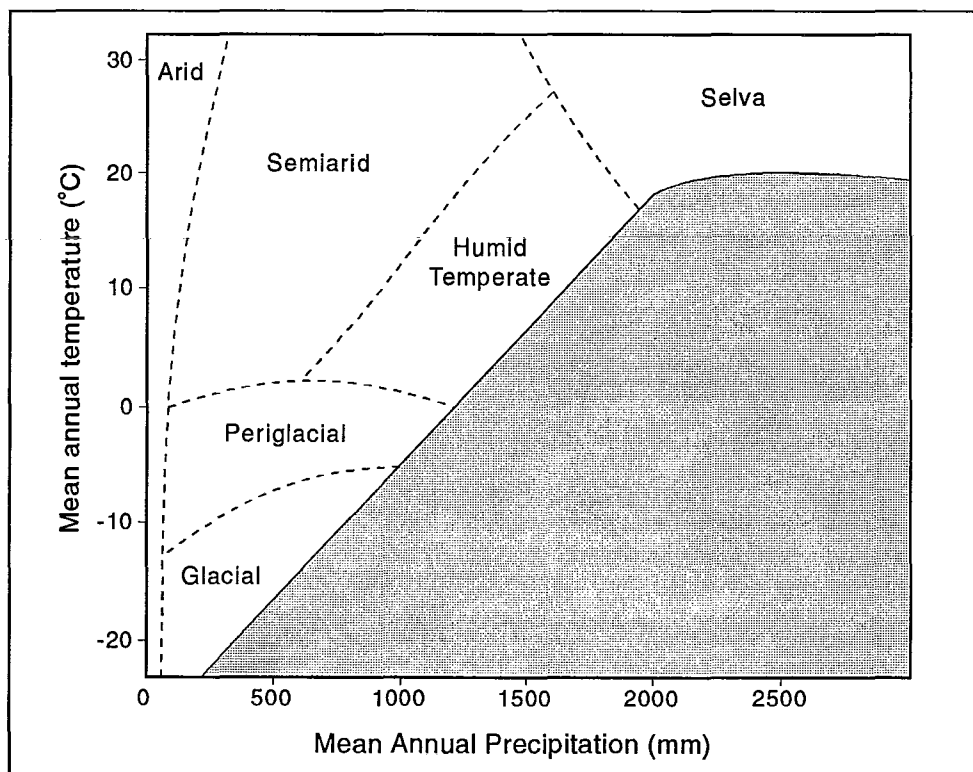


Figure 1.2: Morphoclimatic regions as proposed by Wilson (1968).

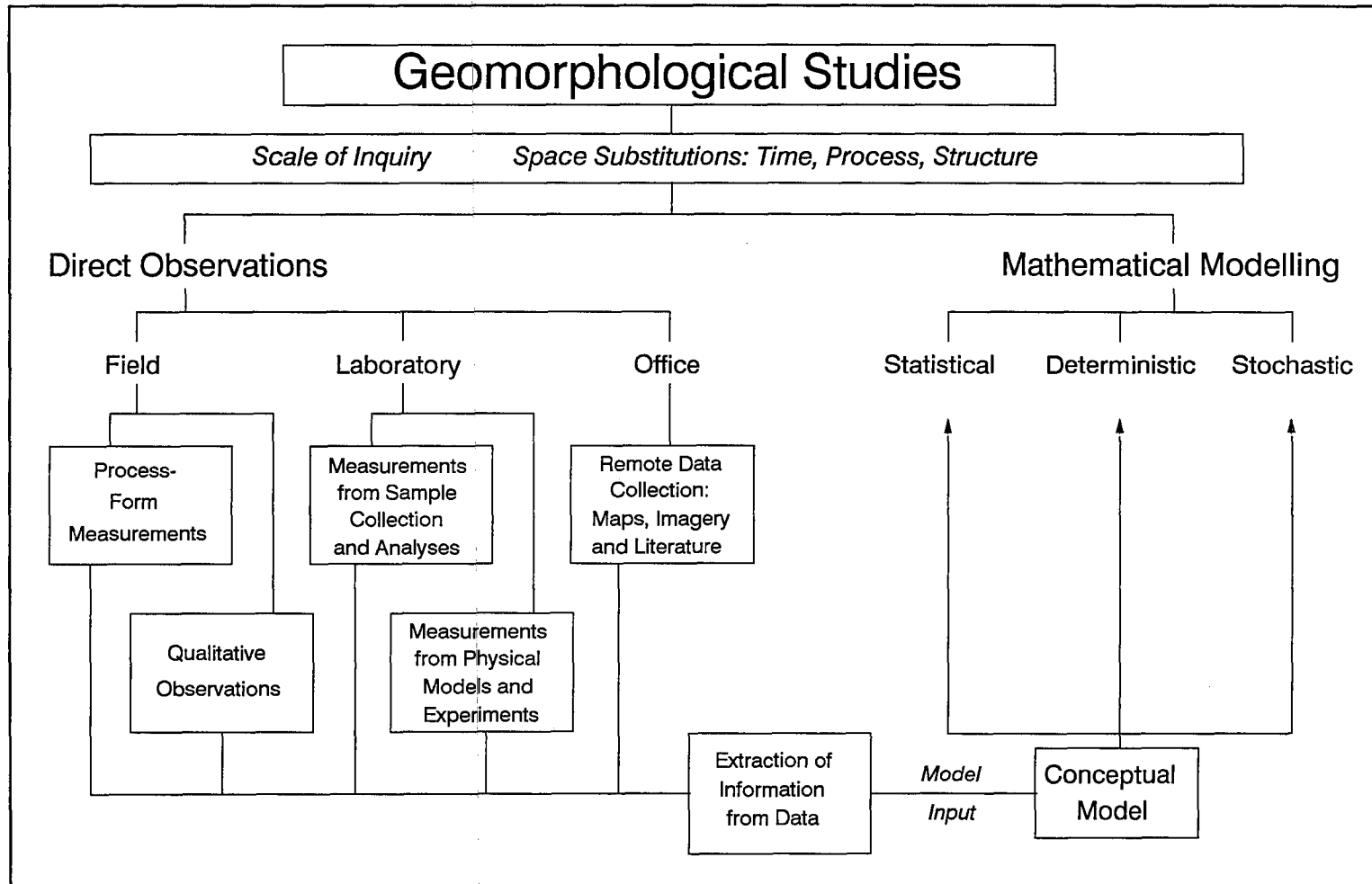


Figure 1.3: The branches of geomorphic inquiry (after Chorley, 1966).

CHAPTER II

KARST IN PERMAFROST TERRAIN

2.1 Introduction

In karst systems, rates of bedrock dissolution and mass transport are a function of several physical and biological factors. The bedrock characteristics of rock purity and solubility, primary and secondary porosity, formation thickness and geometry influence the manner in which surface waters infiltrate into, move, and dissolve minerals in the subsurface. Climate controls the volume, seasonality, temperature and, in part, the carbon dioxide content of recharge waters. In the soil zone, biological sources of carbon dioxide play an important role in the solution chemistry of carbonate rocks. Variations in external factors account for much of the morphological differences that exist between karst terrains of different climatic regimes (e.g., Table 1.2). Karst of the periglacial or permafrost region is characterized by debris mantled pavements, micro-karren, slope caves, and few depressions.

The intent of this chapter is to briefly review materials that relate to the development of karst forms in cold regions. Specific topics considered include mineral dissolution and denudation, as well as karst and permafrost hydrology. The relationships between karst, permafrost, and glaciation are discussed.

2.2 Dissolution of Karst Rocks

Studies of the dissolution chemistry of karst bedrock focus on the behaviour of the dominant carbonate and evaporite minerals: calcite, dolomite, gypsum, and halite. Much research has focused on modelling the dissolution processes and the important rate controls. Equilibrium models are based on thermodynamic principles and they

describe the relative distribution of mass between reactants and products in a given reaction. When mineral dissolution rates are rapid relative to the rate of mass transport, the system is best modelled by an equilibrium approach (Domenico and Schwartz, 1990). When transport rates are high, mineral dissolution is surface reaction controlled (Berner, 1978). The system approaches, but does not achieve, equilibrium and is best described by kinetic methods. This may be observed in a karst where groundwater velocities are high. Most groundwater mineral reactions are characterised by transport control and are modelled by thermodynamics. Importantly, this approach yields information on the direction of reactions but not reaction rate.

2.2.1 Deviations from Equilibrium

A primary concern of karst geomorphology is measuring work accomplished by circulating groundwaters. An understanding of the development and distribution of secondary porosity within an aquifer requires a knowledge of the equilibrium state of groundwater to the major minerals that comprise the aquifer. There are two principal techniques used to assess equilibrium. The first is a direct method that involves introducing powdered mineral into the water sample (Stenner, 1969). If the water is undersaturated with respect to that mineral then there will be additional dissolution. Chemical analyses of the spiked and unspiked specimens reveal if the sample was close to equilibrium, supersaturated, or undersaturated.

The second technique involves the measurement of pH, temperature, and ion concentrations. Equilibrium is determined by a graphical method (Trombe, 1952) or by calculation of saturation indices. The latter are based on thermodynamic principles. Discussions of this method are provided by a variety of karst and hydrogeological texts (Freeze and Cherry, 1979; Dreybrodt, 1988; White, 1988; Ford and Williams, 1989). Detailed accounts of aqueous geochemistry are also available (Garrels and Christ, 1965; Stumm and Morgan, 1980; Plummer and Busenberg, 1982; Faure, 1991).

In the calculation of saturation indices from karst waters, it is necessary to accurately measure pH, temperature, and the concentrations of calcium, magnesium, bicarbonate, sulphate, sodium, chloride, and potassium ions. This technique has been criticised for: (i) difficulties encountered in the accurate determination of pH under field conditions, (ii) the frequent use of partial chemical analyses used as input to equilibrium programs and, (iii) potential interferences from trace metals (Worthington, 1991). These concerns can be accommodated with careful fieldwork using precise instruments to measure pH and by comprehensive chemical analyses (Chapter III). While the Stenner technique is attractive in its simplicity, it is not practical to determine the aggressiveness of the sample water toward several different minerals concurrently. This may be desired where aquifer lithology is complex. Further, when groundwater is close to equilibrium the reaction kinetics following the addition of powdered mineral are very slow.

This study uses saturation indices to express the state of the reaction between the solid and aqueous phase for a number of minerals. Deviations from equilibrium are defined by the ratio of the ion activity product to the equilibrium constant (solubility product). The ion activity product is computed from the mass law expression using activities calculated from the molarities of the products and reactants in the sample water. A logarithmic form of the saturation index is used:

$$SI_m = \log \frac{IAP_m}{K_{eq_m}} \quad (2.1)$$

where SI , IAP and K_{eq} are the saturation index, ion activity product, and equilibrium constant for mineral m , respectively. At equilibrium, the SI equals 0.0. Aggressive solutions have negative SI values, and saturated solutions have positive values.

2.2.2 Anhydrite and Gypsum

Anhydrite (CaSO_4) and gypsum ($\text{CaSO}_4 \cdot 2\text{H}_2\text{O}$) are highly soluble minerals. In

subcrop they are often associated with the development of interstratal karst. This section reviews the controls on solubility and calculation of the saturation index for gypsum. The development of solution breccias is discussed in Chapter IV.

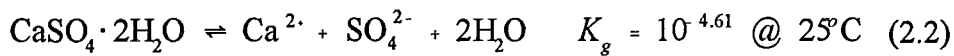
Deposition of calcium sulphate in a sabkha or enclosed basin largely occurs as the mineral gypsum. Upon deep burial, gypsum is dehydrated to form anhydrite, which in turn may be rehydrated as the rock is exhumed. The gypsum-anhydrite relationship is important due to a substantial volume change that may accompany hydration (up to 34%). There are also differences in mineral solubility and dissolution. The stability fields of anhydrite and gypsum are controlled by temperature, salinity, and pressure (Blatt *et al*, 1980). Gypsum is stable at low temperatures and salinity; anhydrite is stable at high temperatures and salinity (Blount and Dickson, 1973). Thus, anhydrite is usually found in the deep subsurface, and gypsum in the shallow subsurface and as outcrop. Gypsum may persist metastably within the anhydrite stability field for tens to hundreds of years. When anhydrite is the unstable phase, it can be rapidly converted to gypsum in the presence of water (Kinsman, 1974). The hydration rate is influenced by bedrock porosity. In compact, massive beds of low primary porosity, the rate of hydration is slow and anhydrite may occur as outcrop. Examples are observed in quarries from western Nova Scotia. In fresh exposures of the Carboniferous Windsor Group, gypsum occurs on the land surface and along fractures and fissures of quarry walls where meteoric waters have infiltrated. Anhydrite forms the unweathered core-stones between the gypsum pipes (Ford, personal communication, 1992).

In distilled water, anhydrite solubility is inversely proportional to temperature. However, gypsum solubility increases with temperature to approximately 40°C and then declines (Quinlan, 1978). Both gypsum and anhydrite are more soluble as salinity increases. Despite the higher solubility of anhydrite at low temperatures, it has been shown by Priesnitz (1969, 1972) that the solution rate of gypsum is higher than that for anhydrite; gypsum was found to enter solution at a rate almost double that of anhydrite. Navas (1990) suggests the factors that

influence the dissolution rate of gypsum are, in order of importance: the flow velocity, ionic strength of the solution, and gypsum saturation. In a system with high flow velocities, gypsum dissolution is surface reaction controlled. Only where flow velocities are extremely slow and the flow paths long will the concentrations of dissolved Ca^{2+} and SO_4^{2-} approach equilibrium values.

2.2.2.1 Gypsum Saturation Index

Gypsum dissociates in the presence of water:



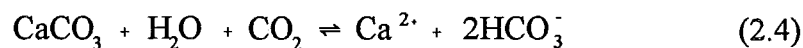
The saturation index for gypsum is calculated from:

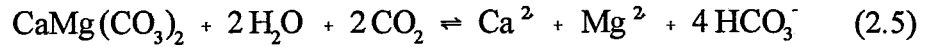
$$SI_g = \log(\text{Ca}^{2+}) + \log(\text{SO}_4^{2-}) + pK_g \quad (2.3)$$

where p denotes negative logarithm, standard parentheses represent activities.

2.2.3 Calcite and Dolomite

In pure water, the solubilities of calcite (CaCO_3) and dolomite ($\text{CaMg}(\text{CO}_3)_2$) are very low. They are approximately 6 and < 1 mg L⁻¹. Meteoric waters commonly have concentrations of these minerals as high as a few hundred mg L⁻¹. The majority of this enhancement is related to the effect of increased hydrogen ion activity on solubility. In meteoric systems, hydrogen ions are supplied by the dissociation of water and weak acids, the latter source normally accounting for a substantial increase in hydrogen ion activity. Carbonic acid is the most important of these weak acids and its activity is a function of the partial pressure of carbon dioxide in the coexisting gas phase. The net reactions for the dissolution of calcite and dolomite are:





The saturation index for calcite is:

$$SI_c = \log(\text{Ca}^{2+}) + \log(\text{HCO}_3^-) + \text{pH} - \text{p}K_2 + \text{p}K_c \quad (2.6)$$

The saturation index for dolomite is:

$$SI_d = \log(\text{Ca}^{2+}) + \log(\text{Mg}^{2+}) + 2\log(\text{HCO}_3^-) + 2\text{pH} - 2\text{p}K_2 + \text{p}K_d \quad (2.7)$$

2.2.3.1 Carbon Dioxide

In carbonate waters, the concentration of carbon dioxide and the production of carbonic acid are of great importance in the solution process. The solubility of CO_2 is directly related to the partial pressure of CO_2 in the gas phase and inversely related to water temperature (Figure 2.1). In most karst systems, CO_2 originates only in the atmosphere and soil. The partial pressure of CO_2 in the atmosphere is approximately $10^{-3.47}$ atmospheres. Soil CO_2 can vary from atmospheric levels to partial pressures of $10^{-1.0}$ in tropical environments (Figure 2.1). The increased CO_2 solubility at low temperatures is an important boost in cold regions where soil CO_2 levels are generally low.

In cold regions, the equilibrium concentrations of calcite, for a given $P\text{CO}_2$, are elevated due to the increase of CO_2 solubility in cold water (Figure 2.2). However, it is clear that $P\text{CO}_2$ exercises greater control on calcite solubility than temperature. Where the soil atmosphere has high $P\text{CO}_2$ values, the potential for dissolution is greater. Based on field measurements of temperature, bicarbonate ion, and pH, it is possible to calculate the $P\text{CO}_2$ of the gas phase that is in equilibrium with the groundwater.

Soil CO_2 levels are a function of a variety of biological factors that are influenced by climate and soil properties. Field measurements from regions of periglacial climate yield values between $10^{-3.4}$ and $10^{-2.3}$ for alpine tundra in the

Rocky Mountains (Miotke, 1974), between $10^{-2.7}$ and $10^{-2.0}$ from arctic tundra (Woo and Marsh, 1977), and $10^{-2.5}$ from the Nahanni karst (Brook, 1976). Considerable effort has been directed to the correlation between PCO_2 and climate. The relationship between PCO_2 in the discharge waters of closed systems and mean annual temperature was evaluated by Drake and Wigley (1975) and Drake (1980). It was suggested that the soil PCO_2 could be back calculated from the PCO_2 of the discharge waters. The following statistical model was proposed:

$$\log P_{CO_2} = -2 + 0.04T \quad (2.8)$$

where T is the mean annual temperature in °C and PCO_2 is the partial pressure of carbon dioxide in the soil in atmospheres. At Norman Wells, the mean annual temperature is -6.0 °C. The expected PCO_2 is $10^{-2.24}$. A correction to account for the inhibition of respiration at low PCO_2 produces a minor difference in the calculation. This model assumes that all CO_2 in the system is derived from the soil zone. It probably overestimates soil CO_2 content in climates influenced by strong seasonal variations (Bakalowicz, 1976). Brook *et al* (1983) examined soil CO_2 as a function of several climatic variables, including temperature, precipitation, potential and actual evapotranspiration. From a data set of 19 widely dispersed locations, a significant relationship was found between PCO_2 and actual evapotranspiration (Figure 2.3). In the arctic region, the predicted PCO_2 at the peak of growing season is below $10^{-3.0}$. In the subarctic, the predicted range is between $10^{-3.0}$ and $10^{-2.6}$.

In this study, soil PCO_2 was measured at four locations at the Dodo Canyon Site (Chapter VII) and at six locations at the Bear Rock Site (Chapter X). Sampling was done on July 8 and August 5, 1988. A variety of soil types were tested, ranging from coarse textured regosols on unvegetated exposed areas, to organic-rich brunisols occurring on doline floors below treeline. A hollow steel probe was driven into the soil and a sample of the soil atmosphere was drawn into a Draeger device, which reports soil CO_2 in volume percentage (Miotke, 1974). Samples were taken at 5 cm intervals below the surface to depths ranging from 10 to 35 cm. The soil

atmosphere in unvegetated areas showed near atmospheric concentrations of CO_2 . Values from sites below treeline ranged from 0.06 to 0.20%. At the Dodo Canyon Site, the average CO_2 for samples from vegetated soils between the depths of 10 and 35 cm was 0.12% ($n=16$). The same figure from the Bear Rock Site was 0.10% ($n=14$). Overall, the average $P\text{CO}_2$ value from this data set is $10^{-2.9}$. Actual evapotranspiration in the region is between 200 and 300 mm (Chapter III) it is plotted against $P\text{CO}_2$ on Figure 2.3.

It is common to find the $P\text{CO}_2$ values of discharge waters are higher than those directly measured in the soil of a karst basin. This indicates there may be additional sources of CO_2 in the system. Atkinson (1977) suggests that the oxidation of organic material in the vadose zone is a possible source of CO_2 , it may also be delivered from groundwaters of deep origin and connate waters. Other weathering processes may contribute CO_2 , particularly the reduction of sulphates in the presence of organic material.

2.3 Karst Hydrology and Aquifers

The hydrology of karst and non-karst terrains differ through the allotment of water between surface and subsurface pathways. The high secondary porosity of karst bedrock permits capture of all surface runoff in areas of holokarst, and a lesser fraction in a fluviokarst. The development and characteristics of karst aquifers are strongly influenced by the physical attributes that control the style and rate of recharge, transmission, and discharge. Climate, vegetation, soils, geomorphology, geology, and boundary conditions constitute important controls (Figure 2.4). Climate governs the volume, temperature, and seasonality of recharge. Vegetation and soil function as a filter and store, regulating infiltration and increasing the dissolved CO_2 content of percolating waters. Geomorphology controls allogenic and point recharge through linkage of the surface drainage network to sink points. These three factors are interrelated and are subject to complex feedback mechanisms. In aggregate, they determine the properties of the recharge to the bedrock (Figure 2.4).

The processes of karstification will proceed when recharge is aggressive towards the minerals which comprise the aquifer. How the bedrock is modified is related to mineral solubility, purity, texture, and the primary porosity and geometry of the rock units. Solution occurring along bedding planes, joints, and fractures increases the secondary porosity and surface waters are progressively diverted into the enlarging subsurface drainage network. The hydraulic conductivity, effective porosity, storativity, and transmissivity of the aquifer are increased. Positive feedbacks to the recharge variables reinforces these modifications. Of particular importance are the boundary conditions imposed on the flow system: the position and elevation of springs points and the amount of local relief from the recharge to discharge areas (Figure 2.4). These variables influence the depth and length of flowpaths, and consequently the physical properties of the aquifer discharge.

It is common practice to classify karst aquifers based on their porosity and the conditions which characterize flow within them. Atkinson (1985) recognizes three types: (i) diffuse, (ii) fissure and, (iii) conduit (Figure 2.5). Aquifer structure strongly influences the style of recharge and their hydrological behaviour. Diffuse flow occurs through the bulk of a bedrock mass within small interconnected pores and fissures, the flow is laminar and linear velocities low. Discharge from these systems tends to be consistent in flow and chemistry (Jackucs, 1959). In the case of a well developed conduit aquifer, groundwater movement occurs almost exclusively through solution conduits, flow is often turbulent and velocities within conduits may exceed 0.1 m s^{-1} . Discharge from these aquifers is highly variable in flow and chemistry. Fissure aquifers are characterized by a mixed flow regime, where the majority of groundwater movement occurs through solution altered joints, fractures, bedding planes, and other fissures.

There is substantial literature available on the modelling of groundwater flow. For diffuse aquifers the most successful deterministic approaches are based on the application of Darcy's Law. However, within conduit aquifers the use of Darcy's Law is inappropriate. Flow in conduits is described by the Poiseuille and Darcy-

Weisbach equations. Modelling groundwater flow in any karst is complicated by difficulties encountered in establishing the fundamental spatial properties of the system. The delineation of catchment areas for springs is problematic. Dye tracing and natural isotopes may aid in that task but often catchment areas and flow vectors within aquifers will change with small fluctuations in the level of the potentiometric surface. Also, porosity need not be uniform within a given aquifer.

2.3.1 Hydrological Components of the Karst System

The hydrological and solute inputs, stores, outputs, and linkages within the karst system are depicted on Figure 2.6. Precipitation and allogenic streams constitute the hydrological inputs. Infiltration occurs via point recharge landforms or as diffuse recharge through the soil, bedrock, or along losing stretches of stream channel. Partitioning of inputs between detention, runoff, and infiltration will vary. Under storm conditions the infiltration capacity of sink points may be exceeded, increasing surface detention and runoff. In conduit aquifers, vadose cave passages may develop beneath point recharge locations. Conduits provide a high velocity pathway from the surface to the phreatic zone or to spring points. Stores within the vadose zone include the soil and subcutaneous aquifer. The subcutaneous zone is a shallow subsoil aquifer that is characterized by high effective porosity and hydraulic conductivity (Williams, 1983). It functions as a source area for percolation to the phreatic zone and as a discharge source from the system. Evapotranspiration will remove moisture from the intercepting vegetation, surface, soil, and subcutaneous zone.

Hydrological outputs include discharge from vadose and phreatic spring points, spring lines, and seeps, as well as surface runoff. A hierarchy of springs may be present in the discharge area of a conduit aquifer (Smart, 1983). In response to a recharge event, higher elevation spring points are activated, these overflow springs are ephemeral and experience rapid changes in flow volume and chemistry. The lower elevation underflow springs exhibit less variability in discharge and solute

contents.

Solutes in the system include contributions from wet and dry fallout, biomass, and weathering products. The atmospheric inputs usually comprise a small percentage of the total solute budget. Much of the dissolution of soluble minerals is accomplished in the soil and the subcutaneous zones, although this is dependent on the spatial distribution of soluble materials within the aquifer. While solution and precipitation dominate weathering, redox reactions involving sulphur compounds can be locally significant.

2.3.2 Spring Analyses

A variety of direct and indirect measures provide data on the physical characteristics of aquifers. Pumping and injection tests produce estimates of storativity, transmissivity, and hydraulic conductivity. A water balance approach may be used to estimate annual recharge. However, many standard hydrogeological methods perform poorly in the study of karst aquifers (Quinlan and Ewers, 1985). Karst researchers frequently employ methods that involve spring analyses. Variations in discharge, hydrochemical facies, ion concentrations, temperature, and isotope ratios of spring points are related to the characteristics of recharge and its transmission through the aquifer. Monitoring these variables at spring points may yield information regarding the aquifer structure. Complications occur when only a fraction of the total discharge may be measured, as spring locations may be obscured beneath a cover of sediment, in stream channels, or in lake beds. In addition, flow at monitoring stations may incorporate a mixture of any number of the potential inputs indicated in Figure 2.6 and the relative proportions of these inputs across stage need not be constant. Basic techniques in spring hydrograph analyses are employed on data from the Dodo Canyon Site (Chapter VII).

2.4 Permafrost

Permafrost is defined as ground (soil or rock) that remains at or below 0°C for at

least two years (Harris *et al*, 1988) or as ground that remains frozen for more than one year (Williams and Smith, 1989). The term cryotic is used to describe ground at a temperature below 0°C. The freezing point of pure water is 0°C. Meteoric waters contain dissolved solids which typically depress the freezing point by 0.1 to 0.2°C. Freezing occurs across a range of temperatures. Ice nucleation initially occurs in large pores and fissures where water is held at relatively low pressures. As freezing continues, the remaining liquid water is held at increasingly higher pressures within capillaries and adsorbed onto solid surfaces. Usually when ground temperatures drop below -1.5°C most of the remaining liquid water is held as adsorbed water. However, the unfrozen water content may exceed 10% in fine grained soils to temperatures as low as -5°C (Williams and Smith, 1989). Much permafrost, particularly that of recent (Holocene) origin is relatively warm, >-5°C, and a significant amount of liquid water can coexist with the ice. This liquid water will move in response to temperature gradients, although as the unfrozen water content decreases, so too does the hydraulic conductivity of permafrost. In common usage, the term frozen ground describes permafrost where the majority of water in the system exists as ice. However, by the thermal definition, permafrost need not contain any ice.

2.4.1 Permafrost Distribution

The distribution of permafrost is usually mapped as a series of zones or regions depicting proportions of the surface that are perennially cryotic (Figure 2.7). The continuous zone is recognized as that area where >80% of the surface is underlain by permafrost (Harris *et al*, 1988). Permafrost extent and thickness varies from relict isolated patches in the sporadic discontinuous zone to continuous coverage in the high Arctic where the thickness can exceed 1000 m (Washburn, 1979). At the macro-scale, permafrost at the boundary between the continuous and discontinuous zones is on average 60 to 100 m thick and approximates the -8.5°C mean annual air isotherm (Prowse, 1990). However, at the local scale, variations in permafrost

thickness and extent can be substantial. On an annual basis, ground temperatures are typically several degrees warmer than air temperatures. Due to the complex relationship between these variables, air temperature does not describe small variations in permafrost distribution, particularly in the discontinuous zone (Williams and Smith, 1989).

Factors which influence permafrost extent and thickness include: climate, ground cover, hydrology, topography, and geology. Ground surface temperature is regulated by the surface energy balance and by site specific properties that influence energy partitioning. The temperature regime within a soil or bedrock unit is a function of the thermal properties of that unit and the action of external heat and mass transfer processes, particularly geothermal heat and surface temperature (Figure 2.8). The surface energy balance is given by:

$$Q^* = Q_H + Q_E + Q_G = K\downarrow(1 - \alpha) - L\uparrow + L\downarrow(1 - \epsilon) \quad (2.9)$$

where Q^* is net radiation, Q_H is sensible heat flux, Q_E is latent heat flux, Q_G is ground heat flux, $K\downarrow$ is incoming shortwave radiation, α is surface albedo, $L\downarrow$ is incoming longwave radiation, $L\uparrow$ is outgoing longwave radiation and ϵ is surface emissivity.

Climate controls large scale variations in permafrost extent. Important variables include: latitude, cloudiness, humidity, windspeed, and temperature. Permafrost is more extensive where $K\downarrow$ is minimized and Q_E and Q_H are maximized. These conditions occur at moist high latitude sites where there are strong winds. Topography influences permafrost through variations in aspect and slope, permafrost is least extensive on steep southerly facing slopes where the duration of insolation is greatest and the angle of incidence acute. Geology exercises control on permafrost through geothermal heat flux and thermal conductivity of the soil or bedrock unit. In localized areas where heat flux is high, permafrost thickness and extent are reduced. Given a constant heat flux, the vertical temperature gradient in a bedrock unit is inversely proportional to thermal conductivity. Thus, for a given surface temperature, formations with high thermal conductivities will support thicker

permafrost.

In the discontinuous zone, the distribution of permafrost is largely governed by surface characteristics that influence energy exchange and consequently the ground surface temperature. Critical ground variables are snow cover, vegetation, and organic material. The thermal conductivity of snow is low and it functions as an insulator, reducing heat loss from the ground during the winter season (Smith, 1975). This variable is perhaps the most important control on the magnitude of the difference between air and ground temperatures. In areas of rugged topography, snow is subjected to redistribution and therefore permafrost beneath topographic snow traps tends to be less extensive.

Vegetation reduces $K\downarrow$ through shading and increases Q_E through evapotranspiration. Thus in the summer, soil temperatures beneath a forest canopy tend to be cooler than those in open sites (Rouse, 1984). However, these surfaces are much warmer during the winter period as vegetation will tend to accumulate snow (Smith, 1975). The net annual effect is that ground temperatures beneath a vegetation canopy are commonly a few degrees warmer than adjacent open surfaces (Williams and Smith, 1989).

Thick organic soils will also influence the surface energy balance and have the effect of lowering the annual ground temperature. The thermal conductivity of peat is strongly governed by moisture content. On average, peaty soils have a lower moisture content in the summer period when rates of evapotranspiration are high. During this period the organic layer functions as an insulator and Q_G to the surface is reduced. This contrasts with the behaviour of wet and frozen peat which has a very high thermal conductivity. In the sporadic portion of the discontinuous zone, cryotic ground is largely confined to positions underlying peatlands (Zoltai and Tarnocai, 1975).

Although not depicted in Figure 2.8, water bodies also constitute an important control on the distribution of permafrost. Noncryotic ground occurs beneath water bodies that are sufficiently deep so that bottom freezing does not

occur. The dimensions of the underlying talik are a function of the size and temperature of the water body, and the temperature of the surrounding permafrost (Gold and Lachenbruch, 1973). In the continuous permafrost zone, taliks are present beneath major rivers and lakes. The hydrological significance of these taliks is addressed in the following section.

2.5 Hydrology of Permafrost Terrain

Permafrost hydrology is the study of the distribution, movement, and storage of water as influenced by the presence of perennially frozen ground (Woo, 1986). This section will review permafrost hydrology focusing on the properties of groundwater aquifers with particular emphasis given to carbonate terrains.

Several characteristics differentiate the hydrology of the permafrost zone from the temperate zone. The following are identified by Woo (1990): (i) frozen ground functions as an aquiclude because of limited permeability, (ii) the majority of hydrological processes are confined to the active layer, (iii) many surface hydrological processes are effectively idle during the winter, (iv) the flux of energy and water are linked as freeze-thaw events influence water storage and distribution, (v) snow and ice function as a store on a seasonal, annual, or multi-annual basis, thereby influencing the temporal availability of surface water through melt.

Stream response to precipitation is related to the physical characteristics of basins, such as the geology, vegetation, watershed shape, topography, and soil moisture conditions. Studies of surface hydrology of Arctic and Subarctic catchments have shown that they are influenced by the additional factor of permafrost. Catchments underlain by permafrost show a rapid stream discharge response to inputs, usually snowmelt, glacier melt, rain, or some combination. Maximum specific discharges are high (peak discharge per unit area) as is the runoff to precipitation ratio (e.g. McCann and Cogley, 1972; Dingman, 1973; Newbury, 1974; Slaughter *et al*, 1983). Typically, a discharge hydrograph is flashy, quickly rising to a peak and followed by a short recession to baseflow, which may be

minimal (Slaughter and Kane, 1979). The rapid response is related to the reduced permeability of frozen ground and the resultant translation of precipitation, snow and ice melt to the stream channel by the pathways of overland flow (Price et. al., 1978) or in the shallow subsurface as throughflow (Lewkowitz and French, 1982; Woo and Steer, 1983). In areas of discontinuous permafrost, the contribution of baseflow to the total hydrograph is greater than in continuous permafrost (MacKay and Loken, 1974), as is the relative contribution to runoff by rainfall events rather than snow or ice melt.

2.5.1 Basin Hydrology

There are four commonly recognized streamflow regimes in permafrost terrain (Church, 1974): (i) Subarctic nival, (ii) Arctic nival, (iii) proglacial, (iv) muskeg or wetland. Craig and McCart (1975) recognize a fifth regime: (v) spring-fed. Annual hydrographs for basins that are representative of the above regimes are presented in Figure 2.9. The nival regimes have a marked snowmelt flood with secondary rainfall generated peaks, the latter being more significant in the subarctic as are groundwater inputs to discharge. This contrasts with the arctic region where baseflow contribution is minor. In the nival regime, short duration high magnitude flows may be associated with the failure of snow and ice dams or ice jams. The proglacial regime is seen in glacierized basins. There is a snowmelt peak with subsequent peak flows due largely to ice melt. The latter peaks may exhibit a diurnal variation driven by radiation input, in some instances jökulhlaups occur. Streams of the wetland or muskeg regime are also characterized by a marked snowmelt pulse, but wetlands tend to attenuate melt and storm peaks due to high levels of detention storage and evapotranspiration. The spring-fed regime is the most relevant to this study, it is discussed in the following section in conjunction with groundwater.

2.6 Groundwater in Permafrost Terrain

The occurrence and characteristics of groundwater in permafrost terrain have been

reviewed by numerous authors (e.g., Cedarstrom, 1953; Williams, 1965; Williams, 1970; Williams and van Everdingen, 1973; Tolstikhin and Tolstikhin, 1976; van Everdingen, 1974, 1987, 1990; Michel and Wilson, 1988). The characteristics of groundwater flow systems are influenced by topography, lithology, and the extent of frozen ground. The latter is the dominant control on the distribution and seasonality of recharge into the soil and underlying aquifers. Following a scheme originally outlined by Tolstikhin (1941, as referenced in Shepelev, 1983) groundwater aquifers are differentiated on the basis of their position relative to the permafrost (Figure 2.10). Three main types of aquifers are recognized: (i) suprapermafrost aquifer, (ii) intrapermafrost aquifer, and (iii) subpermafrost aquifer.

2.6.1 Suprapermafrost Aquifer

Suprapermafrost aquifers occupy the zone above the permafrost. Based on their freezing regimes van Everdingen (1990) recognizes three subtypes, these are called *Ia*, *Ib*, and *Ic* in this text. Groundwater of subtype *Ia* is confined to the zone that is subjected to annual freezing and thawing, the active layer. The annual thickness of this aquifer is related to the surface energy balance and the thermal properties of the material. The active layer achieves its maximum thickness in late summer. Subtype *Ib* encompasses a portion of the active layer and the unfrozen ground beneath it. This aquifer is found in closed taliks beneath shallow streams, lakes, and alluvial fans and undergoes only partial seasonal freezing. Subtype *Ic* is located below the active layer and above the permafrost. It is not subjected to seasonal freezing. This aquifer is found in taliks that may be associated with larger streams and lakes and where thermal water discharges. In the discontinuous permafrost zone, the thickness of this aquifer may be several metres where the permafrost table is located well below the depth of seasonal freezing.

Alternate classifications of suprapermafrost aquifers are provided by Shepelev (1983) and Pengfei (1988). Shepelev differentiates between active layer suprapermafrost water (termed suprapermafrost vadose water) and water in taliks

above the permafrost table but confined by the active layer (termed supraperafrost groundwater). The former is divided based on the continuity of the permafrost and the latter into three subtypes based on the degree of freezing within the talik. Shepelev emphasizes the importance of unfrozen supraperafrost waters found in taliks beneath major water bodies. Pengfei (1988) recognizes the supraperafrost aquifer as one confined to the active layer. Division is based on porosity. Supraperafrost water exists within the pores of sediment in an open or confined state or in the pores and fractures of bedrock. Taliks are considered independently of supraperafrost waters.

2.6.1.1 Surface and Subsurface Flow

The hydrology of the active layer is strongly influenced by frozen ground. Upon freezing, a moist soil experiences a decrease in hydraulic conductivity (Kane and Stein, 1983b). The magnitude of the reduction is related to soil texture, degree of saturation, and temperature. Burt and Williams (1976) demonstrated that freezing saturated soils to approximately -0.5°C resulted in a decline in hydraulic conductivity by four or five orders of magnitude. Very coarse soils and porous and fractured bedrock are less influenced by freezing (Mackay, 1983; Olovin, 1988; van Everdingen, 1990). In addition, dry soils will maintain their permeability despite freezing (Cary and Mayland, 1972; Kane and Stein, 1983a, 1983b). The unfrozen water content of a soil declines with temperature. In a frozen soil, liquid water is restricted to capillaries and thin films around soil particles (Anderson and Morgenstern, 1973; Williams and Smith, 1989). This water will move in response to thermal gradients but due to poor interconnections between water films the velocity of flow is very low. It is also possible for water to travel as vapour through the soil media or for regelation processes to transfer water across ice lenses. Thus, when assessing the hydraulic conductivity of frozen materials a wide range of possibilities exist. In fine grained saturated media, conductivity is sharply reduced but these materials should not be considered absolutely impermeable. Use of the

term aquitard is suggested to describe the hydrogeological role of frozen ground (Harlan, 1974; van Everdingen, 1990). In dry soils or in very coarse debris or fractured and porous bedrock, hydraulic conductivity may remain high. This is particularly the case for bedrock with solution conduits.

Early in the melt season the active layer is frozen to the surface. Meltwater infiltrates into air filled pores and fissures. The infiltration rate is a function of the properties discussed above. Refreezing of percolating waters releases latent heat and warms the active layer (Woo and Heron, 1981; Wright, 1981). This may also seal pores with ice which reduces infiltration. In areas of continuous permafrost, it is common for a layer of ice to develop at the base of the snow cover which further retards infiltration (Marsh and Woo, 1984). Where the active layer contains abundant ice, incremental increases in thaw depth require greater inputs of energy (Wright, 1981). The active layer tends to thaw unevenly and the frost and water table do not perfectly mimic surface topography (Woo and Steer, 1983). If the supply of meltwater and rainfall exceeds the infiltration capacity or the water table reaches the surface, water will pond, first satisfying detention storage, and then run off as overland flow. This is most important in the spring when the thaw depth is shallow and the supply of water high (Lewkowicz and French, 1982). Water may infiltrate into the active layer at one point and re-emerge downslope in response to the changing configuration of the frost and water table relative to the surface (Woo and Steer, 1983). Dingman (1973) described the importance of the active layer water table in the generation of surface flow and applied the variable source area concept to permafrost basins to account for discharge variations.

As the melt season progresses, the thickening thawed zone serves as a store for meltwater and rainwater. Infiltrating waters may percolate to the active layer water table and be stored as suprapermafrost groundwater. The thickness of this aquifer is not consistent and flow within it may not correspond with surface drainage divides. This groundwater will move laterally in response to hydraulic gradients until it is discharged at the surface or encounters a talik. Studies from continuous

permafrost have shown that variations in supraperafrost flow are contemporaneous with those observed in surface flow and may comprise over 50% of the volume of discharge from a system (Lewkowicz and French 1982; Steer and Woo, 1983). As recharge to the active layer is reduced, the aquifer dewateres from the top down and flow declines to minimal levels through the summer period.

2.6.1.2 Chemistry and Discharge of Supraperafrost Groundwaters

Where the water table of the supraperafrost aquifer outcrops on the topographic surface, water flows out as either seeps or springs. These waters are almost exclusively meteoric in origin and their solute content reflects the lithology of aquifer materials and a relatively short residence time in that media. Typically the chemistry is simple with Ca^{2+} and HCO_3^- as the dominate ions. Total solute load and electrical conductivity are low as is temperature. Where the flow velocity is slow, solute content may be relatively high. Lewkowicz and French (1982) report an inverse relationship between discharge and solute concentration. In wetland areas, supraperafrost waters may have higher concentrations of organic acids. In some circumstances there may be mixing between permafrost groundwaters of deep origin and supraperafrost groundwater.

Discharge from springs and seeps draining the supraperafrost aquifer is restricted to the period of thaw and is of variable magnitude. Individual discharge points rarely exceed a few litres per second. In the continuous permafrost zone, snowmelt is responsible for the majority of the discharge, while in the subarctic, rainfall events may produce substantial discharge from the aquifer (van Everdingen, 1987, 1990).

2.6.2 Intrapermafrost Aquifer

Intrapermafrost water occupies unfrozen zones within the permafrost (Figure 2.10). This includes water in open, lateral, or transient taliks and in basal, isolated, and marine cryopegs. The dimensions of these aquifers vary with seasonal freezing and

will respond to long term shifts in the factors that control permafrost extent.

Open taliks provide an important link between the supra and subpermafrost aquifers through which groundwater may be exchanged. They occur in a variety of hydrogeological settings: beneath large lakes and rivers, along the flowpaths of rising hydrothermal (temperature $>0^{\circ}\text{C}$) or hydrochemical (temperature $< 0^{\circ}\text{C}$) subpermafrost waters, or where the downward flow of surface or suprapermafrost water is sufficient to restrict freezing (van Everdingen, 1990). Flow between the aquifers often exploits large fissures, faults, and solution conduits (Cedarstrom, 1953).

Lateral taliks are overlain and underlain by perennially frozen ground and may be cryotic or noncryotic. They are often found in association with alluvial fans and braidplains and with zones of mineralized water in the cryopeg. Alluvial taliks may form when surface and suprapermafrost waters infiltrate into the permeable sediments of a fan or floodplain and travel laterally at depth. The heat content of the flow maintains the integrity of the talik. It is possible to bring subpermafrost water into this pathway via an open talik, and consequently onto the surface. Taliks that are completely surrounded by permafrost are isolated. They may be hydrothermal and transient, or hydrochemical. The former is seen below recently drained lake basins and the latter in the marine cryopeg (Figure 2.10).

Shepelev (1983) classifies intrapermafrost waters into categories which are broadly analogous to lateral (horizontally bound) and open taliks (vertically bound). Horizontally bound waters are subdivided based on the freezing regime in the talik and on the nature of the hydraulic connection to the rest of the system. Vertically bound intrapermafrost waters are subdivided based on the setting, either subaerial or subaquatic, and on the direction of flow through the talik, either downward, upward, or mixed.

2.6.2.1 Chemistry and Discharge of Intrapermafrost Groundwater

The chemistry of intrapermafrost groundwater reflects its flowpath and residence

history. The chemistry of groundwater discharging from a lateral talik that is located beneath an alluvial fan will be similar to the surface and suprapermafrost waters that infiltrate into the talik upslope. A significant change may indicate subpermafrost groundwater is introduced into the talik. Thus, intrapermafrost groundwaters can have a variable chemistry. Discharge from intrapermafrost taliks will terminate during the winter season if the aquifer storage is depleted or if the outlets freeze. This is particularly marked when the output is distributed to numerous low discharge spring points.

2.6.3 Subpermafrost Aquifer

Subpermafrost aquifers are water bearing media occurring in the noncryotic zone below the permafrost (Harris *et al*, 1988). In the zone of discontinuous permafrost, recharge to the subpermafrost aquifer is achieved through open taliks. Recharge is least inhibited where the sediment or bedrock is highly permeable. In karst areas, well developed solution conduits provide routes for the rapid recharge of subpermafrost aquifers by surface waters. In the zone of continuous permafrost, where materials are fine grained, the subpermafrost aquifer is effectively decoupled from suprapermafrost and surface waters.

Subpermafrost aquifers are differentiated by van Everdingen (1990) on the basis of their composition into aquifers of unconsolidated sediments, and sedimentary and crystalline bedrock. Carbonates and evaporites are treated separately as karst rocks and are discussed later in this section. Sediment aquifers are found where the thickness of unconsolidated materials exceeds the permafrost thickness. Cedarstrom (1953) and Williams (1970) provide examples of such aquifers in deep alluvial fills in Alaska where recharge is achieved through open taliks beneath active streams. Sedimentary rocks provide a variety of hydrogeological settings for these aquifers, from basins to folded and faulted strata. Where aquifers are interbedded with aquicludes and aquitards, recharge is reduced. Aquifers in crystalline bedrock have variable properties depending upon the degree

of fracture. Where fissure frequency is high, flow within these aquifers may be similar to that in sedimentary rocks.

Shepelev (1983) classifies subpermafrost waters based of their relationship with the lower boundary of the overlying permafrost. They are either in contact (Type 1) or without contact (Type 2). Type 1 is divided into degrading, aggrading, and stable classes which describe changes of the permafrost boundary. Cryopegs are not treated as intrapermafrost aquifers but rather as subzero subpermafrost water. Type 2 waters are subdivided into confined and unconfined aquifers. The confining layer may be an unfrozen aquitard or aquiclude, below which the subpermafrost waters are under pressure. The unconfined aquifers are separated from the base permafrost and are normally non-cryotic. Pengfei (1988) recognized six varieties of subpermafrost water based on the material, the state of the aquifer, and the porosity characteristics.

2.6.3.1 Chemistry and Discharge of Subpermafrost Groundwater

Discharge from the subpermafrost aquifer is generally perennial. Subpermafrost springs are often noted by the presence of large icings and or frost blisters which develop in the winter months at their spring points (van Everdingen, 1978, 1982; Pollard and French, 1983, 1984; Michel, 1986). The chemical characteristics of subpermafrost waters are variable and are related to the underground residence time and the lithology of the aquifer. It is not uncommon for these waters to have high solute concentrations. Subpermafrost waters flowing through an open talik and discharging at the surface often satisfy one or more of the following criteria: (i) discharge $>5 \text{ L s}^{-1}$, (ii) temperatures thermal ($>10^\circ\text{C}$ above the mean temperature of recharge waters), and (iii) TDS $>1 \text{ g L}^{-1}$. However, some subpermafrost waters will not exhibit these characteristics.

2.6.4 Spring-fed Regime in Permafrost

The spring-fed regime is the least documented of the commonly recognized

streamflow regimes occurring in permafrost terrain. Streams that are predominantly spring-fed are concentrated in the zone of discontinuous permafrost, particularly in association with basins of carbonate bedrock. The first comprehensive study of this regime was conducted by Craig and McCart (1975). They monitored discharge, turbidity, temperature, and the specific conductance of waters emerging from two large springs on the Alaskan north shore. Their observations indicated that discharge from the springs was constant and exhibited peaks only when overflow from surface waters affected the spring outlet. Turbidity levels were low and stable, spring temperatures were less variable than that of surface streams, as were the conductance and chemistry. The main springs were perennial, subpermafrost and could be differentiated from springs of shallow or suprapermafrost origin.

Much of the subsequent work on springs has been undertaken at a number of locations in northwestern Canada in the zone of discontinuous permafrost (Brook and Ford, 1980; Brook, 1976, 1983; van Everdingen, 1974, 1978, 1981, 1982, 1987, 1988; Hamilton *et al*, 1988; Michel, 1977, 1983, 1986; Michel and Fritz, 1978). The majority of these studies involved springs supplied by water circulating through carbonate rocks. Discharge and physical properties of the spring waters reflect aquifer structure and the style and rate of recharge. High discharge, cold springs tend to drain karstified subpermafrost aquifers that are supplied by abundant recharge through open taliks. In most cases, the chemistry of these springs are characterized by a low dissolved solids concentration, this reflects the high flow velocity through a conduit aquifer. High discharge springs are also observed in alluvial environments as discharge points of intrapermafrost aquifers. Subpermafrost karstic aquifers may also be drained by low discharge springs. These usually have a high dissolved solids content and may be thermal. Through examination of the flow regime and the temperature, chemical, and isotopic signature of spring waters it is possible to trace springflow to one of the three permafrost aquifers (Michel, 1977; Michel and Fritz, 1978; van Everdingen *et al*, 1979).

2.7 Glaciation, Permafrost, and Karst

Many karst areas of the temperate and periglacial regions were glaciated in the Quaternary, some karsts are currently influenced by permafrost. Each of the study sites examined in this thesis were glaciated and are in permafrost. The interactions between glaciers and karst landforms and aquifers fall on a continuum from total destruction to complete preservation (Ford, 1983). The occurrence of permafrost influences groundwater circulation. Physical processes that contribute to the development of karst features in cold climates and their characteristics are reviewed by Ford (1993). The following sections describe the impact of glaciation on karst and the role of permafrost. Subsequent sections review examples of karst from permafrost terrain.

2.7.1 Glacial Thermal Regime

The glacial thermal regime influences motion, hydrology, erosion, and deposition. The simplest models of thermal behaviour are based on heat transfer by conduction. For a stationary horizontal ice mass of uniform thermal properties and under steady state conditions, the temperature gradient within an ice mass, dT/dh , is:

$$(dT/dh) = (T_1 - T_2)/h \quad (2.10)$$

where T_1 is the mean temperature at the ice surface, T_2 is the mean temperature at the ice bed interface, and h is the ice thickness (Drewry, 1986). The surface temperature is a function of climatic variables, and the basal temperature is influenced by the geothermal heat flux through the underlying substrate. Assuming conduction occurs in the vertical direction only, the geothermal heat flux delivered to the base of the glacier is:

$$Q_G = -K_r (dT/dh) \quad (2.11)$$

where Q_G is the geothermal heat flux, K_r is the thermal conductivity of the underlying bedrock unit and dT/dz is the geothermal gradient.

The temperature profile within a moving ice mass is complicated by additional heat contributed from internal shear and from friction due to sliding. This has the effect of elevating the temperature of the basal ice. A glacier is cold based when the rate of heat production from geothermal, strain, and sliding sources are less than the product of the thermal conductivity of the ice and the basal ice temperature gradient (Drewry, 1986). When the heat production is greater, the glacier will be warm based with melting at the bed.

2.7.2 Glacial Erosion and Deposition

Glaciers are composed of polycrystalline ice. Motion is achieved by internal shear (creep) and by basal sliding (Drewry, 1986). The latter consists of a combination of processes including enhanced creep, regelation, and slippage. Creep velocity is a function of the ice temperature and the surface slope. Basal sliding is related to ice temperature, bed roughness, and the supply of meltwater to the ice-bed interface. In general, flow velocity increases with temperature and at glacier margins.

In cold based glaciers, motion is wholly by creep. Warm based glaciers will move by a combination of creep and basal sliding. The style of motion influences erosion and deposition at the bed. Sliding glaciers may erode bed material by abrasion and plucking. The abrasion rate is related to the hardness of the bedrock and tools, debris concentration in the basal environment, pressure, velocity, and bed roughness (Hallet, 1981; Drewry, 1986). Abrasion tends to occur on the stoss side of bed obstacles and plucking on the lee side. Cold based glaciers are frozen to their beds and erosion is limited to large bed obstacles that protrude into the basal ice. Erosion of sediment and bedrock may also be accomplished by meltwaters in the subglacial and supraglacial environments.

Deposition occurs in subglacial, ice contact, and ice marginal environments (Shaw *et al.*, 1985). The subglacial environment is characterized by lodgement and melt-out tills, and a variety of glaciofluvial sediments (Boulton, 1982; Dreimanis *et al.*, 1987). The subglacial landform assemblage includes flutes, drumlins, eskers, and

Rogen moraine (Sugden and John, 1976). The ice contact environment consists of an assemblage of kame, end, and hummocky ground moraines. Mass flow deposits (flow till) and glaciofluvial sediments are most common. The ice marginal environment is dominated by glaciofluvial and glaciolacustrine sediments and landforms.

2.7.3 Glacial Hydrology

From a hydrogeological perspective, the movement of water within glaciers is very similar to that of karstified bedrock aquifers. Recharge to the glacial aquifer is achieved through a diffuse network of inter-crystalline veins and fissures, and through discrete input points at crevasses and moulins. It is convenient to subdivide the glacial system into supraglacial and subglacial components. These are decoupled in the accumulation zone but become linked towards the glacier margin in the melt season. In the supraglacial environment, liquid water is provided by surface melt and precipitation. Much of this water is refrozen in the firn aquifer or migrates laterally towards the ablation zone where it supplies supraglacial streams. A limited amount of vertical percolation from the firn aquifer to englacial and subglacial positions occurs through a network of diffuse veins (Berner *et al*, 1977). The PCO_2 of supraglacial meltwaters are typically lower than atmospheric, but become equilibrated with atmospheric concentrations in turbulent supraglacial streams (Raiswell, 1984). Due to the PCO_2 , the solution capacity of this water is low. However, the concentration of dissolved solids are generally very low and supraglacial waters are aggressive toward the carbonate minerals (Palmer, 1984). In the ablation zone, the frequency of crevasses, fissures, and moulins increase. These are discrete input points to vertical conduits. A portion of the supraglacial flow is diverted through these conduits into networks of Nye and Röthlisberger channels at the glacier bed. At glacier margins, these channels coalesce into large streams.

Meltwater is generated in the subglacial environment by geothermal and

mechanical heat. These waters quickly approach equilibrium concentrations with respect to carbonate minerals in the subglacial sediments and bedrock. Much of this flow occurs in thin films at the ice-rock interface (Weertman, 1972). In volumetric terms, the production of meltwaters in the supraglacial environment is several orders of magnitude greater than subglacial film flow (Smart, 1984).

Water may also be contributed to the glacial system by groundwater and surface flow from surrounding uplands or dammed river systems. Subglacial meltwaters may infiltrate into underlying permeable bedrock. The occurrence of an ice mass may alter preglacial surface drainage patterns and produce ice contact and ice marginal ponding. Discharge from the system is seasonal and occasionally catastrophic and is capable of the rapid generation of spillway landforms.

2.7.4 The Influence of Glaciation on Permafrost

Under steady state conditions, a linear temperature gradient is established in permafrost. Disequilibrium in the temperature profile would result from the superimposition of an ice mass. Under warm based ice, permafrost may completely degrade. This is demonstrated using the simple model presented in Section 2.7.1 (Figure 2.11). Permafrost thickness is controlled by surface temperature, geothermal heat flux, and the thermal properties of the bedrock. It is assumed the permafrost is dry and of homogeneous thermal properties. Heat flow by conduction is given by Equation 2.10. Convective and latent heat transfers within the permafrost are ignored. Over geomorphic timescales this is a reasonable exclusion (Williams and Smith, 1989). When a stationary ice mass comes to rest over a permafrost substrate, the initial basal temperature of the ice mass (T_2) is the surface temperature of the permafrost. In response to this change in surface conditions, a new equilibrium is established. It is assumed that the rate of heat flow into the base of the permafrost is equal to the rate of heat flow into the base of the glacier, and that the rate of change of heat storage in the system can be ignored. The equilibrium temperature at the ice bed interface is:

$$T_s = T_2 = T_1 - \frac{(Q_G \cdot h)}{K_i} \quad (2.12)$$

where K_i is the thermal conductivity of glacial ice. Under the new conditions the permafrost thickness, z , is:

$$z = \frac{K_r(T_s - T_b)}{Q_G} \quad (2.13)$$

where T_b is the temperature at the base of the permafrost (0°C). Solutions to Equations 2.12 and 2.13 are solved for a number of conditions and presented in Figure 2.12. The time period for a new temperature equilibrium to become established is long, perhaps as much as several thousand years (Lunardini, 1981).

The model presented is very simple but it does show that, given a long period of time, permafrost beneath a warm based glacier will degrade. Measurements of permafrost thickness from northwestern Canada and Alaska show relatively thin permafrost occurs in those areas that were glaciated in the Late Quaternary (Washburn, 1979).

2.7.5 Glaciation and Karst

The influence of glaciation on pre-existing karst landforms and aquifers is reviewed by Ford (1979, 1983, 1984, 1987, 1993). Based on field studies from a number of karst regions in Canada, nine different glacial impacts are identified (Table 2.1). Destructive and deranging effects result from erosion and deposition. Input and residual landforms and portions of conduit systems may be removed. Karren scale features are most susceptible, large depression landforms are rarely completely eroded by a single glacial event. Where glacial ice or meltwaters are channelled, significant valley erosion may occur. This can dissect and disrupt pre-existing integrated conduit networks and expose spring points on valley sides. Fragments of

cave systems are preserved in positions well above the current valley bottoms. These phenomenon are observed at the Castleguard and Crowsnest Karsts (Ford, 1979; Smart, 1983).

Sedimentation can strongly influence a karst system. Input landforms are commonly partially or completely infilled with glacial deposits. Sediment permeability will determine if the hydrological function of the feature is altered. In some cases, the sediments will have a low permeability and the original holokarst terrain will function as a fluviokarst or fluvial landscape for a period of time. Clastic debris may also be injected into conduit systems. The fill may be flushed out if recharge to the aquifer is re-established. Sedimentation is also commonly responsible for the aggradation of springs in rugged terrain (Worthington, 1991).

The deposition of carbonate or sulphate rich glacial materials will effectively shield underlying bedrock from karstification. The solvent capacity of infiltrating water is spent on soluble glacial materials in the overburden (Drake, 1984). Lastly, a very fine grained and relatively thick sediment will seal and preserve a karst surface.

Additional glacial effects can have a stimulative impact on karst aquifers. Under a warm based glacier, permafrost may degrade which may increase bedrock permeability. The superimposition of an ice mass will also alter the boundary conditions of the karst aquifer, including: (i) the geometry of the catchment area, (ii) the PCO_2 of recharging waters, (iii) the style and volume of recharge, and (iv) the hydraulic gradient and potential. The glacial hydrological system is linked to that of the karst system. Much of the water in the subglacial environment has a supraglacial origin, these waters are normally unsaturated with respect to carbonate and sulphate minerals. Subglacial recharge into a permeable aquifer is capable of the dissolution of aquifer bedrock, thus karstification need not halt beneath glacial ice. Subglacial recharge will infiltrate into the bedrock where the secondary porosity is greatest and the hydraulic head lowest. This occurs at the locations of subglacial dolines and where fractures intersect in the lee of bedrock obstacles (Smart, P, 1986;

Lauritzen, 1986). The structure of the glacial conduit network will be influenced by the locations of these sinking points. Nye channels focus inputs to these locations. When meltwaters are routed directly or focused to sink points, subglacial karstification can produce small bedrock conduits within the order of 10 ka (Palmer, 1981). In the case of an evaporite or interstratal karst, PCO_2 is irrelevant and karstification can proceed at very rapid rates. Recharge to the karst aquifer will also be supplied by subglacial film waters as diffuse flow, although it is a minor contributor (Smart, 1983).

Glaciation may also affect the flow regime within a karst aquifer. When a glacial aquifer is superimposed upon a pre-existing karst system and connections between them are established, the hydraulic gradient and potential of the system will change. The gradient is increased when the ice mass is superimposed upon the recharge area but does not influence the discharge zone (Pyrenean Type). This has the effect of raising the potentiometric surface and increasing flow velocities and depth (Ford, 1979). However, if the ice mass is confined by valley walls to the former discharge zone, the net effect is a reduction of hydraulic gradient (Lauritzen, 1986). In some circumstances the direction of flow within an aquifer may be reversed.

Postglacial gradients and potentials will be influenced by elevation changes to the recharge and discharge areas through glacial erosion and deposition. Particularly important are modifications to the discharge zone. Valley erosion will produce a steeper gradient, valley aggradation a gentler gradient. Karst conduits are graded to the valley floor, thus a change in local base level may produce changes in the flow system (Borneuf, 1981). Vertical spring hierarchies result, in part, from base level fluctuations.

A number of karst landforms are generated or modified during glaciation. In the subglacial environment, small solution furrows and rills are produced on the stoss side of bedrock obstacles, calcite is precipitated on the lee side. Pressure melting on the stoss face and refreezing in the obstacle lee account for these phenomena (Hallet,

1976). Conduits, Nye channels, and dolines are also produced through subglacial karstification, these often occupy anomalous drainage positions (Smart, 1986). Ford (1984) suggests that linear, joint guided solution corridors located in continuous permafrost are also produced subglacially. In regions that have been subjected to repeated glaciation, the morphology of depression landforms may be wholly or partially related to glacial processes. Localized scour may enlarge and deepen pre-existing depressions. This is important in the periglacial regime where the interglacial process set is dominated by frost action and solifluction which tends to infill topographic lows.

In a permafrost region immediately following deglaciation, the exposed bedrock is subjected to a period of relatively unimpeded recharge prior to the aggradation of a significant thickness of permafrost. This paraglacial karstification will be influenced by the amount and mobility of glacial debris on the bedrock surface. These sediments can shield the underlying bedrock or retard infiltration. The paraglacial environment is characterized by accelerated erosion and the establishment of an equilibrium between geology and the new process set (Church and Ryder, 1972).

2.8 Permafrost Karsts

The development of karst features is influenced by the characteristics of groundwater flow systems. The distribution of permafrost is an important control on those systems (Figure 2.13). The following sections review the characteristics of karst terrains across a variety of climatic, permafrost, and geological environments.

2.8.1 Karst of the Continuous Permafrost Zone

Where permafrost is continuous and hundreds of metres thick, there are few hydrological connections between the supra and subpermafrost aquifers. Groundwater circulation and karstification are normally limited to the active layer with karren forms dominating the landform assemblage (Ciry, 1962). Despite the

restrictions on groundwater movement, karst features and active circulation do occur in the zone of continuous permafrost, particularly within isolated taliks or where permafrost is locally thin. Examples are discussed below.

Akpatok island is a 40 by 25 km outlier of 600 m thick undeformed Ordovician limestone located in Ungava Bay, N.W.T. An undulating plateau surface supports a variety of karst landforms (Lauriol and Gray, 1990). The karst is located within the zone of continuous permafrost and was glaciated in the Late Wisconsinan (Gray and Pilon, 1976; Gray *et al.*, 1979). Annual precipitation is very high, approximately 1600 mm a⁻¹, mean annual temperature is -7°C, and the plateau surface is under tundra vegetation.

The karst landform assemblage includes a variety of dolines, dry valleys, and gorges. Many of the dolines are flooded following the snowmelt period, those underlain by relatively thin permafrost drain readily. Recharge is also accomplished through fissures in the floors of dry valleys and through ponors in ephemeral lakes. Recharge is limited where input landforms are underlain by ice-rich permafrost. The hardness of spring waters average 100 mg L⁻¹ CaCO₃. This is consistent with measurements from similar environments (e.g., Smith, 1972; Woo and Marsh, 1977). Relatively little of the apparent recharge is accounted for by the discharge of the visible springs. A model is suggested where much of the plateau serves as a recharge area for an intermediate flow system with discharge routed to submarine spring points around the perimeter of the island (Lauriol and Gray, 1990). This model requires that percolating waters move through approximately 100 m of permafrost.

The Tsi-it-toh-Choh karst is located in the upper Porcupine Valley of the Ogilvie Mountains at a latitude of 67°N in the Yukon Territory (Cinq-Mars and Lauriol, 1985; Roberge *et al.*, 1986; Lauriol *et al.*, 1988). Several caverns are developed in massive limestone along the flank of a breached anticline. Mean annual temperature at Old Crow, 100 km to the north, is -14°C and precipitation is 215 mm a⁻¹. Much of the karst area is located at or below treeline, where the mean annual temperature is probably 2 to 4 degrees warmer than at Old Crow. The region

was not glaciated in the Pleistocene.

There is no evidence from the accessible cave passages of active diffuse recharge into the limestone. Thick accumulations of speleothem occur in some passages, unpublished dates indicate these are probably of Tertiary age (Ford and Williams, 1989). Point recharge is accomplished at several dolines and at valley bottom ponors that function as thermal taliks. Discharge from these local flow systems is accomplished at nearby subpermafrost springs. Few hydrological data are available from this site. The characteristics of this karst indicate that the solution features are inherited from a period of warmer climate, probably Tertiary. This karst is a significant example of inherited groundwater circulation.

A number of permafrost karsts are also found on the Siberian Platform (Popov *et al*, 1972). Permafrost thickness is variable, where unglaciated it may exceed 1000 m. Karst features are best developed where limestone and dolomite are interbedded with gypsum and salt. The solution of evaporite minerals are reported at a number of locations. Groundwater circulation is largely restricted to isolated taliks beneath and surrounding water bodies. In some locations, the dissolution of evaporite beds located within taliks feed suprapermafrost springs with solute concentrations that are typical of subpermafrost waters. It is suggested by some Russian workers that many of the shallow elements of these karst landscapes have developed under the conditions of continuous permafrost, but the larger karst features are inherited from the Tertiary (e.g., Filippov, 1989). Recharge to the subpermafrost aquifer is currently limited to infiltration along the positions of major faults.

Karst features and drainage are also reported from Spitsbergen (Salvigsen *et al*, 1983; Salvigsen and Elgersma, 1985). Mean annual temperature is roughly -5°C , precipitation is 400 mm a^{-1} . The karst landforms consist of dolines and shallow depressions located on raised beaches and shore platforms that are below the Holocene marine limit. A surficial deposit of beach sands and gravels mantle interbedded Carboniferous and Permian limestone and gypsum. The glacial record

indicates that the region was probably glaciated in the Late Wisconsinan. Groundwater recharge occurs at input features. The distribution of permafrost is continuous over much of the region, however it is reasonable to suspect that in the area below the Holocene marine limit permafrost is thinner. It is suggested by Salvigsen and Elgersma (1985) that rising geothermal waters are responsible for the maintenance of the open taliks. Data supporting this hypothesis are not available. It is probable that these depressions were rapidly developed following the Holocene regression, prior to the aggradation of permafrost. Once established, snow accumulation and ponding minimize permafrost aggradation below these features.

2.8.2 Karst of the Discontinuous Permafrost Zone

In the zone of discontinuous permafrost, taliks constitute important linkages between the permafrost aquifers. The most spectacular example of karst under these permafrost conditions is observed north of the South Nahanni River, N.W.T. at a latitude of 61-62°N (Brook, 1976; Ford, 1984). The karst is developed in a 200 m thick package of Devonian limestone and interbedded shale. Groundwater circulation extends into underlying dolomite. Mean annual temperature is approximately -5°C, precipitation is 550 mm a⁻¹. The region has been ice free for at least 350 ka. A wide variety of karst features are present, including karren, vertical-walled dolines, solution streets or corridors, cave systems, towers, platea, and polje. The entire assemblage is referred to as a labyrinth karst (Brook and Ford, 1978).

The karst occurs over an elevation range of several hundred metres. Permafrost is more extensive at the higher elevation sites, above treeline. The vertical permafrost zonation strongly influences infiltration (Figure 2.14). In the upper zone, there is very little recharge into bedrock. Ice plugs in relict cave passages are observed. The intermediate zone is characterized by periodic impedance of recharge. When ice rich permafrost aggrades into depression bases, temporary ponding results. Depressions drain following thawing of the ice plugs. Runoff into large depressions and poljes of the lowest zone is routed via conduits to

two large subpermafrost springs. Seasonal flooding generated by heavy summer rainfall is an important process at this site. Water levels in dolines and lakes experience rapid fluctuations (Brook and Ford, 1980; Brook, 1983a, 1983b). However, these fluctuations are not synchronous across the karst. Variability in the extent of permafrost may partially account for the varied response to recharge events.

Karst features also occur across an extensive area in the Franklin Mountains, Colville Hills, and Great Bear Plain within the N.W.T. (van Everdingen, 1981). The region was glaciated in the Late Wisconsinan, mean annual temperature is -6°C , precipitation is 350 mm a^{-1} . The distribution of permafrost is variable, most of the terrain is in the discontinuous zone. The area includes portions of the Northern Interior Platform and the Cordilleran Orogen. In general, fine grained clastic rocks of Devonian to Permian age outcrop in the low elevation areas, these are underlain by Paleozoic limestone, dolomite, gypsum, halite, and shale. The carbonates and evaporites outcrop in the mountainous areas. Where the evaporites are found in subcrop, the dominant karst landforms are dolines and large depressions. The morphology results from the collapse of the surficial bedrock into underlying solution cavities. The most impressive topography is associated with outcrops of limestone and dolomite solution breccia. Gypsum dissolution has produced a draped and foundered collapse karst where these highly soluble rocks are found in the shallow subsurface. The overall distribution of karst features is controlled by the presence of evaporite formations within the zone of active groundwater circulation.

In some local areas, the density of input landforms is high and permafrost does not constitute a significant barrier to groundwater recharge. Hydrological investigations suggest that a significant proportion of the total annual precipitation functions as recharge and that snowmelt is a critical event. Local flow systems from sink to spring are apparently independent of regional groundwater fluctuations and residence times within these appear short. Hydrochemical analyses reveal that the dissolution of evaporites is more important to the development of collapse karst than limestone and dolomite solution.

2.8.3 The Effect of Permafrost on Karst

Permafrost may have a positive or negative impact on karstification. Frost shatter and ice wedging increase the porosity and storativity of the suprapermafrost aquifer. This aquifer serves the same role as the epikarst in the temperate zone. The bulk permeability of permafrost is low, thus throughflow and runoff are focused towards dolines and ponors. Recharge may occur at discrete points rather than as a diffuse flow through a network of small discontinuities. This increases the recharge flow volume and concentrates dissolution along conduits and major fissures. However, input landforms are often plugged by ice rich permafrost, and may also be infilled by slow mass wasting processes. Where snowmelt is the most important hydrological event, much of the meltwater leaves the system as surface runoff. During snowmelt, the permeability and storage capacity of the supraglacial aquifer are low. Focused runoff may exceed the infiltration capacity of sinking points and ponding results. When water levels exceed the depth of the sinks, surface overflow results. Over time an original holokarst may be modified to a fluvial terrain.

Karst landforms are observed across the full range of climatic and permafrost conditions. The characteristics of several permafrost karsts suggest that active groundwater circulation is, in part, influenced by the morphology of input landforms that may be inherited from either a warmer climato-genetic regime or a radically different environment (e.g., subglacial). In some cases from the continuous zone, it is unlikely that many of the solution features present would be generated under the current process set. Where glaciation, permafrost, and karst interact, much of the land surface consists of complex polygenetic forms.

Table 2.1: Effects of glaciation upon karst systems (after Ford, 1983, 1987).

Process	Effect
Destructive	
1. Erasure	Removal of shallow karren and residual landforms (e.g., pinnacles)
2. Dissection	Fragmentation of an integrated preglacial conduit network
3. Infilling	Burial of depressions by sedimentation, aggradation of spring points
4. Injection	Clastic sedimentation within conduit networks
Inhibitive	
5. Shielding	Sedimentation of carbonate or sulphate rich glacial materials
Preservative	
6. Sealing	Fine grained deposits seal and confine epikarst aquifers
Stimulative	
7. Focusing	Focusing inputs, increasing hydraulic head by superimposition of glacier
8. Springs	Spring elevations and aquifer base level lowered by glacial erosion
9. Injection	Deep circulation of glacial meltwaters

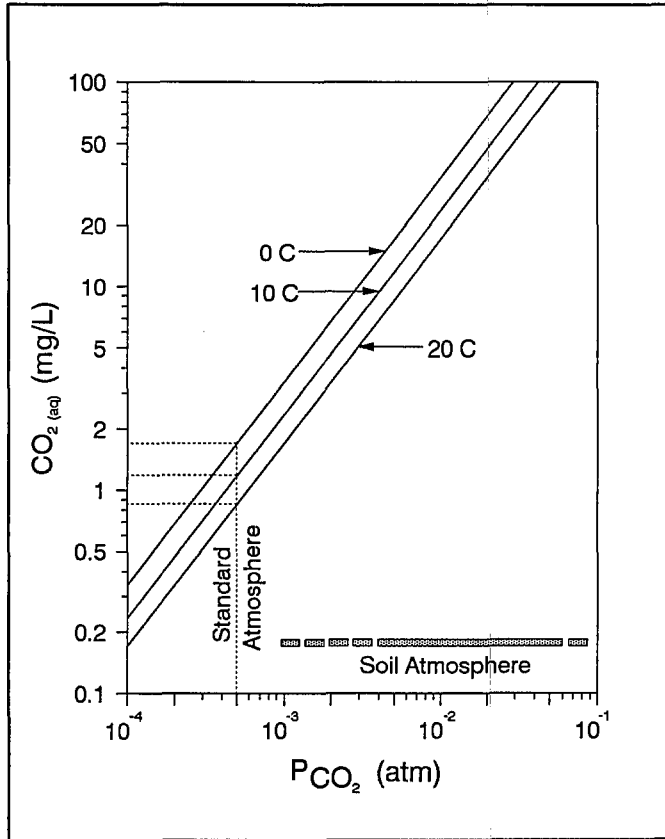


Figure 2.1: Solubility of carbon dioxide as a function of the partial pressure of CO_2 in the coexisting gas phase (after White, 1988).

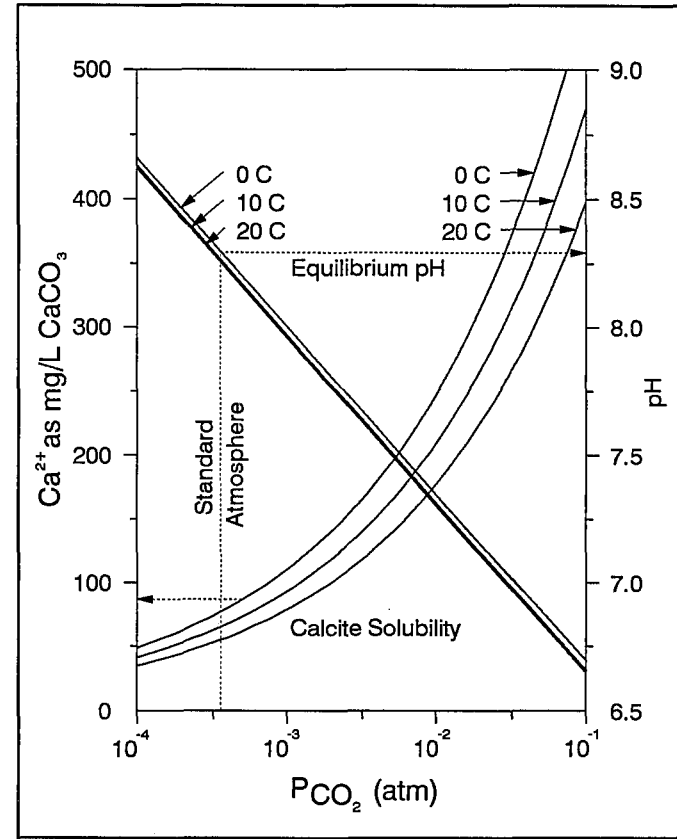


Figure 2.2: Solubility of calcite as a function of carbon dioxide partial pressure. Conditions are open (after White, 1988).

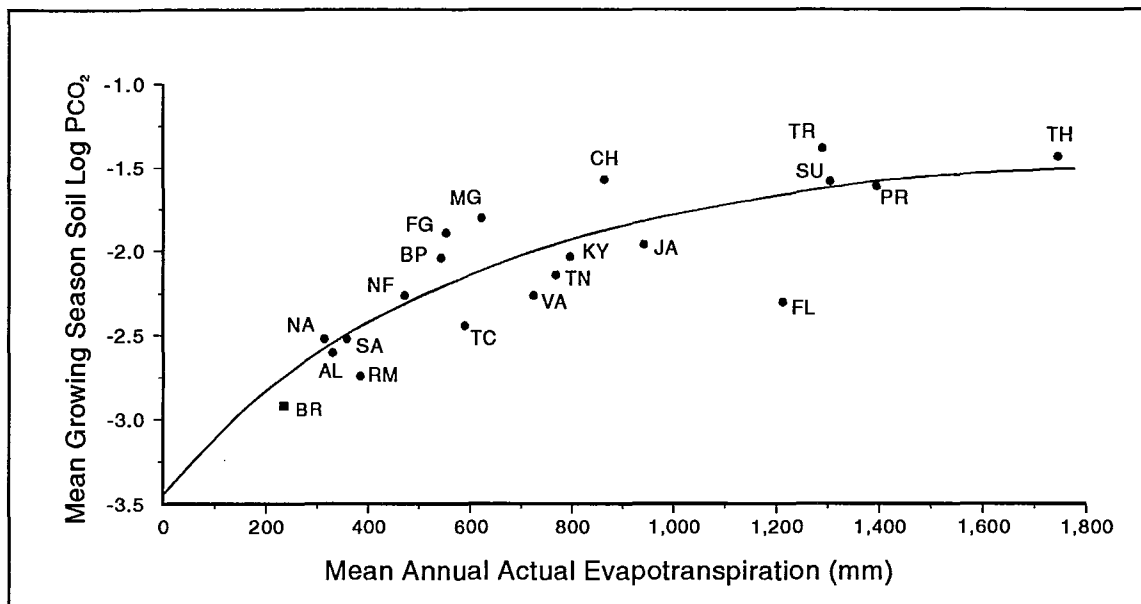


Figure 2.3: Mean growing season soil log P_{CO_2} versus mean annual actual evapotranspiration. Na = Nahanni, N.W.T.; SA = Saskatchewan; RM = Canadian Rocky Mountains; NF = Newfoundland; TC = Trout Creek, Ontario; AL = Alaska; VA = Reston, Virginia; TN = Sinking Cove, Tennessee; KY = Mammoth Cave, Kentucky; FL = southern Florida; FG = Frankfurt-Main, Germany; MG = Mullenbach, Germany; Ja = Jamaica; TR = Trinidad; PR = Puerto Rico; CH = Yuman, China; Sulawesi, TH = Phangnga, Thailand (Brook *et al*, 1983). BR = This Study.

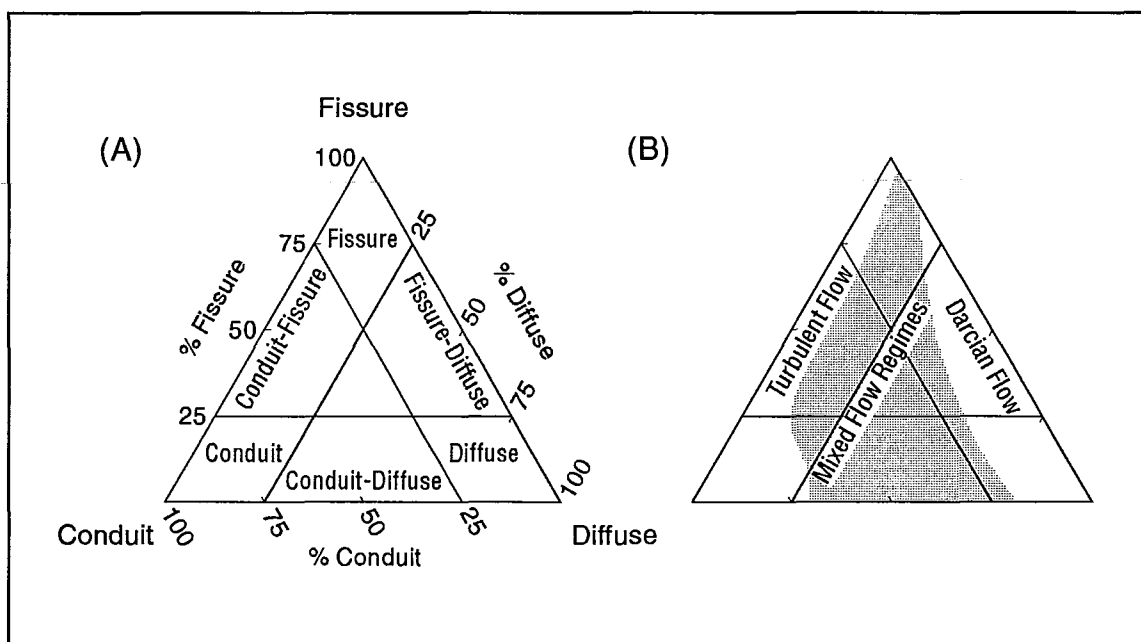


Figure 2.5: (A) A conceptual classification of karst aquifers into diffuse, fissure (mixed), and conduit types. (B) The predominant flow regimes of the aquifer types. The shaded area denotes the range encompassed by karst systems (from Ford and Williams, 1989; after Atkinson, 1985).

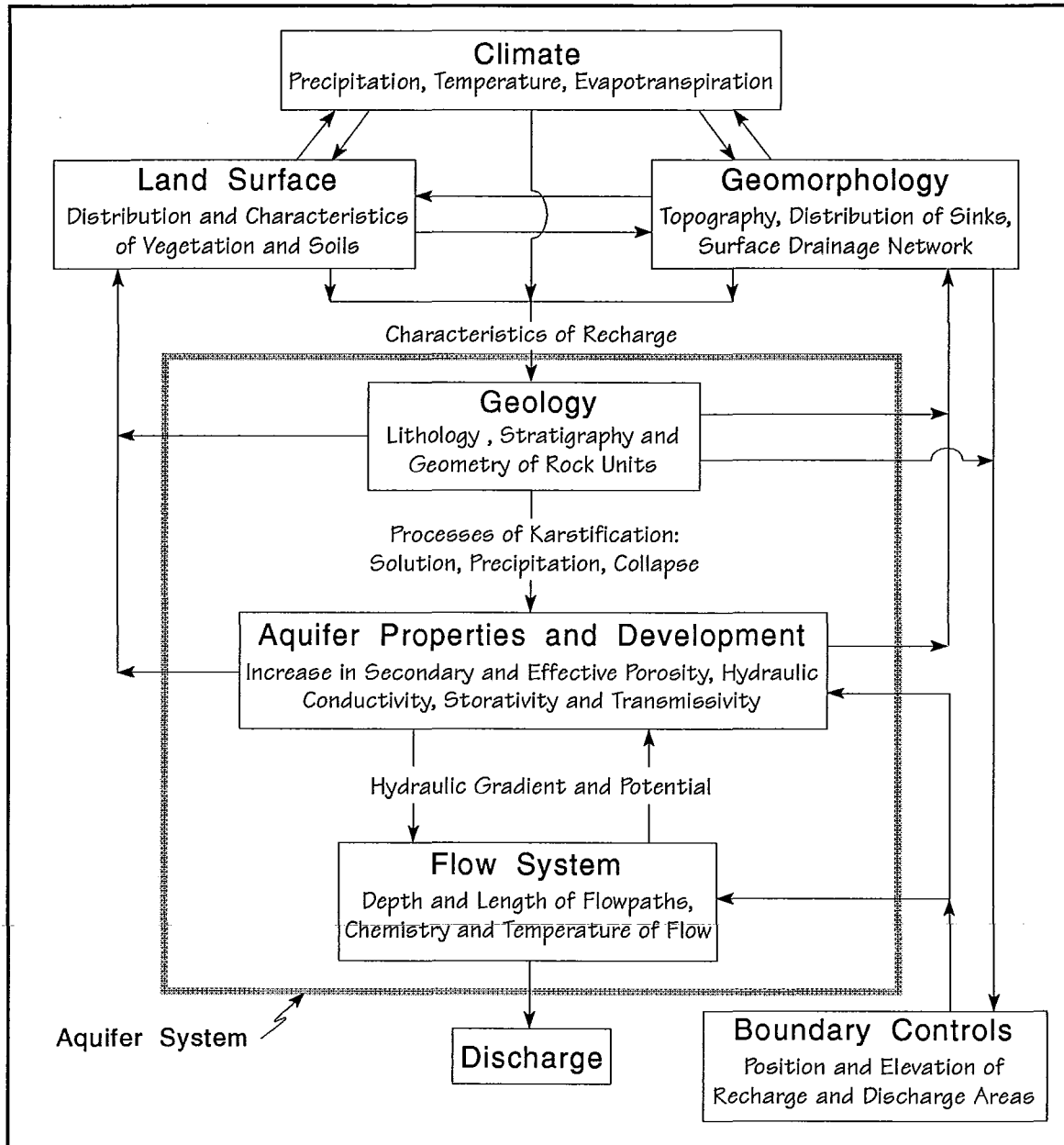


Figure 2.4: Controls on the development of karst aquifer flow systems. In this simple model the aquifer is bounded by the shaded line. The boundary conditions consist of inputs (recharge), outputs (discharge), and the external factors that influence flow within the system. This includes the positions of recharge and discharge areas. The attributes and flux of groundwater through the system are subject to modification with changes in the aquifer properties and boundary conditions. There are complex feedbacks between the system and external factors.

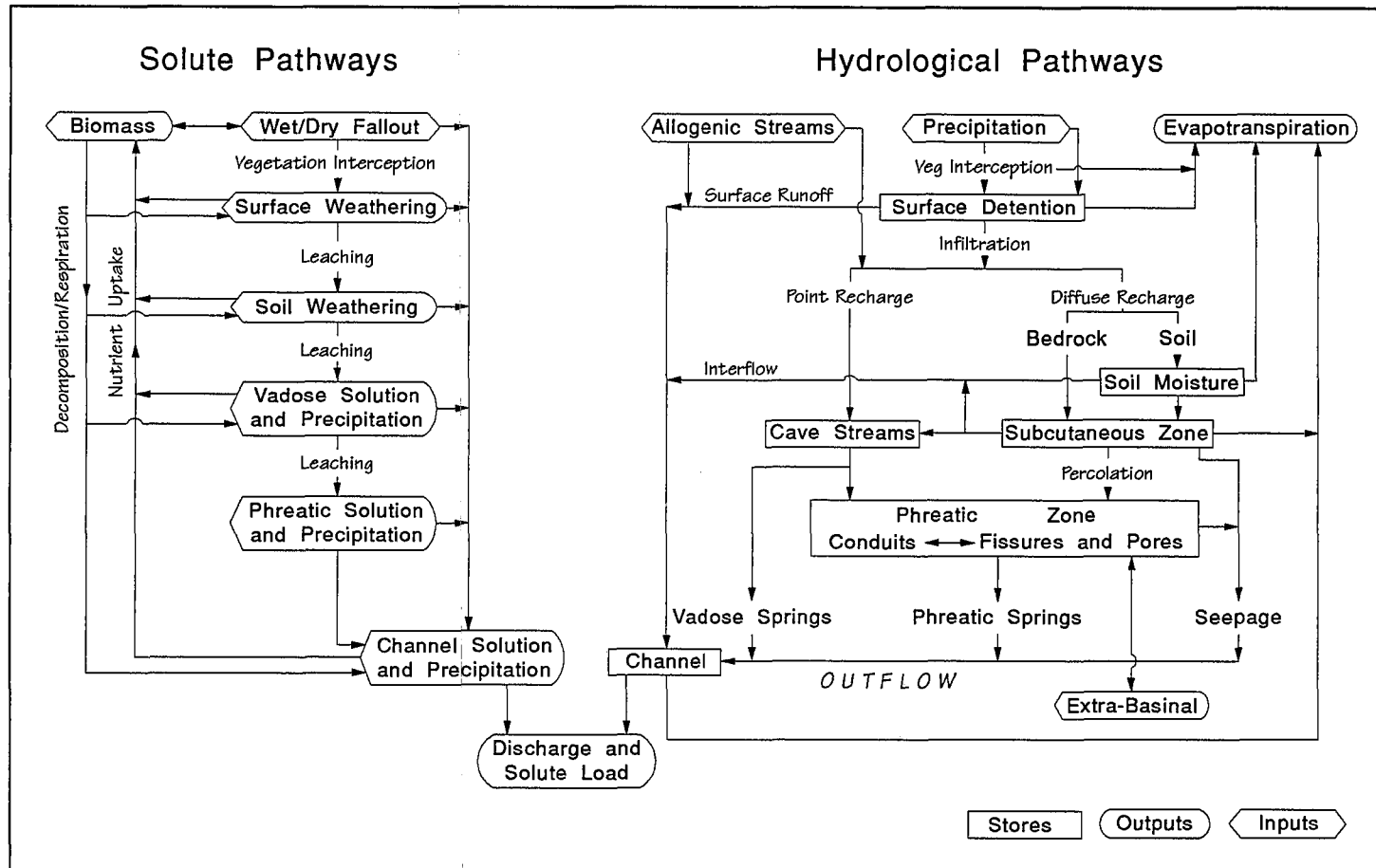


Figure 2.6: Hydrological and solute pathways in a karst system. Inputs, stores, outputs, and linkages are shown (after Ford and Williams, 1989; Walling and Webb, 1986).

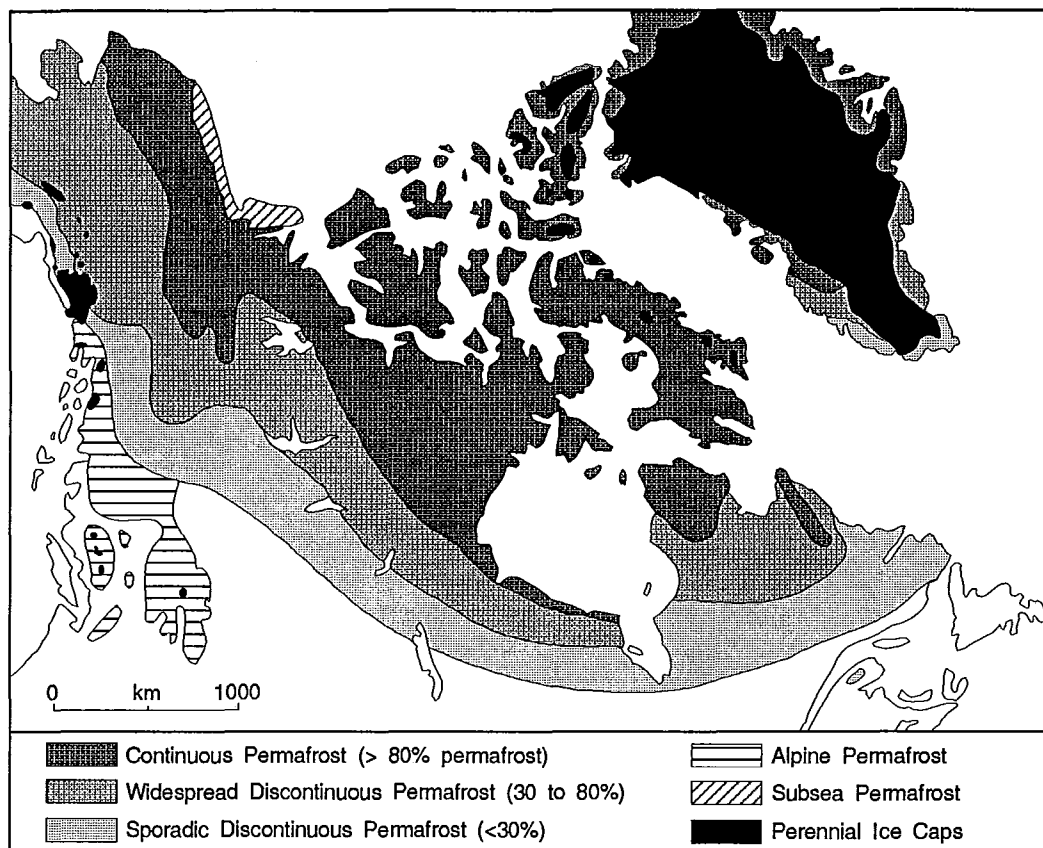


Figure 2.7: Permafrost zones in North America (from Harris *et al*, 1988; after Harris, 1986; Heginbottom, 1984; Johnston, 1981).

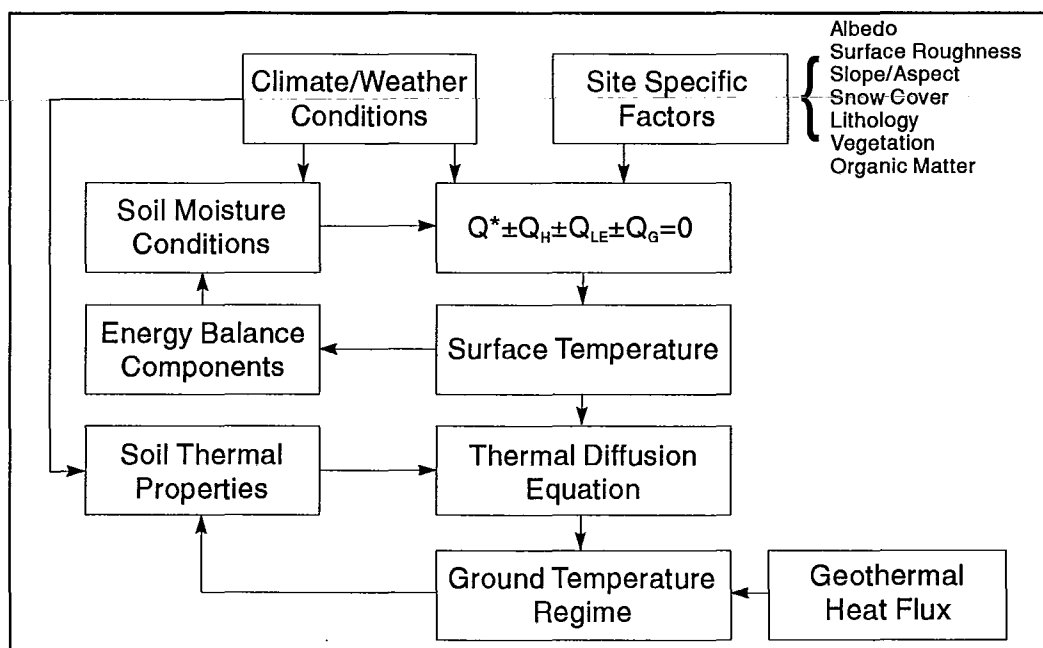


Figure 2.8: Interactions between climate and ground thermal regime (from Williams and Smith, 1989).

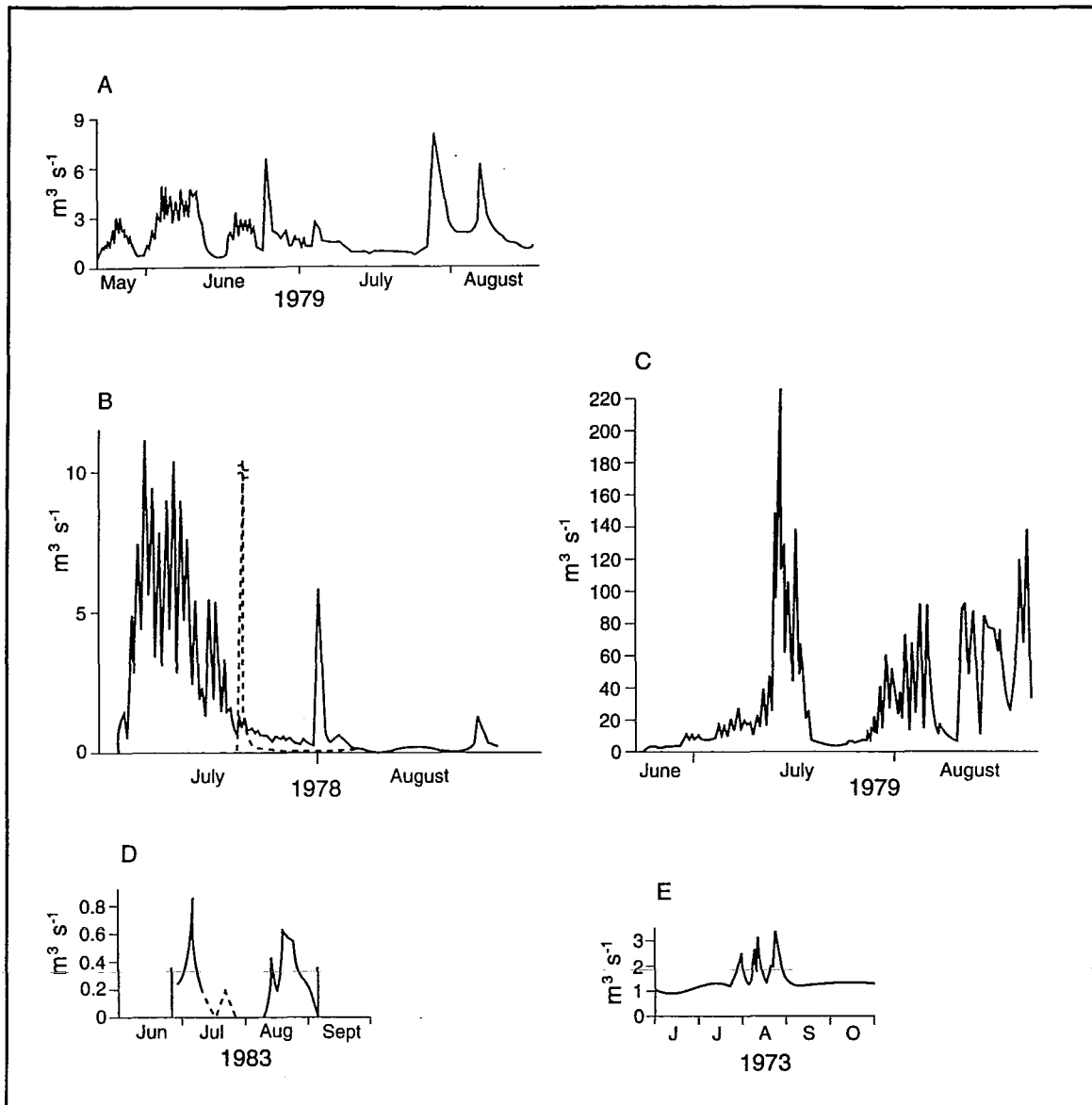


Figure 2.9: Hydrographs from basins representing the five streamflow regimes: (A) subarctic nival regime: Dietrich River, Alaska, (B) arctic nival regime: McMaster River, Cornwallis Island, NWT (C) proglacial regime: Sverdrup River, Ellesmere Island, NWT (d) wetland regime: Barrow watershed, Alaska, and (e) spring-fed regime: Canning Spring-10, Alaska (from Woo, 1986, 1993).

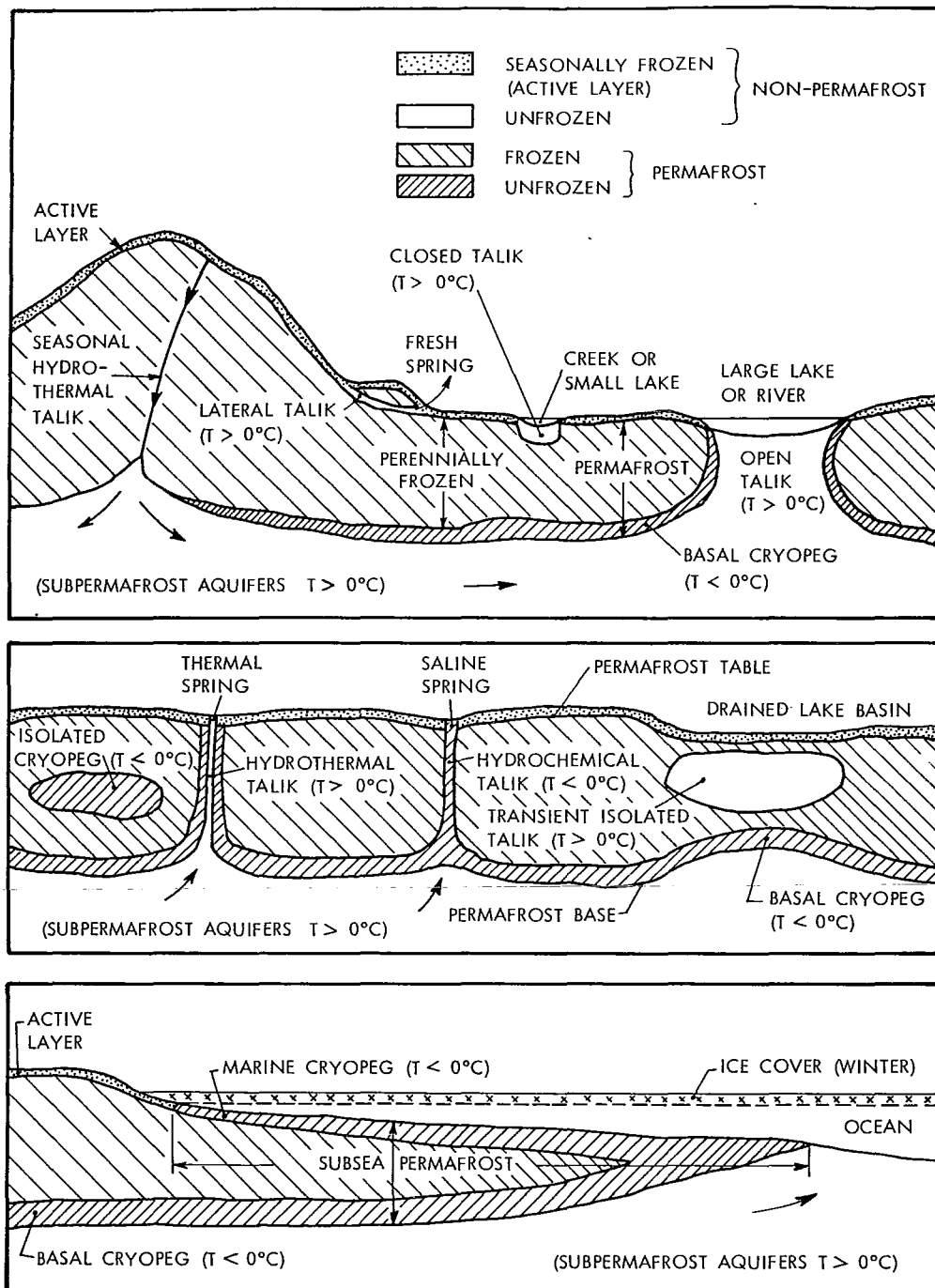


Figure 2.10: Frozen and unfrozen zones in a permafrost environment and their relationships with surface water and groundwater (from Harris *et al*, 1988; after van Everdingen, 1976)

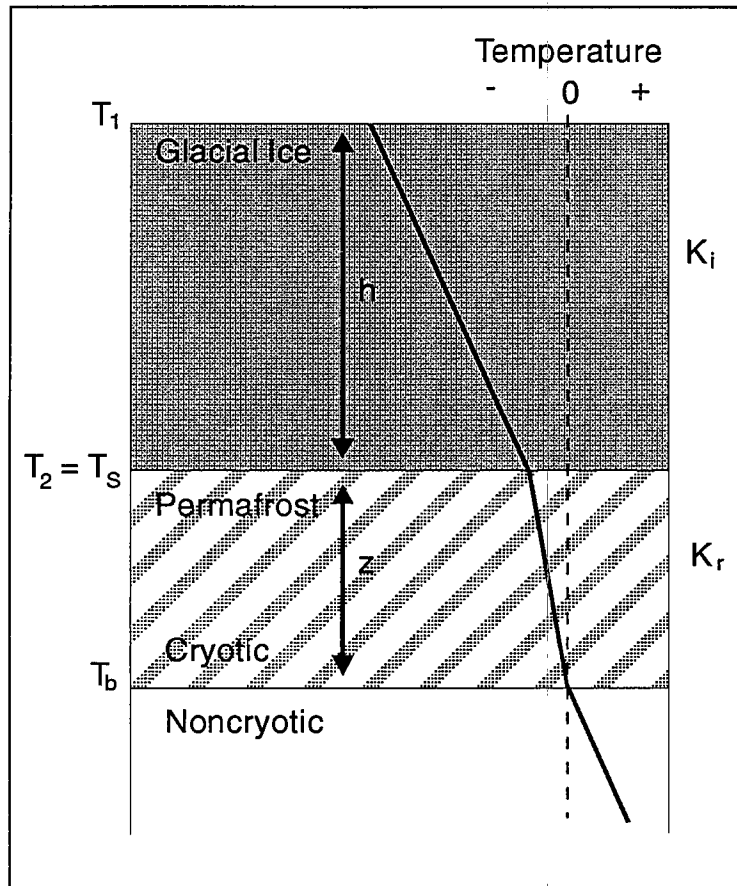


Figure 2.11: A simple model of glacial superimposition on permafrost, variables correspond to equations in text.

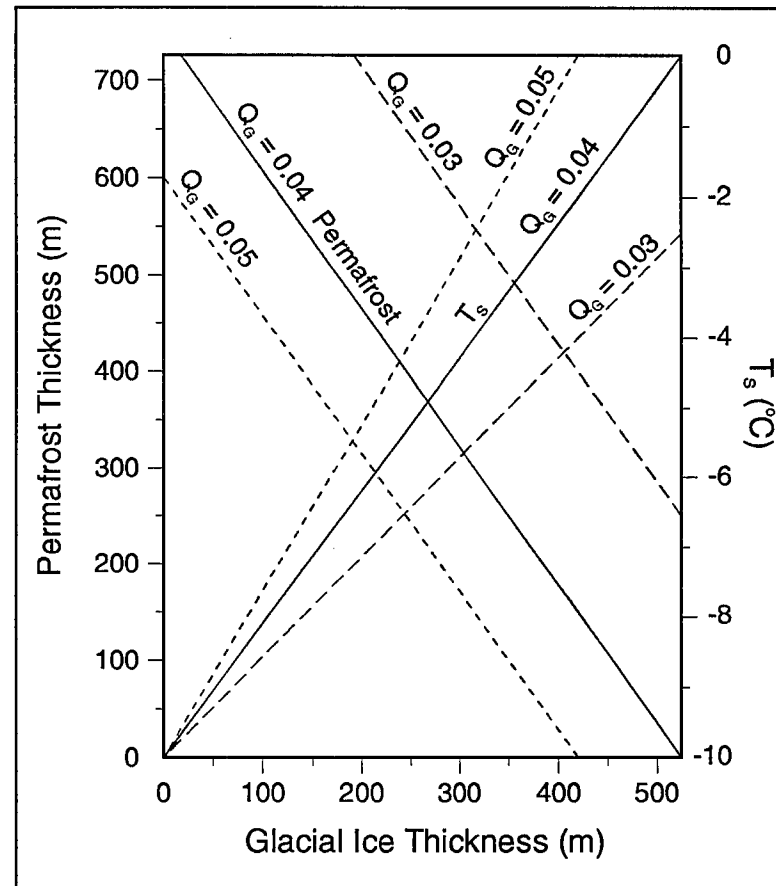


Figure 2.12: Steady state conditions in permafrost and overlying glacial ice solved for three geothermal heat flux conditions ($Q_g = 0.03, 0.04, \text{ and } 0.05 \text{ W m}^{-2}$). The following values are used: $T_1 = -10^\circ\text{C}$, $K_i = 2.1 \text{ W m}^{-1} \text{ K}^{-1}$, $K_r = 3 \text{ W m}^{-1} \text{ K}^{-1}$.

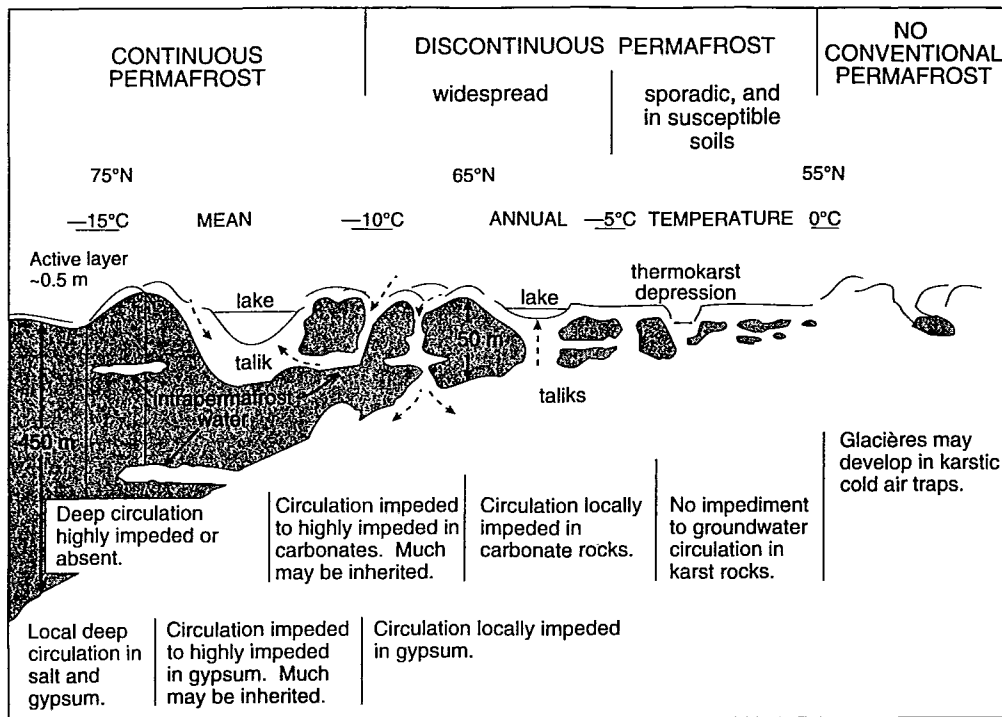


Figure 2.13: A model depicting the relationships between permafrost, groundwater circulation, and karst activity in terrains of low to moderate relief. Permafrost conditions are based on those observed in a transect from the northern Interior Platform to the low arctic (from Ford and Williams, 1989).

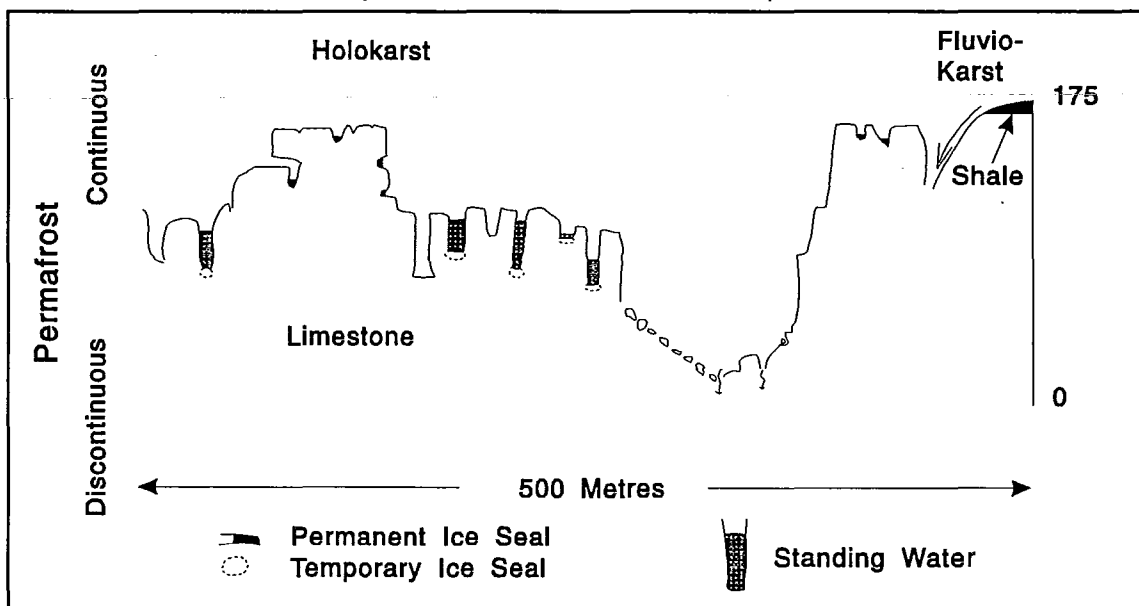


Figure 2.14: A zonal model of permafrost distribution showing the relationship between permafrost and karst drainage in rugged terrain. Based on the Nahanni doline and corridor karst, Mackenzie Mountains, N.W.T. (after Brook, 1976).

CHAPTER III

STUDY AREA AND METHODS

3.1 Introduction

This chapter reviews the biophysical characteristics of the study area and the research methods employed. Investigations were conducted in mountainous terrain of the Mackenzie and Franklin Mountains located near Norman Wells in the District of Mackenzie, N.W.T. The Mackenzie Mountains are broadly divisible into the Canyon and Backbone Ranges. The Canyon Ranges form an eastern arc of low mountains and plateaux between the 61st and 66th parallels. These ranges are dissected by deep canyons that drain runoff from the Backbone Ranges to the west. The Franklin Mountains lie to the east at the margin of the Cordillera and consist of a series of folded, discontinuous, low ranges that extend from the South Nahanni River to Fort Good Hope. The Mackenzie Plain is a wide lowland between the Mackenzie and Franklin chains. Most of the outcrops on the Plain are Cretaceous shales. The Franklin Mountains and the Canyon Ranges are dominated by Cambrian to Devonian carbonates and evaporites, with Proterozoic clastics also present in the Mackenzies. The bedrock geology and geomorphology are discussed in subsequent chapters.

Field sites were selected where karst landforms and evidence of groundwater discharge were clearly visible on aerial photography. Figure 3.1 shows the site locations. Sites 1, 3, and 4 are within the Carcajou Range. Site 1 is at the mountain front adjacent to Dodo Canyon. Sites 3 and 4 are centred on lakes called Bonus and Pyramid Lakes in this thesis. Site 2 is called Bear Rock; it is located in the Norman Range of the Franklin Mountains west of Fort Norman.

3.2 The Biophysical Characteristics of the Study Area

At the study sites, karst occurs across a broad range of elevations. Therefore, it is not possible to provide a simple biophysical description of the area. Much of these data are best organized within an ecoclimatic classification. An ecoclimatic region is a broad area of similar macroclimate that is distinguished by a characteristic assemblage of vegetation, soils, wildlife, and hydrology (Ecoregions Working Group, 1989). There are four ecoclimatic regions in the study area: (i) the Low Subarctic, comprising the Mackenzie Valley northwest of Fort Norman, and the low ground of the Franklin Mountains below 250-300 m elevation, (ii) the High Subarctic, encompassing the bulk of the Franklin Mountains and those areas of the Canyon Ranges generally below 600 m elevation, (iii) the Subalpine Northern Subarctic Cordilleran, consisting of valleys and slopes in the Canyon Ranges between elevations of 600 and 900-1000 m, and, (iv) the Alpine Northern Subarctic Cordilleran, involving the high elevation areas of the Mackenzie Mountains (Ecoregions Working Group, 1989). The following sections provide a review of the climate, vegetation, soils, permafrost conditions, hydrology, and hydrogeology of the central Mackenzie Valley and adjacent highlands. Where appropriate reference is drawn to the ecoclimatic regions defined above.

3.2.1 Climate

The climate is characterized by lengthy cold winters, short warm summers, subfreezing mean annual temperatures, and a total annual precipitation range between 250 and 600 mm. Climate data are available from Norman Wells and Fort Norman in the Mackenzie Valley (Figure 3.2; Table 3.1). There are no stations within the High Subarctic or either of the Cordilleran regions close to the study area. However, a short record is available from Tsichu River in the Backbone Range (Figure 3.1; Table 3.1), and longer data sets are available from Tungsten, N.W.T. and from several stations in the eastern Yukon (Table 3.1). Regional climatic summaries are provided by Wahl *et al* (1987) and Burns (1973). These are compilations of data

from permanent stations and fragmentary records acquired through several field investigations. Variations in temperature and precipitation are related to latitude, elevation, topography, and aspect.

3.2.1.1 Temperature

In the Mackenzie Valley and Canyon Ranges, mean daily temperatures are above freezing from late April/early-May to mid-September (Figure 3.2). River ice clears in late-May and is re-established by early November. On average, there are 70 frost free days during the summer period. Summer temperatures are strongly controlled by elevation with an average lapse rate of approximately $0.8^{\circ}\text{C}/100\text{ m}$. It is common during July for daily maximum temperatures to exceed 25°C at Norman Wells and Fort Norman. In the period between October and March a persistent winter inversion may develop at high elevations. It is most intense during January at elevations around 1500 m, when mountain temperatures may be as much as 10°C warmer than those in the Mackenzie Valley (mean January temperature is -26°C). Local inversions are also frequent within the mountainous terrain. By April the inversions break down, with valley temperatures coming to exceed those in the alpine and subalpine. Over the period 1951 to 1980, mean annual temperatures at Fort Norman and Norman Wells were -6.3°C and -6.4°C , respectively (Table 3.1). Estimates of mean annual temperature in the High Subarctic zone vary between -5 and -7°C . Data from the Subalpine and Alpine Northern Subarctic Cordilleran zones are sparse but are likely in the range -6 to -8°C (Ecoregions Working Group, 1989; Wahl *et al*, 1987; Burns, 1973). The Bear Rock Site is near Fort Norman and lies predominantly within the Low Subarctic zone. Dodo Canyon, Bonus Lake, and Pyramid Lake Sites are located southwest of Norman Wells and extend into the Subalpine Northern Subarctic Cordilleran zone.

3.2.1.2 Precipitation

The mean annual total precipitation at Norman Wells is 317 mm and at Fort Norman

325 mm (Table 3.1). At both stations there is a summer maximum with June to September rainfall accounting for 50 to 55% of the annual precipitation total (Figure 3.2). The timing of precipitation in the Cordillera is similar to that observed in the Mackenzie Valley, but mountain precipitation is strongly influenced by orographic and altitude effects. Total amounts are greater on the western sides of ranges and increase with elevation. A regional gradient of approximately 20 mm/100 m exists to 1500-2000 m and then gradually decreases (Wahl *et al*, 1987). During the summers of 1987 and 1988 recorded precipitation at the Dodo Canyon base camp was approximately 50% higher than values recorded at Norman Wells (Figure 3.3). The stations are separated by only 48 km and 290 m elevation. The data show the difficulty in extrapolating from a Mackenzie Valley location to the Canyon Ranges.

Snowfall accounts for greater percentage of total annual precipitation with increased elevation (Table 3.1). The snowpack reaches its maximum in mid-March/mid-April and is on average approximately 50 to 75 cm in the Mackenzie Valley and 100 cm in the Canyon Ranges. Much of the snow load is subject to drifting and redistribution, particularly in terrain where local wind velocities may be high. Snow re-accumulates in depressions, in the lee of physical obstacles, and under vegetation. Snowfall is a difficult parameter to measure and there are few reliable data from the Cordillera. In the Canyon Ranges, total annual precipitation is estimated to range between 400 and 550 mm and in the Backbone Ranges it is >500 mm (Wahl *et al*, 1987).

The most intense precipitation events occur during July when the frequency of maritime Pacific air is highest. Heavy rainfall is associated with uplift of these air masses. Low pressure cells originating in the north Pacific often track eastward across the southern Yukon over the St. Elias, Selwyn, and Mackenzie Mountains. This flow can bring a large, moist, slow moving, unstable air mass into the Mackenzie Valley. Frontal and convective rainfall can persist for several days. In 1972, heavy rainfall was recorded at the Nahanni Karst in the southern Mackenzie Mountains over the period July 16 to 27 (208 mm) resulting in substantial flooding

of large polje features (Brook, 1976; Brook and Ford, 1980). This heavy precipitation was associated with the orographic uplift of moist unstable air under a northeast wind producing repeated thunderstorm activity. During this period, high pressure usually dominates over the northern Interior Plains and consequently strong easterly and northeasterly surface flows may be generated across the Mackenzie Valley and Mountains. Occasionally, low pressure cells move off the Bering Sea across northern Alaska and Yukon to the northern Mackenzie Mountains. However, far more common is lee side cyclogenesis in the area surrounding and to the west of Norman Wells (Wahl *et al*, 1987). These primary lows may produce heavy rainfall before tracking to the southeast. The greatest recorded precipitation in 24 hours for Norman Wells and Fort Norman are 49.3 mm and 73.7 mm respectively; both records were events occurring in July.

3.2.1.3 Evaporation

Pan evaporation data are collected at Norman Wells, "lake evaporation" is calculated from the observed daily values of pan water loss, mean temperature of the pan water and nearby air, and the total wind run over the pan (Environment Canada, 1984). These values are thought to represent evaporation from small surface water bodies with little heat storage, but overestimate evaporation from lake bodies. Over the period 1951 to 1980 the mean calculated "lake evaporation" for May, June, July, August, and September are: 110.4, 139.9, 123.0, 81.4, and 42.3 mm. The annual total is 497 mm. Burns (1973) estimates the actual annual rate of evaporation from lake sized bodies in the region is approximately 250 mm.

Evapotranspiration can be calculated through use of the Turc (1954) or Thornthwaite equations. In the former equation:

$$E = \frac{P}{[0.9 + (\frac{P}{I_T})^2]^{0.5}} \quad (3.1)$$

where E = annual evapotranspiration in mm, P = annual precipitation in mm. I_T is the evaporation capacity of the air:

$$I_T = 300 + 25T + 0.05T^3 \quad (3.2)$$

where T = mean annual air temperature in °C. Given annual estimates of precipitation and temperature of 400 mm and -7°C for the Canyon Ranges west of Norman Wells, the annual evapotranspiration equals 194 mm. Burns (1973) estimates mean annual actual evapotranspiration in the central Mackenzie Valley at 150 mm.

3.2.2 Vegetation

The study region spans transitions across Boreal, Cordilleran, and Tundra ecosystems. The Low Subarctic of the Mackenzie Valley is dominated by open stands of *Picea mariana* (black spruce) with an understorey of *Betula glandulosa* (dwarf birch), *Ledum groenlandicum* (Labrador tea), and a variety of lichens and mosses. *Betula papyrifera* (paper birch) and black spruce dominate fire-prone sites. Open stands of *Picea glauca* (white spruce) and paper birch are abundant on drier sites, with a discontinuous understorey of *Arctostaphylos uva-ursi* (bearberry), *Vaccinium vitis-idaea* (bog cranberry), *Shepherdia canadensis* (soapberry), *Salix* spp. (willows), *Alnus crispa* (green alder), and mosses. *Populus tremuloides* (trembling aspen) occurs in more protected locations. Bogs and fens, in poorly-drained areas, are composed of black spruce, *Larix laricina* (tamarack) with *Sphagnum* spp. (sphagnum), Labrador tea, *Vaccinium* spp., *Rubus chamaemorus* (cloudberry), and *Andromeda polifolia* (bog rosemary) forming a dense mat of ground vegetation (Ecoregions Working Group, 1989; Ritchie, 1984).

The vegetation of the High Subarctic is similar to that of the Low Subarctic although tree densities and heights decrease, and tundra vegetation increases in frequency and percentage cover. Moss and lichen become more common. Poorly-

drained sites are dominated by tussocks of *Carex* spp. (sedges) and *Eriophorum* spp. (cottongrasses) with sphagnum. Low shrub tundra consisting of dwarf birch and willow along with *Dryas octopetala* (mountain avens) and lichen, have a scattered occurrence. Balsam poplar, white spruce, and paper birch are common along river banks with green alder and willow species (Ecoregions Working Group, 1989; Ritchie, 1984).

The subalpine areas of the Cordilleran region contain several tree species. Where the parent material is calcareous and well drained, very open stands of stunted white spruce occur interspersed with willow and dwarf birch, tamarack may be present. Ground cover is commonly composed of *Ledum decumbens* (northern Labrador tea), *Arctostaphylos rubra* (red bearberry), *Vaccinium uliginosum* (bilberry), *Empetrum nigrum* (crowberry), bog cranberry, moss and lichen. Black spruce krummholz occur on moister sites. Erect spruce, paper birch, balsam poplar, and trembling aspen can still be found in warm, protected areas with adequate drainage. Sedge, cottongrass, sphagnum, and moss are common on poorly-drained sites.

The alpine areas lack trees; they support a tundra assemblage including *Cassiope* spp. (heather), *Lupinus arcticus* (Lupine), *Salix glauca* (dwarf willow), *Salix arctica* (Arctic willow), heaths, lichen, moss, dwarf birch, mountain avens, sedge, and cottongrass. Broad exposed areas of bedrock and scree are only sparsely covered with moss and lichen. (Ecoregions Working Group, 1989; Ritchie, 1984).

3.2.3 Soils

The Cryosol, Brunisol, and Regosol soil orders comprise the soils of the study area. Cryosols occur in either mineral (Turbic and Static Cryosol) or organic materials (Organic Cryosol) where permafrost is in the near subsurface. Turbic Cryosols are strongly cryoturbated soils with an active layer thickness of <2 m; in Static and Organic Cryosols the active layer is <1 m thick (Agriculture Canada, 1987). Brunisols lack the well-developed B horizons of Podzols, Luvisols, and Chernozems

but are sufficiently thick to differentiate them from Regosols. Regosols lack, or possess very thin B horizons due to the age and nature of the parent material, climate, and modifying geomorphic processes.

In the Low and High Subarctic ecoclimatic zones, Brunisols are common on upland, coarse textured, and well-drained sites. Organic and Static Cryosols occur in poorly drained sites. Turbic Cryosols develop locally (Ecoregions Working Group, 1989). In the Subarctic zone, the frequency of Brunisols decreases. Turbic and Static Cryosols are more frequent. Regosols occur on steep slopes. In the Alpine zone, Cryosols are most common. Regosols occur where permafrost is locally absent. At the field sites, valley bottoms and gently sloping areas are characterized by Static Brunisolic Cryosols and Eutric Brunisols, uplands by Static and Turbic Cryosols, and slopes by Turbic Cryosols and Regosols.

3.2.4 Permafrost in the Mackenzie Valley and Area

The regional distribution of permafrost in the Mackenzie Valley is well documented. In the early 1970's, over 11600 shallow boreholes were drilled east of the Mackenzie River to evaluate the geotechnical properties of materials along the proposed routes of roadways and pipelines. Data collection focussed on the occurrence of frozen ground and ground ice within 10 m of the surface. The borehole data were spatially divided using 1:250,000 NTS map areas, and the incidence of frozen ground for classes of surficial materials determined (Heginbottom *et al*, 1978). The data from map areas in the central Mackenzie Valley are presented in Table 3.2.

The regional survey shows that from 61°N to 68°N the extent of permafrost increases and the depth to permafrost decreases. Along this transect, mean annual temperatures drop from -3.5°C to -9.5°C, the length of winter increases from 195 to 245 days, and degree days above 5°C decrease from 1195 to 682 (Burns, 1973; Environment Canada, 1993). At Norman Wells, greater than 80% of the terrestrial area is underlain by frozen ground. However, the area is classified as widespread discontinuous permafrost due to the high proportion of water bodies that are likely

underlain by open taliks. Heginbottom *et al* (1978) suggest that permafrost becomes continuous just north of the Sans Sault Rapids map area (106H). The mean annual temperature at the nearest station, Fort Good Hope (66°16' N), is -7.5°C. Permafrost thickness measurements were not routinely conducted, although figures from the Norman Wells area show that permafrost, where present, averages between 45 and 60 m in thickness (Brown, 1970; Wahl *et al*, 1987).

The frequency of ground ice also increases from south to north with soil texture exercising an important local control. High ice content is associated with organic and fine-grained soils. In map area 96E, the mean winter ice content of peaty soils was 220%, for fine-grained soils 35%, and for clean coarse-grained soils 10-15% (Heginbottom *et al*, 1978). Organic and fine-grained soils usually retain more moisture than coarse-grained soils. During the summer period, water in the active layer can migrate downward into the top of the permafrost producing segregation ice (Mackay, 1983a). This process may be favoured in organic and fine-grained soils.

A geophysical survey undertaken along the full length of the Norman Wells-Zama pipeline right of way detected frozen ground to a depth of 10 m based on sediment conductivity (Kay *et al*, 1983). Genetic terrain types were assigned by using air photo interpretation and borehole control. Data from the construction spread south of Norman Wells show permafrost underlies 83.7% of the terrestrial area (Table 3.3). High percentages of the exposed bedrock, ground moraine, lacustrine plains, and organic veneered sediments are frozen. Coarse glacial, fluvial, and eolian deposits have a lower incidence of permafrost, though the percentage in talus is high. Active floodplains have a high frequency of frozen-unfrozen interfaces. To the south, the frequency of permafrost decreases across all classes.

No direct measurements of permafrost are available from the northern Mackenzie Mountains. Permafrost distribution must be inferred by extrapolation of climatic and terrain relationships from adjacent areas and through the use of diagnostic geomorphic and hydrologic features. The principal difficulties in

mountainous terrain are local variations in microclimate that are related to slope aspect, snow drifting, and variations in ground cover. South facing slopes have a higher mean annual ground temperature. Kay *et al* (1983) noted a higher incidence of permafrost on north facing slopes. The relationship between snow cover and permafrost was not examined in the regional surveys, however, Kershaw (personal communication, 1988) induced palsa formation in unfrozen ground near Fort Norman by removing snow cover.

Karst input and output features are distributed throughout the study area up to elevations of 950-1000 m (Chapter VI). Dolines, sinking streams, and springs points are evidence of active karstic drainage. Data show that meteoric waters circulate to depths of several hundred metres (Chapter VII). Where such groundwater systems operate the distribution of permafrost cannot be considered continuous (Heginbottom, personal communication, 1988).

Harris (1982) suggests that the periglacial landform assemblage may be used as a surrogate for permafrost data. Features exclusive to the zone of continuous permafrost include active felsenmeer (block field), ice wedge polygons in mineral soils, earth hummocks, and lobate rock glaciers. Ice wedges in peat, palsas, sorted and non-sorted stripes and circles, frost blisters, and open system pingos are found extending into the zone of discontinuous permafrost. In the study area, active felsenmeer is found at elevations above 1000 m, corresponding to the boundary between the subalpine and alpine ecoclimatic zones. At the field sites there are frost blisters, stone stripes and circles, palsas, mudboils, and a range of slow mass wasting features. Only at the higher elevations of the Pyramid Lake Site is felsenmeer present.

Recent permafrost mapping by Heginbottom and Radburn (1992) includes the Franklin Mountains and portions of the Canyon Ranges at the 1:1000000 scale. The Bear Rock, Bonus Lake, and Dodo Canyon Sites are mapped as extensive discontinuous permafrost; the Pyramid Lake Site lies outside the mapping limit. The ground ice content is estimated as nil to low due to the high proportion of exposed

bedrock, talus, and coarse glacial and alluvial deposits. The information from the Mackenzie Valley studies, the mountain climate data, and the geomorphic and hydrologic evidence support the general mapping of Heginbottom and Radburn (1992). However, at such a scale, local variations in the distribution of permafrost and ground ice are not captured.

It is expected that the permafrost conditions in the Canyon Ranges should be highly variable across short distances due to changes in elevation, aspect, exposure, substrate, and ground cover. Permafrost will be absent or sporadic beneath major rivers and lakes, on southern exposures at low elevation, and within some depressions where drifting snow and meltwater accumulate. On active floodplains and terraces the distribution will be discontinuous. Continuous permafrost with a low ice content will occur on exposed areas of bedrock, talus, and coarse substrate. Ice-rich permafrost occurs where organic and fine grained sediments accumulate, such as in shallow depressions and wetlands.

3.2.5 Regional Hydrology

There are comparatively few discharge data from the northern Mackenzie Mountains. Records are available from the Redstone, Mountain, Carcajou, Twitya, and Tsichu Rivers (Figure 3.1). These mountain basins are characterized by a subarctic nival regime in which an early snowmelt-driven peak is followed by summer runoff events produced by frontal and convective precipitation. Figure 3.4 shows the mean monthly discharges of the above streams for the period 1980 to 1990. Discharge through the winter period (October to April) is very low, snowmelt begins in May and the monthly values peak in June for all stations. On average, stream flows remain high in July and August but there are marked variations in response to summer rainfall (e.g., Figure 3.5).

Discharge characteristics are influenced by the amount and timing of precipitation, basin topography, lithology, ground cover, and the distribution of permafrost, lakes, and wetlands. Calculation of discharge per unit area (specific

discharge: Q_s) allows a regional comparison. Annual values of specific discharge from permafrost basins of the Northern Interior Plains and Canadian Shield range from 0.001 to 0.006 $\text{m}^3 \text{s}^{-1} \text{km}^{-2}$; mountainous, glacierized basins of southeastern Yukon have values of 0.015 to 0.018 $\text{m}^3 \text{s}^{-1} \text{km}^{-2}$ (Woo, 1986). The annual specific discharge calculated for Tsichu River is 0.016 $\text{m}^3 \text{s}^{-1} \text{km}^{-2}$; it is a small high elevation basin in continuous permafrost with a heavy snowpack (Tables 3.1, 3.4). The values calculated for the Redstone, Mountain, Carcajou, and Twitya Rivers are all approximately 0.010 $\text{m}^3 \text{s}^{-1} \text{km}^{-2}$ (Table 3.4). These large basins span a range of elevations, permafrost conditions, and vegetation zones, and receive less precipitation than the Tsichu basin. The high specific discharge values of the Mackenzie Mountain streams reflect relatively high levels of precipitation and the rapid flux of inputs to stream channels. The latter are aided by high relief and the presence of a permafrost aquitard in the near subsurface. Storage and evaporation are limited by the low area of wetland and lakes, the short summer season, and a high proportion of bare ground and bedrock.

For this thesis, daily maximum specific discharges were calculated using the highest daily peak flow on record. Values for the Mackenzie Mountain streams range from 0.12 to 0.26 $\text{m}^3 \text{s}^{-1} \text{km}^{-2}$ (Table 3.4). These figures are an order of magnitude greater than those from basins of the Northern Interior Plains and Canadian Shield, and exceed values from the Yukon glacierized basins (Woo, 1986). In the northern Mackenzies, the peak flows occur in late June and early July following heavy rainfall. The 1988 hydrograph of Carcajou River is typical (Figure 3.5). Following 58 mm of rainfall over three days, a maximum instantaneous discharge of 1460 $\text{m}^3 \text{s}^{-1}$ ($Q_s=0.2 \text{ m}^3 \text{s}^{-1} \text{km}^{-2}$) and a daily discharge of 1110 $\text{m}^3 \text{s}^{-1}$ ($Q_s=0.15 \text{ m}^3 \text{s}^{-1} \text{km}^{-2}$) were recorded on July 1. Unlike streams of the Northern Interior Plains and Arctic Islands, spring break up does not produce the most significant flow events.

The hydrograph of Jungle Ridge Creek resembles an Arctic nival regime, where snowmelt is the highest annual flow (Figure 3.4). Jungle Ridge Creek is a

small basin on the Mackenzie Plain west of the Bear Rock Site. This shale basin is well below treeline with large areas of wetland. Summer rainfall events produce only minor flows, likely due to high rates of interception, storage, and evapotranspiration. This basin differs greatly from the rugged, lightly vegetated basins of the mountains.

Across northern Canada, water balance calculations are hampered by a lack of detailed hydrometeorological data (Woo, 1986). However, given the information that is available from the study region a first approximation of the water balance components can be derived. Runoff is calculated as the ratio of total annual discharge to basin area (Table 3.4). It is highest for the Tsichu watershed (507 mm), with the other Mackenzie Mountain basins varying between 318 and 363 mm. Total precipitation can be estimated to be 500 mm for the Redstone, Mountain, Carcajou, and Twitya basins and 630 mm for the Tsichu. This yields a runoff to precipitation ratio of 0.80 for Tsichu and a range of 0.64 to 0.73 for the others. These values are characteristic of basins in continuous and discontinuous permafrost (Woo, 1986). If storage is assumed to be zero, then evaporation for the Mackenzie Mountain basins varies between 123 and 182 mm, with the low value being the Tsichu and the highest being Carcajou. The calculated runoff of Jungle Ridge Creek basin exceeds the total annual precipitation at Fort Norman. This basin may receive more precipitation than Fort Norman but it is likely that during May its discharge is overestimated due to channel ice.

3.2.6 Clastic and Dissolved Sediments

There are no lengthy records of sediment concentration from the rivers of the northern Mackenzie Mountains. There are a few spot samples of suspended sediment and total dissolved solids concentrations from the Redstone, Mountain, and Carcajou Rivers (Table 3.5). Water quality data are available from Mackenzie River and from several reconnaissance studies conducted in the region to the east and south of the study area. However, few water quality data are available from the Mackenzie

Mountains, none having been collected since 1974. Data from the Keele, Redstone, and Mountain Rivers are presented in Table 3.6; there are no such data from Carcajou River. Annual values of clastic and solute load cannot be accurately determined from the data set. However, the relationship with discharge can be examined.

Suspended sediment concentration and load are positively correlated with discharge for all rivers (Table 3.5, Figure 3.6); this relationship is steepest for Carcajou River. The trunk branch of the Carcajou and its major tributaries (Little Keele, Dodo, Katherine, and Rouge Mountain) all flow through deep canyons and gullies in sedimentary rocks along their courses. Geomorphic evidence suggests high rates of erosion on these routes. The single highest concentration recorded on the Carcajou is 2070 mg L^{-1} , yielding an instantaneous load of 898 kg s^{-1} . This sample was taken on the falling limb of the July 1, 1988 flood event by the Water Survey Branch. It is likely an underestimate of the maximum concentration and load. The texture of samples from Carcajou average 30% sand, 50% silt, and 20% clay; there are no estimates of bedload (Environment Canada, 1989a). Mountain and Redstone Rivers show a more gradual increase in suspended sediment concentration with discharge. This may be an effect of the sampling dates or it may reflect slight variations in the basin characteristics. The Mountain River watershed is mainly in resistant quartzites while the basin of Redstone River lacks the very rugged canyon topography of the Carcajou Range.

There is an inverse relationship between discharge and total dissolved solids (TDS) concentrations (Table 3.5, Figure 3.6). At low flows, TDS concentrations generally exceed 300 mg L^{-1} , values decrease below 200 mg L^{-1} at high discharge. The solute load does increase with discharge but exceeds the clastic load only during periods of low flow. At peak discharges, the instantaneous clastic load is an order of magnitude greater than the solute load. On average, TDS concentrations are high during winter (October to April) and low in the summer (May to September). During the winter period, discharge of the major streams is maintained at low levels by

groundwater flow (Michel, 1986a). In the summer, the groundwater component is overwhelmed by surface and near subsurface runoff. Spatially the TDS concentrations are highest for Carcajou River (279 mg L^{-1}) and lowest for Redstone River (208 mg L^{-1}). This may reflect differences in geology; evaporite sequences subcrop extensively throughout the Carcajou basin.

Details on ion concentrations, pH, conductivity, and saturation indices are restricted to a few samples from the Keele, Redstone, and Mountain Rivers (Table 3.6). Ion abundances are shown on a trilinear diagram (Figure 3.7) and concentrations on a fingerprint diagram (Figure 3.8). The composition and the ion ratios suggest the principal minerals contributing to the solute component are dolomite, limestone, anhydrite (gypsum), and halite. There are some spatial and temporal differences in the patterns. Across all flow conditions cation abundances are $\text{Ca}^{2+} > \text{Mg}^{2+} > \text{Na}^+ \gg \text{K}^+$. During the low flows of winter, anion abundances are $\text{SO}_4^{2-} > \text{HCO}_3^- > \text{Cl}^-$, in summer they are $\text{HCO}_3^- > \text{SO}_4^{2-} > \text{Cl}^-$ (Figures 3.7, 3.8). These temporal changes in ion abundance and concentration are related to the proportional contribution of baseflow to total stream flow. Overall, Mountain River has lower concentrations of all ions and in particular much less Na^+ and Cl^- . This is a function of the basin geology; halite and anhydrite subcrops are very restricted in that basin.

Saturation indices were calculated using the ion concentrations, temperature, and pH data. Winter groundwater-dominated flows are at equilibrium or slightly oversaturated with respect to calcite, and are at equilibrium or undersaturated with respect to dolomite. The high discharge summer flows are predominantly aggressive towards both minerals.

3.2.7 Regional Hydrogeology

The hydrogeology of the Mackenzie Valley and area has been examined by Brandon (1965) and Michel (1977, 1986a). Surface water chemistry is described by Reeder *et al* (1972) and Hitchon and Krouse (1972). Studies have identified the Devonian Bear Rock Formation as the principal groundwater aquifer in the Mackenzie Valley

region. In outcrop the Bear Rock Formation is a dolomite and limestone breccia, in subcrop it is interbedded dolomite and anhydrite (Fort Norman Formation: Chapter IV). The Cambrian Saline River and Franklin Mountain Formations, and the Ordovician-Silurian Mount Kindle Formation are also recognized as important aquifers. The Saline River is composed of redbeds, salt, and anhydrite in subcrop; outcrops lack the evaporite component. The Franklin Mountain and Mount Kindle Formations are both dolomite. These formations subcrop in the Northern Interior Plains and outcrop in the Franklin and Mackenzie Mountains.

Outcrops and shallow subcrops of the Bear Rock and Saline River Formations are often marked by karst input landforms (Aitken and Cook, 1974). Michel (1986a) describes karstic flow systems on the western slopes of the Franklin Mountains developed in the Bear Rock Formation. Karst captures 15% of the surface flow in the area between the Smith Arm of Great Bear Lake and the Franklin Mountains (van Everdingen, 1981). Drilling reports from Norman Wells have noted circulating groundwaters in the Bear Rock Formation, even to depths as great as 1000 m (Hume, 1954; Hume and Link, 1945).

Many groundwater springs in the region are highly enriched in Ca^{2+} , Na^+ , SO_4^{2-} , and Cl^- ions (van Everdingen, 1981; Michel, 1986a). Dissolution of gypsum and halite in subcrop are principally responsible (Reeder *et al*, 1972). Several subpermafrost groundwater springs in the Franklin Mountains are dominated by Ca^{2+} - SO_4^{2-} or Na^+ - Cl^- waters depending upon the flowpath and strata encountered, Ca^{2+} - Mg^{2+} - HCO_3^- waters characterize springs that drain shallow local flow systems in carbonate rocks and surface waters. The hydrochemical facies described for the Redstone, Keele, and Mountain Rivers confirm subpermafrost waters constitute the bulk of the winter baseflow. The summer facies show a greater contribution from surface and shallow flow systems through carbonates.

3.3 Methods: Data Collection and Analyses

The thesis objectives outlined in Chapter I require that data be collected on: (i) the

regional distribution and morphology of karst landforms, (ii) the lithological and structural controls on that distribution, (iii) the influence of glaciation and permafrost on karst, and (iv) measures of karst landform generating processes.

Regional data on karst landform description and distribution, and on the geological, glacial, and permafrost controls were gathered through literature search, analyses of aerial photography, and low level aerial reconnaissance. Ground checking of these data were accomplished at several field sites. Four sites were visited by the author. In all, 33 weeks were spent on location over the course of three summers (1987, 1988, 1991). Approximately 60 km² of terrain were traversed on foot. The remote character of the field area required transport by helicopter or float plane. The prohibitive cost of air transportation limited the number of locations that could be examined, the frequency of relocation between sites, and the amount of equipment conveyed.

The process oriented investigations focussed on data collection to examine: (i) seasonal and temporal variations in solution and discharge, (ii) the isotopic characteristics of karst waters, and (iii) the movement of water in a permafrost environment. Discharge records were obtained from four springs over portions of one or two summers, and observations were also made of the general hydrology, particularly in response to storm events. There were some attempts at groundwater tracing, with mixed success. Sampling of input (precipitation and sinks) and output (springs) waters provided data on spatial and temporal variability in solutes and isotopes. These data are most valuable when evaluating the rate of landscape development and the characteristics of the groundwater flowpaths. Field work was equally expended between geological and geomorphological mapping, and hydrological and hydrochemical measurements. The following sections describe the methods and techniques that were used to gather the hydrological, solute, isotope, and dye trace data.

3.3.1 Hydrometeorological Measures: Discharge and Precipitation

Most of the streams gauged in this study had low gradient channels with negligible clastic loads. Straight, stable reaches free of obstructions were selected for gauging. In some cases modifications were necessary to ensure stability, including armouring and deepening of channels. Discharge was measured by the velocity area method using Price or Pygmy current meters with a wading rod and was calculated from the velocity, width and depth data using standard techniques (Lewin, 1990; Gardiner and Dackombe, 1983). A FORTRAN program was used to simplify rapid processing of these data. Errors associated with this technique include inaccuracies in channel area measurement, operation of the current meter, and instrument calibration. The accuracy of these discharge measurements is approximately $\pm 5-10\%$. Discharge was occasionally determined by measuring channel geometry and estimating the surface velocity with floats. This method yields results estimated to be accurate to $\pm 25\%$.

At four locations, stage was measured continuously using Leupold-Stevens Type F water level indicators. The number of stations were limited by the logistics of the project. The water level indicators were fixed to 30 cm diameter PVC tubes that functioned as stilling wells. The wells were dug into the bank adjacent to the streams and encircled with gravel to ensure a good response to fluctuations in stage. The top of the wells were capped. Care was exercised to ensure secure footing for well and recorder. In some instances it was necessary to construct additional supports to ensure stability of the instrument. At the locations of the water level indicators, discharge was repeatedly measured and rating curves were generated. Variations in stage were recorded on the graph paper fixed to the rotating drum. In the office, these records were digitized to produce 'instantaneous' records of stage. Depending upon the pen velocity and the rapidity of changes in stage, the sampling interval along the analogue record varied between 1 and 4 hours yielding the 'instantaneous' digital record. Rating curves were then used to generate the discharge series. The digitization procedure is another potential source of error. The

accuracy of the continuous discharge series is estimated at approximately $\pm 15\%$. Precipitation was monitored at the field camp locations using a standard tipping bucket and 5 inch rain gauges. In addition, records are available from Norman Wells and Fort Norman.

3.3.2 Solute Measurements

The acquisition and analyses of water samples for solute studies are reviewed by Cryer and Trudgill (1990). The value of conclusions drawn from these inquiries are related to: (i) the design of the water sampling program, (ii) the collection of the water samples, and (iii) the analytical techniques used to generate data. Error and bias may be introduced at any of the above stages. Representativeness and design are major concerns. The spatial and temporal distribution of samples should be suited to the specific research questions and the samples representative of the population from which they are drawn (Hem, 1985). Sampling frequency is based on the objectives and the logistics of the program. In solute budget, or denudation studies, regular but infrequent sampling may suffice (e.g., weekly samples at the basin outlet). In detailed examinations of storm driven solute variations, more frequent sampling is required, so that substantial changes or events are not missed between sampling times. If the purpose is to examine spatial variability and possibly the relationship between solutes and geology, then infrequent spot or grab sampling may be sufficient. As was discussed earlier, the solute component of this study involves sampling across large areas. However, at a few locations time series of solute, discharge, conductivity, and isotope measurements are available.

3.3.2.1 Sample Collection

Analyses of water samples were undertaken at the collection point, at the base camp, and later at several laboratory facilities. Routinely temperature, pH, conductivity, salinity, and alkalinity were determined on site during sample collection. Conductivity and temperature were measured with a portable analogue device, the

YSI model 33 SCT meter. The conductivity measurements were adjusted in a two-step procedure: (i) the values were corrected using calibration equations that were developed using standard KCl solutions, and (ii) conductivity was expressed to 25°C using the equation:

$$L_R = L_T - 0.02(T - R) L_T \quad (3.3)$$

where L_R is the conductivity at the reference temperature, L_T is the conductivity at the sampled temperature, R is the reference temperature and T is the sample temperature (°C) (Gardiner and Dackombe, 1983). Technical representatives from YSI support the use of a 2% conductivity correction per degree Celsius. Conductivity readability from the analogue scale is approximately 0.5% of the scale maximum (2.5 to 250 $\mu\text{S cm}^{-1}$ depending upon the scale used); the meter accuracy is specified at $\pm 2.5\%$ and the probe at $\pm 2.0\%$. Temperature measurements were also corrected using calibration equations. Temperature scale readability varies between $\pm 0.1^\circ\text{C}$ @ -2°C to $\pm 0.4^\circ\text{C}$ @ 45°C , meter accuracy is $\pm 0.1^\circ\text{C}$ @ -2°C and $\pm 0.6^\circ\text{C}$ @ 45°C , the probe accuracy is $\pm 0.1^\circ\text{C}$ @ 0°C and $\pm 0.3^\circ\text{C}$ @ 40°C . Based on the calibration runs, the mean instrument accuracy, including the probe, was approximately $\pm 4.0\%$ for conductivity (n=18), and $\pm 2.0\%$ for temperature (n=87).

Continuous records of temperature and conductivity were periodically recorded at springs at the Dodo Canyon and Bear Rock Sites using a pHOX System Series 57 Conductivity/T.D.S. meter. This meter features an automatic temperature compensation to 25°C. When in operation the meter samples conductivity at 15 minute intervals. These data were recorded on an analogue tape and were subsequently digitized at 1 to 4 hour intervals. Data correction was accomplished with calibration equations. Accuracy for the meter and probe are specified at $\pm 2\%$. From the calibration runs, instrument accuracy including the probe was approximately $\pm 4.0\%$. Digitization of the analogue record introduced additional error, yielding a total error estimate for the continuous conductivity series of $\pm 10\%$.

On site, pH was recorded using portable 9 volt hand held instruments from

Fisher Scientific. A model 119 was used in 1987 and 1988, and an Accumet 1003 was used in 1991. The first model has a resolution of 0.01 pH units and is accurate to $0.01 \text{ pH} \pm 1$ digit. The Accumet 1003 meter has a resolution to 0.001 pH units and is accurate within 0.002 pH units. Combination gel-filled electrodes were used, the electrode accuracy is better than 0.05 pH units. Fisher certified buffers were used in meter calibrations.

At the field camp, calcium and magnesium hardness and, periodically, sulphate concentrations were measured. Analyses for sodium, chloride, sulphate, and potassium were done later (Section 3.3.2.2). Nalgene brand polyethylene containers were used to transport water from the sample locations to the field laboratory. Borosilicate glass bottles with polyethylene or Teflon lined caps were used to collect water samples for later analyses. All bottles and caps were triple rinsed in the sample water during collection. The bottles were held with their openings upstream of the collectors hand and were completely filled and capped below the water surface to exclude atmospheric gases. In streams or springs, the water was drawn from a mid-channel and mid-depth position where the flow was well mixed. For almost all sites there was very little suspended sediment, therefore a $0.45 \mu\text{m}$ filter was only employed on the few occasions when the water was visibly turbid. Sample agitation during transport to the field laboratory was kept to a minimum, and samples to be transported back for later analyses were kept as cool as possible and out of sunlight.

3.3.2.2 Sample Analyses

A variety of analytical techniques were used to measure the concentrations of the major ions in the sample waters, the techniques employed conform to standard methods (APHA, 1985). Titrations for alkalinity (HCO_3^-) and hardness (Ca^{2+} and Mg^{2+}) were done at the collection site or at the field laboratory. A turbidimetric technique was used to determine SO_4^{2-} concentrations for the 1988 samples. Ion chromatography was used to measure SO_4^{2-} and Cl^- concentrations for the 1991

samples.

Neutron activation analysis (NAA) was used to determine concentrations of Na^+ , Cl^- , K^+ , Ca^{2+} , Mg^{2+} , and a number of trace elements for the 1988 samples. These analyses were done at the neutron activation laboratory at McMaster University (Haskin, 1980; Dostal and Elson, 1980). The technique involves introducing a small volume of sample (<5 ml) into a reactor core where it is bombarded by a carefully monitored neutron flux. Upon irradiation, radioactive isotopes of the above elements are produced. These isotopes decay at known rates and energy levels. The sample is retrieved from the reactor core and gamma emissions across a range of energy levels are monitored by a counter. Software specific to the McMaster facility is then used to select, isolate, and measure the dimensions of energy peaks associated with the radioactive isotopes in question. These data are then used together with counts from standards to determine the concentrations of the elements in the sample. Under optimal conditions accuracy is $\pm 1\text{-}2\%$, when concentrations are low this accuracy is not achieved. From running standards, accuracy for Na^+ and Cl^- were $\pm 3\%$. These analyses were conducted by the author under the supervision of the laboratory coordinator in the fall of 1988.

Alkalinity

Alkalinity is the capacity of water to neutralize acid (Stednick, 1991). In most natural waters alkalinity is contributed by bicarbonate (HCO_3^-), carbonate (CO_3^{2-}), and hydroxide (OH^-) ions. Across the pH range that characterizes karst waters the bicarbonate ion is the dominant species and alkalinity is usually expressed as a mass or equivalence of HCO_3^- per unit volume. It may also be quoted in mg L^{-1} as CaCO_3 . It is important that alkalinity be measured as quickly as possible following sample collection (Cryer and Trudgill, 1990). It is determined by potentiometric or colorimetric titration methods; the latter was used in this study. Samples collected in 1987 were transported to base camp where total alkalinity was determined within 24 hours of collection. Sample volumes of 50 ml were used. Titration to pH 4.5 was

accomplished with 0.02 N HCl; BDH 4.5 was used as an indicator. Titrations were conducted until there was agreement within 0.5 mg L^{-1} as CaCO_3 . The acid was periodically standardized with a borax solution (Stenner, 1969). In the field seasons of 1988 and 1991, total and phenolphthalein alkalinities were determined on site with portable apparatus and reagents supplied by HACH company. This apparatus was capable of delivering small volumes of titrant and therefore more concentrated acids could be used. Sample volumes were dependent upon the site; normally 50 ml were used. The acid was 0.16 or 1.6 N H_2SO_4 , bromcresol green-methyl red was used as an indicator for total alkalinity, titrations were done to pH 4.5 and repeated until agreement was within 1 mg L^{-1} as CaCO_3 . Titrations using standards showed that the accuracy was approximately $\pm 2\%$. Phenolphthalein alkalinity was always zero or very close to it. Total alkalinity was then expressed as mg or meq $\text{L}^{-1} \text{HCO}_3^-$. Occasionally field conditions were so adverse that the samples were transported to base camp for alkalinity determination.

Calcium and Magnesium Hardness

Total hardness is the most commonly measured water quality parameter in karst areas, being the sum of divalent cations ions expressed as calcium carbonate. In surface waters from the Mackenzie Mountains calcium and magnesium are the only ions of this group that are present in significant concentrations (Table 3.6). In this study, total and calcium hardness were determined on site or at the field laboratory within 24 hours of sample collection. Apparatus and reagents for on site determinations were purchased from HACH chemicals. Reagents used in the field laboratory were purchased from BDH chemicals. Titrations were repeated until agreement was within 1.0 mg L^{-1} as CaCO_3 . At the field laboratory, total hardness was determined using a standard complexometric titration with EDTA (Stenner, 1969). The sample pH is adjusted to 10.1 with an ammonia buffer; Eriochrome Black T was used as an indicator and 0.02 N EDTA as titrant. Calmagite was found to yield a more distinct end point, and for most of the 1988 and 1991 field seasons

it was used as the indicator. When total hardness was determined on site, 2-amino-2-methyl-1-propanol was used as the buffer and calmagite as the indicator.

The calcium hardness titration is very similar to the total hardness procedure. In the field laboratory, buffering of the sample to a pH above 12 was accomplished by 2 N sodium hydroxide, and murexide was used as the indicator. The end point with this indicator is difficult to detect and a switch was made in 1988 to hydroxy naphthol blue which has a sharper end point. The on-site procedure used 8 N potassium hydroxide as buffer and hydroxy naphthol blue as an indicator. Total and calcium hardness were determined separately and magnesium hardness was calculated as the difference between them. Calcium and magnesium concentrations are expressed in mg or meq L⁻¹.

The samples from 1988 that were retained in borosilicate glass vials were not acidified in the field. However, analyses for calcium and magnesium ions by NAA were in good agreement with the field determinations. Data from the Dodo Canyon Site are:

$$\text{Ca}_i^{2+} = 1.09\text{Ca}_f^{2+} - 0.06 \quad (n=56, R^2=0.92)$$

$$\text{Mg}_i^{2+} = 1.01\text{Mg}_f^{2+} - 0.53 \quad (n=56, R^2=0.84)$$

where Ca_i^{2+} and Mg_i^{2+} are concentrations in mg L⁻¹ determined in the field and Ca_f^{2+} and Mg_f^{2+} are concentrations in mg L⁻¹ determined by NAA.

Not all samples collected in 1991 could be analyzed in the field for calcium and magnesium. Replicate samples were retained from each site. These were acidified with 2 N HCl. Calcium and magnesium concentrations were determined from the acidified samples by the titration methods described above. There was excellent agreement between field and laboratory determinations:

$$\text{Hd}_i = 0.97\text{Hd}_f + 5.3 \quad (n=22, R^2=0.99)$$

$$\text{Ch}_i = 0.98\text{Ch}_f + 4.0 \quad (n=17, R^2=0.99)$$

where Hd_i and Ch_i are total and calcium hardness determined in the lab as CaCO₃, and Hd_f and Ch_f are the same measures from the field.

Sulphate

Samples from 1987 were not analyzed for sulphate. Samples from 1988 were analyzed by three methods, two of which involved the introduction of barium chloride (BaCl_2) into the sample. If sulphate ion is present, crystals of barium sulphate (BaSO_4) are precipitated. In the first technique the sample was first pretreated to remove potentially interfering cations, then barium chloride was added, the sample was then heated and the excess barium chloride titrated with EDTA. The apparatus used for this test is not precise and the results of poor quality. Data generated by this method were not used. The second technique used was a turbidimetric method. Barium chloride was introduced into a vial containing the sample. The amount of turbidity produced by the barium sulphate precipitate was proportional to the sulphate concentration. A stabilizing agent was added to hold the precipitate in suspension. Light absorbance of the barium sulphate suspension was measured by a photometer and sulphate concentration was determined from a standard curve. A HACH DR100 colorimeter was used for these measurements. An attempt was also made to measure total sulphur in the water samples by NAA. However, while standards yielded reasonable results the sulphur peaks were poorly developed when the concentrations of sulphate in the samples were low.

Ion chromatography was used to measure sulphate concentrations for the 1991 samples. These analyses were conducted by the Lethbridge Office of the Earth Sciences Division, Department of Environment, Province of Alberta. The device used was a Dionnex Ion Chromatograph with a detection limit of approximately 0.25 meq L^{-1} and an accuracy of $\pm 2\%$.

Sodium and Chloride

Samples collected in 1987 were not analyzed for sodium and chloride. For the 1988 samples, these ions were measured using NAA. Chloride from the 1991 samples was measured with ion chromatography by the Earth Sciences Division, Department of Environment, Province of Alberta. The detection limit and accuracy are similar to

that for sulphate. Sodium ion concentrations for the 1991 samples were measured by the water quality laboratory of Moneco Limited, Mississauga, Ontario. The method used was plasma emission spectroscopy, accuracy is specified at $\pm 0.05 \text{ mg L}^{-1}$, the detection limit varies depending upon the sample.

Potassium and Other Ions

Regional water quality data (Table 3.6) show that the potassium ion is a minor constituent in stream waters of the Mackenzie Mountains. Samples from 1988 were analyzed for potassium using NAA. However, given the irradiation times that were selected, the resulting potassium counts were very low and the peaks ill defined. This yielded detection limits of between 0.5 and 10 mg L^{-1} , and for more than 95% of the samples the potassium concentrations were below the detection limit. Runs with standards of low potassium concentration yielded inconsistent results. For economic and practical reasons other methods were not used to measure potassium, and potassium concentrations are not reported in this study. Other ions and dissolved species were not measured for this work since they are a very small percentage of the total solute load.

3.3.2.3 Treatment and Presentation of the Solute Data

The solute data generated by this study are presented in a series of tables and figures in Chapters VI through XI, and the Appendix. The program WATCHEM was used to calculate saturation indices for calcite, dolomite, and gypsum as well as $p\text{PCO}_2$, ion balance error, and the ratios $\text{Ca}^{2+}/\text{Mg}^{2+}$, $\text{Ca}^{2+}/\text{SO}_4^{2-}$, and Na^+/Cl^- . WATCHEM is an unpublished FORTRAN-66 program written by John Drake and Tom Wigley, the author updated the code to FORTRAN-77 standard. The saturation indices and $p\text{PCO}_2$ were calculated using equations described in Chapter II, ion balance was calculated from:

$$IBE = \frac{\sum m_i z_{i \text{ cations}} - \sum m_i z_{i \text{ anions}}}{\sum m_i z_{i \text{ cations}} + \sum m_i z_{i \text{ anions}}} \times 100 \quad (3.4)$$

where m is molarity and z is valance of species i . Ion ratios were calculated using species concentrations.

3.3.3 Dye Tracing

There is a substantial literature available on dye tracing in karst environments (e.g., Drew and Smith, 1969; Back and Zotl, 1975; Quinlan, 1986). Dye tracing can yield information regarding the characteristics of porosity within an aquifer. Specific objectives of tracing are commonly: (i) to establish point to point connections between recharge (dolines) and discharge areas (resurgences), (ii) to aid in the delineation of catchment boundaries, (iii) to provide information on the geometry of the conduit network, and (iv) to enable certain aquifer characteristics, such as groundwater velocity, to be quantified.

A variety of natural and artificial tracers may be used in a karst environment. Naturally occurring isotopes (e.g., ^{18}O) are particularly useful in establishing the time of residence, depth of travel, and the seasonality of the recharge into a karst aquifer. How pulses of discharge, solutes, or clastic sediments are translated through an aquifer to spring points is related to its structural characteristics. Artificial tracers may be introduced into an aquifer and can be observed at springs or within observation wells. Several criteria should be considered when selecting a tracer. Drew and Smith (1969), Smart and Laidlaw (1977), and Ford and Williams (1989) discuss the properties of a variety of tracers. Generally the tracer should be environmentally safe, easily detectable at low concentrations, and simple and inexpensive to use. Fluorescent dyes were selected as artificial tracers in this study. Based on reviews of dye performance it was decided to select Rhodamine WT to minimize interference from background fluorescence.

In this study, the main objective of artificial tracing was to establish point to point connections between sinks and springs. Much effort was concentrated on outcrops of the Bear Rock Formation. Due to logistics, quantitative tracing using continuous fluorometry was not used. Granular activated charcoal was used to absorb dye at potential resurgences. Approximately 30 to 40 grams of charcoal were placed in nylon mesh bags and were suspended in areas of moderate flow. Through frequent replacement of these detectors there was an opportunity to qualify the speed of groundwater flow in the systems. Absorbed dye was eluted from the charcoal by an alcoholic KOH or NH₄OH solution and detected under an ultraviolet light or by a fluorometer. Smart and Brown (1973) recommend an elutant of equal parts 10% NH₄OH in a 50% aqueous I-propanol solution for use with Rhodamine WT. The elutant was checked for fluorescence using a Turner III fluorometer and/or by checking for visible fluorescence under exposure to UV radiation. Duplicate sets of analyses were run for each detector.

3.3.4 Stable Isotopes

The uses of the stable isotopes of hydrogen, oxygen, and sulphur in groundwater hydrology are reviewed by Fritz and Fontes (1980), Payne (1988), and Mazor (1991). Isotopic analyses of discharge waters from an aquifer can provide information on the source and seasonality of recharge, secondary fractionation effects, mixing, and flow path history of groundwater. The most commonly utilized stable isotopes are deuterium (²H or D), oxygen-18, and sulphur-34. The ratios between D/H, ¹⁸O/¹⁶O and ³⁴S/³²S are expressed in delta units, these are parts per thousand (per mil) departures from a standard, delta units are calculated from:

$$\delta\text{‰} = \frac{(R_{\text{sample}} - R_{\text{standard}})}{(R_{\text{standard}})} \times 1000 \quad (3.5)$$

where R is the isotopic ratio of interest. Sulphur isotope abundances ($\delta^{34}\text{S}$) are

expressed as per mil deviations relative to the Cañon Diablo meteorite troilite standard. Isotope abundances of oxygen ($\delta^{18}\text{O}$) and hydrogen (δD) are expressed as per mil deviations relative to standard mean ocean water (SMOW).

$\delta^{18}\text{O}$ was determined for water samples collected in 1983, 1987, and 1988. The analyses were done in the Isotope Laboratory of the Department of Geology, McMaster University. It was originally intended that δD also be measured for the 1988 samples, however the time between collection and potential completion of the analyses was too long. $\delta^{18}\text{O}$ and δD were determined for most of the samples collected in 1991. These analyses were done by Dr. R. Krouse, Department of Physics and Astronomy, University of Calgary. In addition, $\delta^{34}\text{S}$ was determined for several 1991 samples. The sulphur isotopes were done to differentiate groundwaters that had encountered either the Lower Devonian Bear Rock or Upper Cambrian Saline River Formations. The $^{34}\text{S}/^{32}\text{S}$ abundance ratios of sulphates in these two formations differ (van Everdingen and Krouse, 1977; van Everdingen *et al*, 1982).

Table 3.1: Mean daily temperature, annual rainfall, snowfall, and precipitation for selected stations in the western N.W.T. and eastern Yukon (Environment Canada, 1982; Environment Canada, 1993).

Station	Location and Elevation (m)	Climate Normals			
		Mean Daily Temperature (°C)	Annual Rainfall (mm)	Annual Snowfall (cm)	Annual Precipitation (mm)
Elsa, YT	63°55'N 135°29'W 814	-4.4	219.5	202.9	413.0
Keno Hill, YT	63°44'N 135°40'W 1472	-5.0	241.3	365.7	590.2
Fort Norman, NWT	64°53'N 125°34'W 74	-6.3	186.4	144.3	324.9
Mayo, YT	63°37'N 135°52'W 504	-4.0	185.1	130.5	306.3
		-3.6	201.4	145.0	318.4
Norman Wells, NWT	65°17'N 126°48'W 67	-6.4	188.3	146.8	328.4
		-6.0	183.2	148.9	316.6
Tsichu River, NWT	63°18'N 129°49'W 1265	-8.3	244.0	386.5	630.5
Tungsten, NWT	61°57'N 128°15'W 1148	-5.7	333.6	316.7	644.7

Data from Mayo and Norman Wells include climate normals from the period 1951-80 and 1961-90 (second line). The figures from Tsichu River are based on a fragmentary record.

Table 3.2: Occurrence of frozen ground for surficial materials in NTS map areas 96C, 96E, and 106H; data in percentages (Heginbottom *et al*, 1978).

Surficial Material	96C	96E	106H
	Fort Norman	Norman Wells	Sans Sault Rapids
	64°-65° N Lat 124°-126° W Long	65°-66° N Lat 126°-128° W Long	65°-66° N Lat 128°-130° W Long
Alluvial	42	82	85
Glaciofluvial	43	82	73
Morainal	92	93	83
Organic	*	*	87

* insufficient data

Table 3.3: Occurrence of frozen ground for genetic terrain types in construction spread 1 (km 0 to km 149.5) of the Norman Wells-Zama pipeline (Kay *et al*, 1983).

Terrain Type	Distance (km)	% of Spread	% Frozen	Taliks per km
AF: Alluvial Fan*	4.86	4.06	94.3	1.4
AP: Alluvial Floodplain	0.51	0.34	19.4	7.8
AT: Alluvial Terrace	1.64	1.10	63.6	4.9
CM: Colluvial Slopewash	1.96	1.31	84.3	5.1
CT: Colluvial Talus**	1.40	1.26	89.5	4.3
ED: Eolian Dunes	2.03	1.36	43.3	0.5
GO: Glacial Deposits	4.31	2.88	62.9	1.4
LB: Postglacial LP	0.97	0.65	40.0	7.3
LP: Lacustrine Plain	41.66	27.86	79.3	1.3
LP-MG: Combination	14.66	9.82	78.1	1.9
MG: Ground Moraine	23.30	15.64	90.5	1.5
OU: Organic Undifferentiated	1.05	0.70	47.4	4.8
OU-LP: Combination	8.48	5.67	79.8	2.1
OV-LP: Organic Veneer on LP	25.02	16.74	94.3	1.1
OV-MG: Organic Veneer on MG	3.12	2.02	93.8	1.7
RK: Bedrock	17.22	11.52	92.1	2.6
OV-SP: OV on Other Deposits	0.12	0.08	9.8	8.2
MG-RK: Combination	3.45	2.31	89.5	1.5
Total***	149.5	100.0	83.7	259

Distance is the length of that terrain type for the whole of construction spread 1

* data from construction spread 2; km 149.5 to km 269.3

** data from construction spread 3; km 269.3 to km 380.4

*** totals do not include the terrain types from construction spreads 2 and 3

Table 3.4: Discharge characteristics from streams in the study area. Runoff and annual specific discharge are calculated from the annual means. The daily maximum specific discharge is based on the highest daily discharge on record (Environment Canada, 1991).

Station	Basin Area (km ²)	Runoff (mm)*	Specific Discharge (m ³ s ⁻¹ km ⁻²)		Maximum Daily Discharge (m ³ s ⁻¹)	1988 Max Q (m ³ s ⁻¹)	
			Daily Max	Annual	date		
Redstone R	15,400	363	0.22	0.01	3,390	010788	3,390
Mountain R	11,100	348	0.12	0.01	1,320	240690	762
Carcajou R	7,400	318	0.26	0.01	1,930	250690	1,110
Twitya R	5,590	349	0.14	0.01	760	010683	321
Tsichu R	219	507	0.22	0.02	47.9	280584	27.8
Jungle Ridge Ck	41.3	349	0.3**	0.02	12.3	190582	3.6

* calculated as the ratio of total annual discharge to basin area

** daily maximum discharge is suspect due to channel ice

Table 3.5: Instantaneous sediment data for the Redstone, Mountain, and Carcajou Rivers, 1987-89 (Environment Canada, 1988, 1989, 1990).

River	Date	Discharge (m ³ s ⁻¹)	Suspended Sediment		Total Dissolved Solids	
			(mg L ⁻¹)	(kg s ⁻¹)	(mg L ⁻¹)	(kg s ⁻¹)
Redstone	060689	774	1,955	1,513	159	123
	110588	172	172	30	204	35
	250588	385	758	292	172	66
	100888	385	200	77	203	78
	230888	233	87	20	242	56
	190687	198	65	13	234	46
	200787	369	240	89	185	68
	250987	166	21	3	263	44
Mountain	070689	418	290	121	208	87
	060788	720	1,330	958	201	145
	210787	187	23	4	273	51
	220987	129	8	1	326	42
Carcajou	070689	203	459	93	241	49
	200689	304	731	222	264	80
	120588	75	128	10	298	22
	250588	285	1,440	410	183	52
	060788	434	2,070	898	209	91
	180687	105	132	14	303	32
	210787	70	19	1	355	25
	220987	61	13	1	378	23

Table 3.6: Water quality data from Keele, Redstone, and Mountain Rivers (Environment Canada, 1977).

Date	Temp	SPC	pH	Ca ²⁺	Mg ²⁺	HCO ₃ ⁻	SO ₄ ²⁻	Na ⁺	K ⁺	Cl ⁻	Ca/Mg	Na/Cl	SI _c	SI _D	pPCO ₂	IBE
KEELE R																
260274	0.3	673	7.7	4.59	2.40	2.84	3.96	1.35	0.02	1.41	1.9	1.0	0.01	-0.37	2.67	1.1
270374	0.3	720	7.8	4.69	2.04	2.70	4.48	1.35	0.02	1.35	2.3	1.0	0.09	-0.29	2.79	-2.8
220574	4.0	168	8.0	1.60	0.56	1.46	0.83	0.18	0.02	0.16	2.9	1.2	-0.28	-1.08	3.21	-1.9
260674	14.0	190	7.9	1.65	0.91	1.66	0.83	0.18	0.01	0.16	1.8	1.1	-0.20	-0.62	2.97	2.1
240774	12.5	160	7.9	1.80	0.82	1.70	0.83	0.20	0.01	0.21	2.2	0.9	-0.17	-0.65	2.97	1.4
120974	13.5	402	8.2	2.50	1.37	2.31	1.73	0.32	0.01	0.24	1.9	1.3	0.36	0.50	3.15	-1.1
301074	0.3	531	8.2	3.09	2.02	2.80	2.19	0.57	0.02	0.48	1.6	1.2	0.37	0.44	3.18	2.3
REDSTONE R.																
260274	0.3	600	7.6	4.49	2.00	3.10	3.54	1.17	0.02	1.10	2.3	1.1	-0.05	-0.56	2.53	-0.4
270374	0.3	624	8.0	3.49	3.10	3.11	3.54	1.17	0.02	1.21	1.1	1.0	0.23	0.30	2.94	-0.5
220574	6.4	235	8.3	1.50	0.58	1.66	0.69	0.22	0.02	0.17	2.6	1.3	0.07	-0.31	3.44	-4.2
260674	14.0	265	7.4	1.65	0.83	1.88	0.69	0.23	0.02	0.11	2.0	2.1	-0.64	-1.53	2.41	0.9
240774	13.5	275	7.4	1.65	0.91	1.84	0.73	0.22	0.02	0.16	1.8	1.4	-0.65	-1.53	2.43	1.5
120974	12.0	369	8.2	2.15	1.37	2.44	1.29	0.33	0.02	0.25	1.6	1.3	0.32	0.45	3.13	-1.6
301074	0.3	532	8.3	3.09	1.94	3.00	1.92	0.65	0.02	0.56	1.6	1.1	0.50	0.68	3.25	2.2
MOUNTAIN R.																
270274	0.3	473	8.0	3.49	1.55	2.80	2.42	0.30	0.02	0.25	2.3	1.2	0.22	-0.01	2.97	-1.0
280374	0.3	467	8.1	2.20	1.98	1.78	2.35	0.33	0.02	0.25	1.1	1.3	-0.06	-0.28	3.27	1.7
240574	3.3	222	7.8	1.55	0.55	1.46	0.77	0.09	0.02	0.05	2.8	1.7	-0.49	-1.51	3.01	-1.8
270674	12.0	317	8.3	2.10	1.10	2.06	1.12	0.13	0.02	0.06	2.0	2.1	0.34	0.42	3.31	1.6
250774	14.0	242	7.9	1.65	0.85	1.78	0.62	0.11	0.02	0.05	2.0	2.1	-0.16	-0.57	2.94	3.5
120974	13.5	380	8.2	2.54	1.25	2.44	1.58	0.20	0.02	0.06	2.1	3.4	0.40	0.52	3.12	-0.9
311074	0.3	435	8.0	3.79	0.18	2.38	1.85	0.29	0.02	0.12	21.1	2.3	0.22	-1.00	3.04	-0.9

Temp: Temperature in °C

SPC: Specific Conductivity in $\mu\text{S cm}^{-1}$

Ion Concentrations in meq L^{-1}

Ca/Mg, Na/Cl: Ion Ratios

SI_c: Saturation Index of Calcite

SI_D: Saturation Index of Dolomite

pPCO₂: -log of CO₂ partial pressure

IBE: Ion Balance Error

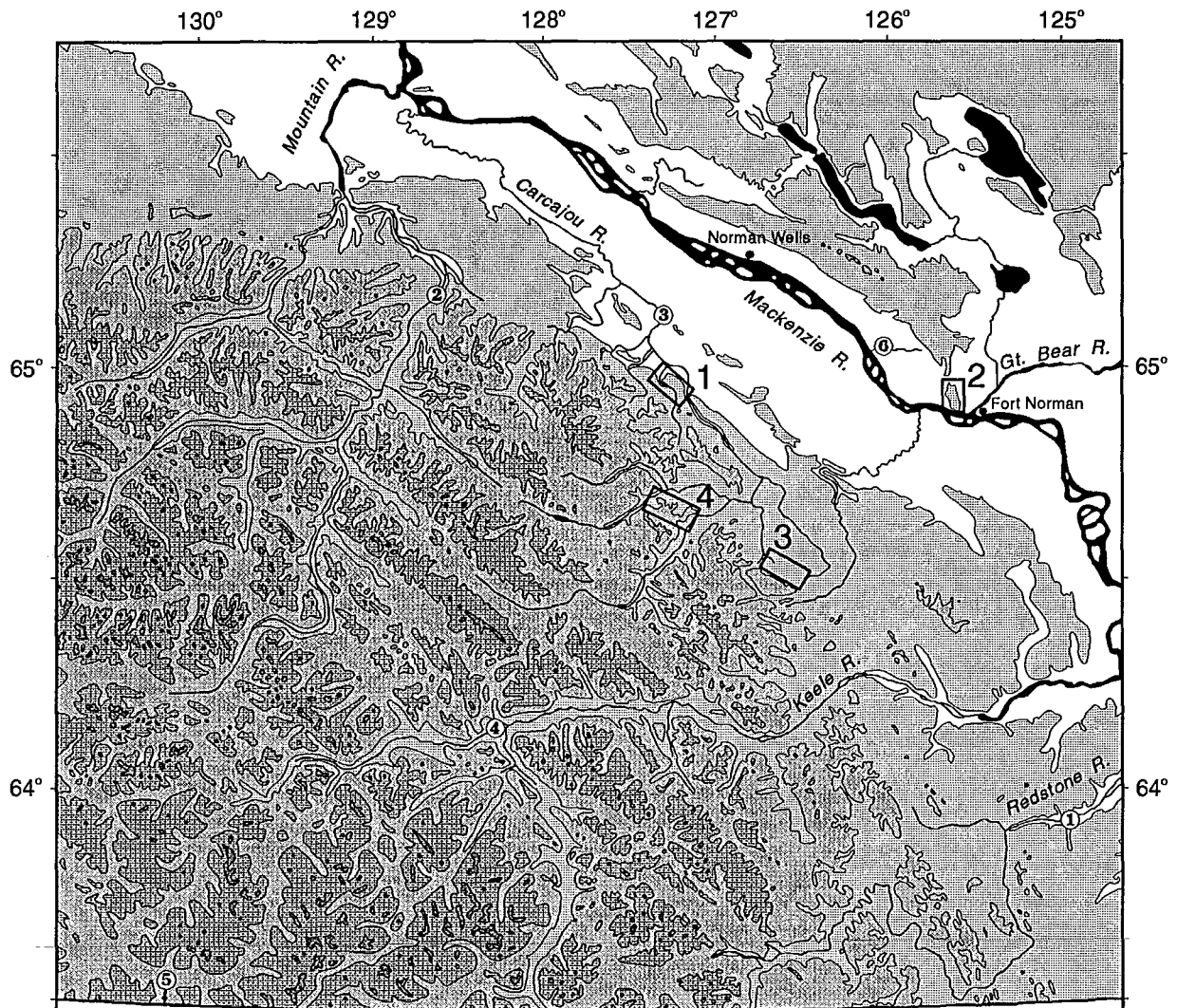
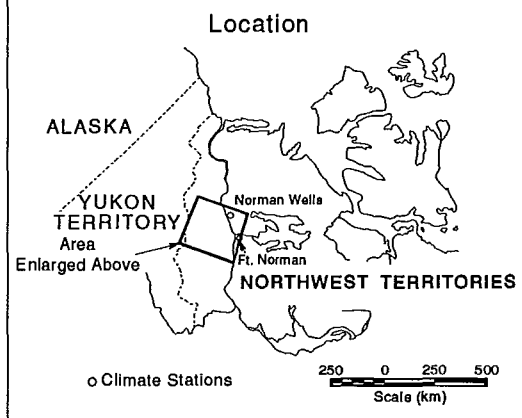
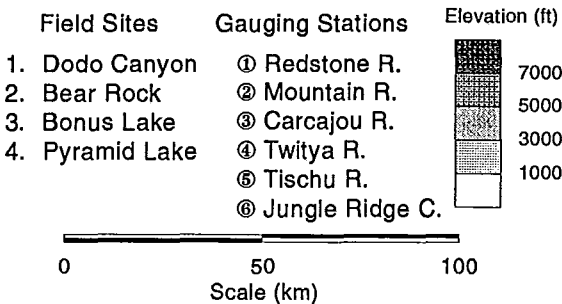


Figure 3.1: Topography, drainage, field site locations, and gauging stations in the northeastern Mackenzie Mountains.



130° 129° 128° 127° 126° 125°

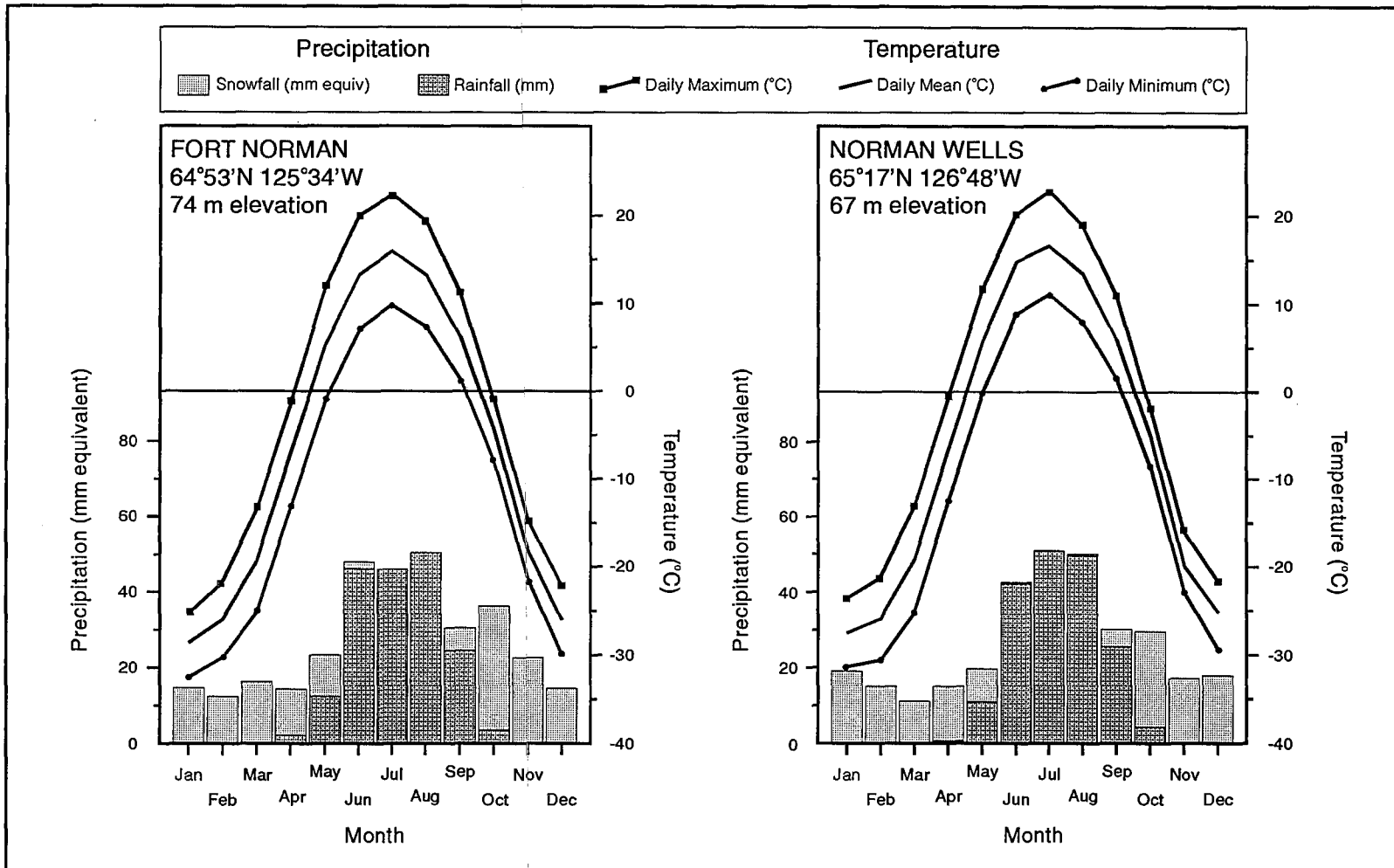


Figure 3.2: Mean monthly rainfall and snowfall, daily maximum, mean, and minimum temperatures for Norman Wells and Fort Norman. The data from Norman Wells are 1961-90 normals, the data from Fort Norman are 1951-80 normals (Environment Canada, 1982, 1993).

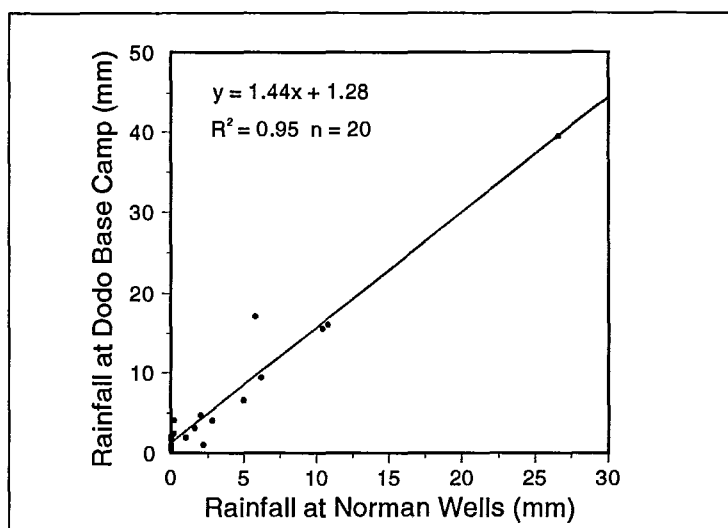


Figure 3.3: Rainfall at Dodo Base Camp vs Rainfall at Norman Wells. Data are from June and July of 1987 and 1988. The relationship indicates that summer rainfall recorded at Norman Wells underestimates levels in the Carcajou Range.

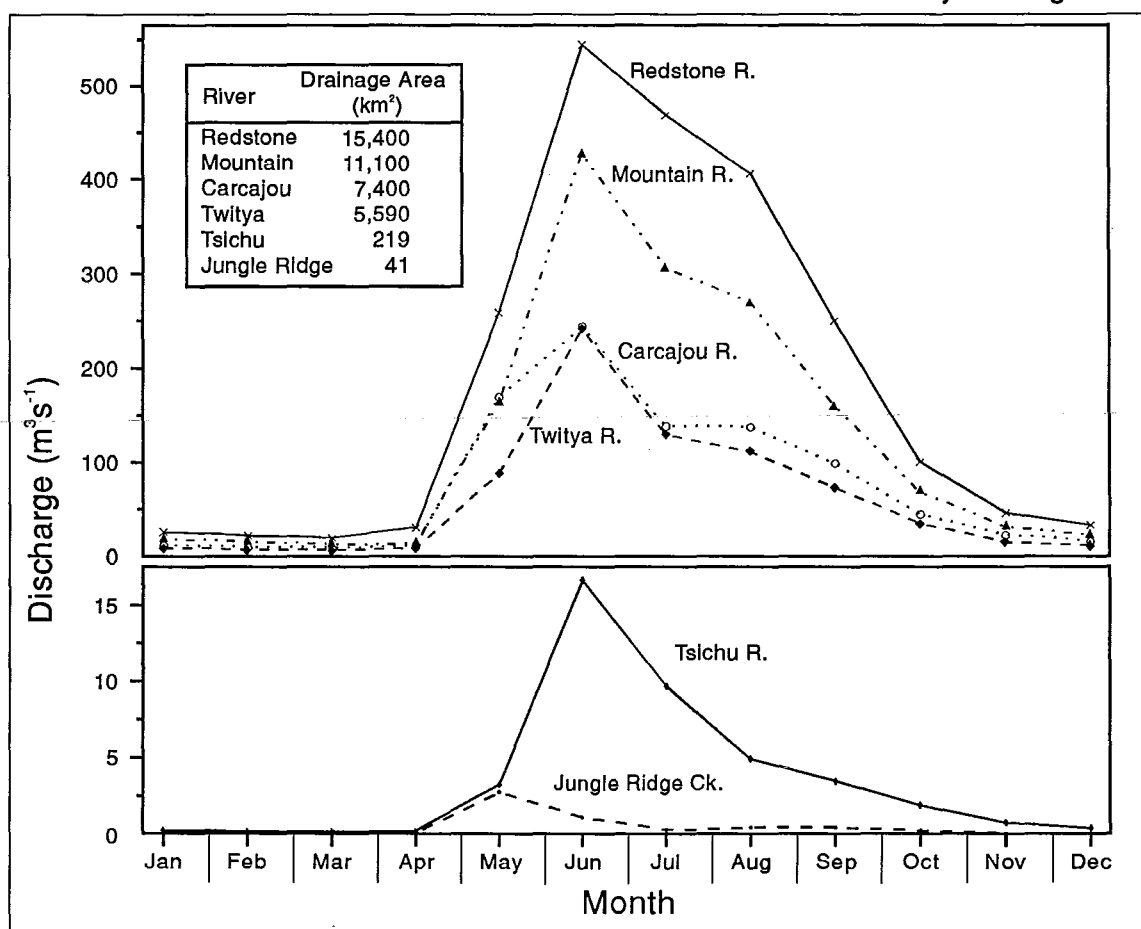


Figure 3.4: Mean monthly discharges over the period 1980-90 for Mackenzie Mountain Rivers: Redstone, Mountain, Carcajou, Twitya, and Tsichu. Jungle Ridge Creek is on the Mackenzie Plain west of Bear Rock (Environment Canada, 1991).

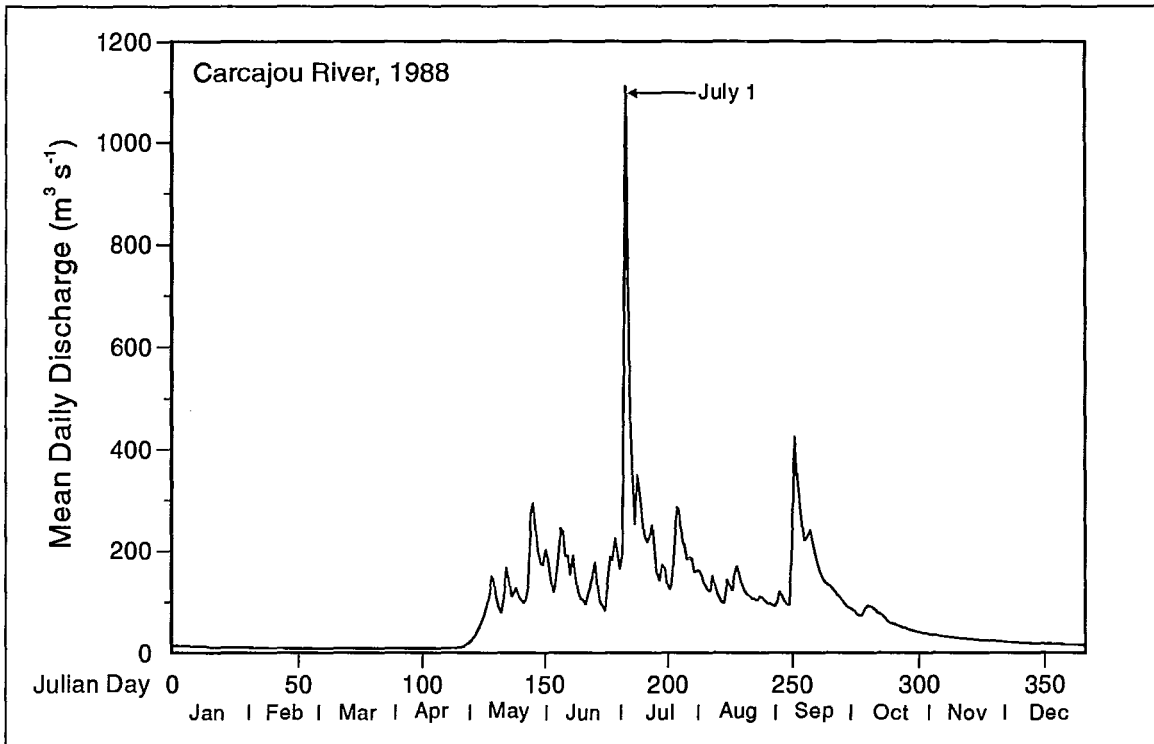


Figure 3.5: Hydrograph of Carcajou River, 1988. Snowmelt occurred from early May to early June. The peak flows are rainfall generated. The major flood on July 1 followed 58 mm of rainfall at the Dodo Canyon Site from June 29 to July 1 (discharge data from Environment Canada, 1989)

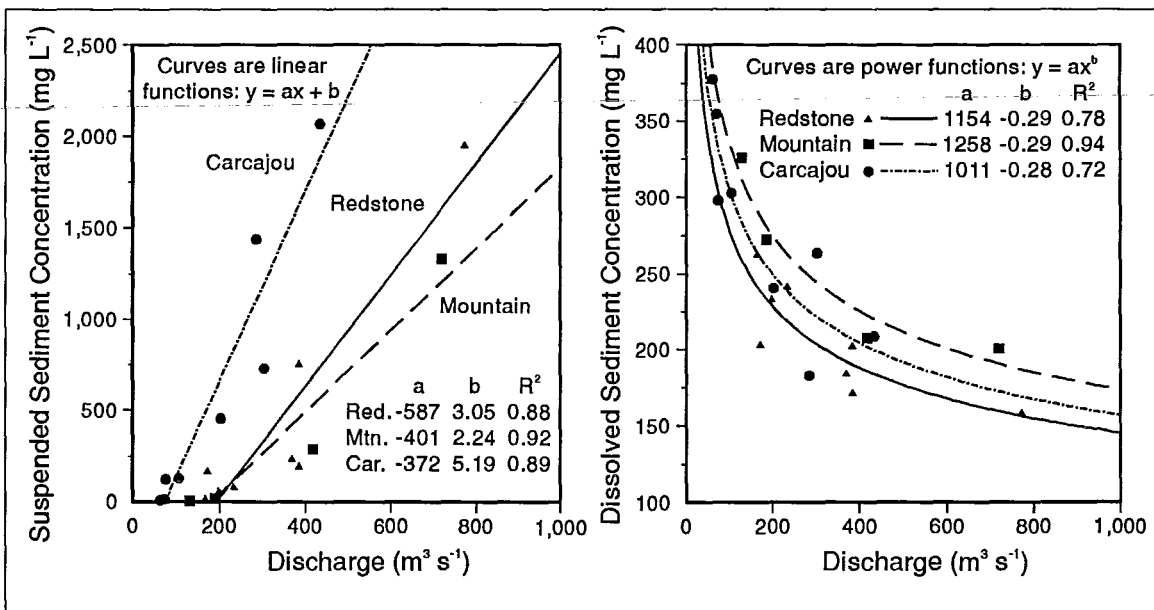


Figure 3.6: Suspended sediment and dissolved sediment concentrations vs discharge for Redstone, Mountain, and Carcajou Rivers (data from Table 3.5).

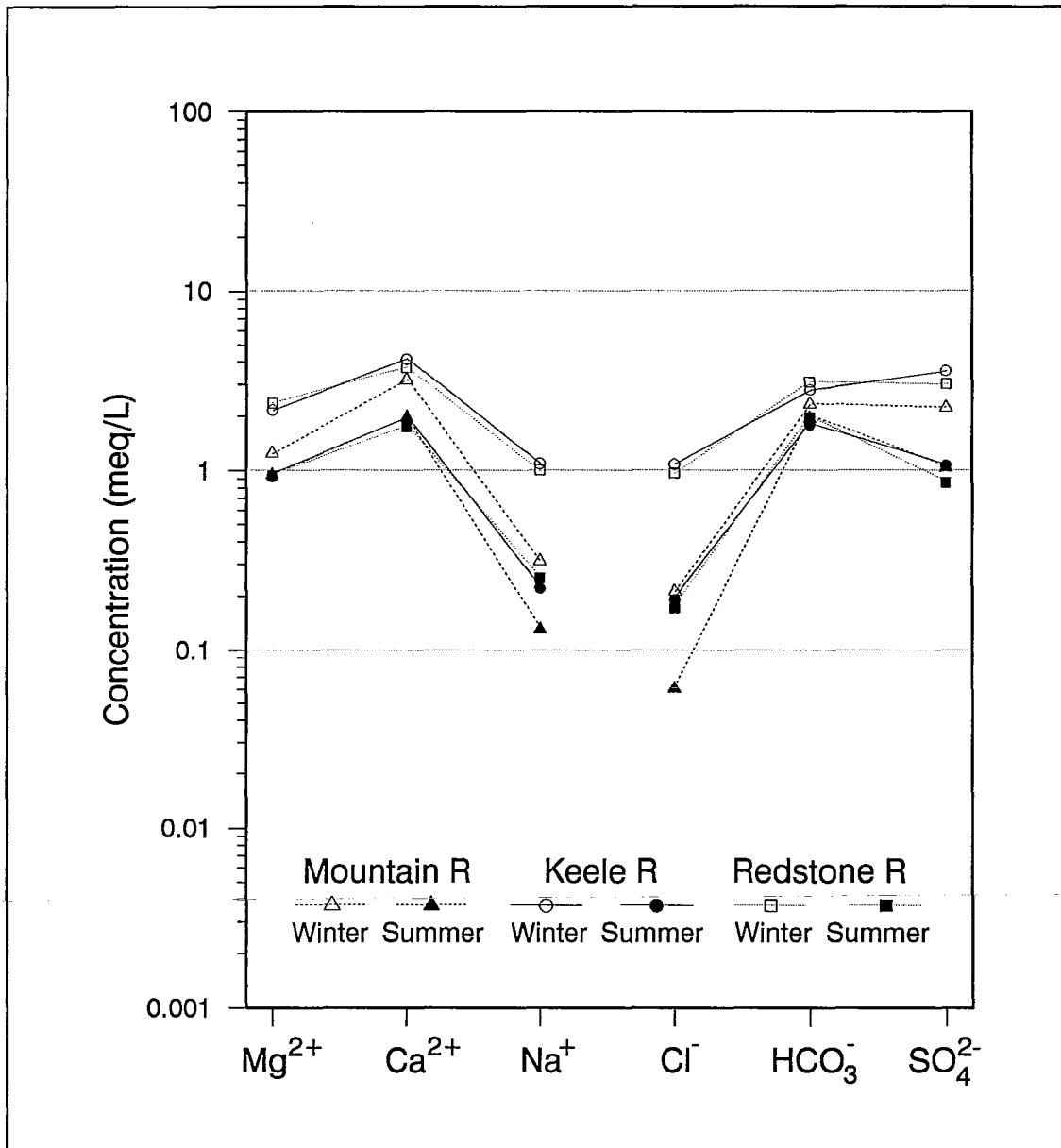


Figure 3.8: Mean ion concentrations for summer and winter samples from Mountain, Keele, and Redstone Rivers. Winter samples are from October to April, summer samples from May to September. Ion concentrations in meq/L (raw data in Table 3.6).

CHAPTER IV

GEOLOGY OF THE NORTHEASTERN MACKENZIE MOUNTAIN REGION

4.1 Introduction

This chapter reviews the bedrock geology of the northern Mackenzie and Franklin Mountains in the District of Mackenzie. The depositional and tectonic histories of the region are examined with an emphasis given to Paleozoic carbonate and evaporite sequences. The distribution, lithology, and weathering characteristics of several formations are described.

4.2 Previous Work

Initial detailed geological investigations in the District of Mackenzie were undertaken with the discovery of oil at Norman Wells in 1920. The Geological and Topographical Surveys of Canada produced several stratigraphic reports on formations exposed along the Mackenzie River (Camsell and Malcolm, 1921; Dowling, 1922; Hume, 1921, 1923; Kindle and Bosworth, 1921). During the Second World War, exploration moved into the mountains accompanying the construction of the Canol Road and pipeline. A series of unpublished reports were produced in 1944 by the Canol geologists; these are summarized by Hume and Link (1945) and Hume (1954).

In the 1950's and 60's the Geological Survey undertook helicopter supported reconnaissance studies in the Northwest and Yukon Territories. Operation Norman (1968-1970) investigated the western portion of the District of Mackenzie between the Arctic coastline and the 64th parallel. The geology of individual map areas in that region are presented in a series of reports. Those most pertinent to this work

include: Carcajou Canyon (map area 96D; Aitken and Cook, 1974a), Fort Norman (map area 96C; Cook and Aitken, 1976), Norman Wells (map area 96E; open file 304), and Upper Ramparts River and Sans Sault River (map areas 106G and 106H; Aitken *et al*, 1982).

Reviews of regional stratigraphy, structure, and paleogeography include the works of Bassett (1961), Gabrielse (1967), Douglas *et al* (1970), Law (1971), and Gilbert (1973). Proterozoic and Cambrian stratigraphy are described by Aitken *et al* (1973, 1978), Aitken (1981), Aitken and McMechan (1991), and Gabrielse and Campbell (1991). The Paleozoic of the Selwyn Basin (Mountains) is examined by Cecile (1982), and the southern Mackenzie Mountains by Morrow and Cook (1987). The Silurian and Devonian of the northern Mackenzie Mountains is reviewed by Morrow (1991), and the Cretaceous and Tertiary of the Northern Interior Plains by Yorath and Cook (1981). The characteristics and distribution of evaporite deposits in western Canada are reported by Meijer Drees (1986). Aspects of the subsurface geology of the Mackenzie Valley area are reviewed by Tassonyi (1969), Meijer Drees (1989, 1993), and Pugh (1983, 1993). Structural elements of the eastern Cordilleran foldbelt are described by Norris (1972; 1985a) and Park *et al* (1989). In addition, there are a number of reports and papers that are concerned with individual rock formations or tectonic features.

4.3 Regional Geological Setting

The northeastern segment of the Cordilleran Orogen consists of the rugged terrain of the Mackenzie and Selwyn Foldbelts (Figure 4.1). The Selwyn Foldbelt is bordered by the Tintina Fault to the west and the Backbone Ranges of the Mackenzie Mountains to the east. The Mackenzie Foldbelt is a broad arc of variable terrain extending from Liard Plateau in northern British Columbia, through the District of Mackenzie, to eastern Yukon. The total length of the foldbelt is approximately 950 km and it is bordered to the east by the Northern Interior Platform. The Mackenzie Foldbelt contains several tectonic/physiographic elements, including the Mackenzie

and Franklin Mountains and the Mackenzie Plain.

4.3.1 Physiography

The physiography of the region is reviewed by Bostock (1948, 1970). The periglacial geomorphology is discussed by Priesnitz and Schunke (1983). The most comprehensive treatment of the glacial history is Duk-Rodkin and Hughes (1991).

The Mackenzie Mountains are broadly divisible into the Canyon and Backbone Ranges (Figure 4.1). The latter is an interior arc of rugged northwest trending ridges rising to 2600 metres elevation. Morphology is strongly controlled by structure and also reflects the influence of cirque and valley glaciation. At present, the glacierized portion of the range is restricted to several small alpine glaciers along the continental divide. The ridges are separated by a few broad valleys and there are limited areas of plateaux.

The Canyon Ranges are an eastern arc of low mountains and plateaux. These ranges are characterised by widely separated smooth profiled mountain ridges and plateaux that are dissected by numerous steep valleys and deep canyons. The northwest portion of the Canyon Ranges are rugged with numerous cirques and large troughs. The area southeast of Mountain River is a region of high plateaux where the remnants of an old erosion surface are easily seen on many of the ridge summits (Bostock, 1948). Summit elevations gradually decrease towards Keele River. South of the Keele River there is an area of low hills where the plateaux are less prominent. The Canyon Ranges have been influenced to a minor degree by glaciation. Ice spreading from the Backbone Ranges occupied many of the broad valleys and canyons. Laurentide ice advanced to the mountain front and penetrated westward along the main valleys. In some areas, Montane and Laurentide ice coalesced (Duk-Rodkin and Hughes, 1991). The glacial record is discussed in detail in Chapter V.

The Mackenzie Plain is a low elevation area between the Mackenzie and Franklin Mountains. It is best described as an isolated strip of the Interior Platform within the Mackenzie Foldbelt. The surface is rolling with local relief due to a

mantle of glacial deposits and minor folds. The Mackenzie River and its major tributaries are incised 50 to 150 metres below the surface of the plain.

The Franklin Mountains are a series of discontinuous low ranges stretching from Nahanni Butte to Fort Good Hope. The Norman Range extends northward from Bear Rock, located at the confluence of the Mackenzie and Great Bear Rivers. The summit elevations of these ranges vary from a few hundred to 1500 metres. During glaciation, the Franklin Mountains were completely overrun by continental ice.

4.3.2 Depositional Setting, Stratigraphy, and Structure

The Cordilleran Orogen is subdivided into five distinct morphogeological belts. These belts are differentiated on the basis of their tectonic history and stratigraphic composition. The Foreland Belt encompasses the eastern ranges of the Cordillera: the Rocky Mountains and the mountains of the Mackenzie Foldbelt. This belt consists of a sequence of faulted and folded miogeoclinal, rift, and clastic assemblages. The miogeocline is a wedge of deposits that accumulated on the continental margin of Ancestral North America from Middle Proterozoic to Middle Jurassic time (Gabrielse *et al*, 1991). Across the Interior Platform this succession is thin and uniform, gradually increasing in thickness westward. A hinge line or zone is the tectonic boundary separating the platform sequence from the shelf and slope sediments of the Foreland. Basinward of the hinge line, deposits thicken markedly toward the position of the former shelf edge with accompanying changes in facies. Sediments of the miogeocline are overlain by an eastward tapering wedge of foredeep clastics that are derived from western regions influenced by orogeny in the Cretaceous and Tertiary.

Within each of the morphogeological belts, the major sedimentary sequences are divided into tectonic assemblages. Each assemblage is a distinctive collection of lithostratigraphic units that are bound by regional unconformities or faults, and represent a period of deposition in a specific tectonic environment (Gabrielse *et al*,

1991; Wheeler and McFeely, 1991). Most commonly an assemblage consists of several equivalent formations or groups from a number of regions, names being assigned on the basis of where assemblages are best expressed.

The sedimentary succession of the Mackenzie Foldbelt spans Middle Proterozoic to Cenozoic time and is assumed to rest unconformably on a Lower Proterozoic crystalline basement (Douglas, 1980). It is approximately 7 km in thickness at the eastern boundary of the foldbelt and approaches 20 km in the mountain interior. The known sedimentary package may be divided into an infrawedge and a suprawedge (Norris, 1985a). The infrawedge consists of a series of tectonic assemblages that record sedimentation on a continental margin called the Mackenzie Shelf. The suprawedge represents clastic deposition in a foredeep environment.

Tectonic assemblages of the study region are illustrated on Figure 4.2. Stratigraphic columns from the Sans Sault Rapids (106H), Carcajou Canyon (96D), Norman Wells (96E), and Fort Norman (96C) map areas are presented on Figure 4.3. There are considerable variations in strata across these map areas. Sedimentation on the Mackenzie Shelf was influenced by relative sea level variations and intra-shelf topographic or tectonic features (Morrow, 1991). The distribution of intra-shelf features accounts for much of the regional variability in facies observed in the Mackenzie Foldbelt (Figure 4.4). The position of the shelf edge varied but it likely persisted near the boundary between the Canyon and Backbone Ranges, now marked by the Plateau Fault zone (Figure 4.2). The area northeast of Plateau Fault functioned as a shelf-platform from Middle Proterozoic through Middle Devonian time (Aitken *et al*, 1982). The total exposed stratigraphic column is relatively thin with several major hiatuses present. The area to the southwest is represented by a thick sequence that includes several formations that are absent from the shelf-platform area (Figure 4.5). This is represented by a facies change from carbonates to shales southwest of the fault zone (Franklin Mountain to Road River Formations: Figure 4.5). On the shelf proper, other elements influenced sedimentation. An

example is the Mackenzie Arch, a positive tectonic element that extended from Keele River to Mountain River in the northeastern Mackenzie Mountains (Aitken *et al*, 1973). This arch was active during the Upper Proterozoic and Cambrian and produced a restricted basin northeast of the arch where shallow water carbonates and evaporites accumulated. To the southwest, deeper water basinal facies were deposited in Selwyn Basin. Other important topographic elements include Redstone Arch, Keele Arch, and Twitya Uplift. The influence of these features on individual formations are discussed in subsequent sections. In general, the strata of the Canyon Ranges are primarily carbonates, evaporites, and coarse clastic lithologies, while the thicker succession of the Backbone and Selwyn Foldbelt are largely fine grained clastics.

In the sedimentary succession, depositional hiatuses, faulting, and deformation are associated with orogenic events in the Middle and Upper Proterozoic, mid-Cretaceous, and Upper Cretaceous to early Tertiary (Figures 4.2, 4.3, 4.5). The Proterozoic Racklan Orogeny is recorded by a series of steeply dipping faults in Middle Proterozoic strata (Aitken *et al*, 1973; Aitken *et al*, 1982; Cook, 1992). The Upper Cretaceous to Eocene orogeny ("Laramide Orogeny") formed the Mackenzie and Franklin Mountains, and may have occurred in two distinct pulses (Figure 4.3). This was marked by shortening of the sedimentary cover through widespread folding and faulting, and included reactivation of Proterozoic faults. Epeirogenic events produced unconformities in the Middle Cambrian, Middle Ordovician, mid-Silurian, and Upper Devonian (Aitken and Cook, 1974; Aitken *et al*, 1982).

The Mackenzie Foldbelt is an orocline. The overall arcuate shape reflects the original geometry of the shelf, rather than later bending of the sedimentary pile (Park *et al*, 1989). It can be divided into four structural subregions: (i) Plateau Sheet, (ii) Outer Fold Belt, (iii) northern Franklin Mountains and Mackenzie Plain Synclitorium, and (iv) Peel Plateau and Plain (Aitken *et al*, 1982). The Plateau Sheet lies to the southwest of Plateau Fault, and the Outer Foldbelt between Plateau

Fault and the Mackenzie Mountain Front (Figure 4.3). Peel Plateau is north of the area of study.

The Plateau Sheet comprises strata deposited within Selwyn Basin and on the Mackenzie Shelf edge. It extends from the Root River area toward Arctic Red River. To the southeast, it is largely unfractured but becomes progressively faulted northwestward. In the northern Mackenzies, it consists of a series of slices bounded by imbricate thrust and reverse faults. These faults are represented on the surface by traces parallel to Plateau Fault (Figures 4.2, 4.6). The main failure surface associated with these faults is a gypsum sub-unit of an unnamed Middle Proterozoic formation (map unit H₅). It is suggested that horizontal displacement in the northern Mackenzies is on the order of several kilometres (Aitken *et al*, 1982), to the south it may be as much as 35 km (Cecile *et al*, 1982). There are few major folds in the Plateau Sheet.

The Outer Foldbelt is dominated by bundles of flexural slip, cylindrical folds, and associated contraction faults (reverse and thrust) (Norris, 1972, 1985a). Strike-slip and normal faults are less common and usually of low displacement. The majority of folds have curvilinear and sinuous axial surfaces that commonly dip to the southwest. Individual folds or fold pairs are arranged in a parallel or subparallel alignment; an en échelon pattern. In the southern Mackenzie Mountains, folds are right-hand en échelon. In the Carcajou Range, right and left-hand styles are equally common, while left-hand en échelon occur to the northwest (Figure 4.6). These folds involve strata as old as Late Proterozoic. Their structure suggests there is a deep surface of décollement below the oldest known Middle Proterozoic unit (Aitken *et al*, 1982).

Broad, flat topped anticlines are typically separated by narrow, steep limbed, complex synclines. In the northeastern Mackenzie Mountains, directly opposite Norman Wells, the full width of the Outer Foldbelt (95 km) is occupied by only four major anticlines and synclines. The major folds are persistent along strike; Stony (Foran) anticline extends for 170 km, Tawu Anticline greater than 200 km.

Laramide shortening of the sedimentary cover in this area is estimated between 12 and 15% (Aitken *et al*, 1982). Through much of the Outer Fold Belt, this shortening is due to folding but between Mountain and Arctic Red Rivers the numerous reverse and thrust faults are the main agents. The Mackenzie Mountain front is usually marked by steep monoclines that dip toward the westernmost synclinal structures of Mackenzie Plain, such as the Gayna Flexure and Imperial Syncline. Locally, the mountain front is defined by thrust and reverse faults (e.g., Deadend and Gambill Faults).

The structure of Mackenzie Plain and Franklin Mountains are reviewed by Cook and Aitken (1972, 1973). The Mackenzie Plain is a large gently dipping synclinorium punctuated by sharp anticlinal uplifts such as Imperial Anticline and MacKay Range. The northern Franklin Mountains are a series of narrow, linear, anticlinal ridges separated by broad flat bottomed synclines. Stratigraphic sequences are repeated by steep reverse faults that are commonly found on the northeastern limbs of these uplifts. No strata older than Cambrian are exposed in these structures. Unlike the Outer Foldbelt, the surface of décollement is relatively shallow. Stratigraphic evidence suggests structural detachment occurred in the Cambrian Saline River Formation (Cook and Aitken, 1973; Aitken *et al*, 1982).

The following sections of this chapter describe each of the tectonic assemblages represented in the study area. Formation lithology, distribution, and weathering characteristics are reviewed. Detailed information is limited to those strata that host karst features, essentially the Saline River, Franklin Mountain, Mount Kindle, Bear Rock, and Hume Formations.

4.4 Proterozoic

The Proterozoic succession of the Cordillera is divided into three sequences: (i) Middle Proterozoic (1.7 to 1.2 Ga), (ii) Middle to Upper Proterozoic (1.2 to 0.78 Ga), and (iii) Upper Proterozoic (0.78 to 0.57 Ga) (Young *et al*, 1979; Aitken and McMechan, 1991). Dating and correlation of these sequences are not complete. In

the Mackenzie Foldbelt, assemblages of the first sequence occur in the Wernecke and Ogilvie Mountains, and at Cap Mountain of the Franklin Mountains. The Cap Mountain and Wernecke assemblages are a record of clastic and carbonate sedimentation on a continental margin, and are broadly equivalent to the Purcell Supergroup of the southern Rocky Mountains.

4.4.1 Mackenzie Mountain Assemblage

The second Proterozoic sequence (1.2 to 0.78 Ga) is represented in the Mackenzie Foldbelt by the Mackenzie Mountain Assemblage (Figure 4.2). This sequence only occurs in the District of Mackenzie and it includes the Mackenzie Mountain Supergroup, Upper Proterozoic gabbro intrusions, and possibly the Pinguicula Group (Young *et al.*, 1979; Aitken and McMechan, 1991). The latter group does not occur in the study region. The Mackenzie Mountain Supergroup has not been formerly defined, but is generally recognized as the strata bound between the regional unconformity at the base of the Upper Proterozoic Coates Lake Group and the underlying Wernecke-Cap assemblages (Aitken, 1981; Morris and Aitken, 1982; Aitken and McMechan, 1991). It consists of four main units: Map Unit H₁, the Tsezotene Formation, the Katherine Group, and the Little Dal Group (Figure 4.3).

The Mackenzie Mountain Supergroup is widely exposed in the Mackenzie Mountains and is thought to extend in the subsurface of the northern Franklin Mountains and Great Bear Plain (Figure 4.5). Isopachs indicate the trend of the supergroup is congruent with the broad foldbelt arc (Aitken and Long, 1978). It gradually thickens to the southwest, exceeding 4 km in the mountain interior. Much of the assemblage displays slight lateral variation in facies. It is a platform sequence of shallow water clastics, carbonates, and evaporites deposited in a broad epicratonic basin or at a passive continental margin (Aitken and McMechan, 1991).

4.4.1.1 Map Unit H₁

Map Unit H₁ is the oldest formation exposed in the Mackenzie Mountains. Outcrop

is limited to the crestal areas of three major anticlines. The total thickness of the formation is not known. At Tawu Anticline 400 m are exposed, and based on the anticline structure it is suggested at least 1 km of bedded folded strata underlie Unit H₁. The underlying strata may be Wernecke equivalents (Aitken *et al*, 1982; Aitken and McMechan, 1991). Unit H₁ is a massive and resistant dolomite with chert, deposited on a shallow platform or shelf. It is informally divided into three members: (i) a lower member of interbedded silty dolomite and dolomitic shale, (ii) a middle member of stromatolitic grey dolomite and sandy dolomite, and (iii) an upper member of chert, with sandy dolomite and dolomitic sandstone. The uppermost beds grade conformably into shale of the overlying Tsezotene Formation (Aitken and McMechan, 1991).

4.4.1.2 Tsezotene Formation

The Tsezotene Formation is a lithologically diverse succession of shale, argillite, and mudstone with minor intervals of sandstone, quartzite, siltstone, dolomite, and limestone. The formation is widely distributed in the Canyon and Backbone Ranges where it is exposed in the cores of major anticlines. Thickness ranges from 750 to 1500 m. Gabbro sills occur locally within the Tsezotene, a single sill in the upper part of the formation is possibly of regional extent (Aitken and Cook, 1974). A twofold division of the Tsezotene is informally recognized. The lower member is mainly a recessive grey and black shale. The upper member is red, green, and grey shale (Aitken and McMechan, 1991). Where present, intervals of sandstone and dolomite are resistant, with the latter weathering a bright orange. The Tsezotene Formation forms the lower portion of a coarsening upward cycle that is superimposed on the platform carbonates of Map Unit H₁. The formation passes conformably into the overlying Katherine Group.

4.4.1.3 Katherine Group

The Katherine Group is a widespread succession of resistant quartzite, with minor

shale and dolomite. Group thickness ranges from 700 to greater than 1900 m. Stratigraphic practise has been to divide the Group into two broad units, although seven units of formation and member rank have been described (Aitken *et al*, 1978). The lower Katherine is a thick sequence of orthoquartzite with intervals of shale and dolomite. The upper unit has a base of recessive shale overlain by quartzite (Aitken *et al*, 1973). The quartzites are well sorted with very fine sand as the modal grain size. Sedimentary structures indicate much of the Katherine Group is a record of a prograding fluvial-deltaic sequence with subsequent reworking in the littoral zone (Aitken and McMechan, 1991). The upper Katherine Group is missing over the crestal area of the Mackenzie Arch where it was eroded in the Upper Proterozoic (Figure 4.5). The upper contact with the Little Dal Group appears conformable but may represent an erosional hiatus.

4.4.1.4 Little Dal Group

The Little Dal Group includes the former subdivisions of the now obsolete Map Unit H₃ and the Little Dal Formation (Aitken *et al*, 1978; Aitken, 1981). The Group is informally divided into seven units of formation rank comprising 2 km of platform and basin deposits. The Mudcracked Formation is widely distributed at the base of the Group, it is 20 to 60 m of grey, brown, and black mudstone with minor fine grained sandstone. In the southeastern portion of its distribution, the Mudcracked Formation grades into an overlying platform sequence of stromatolitic limestone and calcareous mudstone. This platform sequence ranges in thickness from 450 to 800 m. Westward, the platform sequence passes through a thick biostrome complex, interpreted as a shelf edge, and adopts a basin character (Aitken and McMechan, 1991). This 430 to 630 m thick basinal sequence is devoid of shallow water facies and structures. The lithology is dominated by carbonate-clastic rhythmites and nodular limestone. Some thick stromatolite reefs are present within the unit. Both the basinal and platformal sequences grade into the overlying Grainstone Formation.

The Grainstone Formation is 425 m of massive dolomitized ooid grainstone

with thinly bedded and platy weathering sandy dolomite. Minor gypsum and local solution breccia are recorded in some cores that have encountered the Grainstone Formation (Aitken and McMechan, 1991). It is succeeded conformably by the Gypsum Formation, a recessive unit of laminated and nodular grey gypsum and anhydrite. At least 90% of this unit consists of evaporite minerals and the maximum thickness approaches 530 m. Clastic materials are largely restricted to the top and base of the formation. The Little Dal Group is absent across the Mackenzie Arch, only the lower units of the Group extend eastward into the Canyon Range. The northeastern limit of the Gypsum Formation is just east of Plateau Fault (Aitken *et al.*, 1982).

The Rusty Shale Formation overlies the Gypsum Formation. It is 180-270 m of varicoloured shale and very fine sandstone. This is overlain by the Upper Carbonate Formation, a 300 to 750 m thick, resistant, stromatolitic dolomite with minor interbeds of shale. Locally the Little Dal Group is topped by basaltic lava, partially pillowed. There is a significant erosional hiatus between the Little Dal and overlying units.

4.4.2 Windermere Supergroup

The third Proterozoic sequence is the Windermere Supergroup. In the Mackenzie Mountains this incorporates the Coates Lake Group, Rapitan Group, and the Sheepbed and Backbone Ranges Formations. These units are represented by the Pinguicula, Rapitan, Windermere, and lower Gog assemblages (Figure 4.2). The Pinguicula assemblage is largely confined to the Wernecke Mountains. The Coates Lake Group is restricted to a narrow band of outcrop at the eastern margin of the Upper Proterozoic, in the vicinity of the Plateau Thrust (Jefferson and Ruelle, 1986; Gabrielse and Campbell, 1991). This group has been mapped as either Mackenzie Mountain, Rapitan, or Windermere Assemblages on Figure 4.2. It is a succession of basalt, clastics, carbonates, and evaporites deposited in a rift basin.

The Rapitan Group overlies the Coates Lake or Little Dal Groups with sharp

unconformity. It consists of four units: the Sayunei, Shezal, Twitya, and Keele Formations (Eisbacher, 1981; Gabrielse and Campbell, 1991). The basal Sayunei Formation (700 m) is a sequence of turbidites and argillite, with glacial dropstones and ironstone. The Shezal Formation is 500 m of tillite, diamictite, sandstone, and shale. These two units comprise the Rapitan Assemblage (Figure 4.2) and were deposited in a rift environment. These units are conformably overlain by the Twitya Formation, a clastic unit of shale, siltstone, sandstone, and conglomerate. The Twitya Formation grades into the Keele Formation, 100 to 500 m of carbonates, quartzite, and minor tillite. Shale and siltstone of the Sheepbed Formation (900 m) overlie the Keele. The latter three units constitute the Windermere Assemblage (Figure 4.2) and represent a period of clastic deposition on the rifted continental margin. In the western Mackenzie Mountains the Sheepbed is succeeded by the clastic Backbone Ranges and Sekwi Formations, comprising the Gog Assemblage (Figure 4.2). During the Lower Cambrian deposition was restricted to Selwyn Basin.

4.5 Cambrian

The Rocky Mountain assemblage of the Foreland Belt is a miogeoclinal platform-shelf succession spanning the Lower Cambrian to Devonian (Figure 4.2). In the Mackenzie Foldbelt this sequence is referred to as the Franklinian assemblage (Norris and Yorath, 1981; Norris, 1985a). Regional unconformities in the Lower and Middle Cambrian, Lower Ordovician, Lower Silurian, and at the base of the Devonian divide the package into a series of carbonate and evaporite formations. Clastic units are present at the base and top of the sequence. The Systems of the Rocky Mountain (Franklinian) assemblage are described in the following sections.

The Proterozoic of the Mackenzie Foldbelt is unconformably overlain by a platform sequence of Cambrian sandstone, shale, evaporite, and dolomite. During much of Cambrian time, the Mackenzie and Mahoney Lake Arches were topographic highs and strongly influenced sedimentation. The latter feature occupied a position similar to that illustrated for Keele Arch on Figure 4.4 (Pugh, 1993). The basal

clastic units, the Mount Clark and Mount Cap Formations, are absent across both arches. The Upper Cambrian Saline River Formation thins over the area of Mahoney Lake Arch and occurs east of Mackenzie Arch. The Franklin Mountain Formation (Upper Cambrian-Lower Ordovician) is a platform carbonate that extends westward across Mackenzie Arch to Selwyn Basin (Figure 4.5).

4.5.1 Mount Clark and Mount Cap Formations

The basal Cambrian unit is the Mount Clark Formation, a massive and resistant quartz sandstone with minor conglomerate, siltstone, shale, and arenaceous dolomite (Williams, 1923; Douglas and Norris, 1963; Aitken *et al*, 1973). The distribution of the Mount Clark Formation in the study area is poorly documented, there are scattered outcrops in the Franklin Mountains and it occurs in the subsurface of Great Bear Plain. Formation thickness is highly variable with a maximum value of >215 m at the type section near Wrigley.

The Mount Clark Formation is abruptly overlain by the Middle Cambrian Mount Cap Formation (Williams, 1922, 1923). Northeast of Mahoney Lake Arch, the Mount Cap Formation has a diverse lithology, including: shale, dolomite, limestone, siltstone, glauconite, and sandstone. Pugh (1993) divides that portion of the formation into eight members. Southwest of Mahoney Lake Arch the formation is grey, grey-green, and brown shale with minor argillaceous dolomite and siltstone. This shale facies is widely distributed and onlaps the eastern flank of Mackenzie Arch (Figure 4.5). In Dodo Canyon, on the southwestern flank of MacDougal Anticline, the thickness of the Mount Cap Formation is between 100 and 110 m (Section MQ-6: 64°57'N Lat., 127°16'W Long.: Aitken *et al*, 1973). A borehole near the confluence of Mackenzie and Keele Rivers yields a thickness of >595 m. The thicker accumulation may have occurred along the centre of a narrow linear trough (Keele Trough) between Mackenzie and Mahoney Lake Arches (Pugh, 1993).

4.5.2 Saline River Formation

The Upper Cambrian Saline River Formation (Williams, 1923) overlies either the Mount Cap Formation or Proterozoic strata. Across the study area, the contact between the Saline River and Mount Cap has been described as disconformable (Aitken *et al*, 1973; Aitken and Cook, 1974; Aitken *et al*, 1982) (Figure 4.3) but Pugh (1983, 1993) argues for a depositional hiatus of short duration. In outcrop, the Saline River Formation is a recessive unit of redbeds and gypsum, red and green gypsiferous shale, mudstone, siltstone, and thin dolomite. It is locally brecciated and contains abundant salt casts (Williams, 1923; Aitken *et al*, 1973; Aitken and Cook, 1974; Aitken *et al*, 1982). Brine is observed discharging from exposures at the type section near the confluence of Saline and Mackenzie Rivers (Williams, 1923). The formation is exposed in the Canyon Ranges and Franklin Mountains and is extensive in the subsurface of the region (Tassonyi, 1969; Meijer Drees, 1975, 1986; Pugh, 1993). Subcrops often exhibit thick intervals of halite and anhydrite. The thin, recessive, and contorted surface exposures are indicative of subsrosion of evaporite by circulating meteoric groundwaters (Aitken *et al*, 1982).

Tassonyi (1969) established Imperial Vermillion Ridge No. 1 well (elevation 282 m, 65°07'51" N Lat., 126°05'00" W Long.) as the type locality for the subsurface Saline River Formation. The well is located 8 km northeast of the mouth of Vermillion Creek. The Saline River Formation is encountered at depths between 853 and 1701 m. Tassonyi recognized two members of different lithology: an upper Shale Member (171 m thick), and a lower Salt Member (671 m thick). It is suggested by Meijer Drees (1986) that due to very steeply dipping beds or tectonic thickening Tassonyi's estimate greatly inflates the true stratigraphic thickness.

The Shale Member consists of red, pink, and green shale, dolomitic shale, gypsiferous and grey shale. The shale is interbedded with light coloured anhydrite and some anhydritic or gypsiferous dolomite. Salt casts are observed. The Salt Member is dominated by white and orange-red halite. Beds and laminae of argillaceous, gypsiferous, and silty anhydrite infrequently occur in the upper half of

the member. Impurities become more significant lower in the member and include evaporitic beds of mixed lithology: anhydrite, light pale grey gypsiferous shale, light buff anhydritic dolomite, buff and grey dolomitic argillaceous siltstone, and red and green shale.

Meijer Drees (1975, 1986) divides the subsurface Saline River Formation into three similar units: a Lower Clastic Member, an Evaporitic (salt) Member, and an Upper Clastic Member. The Mobil Colville E-15 well (67°14'18" N Lat., 126°18'26" W Long.) and the CDR Tenlen Lake A-73 well (67°52'08" N Lat., 130°43'22" W Long.) completely core the formation. The Colville well is representative of subcrop throughout the central portion of its distribution and includes all three members. The Lower Clastic Member is approximately 10 m of thinly bedded, greenish grey, and reddish brown dolomitic shale, light brown arenaceous dolomite, and greenish grey anhydrite. Halite is present as cement and veins. The Evaporitic Member is 113 m of interbedded and interlaminated light brown, light grey, and semi-translucent, coarsely and very coarsely crystalline halite; light grey, finely to coarsely crystalline nodular anhydrite with interbeds of brown, halite-cemented dolomite; and greenish grey, dolomitic shale. Anhydrite, siltstone, and halite occur within the shale. The Upper Clastic member is 115 m of greyish, green breccia of dolomitic anhydrite fragments in an anhydrite or shale matrix, and includes varicoloured shale and very light grey, dolomitic siltstone. The Evaporitic Member is absent in the Tenlen Lake core. It includes reddish brown and greyish green dolomitic shale, and very thinly interbedded light grey, silty and anhydritic dolomite. An occasional conglomerate of dolomite clasts in an anhydrite matrix is observed.

The average subsurface thickness of the Lower Clastic Member is 20 to 40 m, with marked thinning over Mahoney Lake Arch (Pugh, 1993). The Evaporite (salt) Member has a highly variable thickness. It is absent from the lower Keele River area and is >300 m thick north of Smith Arm of Great Bear Lake and below the Mackenzie Plain. The Upper Clastic Member ranges between 13 and 120 m in thickness. The whole sequence represents a period of continuous sedimentation

(Pugh, 1993). Thickness variations between the Evaporite and Upper Clastic Member reflect local facies changes within an evaporite basin. The basin was separated from the open sea by the topographic high of the Mackenzie Arch. Lobes extend to the southeast along the Mackenzie Valley and Great Bear Lake, deposition was absent over the emergent Bulmer Lake Arch (Meijer Drees, 1975, 1986; Pugh, 1993). The periphery of the basin is represented by a redbed facies of silty sandstone and shale (Figure 4.7). Included are sedimentary structures indicative of a lagoonal and intertidal environment (Meijer Drees, 1986). Thick evaporite deposits characterize the central portion of the basin. They are divisible into primary and secondary deposits. The primary precipitation of halite occurred during extreme periods of basin wide evaporation. Secondary deposits of halite, gypsum, and anhydrite were precipitated from groundwater brines during desiccation. Periods of clastic sedimentation are correlated with relatively high water levels. The formation becomes sandy towards its zero edge of deposition.

There are sufficient data available to produce an isopach map of the formation and Evaporite Member (Figure 4.8). The Evaporite Member is thickest beneath the Mackenzie Plain and northeastern Franklin Mountains. The southern and western limits of the salt deposits are depositional, the northern limits are not completely known, and the eastern limit is a dissolution edge. There are no data on subsurface thicknesses from the Canyon Ranges.

Outcrops of the Saline River Formation approach a maximum thickness of 180 m in the Canyon Ranges. At the MacDougal section in Dodo Canyon, the formation is 128 m thick (Aitken *et al*, 1973). The Saline River Formation is conformably and gradationally overlain by the basal member of the Franklin Mountain Formation.

4.5.3 Franklin Mountain Formation

Williams (1922, 1923) assigned the name Franklin Mountain Formation to 100 m of calcareous shale and limestone overlying the Saline River Formation at Mount

Kindle of the southern Franklin Mountains. At the same location, Douglas and Norris (1963) measured 400 m of dolomite, shale, limestone, and sandstone. During Operation Norman, four informal members were recognized: Basal Redbeds, a Cyclic Member, a Rhythmic Member, and a Cherty Member (Macqueen, 1970; Macqueen and MacKenzie, 1973; Aitken *et al*, 1973). MacKenzie (1974) noted a thin and discontinuous fifth unit, the Upper Dolomite Member, but it has rarely been mapped by subsequent workers. Norford and Macqueen (1975) provide a full description from the type section near Wrigley.

The Franklin Mountain Formation is widely distributed in the study region and overlies strata ranging in age from Proterozoic to Upper Cambrian. In the Canyon Ranges and at Bear Rock, it rests on the Saline River Formation and has an average thickness of 400 m. The Cyclic Member, Basal Redbeds, and Rhythmic Member are Upper Cambrian, the Cherty Member is Lower Ordovician (Norford and Macqueen, 1975).

The Cyclic Member is a recessive, yellowish orange weathering, dolomite and argillaceous dolomite. It occurs, with few exceptions, where the Franklin Mountain Formation overlies the Saline River Formation. Near the western depositional edge of the Saline River Formation (Mackenzie Arch), or where the Franklin Mountain Formation overlies older formations, the Cyclic Member does not occur (Aitken *et al*, 1974). Where present in the Franklin and Mackenzie Mountains, it averages 40 m in thickness. Locally the Cyclic Member is replaced by the Basal Redbeds unit. This discontinuous unit is orange and red weathering, argillaceous dolomite and dolomitic mudstone, with some minor quartzite and chert.

The Rhythmic Member is a medium to thick bedded pale grey and brown, finely to very finely grained dolomite, with minor chert present as nodules and thin beds. In the Mackenzie and Franklin Mountains, some outcrop have a pronounced rhythmic colour banding. Typically this unit has a thickness of 250-300 m in the study region (Norford and Macqueen, 1975). In the area of the Mackenzie Arch, the basal part of this member contains some sandstone.

The Cherty Member weathers darker than the rhythmic unit, is more resistant, and contains a higher incidence of siliceous material. Chert occurs as nodules, thin beds, and quartz filled vugs, although in the Canyon Ranges the amount of chert remains relatively low. The member is predominantly a pale grey, finely crystalline dolomite. Thickness is highly variable, ranging between 0 and 200 m in the study region (Aitken *et al*, 1974; Aitken *et al*, 1982; Pugh, 1993).

4.6 Ordovician-Silurian

The Cherty Member (or Upper Dolomite Member) of the Franklin Mountain Formation is unconformably overlain by the Upper Ordovician-Lower Silurian Mount Kindle Formation (Figure 4.3) (Norford and Macqueen, 1975; Ludvigsen, 1975). Formerly, these two platform units constituted the Ronning Group (Hume and Link, 1945; Hume, 1954), or Ronning Formation (Tassonyi, 1969). Use of the term "Ronning Group" is now confined to subsurface mapping (Pugh, 1983, 1993) and is obsolete in surface studies (Morrow, 1991). Where the Mount Kindle Formation is absent, younger strata directly overlie the Franklin Mountain Formation. The Ordovician unconformity is of regional extent and there is evidence of substantial relief at that contact (Aitken *et al*, 1974).

4.6.1 Mount Kindle Formation

The type section of the Mount Kindle Formation is in the southern Franklin Mountains near Wrigley (Williams, 1922, 1923; Douglas and Norris, 1963; Norford and Macqueen, 1975). The Mount Kindle Formation is a fossiliferous, medium to dark brownish grey, finely to medium crystalline, thin to thick bedded dolomite that contains abundant chert (Norford and Macqueen, 1975). Silicified fossils (corals, brachiopods, and cephalopods), chert nodules and beds are common, vug porosity is well developed. Norford and Macqueen (1975) divided the section into three informal units: a basal member of argillaceous dolomite and shale, a middle resistant member of dark grey dolomite and chert, and a thick upper member of light grey

dolomite. Meijer Drees (1975) and Pugh (1993) adopted the threefold division in the subsurface to the south and east of the study area. In the northernmost Franklin and eastern Mackenzie Mountains, the Mount Kindle Formation is undivided, consisting of a uniform sequence of medium to dark brownish grey, fine to medium grained dolomite with chert and silicified corals (Macqueen, 1970). In the western Mackenzie Mountains, it is informally divided into two members: a lower dark grey cherty dolomite and an upper light grey reefoid dolomite (Cecile and Norford, 1991). In general, across the study area outcrops are brownish grey, massive, blocky, and resistant (Aitken *et al*, 1982). Karst pavements may occur where bedding is gently dipping (Chapter VI).

The Mount Kindle Formation is widely distributed in the Mackenzie Mountains. It is absent over much of the Franklin Mountains, in the subsurface of the eastern Mackenzie Plain, and the lower Keele River area. This distribution is related to pre-Devonian erosion over the area of Keele Arch (Figure 4.4)(Cook, 1975). At the Bear Rock Site, the Franklin Mountain Formation is directly overlain by Devonian strata. In the study area, the thickness of the Mount Kindle is variable. Maximum values approach 250 to 300 m (Aitken and Cook, 1974; Aitken *et al*, 1982); a single exposure 35 km southeast of Keele River is 407 m thick (Morrow, 1991). The upper contact of the Mount Kindle Formation with overlying units is unconformable. At some locations, including exposures in Dodo Canyon, the contact is sharply angular and represents an erosion surface of substantial relief.

4.7 Upper Silurian and Devonian

The Silurian succession of the Mackenzie Foldbelt is limited to the upper portion of the Mount Kindle Formation and the base of the overlying Tsetso Formation. The Mackenzie Platform was exposed to erosion for much of Silurian time. The Devonian is recorded by several formations, and a number of studies have examined the regional stratigraphy (Bassett and Stout, 1966; Law, 1971; Aitken and Cook, 1974; Williams, 1975; Aitken *et al*, 1982; Pugh, 1983, 1993; Meijer Drees, 1989,

1993; Morrow, 1991). Much debate has focussed on determining the nature of the stratigraphic relationships between Upper Silurian and Lower Devonian units (Figure 4.3).

In Operation Norman, the base of this sequence was mapped as either an Unnamed Silurian-Devonian unit or a subdivision of the southern Mackenzie Mountain Delorme Formation. The latter term has been rendered obsolete and Tsetso Formation is formally recognized as the basal dolomite (Morrow, 1991). The overlying Camsell and Bear Rock Formations are carbonate breccias and there is now general agreement that despite lithological similarities the Camsell underlies the Bear Rock (Blusson, 1971; Gabrielse *et al*, 1973; Williams, 1975; Meijer Drees, 1989, 1993; Morrow, 1991). The Arnica Formation is a lateral equivalent of the Bear Rock Formation and both are overlain by the Landry Formation (member). The three members of the subsurface Gossage Formation (Tassonyi, 1969) are recognized on the surface as the Tsetso, Arnica, and Landry Formations (Aitken *et al*, 1982; Pugh, 1983), and use of "Gossage" has been abandoned (Morrow, 1991).

It is convenient to divide the Devonian succession into four sequences, each constituting a distinctive facies and period of sedimentation on the Mackenzie Platform: (i) the Delorme Sequence (Gedinnian-Siegenian), (ii) the Arnica-Bear Rock Sequence (Emsian), (iii) the Hume Sequence (Eifelian), and (iv) the Fairholme Sequence (Givetian-Frasnian) (Morrow and Geldsetzer, 1991).

4.7.1 Delorme Sequence (Group)

In the northern Mackenzie Foldbelt, the Delorme Sequence includes the strata of the Delorme Group, which comprises the Tsetso and Camsell Formations and strata previously mapped as Delorme Formation (Morrow, 1991). In the southern Mackenzie Mountains, the group has been allocated between the Road River, Cadillac, and Vera Formations (Morrow and Cook, 1987).

The Delorme Group is a record of the earliest Devonian transgression (Gedinnian and Siegenian) onto the Mackenzie Shelf (Platform). This followed an

interval of erosion in the Upper Silurian (Ludlovian and Pridolian) (Pugh, 1983). The sequence is characterized by argillaceous, yellow and orange weathering, peritidal and supratidal dolomite and evaporite (Morrow and Geldsetzer, 1991). The colour and terrigenous content are the result of the transport of hematitic sand from the craton onto the platform (Morrow and Geldsetzer, 1991). Variability in thickness is considerable, ranging from a few hundred metres in the area of the Redstone Arch to in excess of 1500 m in Camsell Sub-Basin and Godlin Salient (Morrow, 1991). The group is distributed extensively, being absent only over the Norman Wells High (Figure 4.4). The Delorme Group overlies the Mount Kindle Formation with profound unconformity. In the region of the Twitya Uplift, it rests on the Franklin Mountain Formation or older strata.

4.7.1.1 Tsetso Formation

The Tsetso Formation occupies the uppermost Silurian and lower Devonian (Gedinnian and Siegenian) (Meijer Drees, 1989, 1993). It is a light yellow to orange weathering, argillaceous and silty, thin to medium, planar bedded dolomite (Morrow, 1991). There are also intervals of thick bedded and vuggy dolomite, dolomicrite, and dolomitic siltstone. In the area of Twitya uplift, sandstone is a common constituent. Minor anhydrite is recorded at the type section (Meijer Drees, 1989). Dolomicrite units contain small solution pipe features developed at minor unconformities within the formation.

4.7.1.2 Camsell Formation

The Camsell Formation was initially applied to a resistant breccia located between the Delorme and Sombre Formations in the southern Mackenzie Mountains (Douglas and Norris, 1961). This formation grades laterally into and locally overlies the Tsetso Formation. It is absent from the Norman Wells High, Redstone Arch, and Twitya Uplift (Figure 4.4). Two facies are represented: a silty carbonate facies, and an evaporite facies (Morrow, 1991). The silty carbonate intervals are repeating

cycles of dark calcareous mudstone and dolomite that grade vertically into light coloured, laminated and thinly bedded, silty and argillaceous dolomite. These repeating intervals are several metres thick and represent sequences of subtidal and intertidal deposition following minor transgressions (Morrow and Cook, 1987).

The evaporite facies are restricted to Godlin Salient and Camsell Sub-Basin, maximum thicknesses in these areas exceed 1000 m. In well sections, this facies is represented by interbedded anhydrite and silty dolomite. Surface exposures are recessive and yellow weathering, and all outcrops are brecciated. The calcareous solution breccias are lithologically similar to those of the Bear Rock Formation (Morrow, 1991). Development of such breccias is discussed in following sections.

4.7.2 Arnica-Bear Rock Sequence

A significant change in facies occurs across the Mackenzie Shelf (Platform) at the Siegenian Emsian transition. The Arnica-Bear Rock Sequence spans the stratigraphic interval between the Delorme Group and the Hume Formation, this includes the Arnica, Sombre, Bear Rock (Fort Norman), and Landry Formations (Morrow, 1991). The sequence has an average thickness of about 500 m and is a record of sedimentation on a subsiding shelf. Carbonates of the Arnica and Sombre Formations occur predominantly on the outer reaches of the shelf, and the breccia and associated evaporites of the Bear Rock (Fort Norman) Formation are located on the inner shelf (Figure 4.9). The contact between the brightly weathering terrigenous carbonates of the underlying Delorme Group and the grey units of the Arnica-Bear Rock Sequence is abrupt. However, brecciated exposures of the Camsell and Bear Rock Formations can appear identical.

The nomenclature of the Lower Devonian in the study region has seen recent revision. Pugh (1983) advocated inclusion of the subsurface equivalents of the above strata into a Bear Rock Group, which was supported by Norris (1985b) for surface exposures. On the basis of the geographic isolation and definitions of individual units, Morrow (1991) and Meijer Drees (1989, 1993) do not support the

establishment of a group ranking. However, the term "Fort Norman Formation" has been adopted for the thick interval of anhydrite that characterizes the subsurface Bear Rock Formation (Figure 4.10) (Meijer Drees, 1989, 1993; Morrow, 1991; Pugh, 1993). The latter term is now restricted to brecciated intervals at the surface and in the near subsurface. The stratigraphic nomenclature used in this thesis is taken from Morrow (1991).

4.7.2.1 Arnica and Sombre Formations

The Arnica Formation is a resistant dolomite, widely distributed in the western portion of the southern and northern Mackenzie Mountains (Figure 4.9). It is described in type section at Virginia Falls (Douglas and Norris, 1961). Formation thickness is uniform, approaching a maximum of 500 m. In outcrop, the Arnica Formation grades laterally eastward with the Bear Rock Formation. A 100 to 200 m thick member extends below the Bear Rock, or the Fort Norman Formation, in the area of Camsell Sub-Basin. This unit is called Arnica Platform (Dolomite) (Williams, 1975). In addition, a thin tongue of Arnica extends over much of the area where the Lower Devonian is represented by the Bear Rock or Fort Norman Formation. In the subsurface of Mackenzie Plain near Norman Wells, 20 to 30 m of Arnica are recognized above the Fort Norman Formation (Table 4.2) (Pugh, 1993). The Arnica Platform member is absent from the study area.

The Arnica Formation consists of repeated intervals of dark grey, medium to thick bedded, slightly vuggy dolomite that grade vertically into light grey, thinly laminated dolomite. This sequence is a record of periods of subtidal and intertidal deposition (Morrow, 1991). The incidence of limestone increases towards the top of the formation, with a gradational contact with the overlying Landry Formation. The Arnica Formation overlies the Delorme Group sharply and conformably.

The Sombre Formation is a thick bedded, grey dolomite extending from the southern Mackenzie Mountains along the western border of the Mackenzie Shelf to the region west of Godlin Salient. Thickness in the area of Godlin Salient is between

700 and 1000 m.

4.7.2.2 Bear Rock and Fort Norman Formations

The Bear Rock Formation was defined by the Canol geologists as intervals of brecciated, non-bedded dolomite and limestone, lying between the Middle Devonian and Silurian (Hume and Link, 1945). A steeply dipping type section was established in the hanging wall of a reverse fault at the southern flank of the Norman Range, 4 km downstream of the confluence of Great Bear and Mackenzie Rivers. This exposure was described by Stelck (1944, cited in Hume and Link, 1945) as 53 m of brecciated dolomite and limestone overlying 9 m of poorly bedded dolomite and 12 to 18 m of non-bedded gypsiferous dolomite.

This same section was later remeasured by Morrow and Meijer Drees (1981) adopting Bassett's (1961) definition of the Bear Rock Formation as all strata between the Hume Formation and the Ronning Group. This had been the working definition for regional mappers of Operation Norman (e.g., Aitken and Cook, 1974; Cook and Aitken, 1976; Aitken *et al*, 1982). This remeasurement yielded a thickness of 154 m for a lower brecciated interval, a substantial increase from the original estimate of 80 m. In addition, 45 m of bedded, non-brecciated, pelletal limestone were observed between the Hume and the brecciated sequence. This unit had been noted during Operation Norman but had not been mapped separately from the Bear Rock Formation.

In the subsurface, the Bear Rock Formation has been described by Tassonyi (1969), Meijer Drees (1980, 1986), and Pugh (1983). Tassonyi established Imperial Vermillion Ridge No. 1 well (65°07'51" N Lat., 126°05'00" W Long.) as the subsurface reference for the Bear Rock Formation (Tables 4.2,4.3). The section was divided into two informal members: an upper brecciated member, and a lower evaporitic member. The top of the brecciated member was taken at the base of a bedded pelletal limestone, which was the lower portion of the now obsolete subsurface Gossage Formation. This limestone unit is now recognized as the Landry

Formation (member). The brecciated member consists of brown and grey, micro to finely crystalline micro-brecciated dolomite. The matrix is calcareous and interbedded limestone rare. Minor amounts of anhydrite are recorded. The evaporitic member is a thick sequence of interbedded white to grey nodular dolomitic anhydrite and light brown, laminated, microcrystalline to very finely crystalline, anhydritic dolomite. In the Fort Norman area the evaporitic member contains relatively little dolomite but does include dolomitic and anhydritic mudstone. Meijer Drees (1980) recognized a third unit of the subsurface Bear Rock Formation; a basal dark greyish brown fossiliferous dolomite with little anhydrite. This unit is the Arnica Platform of Williams (1975) and it is largely confined to the Camsell Sub-Basin region, though recent work suggests it extends into western Mackenzie Mountains (Morrow, 1991).

The most detailed sedimentological study of this sequence is based on a cored interval from the Dahadinni M-43A well (63°52'59" N Lat., 124°39'15" W Long.; Meijer Drees, 1980, 1989). Repetitive sequences of interbedded dolomite and anhydrite are recorded at intervals of one to several metres. Dolomitic mudstone grades upward through nodular and recrystallized anhydrite to contorted and desiccated anhydritic mudstone. This sequence is characteristic of periods of regressive sedimentation under peritidal to supratidal conditions (James, 1984). Meijer Drees (1980) draws a parallel with the sabkha environments of the Persian Gulf. Minor intervals of breccia are observed in these sequences, but Meijer Drees suggests they constitute a small percentage of the total brecciation observed in outcrop (1990, personal communication).

The contrast between the surface and subsurface expression of the Bear Rock Formation has been attributed to near surface solution of anhydrite and gypsum by meteoric groundwater (e.g. Aitken *et al*, 1974; Morrow, 1991, Meijer Drees, 1993). This contrast has required the introduction of separate nomenclatures. The pelletal limestone unit of the surface type section is considered to be the lateral equivalent of the Landry Formation and the lower member of Tassonyi's subsurface Gossage

Formation (Morrow and Meijer Drees, 1981). This unit is mapped as Landry Formation in the subsurface (Meijer Drees, 1993; Pugh, 1993). In outcrop, the Landry is assigned to member status within the Bear Rock Formation (Figure 4.3) (Morrow, 1991). Tassonyi's subsurface brecciated member is predominantly bedded dolomite, and current subsurface mapping identifies this unit as the Arnica Formation (Pugh, 1993). The term Fort Norman Formation has been introduced for the subsurface evaporitic member (Meijer Drees, 1989, 1993). It is defined as the sequence of interbedded anhydrite and dolomite that underlies the Arnica Formation and overlies the Tsetso or equivalent Formations (Meijer Drees, 1989, 1993). The Fort Norman Formation consists of light brown or greyish brown, micro to fine crystalline, anhydritic dolomite, and light grey or greenish grey, dolomitic, microcrystalline anhydrite, and white to translucent, nodular-bedded, fine to coarse crystalline anhydrite (Meijer Drees, 1993). Where the Delorme Group is absent the Fort Norman Formation rests on Silurian or older strata. Where present, the Arnica Platform unit may be considered part of the Fort Norman Formation (Meijer Drees, 1980; Pugh, 1993). The term Bear Rock Formation is now confined to surface or near subsurface exposures.

The Bear Rock Formation is composed of two informal members: the Landry Member (section 4.7.2.4), and the Brecciated Member (Morrow, 1991). Exposures of the Brecciated Member are predominantly light to medium grey, massive and chaotic, cavernous and vuggy weathering, carbonate breccias (Figures 4.11, 4.12). There are also thin sequences of pale brown and grey, thick to thinly bedded dolomite and limestone. Bedded intervals are more common at the top of the member. Rarely is gypsum or anhydrite exposed at the surface. In the Dodo Canyon area, the formation is yellow orange weathering due to a high incidence of terrigenous material. The relative proportion of limestone to dolomite in the brecciated intervals varies considerably between and within sections, much of the matrix is calcareous. Calcite occurs as vein and vug fill, or as spar and micrite cement. In the shallow subsurface the Bear Rock Formation includes gypsum and

secondary calcite (dedolomite) (Meijer Drees, 1989, 1993).

The description of breccia exposures are based on: (i) the nature of the fill in the interfragmentary spaces (the matrix), (ii) the spatial relationship of fragments relative to their original positions, and (iii) the mutual proximity of fragments (Table 4.1). Classification of a given breccia interval may incorporate any combination of the three terms. The most resistant intervals of the Bear Rock Formation are composed of calcite cemented crackle packbreccia. The Landry Member commonly has a crackle breccia fabric (Figure 4.13). Mosaic and rubble packbreccias form the resistant intervals of the Brecciated Member. Fragments in packbreccias tend to be poorly sorted, equant, and angular. Clast sizes vary from granules to boulders. Morrow (1991) notes the presence of rounded corners on some clasts. Floatbreccias are less resistant, the most recessive exposures being composed of particulate rubble floatbreccia. The fragments tend to be platy, angular, granule to cobble sized, and subparallel to crude bedding: rounding of fragments is less common (Morrow, 1991). Relative to bounding strata the Brecciated Member is recessive and exposures are of poor quality, consequently characterization of the breccia fabric was often difficult.

Stratigraphic issues regarding these formations are not resolved. The Arnica Formation is recognized in the subsurface, but in the study area it is not well expressed in outcrop. At the Dodo Canyon Site, the Landry Member is easily discerned on the basis of colour, weathering pattern, and lithology. Bedded dolomite is also observed near the top of the Brecciated Member; it is assumed to be the Arnica equivalent. However, the latter exposures are scattered and the Arnica is consequently grouped into the Brecciated Member of the Bear Rock Formation. The relationship between the Fort Norman and Bear Rock Formation presents another difficulty. In most well sections the Fort Norman is represented by sequences of anhydrite and dolomite. There are cases though where the Fort Norman has the lithological characteristics of the Brecciated Member (e.g., K-29, Table 4.2).

The Bear Rock and Fort Norman Formations are widely distributed in the District of Mackenzie (Figures 4.9, 4.10). Maximum subsurface thicknesses are

recorded in Camsell Sub-Basin, where >1000 m of evaporites are present. In the subsurface of the Mackenzie Plain, the Fort Norman Formation averages between 250 and 300 m thickness (Tables 4.2, 4.3). The Arnica and Landry Formations are relatively thin, totalling 30 to 60 m. The only subsurface data close to the northern Mackenzies are from Imperial Whirlpool No. 1 well (65°32'25" N Lat., 129°13'17" W Long.). This well records 45.7 m of the Landry Formation and 134 m of the Fort Norman Formation (nomenclature altered from Tassonyi, 1969). However, there is no anhydrite, the Fort Norman is represented by bedded dolomite and brecciated dolomite and limestone. Nearby, surface exposures of the Bear Rock Formation are approximately 120 to 130 m in thickness (Hume and Link, 1945; Tassonyi, 1969). In the area of Twitya uplift, surface exposures vary from 85 to 140 m. The thickness gradually increases towards Keele River and Camsell Sub-Basin.

At the type section, the Bear Rock Formation unconformably overlies the Franklin Mountain Formation. There is considerable relief at that contact with large tabular masses of breccia extending several metres vertically into the Franklin. Elsewhere in the study region, the Bear Rock Formation overlies the Mount Kindle Formation or the Delorme Group. Generally across the Keele Arch and Norman Wells High, the lower contact is unconformable. The Bear Rock Formation grades laterally into the Arnica and Landry Formation and the contact with the overlying Hume Formation is conformable.

4.7.2.3 Origin and Development of Bear Rock Breccias

There are several genetic types of carbonate breccias, including: (i) early diagenetic solution or collapse breccias, (ii) late diagenetic solution breccias, (iii) depositional breccias, (iv) tectonic and fault breccias, (v) caliche breccias, and (vi) karst collapse breccias (Blount and Moore, 1969; James, 1984, James and Choquette, 1988). Early diagenetic solution, or collapse breccias, are generated within supratidal carbonate-evaporite sequences through evaporite removal and subsequent collapse of overlying materials (James, 1984). Typically these breccia intervals are limited to the upper

portions of regressive cycles. At a larger scale, subsurface solution of thick evaporite units by circulating meteoric groundwater and the resulting subsidence and collapse of overlying carbonate strata can form extensive late diagenetic solution breccias. This process is reviewed by Stanton (1966).

Meijer Drees (1980, 1989, 1993) notes the occurrence of early diagenetic breccias and very small mass flow deposits in the Bear Rock and Fort Norman Formations but suggests that late diagenetic solution breccias of the type described by Stanton are overwhelmingly dominant. Several lines of petrographic and stratigraphic evidence favour this interpretation.

Descriptions of solution breccias have emphasized the following characteristics: (i) the clasts are very poorly sorted angular fragments of dolomite and limestone, (ii) there is a wide range of clast sizes, (iii) clasts are most often set into a fine grained matrix or calcite cement, (iv) dedolomite is common, (v) the upper contacts are often indistinct and gradational, while lower contacts are sharp and well defined, (vi) breccia intervals are stratigraphically represented by evaporite sequences (particularly interbedded anhydrite and dolomite) in surrounding areas, and (vii) breccia is restricted to areas proximal to an erosion surface (Middleton, 1961; Stanton, 1966; Blount and Moore, 1969; Quinlan, 1978). The Bear Rock breccias possess each of these characteristics and they are discussed below.

The most common breccia fabrics observed in the field area are: crackle breccias, cemented and particulate mosaic packbreccias, and particulate rubble floatbreccias (after Table 4.1). The crackle breccias are found in the Landry Member and occasionally in the overlying Hume Formation. These resistant intervals have angular limestone clasts set in a calcite cement. Intervals of cemented mosaic or rubble packbreccias display clasts that are angular, with a size range from granules to boulders. Many clasts show minor rounding. This may be attributed to either abrasion or in situ solution, Morrow (1991) favours the latter. Primary depositional textures within clasts are few and where present the clasts tend to be dolomitic. Calcite cements that partially or completely fill the interfragmentary spaces tend to

be equant to weakly bladed and isopachous, and coarsen toward pore centres (Morrow, 1991). These characteristics are indicative of cementation in a freshwater phreatic diagenetic environment (Longman, 1980; Morse and Mackenzie, 1990). Intervals of particulate rubble floatbreccia are recessive. Most of the angular platy clasts are held in a particulate carbonate matrix (micrite). In some sections there appears to be a preferred orientation of fragments parallel to crude bedding.

Morrow (1991) explains variations in breccia fabric as a result of solution collapse in dipping interbedded sequences of anhydrite and dolomite (Figure 4.15). Subsurface intervals that are thinly bedded and anhydrite-rich experience much solution, subsidence, and gravitational compaction, relative to bounding intervals where anhydrite is less common or absent. Interbedded dolomite in these sections fractures and clasts are displaced from their original positions. These anhydrite-rich units are predominantly represented in outcrop by particulate rubble floatbreccias, where clasts are preferentially oriented parallel to bedding. At the boundary between compactable units of anhydrite and noncompactable dolomite units, a component of shear stress develops down dip. This shear is transmitted through the fine grained matrix and clasts are rotated parallel to bedding. Mosaic and rubble packbreccias are the result of solution compaction of anhydrite-poor dolomite sequences while crackle breccias develop by subsidence of thicker carbonates.

Lithologically, the Bear Rock breccias are primarily limestone while in the subsurface dolomite comprises the carbonate component of the Arnica and Fort Norman Formations. This suggest that dedolomitization (calcitization) accompanied the solution collapse process. This would be driven by an increased concentration and activity of Ca^{2+} ion in groundwaters that encounter anhydrite. Hydrochemical data from the Dodo Canyon Site support this model (Chapter VII). In addition, there are few primary depositional structures preserved in the breccia clasts indicating replacement of dolomite by calcite. Meijer Drees (1993) describes cores where calcite has replaced anhydrite crystals.

In the study area, the upper contact of the Brecciated Member with the

Landry Member and the Hume Formation is gradational. Particulate floatbreccias pass upward through packbreccias to crackle breccias over a distance of several metres. Morrow (1991) has noted similar transitions in western Mackenzie Mountains where intervals of particulate rubble floatbreccia grade into sequences of cemented packbreccia. The basal contact with the underlying Mount Kindle Formation is abrupt (Figure 4.11). These contact relationships are consistent with those of solution breccias described elsewhere.

The relationship between the surface Bear Rock Formation and the subsurface Fort Norman Formation is consistent throughout the study area. With some exceptions the Fort Norman is represented by an evaporite facies and the Bear Rock by a massive carbonate breccia. On the basis of this distribution, a mass flow origin for the Bear Rock breccias can be rejected.

In a few wells, the Fort Norman Formation is represented by intervals of carbonate breccia or displays features that are indicative of groundwater circulation. Imperial Whirlpool No. 1, Amoco Red Dog K-29, Decalta Keele River I-01, Imperial Sans Sault No.1, and the Candel Tate J-65 wells all possess solution breccia (Table 4.5). In Imperial Morrow Creek No. 1 and Sans Sault No. 1 groundwater is noted in the Landry or Fort Norman Formations at depths greater than 900 m. The log from Amoco Red Dog K-29 indicates solution breccia is actively forming between 415 and 685 m depth (Morrow, 1991). These records show that active circulation of meteoric groundwater generates solution breccias in the near subsurface to depths in excess of 500 m. However, this is not observed in all situations where the Fort Norman Formation is present at such depths. The log of Shell Blackwater Lake G-52 (64°01'20" N Lat., 122°55'12" W Long.) records bedded anhydrite and dolomite between 314 and 553 m depth; Banff Oscar Creek H-71 (65°30'20" N Lat., 127°13'26" W Long.) registers the same at depths below 357 m; Buttes Blackwater Lake I-54A (64°33'44" N Lat., 122°39'40" W Long.) has anhydrite between 268 and 595 m depth, and Imperial Vermillion Ridge No. 1 (N-28: Tables 4.2, 4.3) records anhydrite and dolomite between 315 and 564 m (Pugh, 1993). These and other well

logs indicate breccias occur to depths of several hundred metres but are more prevalent in the shallow subsurface where exposure to circulating meteoric water is more probable.

In the Candel Tate and Decalta Keele River wells, the top of the breccia occurs at depths of 2002 and 1305 m respectively, certainly below the depth of fresh groundwater circulation. However, the thickness of Devonian strata above the Fort Norman Formation is only 277 m for the Candel well and 187 m for Decalta. The occurrence of breccias in the deep subsurface may be attributed to groundwater leaching that occurred during uplift and erosion between the Upper Devonian and Cretaceous. These deep breccias are in fact in close proximity to the erosion surface that cuts across Devonian and Silurian strata in the region. Much of the secondary porosity and breccia observed in deep subcrops of the Fort Norman Formation may be attributed to this sub-Cretaceous unconformity (Meijer Drees, personal communication, 1990).

4.7.2.4 Landry Formation and Landry Member

The Landry Formation is a resistant platform limestone of Eifelian age widely distributed in the Mackenzie Mountains (Douglas and Norris, 1961; Morrow, 1991). Where it overlies the Arnica Formation it is treated as a separate unit. Across the distribution of the Bear Rock Formation the Landry is granted member status within that sequence (Morrow, 1991). In the area of the Norman Wells High, the Landry has a thickness of approximately 20 m. It thickens to the west and south at the expense of the Arnica Formation and approaches a maximum of 500 m. Contact with the Sombre and Arnica Formations is gradual and conformable (Aitken *et al*, 1982). The upper contact with the overlying Hume Formation is abrupt and conformable.

The Landry Formation (member) is a fossiliferous, very resistant, buff to blue grey weathering limestone. It consists of alternating sequences of thick resistant planar beds of tan, pelletal lime wackestone or lime mudstone and thin recessive very

thinly bedded, brown lime mudstone and pelletal mudstone (Morrow, 1991). The resistant and recessive couplets impart a ribbed appearance to outcrop (Figure 4.13). They are interpreted as shallowing upward cycles representing periods of subtidal and intertidal deposition following minor rises in sea level. Locally the member is brecciated where it overlies the Brecciated Member of the Bear Rock Formation.

4.7.3 Hume Sequence (Formation)

The Hume Formation is an argillaceous and fossiliferous limestone deposited under open marine conditions on the Mackenzie Shelf in late Eifelian to earliest Givetian time (Bassett, 1961; Lenz and Pedder, 1972; Chatterton, 1978; Morrow, 1991; Pugh, 1993). The Hume Formation is described in the subsurface by Tassonyi (1969), Meijer Drees (1980), and Pugh (1983, 1993). In outcrop the formation is divided into three members: the Upper, Middle, and Headless (Lower) Members (Pugh, 1983, 1993). In the study area, the Headless Member is a recessive, fossiliferous lime mudstone with interbeds of grey and black calcareous shale. The Middle Member is a fossiliferous wackestone interbedded with varying amounts of lime mudstone and calcareous shale. In outcrop, the Headless and Middle Members are commonly grouped as a recessive lower unit. Across the northern Mackenzie Mountains, this lower unit is described as a recessive, dark greyish brown to orange weathering sequence of fossiliferous nodular bedded skeletal micritic limestone with irregular thin to medium interbeds of brown and grey shale (Morrow, 1991). The Upper Member (upper unit) is a resistant cliff forming, pale grey weathering, thick bedded, medium to dark grey skeletal wackestone and fossiliferous lime mudstone (Aitken and Cook, 1974; Morrow, 1991).

In the northern Mackenzie Mountains, the thickness of the Hume Formation ranges from 90 to 150 m with the recessive units constituting approximately 50 to 60% of that total. The formation thickens to the south and west to a maximum of 350 m near Root River with much of the increase recorded in the resistant unit. The Hume Formation grades laterally into the Headless and Nahanni Formations in the

southern Mackenzie Mountains (Tassonyi, 1969; Pugh, 1993).

4.7.4 Fairholme Sequence

In early Givetian time, there was a marked change from carbonate to siliclastic sedimentation on the Mackenzie Shelf (Platform). This is represented by shales overlying the Hume Formation. The clastic dominated portion of the Devonian-Mississippian succession is the Fairholme Sequence, it is composed of the Imperial and Earn Assemblages (Figure 4.2). During this time, uplift associated with tectonic activity in the region of Selwyn Basin provided source materials for prograding clastic wedges (Gordey, 1978; Gordey *et al*, 1982). The Earn Assemblage consists of the clastic strata of the Earn Group. In the Backbone Ranges and Selwyn Mountains, this includes the Portrait Lake and Prevost Formations (Abbott, 1982, 1983; Gordy *et al*, 1982; McClay, 1984). The Portrait Lake Formation (40 to 880 m) is siliceous shale and chert. The Provost Formation (up to 900 m) is brown weathering shale, siltstone, cherty sandstone, and conglomerate. These formations are restricted to areas southwest of Plateau Fault.

The Imperial Assemblage includes shale, siltstone, and limestone of the Hare Indian, Ramparts, Canol, and Imperial Formations. These formations outcrop along the axes of tight synclines in the Canyon and Backbone Ranges and on the flank of the Mackenzie Plain Synclinorium.

4.7.4.1 Hare Indian Formation

The Hare Indian Formation is a recessive unit of grey-green and black, bituminous shale (Bassett, 1961). Thin interbeds of siltstone and limestone occur in the upper portion of the formation. The lower contact with the Hume Formation is conformable. The Hare Indian Formation is overlain by either the Ramparts or Canol Formations. The former contact is conformable and gradational, and the latter is unconformable. In the study region, the formation thickness varies between 140 and 190 m, some of this variability is due to the sub-Canol unconformity.

4.7.4.2 Ramparts Formation (Kee Scarp Formation)

The Ramparts Formation is a limestone unit that exhibits considerable variation in thickness and a discontinuous distribution (Bassett, 1961). It is the host stratum for the hydrocarbons of the Norman Wells oil field. It is divided into a lower platform member of brown and brownish grey limestone with interbedded shale, and an upper reefal member of fossiliferous, resistant, very thick bedded, pale brown limestone. The overlying contact with the Canol Formation is unconformable; in some locations the Ramparts Formation is overlain directly by the Imperial or younger formations (Aitken *et al*, 1982). The thickness of the platform member is typically 90 m and the reef member 150 m, it is Givetian in age.

4.7.4.3 Canol Formation

The Canol Formation is a dark grey and black, bituminous, siliceous shale that in outcrop resembles the lower Hare Indian Formation (Bassett, 1961; Tassonyi, 1969). This unit may reflect an abrupt change from shallow to deep water sedimentation on the Mackenzie Shelf (Platform) (Gordy, 1991). It is separated from underlying strata by an unconformity of variable magnitude. Locally, the Canol rests on strata as old as the Hume Formation. The thickness ranges from 80 to 225 m and is Frasnian in age (Lenz and Pedder, 1972).

4.7.4.4 Imperial Formation

The Imperial Formation is a thick sequence of grey and greenish grey shale, siltstone, and sandstone that is in conformable contact with the underlying Canol Formation (Bassett, 1961; Tassonyi, 1969). Thickness along the Mackenzie Mountain front approaches 850 m and increases southward to over 1500 m, but values of 300 to 400 m are typical of the study area. The formation outcrops on the eastern flank of the Mackenzie Mountains, locally within the Mackenzie Plain, and on the western flank of the Franklin Mountains. It is present in the subsurface of the Mackenzie Plain where it is overlain by Cretaceous strata. The unconformity at the base of the

Cretaceous is of regional extent. The Imperial Formation is Frasnian and Famennian age (Lenz and Pedder, 1972).

4.8 Upper Jurassic to Paleogene Assemblages

In the Mesozoic and early Cenozoic, terrane accretion onto the western margin of ancestral North America subjected the miogeoclinal strata of the Foreland Belt to compressive thickening, faulting, and folding. Easterly tapering clastic wedges were deposited in foredeep environments along the eastern margin of the Foreland Belt as a result of periods of orogeny (Norris, 1985a). Collectively, these clastic wedges are divisible into three groups of tectonic assemblages that are separated by regional unconformities; they are: (i) Upper Jurassic to Lower Cretaceous, (ii) Mid and Upper Cretaceous, and (iii) Upper Cretaceous to Oligocene (Yorath, 1991). Each represents a period of orogenic activity in the Cordillera.

In the northern Foreland Belt, uplift was delayed until the mid-Cretaceous. Clastic assemblages of the first group are not recorded in the study region. By Late Aptian to Early Albian time, several foreland basins and troughs were receiving sediment from uplifts in the Mackenzie Mountains and Keele Arch. Peel Trough was an elongated foredeep that developed east of the Mackenzie Mountains. Strata of Aptian and Albian time are represented by the Blairmore and Trevor Assemblages. The Brazeau Assemblage comprises units from the Upper Cretaceous to Oligocene. The stratigraphic relationships between formations of the above assemblages, along the axis of Peel Trough, are depicted in Figure 4.16. A thick and isolated fault bounded sequence of Cretaceous fluvial deposits are described from the western Mackenzie Mountains by Blusson (1971). Few data are available on these strata and they are not mapped separately on Figure 4.2.

4.8.1 Blairmore and Trevor Assemblages

The Blairmore Assemblage includes the Arctic Red and Sans Sault Formations, the Trevor Assemblage consists of the Slater River and Trevor Formations (Stott *et al*,

1991). The Arctic Red Formation is a thick sequence of concretionary, fossiliferous, and silty mudstone overlying a basal unit of glauconitic sandstone and conglomerate (Mountjoy and Chamney, 1969; Yorath and Cook, 1981). It disconformably overlies the Devonian in the Mackenzie Plain and possibly older units on the flank of Keele Arch. Thickness is variable with a maximum of 1600 m and an average of approximately 600 to 800 m in northern Peel Trough. The Arctic Red Formation pinches out 48 km southeast of Norman Wells. The upper part of the formation is the lateral equivalent to sandstones and mudstones of the Sans Sault Formation (Yorath and Cook, 1981).

The Sans Sault Formation developed on the western border of Keele Arch and extended into Peel Trough. In distribution it is limited to the Mackenzie Plain between Fort Good Hope and Norman Wells (Aitken *et al*, 1982). The maximum surface thickness is approximately 450 m and in the subsurface 700 m. The formation thins to the north, south, and west due to a facies change with the Arctic Red Formation. The Sans Sault Formation unconformably overlies Devonian units and is, in part, a lateral equivalent to and overlain by the Arctic Red Formation. The Sans Sault and Arctic Red Formations do not occur across Keele Arch.

By late Middle Albian time, coarse sediments of the Trevor Formation were accumulating in Peel Trough (Yorath and Cook, 1981). The Trevor Formation consists of interbedded sandstone and mudstone. The uppermost sandstone units are very resistant. The Trevor Formation is preserved in the broad synclines of the Mackenzie Plain west of the Mackenzie River and on Peel Plateau. An equivalent unnamed conglomerate occurs across the crest of Keele Arch. Thickness of the Trevor Formation ranges from 300 to 1150 m. Over much of its occurrence, it is overlain by a thin veneer of Quaternary deposits. The Trevor Formation and the unnamed conglomerate grade laterally southward along the Mackenzie Valley into the mudstone and siltstone of the Slater River Formation. The underlying contact with the Arctic Red is gradational.

The Slater River Formation is a very poorly exposed sequence of black,

concretionary, bentonitic shale (Yorath and Cook, 1981). Its distribution is extensive in the southern Mackenzie Plain and it extends across Keele Arch. The Slater River Formation unconformably overlies Paleozoic strata ranging in age from the Cambrian to Devonian. In the southern area of Peel Trough, bentonitic shales of the lower Slater River Formation comprise the basal unit of the Cretaceous Succession (Yorath and Cook, 1981, 1984).

4.8.2 Brazeau Assemblage

In the study region, the Brazeau Assemblage includes the Little Bear, East Fork, and Summit Creek Formations. Across much of the Northern Cordillera and the Northern Interior Platform, there is an unconformity between the Mid and Upper Cretaceous. However, evidence from Peel Trough suggests sedimentation through this interval was not interrupted by a significant hiatus (Yorath and Cook, 1981). The contact between the Slater River Formation and the overlying Little Bear Formation may be conformable. The Little Bear Formation is a unit of interbedded sandstone, siltstone, and mudstone. It occurs in the southeastern portion of Peel Trough. At the type section in the Canyon Range, the Little Bear Formation is 228 m thick, in the subsurface as much as 482 m are recorded. The formation comprises an easterly tapering wedge that thins towards Keele Arch and is replaced to the northeast by shale of the East Fork Formation (Yorath and Cook, 1981).

The East Fork Formation is a unit of black shale and minor sandstone and siltstone. It is distributed in the Mackenzie Plain in the Norman Wells area. Outcrops are few and recessive, and differentiation from the Slater River Formation on the western flank of Keele Arch is difficult. Subsurface thickness averages several hundred metres with a maximum of 1055 m. The East Fork Formation is Campanian to Maastrichtian age (Aitken and Cook, 1974). Contacts with the underlying Little Bear and overlying Summit Creek Formations are poorly exposed. The latter contact represents a change from marine to nonmarine conditions and is disconformable (Yorath and Cook, 1981).

The Summit Creek Formation is a Late Maastrichtian and Paleocene (Eocene?) succession of nonmarine conglomerate, sandstone, tuff, and coal. The formation is restricted to the Mackenzie Valley between Fort Norman and Keele River. The facies and geometry of the Summit Creek Formation suggest it represents deposition on broad alluvial fans and bajadas. These strata are deformed and tilted by positive tectonic elements on the Mackenzie Plain, such as the MacKay Range, demonstrating much of the thrust faulting in the eastern foldbelt is post-Paleocene (Yorath and Cook, 1981). Units equivalent to the Summit Creek Formation were presumably deposited throughout the foredeep, but have been largely removed by Quaternary glacial erosion (Hughes, personal communication, 1991).

4.9 Tertiary to Quaternary

There are no deposits of the Oligocene, Miocene, or Pliocene epochs recognized in the study region. To the north, sediments from southeastern Banks Island record changes from temperate to periglacial conditions over the Neogene to Quaternary. The Upper Miocene to Lower Pliocene Beaufort Formation is a poorly consolidated unit of sand and gravel, it includes a fauna indicative of mixed temperate forest (Hills, 1975; Vincent, 1990). This formation extends southward into Anderson Plain (Yorath and Cook, 1981). The Beaufort Formation is overlain by the preglacial Upper Pliocene to early Pleistocene Worth Point Formation (Vincent, 1989, 1990). Paleocological data from the Worth Point Formation indicate an environment of open, subarctic forest-tundra, similar to that of the northern boreal forest (Kuc, 1974; Vincent, 1990). This formation represents a period of warm climate relative to the subsequent Quaternary interglacials (Matthews *et al*, 1986). The occurrence of ice wedge pseudomorphs provide a minimum date for permafrost aggradation in the Northern Interior Plains (Vincent, 1983, 1990; Matthews *et al*, 1986). The Worth Point Formation is overlain by the early Pleistocene Ducks Hawk Formation, deposits of the oldest recognized glaciation in the region (Vincent, 1983, 1989, 1990; Vincent *et al*, 1983).

There are no such data from the northern Mackenzie Mountains. The chronology from the Arctic coast is probably a reasonable account of the regional climatic changes that occurred from the Miocene to Pleistocene. In the Mackenzie Mountains, it is assumed that permafrost was aggrading at high elevations by the Upper Pliocene. In the Upper Cretaceous and Paleocene the mountainous region was subjected to a long period of erosion, remnants of that erosion surface are preserved on the plateau-like summits of the Canyon Ranges (Bostock, 1948, 1970). A change in climate at the end of the Tertiary and the onset of glacial conditions in the Quaternary have had a substantial impact on the geomorphology of the region. The following chapter focusses on the Quaternary glacial record.

Table 4.1: Descriptive classification of breccia fabrics (Morrow and Meijer Drees, 1981).

Interfragment Space	Spatial Relationship of Fragments	Mutual Proximity of Fragments
Open: unfilled void space between fragments	Crackle: little relative displacement of fragments	Packbreccia: fragments largely in contact
Cemented: chemically precipitated mineral in void space	Mosaic: fragments largely but not wholly displaced	↓
Particulate: voids filled with subgranule sized grains	Rubble: fabric where no fragments match	Floatbreccia: fragments not in contact

Table 4.2: Locations of wells in Table 4.3. Surface elevations are in metres (Pugh, 1993).

Well	Name	Latitude	Longitude	Elevation
A-37b	Imperial Bluefish No. 1-A	64°56'01"N	125°50'54"W	67.1
A-52	Imperial Loon Creek No. 1	65°11'06"N	126°54'23"W	116.4
G-12	Imperial Loonex No. 1	65°11'19"N	127°02'33"W	133.2
G-44	Imperial Morrow Creek No. 1	65°23'15"N	127°23'07"W	55.8
G-78	Imperial Loon Creek No. 2	65°07'20"N	126°28'51"W	110.6
H-15	Imperial Hossier Ridge No. 1	65°24'16"N	127°32'14"W	131.1
H-34	Arco W. Whitefish River H-34	65°33'24"N	127°35'45"W	230.7
I-01	Decalta Keele River I-01	64°20'40"N	125°00'07"W	289.9
J-65	Candel Tate J-65	64°24'39"N	125°26'48"W	607.5
K-03	Aquit. Dodo Canyon K-03	65°02'33"N	126°46'14"W	308.5
K-29	Amoco Red Dog K-29	64°08'43"N	125°34'55"W	560.5
N-28	Imperial Vermillion Ridge No.1	65°07'51"N	126°05'00"W	281.9
S-01	Imperial Sans Sault No. 1	65°43'19"N	128°49'08"W	57.3
W-01	Imperial Whirlpool No. 1	65°32'25"N	129°13'17"W	99.4

Table 4.3: Thickness of Mesozoic to Lower Cambrian units from several cores in the Mackenzie Plain area. Data are in metres. In each well the upper unit may be erosionally truncated. The lower unit may be only partially represented. Tables 4.2 and 4.4 provide a legend, well locations are indicated on Figure 4.9 (data from Pugh, 1993).

Unit	Well Sections													
	A-37b	A-52	G-12	G-44	G-78	H-15	H-34	I-01	J-65	K-03	K-29	N-28	**S-01	**W-01
Mes	383.4	146.3	399.3				663.2	1113.1	1664.8	907.1			393.2	
uDi	87.4	528.8	537.4	>216.1	323.1		0.0	0.0	0.0	675.4			29.6	289.6
uDc	28.0	79.2	60.7	74.1	46.6	3.0	0.0	0.0	0.0	52.1			34.4	0.0
mDr	18.6	84.4	0.0	30.5	0.0	170.7	0.0	0.0	0.0	0.0			125.0	131.1
mDhi	141.7	125.9	212.1	153.6	134.1	139.6	0.0	0.0	78.3	135.9		143.3	207.3	216.4
mDh	114.0	102.1	100.0	101.8	114.3	104.2	0.0	91.7	123.4	118.6	33.5	115.8	96.0	160.0
ImDI	7.0	21.3	21.0	6.1	19.5	10.4	18.9	56.1	50.6	17.7	204.2	25.9	13.7	65.5
ImDa	6.1	14.6	22.9	>19.5	28.7	32.6	47.9	38.7	24.4	29.0	176.2	30.5		
ImDf	>*182.6	274.9	>34.7		309.1	303.5	*199.3	*154.2	*167.6	353.6	*271.9	248.4	*>103.9	*134.0
ImDap		0.0			0.0	0.0	0.0	94.5	123.1	0.0	204.2	0.0		0.0
SDd		0.0			0.0	0.0	177.1	0.0	0.0	0.0	>1258.8	0.0		0.0
OSk		7.0			0.0	0.0	132.0	0.0	0.0	23.8		9.1		0.0
COf		>265.8			386.5	>45.4	186.5	>118.9	>516.3	419.7		278.9		>600.0
uCs					>143.9		63.1			>13.4		885.4		
ImCc							29.3					>82.3		
ICc							31.4							

* Fort Norman Formation with breccia or other evidence of groundwater solution (see Table 4.5).

** Data from wells S-01 (Imperial Sans Sault No. 1) and W-01 (Imperial Whirlpool No. 1) are after Tassonyi (1969) and Hume (1954), the Arnica is not present because unit definitions do not precisely match those used by Pugh (1993).

Table 4.4: Abbreviations used for lithostratigraphic units in Table 4.3.

Abbreviation	Erathem, System, Series	Group and or Formation (s)
Mes	Mesozoic	Arctic Red, Sans Sault, Trevor, etc.
uDi	Upper Devonian	Imperial
uDc	Upper Devonian	Canol
mDr	Middle Devonian	Ramparts
mDhi	Middle Devonian	Hare Indian
mDh	Middle Devonian	Hume
ImDI	Lower Middle Devonian	Landry
ImDa	Lower Middle Devonian	Arnica
ImDf	Lower Middle Devonian	Fort Norman
ImDap	Lower Middle Devonian	Arnica Platform
SDd	sub-Devonian	Delorme Group: Tsetso, Camsell
OSk	Ordovician-Silurian	Mount Kindle
COf	Cambrian-Ordovician	Franklin Mountain
uCs	Upper Cambrian	Saline River
ImCc	Lower Middle Cambrian	Mount Cap
ICc	Lower Cambrian	Mount Clark

Table 4.5: Well records from the Mackenzie Plain area that display evidence of groundwater solution in Devonian strata, in particular the Fort Norman Formation.

Well	Mes	Dev	FN	Description
A-37b	383.4	402.8	896.1	Lost circulation during drilling in the Ramparts Fm at 774 m, water encountered in Landry or Arnica Fm at 892 m (1)
G-44	0.0	601.7	*	At 616.9 m sulphate rich groundwater encountered with a temperature of 32°C, and a flow volume of 55-60 L s ⁻¹ (1)
H-34	663.2	66.8	830.5	Vug porosity in Arnica Fm, vug and intercrystalline porosity in interbedded anhydrite and dolomite of the Fort Norman Fm (2)
I-01	1113.1	186.5	1305.8	Fort Norman Fm represented by brecciated dolomite and limestone, the underlying Arnica Platform is also brecciated (2)
J-65	1664.8	276.7	2002.6	Fort Norman Fm represented by becciated dolomite with appearance of solution breccia (2)
K-29	0.0	413.9	413.9	Arnica Fm with high porosity, Fort Norman Fm represented by brecciated dolomite and anhydrite also has high porosity (2,3)
S-01	393.2	506.0	956.5	Groundwater in Fort Norman (Bear Rock Fm)(1), Fort Norman Fm represented by brecciated dolomite and limestone (4)
W-01	0.0	862.6	965.0	Fort Norman Fm represented by brecciated gypsiferous dolomite (4)

Mes: Thickness of Mesozoic strata above the Devonian (in metres)

Dev: Thickness of Devonian strata above top of the Fort Norman Formation (in metres)

FN: Depth of the Fort Norman Formation below the surface (in metres). The thickness of surficial sediments are not listed separately, thus the sum of columns Mes and Dev may not equal FN.

* The base of well G-44 was assigned to the Bear Rock Formation by Hume (1954). Pugh (1993) assigns the base to the Arnica Formation near the transition with the Fort Norman Formation.

(1) Hume (1954) (2) Pugh (1993) (3) Morrow (1991) (4) Tassonyi (1969)

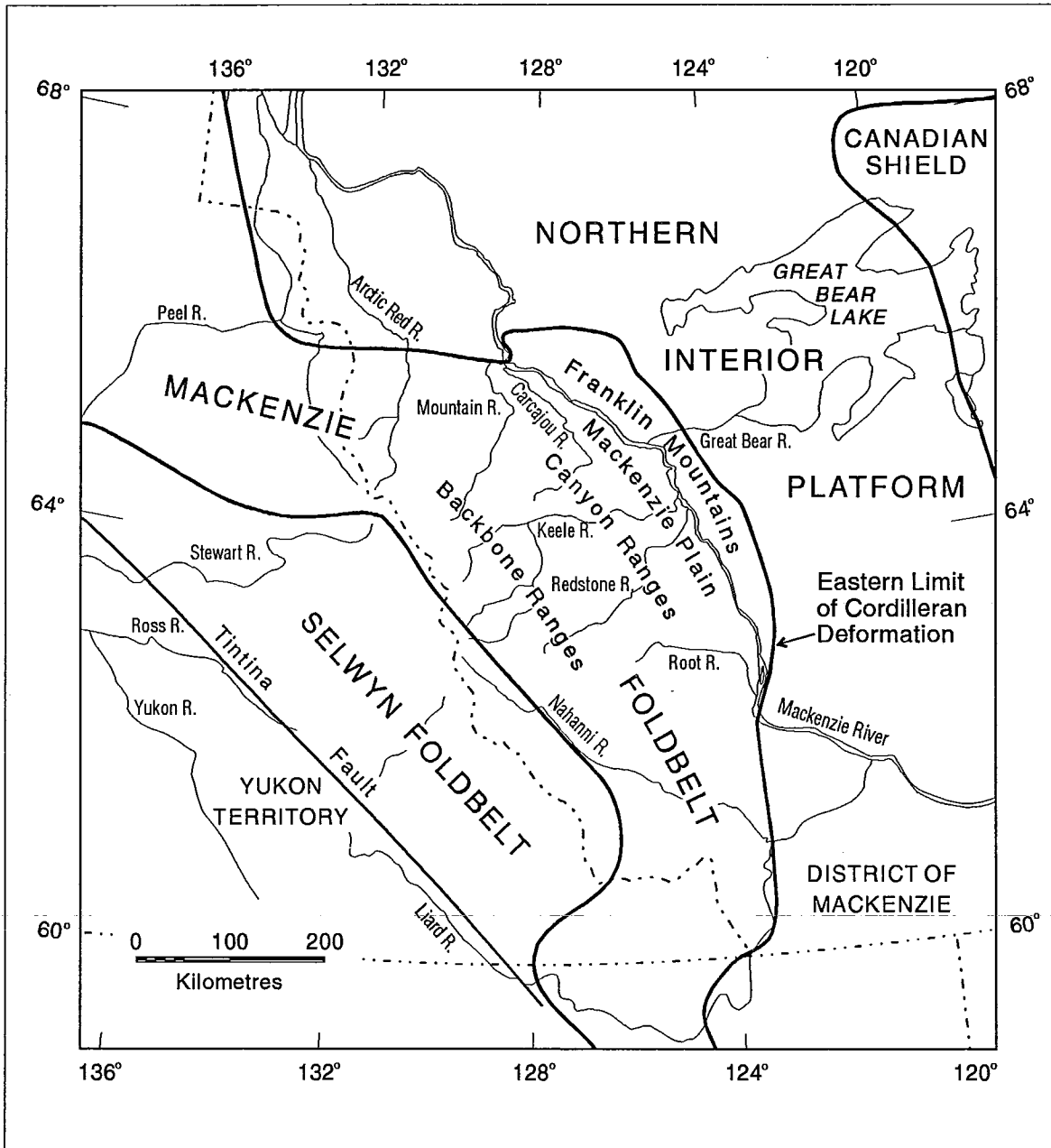


Figure 4.1: Major physiographic and tectonic divisions in western District of Mackenzie and eastern Yukon. The Mackenzie Foldbelt incorporates the Mackenzie and Franklin Mountains and the Mackenzie Plain. The eastern limit of the Cordillera is marked by a series of thrust faults on the eastern slopes of the Franklins (after Gabrielse *et al*, 1991; Bostock, 1970).

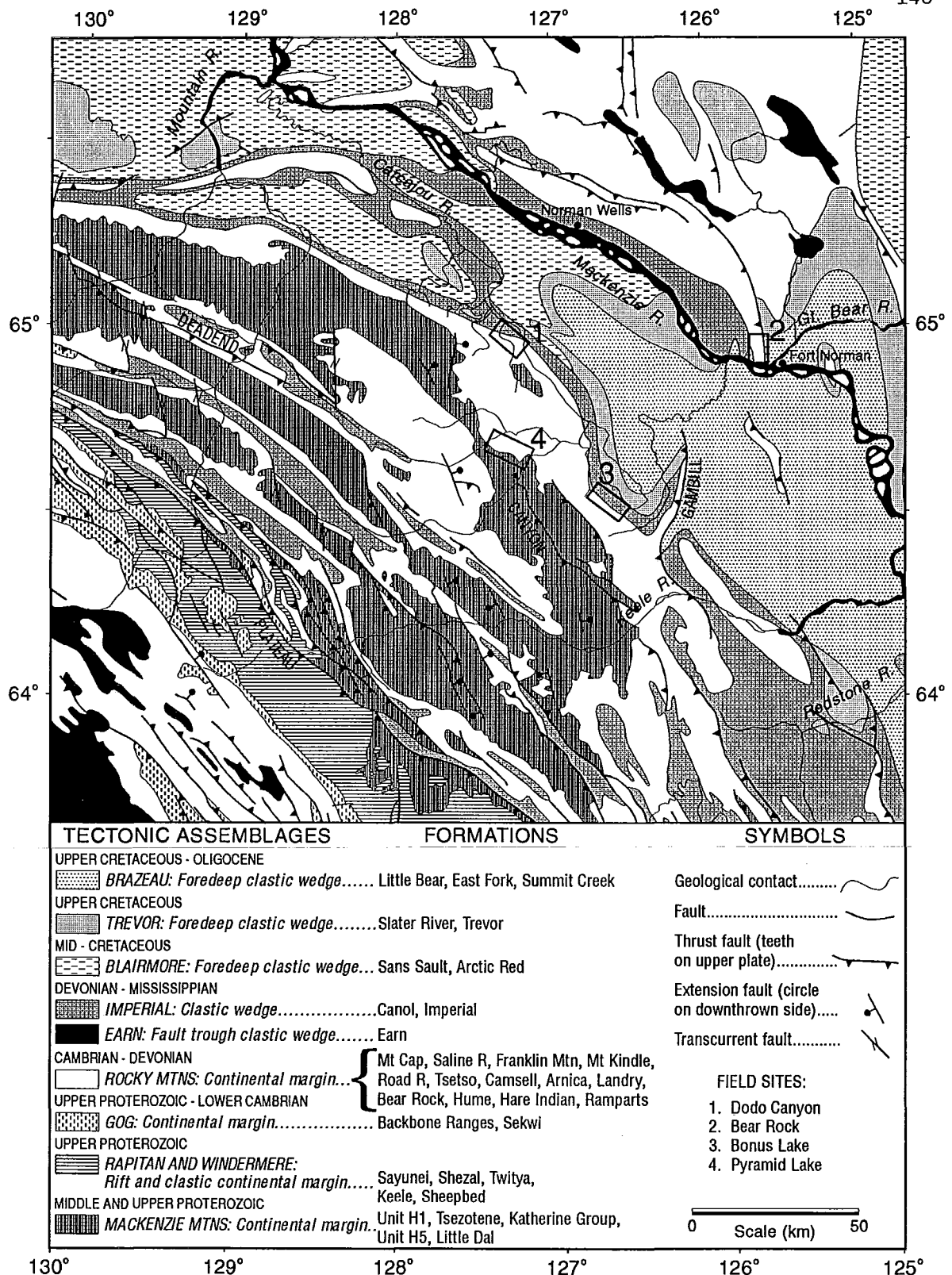


Figure 4.2: General geology of the study region, map shows the distribution of tectonic assemblages and major faults. Where known fault type and sense of displacement are illustrated. Formation lithologies are given on Figure 4.3 (Wheeler and McFeely, 1991).

LOCATION (Map Area)

ERATHEM		SYSTEM AND/OR STAGE		Sans Sault Rapids, (106H)	Carcajou Canyon, (96D)	Norman Wells, (96E)	Fort Norman, (96C)
CENOZOIC	QUATERNARY	HOLOCENE		erosion	all	erosion	all
		PLEISTOCENE			gl	gl	gl
	TERTIARY	EOCENE				folding	folding
		PALEOCENE			UNNAMED cg ss 4.5		SUMMIT CREEK cg ss 3.0
MESOZOIC	CRETACEOUS	UPPER		Folding and Thrusting	EAST FORK sh ss 2.0		EAST FORK sh ss 9.0
					LITTLE BEAR ss sh 1.0	Folding and Thrusting	LITTLE BEAR ss silt sh 3.0
			TREVOR ss 11.0		SLATER R. sh 3.0		SLATER R. sh 3.0
	LOWER		ARCTIC RED sh silt ss 13.0	SANS SAULT ss 5.0	SANS SAULT ss 4.0	SANS SAULT ss 4.0	ARCTIC RED sh 4.5
PALEOZOIC	DEVONIAN	UPPER	FRASNIAN	IMPERIAL sh ss 6.0	IMPERIAL sh ss 11.0	IMPERIAL sh ss 2.5	
				CANOL sh ch 0.5	CANOL sh ch 0.9	CANOL sh ch 0.7	CANOL sh 0.3
				RAMPARTS ls 1.0		RAMPARTS ls 1.0	RAMPARTS ls 0.3
				HARE INDIAN sh ls 2.0	HARE INDIAN sh ls 1.3	HARE INDIAN sh ls 2.0	HARE INDIAN sh ls 2.0
		EIFELIAN	HUME ls ch 1.2	HUME ls ch 1.7	HUME ls ch 1.2	HUME ls ch 1.2	
	LOWER		LANDRY ls 2.0	Landry ls ↑	LANDRY ls 1.0	Landry ls ↑	Landry ls 0.2 ↑
			ARNICA dol	BEAR ROCK ls dol bx anh gyp ↓	ARNICA dol 1.0	BEAR ROCK ls dol bx anh gyp ↓	Fort Norman BEAR ROCK ls dol bx anh gyp ↓
			TSETSO dol ss ls 0.5		CAMSELL ls bx anh 3.0		TSETSO dol ss ls 0.5
					TSETSO dol ss ls 2.5		
	SILURIAN	UPPER					
LOWER							
ORDOVICIAN	UPPER			MOUNT KINDLE dol ch 2.5	MOUNT KINDLE dol ch 3.0	MOUNT KINDLE dol ch 1.0	MT KINDLE dol ch 1.0

Figure 4.3: Table of formations from Sans Sault Rapids, Carcajou Canyon, Norman Wells, and Fort Norman map areas (various references in legend).

ERATHEM		SYSTEM AND/OR STAGE	Sans Sault Rapids, (106H)	Carcajou Canyon, (96D)	Norman Wells, (96E)	Fort Norman, (96C)	
PALEOZOIC	ORDOVICIAN	LOWER	1,4,7	1,2,6,7	1,5,6,7	1,3,6,7	
		UPPER	FRANKLIN MOUNTAIN dol ch 8.0	FRANKLIN MOUNTAIN dol ch 4.5	FRANKLIN MOUNTAIN dol ch 5.0	FRANKLIN MOUNTAIN dol ch 4.0	
	CAMBRIAN		SALINE RIVER sa anh redbeds	SALINE RIVER sa anh redbeds	SALINE RIVER sa anh redbeds 3.5	SALINE RIVER sa anh redbeds 3.5	
		MIDDLE	MOUNT CAP sh slt ss 0.3	MOUNT CAP sh ls slt ss 1.1	MOUNT CAP sh ls slt ss 1.0	MOUNT CAP?	
		LOWER			MT CLARK ss qte 2.0	MT CLARK ss qte 2.0	
	PROTEROZOIC	UPPER	Gabbro intrusions	LITTLE DAL dol sh qte gyp ls slt 14.6	LITTLE DAL dol sh qte gyp ls slt 10.2		
				KATHERINE qte dol sh 7.1	KATHERINE qte dol sh 24.0		
		MIDDLE	Gabbro intrusions	TSEZOTENE sh ss dol 7.5	TSEZOTENE sh ss dol ls 12.2		
			UNIT H1 dol ch 4.0+	UNIT H1 dol ch			

LITHOLOGICAL ABBREVIATIONS		LEGEND	
all alluvium	gyp gypsum	Group or Supergroup.....	MACKENZIE
anh anhydrite	ls limestone	Formation.....	HUME
bx breccia	qte quartzite	Member.....	Landry
cg conglomerate	sa salt	Maximum Thickness (100's of m)..	3.5
ch chert	sh shale	Facies change.....	
dol dolomite	slt siltstone	Non-marine.....	
gl glacial drift	ss sandstone	Relationship not known.....	

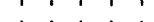
STRATIGRAPHIC CONTACTS		REFERENCES
	Established Uncertain	1 Aitken et al, 1973
Conformable	 	2 Aitken and Cook, 1974
Disconformable	 	3 Cook and Aitken, 1976
Unconformable	 	4 Aitken et al, 1982
Nonconformable	 	5 Cook and Aitken, 1975
		6 Morrow, 1991
		7 Gabrielse and Brookfield, 1992

Figure 4.3 (con't): Table of formations from Sans Sault Rapids, Carcajou Canyon, Norman Wells, and Fort Norman map areas (various references).

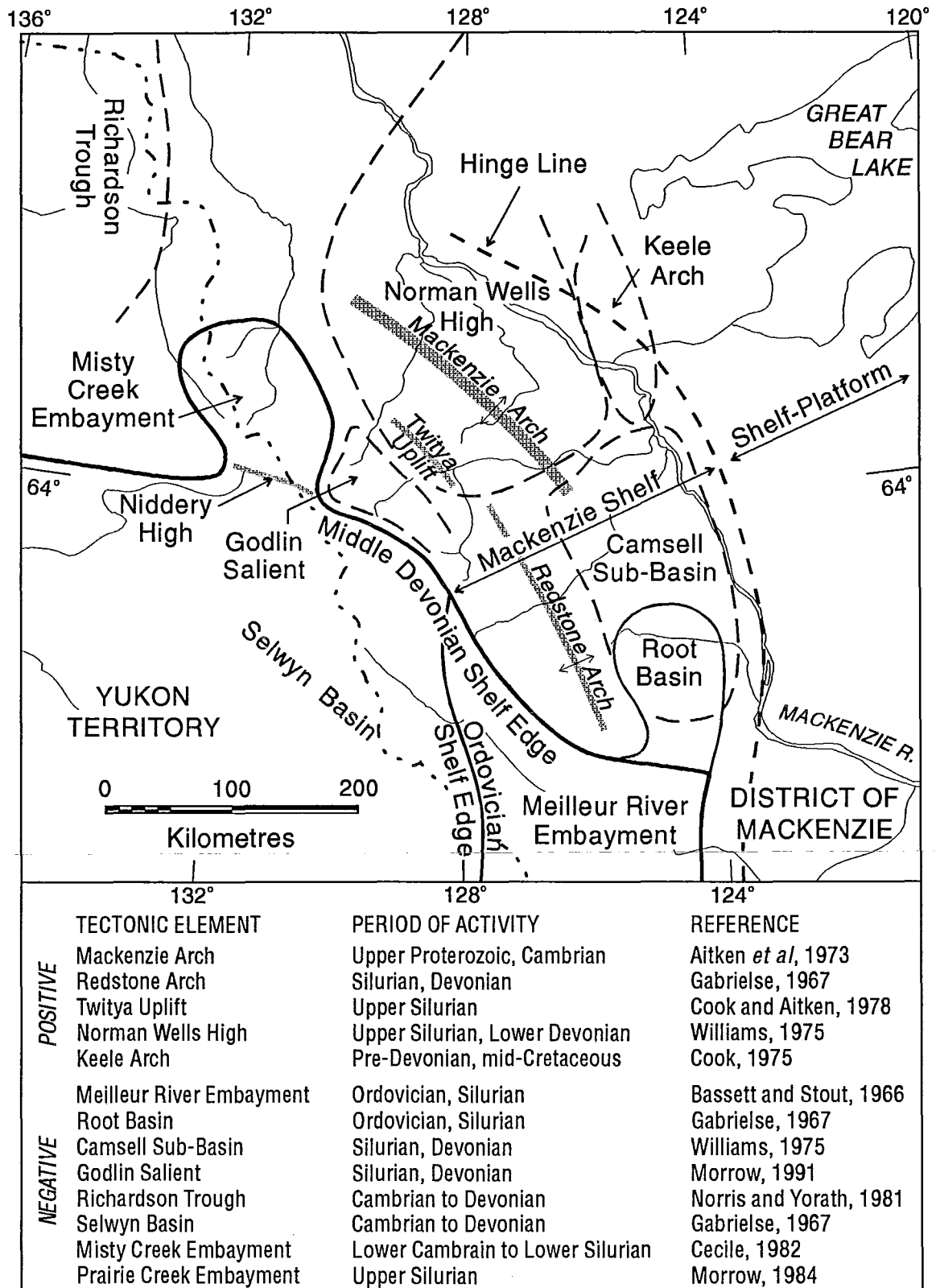


Figure 4.4: Distribution of positive and negative tectonic features on the Mackenzie Shelf. Negative elements were centres of subsidence and thick sediment accumulation, positive elements were exposed during the periods indicated. The position shown for the hinge line was during the Silurian and Devonian (after Morrow, 1991).

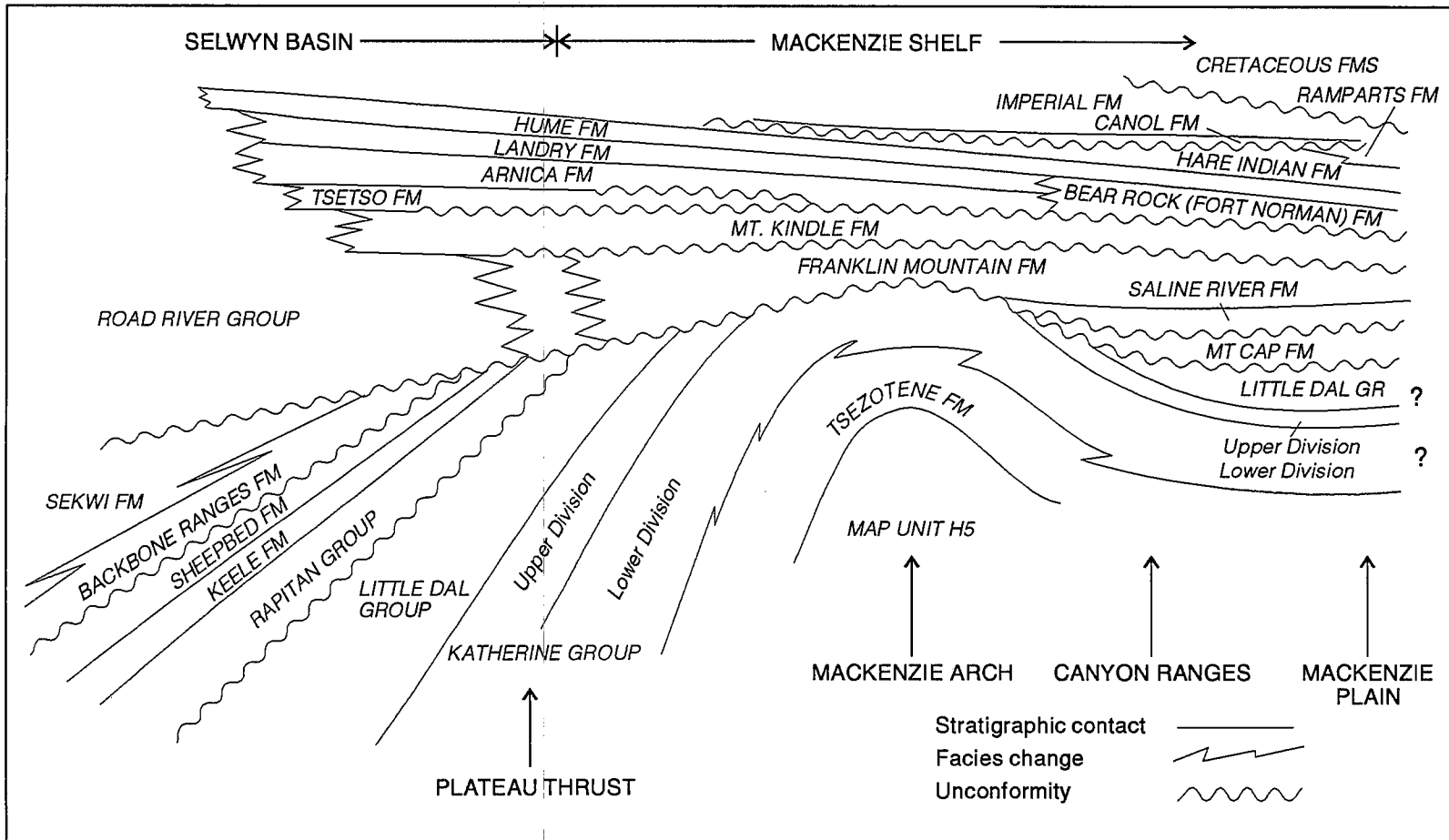


Figure 4.5: Stratigraphic relationships in the northeastern Mackenzie Mountains. The cross section is from Mackenzie Plain across the Mackenzie Arch to Selwyn Basin. The thick sequence west of Plateau Thrust includes a number of formations absent from the Canyon Ranges and Mackenzie Plain. Over the area of Mackenzie Arch the Upper Cambrian Franklin Mountain Formation rests unconformably on the Middle Proterozoic Katherine Group. In the study area evaporites occur east of the Arch in the Bear Rock (Fort Norman) and Saline River Formations (after Aitken *et al*, 1973, 1982).

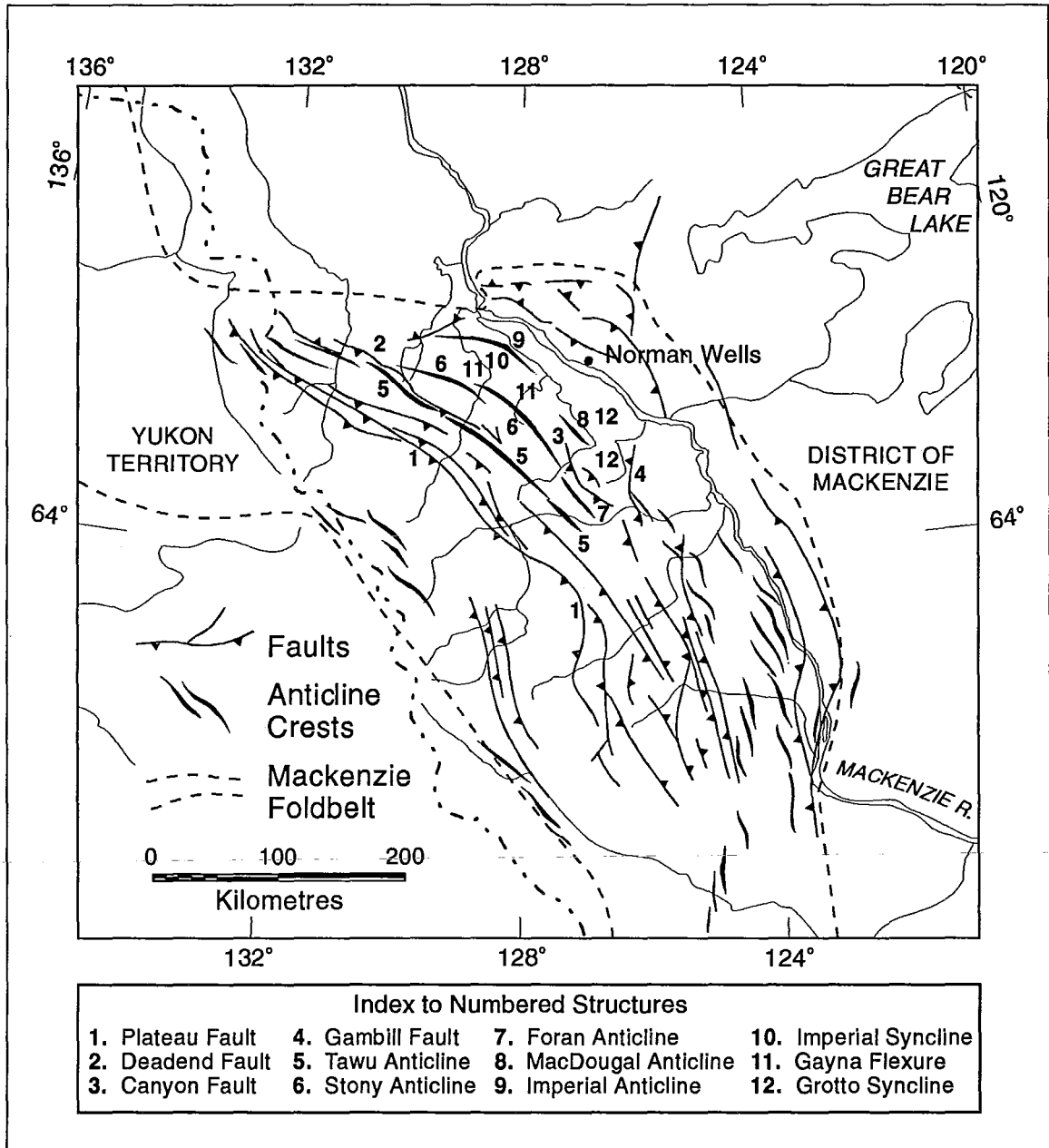


Figure 4.6: Distribution of major faults and anticlines in the Mackenzie Foldbelt. The features depicted are representative of the total population. Cusp marks on the fault symbols indicate the hanging walls of thrust or reverse faults. Syncline and monocline traces are not shown. Plateau Fault separates the Outer Fold Belt of the Canyon Ranges from the Plateau Sheet of the Backbone Ranges. The fold pattern changes from right-hand to left-hand en échelon from the southern to northwestern Mackenzies. The labelled features are the dominant structural forms in the area of the field sites (after Norris, 1972; Aitken *et al*, 1982; Park *et al*, 1989; Wheeler and McFeely, 1991).

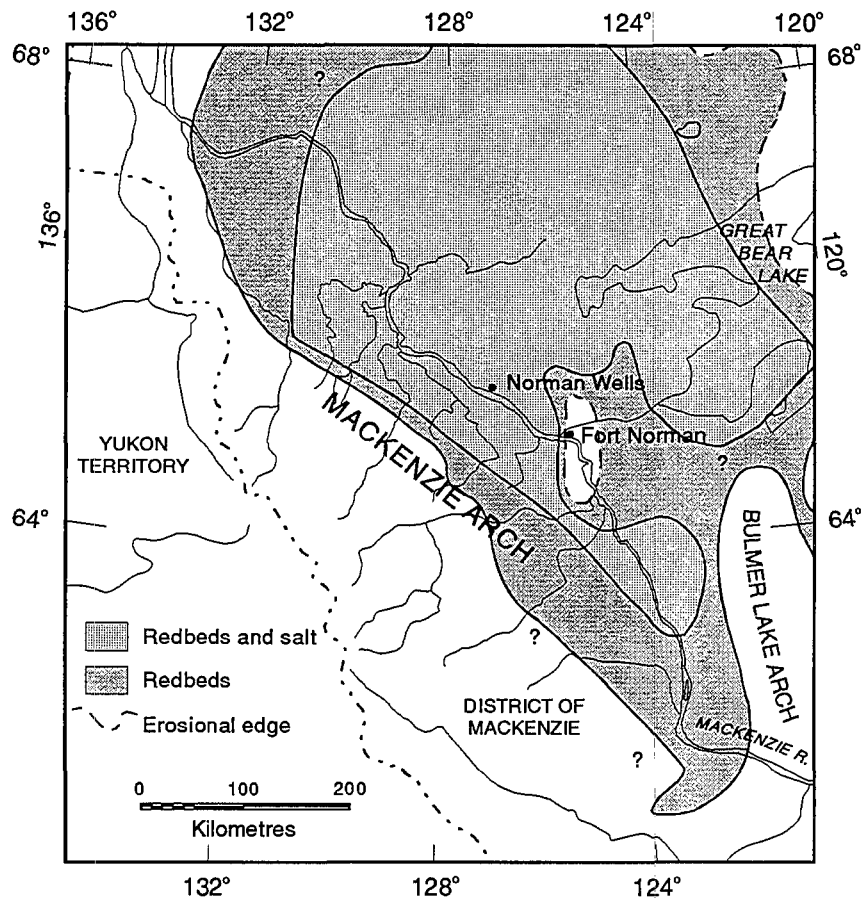


Figure 4.7: Approximate configuration of the Saline River Formation depositional basin. Evaporite facies were restricted to the central portions of the basin, redbed facies occur on the periphery (Meijer Drees, 1986).

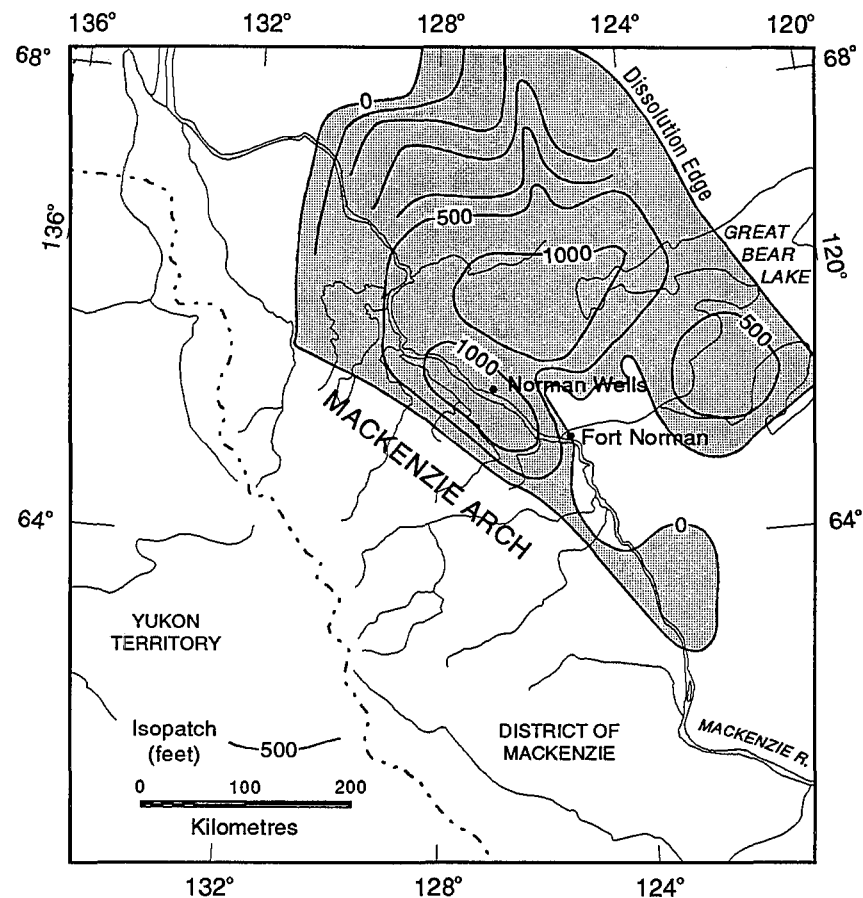


Figure 4.8: Isopach map of the Evaporite Member of the Saline River Formation. The depositional edge of the evaporite extends into the Canyon Ranges of the northern Mackenzie Mountains. The evaporite is thickest under Mackenzie Plain (Meijer Drees, 1986).

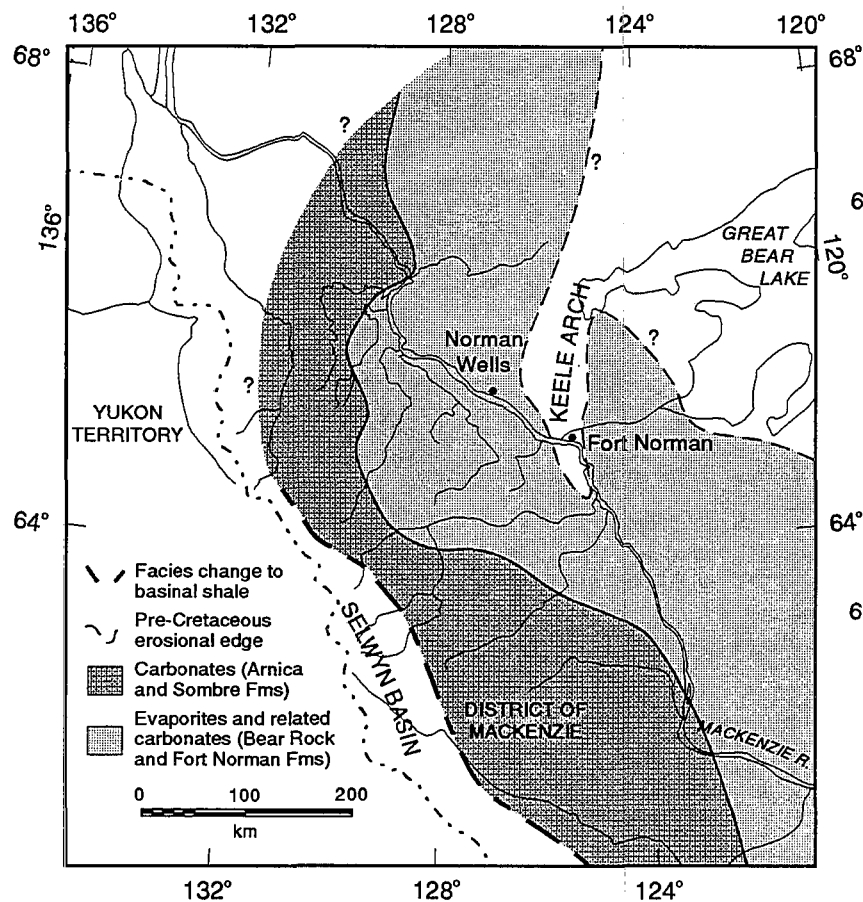


Figure 4.9: Distribution of upper Lower to lower Middle Devonian rocks. Anhydrite and dolomite were deposited on the inner Mackenzie Shelf, carbonates in deeper water near the shelf edge. The subsurface Fort Norman Formation has an evaporite facies, the Bear Rock Formation is the brecciated surface equivalent. Though not depicted in the diagram a tongue of the Arnica Formation does extend over the area of the evaporite facies (Meijer Drees, 1993).

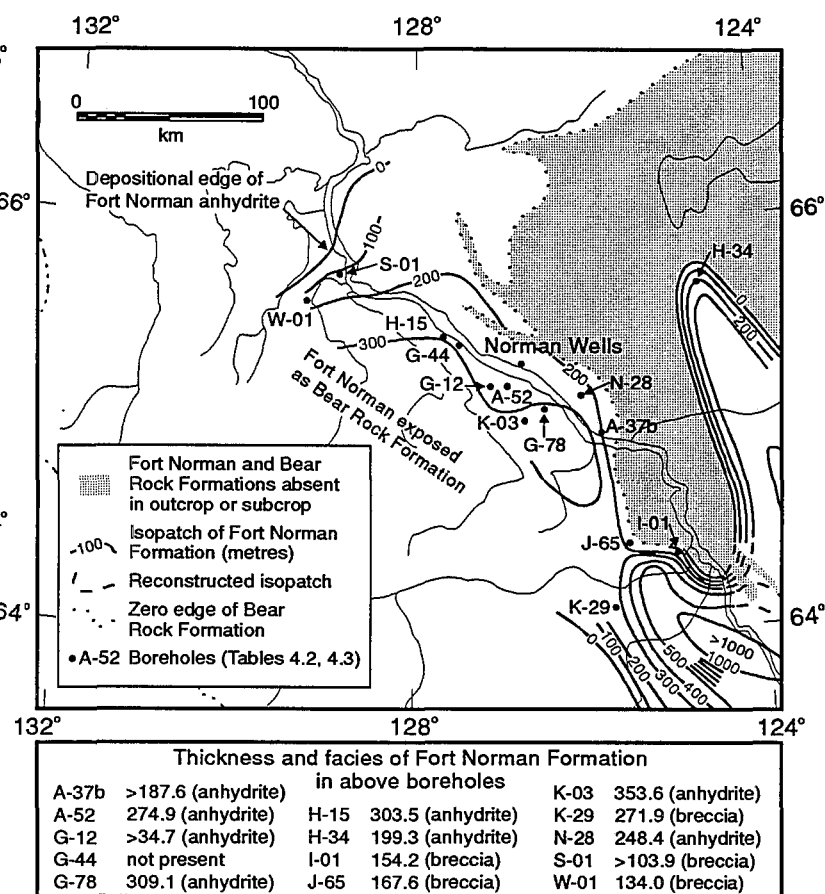


Figure 4.10: Isopach map of the Fort Norman Formation. Subsurface thickness is greatest southeast of Keele River, the formation is absent over the area of Keele Arch. The thickness under Mackenzie Plain ranges between 200 and 350 m. No subsurface data exist from the northern Canyon Ranges. The brecciated Bear Rock Formation occurs where the Fort Norman Formation is, or has been, exposed to circulating meteoric groundwater (Pugh, 1993).

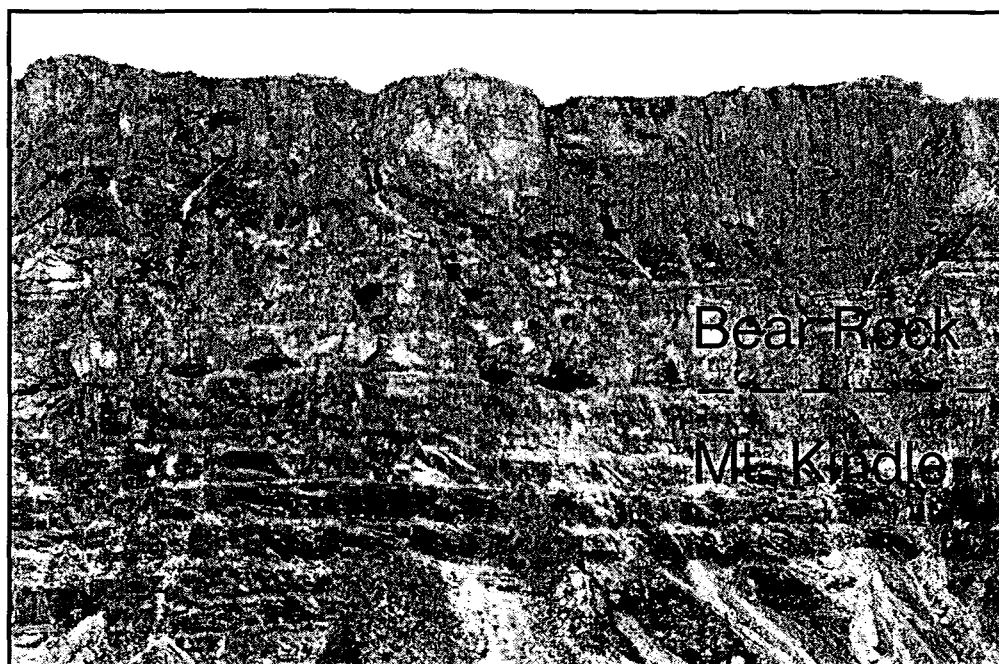


Figure 4.11: Exposure of the Mount Kindle and Bear Rock Formations on the north wall of Carcajou Canyon near the Dodo Canyon Site. The bedded dolomites of the Mount Kindle are sharply overlain by the Brecciated Member of the Bear Rock. Cavernous porosity is evident along the contact. The degree of brecciation decreases toward the Landry Member which is discontinuously exposed at the cliff top.

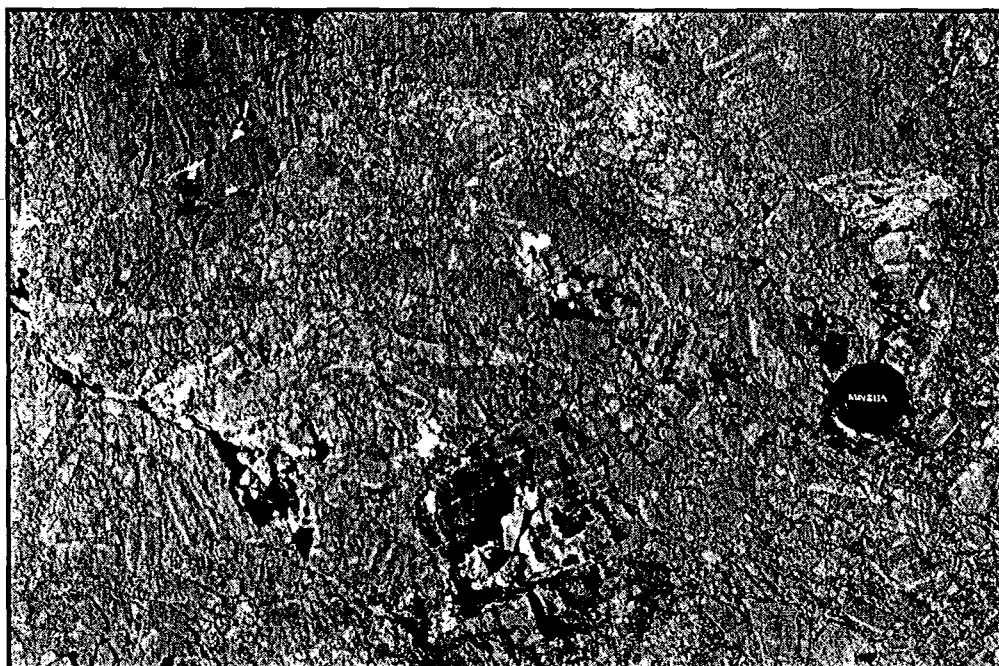


Figure 4.12: The Brecciated Member of the Bear Rock Formation at the type section near Fort Norman. This photo was taken approximately 20 metres below the base of the Landry Member. The exposure is predominantly medium to dark grey rubble packbreccia. The dolomite and limestone clasts are angular, granule to boulder sized, and set in a matrix of lime mudstone (micrite).

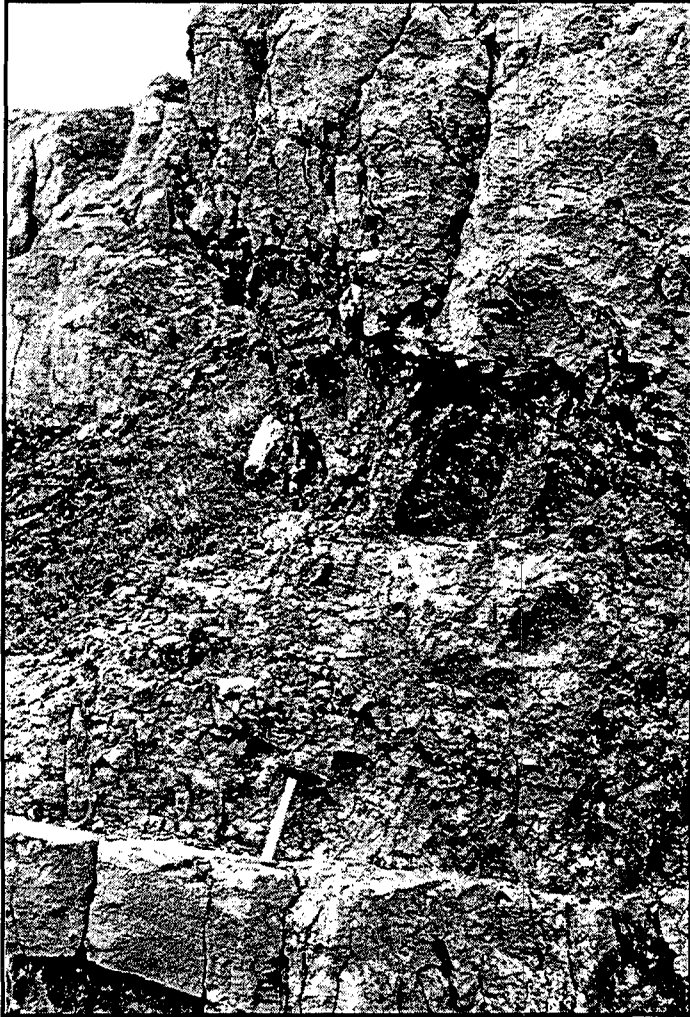


Figure 4.13: The Landry Member of the Bear Rock Formation. This exposure is on the east wall of Dodo Canyon at the Dodo Canyon Site. The Landry consists of alternating sequences of massive, resistant, blue-grey weathering lime mudstone and recessive, thinly bedded, lime mudstone. The hammer is resting on a resistant bed, a crackle breccia fabric occurs throughout the section.

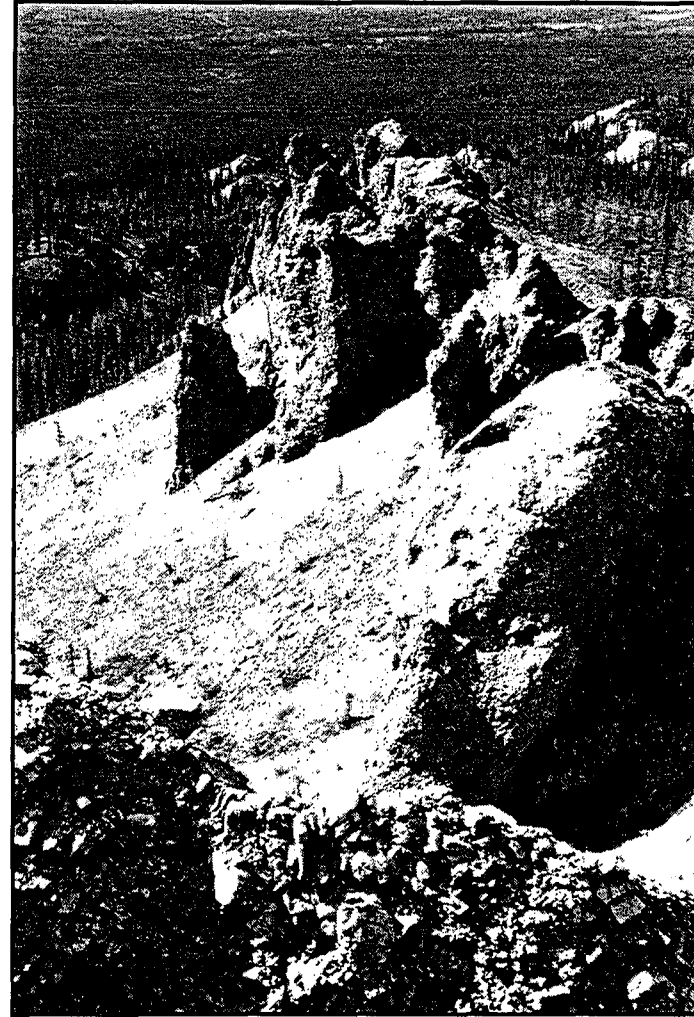


Figure 4.14: The Brecciated Member of the Bear Rock Formation at the Bear Rock Site. Much of the exposure is particulate rubble floatbreccia, though many of the clasts are in close proximity (foreground). Rounding of clasts is due to solution following exposure. The pinnacles occur on the crest of a whaleback ridge and are Holocene features. They are generated by solution and frost action.

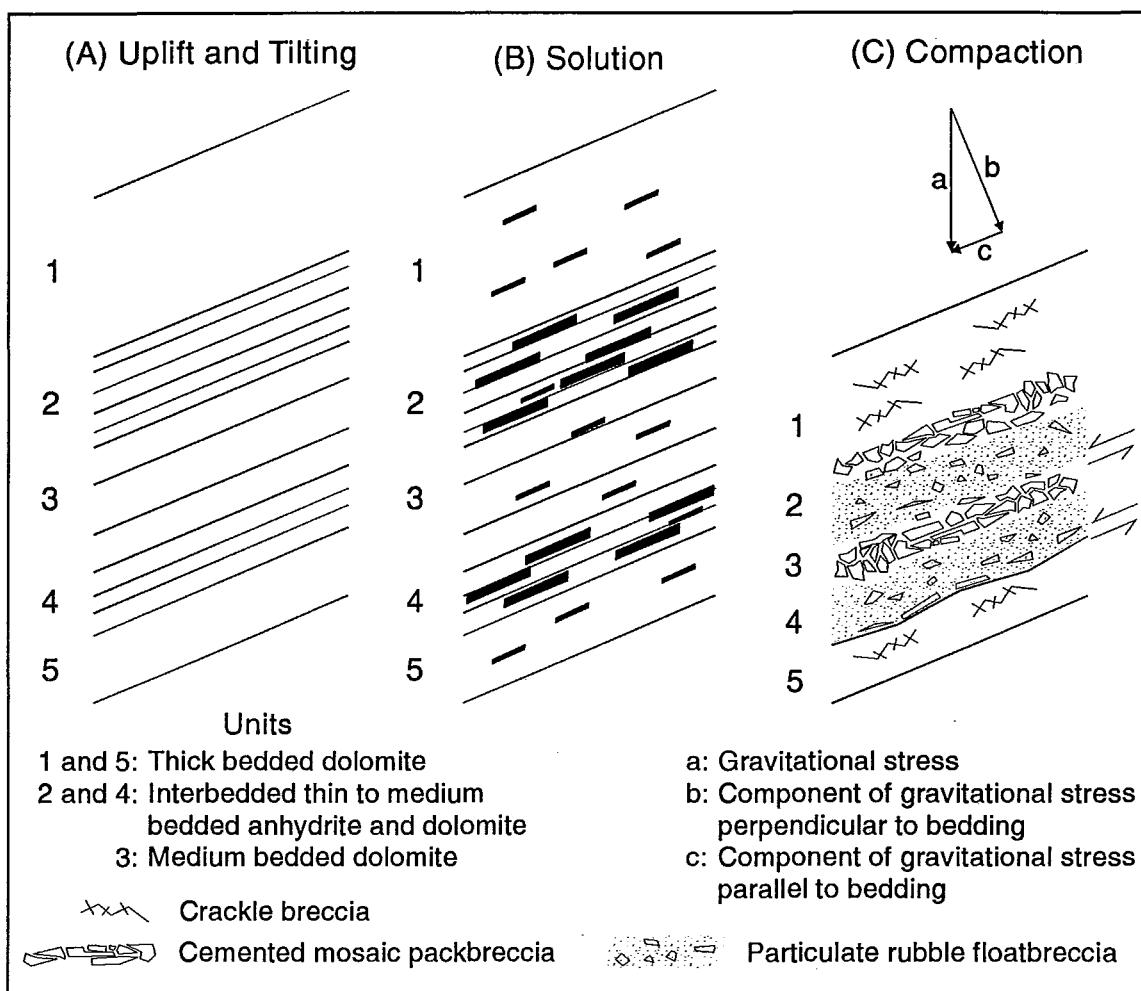


Figure 4.15: The solution brecciation process as outlined by Stanton (1966) involves: (i) initial solution of evaporite minerals (in the order: sodium and potassium salts, hydration of anhydrite to gypsum, expansion, solution of gypsum); (ii) initial subsidence of overlying strata into void spaces; (iii) fragmentation of strata accompanying subsidence; (iv) deformation of evaporite, entrainment of carbonate clasts through the evaporite; (v) continuing solution, gradual development of a grain or clast supported mass; (vi) compaction and subsidence of the mass; (vii) complete solution of evaporite. The above model is from Morrow (1991), it illustrates the early and late stages of Stanton's process and accounts for variations in breccia fabric observed in the Bear Rock Formation. Brecciation of the unweathered interbedded dolomite and anhydrite follows exposure to meteoric groundwater. (A) Uplift brings these strata to the shallow subsurface, steepens the hydraulic gradient, and increases the depth of groundwater circulation. (B) Anhydrite is preferentially dissolved creating voids parallel to bedding (shown as black). (C) Gravitational compaction of thin dolomite beds generates platy fragments that are oriented parallel to bedding by a component of shear (c) developed against less compactable, thicker dolomite beds. Intervals of thinly bedded dolomite and anhydrite are altered to particulate rubble floatbreccia, while intervals of medium and thick bedded dolomite are represented by cemented mosaic packbreccia. Overall the degree of brecciation decreases from the base of the lowest anhydrite rich beds to the overlying thick bedded dolomites, which are crackle breccia.

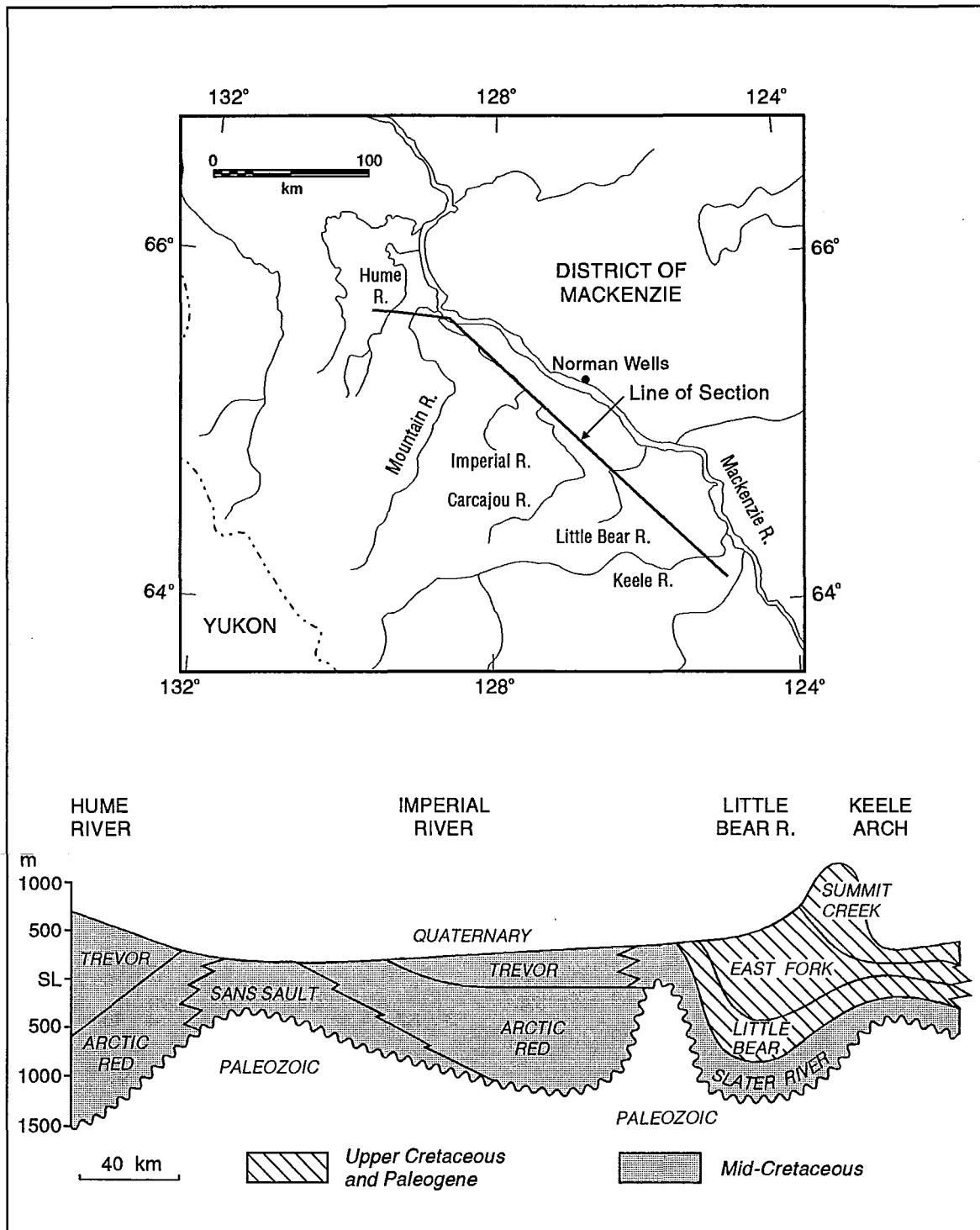


Figure 4.16: Schematic diagram showing the distribution of formations comprising the Cretaceous and Tertiary clastic wedges of the Peel Trough. The line of section passes from Hume River down the length of the Mackenzie Plain to Keele River (from Yorath, 1991; after Yorath and Cook, 1981).

CHAPTER V

QUATERNARY OF THE NORTHEASTERN MACKENZIE MOUNTAINS

5.1 Introduction

This chapter reviews the Quaternary of the District of Mackenzie with a focus on glaciation of the northern Mackenzie Mountains. Mackay (1958, 1963) and Craig (1960, 1965) conducted the first extensive Quaternary studies in the Mackenzie Valley. Terrain mapping accompanied Project Norman and the Northern Pipeline Study (Hanley and Hughes, 1973a, 1973b, 1973c; Hanley *et al.*, 1975; Hughes, 1970; Hughes *et al.*, 1972a, 1972b; Hughes and Pilon, 1973; Rutter, 1974). Data on regional glacial limits and chronology are reviewed by Hughes (1972, 1987, 1989), Hughes *et al.* (1981), Rampton (1982, 1988) and Vincent (1989). Duk-Rodkin and Hughes (1991) and Ford (1976) describe the glacial records of the northern and southern Mackenzie Mountains. Vincent (1982, 1983, 1984) and Vincent *et al.* (1983) review the glaciation of Banks Island, and Catto (1986) that of the Richardson Mountains. The glacial history of Yukon Territory is reviewed by Hughes *et al.* (1989a), the eastern Cordillera by Jackson *et al.* (1989), and unglaciated areas by Hughes *et al.* (1989b).

Ice sources that have influenced northwestern Canada include the Cordilleran Ice Sheet, small montane cirque and valley glaciers, and the Laurentide Ice Sheet. These ice masses have repeatedly fluctuated in the Pleistocene, producing a terrestrial stratigraphic and geomorphic record that is complex and displays considerable spatial variation. The approximate Wisconsinan limits of the Laurentide and Cordilleran Ice Sheets show much of the Canyon Ranges are unglaciated (Figure 5.1).

In the Wisconsinan, Laurentide ice advanced northwesterly from Great Bear

and Great Slave Lakes across the Mackenzie Valley to the Mackenzie Mountains. The Mackenzie Lobe spread north to the Beaufort Sea and Yukon Coastal Plain. In the low Arctic, ice lobes advanced westerly through Amundsen Gulf and M'Clure Strait to Banks Island. Laurentide Ice was deflected south of Nahanni River and coalesced with the Cordilleran Ice Sheet on the Liard Plateau. Cordilleran ice spread from the Selwyn and Pelly Mountains to the Yukon Plateau and Backbone Ranges of the Mackenzie Mountains.

5.2 Regional Glacial Chronologies

The following sections review the glacial chronologies and ice limits from several areas in northwestern Canada (Figures 5.2, 5.3). With exception of the most recent events, glacial limits are poorly defined and controls on dating few. Thus, interpretations of the available evidence vary. Table 5.1 lists chronological data discussed in this text. Site locations are indexed on Figures 5.1 and 5.3. Late Wisconsinan retreat positions of the Laurentide Ice Sheet are indicated on Figure 5.4.

5.2.1 Yukon Territory

Bostock (1966) identified four Cordilleran glacial advances in Yukon Territory. From oldest to most recent they are: Nansen, Klaza, Reid, and McConnell Glaciations (Figure 5.2). Lava and tephra separate deposits of the Nansen and Klaza events at Fort Selkirk (0.84 to 1.08 Ma, Naeser *et al*, 1982). Both glaciations are recognized as pre-Illinoian (middle and early Pleistocene; Vincent, 1989; Tarnocai and Schweger, 1991). The limits of the Nansen and Klaza are mapped only in the western Yukon (Figure 5.3). Thick luvisols have developed on these deposits, brunisols and regosols characterize younger surfaces (Hughes *et al*, 1972c; Tarnocai *et al*, 1985).

The limits of the Reid and McConnell Glaciations are well defined across the Yukon Plateau and correlate with the Mirror Creek and Macauley Glaciations of the Snag-Klutan region (Hughes *et al*, 1969, 1983; Rampton, 1971), and with a series of

tills in southeastern Yukon (Hughes *et al*, 1989a). Dating from Mayo and Stewart River provide minimum ages for the Reid Glaciation of >46,580 BP (GSC-331) and >42,900 BP (GSC-524). A K-Ar date of 0.23 Ma from basalt underlying the southeastern Yukon equivalent provides a maximum age (Klassen, 1978, 1987). At the Stewart River site, Sheep Creek tephra overlies the Reid deposit (~75-80 ka: Hamilton and Bischoff, 1984), and at Kluane Lake, Old Crow tephra mantles the Mirror Creek drift (~80-130 ka: Schweger and Matthews, 1985; Wintle and Westgate, 1986; Berger, 1987; Hughes *et al*, 1989a). The Reid Glaciation is no younger than Early Wisconsinan and many researchers favour an Illinoian assignment (Hughes, 1989; Hughes *et al*, 1989a; Vincent, 1989; Matthews *et al*, 1990). The McConnell Glaciation is recognized as Late Wisconsinan, maximum dates of 29,600 BP (GSC-769) and 23,900 BP (GSC-2811) occur at Kluane Lake and Liard Lowland. Deglaciation in the southern Ogilvie Mountains and the Snag-Klutan region began before 13.7 ka (Vernon and Hughes, 1966; Rampton, 1971).

5.2.2 Banks Island, Tuktoyaktuk Coast

In the western Arctic there is evidence of several glaciations, data are available from Banks Island where the limits of three major glaciations are mapped (Vincent, 1978, 1982, 1983, 1984, 1989; Vincent *et al*, 1983; Figures 5.2 and 5.3). The relative ages of these events are established but absolute dating is not conclusive. On Banks Island, a series of Laurentide tills overlie the Late Pliocene Worth Point Formation. These tills represent the oldest and most extensive glacial event, the Banks Glaciation. The deposits are magnetically reversed and are therefore Early Pleistocene in age (Vincent and Barendregt, 1987). The following Middle Pleistocene Thomsen Glaciation and the equivalent Mason River Glaciation of western Bathurst Peninsula were less extensive events (Rampton, 1988). Paleocological data suggest the Banks and Thomsen Glaciations were followed by interglacials that were warmer than present (Vincent, 1989).

The Wisconsinan Stage of Banks Island is subdivided into the McClure and

Russell Stadials of the Amundsen Glaciation (Vincent, 1983, 1984). During the M'Clure Stadial, Laurentide ice expanded to eastern and northern Banks Island (Vincent, 1983). On the northern mainland, ice was wholly absent from Bathurst Peninsula, Brock Upland, and much of Tuktoyaktuk Peninsula (Toker Point Stadial; Rampton, 1988). The Russell Stadial is the least extensive of the recognized glacial advances, influencing only the northeastern extreme of Banks Island. During the equivalent mainland event (Sitidgi Stadial), Laurentide ice advanced northwestward from Great Bear Lake to the Mackenzie Delta (Rampton, 1988). Two distinct limits occur in association with the Sitidgi Stadial. They are the Tutsieta and Kelly Lake Phases (Hughes, 1987).

Dating of these stadials and equivalent events in the northern Cordillera have been the subject of considerable debate. The M'Clure Stadial is considered either Early Wisconsinan (Vincent, 1982, 1983; Vincent and Prest, 1987), or Late Wisconsinan (Denton and Hughes, 1983; Dyke, 1987). Evidence supporting the former interpretation include a number of absolute dates and correlation of glacial units with adjacent regions. Shells collected from marine sediments directly underlying a M'Clure till in southern Banks Island provide a maximum date (>37,000 BP: GSC-3698, and U/Th 92.4 ka: UQT-143; Vincent, 1989). On northern Banks Island, autochthonous moss overlying marine sediments, associated with the M'Clure Stadial, provide a minimum date (>41,000 BP: GSC-1088). Shells thought to be contemporaneous are >19,000 BP, 24,730 BP, and 46 ka (GSC-1478, TO-650, UQT-142; Vincent, 1989). Based on these dates and additional amino acid ratio data, Vincent and Prest (1987) favour a pre-Late Wisconsinan assignment. Tills on Melville Island thought to be equivalent to M'Clure units are overlain by shells that support this interpretation (Hodgson *et al*, 1984).

Glacial ice of the M'Clure/Toker Point Stadial was too thin to cover Bathurst Peninsula and Brock Upland of the northern District of Mackenzie. There are two glacial limits recognized around the perimeter of Brock Upland, an upper limit at 450-600 m, and a lower limit at approximately 300 m. Vincent (1984) suggests the

upper limit is Early Wisconsinan and the lower, Late Wisconsinan. Hughes (1987) assigns the upper limit to the Tutsieta Lake Phase of the Russell/Sitidgi Stadial. St-Onge (1987) also considers both limits to be Late Wisconsinan. The Tutsieta limit is traced to the south and west into the Mackenzie Valley.

M'Clure/Toker Point Stadial ice also advanced across the Mackenzie Delta to southern Tuktoyaktuk Peninsula (Rampton, 1988). Shell fragments lying above sediments associated with this stadial have yielded minimum dates of >35,000 BP (GSC-562) and >37,000 BP (GSC-690) from Garry and Kendall Islands. These fragments may, however, be reworked from older deposits (Hughes, 1987). Additional dates from shells overlying till on Garry and Kendall Islands suggest a pre-Late Wisconsinan assignment for the Toker Point Stadial (43,550 BP: TO-796; 48,200 BP: RIDDLE-801; Vincent, 1989). Rampton (1982) mapped the glacial limit of the Toker Point equivalent on the eastern Yukon Coastal Plain, locally termed the Buckland Glaciation. Based on correlation with glaciomarine sediments in coastal Alaska, Vincent (1989) suggests an Early Wisconsinan date. However, the oldest minimum date on the Buckland Glaciation is 22,400 BP (GSC-1262) and Hughes (1987) argues the Buckland Glaciation is synchronous with the Hungry Creek Glaciation of Bonnett Plume Basin.

5.2.3 Bonnett Plume Basin, Richardson and Franklin Mountains, Mackenzie Valley

Bostock (1948) traced the limit of the last glaciation on the eastern slopes of the Richardson Mountains to 1000 m elevation. Mapping by Hughes (1972) placed the Wisconsinan limit farther east, at a series of moraines that are approximately equivalent to the Sitidgi Lake Stadial of the Arctic coast (Rampton, 1982). Subsequent reinterpretation by Hughes *et al* (1981), Catto (1986), and Hughes (1987) has moved the Wisconsinan margin westward to 900 m elevation south of Rat River and approximately 1100 m in Bonnett Plume Basin. This is recognized as the local all-time limit of the Laurentide Ice Sheet.

Till of this advance is preserved in the upper Rat River Valley where it underlies proglacial lacustrine sediments (Catto, 1986). Organic material incorporated into the lake deposits provides a minimum date on this glaciation (21,300 BP: GSC-3371; 21,200 BP: GSC-3813). At Hungry Creek in Bonnett Plume Basin, a single Laurentide till and a sequence of glaciofluvial sediments overlie deltaic and fluvial deposits (Hughes *et al*, 1981). Allochthonous wood fragments in the lower unit provide a maximum date on the Hungry Creek Glaciation (36,900 BP: GSC-2422).

During this glaciation, Laurentide Ice advanced across the Franklin Mountains and Mackenzie Valley to the eastern Richardson Mountains. Glacial ice infilled Bonnett Plume Basin and impeded drainage of eastward flowing rivers. Peel River backed up via the Eagle River into the Porcupine system. The route of the latter through McDougall Pass was blocked. As a result, lake basins developed in portions of the Porcupine watershed in the unglaciated Yukon (Hughes, 1972; Hughes *et al*, 1989b). The sediments of Old Crow and Bluefish Flats record a history of flooding related to the damming of the ancestral Porcupine River by Wisconsinan Laurentide advances. Based upon sedimentation in the Porcupine River in Alaska, Thorson and Dixon (1983) conclude there were at least three glacial lacustrine phases in the Wisconsinan, with two events after 31 ka. Morlan (1980) and Hughes *et al* (1981) have found evidence for only one event in the Late Wisconsinan. Maximum dates on the most recent inundation are provided by: (i) organic debris underlying lacustrine sediments at Old Crow Flat (31,300 BP: GSC-1191), (ii) a mammoth tusk underlying lacustrine sediments at the nearby Cadzow Bluff (25,170 BP: NMC-1232), and (iii) plant debris occupying the same stratigraphic position at Bluefish Flats (20,800 BP: GSC-3946). At Doll Creek, organic silts overlying deposits of the Hungry Creek Glaciation suggest Laurentide ice was retreating from Bonnett Plume Basin by 16,000 BP (GSC-2690). At Old Crow Flats, fluvial sediments dated at 12,460 BP (I-3574) overlie the lacustrine deposits.

The Hungry Creek Glaciation may have culminated as early as 25 ka ago (Schweger, 1989), and is considered by Hughes (1987) and Duk-Rodkin and Hughes (1991) to represent the all-time Laurentide advance in the northwestern District of Mackenzie. Vincent (1989) favours assigning the glaciation to the late Middle Wisconsinan or the early Late Wisconsinan. Moraines of the Hungry Creek Glaciation are approximately contiguous with the Early Wisconsinan Buckland Glaciation of Rampton (1982). Hughes (1987) and Tarnocai and Schweger (1991) assign the Buckland to the Late Wisconsinan. The glacial advance denoted by these moraines was extensive enough to cover the entire Mackenzie Delta and the southern Beaufort Sea. However, data do not support an extensive ice advance on the Arctic coast in Late Wisconsinan time (Vincent, 1989). There remains some debate regarding the timing of this event.

Following retreat from the Hungry Creek maximum, a readvance of the Mackenzie Lobe is marked by a series of moraines east of the Mackenzie River (Hughes, 1987). At Tutsieta Lake, well-preserved moraine ridges and hummocky features extend to the north and are continuous with moraines mapped by Rampton (1980) at Sitidgi Lake in the Inuvik area. Eastward, the Tutsieta moraines extend through the Anderson River basin to the western flank of Brock Upland. Minimum dates on the Tutsieta Lake Phase are derived from organic materials in the Sitidgi Lake region (12,900 BP: GSC-1784-2; 13,000 BP: GSC-1995; 13,100 BP: GSC-3387). Hughes (1987) assigns a date of 13 ka to the Tutsieta Moraine. The position of the ice margin west of the Mackenzie River during the Tutsieta Phase is uncertain. A series of moraines just west of Peel River on the eastern slopes of the Richardson Mountains may be correlative (Hughes, 1987).

A major stillstand or minor readvance of Laurentide ice is marked by a single sharp moraine or a belt of hummocky moraine extending from Kelly Lake northward in the Norman Range. The area west of Kelly Lake (Franklin Mountains) was deglaciated well before 11 ka. Wood fragments dated at 10,600 BP (GSC-2328) occur in deltaic sediments associated with Glacial Lake Mackenzie in the Fort

Norman area. On this basis, Hughes (1987) assigns a minimum date of 10.6 ka to the end of the Kelly Lake Phase. In addition to moraines marking the Hungry Creek, Tutsieta, and Kelly Lake events, there are many fragments of hummocky moraine present in the Mackenzie Valley that are not assigned to a particular phase or stadial.

Glaciolacustrine deposits mantle much of the surface of the Mackenzie Plain (Mackay and Mathews, 1973). Following the Kelly Lake Phase and retreat of the Mackenzie Lobe, a long linear proglacial lake developed in the Mackenzie Valley between Fort Good Hope and Fort Simpson (Smith, 1992). The Mountain River area was deglaciated before 11,760 BP (TO-1190) and Fort Norman by 11,530 BP (I-15020). Glacial Lake Mackenzie persisted between at least 11.8 and 10.3 ka and achieved a maximum depth of 80 m in the Fort Norman region. Deltaic sequences occur along most tributaries at the former shoreline of this glacial lake (Smith, 1992). Given the older dates associated with Glacial Lake Mackenzie, the Kelly Lake moraine must date to at least 12 ka.

5.3 Mackenzie Mountains

The geomorphic and stratigraphic records of the Mackenzie Mountains show repeated glacial advances from three sources: (i) the Laurentide Ice Sheet, (ii) large montane glaciers emanating from the Backbone Ranges, and (iii) small cirque, valley, and piedmont glaciers in the Canyon Ranges (Ford, 1976; Duk-Rodkin and Hughes, 1991). The all-time limit of the Laurentide Ice Sheet extends to approximately 1500 m on the eastern flank of the Mackenzie Mountains (Hughes, 1972). It is considered Wisconsinan by many workers, but there is considerable debate regarding timing of the event (Rutter, 1974; Hughes *et al*, 1981; Prest, 1984; Hughes, 1987; Vincent and Prest, 1987; Vincent, 1989). In the Nahanni region, older Laurentide deposits (Illinoian) occur beyond the Wisconsinan limit (Ford, 1976), but equivalent units are not recognized northward. The behaviour of montane ice in the Mackenzie Mountains was largely independent of the Cordilleran Ice Sheet, and topography strongly controlled ice flow. Extensive areas in the Canyon

Ranges are characterized by cryoplanation features and tors, suggesting a history of infrequent or no glaciation (Hughes, 1972; Hughes *et al.*, 1989b).

5.3.1 Southern Mackenzie Mountains

Laurentide glacial deposits identified in the Nahanni region are assigned to a series of three glaciations (Figures 5.2, 5.3) (Ford, 1973, 1976; Brook, 1976). The oldest and most extensive deposit is a thin lag of scattered till and erratics occurring as far west as the eastern flank of Nahanni Plateau. At First Canyon, shield erratics are found to an elevation of 1400 m and occur at elevations between 1400 and 1600 m across the plateaux to the north (Ford, 1976). This unit is assigned to the First Canyon Glaciation. During this advance, Laurentide Ice pushed across the Nahanni Range to Nahanni Plateau. The thin, discontinuous, and highly weathered state of the till is interpreted as evidence of the event's antiquity (Ford, 1976). Uranium thorium ages on cave speleothem from First Canyon provide dating control on this glaciation. Speleothem growth occurred between 320-275 ka and 220-190 ka, these intervals represent interglacial periods (Grotte Valerie Interglacials I and II). Samples of older speleothem overlie fluvial sediments that are dominated by shield erratics. This fill is attributed to the First Canyon Glaciation and based on the speleothem data it is given an age >350 ka (Ford, 1976; Harmon *et al.*, 1977). Geomorphic evidence from Virginia Falls indicates a concurrent montane advance correlating with the First Canyon Glaciation.

West of Yohin Ridge, a belt of hummocky ground moraine marks the terminal position of the Clausen Glaciation (Ford, 1976). During this advance, Laurentide ice blocked the outlet of the eastward flowing Nahanni River, impounding a lake in the Nahanni and Flat River Valleys (Glacial Lake Nahanni). There is evidence of two lake phases separated by a period of erosion. In Grotte Valerie, Glacial Lake Nahanni deposits onlap in situ speleothem dated between 220 and 190 ka. This provides a maximum date for the early lake phase and glaciation (Ford, 1976). In the Upper Nahanni and Flat River Valleys, the Clausen Glaciation

was preceded by at least one montane glaciation, the Flat River Glaciation. Ice advanced to the east from the Ragged Range and Logan Mountains. The limits of this event are marked by ice marginal channels and breached divides. Lacustrine deposits from Glacial Lake Nahanni overlie and infill some Flat River glacial meltwater features. Ford (1976) favours an Illinoian assignment for the Clausen/Flat River Glaciation (>145 ka) but does not oppose the view that it is Wisconsinan. It may be correlative with the Reid glaciation of the Cordilleran Ice Sheet in Yukon Territory (Jackson *et al*, 1989) and the Thomsen Glaciation of the western Arctic (Vincent, 1989).

The limit of the third Laurentide advance is marked by a sharp ice-contact moraine at an elevation of 500 to 800 m on the eastern flank of the mountain front. This Jackfish Glaciation confined a lake in the lower South Nahanni Valley, Glacial Lake Tetcela. The penecontemporaneous montane Hole-in-the-Wall Glaciation was of limited extent, with valley glaciers extending only a few kilometres from cirques in the Ragged Range. The Jackfish/Hole-in-the-Wall Glaciation is considered Late Wisconsinan by Ford (1976).

Reconnaissance work in the southern Mackenzie Mountains has also been undertaken by Rutter and Minning (1972), Rutter and Boydell (1973), and Rutter, (1974). Meltwater channels at an elevation of 1525 m west of the Nahanni Range and 1295 m near Wrigley Lake define the extent of the all-time Laurentide advance. The limit of a more recent advance is observed at a lower elevation. Unlike the chronology presented by Ford (1976) and Harmon *et al* (1977), both events are considered Late Wisconsinan by Rutter (1974). Vincent (1989) suggests the Clausen Glaciation may be Wisconsinan and approximately equivalent to the upper limit described by Rutter.

5.3.2 Northern Mackenzie Mountains

Operation Norman and the Northern Pipeline Study included preliminary examinations of the surficial geology of the northern Mackenzie Mountains (Hughes,

1970; Hughes *et al* 1972a, 1972b). Duk-Rodkin initiated a comprehensive glacial study in 1986, involving detailed aerial photograph interpretation and several summers of field work in the Canyon Ranges between Redstone and Arctic Red Rivers (Duk-Rodkin and Hughes, 1991). Tarnocai and Schweger (1991) review data on Middle Pleistocene deposits from the Canyon Ranges. In addition, the present author has undertaken mapping in the area east of the Laurentide limit between Little Bear River and Katherine Creek (Figure 5.6).

Topography controlled the extent of Laurentide ice penetration into the Mackenzie Mountains. Ice tongues advanced tens of kilometres past the mountain front into Redstone, Keele, Carcajou, Little Keele, Imperial, Mountain, and Gayna River Valleys. Large icefields in the Backbone Ranges supplied eastward advancing montane valley glaciers. Also, high cirques in the Canyon Ranges supported valley and piedmont glaciers. The morphology of ice marginal features, the distribution of erratics, and the occurrence of extraglacial features, such as cryoplanation surfaces and tors, are used to establish the limits of montane and Laurentide ice. Moraines and meltwater channels delimit advance positions and stillstands during retreat. Erratic lithology defines source areas for glacial deposits; sediments of montane origin lack shield clasts. In some areas, extensive deposits of glaciolacustrine and glacial diamictons are identified. Stratigraphic relationships, relative dating and correlation with areas to the north and west provide control on event chronology.

The following sections review the salient characteristics of the glaciation of the northern Mackenzie Mountains. Figure 5.5 illustrates the regional limits of Laurentide and montane ice during the Late Wisconsinan. Figure 5.6 shows the distribution of moraines and meltwater channels in the study area.

5.3.2.1 Pre-Wisconsinan Events

There are no pre-Wisconsinan Laurentide deposits recognized in the northern Mackenzie Mountains. However, the morphology of numerous glacial troughs, stoss and lee forms, and large meltwater channels suggest it is highly probable that in the

Pleistocene, Laurentide ice has repeatedly advanced to the eastern ranges of the Mackenzie Mountains.

Evidence of Early and Middle Pleistocene montane glaciations in the Canyon Ranges are preserved at a section located above treeline on the south bank of Little Bear River (64°27'42"N Lat., 126°43'18"W Long.). The surface material is outwash from a Wisconsinan Laurentide event. It overlies five glacial diamictons of montane origin that rest locally on colluvium of the Franklin Mountain Formation. Valley glaciers advancing from high ground in the Carcajou Range deposited these tills. Paleosols are present at the upper surface of each of these till units (Tarnocai and Schweger, 1991). These paleosols lack A horizons and the upper portions of the B horizons, but they are considerably thicker than the modern soil. They represent periods of pedogenesis during interglacials. There are no indications of cryoturbation and the pollen record suggests closed boreal forest conditions. Solum thickness, rubification, and the occurrence of argillans increase from the youngest to the oldest paleosols. Tarnocai and Schweger (1991) speculate they may represent a gradual deterioration in interglacial climate. This is consistent with observations in Yukon Territory where paleosols of the Late Tertiary and Early Pleistocene are indicative of a much warmer and moister climate.

At the Little Bear Site, an infinite radiocarbon date of >47,000 BP (GSC-1618) occurs between the uppermost montane tills (units five and four). Wood dated at 44,420 BP (TO-195) underlies the Laurentide deposit, but the wood fragments are detrital and may not accurately date the Laurentide event (Duk-Rodkin and Hughes, 1991). The upper montane till (unit five) may correlate with the Yukon Reid Glaciation. The lower four units are considered pre-Reid age (Tarnocai and Schweger, 1991). Of the three montane glaciations recorded in the southern Ogilvie Mountains (Vernon and Hughes, 1966) only the oldest is pre-Reid. The others are equivalent to the Reid and McConnell Glaciations (Duk-Rodkin and Hughes, 1991). At Katherine Creek, a series of montane tills underlying Laurentide deposits provide additional evidence of multiple pre-Wisconsinan advances of montane ice.

Moraines of montane origin occur at several other locations in the Canyon Ranges. Many of these represent deposition from small local glaciers and others from large valley glaciers spreading eastward from the Backbone Ranges. At Dark Rock Creek, south of Keele River, lateral moraines of a montane glaciation emanate from an area of cirques in the Tigonankweine Range. These moraines are truncated by a Laurentide advance of Hungry Creek age (see below). A second set of montane features extends onto the Hungry Creek deposits. The penultimate montane event, the Dark Rock Creek I, is considered Reid (Illinoian) age (Duk-Rodkin and Hughes, 1991). The second montane glaciation is considered equivalent to the McConnell Glaciation (Dark Rock Creek II). In general, moraines of the penultimate montane glaciation are subdued in their morphology and contrast with the sharp forms of McConnell age.

5.3.2.2 Hungry Creek Glaciation

The limit of the most extensive Laurentide glaciation in the Canyon Ranges is delineated by ice marginal features and shield erratics (Figures 5.5, 5.6). This limit occurs to elevations of approximately 1550 m in the Landry Range, 1430 m in the Carcajou Range, 1200 m near Katherine Creek, and 1100 m at Arctic Red River. In all, the limit declines at a rate of about 1.2 m km^{-1} northward from Keele River (Duk-Rodkin and Hughes, 1991). Laurentide deposits from this event are generally thin and discontinuous. Well rounded, granule to boulder sized erratics of granite gneiss comprise less than 5% of the coarse fraction of surficial materials. Moraine features are subdued but are traceable northward where they are contiguous with moraines of the Hungry Creek Glaciation mapped around the perimeter of Bonnett Plume Basin (Duk-Rodkin and Hughes, 1991). These moraines are correlated with the Buckland Glaciation of the Yukon Coastal Plain. Soils developed on these deposits are primarily thin brunisols and regosols, weathering rinds on shield erratics are 1 to 2 mm in thickness. These data indicate the most extensive Laurentide event is Wisconsinan age and Duk-Rodkin and Hughes (1991) assign it to the Hungry Creek

Glaciation. Downslope of the Hungry Creek maximum, there are sets of moraines denoting stillstands and minor readvances during the Late Wisconsinan.

The intrusion of Laurentide ice into mountain valleys profoundly influenced drainage. During the Hungry Creek Glaciation and subsequent stadials, proglacial lakes were impounded and drainage was diverted to the northwest along passes that join the main valley systems (Figure 5.5). Major spillways extended from the headwaters of the Little Keele and Carcajou Rivers to Mountain and Gayna Rivers. These channels incise deposits of piedmont glaciers that are likely of Reid age. Thick sequences of glaciolacustrine deposits mark the extent of the largest glacial lakes in the Keele and Mountain River Valleys. As the Laurentide Ice Sheet retreated, the positions and extent of proglacial lakes and ice marginal meltwater channels shifted frequently, utilizing lower passes as they were deglaciated. In the Canyon Ranges, numerous underfit channels and canyons occupy anomalous drainage positions that were carved by ice marginal and subglacial meltwaters (Section 5.3.2).

Bracketing dates on the Hungry Creek Glaciation in Bonnett Plume Basin are 36,900 BP (GSC-2422) and 16,000 BP (GSC-2690) (Section 5.1.3). In the northern Mackenzie Mountains, dates from outside this limit are available from Keele and Andy Lakes (Szeicz, personal communication, 1993). Keele Lake is located approximately 2 km south and 300 m above the Hungry Creek maximum in Keele River Valley. Basal sediments were expected to yield an infinite age but were dated at 11,900 BP (TO-2298). This lake could have been affected by the Dark Rock II montane advance that followed the Hungry Creek maximum. Andy Lake is located near the headwaters of Little Keele River and has a basal date of 12,060 BP (TO-2295). It is also likely this lake received sediments from the most recent montane advance.

5.3.2.3 Katherine Creek Phase

Following the Hungry Creek maximum, Laurentide ice retreated eastward. Montane

ice then advanced from high ground to positions down slope of the Hungry Creek limit. This is recorded at Dark Rock Creek, Little Bear River, Katherine Creek, and at other locations. The duration and extent of the Dark Rock Creek II event is not known. A readvance of Laurentide ice ensued, termed the Katherine Creek Phase (Duk-Rodkin and Hughes, 1991). In the Moose Horn Valley, tributary to the Redstone River, a belt of hummocky moraine and kame occurs where montane and Laurentide ice coalesced during this phase.

At the Katherine Creek type location, lateral moraines, outwash, and meltwater channels of montane origin extend beyond the Hungry Creek limit (Figure 5.6). In turn, ice marginal Laurentide moraines truncate these montane features. Similar Laurentide features occur sporadically to the southeast on the flanks of the ranges stretching to Rouge Mountain River (Figure 5.6). Those occurring between Katherine Creek and Little Bear River were located on aerial photographs. These data were transferred to 1:50000 and 1:250000 scale maps. The topographic base maps available from this region are provisional and elevations poorly controlled. Errors of ± 50 m are expected in data transfer.

Small meltwater channels occur on mountain slopes and across high passes to elevations of 1080 m, and are common between 1020 and 1070 m (3350 to 3500 ft) (Figure 5.6). These represent drainage routes at the upper margin of Laurentide ice mass during the peak of the Katherine Creek Phase. The Katherine Creek moraine attains a maximum elevation of 1020 m (3350 ft) at the type area; approximately 160 vertical metres below the Hungry Creek limit. Elsewhere, moraine elevations vary with local topography. A large number occur between 915 and 975 m (3000 to 3200 ft) and a second group between 1000 and 1070 m (3300 to 3500 ft). While those of the latter group are less continuous, there are no apparent differences in the degree of preservation of these moraine sets, and all are interpreted as deposits of the Katherine Creek Phase. Duk-Rodkin and Hughes (1991) favour a contemporaneous age assignment for similar features to the south.

Tills from the Hungry Creek and Katherine Creek events are sparse, and

fragments of recessional moraine uncommon. Large areas are characterized by a thin patchy veneer of waterlain sediments of glaciolacustrine and fluvioglacial origin. During ice retreat, much of the landsurface was exposed to meltwater erosion and drift remobilized. Materials deposited in canyons and large valleys have been reworked since deglaciation. However, local glacial deposits may approach tens of metres in thickness. Many higher peaks and cirques in the Carcajou Range would have existed as nunataks during the Katherine Creek Phase. Relatively thick morainal and glaciolacustrine deposits occur where Laurentide ice advanced up narrow valleys into small cirques, creating sediment traps. Moraine morphology suggests that in some instances these cirques may have been occupied by small ice bodies. Other montane moraines extend down valley, below the Katherine limit, implying that a minor advance of cirque glaciers followed the Katherine Creek maximum. Evidence suggests that proglacial lakes were impounded in the Little Keele, Carcajou, and Rouge Mountain River Valleys by ice dams in Carcajou Canyon. At Bonus Lake, sediments from a lake phase partially infill sinkholes developed in the Hume Formation. Excavations show these materials are massive silts, revealing periods of rapid sedimentation (Section 5.2.2.6).

Dating control of the Katherine Creek Phase is provided by a single radiocarbon age, correlation with nearby areas, and the weathering state of deposits. Bells Lake is located north of Katherine Creek about 16 km west of the Dodo Canyon Site. The lake is at the limit of the Katherine Creek Phase. Basal sediments provide a minimum age of 10,230 BP (TO-2375; Szeicz, personal communication, 1993). The Katherine Creek Phase is younger than the Hungry Creek Glaciation and older than the 13 ka Mackenzie Valley Tutsieta Lake Phase. Duk-Rodkin and Hughes (1991) speculate the Katherine Creek Phase may be equivalent to the extensive Sabine Stadial of the Yukon Coastal Plain Buckland Glaciation (Rampton, 1982).

5.3.2.4 Tutsieta and Kelly Lake Phases

Moraines of the Tutsieta Lake Phase are strongly developed east of the Mackenzie Delta. Extrapolation of that limit to the Mackenzie Mountains places the ice margin between 450 and 600 m elevation. There is some evidence of a prolonged stillstand of Laurentide Ice at that position in the Canyon Range. A series of narrow, discontinuous, parallel benches extends on the eastern flank of MacDougal Anticline, across Dodo Mountain, northward to Katherine Creek. These benches cut across structure at elevations between 580 and 600 m and are interpreted as ice marginal channels. West of Dodo Mountain, large intact blocks of the Mount Kindle Formation have been displaced forming a moraine at 620 m. These features may be above the Tutsieta limit. In addition, there is a series of large meltwater channels occurring between 550 and 600 m that link drainage from Rouge Mountain River to Katherine Creek. This route is situated just west of a postulated Tutsieta limit and includes sections of canyon that are currently dry (Figure 5.6).

Laurentide ice experienced a minor readvance during the Kelly Lake Phase. Moraines and meltwater channels at the mountain front occur between 300 and 375 m and may define the position of ice during this stillstand. Glacial ice had retreated from the mountain front by at least 12 ka (Section 5.1.3, Figure 5.4).

5.3.2.5 Chronological Summary

Data from the northern Mackenzie Mountains are summarized by the following chronology: (i) several montane advances occurred in the Early and Middle Pleistocene, (ii) Dark Rock Creek I advance, the penultimate montane event of Illinoian age, extended to the eastern Canyon Ranges, (iii) the all-time Laurentide advance, the Wisconsinan Hungry Creek Glaciation, truncated moraines of the Dark Rock Creek I event, (iv) a second montane advance, Dark Rock Creek II, extended downslope of the Hungry Creek limit, kame and other ice marginal features define positions near Redstone and Keele Rivers where montane valley glaciers and Laurentide ice coalesced, (v) Laurentide ice readvanced during the Katherine Creek

Phase, truncating moraines of the Dark Rock Creek II event, and (vi) retreat and/or readvance of Laurentide ice in the mountain front region is marked by ice marginal channels, two possible stillstands are associated with the Tutsieta and Kelly Lake Phases.

The sequence of events presented in this interpretation is grounded on stratigraphic and geomorphic evidence, however, controls on dating are few. Much hinges on the date assigned to the Hungry Creek Glaciation, and this remains a matter of some controversy. There is a possibility of older Laurentide advances, though their deposits are not recognized.

5.3.2.6 Glacial Thermal Conditions

Geomorphic evidence from the field areas suggests that Laurentide ice of the Katherine Creek and subsequent phases was warm based. There are numerous examples of roche moutonnée, drumlinoid, and crag and tail features, all indicative of basal sliding. Meltwater channels are predominantly ice marginal but examples of subglacial Nye channels and p-forms provide evidence of subglacial flow. At the Bonus Lake and Bear Rock Sites, fine-grained sediments were found in conduits and cavities in the Bear Rock and Hume Formations. The materials were primarily massive fine and medium silts but also included some coarse silt and sand, and thin sequences of laminated clay. These deposits were similar in texture and colour to glaciolacustrine and fluvial materials found on the surface. The fine silt and clay could have been deposited near openings of larger conduits during glacial lake phases. However, the distribution and massive structure of the coarser silts suggests that deposition occurred subglacially. At Bonus Lake these deposits are found more than 30 m from cavern openings, through conduits of high sinuosity, and exceed 2 m in thickness, completely infilling some passages. These materials were probably flushed into conduits in a subglacial phreatic environment by meltwaters operating under the hydraulic gradient provided by the overlying glacial aquifer.

The evidence of warm-based ice and subglacial groundwater circulation are

important to the karst geomorphology of the region. While the infilling of conduits with sediment would inhibit karstification, the occurrence of basal melting at the ice rock interface would have had a positive effect. This is of particular significance where strata are evaporites and dissolution is largely controlled by groundwater flux rather than by the carbonic acid content. There are no data available regarding the rate of subglacial meltwater production that would characterize the Laurentide Ice Sheet in this region.

5.4 General Geomorphology, Canyon Ranges

The geomorphology of the Canyon Ranges reflects the balance between process and structure across a variety of spatial and temporal scales. At the macroscale, structure exercises the dominant control on topography. The general distribution of ridges and valleys is coincident with the structural trend. Overall, the regional drainage has a trellis pattern (Figure 3.1). Subsequent streams tend to be developed along recessive Devonian units that occupy synclinal axes while, ridges are primarily in resistant Proterozoic strata exposed along anticlines. The largest plateau features (e.g., Plains of Abraham) are formed by gently dipping synclinal and monoclinical structures. However, exogenic processes have generated large geomorphic features. Combinations of periglacial, fluvial, glacial, and slope processes have generated cryopediments, planation surfaces, meltwater channels, and canyons. Locally, solution has produced karst landforms. This section provides a brief discussion of the major non-karst elements of the geomorphology.

5.4.1 Pediments and Planation Surfaces

Strata of the northern Cordillera were subjected to folding, faulting, and uplift during the Cretaceous and Tertiary, with the last major phase ending as recently as the Paleocene (Eocene?). In response to uplift, erosion occurred over the Mackenzie Mountain area, initiating sedimentation in the adjacent foredeep (Chapter IV). Bostock (1948, 1970) noted the remnants of erosion surfaces across much of the

northern Cordillera. Hume and Link (1945) describe the predominance of plateau forms in the Dodo Canyon region. Alpine terrain is limited to the highest of the ranges, where resistant Proterozoic strata outcrop along the axial traces of major anticlines. Most of the low ranges are flat topped and broad uplands are common. In many areas, these gentle surfaces cut across structure and slope toward Mackenzie Plain (Aitken and Cook, 1974). They may be attributed to a long interval of fluvial erosion in the Upper Cretaceous and Tertiary and to cyroplanation during the Tertiary and Quaternary.

Ice wedge pseudomorphs in the Worth Point Formation show permafrost was present in the northern District of Mackenzie by the Upper Pliocene to early Pleistocene (Vincent, 1989, 1990). Under the conditions of a periglacial climate, bedrock weathering is dominated by frost action. Sediment is transferred by slow mass wasting and seasonal fluvial activity. Regions of the Canyon Ranges that have been infrequently glaciated, or are unglaciated, display the characteristic morphologies often attributed to periglaciation (e.g., French, 1976; Büdel, 1982). Planation surfaces and pediments are common and areas of high plateau are sharply dissected by deep valleys. Many of these valleys are flat floored and have steep rectilinear slopes that approach 30°. Talus and blockfields (felsenmeer) are observed. Braided channel patterns are common. Tors occur on plateau and planation surfaces. Steep mountain sides are bounded by gently sloping pediments (cryopediments) (Hughes, 1972; Priesnitz and Schunke, 1983).

Mountain and hillslope morphologies reflect parallel slope retreat. The general model suggests slope retreat is accomplished by frost wedging, slow mass wasting, and rillwash, and that slope debris is transported over the pediment surface by solifluction and sheetwash (Priesnitz, 1981, 1988). Many argue activity on pediments and planation surfaces under current climatic conditions is limited. Büdel (1982) finds no evidence to support pedimentation as an important process in modern periglacial regions, and favours fluvial dissection as the dominant process. Evidence of sediment erosion and transport is restricted to steep pediments in the Mackenzie

and Richardson Mountains, with little activity on gently sloping vegetated surfaces (Priesnitz and Schunke, 1983). Fried *et al* (1993) contend that pediments of the Richardson Mountains are relict features developed during colder periods of the Pleistocene. Pediments of the unglaciated Barn Mountains of northern Yukon are also currently inactive (French and Harry, 1992). Given typical rates of backwearing commonly attributed to periglacial regions (e.g., French, 1976), cryopediments of the dimensions observed in the Mackenzie Mountains could be developed in the Quaternary (Priesnitz and Schunke, 1983). However, these estimates are based on few data. French and Harry (1992) support assigning a middle or upper Tertiary age to the original pediment features of the Barn Mountains. The initial formation processes are not known but it is suggested the pediments were reactivated during the wet and cold periods of the Pleistocene.

5.4.2 The Valleys and Canyons

Elements of two drainage systems are recognized in the northern Mackenzie Mountain region, an older system consisting of gently sloping valleys, and a younger network of incised channels that are expanding retrogressively into the older system (Priesnitz and Schunke, 1983). Elements of the former are observed on the plateau and low mountains of the Canyon Ranges, while the upland blocks are dissected by the younger steep sided valleys and deep canyons. It is likely that expansion of these canyons has occurred throughout the Quaternary. The long profiles of Dodo Creek, Carcajou River, and Little Keele River are steep, with prominent knick points. The rapid downcutting is attributed to recent uplift and ongoing adjustment to the current base level. Ford (1973) documents 500 m of Quaternary uplift in the southern Mackenzie Mountains. Between 100 and 200 m occurred in the Richardson Mountains over the same interval (Priesnitz and Schunke, 1983). There are no data on Quaternary epeirogeny in the northern Mackenzies; however, it is reasonable to suspect uplift, tectonic and isostatic, is at least on the order of 100 metres.

On the South Nahanni River, meanders have cut through several hundred

metres of bedrock following uplift. There are equivalent meanders on the Carcajou and Little Keele Rivers, although not of the number or dimension observed on the South Nahanni. These meanders occur just east of a major break in slope in the long profile. Above the knick point, channels are wide and braided with cryopediments extending to their boundaries. Priesnitz and Schunke (1983) argue that these reaches are at equilibrium and provide a model for channel development under periglacial conditions. However, much sediment on the braidplains is reworked glacial deposits and this material must be flushed through the system before a dynamic equilibrium will be established between periglacial processes and channel form. Below the knick points, the river channels are confined to canyons and the morphology ranges from straight and meandering single channels to braided.

The conditions favouring incision are not limited to uplift. During the Pleistocene the Mackenzie Plain was repeatedly glaciated by Laurentide Ice advancing from the Great Bear Lake region. Mackay and Matthews (1973) speculate that a pre-glacial Mackenzie River may have followed a course through the eastern Franklin Mountains. Hughes (personal communication, 1990) and Duk-Rodkin and Hughes (1993) contend that the present configuration of the Mackenzie River system is of Quaternary age. Ice of the Mackenzie Lobe progressively removed Cretaceous and Tertiary strata from the Mackenzie Plain. This altered the position of the Mackenzie River and the local base level for streams of the Mackenzie Mountains. The major effect on mountain drainage was a disturbance to the pre-glacial river profiles, causing incision and the headward propagation of knick points.

While canyon development was in response to a combination of uplift and base level change, the positions and characteristics of these canyons have been strongly influenced by glaciation. These features generally fall into one of three classes: (i) major river canyons and valleys, (ii) glacial marginal canyons, and (iii) mountain front canyons. Canyons of the latter group are small narrow features that are typically 1 to 3 km in length and up to 300 m deep. Rapids and falls are common down their length and alluvial fans occur at the outlets. Many of these fans continue

to aggrade. Canyon orientation is either normal to a larger canyon or to the mountain front. They are best expressed on the Bear Rock and Hume Formations where small springs and seeps are visible on canyon walls. Spring head sapping appears responsible for the development of one box canyon tributary to Dodo Canyon.

The largest valleys of the first group have relatively smooth river profiles with few abrupt changes in slope, and cut across structure deep into the core of the foldbelt. They may represent the Tertiary drainage routes of the major rivers. The Arctic Red, Keele, and Redstone Rivers fall into this category. The courses of other major rivers are partially controlled by structure and do not possess a graded profile over their entire length. The upper Carcajou and Mountain Rivers follow a trellis pattern, though the trunk channels do cut across most of the outer ranges. All of these valleys have been scoured by montane ice.

Glacial marginal canyons occur where mountain drainage and meltwaters were diverted and focused during glaciation. They are most common between the mountain front and the all-time Laurentide limit (Figures 5.5, 5.6). Included in this group are: (i) reaches of major river canyons currently integrated into the drainage network, (ii) sections of canyon now underfit or dry and abandoned, and (iii) canyons or channels cutting across drainage divides or occupying anomalous positions on mountain slopes. The lower reaches of many of the major rivers and abandoned canyons show a deflection to the northwest. Carcajou River abruptly turns into a canyon paralleling the mountain front despite the presence of a more direct route onto the Mackenzie Plain. Dodo and Grotto Canyons, Katherine Creek, and Mountain River also have a northwest deflection near the mountain front. The location and orientation of these drainage elements have been strongly influenced by Laurentide Ice blocking pre-glacial drainage routes.

Sections of dry and abandoned canyon are found in positions where they have drained proglacial lakes or functioned as ice marginal channels. One example is a canyon linking the drainages of Little Keele River and Dodo Creek. It is illustrated in a sequence of photographs on Figure 5.7, the location is shown on Figure 5.6. The

canyon cuts through the Mount Kindle and Franklin Mountain Formations. The Bear Rock Formation is exposed along its rim. At its southeastern end is a large plunge pool developed beneath a dry 30 m waterfall. Since its abandonment, the canyon floor has been partially buried by slumps and talus. A small lake has been impounded at the north end by aggrading fans. This canyon was probably carved as a gorge that drained proglacial lakes and streams that were impounded and diverted by Laurentide Ice dams. This route was active when the ice position was between the limits mapped for the Katherine Creek and Tutsieta Lake Phases. This would produce an ice dam in Carcajou Canyon near the confluence with Rouge Mountain River. The lake generated would inundate portions of the Little Keele and Carcajou River Valleys to approximately 650 m elevation, and receive drainage from as far south as Little Bear River. There are other examples of abandoned canyons in the study area (Figure 5.8, 5.9). Above and parallel to segments of Carcajou and Dodo Canyons are channel fragments that also held mountain drainage and meltwaters when ice was present in the main canyons. Some stretches are represented by deep canyons and others by lightly vegetated braidplains and sequences of fluvio-glacial sediments.

Channels and canyons also cut across divides. A canyon headed in Carcajou Lake extends to the northwest across a divide to the Mountain River basin. This drainage route was active during the Hungry Creek and possibly the Katherine Creek events. Most of these features occur at the limit of the Hungry Creek, Katherine Creek, or Tutsieta Glaciations. They are small in their dimensions, but some major canyon features may have been initiated as such channels. Dodo Canyon cuts sharply through the northwestern flank of Dodo Mountain from a position up high on the slope. The canyon cuts through older drainage elements in the area of the Dodo Canyon Karst. Much of the area now included in the Dodo Creek watershed was formerly drained by streams to the south of Dodo Mountain. Dodo Canyon may have evolved from an initial small ice marginal channel, and was enlarged during subsequent glaciations to a position where it progressively captured drainage.

The major canyons of the northern Mackenzie Mountains are of Quaternary age. The sharpness of their morphology makes them the most striking mesoscale geomorphic features of the Canyon Ranges. The role of such relief development as an influence on karst will be discussed in subsequent chapters.

Table 5.1: Map reference, lab numbers, and location of radiocarbon dates in the District of Mackenzie (various sources).

Map	Lab #	Date (years BP)	Locality	Reference	Material	Significance
1	GSC-331	>46,580	Mayo, Yk	Dyck <i>et al</i> , 1966	wood	minimum date for Reid Glaciation
2	GSC-524	>42,900	Stewart River, Yk	Lowdon and Blake, 1968	wood	minimum date for Reid Glaciation
3	GSC-562	>35,000	Garry Island, NWT	Lowdon <i>et al</i> , 1971; Rampton, 1988	shells	minimum date for Toker Point Stadial
4	GSC-690	>37,000	Kendall Island, NWT	Lowdon and Blake, 1968; Rampton, 1988	shells	minimum date for Toker Point Stadial
5	GSC-769	29,600 ± 460	Silver Creek, Yk	Lowdon and Blake, 1970	plants	maximum date for Kluane (McConnell) Glaciation
6	GSC-1088	>41,000	Banks Island, NWT	Vincent, 1983, 1984	moss	minimum date for M'Clure Stadial
7	GSC-1191	31,300 ± 640	Old Crow Flats, Yk	Lowdon and Blake, 1979	plants	maximum date for proglacial lake
8	GSC-1262	22,400 ± 240	Stokes Point, Yk	Lowdon and Blake, 1976; Rampton, 1982	peat	minimum date for Buckland Glaciation
9	GSC-1478	>19,000	Banks Island, NWT	Lowdon and Blake, 1973; Vincent, 1983	shells	minimum date for M'Clure Stadial
10	GSC-1618	>47,000	Little Bear R, NWT	Duk-Rodkin and Hughes, 1991	wood	minimum date Dark Rock Creek I
11	GSC-1784-2	12,900 ± 150	Eskimo Lakes, NWT	Blake, 1987; Rampton, 1988	grass	minimum date for Tutsieta Lake Phase
12	GSC-1995	13,000 ± 130	Eskimo Lakes, NWT	Blake, 1987; Rampton, 1988	plants	minimum date for Tutsieta Lake Phase
13	GSC-2328	10,600 ± 260	Great Bear R, NWT	Lowdon and Blake, 1979; Smith, 1992	plants	minimum age of Glacial Lake Mackenzie
14	GSC-2422	36,900 ± 300	Hungry Creek, Yk	Hughes <i>et al</i> , 1981	wood	maximum date for Hungry Creek Glaciation
15	GSC-2690	16,000 ± 420	Doll Creek, Yk	Lowdon and Blake, 1981; Ritchie, 1982	mud	minimum date for Hungry Creek Glaciation
16	GSC-2811	23,900 ± 1,140	Tom Creek, Yk	Klassen, 1978; Lowdon and Blake, 1981	plants	maximum date for McConnell equivalent
17	GSC-3371	21,300 ± 270	Rat River, NWT	Catto, 1986	plants	minimum date deglaciation, Rat River
18	GSC-3387	13,100 ± 150	Tamarack Lk, NWT	Blake, 1983; Ritchie <i>et al</i> , 1983	mud	minimum date on Tutsieta Lake Phase
19	GSC-3698	>37,000	Banks Island, NWT	Vincent, 1984; Blake, 1987	shells	minimum date for M'Clure Stadial?
20	GSC-3813	21,200 ± 240	Rat River, NWT	Catto, 1986	plants	minimum date for deglaciation, Rat River
21	GSC-3946	20,800 ± 200	Bluefish Flats, Yk	Blake, 1987	plants	maximum date for proglacial lake
22	I-3574	12,460 ± 440	Old Crow Flats, Yk	Harrington, 1977	bone	minimum date for proglacial lake
23	I-15,020	11,530 ± 170	Fort Norman, NWT	Smith, 1992	wood	deglaciation from Fort Norman
24	NMC-1232	25,170 ± 630	Cadzow Bluff, Yk	Morlan, 1986	bone	maximum date for proglacial lake
25	RIDDL-801	48,200 ± 1,110	Kendall Island, NWT	Vincent, 1989	shells	minimum date on Toker Point Stadial
26	TO-195	44,420 ± 630	Little Bear R, NWT	Hughes <i>et al</i> , in press	wood	maximum age for Hungry Creek Glaciation?
27	TO-650	24,730 ± 260	Banks Island, NWT	Vincent, 1989	shells	minimum date for M'Clure Stadial
28	TO-796	43,550 ± 470	Garry Island, NWT	Vincent, 1989	shells	minimum date on Toker Point Stadial
29	TO-1190	11,760 ± 90	Mountain R, NWT	Smith, 1992	wood	deglaciation from Mountain River
30	TO-2298	11,900 ± 80	Keele Lake, NWT	Szeicz, personal communication, 1993	shells	minimum date for Hungry Creek Glaciation
31	TO-2295	12,060 ± 80	Andy Lake, NWT	Szeicz, personal communication, 1993	wood	minimum date for Dark Rock Creek II
32	TO-2375	10,230 ± 150	Bells Lake, NWT	Szeicz, personal communication, 1993	wood	minimum date on Katherine Creek Phase

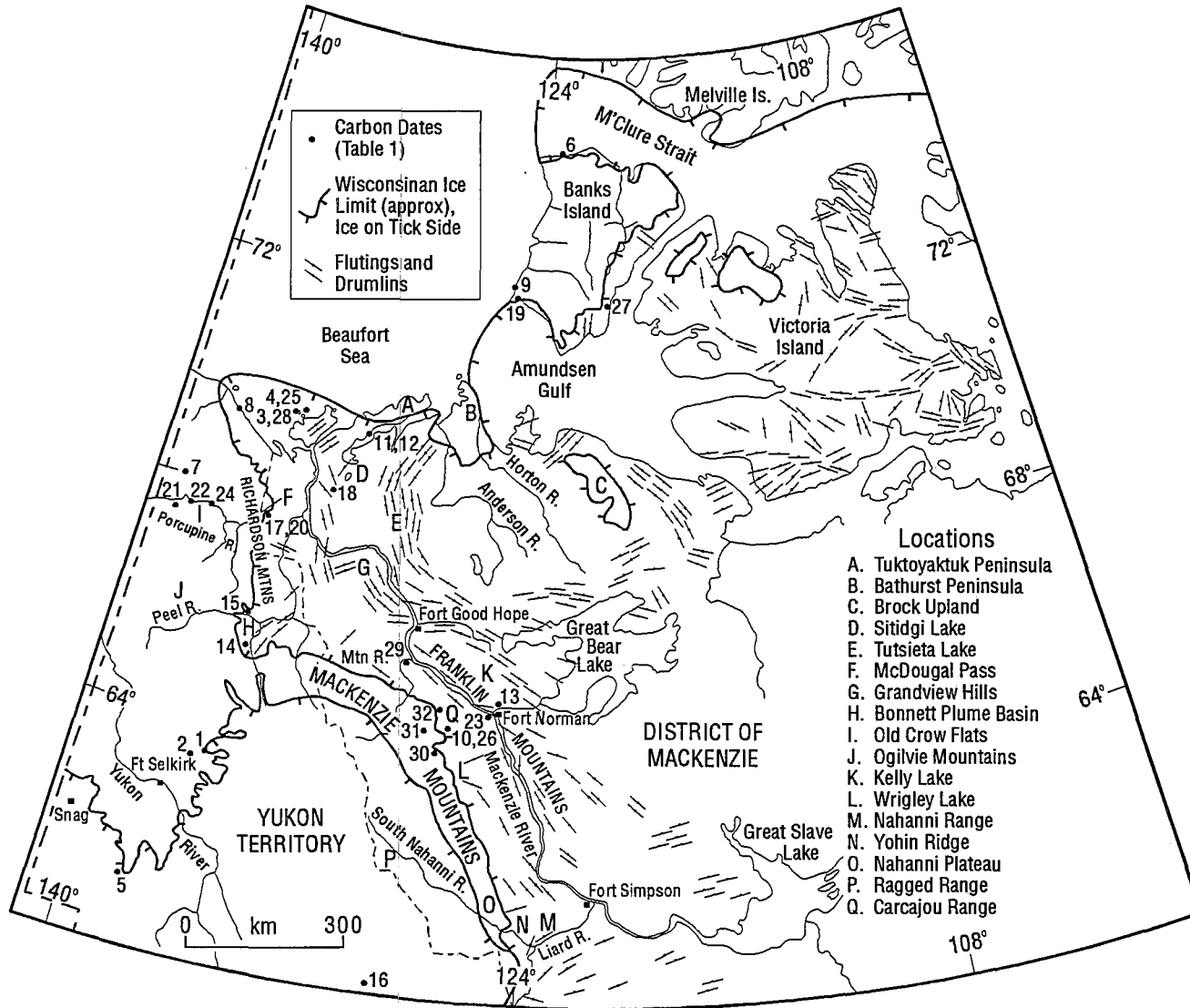


Figure 5.1: Wisconsin ice limits in northwestern Canada. The numbered carbon dates are indexed to Table 5.1. Locations are discussed in the text (data from Hughes, 1987; Vincent, 1989).

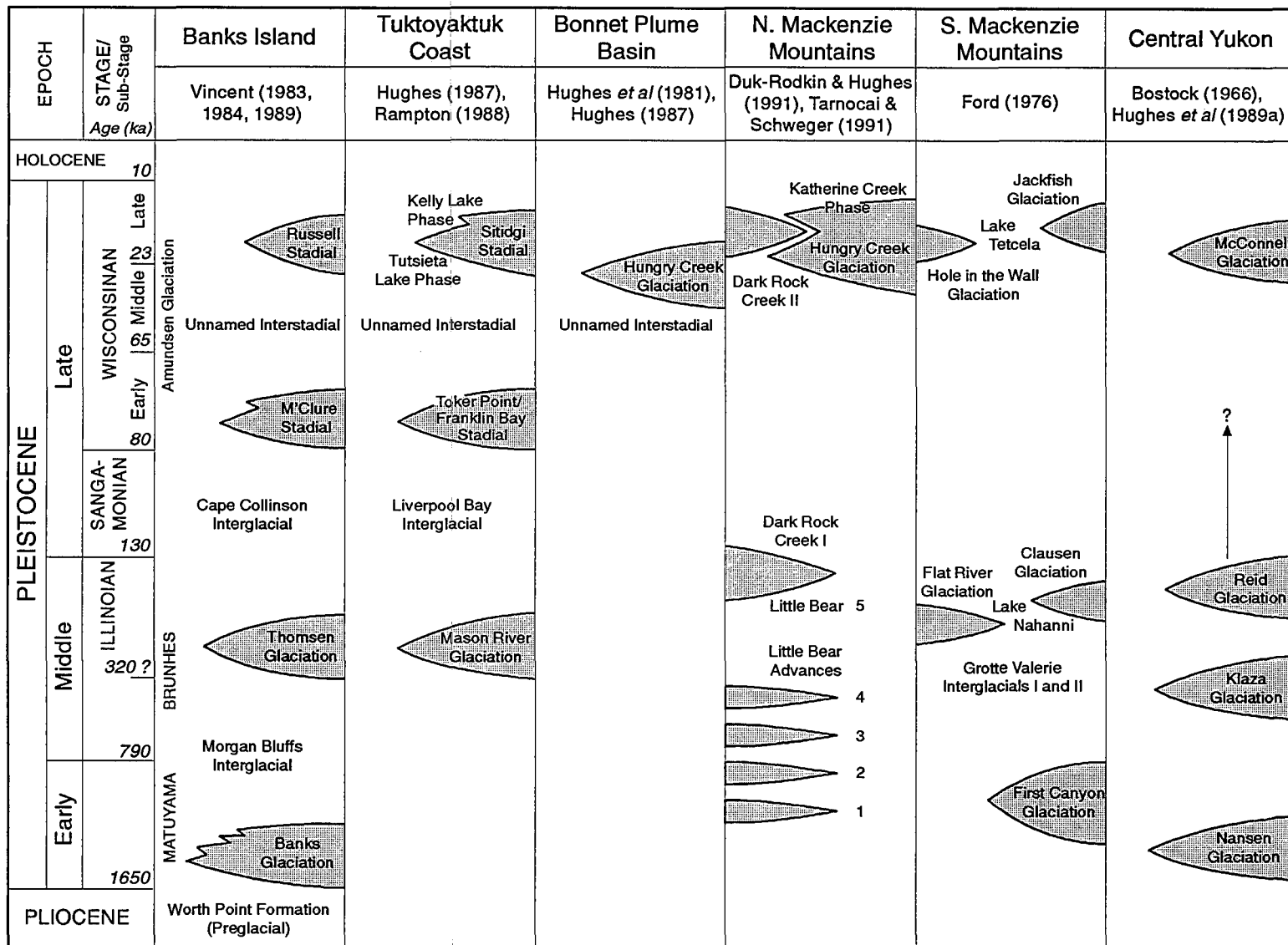


Figure 5.2: Regional correlation of glacial deposits and events in northwestern Canada (various sources).

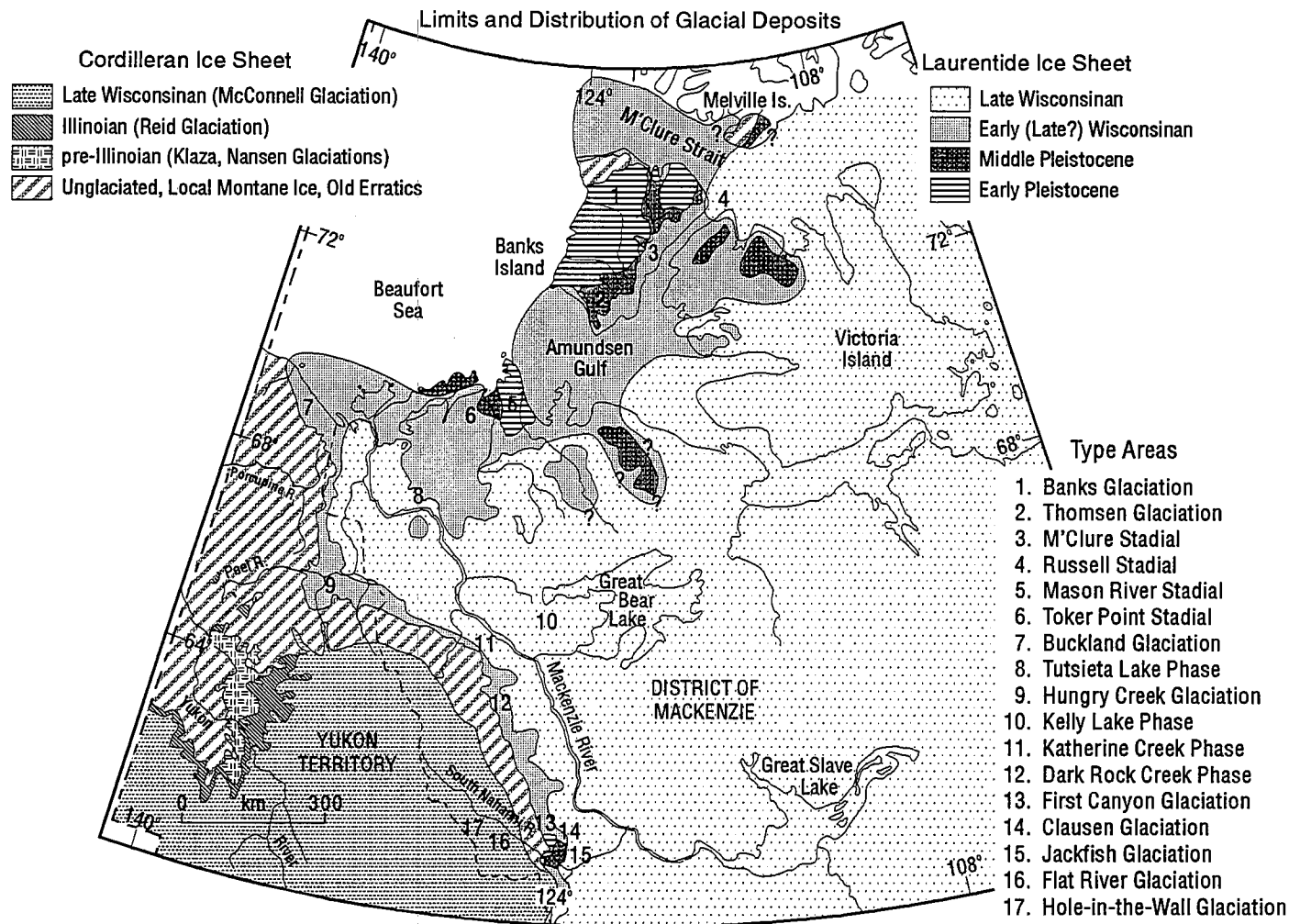


Figure 5.3: Glacial limits, type areas, and distribution of deposits in northwestern Canada (after Hughes, 1987; Vincent, 1989; Tarnocai and Schweger, 1991). The Late Wisconsinan limit shown for the Laurentide Ice Sheet is a conservative view. Hughes (1987) argues for an all time Laurentide maximum at c. 25 ka that would include much of the area mapped as Early Wisconsinan on this diagram.

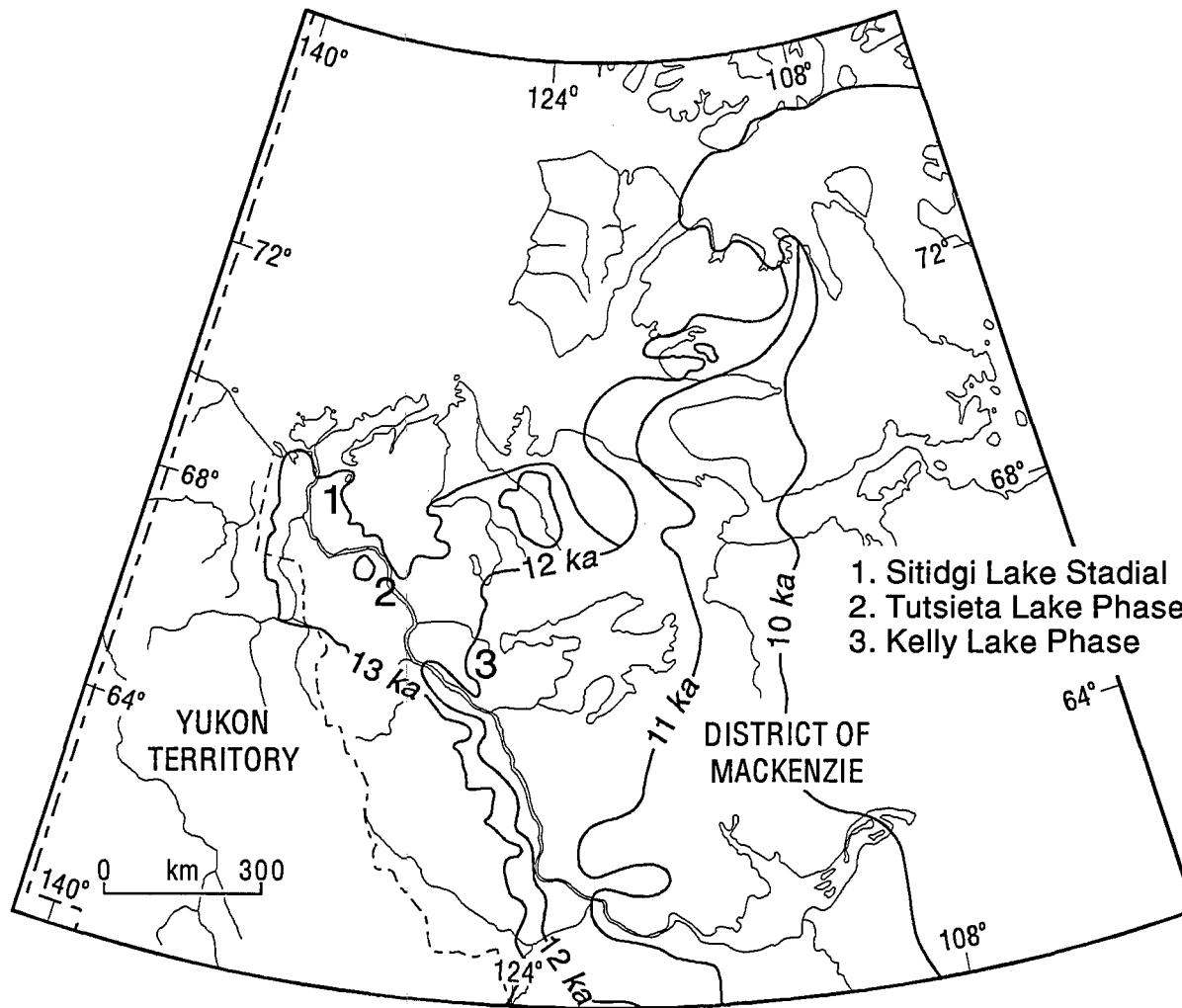


Figure 5.4: Retreat positions of the Laurentide Ice Sheet in the Late Wisconsinan, and the locations of the type areas for the major stadials (Vincent, 1989).

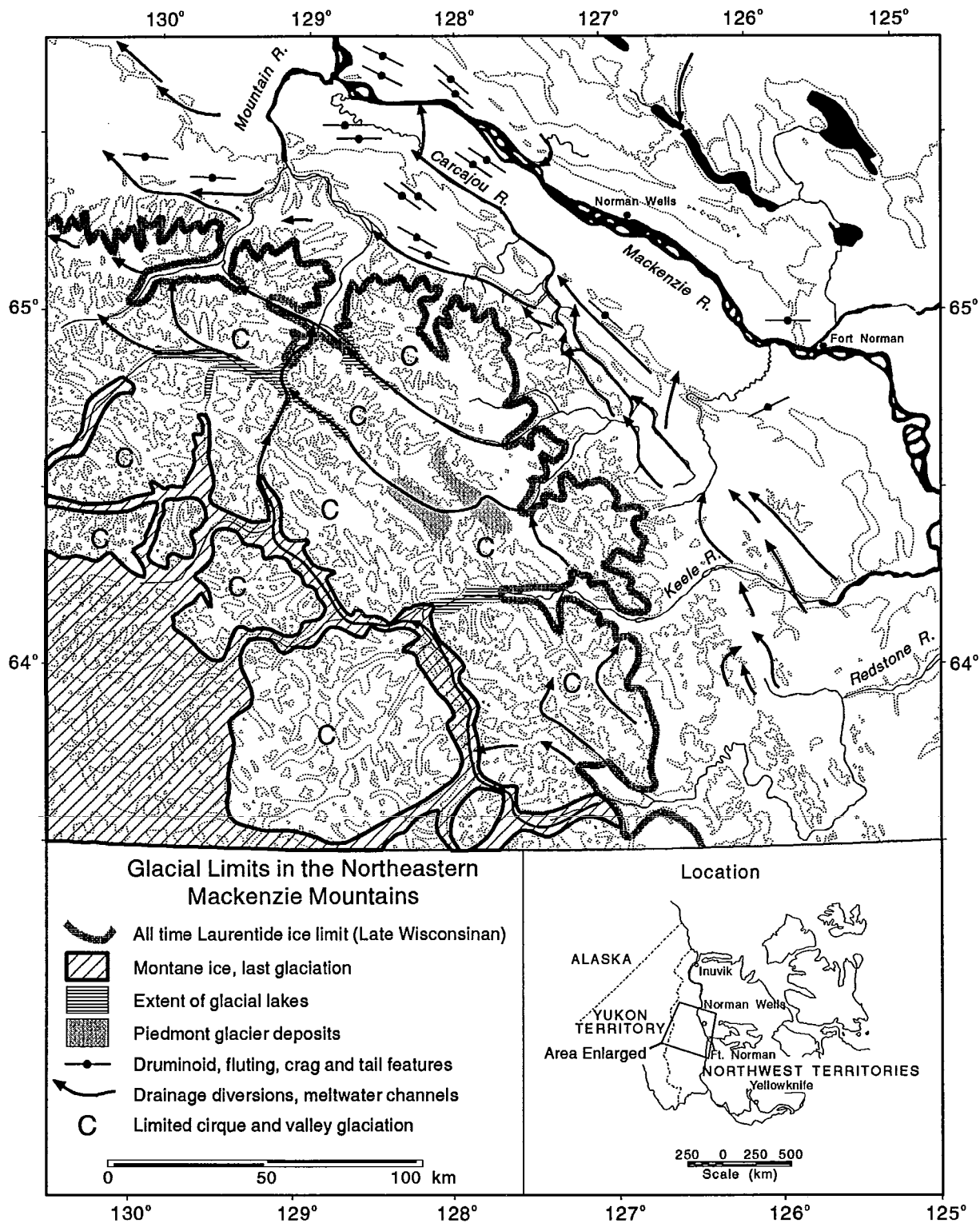


Figure 5.5: Limits of the Hungry Creek Glaciation (all time Laurentide maximum) and the Dark Rock Creek II montane glaciation. The extent of the largest glacial lakes and piedmont glacier deposits are indicated as are the major drainage diversions and spillways (modified after Duk-Rodkin and Hughes, 1991)



Figure 5.6: Glacial landforms in the Carcajou Range, Mackenzie Mountains, N.W.T. The approximate limits of the Hungry Creek, Katherine Creek, and Tutsieta Glaciations are shown, as are the distributions of moraine fragments, meltwater channels, and erratics. Data are from aerial photograph interpretation and from Duk-Rodkin and Hughes (1991).

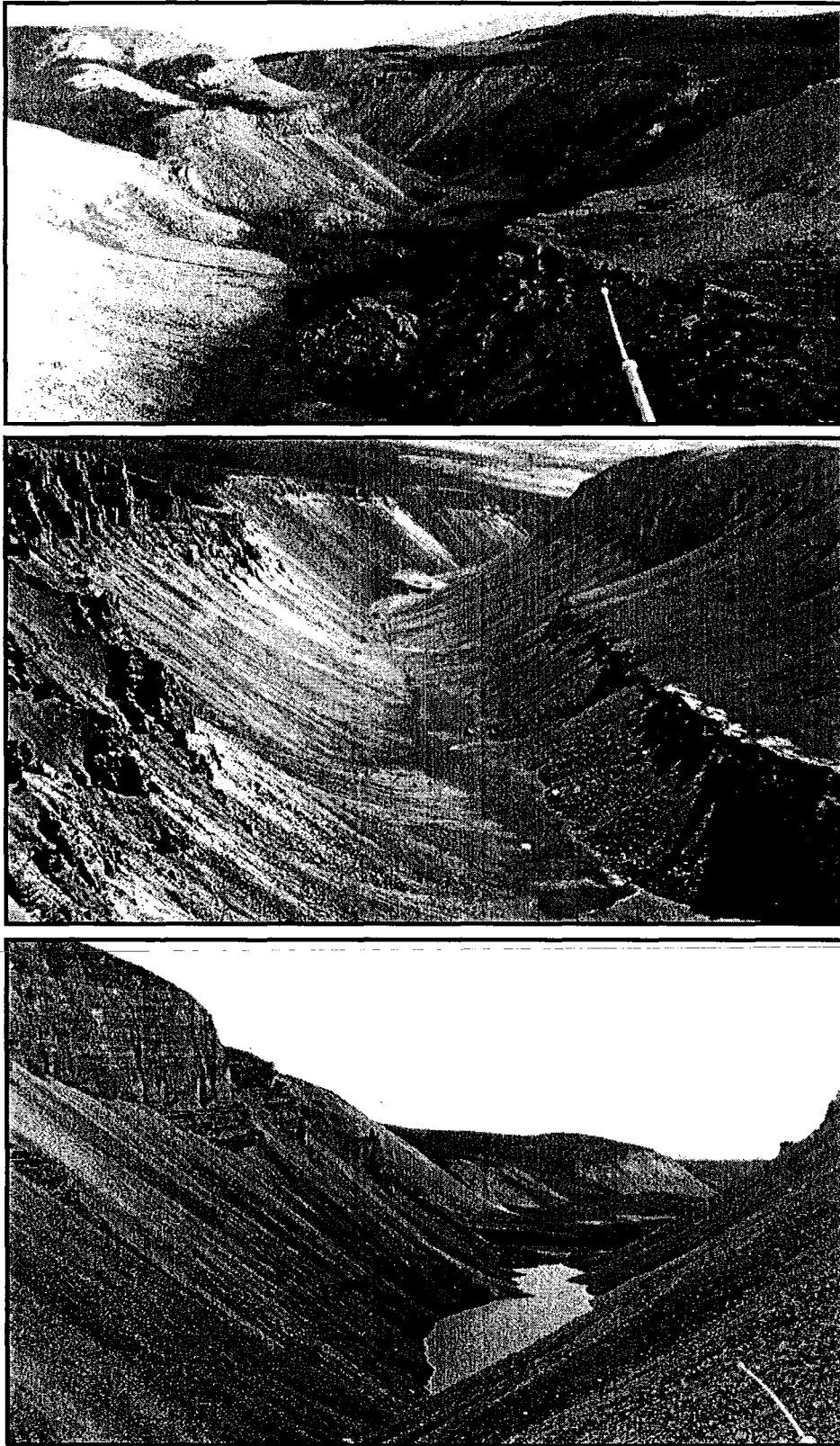


Figure 5.7: A south to north transect of the abandoned canyon between Little Keele River and Dodo Creek (top to bottom). The Bear Rock, Mount Kindle, and Franklin Mountain Formations are seen in outcrop.



Figure 5.8: The photo is looking northwest through "Dry Canyon" to Katherine Creek. The floor of Dry Canyon is at 580-590 m elevation, about 20 m above the level of the adjacent Katherine Creek floodplain. From aerial photography a braided channel pattern is seen on the area of the floor now vegetated. This meltwater channel is just beyond the limit of the Tutsieta Lake Phase. The rotational slump is in the Mount Kindle Formation.

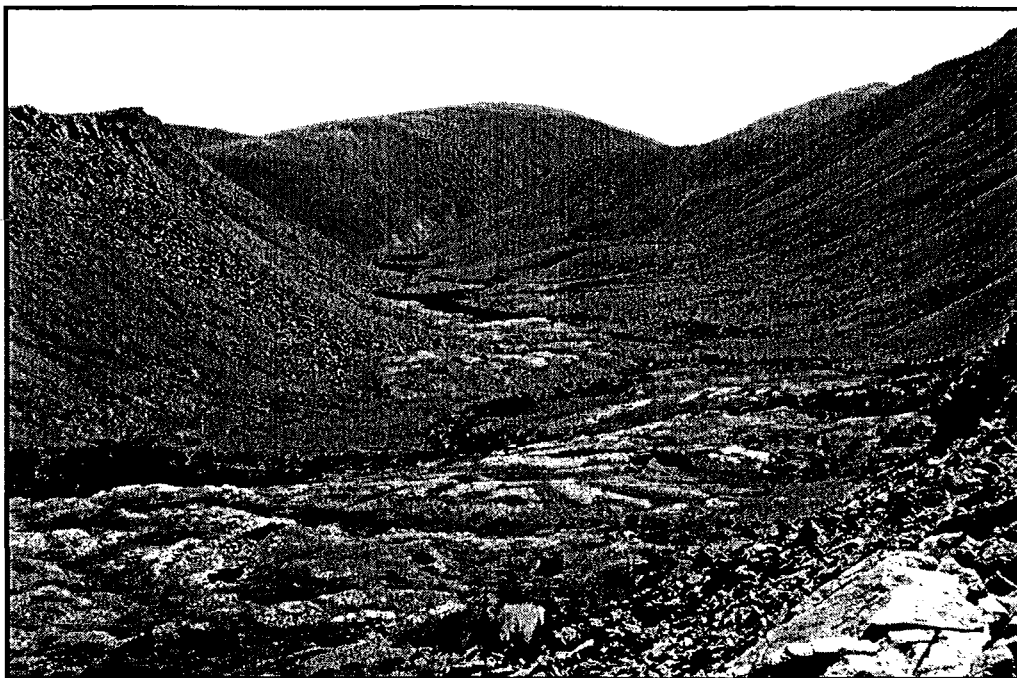


Figure 5.9: Photograph of "Kindle Canyon", the view is to the north. The canyon cuts through the Mount Kindle Formation, there are numerous mass movement deposits along its length. The canyon floor is at 630-640 m elevation. This channel was last active when drainage from the dry canyon of Figure 5.7 was routed via Dodo Canyon to this location.

CHAPTER VI
KARST LANDFORMS OF THE NORTHEASTERN MACKENZIE
FOLDBELT

6.1 Introduction

Karst landforms and drainage systems are typically of limited extent in periglacial regions. Bedrock depressions are gradually infilled by the slow flux of frost shattered debris through the processes of solifluction, creep, sheet and rillwash. Where permafrost is continuous, the development of karst may be inhibited by the presence of an aquitard in the near subsurface. Despite these factors, karst does occur in areas of periglacial climate, particularly where permafrost is discontinuous. This chapter describes the range and characteristics of karst input, throughput, and output landforms observed in the study region.

Karst is widely distributed in the northern Mackenzie Foldbelt (Figure 6.1). Mapping of karst features is not complete over the whole region. A range of features are present: karren, dolines, dry valleys, caves, springs, and tufa deposits. While the focus was on sites in the Carcajou Range, comments in this section are extended to karst from adjacent areas. Geomorphological maps from the individual study sites are provided, with hydrochemical data presented in subsequent chapters.

6.2 Karren

Small linear dissolution features of the surface and shallow subsurface are collectively called karren. They function as input landforms to the epikarst and normally range in size between 1 cm and 10 metres, but may approach lengths of several hundred metres. Microkarren occurs at the millimetre scale. There are several types of karren and they are classified morphologically (Ford and Williams,

1989). A karrenfield is an assemblage of individual features extending over areas as broad as several square kilometres. Rarely are karren described on a regional scale, particularly where bedrock is mantled by soil and vegetation. The following discussion of karren is not exhaustive, only the most common forms associated with the Mount Kindle and Bear Rock Formations are described.

6.2.1 Karren on the Mount Kindle Formation

A karst pavement is a level or stepped karrenfield dominated by an orthogonal or polygonal network of vertical, solutionally enlarged fissures (grikes and splitkarren) occurring along joints, fractures, and minor faults (Figure 6.2)(Williams, 1966). Intervening bedrock areas (clints) support several lesser karren forms. Pavements are best developed on flat lying or gently dipping, massive, fine grained limestones that have been scoured by glaciation or other geomorphic processes that expose unweathered bedrock surfaces. Pavements are also present on dolomite, but typically support a smaller range and lower density of karren forms. Old pavement surfaces may become mantled by insoluble residue and irregular bedrock fragments of shillow that result from solution along minor discontinuities (Figure 6.3). Shillow production is most rapid where bedding is thin and flaggy, the insoluble content high, and where frost wedging and shatter are intense. Pavements may also develop under the cover of thin, acidic soils that contribute carbonic acid and accelerate subsoil solution.

Karst pavements occur at several locations in the Carcajou Range, developed on bare, flat to gently dipping dolomite of the Mount Kindle Formation. The formation is predominantly a medium to fine grained, vuggy, fossiliferous dolomite with minor chert. The most extensive pavement is at the Dodo Canyon Site and it is adopted as the type area for this karren assemblage. The site lies at an elevation between 600 and 800 m, at or just above the glacial limit of the Tutsieta Lake Phase (13 ka). Large meltwater canyons occur south and north of the pavement and several smaller channels cut across its eastern portion. The occurrence of large plucked and

bulldozed blocks, and numerous stoss and lee forms, suggest the last glacial ice was warm based. The area is above treeline and is largely free of soil and sediment. Lichen and moss are locally observed on the bedrock surface. Moist locations are characteristically dark grey and black weathering, indicating the presence of an organic coating. Massively bedded intervals are separated by flaggy, thinly bedded, chert-rich units. This bedding pattern imparts a stepped appearance to the pavement (Figure 6.2). Strata dip northward at 5° to 10°.

The morphological characteristics of the Dodo Pavement are similar to those of other stepped pavements (*schichttreppenkarst*) that occur in glaciated and cold regions of Europe and North America (Bögli, 1980; Ford and Williams, 1989). Large karren features on the Dodo Pavement include grikes, splitkarren, solution pits and pans. There are few subsoil (*rundkarren*) features. Grikes are angular and sharp and are the dominant solution forms. Major grikes typically penetrate from the surface of the massive beds to the thin cherty units that are 1 to 2 metres below. These grikes spread orthogonally from several large fractures and lineaments that dissect the pavement area from the north to south. An *en échelon* pattern of smaller grikes and splitkarren intersects the main set at oblique angles, forming many triangular clints (Figure 6.2). A variety of closed and open splitkarren are developed along minor fissures.

On the surface of clints there are a variety of minor features including small solution pits, grooves, shallow *rillenkarren*, and solution pans. Cockling and rippling may occur on steep slopes. In some areas thin bedded intervals break down into an almost complete cover of shillow, particularly where chert is abundant along bed partings. The solution pans observed were typically 15 to 25 cm in diameter and 3 to 8 cm deep with an outer rim raised 2 to 5 cm above the general surface of the pavement (Figure 6.5). A thin layer of precipitated calcite commonly occurs at the rim crest due to the wicking of moisture from the pan base and subsequent evaporation. Pan bases are often covered in lichen and cyanobacteria contributing to accelerated local erosion. Overflow channels run outward from the pan centres

and small rillenkarren may develop on the rim edges. The rillenkarren are discontinuous and typically only 1 to 2 cm in length. The Mount Kindle Formation contains a diverse fauna; particularly abundant are silicified hemispherical coral of the genus *Favosite*. Individual coral heads approach diameters of 15 cm. Many solution pans appear to have developed within depressions that were formerly occupied by coral specimens. The heads were dislodged from the rock mass by either glaciation or frost wedging. Solution has enlarged these depressions.

Small scale solution features are best developed, and the shillow frequency lowest, on clints where bedding is massive, the dolomite fine grained and homogeneous, and the chert content low. Lundberg (personal communication, 1988) identified an unusual microkarren form on the windward surface of smooth clints. These positive relief features, called wind streaks, are oriented parallel to the direction of major storm winds and averaged 1 mm in height, 20 mm in length, tapering in a down wind direction. Lundberg speculated that these forms result from solution by wind driven rain and sheetflow across the rock surface. Flow is diverted around minor inhomogeneities or impurities, focusing solution in intervening areas. Wind oriented microkarren are also reported on limestones from the Tibetan Plateau (Zhang *et al*, 1993).

At the Pyramid Lake Site, much of the Mount Kindle outcrop is debris covered, however, in some areas the weathering of the formation is characterized by dense pitting (Figure 6.4). The morphology is similar to that of phytokarst, outcrops pocked by a dense irregular network of concavities generated in part through the boring action of microflora (Folk *et al*, 1973). Jones (1989) identified a variety of fungi, algae, and bacteria responsible for these features on dolomite in the Cayman Islands. Although Viles (1987) has questioned the importance of biokarst processes in non-coastal areas, Jones (personal communication, 1993) supports the argument that these processes operate across a full range of environmental conditions. Identification of the particular organisms involved would require examination by a scanning electron microscope.

Measurements of grike widths provide an assessment of the rate of epikarstification following a glacial event. Lundberg and Ford (personal communication, 1988; 1994) identified two populations of grikes at the Dodo Pavement, a set of smaller, less well-developed grikes with an average width of 39 mm and a group of large grikes with an average width of 72 mm. Goldie (1981) established the rate of grike widening on limestone pavements in Britain as 13 mm ka^{-1} . If it is assumed that the Dodo Pavement was a pristine surface following deglaciation, the rate of grike widening would vary between 3 and 5.5 mm ka^{-1} . It is probable that the larger grikes were not completely removed by the last glacial event and that they represent a preglacial population.

The largest silicified corals rise between 60 and 80 mm above the level of the dolomite pavement. Erratic pedestals approach 70 mm in height. These data yield a postglacial surface lowering rate of approximately 5 mm ka^{-1} . This rate is much lower than those observed on limestone pavements in warmer, moister climates. Bogli (1961) calculated a rate of 15 mm ka^{-1} in the Maren Mountains of the Swiss Alps. Williams (1966) determined a rate of 12.5 mm ka^{-1} in County Clare, Ireland. At other temperate locations rates range between 30 and 50 mm ka^{-1} (Ford and Williams, 1989). Akerman (1983) estimated surface lowering on a dolomitic limestone at Spitsbergen of 2.5 mm ka^{-1} , which is comparable to the Dodo value.

Compared to limestone pavements of the temperate zone, there are a smaller range and lower density of karren on the Dodo Pavement. The frequency and size of pits and pans are low, while rillenkarren, runnels, and shafts are largely absent. This distribution may be related to the slow rate of surface corrosion at the Dodo Pavement, which is likely a function of dolomite solubility and the semi-arid level of precipitation. However, the site does show the general characteristics of dolomite pavements found elsewhere in southern Canada. It is significant because it has developed under the conditions of a permafrost climate.

6.2.2 Karren on the Bear Rock Formation

On the Bear Rock Formation, karren are restricted to the massively bedded limestone intervals of the Landry Member. The major karren features identified include solution pans, pits, rillenkarrren, and cockling. No extensive areas of pavement occur due to the restricted area and the highly variable attitude of the Landry outcrop, the latter resulting from the underlying interstratal dissolution of evaporites. Solution pans are rare and are similar in morphology to those described on the Mount Kindle Formation.

Rillenkarrren are rainfall-generated linear solution channels. They extend downslope from crest line positions on bare rock outcrops and may grade into either cockling, consisting of a mixture of scallops, ripples, and discontinuous rills, or into a belt of smooth planar erosion (*ausgleichflache*). These are equilibrium features and once established subsequent retreat is parallel to the surface. Laboratory experimentation suggests rill length is directly proportional to surface slope (Glew and Ford, 1980). However, many field studies have not proven that relationship (Ford and Lundberg, 1987; Ford and Williams, 1989).

Rillenkarrren occur on the Landry Member at the Dodo Canyon Site (Figure 6.6). This site was deglaciated at approximately 13 ka. Rill lengths were measured from the crest tops to *ausgleichflache* or cockling. Rill depth and width were determined at the rill midpoint. Data from the Dodo Canyon Site show: (i) there is no relationship between surface slope and rill length, (ii) rill width increases with rill length ($r=0.62$, $n=87$), and (iii) rillenkarrren occur on crackle breccias (Figure 6.7). The rillenkarrren depicted on Figure 6.6 and similar frost shattered exposures were not used for sampling length and width. The measured rill widths are consistent with the range expressed in the literature, although the relationship with length is not usually reported (e.g., Lundberg, 1977; Dunkerly, 1979). The Landry Member at the rill site is predominantly a homogeneous crackle breccia of calcite cemented fossiliferous pelletal lime wackestone. Solution across the fragments and cement were observed to be congruent. Rillenkarrren were not found on the recessive lime

mudstone units of the Landry Member or where there was a mosaic or rubbly breccia fabric.

The frequent occurrence of rillenkarren on the massive units of the Landry Member is in sharp contrast with the absence of these forms across extensive areas of dolomite on the Dodo Pavement. This is consistent with observations on dolomite outcrop elsewhere in Canada (Ford, personal communication, 1992). Presumably the dolomite is not sufficiently soluble to host such features.

The highly fractured and heterogeneous outcrops of the Brecciated Member of the Bear Rock Formation do not support karren forms. Massive intervals of mosaic packbreccia tend to weather with a blocky spheroidal form. Rubble packbreccias and floatbreccias support sharp ridges and pinnacles at some locations (e.g., Figure 4.14). The heights of individual pinnacles were measured at the Bear Rock, Dodo Canyon, and Bonus Lake Sites. Pinnacle heights ranged from 1 to 15 m, with a mean of approximately 6 m (n=20). A weak relationship was observed between pinnacle height and circumference, but measuring the latter was often difficult. Pinnacles were observed with a lower frequency on the more resistant intervals of the Bear Rock Formation, and on the Franklin Mountain, Mount Kindle, and Hume Formations.

In a karst context, most pinnacles develop in a subsoil environment. Clints are gradually rounded by rundkarren developing wide tapering subsoil grikes called cutters. This process reduces the clints to rounded pinnacles. Subsequent exhumation and exposure to rainfall may sharpen features with the development of hydraulic karren. Alternatively, pinnacles may develop as tower remnants in giant grikeland, corridor, or labyrinth karsts (e.g., Brook and Ford, 1978). At the Dodo Canyon Site, there are examples of pinnacles or small towers on the Mount Kindle Formation. These are found where mountain drainage and glacial meltwaters were routed near the limit of the Tutsieta Lake Phase. The Mount Kindle Formation at this site is strongly jointed and tower development accompanied toppling failures at the margins of meltwater channels.

There were several subsoil cutters or grikes located in the Hume Formation at the Bonus Lake Site. Vertically tapering fissures infilled with sediment are observed in canyon exposures. Most of these features have a maximum width of less than 1 m and a vertical dimension of 1 to 3 m. While there are some morphological similarities to cutters, the origin of these features is not attributed to subsoil solution during the Holocene. The infilling sediments are fluvioglacial and glaciolacustrine materials. The carbonate content of these sediments is high, indicating the relief on the underlying Hume predated deposition. The largest fissures are located where subglacial and glacial marginal channels cross-cut small mountain front canyons. These fissures may have an origin that is attributed to a combination of preglacial solution, erosion by meltwaters, and to tension associated with glaciotectonism. It is unlikely that the cutter forms observed at the Bonus Lake Site developed by recent subsoil solution.

The pinnacles observed in the study region are predominantly frost features. Solution along minor fissures and discontinuities parallel to and dipping out of rock faces increases the susceptibility of outcrop to disintegration through frost wedging. The breccia of the Bear Rock Formation has a very high fissure frequency. Much of the strata that sustain pinnacles are particulate cemented rubble packbreccia and mosaic floatbreccias that contain a high proportion of large (>10 cm diameter) subangular dolomite and limestone clasts (Figure 4.14). The lime mudstone cement is preferentially weathered leaving the clasts partially extruding from the surface; subsequent solution and frost action along fissures then removes these blocks. At 10 locations the geomorphic rock mass strengths of pinnacle strata were determined after the method of Selby (1980). A composite rating is assessed based on: intact rock strength, state of weathering, spacing of discontinuities, joint orientations, joint width, fracture continuity, and outflow of groundwater. The majority of pinnacle hosting strata were rated as weak, the more resistant calcite cemented packbreccias were predominantly rated as moderate and the massive Landry Member as strong.

Pinnacles occur in the following situations: (i) on the flanks or near the tops of

steep valley, doline, and canyon slopes, (ii) on the headwalls of mass movement scars, and (iii) along sharp ridge crests. Pinnacles on steep slopes are locally resistant columns of bedrock, the intervening rock having been removed by frost wedging and rockfall. Typically these pinnacles occur as individuals and are bordered by talus. In active river canyons, talus accumulation is limited as these materials are quickly remobilized by braided streams. Where the pinnacles rim the upper slopes of dolines, the frost shattered debris is gradually moved downslope by solifluction and creep. In some instances, a sufficient accumulation of material has occurred on the doline floor to impede drainage.

On ridge crests, pinnacles may not occur as discrete forms. At the Bear Rock Site there are many examples of sharp ridges supporting pinnacles. These features have developed since deglaciation at this site. Crag and tail features suggest the last ice was warm based and thus it is likely the ridges initially had a smooth whaleback form. Rock weathering has generated sharp ridges and pinnacles as high as 15 m in only 12 to 13 ka.

6.2.3 Karren on the Hume Formation

In the study region, much of the outcrop of the Hume Formation is mantled in glacial deposits or is steeply dipping. Thus, no extensive areas of pavement were located in the field or aerial surveys. Small scale karren forms do occur on the Hume Formation though they were not examined in detail. At the Bonus Lake Site, there are subsoil cutters and an area of giant grikes. The latter area is referred to as a giant grikeland and is described in Chapter VIII.

6.3 Dolines and Depressions

Dolines are mesoscale closed depressions of solution origin that constitute the major input landform to many karst systems. Dimensions and morphology vary, most being circular in plan and conical in section. Four genetic classes are recognized: (i) solution, (ii) collapse, (iii) subsidence, and (iv) suffosion. Solution dolines develop

where bedrock corrosion is unevenly distributed in the epikarst. This may be a function of the localized capture of autogenic drainage due to spatial variations in bedrock porosity (drawdown doline), or the routing of allogenic drainage by cover or bordering rocks into inliers or outcrops of karst rock (point recharge doline). Williams (1983, 1985) argues that in carbonate rocks the enlargement of dolines to the classic topographic form requires the development of proto-conduits to link the epikarstic and main aquifers. This establishes an efficient route for the removal of solutes from the doline catchment.

Dolines of other genetic classes are differentiated from solution dolines based on the secondary processes that accompany their development. Debates on classification have focused on areas of overlap between collapse and subsidence forms. Dolines of the collapse end member develop where bedrock or sediment fails catastrophically into underlying conduits. The resulting topographic feature may be distinguished from solution dolines by morphology. Fresh collapse features tend to be steep to vertical sided and have bordering catchments of limited or no areal extent. Where doline walls are accessible, examinations may reveal the presence of fractures across which coherent blocks of bedrock have been vertically displaced. A morphological similarity to solution dolines may arise when surficial materials accumulate within collapse features and their upper walls become dissected by weathering processes.

Bedrock fracture is an integral component of the collapse process. Subsidence normally involves less fracturing, but between collapse and subsidence exists a continuum of process and form. Subsidence dolines and depressions are generated when solution occurs at depth and is propagated vertically to the surface by either sagging and folding, or by stoping through breccia pipes. The latter may also be produced through the failure of cave passages and be responsible for the origin of surficial collapse dolines, but pipes are far more common where evaporites occur in the subsurface. Essential to subsidence is the condition that a formation of high solubility underlies a less soluble cover and that circulating meteoric groundwaters

encounter the lower unit. Cover often consists of insoluble materials such as clastics and chert. Limestone and dolomite may be considered cover rocks when underlain by evaporites. Forms generated by deep solution are called subjacent karst by Jennings (1971, 1985), solution generated collapse structures by Simpson (1987, 1988), and interstratal karst by Quinlan (1978). The latter term is applied to a range of features associated with solution of karst rock beneath a pre-karst cover of rock or sediment. In practise, the term karstification is attributed to changes in secondary porosity of carbonate rocks that are associated with solution and other processes, and the term subrosion is used to describe solution of evaporites under cover (Quinlan, 1978). Subrosion is of particular significance to the study area where the Fort Norman (Bear Rock) and Saline River Formations occur in subcrop.

Two major classes of interstratal karst are recognized: (i) point solution subsidence features and, (ii) areal solution subsidence features (Quinlan, 1978). Point solution features are produced by the localized corrosion of a karst rock beneath cover. Most of these forms are in limestone and have a vertical morphology. This class includes subsoil karren and pipes, geological organs, pocket deposits, and vertical shafts. Many of these forms are gradually infilled by their cover material as they develop, or the cover may fail abruptly and partially or completely infill the feature. It is emphasized that these features are not formed on the surface and then buried; they are younger than their cover.

Areal subsidence features are associated with solution of evaporites in subcrop. Quinlan (1978) includes a range of planar and linear subsidence forms, and breccia pipes in this category. When evaporite removal is approximately parallel to the cover bedding the extensive subrosion of massive salts and sulphates can occur with little brecciation of overlying strata. Cover rocks and the topographic surface are gradually let down as a consequence of the subcrop erosion. However, subsidence may not be uniform if subrosion is concentrated along the axial traces of folds or along the zero edge of dipping or flat lying evaporite strata. Linear subsidence troughs are recorded at anticline crests where underlying salt has been removed

(Adams, 1940, 1944; Quinlan, 1978) and above the zero edge of salt and anhydrite subcrops (Olive, 1957; Quinlan *et al*, 1986) (Figure 6.8). The topographic expression of these troughs is highly variable. Small troughs developed from subsrosion in the shallow subsurface may be sharp and possess several metres of surface relief. At the margins of extensive evaporite subcrops, the positions of active or former dissolution fronts may be marked by a salt slope. The largest troughs may be infilled as quickly as they enlarge and exhibit no relief. The latter are called solution-induced depositional basins by Quinlan (1978) and are commonly reported in the paleokarst literature (e.g., Tsui and Cruden, 1984; Bosak, 1992).

On Great Slave Plain in the southern District of Mackenzie a large linear subsidence trough is developed above the zero edge of the Cold Lake salt member of the Mirage Point Formation (Meijer Drees, 1993). The Mirage Point Formation is the lateral equivalent of the Fort Norman Formation. The subsurface Cold Lake salt is distributed east of the Mackenzie River, from Wrigley to eastern Great Slave Lake. The salt and the bounding Paleozoic strata dip to the west and are locally overlain by flat lying Cretaceous clastics. The dissolution edge is on the northeast side of the salts distribution where it is within a few hundred metres of the surface or the sub-Cretaceous unconformity. The subsidence trough has a length of approximately 150 km and is expressed as an asymmetrical syncline in Devonian strata overlying the Mirage Point Formation. Its surficial expression is partially masked where the Cretaceous infills the structure. This shows that much of the subsrosion was pre-Cretaceous.

Solution breccias usually develop penecontemporaneously with evaporite subsrosion, and are common where interbedded carbonate and evaporite strata are exposed to meteoric groundwater. The process of solution brecciation is discussed in detail in Section 4.7.2.3. It is topographically significant because of the associated foundering of cover rocks and the development of breccia pipes. Quinlan (1978) in a survey of the latter, found individual pipe diameters ranged from 1 to 1000 m, with upward stoping passing through a maximum 1500 m of cover. They occur in large

numbers wherever there are extensive subcrops of evaporites. In southeastern Saskatchewan, subsidence of salt and anhydrite of the Middle Devonian Prairie Evaporite has generated a variety of fault bounded solution generated collapse forms (Simpson, 1988). In plan view, features exhibit a circular, linear, wedge or blanket shape, while pipe, chimney, sink, dome, wedge and blanket morphologies occur in elevation. Where subsidence is concentrated at the evaporite superface (supraface), lateral expansion of conduits and localized subsidence and collapse has produced extensive blankets of breccia. Wedge, pipe, and linear bodies occur where subsidence is directed at the evaporite margin. Groundwater passing through underlying fractures or carbonate mounds to the evaporite subface produce pipes that slope through overlying strata (Figure 6.8). Pipes extend as much as 975 m from the evaporite into cover rocks and the surficial expression may be marked by topographic depressions and circular ponds (Christiansen, 1971a, 1971b; Gendzwill and Hajnal, 1971; Christiansen *et al*, 1973). These features occur across the full area of salt subcrop although most of the large topographic sinks occur above the anhydrite member (Simpson, 1988). Quinlan and Ford (1973) suggest there may be hundreds of such pipes in the southern prairies, masked topographically by overlying glacial sediments. Large complex depressions are also recorded in the subsurface of the same region. The Rosetown Low is a 370 km² basin developed in the Devonian, 1500 m below the surface (De Mille *et al*, 1964). It represents a large area where the Prairie Evaporite was removed by post-Mississippian subsidence and later infilled with younger sediments. Collapse structures are also associated with subsidence of the Cold Lake Formation in northeastern Alberta, and the Cold Lake salt member of the Mirage Point Formation in southern District of Mackenzie (Meijer Drees, 1986, 1993).

Ford and Williams (1989) identify four possible dynamic/topographic states for breccia pipes: (i) active, upward propagating pipes without a surface expression, (ii) active or inactive pipes expressed at the surface as a closed depression with or without a surface overflow channel, (iii) inactive pipes buried by younger strata, and

(iv) inactive with the pipe standing as a possible relief feature, owing to differential erosion with the surrounding strata.

Suffosion dolines are surface depressions in unconsolidated materials overlying porous bedrock. Fine grained sediments are mobilized by infiltrating autogenic recharge and downwashed into subsoil karren and fissures. This is aided by mineral solution within the sediment cover. Suffosion dolines are common in alluvial and glacial deposits overlying buried karst surfaces, and in the alluvium of dry valleys.

6.3.1 Distribution and Identification of Dolines and Depressions

Karst depressions have been widely reported in the northern Mackenzie and Franklin Mountains, but there are few data available on the distribution and range of features (e.g., Hume, 1954; Aitken and Cook, 1974; van Everdingen, 1981; Michel, 1986; Duk-Rodkin, personal communication, 1990) (Figure 6.1). van Everdingen (1981) has mapped karst from the Norman Range eastward to Great Bear Lake. Many landforms identified were simply depression contours shown at 50 foot intervals on 1:50000 scale topographic maps. This study involves mapping dolines and depressions in the Carcajou Range (Figure 6.9) and at the southern extent of the Norman Range (Bear Rock Site, Chapter X). The products of this work are viewed as a substantial improvement on earlier surveys in the region.

Field sites were traversed by foot and the locations of depressions and ponors recorded. Mapping of intervening areas was accomplished by aerial photographic interpretation, ground truthed on data gathered during field surveys. The scale of photography varied from 1:15000 to 1:35000. Depressions were identified based on topography, drainage, and vegetation. The most distinctive features were enclosed in bedrock and had topographic catchments that were easily defined from the photography; ponded drainage and overflow channels occurred in some instances. Where the surface is mantled by sediment and the relief low, drainage channels and solifluction lobes were used to determine the direction of surface flow and the points of convergence functioning as sink points. On flat or gently sloping terrain, dolines

were often identified as shallow, partially drained or empty ponds. These were normally linked by a series of overflow channels. Vegetation on protected and well-drained slopes fringing sink points often included large individuals of black and white spruce, and commonly, trembling aspen. The aspen was notably absent from exposed and moist locations.

In addition to dolines in bedrock, there are several areas in the Carcajou Range where small depressions occur in former meltwater channels or dry valleys. There is a possibility of confusion with kettles in fluvio-glacial outwash. Several characteristics were used to help distinguish between them. Suffosion dolines tended to be clustered in their distribution above outcrops of the Bear Rock and Saline River Formations. Kettles were more often solitary features and demonstrated no bias to a particular formation. Often former meltwater channels and braidplains could be identified in proximity to kettles. Surface drainage was often focussed to suffosion dolines while kettles remained independent. Suffosion dolines were more likely to drain than kettle ponds.

Field work revealed a much higher doline density than was apparent from the photography. Under ideal conditions, features of diameter greater than 10 m could be identified by the latter method. However, below treeline and where local relief was small, features of that dimension were undoubtedly overlooked. Most often the doline markers on Figure 6.9 are disproportionately large given the size of the landform on the ground; some are ponors within larger depressions. Where doline densities were very high, the distribution of markers represents the total population. Maps in subsequent chapters provide detail at the scale of individual study sites.

Often it was possible to recognize dolines and depressions as members of a particular group; however, no attempts were made to index all features mapped. Several genetic categories of depressions are identified: (i) collapse-subsidence dolines, (ii) solution dolines, (iii) suffosion dolines, (iv) compound depressions, blind valleys, and pocket valleys, (v) subsidence troughs, (vi) poljes, and (vii) fault-bounded or structural depressions. The morphology of features between and within

groups are highly variable.

Collapse-subsidence dolines, depressions, and troughs are observed on both karst and non-karst rocks. These strata function as cover over evaporites which are in shallow subcrop and are subroded by meteoric groundwaters. Frequently, cover hosted depressions occur on: (i) the crests and flanks of anticlines, (ii) monocline limbs, and (iii) gently dipping or horizontal strata. Landform density is highest above local zero edges of evaporite subcrops.

Solution dolines and depressions, shallow collapse features, and blind valleys occur on exposed karst rock in a variety of structural situations. The largest depressions and polje are usually fault bounded, moraine dammed, or glacially scoured. The following sections describe the distribution and general characteristics of the depression landform categories and the typical structural situations in which they are found. Emphasis is given to those developed on the Bear Rock Formation.

6.3.2 Collapse-Subsidence Dolines and Depressions

Dolines of collapse origin are characterized by low width to depth ratios, sheer walls, foundered and faulted strata, and small topographic catchments (Figure 6.10). Dolines of this morphology are common in the study region, though it is likely that few have been generated by collapse into underlying conduits. They are predominantly subsidence features of the types described above. There are many examples from Carcajou Range (Dodo Canyon, Bonus Lake, Ration Creek Sites), Great Bear Karst (Kelly Lake, Moon Lake, Vermillion Creek), and Imperial Hills (Figure 6.1). In each case, cover units have failed due to stoping of underlying breccia pipes or with large linear depressions by trough subsidence (Figure 6.8). The cover units include: (i) Tertiary gravels, (ii) Cretaceous clastics (Little Bear and East Fork Formations), (iii) Upper Devonian clastics (Imperial, Canol, Hare Indian Formations), (iv) Middle Devonian carbonates (Hume and Bear Rock Formations), and (v) Cambrian to Silurian dolomites (Franklin Mountain and Mount Kindle Formations). Subrosion occurs in either the Fort Norman (Bear Rock) or Saline

River Formations.

6.3.2.1 Regional Structural Setting

Collapse-subsidence depressions occur in a number of structural situations. The following sections provide a brief description of the regional distribution of these features. This is not a complete inventory but rather a sample that typifies the landform setting.

Vermillion Creek

The most striking regional example of a post-glacial collapse-subsidence doline is the Vermillion Creek Sinkhole (Quinlan and Ford, 1973; van Everdingen, 1981) (Figures 6.1, 6.11). It is the largest of several features that occur near Vermillion Creek on gently sloping terrain, west of Norman Range (Figure 6.1). It is an oval shaped doline approximately 120 m long, 60 m wide, and 40 m deep, occurring in shale of the Canol Formation. At the nearby Imperial Vermillion Ridge No. 1 well, the Fort Norman Formation occurs 300 m below the surface. The local evaporite thickness is approximately 250 m (Table 4.3, Tassonyi, 1969; Pugh, 1993). Water samples taken from within the sink and at nearby subpermafrost springs that flow into Vermillion Creek have high concentrations of Ca^{2+} and SO_4^{2-} ions (Mackenzie Valley Transportation Corridor Study, 1973; van Everdingen, 1981). These data indicate active circulation of groundwater in contact with anhydrite/gypsum. Subrosion in the Fort Norman Formation has developed breccia pipes that have stoped through the Hume and thin intervals of the Hare Indian and Canol Formations to the surface, generating the collapse-subsidence dolines.

Great Bear Karst

West of Smith Arm of Great Bear Lake, east of Moon Lake, and along the eastern Franklin Mountains, there are several hundred dolines and large depressions in gently dipping strata of the Franklin Mountain and Mount Kindle Formations (Figure

6.1, van Everdingen, 1981). Recharge to groundwater flow systems of the Franklin Mountains occurs along mountain crests and flanks with the principal aquifers being the Bear Rock/Fort Norman, Mount Kindle, Franklin Mountain, and Saline River Formations (Michel, 1986). Winter icings show much discharge occurs in down dip valley bottom locations and at fault traces.

Subrosion of the Saline River Formation along groundwater flowpaths has generated the network of dolines in the Franklin Mountain strata. Many of these features are older than the most recent glaciation. The expanding network of dolines and depressions has captured a significant amount of surface drainage. Large scale areal subsidence has occurred over the crests of structural domes, where much of the underlying Saline River Formation has been subroded and the overlying strata let down. Similar features are noted in southern Franklin Mountains where the evaporite units occur in shallow subcrop (e.g., Cap Mountain).

Imperial Hills

There are collapse-subsidence landforms in the Imperial Hills of the Mackenzie Plain (Figure 6.1). The Hills consist of folded Paleozoic strata located between the mountain front and Carcajou River (Imperial Anticline: Figure 4.6). A range of karst features are present. Dolines occur on the crests or limbs of anticlines, where the Bear Rock Formation outcrops or is in shallow subcrop. At some locations, dolines have coalesced to form large lobate depressions or linear troughs that are aligned parallel to strike (Figure 6.12). Figure 6.12 and similar diagrams depict a change in facies and thickness between the Bear Rock and Fort Norman Formations, from solution breccia to anhydrite. The Arnica and Landry Formations are not shown separately though they are commonly recognized in well records as distinct units. In outcrop, their thicknesses do not warrant mapping at these scales. They are included with either the Bear Rock or Fort Norman Formations.

In the eastern Imperial Hills, sharp collapse-subsidence dolines are developed in the Bear Rock, Hume, and Hare Indian Formations on fold limbs and crests.

Recharge passing through cover units has subroded the Fort Norman Formation. At the eastern plunging end of Imperial Anticline, a stream draining an area of several square kilometres on the Hume and Hare Indian Formations sinks into a large depression in the Bear Rock Formation. It is thought to resurge 1.5 km down dip at Sammons Creek, a tributary to Carcajou River (Hume and Link, 1945).

Mountain River

Dolines and compound depressions are found at the Mackenzie Mountain front near Mountain River (Figure 6.1). In this area, the Saline River Formation is near its depositional edge with only red beds and shales locally represented. To the west, the Bear Rock and Fort Norman Formations grade laterally into the Arnica and Landry Formations. Subsidence depressions are confined to those areas where the Fort Norman Formation occurs in subcrop.

A monocline structure forms the mountain front in the region (Gayna Flexure: Figure 4.6). Helikian strata outcrop in the crests of broad anticlines to the southwest (Stony and Tawu Anticlines). Cambrian to Devonian strata outcrop on the monocline limb, and clastics on the Mackenzie Plain to the northeast (Figure 6.13). Karst depressions occur on the reef limestone member of the Ramparts Formation and on the Upper Devonian and Cretaceous formations. The depressions on the Ramparts Formation are probably solution dolines while those on the clastics units are interstratal karst of subsidence origin. Occasionally, linear troughs are developed parallel to strike. Evidently recharge passes down dip through the Hume, Bear Rock, Mount Kindle, and Franklin Mountain Formations bringing meteoric water into contact with the Fort Norman Formation. Across the area of subsidence depressions, the Fort Norman Formation occurs as much as 900 m below the sub-Cretaceous unconformity and 1200 m below the topographic surface. Formation thicknesses depicted in Figure 6.13 are from outcrops and a nearby well record (Imperial Whirlpool No.1). Elsewhere in the region interstratal karst features are recorded in similar structural situations along the Mackenzie Mountain front.

Ration Creek

At the Mackenzie Mountain front east of Little Bear River, the hanging wall of Gambill Thrust forms a prominent ridge. Cambrian to Devonian strata outcrop along the ridge and rest unconformably on Cretaceous clastic units. Dolines and troughs occur on the Hume, Bear Rock, and Mount Kindle Formations above the local zero edge of the underlying Saline River Formation. A sheer 50 m deep circular collapse-subsidence doline in the Bear Rock Formation is the sharpest single feature (Figure 6.14). Strata of the underlying Mount Kindle Formation are exposed at the base of the sink. The Saline River Formation has been identified as a surface of décollement in the region (Aitken and Cook, 1974; Aitken *et al*, 1982), and the planes of thrust faults as routes of regional groundwater flow (Michel, 1986). The deep doline is the obvious surface expression of a breccia pipe passing from the Saline River Formation, through dolomite of the Franklin Mountain and Mount Kindle Formations (subsurface Ronning Group), to the surface Bear Rock Formation. The combined thickness of the Ronning Group in the area is 500 to 600 m (Pugh, 1993).

The terrain east of Gambill Thrust consists of low dissected plateaux in gently dipping Cretaceous and Tertiary clastics. Several shallow dolines occur along the crest of a plateau ridge 10 km east of Ration Creek Sink. These features may owe their origin to subsidence in the Fort Norman Formation. The C.S. Bluefish K-71 well (64°50'30" N Lat., 125°59'30" W Long.) is the closest borehole that penetrates to the Fort Norman Formation. In that well, the Fort Norman is overlain by 1338 m of Devonian and Mesozoic strata, 436 m of which are Mesozoic units (Pugh, 1993). If these dolines are the surficial expression of breccia pipes then subsidence must be propagated through a minimum of 900 to 1100 m of cover. The local hydrogeology is unlike the other cases described. The cover strata are gently dipping, thick impermeable units and there is no clear recharge-discharge zonation as is seen in the monocline, anticline, and fault examples. The possible superimposition of a glacial aquifer would increase the hydraulic potential, or unseen faults may move groundwaters of a regional flow system to the Fort Norman Formation. However,

it is also possible these shallow features are kettles or other pseudokarst forms.

Carcajou Canyon

Several small collapse-subsidence dolines are found on the steeply dipping northeastern flank of MacDougal Anticline above Carcajou Canyon. A series of dolines, each 20 to 30 m in diameter and up to 10 m in depth, are located along a lineament in the Franklin Mountain Formation. These are northeast of the Saline River outcrop, and represent subsidence of the latter beneath approximately 50 to 100 m of cover. Nearby are some very shallow dolines in red beds of the Saline River. These landforms could be considered solution-subsidence features since little collapse of strata accompanied shallow subsidence.

Dodo Canyon North Karst, Bonus Lake

There are collapse-subsidence dolines at the Dodo Canyon Site (Chapter VII). The northern section of this site is called the North Karst. Within that area, individual dolines and compound depressions occur on the northward dipping limb of MacDougal Anticline in the Hare Indian and Hume Formations (Figure 6.10). Many features are steep sided but the slopes are vegetated, suggesting a period of recent stability. At the Bonus Lake Site, collapse-subsidence dolines are confined to the Hume Formation, many are partially infilled with talus. The density is high, exceeding 10 km⁻², they are discussed in Chapter VIII. At both locations, subsidence of the Fort Norman Formation is responsible for subsidence.

6.3.3 Depressions on the Bear Rock Formation

At the Dodo Canyon and Bear Rock Sites, depressions on outcrops of the Bear Rock Formation include single and compound dolines, blind valleys, subsidence troughs, and fault bounded lowlands. These features are sufficiently numerous to warrant separate treatment from the collapse-subsidence depressions described above.

6.3.3.1 Dolines

On the Bear Rock Formation, dolines exhibit forms ranging from sharp vertical walled depressions to broad flat floored shallow features (Figures 6.10, 6.11, 6.15). Ground surveys revealed that many collapse or subsidence dolines were partially infilled with talus, giving them the solution morphology. Consequently, individual or compound dolines could be attributed to combinations of subsidence, collapse, solution, and other processes. At each of the field sites, the general orientation of doline long axes were parallel to local strike. In addition, many dolines occurred within, or were aligned with, glacial meltwater channels (Figures 6.11, 6.17).

There are many shallow, steep sided dolines at the Dodo Canyon Site where the Landry Member is locally present (e.g., Figure 6.10). The Landry functions as a strong cover unit over the Brecciated Member. Dolines occur above local areas of collapse and subsidence into the underlying evaporite breccia. They are generally 20 to 50 m in diameter and 5 to 10 m in depth. Where talus is absent, the walls may be near vertical. There are two main variants of these dolines. The first type usually has a flat to slightly concave bottom that is largely vegetation-free (Figure 6.15a). Many of these held water through the summer period due to a slow rate of infiltration. Overflow channels were common and were activated only following substantial ponding in the early spring. It is likely that water held in these dolines freezes to the bed in winter, and that the underlying permafrost and fine sediments account for the slow summer drainage of the ponds. This situation is similar to that described by Brook (1976) for the Nahanni Karst (Chapter II). The poor hydrological connection between the doline catchments and the underlying breccia results in a slow rate of solute removal from these basins. Data show that surface waters in these slow draining dolines are near saturation with respect to calcite and dolomite (Chapter VII). Thus, recharge through them has little solution potential. The flat floored morphology is preserved as the rate of talus and debris accumulation on basin floors keeps pace with solute removal. In some cases, debris accumulation has reduced the relief of the features, producing very shallow depressions.

The second type of doline is steep sided with a high depth to width ratio and a conical bottom (Figure 6.15b). They are developed in the Landry Member and extend vertically into the underlying breccia. Observations and strandline positions show that these dolines drain rapidly in the spring and early summer. The bottoms are commonly lightly vegetated (Figure 6.11). Hydrochemical data show that waters draining through these depressions are aggressive to calcite and dolomite. The efficient removal of solutes from these basins has contributed to their deepening into the Brecciated Member. These solution-subsidence dolines provide a good contrast with the perched examples.

At the Bear Rock Site, the Landry Member is locally absent over much of the karst area. Consequently, dolines do not have a sharp morphology, instead depressions tend to be large compound features. Sink points are shallow and marked by grasses and tall aspen and spruce (Figure 6.11). Ponors within large depressions have the same characteristics.

At the Dodo Canyon Site, there is evidence that the downslope walls of many former dolines have eroded away, producing cirque shaped basins (Figure 6.16). These features are called breached or horseshoe sinks. A steep backwearing slope gradually intercepts the doline, opening a gap in the depression. The downslope wall is eroded by a combination of surface overflow, solution, and mass wasting. Surface overflows generate channels by solution and abrasion. Local groundwater passes from the sink points to seeps at the base of the slope. Rock is removed along these flowpaths but more importantly slope caves may develop at seep points (Section 6.4.1). Slope cave formation is accompanied by mass wasting and slope retreat. There were several such features observed at the Dodo Canyon Site across several stages of development. Aerial photography showed the recent failure of one such doline. It was intact in 1974 when it ponded water: examination in 1988 revealed a slope cave collapse on the downslope wall and the feature was drained. In some breached sinks, the hydrological functioning of the karst continues, with local sinking on the doline floor and a downslope resurgence as supra and intrapermafrost

springs. In other cases, the seep positions have migrated upslope into the body of the breached doline.

6.3.3.2 Compound Dolines

Depressions are not limited to individual doline forms. Compound dolines (uvalas), fault bounded lowlands, blind valleys, subsidence troughs, and poljes are recorded in the study region. Uvalas result from the expansion and coalescence of adjacent dolines. They occur on the Bear Rock and Hume Formations. In plan view, the long axes of these depressions are often oriented parallel to strike, though their geometry can be irregular (e.g., Big Depression: Figure 7.7). In profile, they are similar in character to single dolines and differ only in scale. At the Dodo Canyon and Bonus Lake Sites, fluvio-glacial deposits are present within several compound dolines. Field observations suggest glacial modification of these features by scour and meltwater erosion.

At the Bear Rock Site (Norman Range) there are three large depressions. The features are an order of magnitude greater in their size than depressions at the Dodo Canyon and Bonus Lake Sites. The largest depression is three kilometres in length and 100 m deep. It is aligned along a reverse (thrust) fault in the Saline River Formation (Chapter X). The Franklin Mountain and Bear Rock Formations are exposed on the hanging wall. Elsewhere on the range, large compound depressions occur on gently dipping strata of the Bear Rock Formation, covering areas up to 1.5 km² with local relief to 100 m.

6.4 Blind Valleys

Valleys may develop on an area of karst rock in response to allogenic stream inputs. Valley morphology is related to: (i) the amount and timing of allogenic discharge, (ii) the infiltration capacity of surficial materials, (iii) the hydraulic conductivity of the karst rock, and (iv) the hydraulic gradient of the system (Ford and Williams, 1989). Through valleys develop where allogenic inputs exceed the infiltration

capacity and hydraulic conductivity of the karst aquifer. The largest through valleys are deeply incised and may function as regional base levels, their streams gaining discharge from springs along their courses.

Where allogenic inputs are less substantial, more of the discharge is captured by stream sinks and influent channel stretches. This fraction increases with progressive karstification of the aquifer. A half or semi-blind valley is one where all of the allogenic discharge is captured under normal flow conditions. During flood events the full valley length will take flow. Semi-blind valleys contain ponors and shallow dolines that function as stream sinks. A reverse step forms in the long profile, due to higher rates of corrosion in upstream reaches. In a fully developed blind valley, the total allogenic input is taken up by the karst aquifer. The hydrological function of a blind valley can be altered by changes in surficial materials that influence infiltration. The deposition of fine grained sediments or the aggradation of permafrost may result in a blind valley changing to semi-blind or through valley status.

There are through, semi-blind, and half-blind valleys on the karst rocks of the study area. Carcajou Canyon is an example of a through valley; it dissects 35 km of the Franklin Mountain, Mount Kindle, Bear Rock, and Hume Formations along the mountain front. Regional thermal springs discharge into Carcajou River where it cuts through onto the Mackenzie Plain. Straight Valley is an example of a semi-blind valley at the Dodo Canyon Site (Chapter VII: Figure 7.7). The incision of Dodo Canyon has cut off its allogenic source. Straight Valley is oriented normal to strike, has several small ponors along its length, and a large doline at its maximum penetration into the Dodo Canyon Karst. It is classified as semi-blind as some allogenic waters are diverted away from ponors and runoff to an adjacent stream course. At the Bonus Lake Site, a small stream on the Bear Rock Formation flows through a strike aligned valley along the contact with the Hume Formation (Chapter VIII: Bear Rock Valley). The stream gradually loses flow along its course and sinks in an exposure of the Hume Formation, a classic example of a blind valley.

However, many of these valleys features have been modified by glacial meltwaters and should be considered polygenetic features.

6.5 Subsidence Troughs

The origin and characteristics of subsidence troughs are discussed in Section 6.3. Troughs in the study area occur in several structural situations but predominantly near the zero edge of the Bear Rock Formation (e.g., Figure 6.8: salt slope) and along the axial traces of anticlines. Troughs of the latter type are developed in either the Bear Rock or in cover units where evaporite is in the shallow subsurface. In morphology, troughs are generally oriented parallel to strike, of variable length and width, and exhibit up to 50 m relief. In many locations, troughs have been modified by glacial meltwaters or diverted mountain drainage.

At the field sites, shallow troughs are recorded along the contacts between the Mount Kindle and Bear Rock Formations (Dodo Canyon Site) and between the Bear Rock and Hume Formations (Bonus Lake Site). Larger examples are seen at Ration Creek, along the MacKay Range (Figure 6.1), and at the Bear Rock Site (Chapter X). At Ration Creek, a linear depression of length 1,100 m, width 50 to 100 m and average depth 20 m, occurs in the Bear Rock Formation on the hanging wall of Gambill Thrust (Figure 6.14). The Bear Rock dips steeply and the trough is developed along the trace of its outcrop. Subrosion of evaporite has contributed to the lateral expansion of a surface depression along strike.

6.5.1 MacKay Range

The MacKay Range is an upthrust inlier of Paleozoic strata on the Mackenzie Plain (Figure 6.1). The range rises 500 m above the level of the surrounding terrain. Steep thrust and reverse faults are exposed on its northeastern side where the Bear Rock and Franklin Mountain Formations are brought to rest upon the Cretaceous Slater River Formation (Figure 4.2). Across the crest area, a tight anticline runs the full length of the range (Figure 6.18). Strata as old as the Cambrian Saline River

Formation are exposed. The fold limbs dip steeply with local values exceeding 70°.

Two large linear depressions are developed along the range; both are close to the range crest southwest of the fault traces. The bounding slopes are steep and mantled in talus. The larger feature is illustrated on Figure 6.18. The depression has a length of 3.2 km, an average width of 1 km and a maximum depth of 160 m. It is developed in the Bear Rock Formation. The Franklin Mountain Formation is exposed at a fault to the northeast. These features are interpreted as subsidence troughs. Post-Paleocene folding and faulting upthrust Paleozoic strata. Subsequent erosion of the Hare Indian, Canol, and Hume Formations over much of the range exposed the Bear Rock Formation to fresh meteoric groundwater. The removal of the evaporite in the Bear Rock and possibly the underlying Saline River Formation has generated the troughs. Well records in the area show the two formations have a combined total of 450 m of anhydrite and halite.

6.6 Poljes

Poljes are karstically drained, flat floored, closed basins that are at least 400 m in width and are bounded by steep valley walls (Gams, 1978). Moraine Polje is the only depression feature in the study area that satisfies this formal definition (Figure 6.1). The basin floor has an area of 5 km² and a maximum width of 1250 m. The total drainage area is 92 km², making it the largest karst watershed in the region. Moraine Polje occupies the limb of a major syncline in Devonian strata and is elongated parallel to its axial trace. Runoff from the Katherine Group, Franklin Mountain, and Mount Kindle Formations sinks on the basin floor near the contact between the Bear Rock and Hume Formations. The basin is dammed by a moraine of Hungry Creek age, deposited by the lobe of the Laurentide Ice Sheet that occupied the Keele River Valley (Chapter V). However, sinking and resurgence points are in bedrock. The feature matches the description of a border polje, where allogenic runoff onto an alluviated basin sinks into underlying karst rock.

There are also examples of small overflow poljes. In these cases, the floors of

the depressions are underlain by relatively impermeable strata. Spring flow from one end of the polje sinks through ponors at the opposite end. At the Dodo and Bonus Lake Sites, there are shallow depressions of this basic morphology (Carcadodo and Bonus Valleys). In both cases, the shale interval of the Hume Formation forms the local aquitard. These features are polygenetic. The flat floors have been produced by combined action of glacial meltwaters and lateral corrosion. In addition, they are not sufficiently wide to qualify as formal poljes, though they do function hydrologically as karst.

6.7 Caves

Conduits are the throughput landforms of the karst system. The widespread distribution of dolines and the discharge behaviour of some springs suggests conduit aquifers occur in the study region. Well records from Mackenzie Valley record cavernous porosity in the Bear Rock (Fort Norman) Formation (e.g., Hume and Link, 1945). Despite this, there are few locations in the study region where enterable relict cave passages are preserved. Solution caves were observed in the Bear Rock and Hume Formations, but only in the latter did they warrant exploration. Far more common were slope caves.

6.7.1 Slope Caves

Cliff and steep exposures of the Brecciated Member of the Bear Rock Formation often appear to possess substantial cavernous porosity (e.g., Figure 4.11). Close investigation of what may be large solution cave openings are usually shown to be shallow rock shelters termed slope caves or frost pockets (Figure 6.19). The cave mouths range from <1 to 10 m in height. The openings are normally backed by inclined subcircular passages that gradually taper to a pinch. Occasionally, rectangular rooms were observed to expand from small openings. In a cave from the Bear Rock Site, a room with a volume of 80 m³ enlarged from an entrance of 0.6 m height.

Total passage lengths are usually <10 m. Interior surfaces are frost riven, rockfall debris mantles the cave floors, and talus ramparts occur at cave entrances. Patterned ground is observed on passage floors and on the talus ramps. Often a sink point as a shallow doline or ponor is located immediately upslope of the cave and groundwater seeps are common in the ceiling rock. There is a tendency for cave openings and passages to develop along large fractures and shear planes (Figure 6.19). Displacement along some of these planes were recorded by the presence of slickenslides. These general observations are consistent with slope cave descriptions from other periglacial regimes (e.g., Schroeder, 1979; Mitter, 1982).

A slope cave at the Dodo Canyon base camp was observed from early spring to late summer. Upslope a shallow doline is present in the Landry Member. This sink functions as a site of depression storage during snowmelt and following rainfall events, and is the likely supply of groundwater flow to the cave (Figure 6.19). The drip rate through the slope cave ceiling increased over the course of the summer, as seasonal frost thawed and flow routes were established between the sink and seeps points. In addition, the drip rate increased following major storm events.

Morphological evidence suggests slope cave initiation occurs on steep slopes at the locations of groundwater seeps and minor springs. Frost action and solution both play a role as they do in pinnacle development. Solution of the limestone clasts and micrite cement gradually increases the effective porosity and rate of water transmission from sink to seepage points. The rock mass strength is reduced as breccia fragments are loosened. Frost wedging and gravitational fallout of these loose clasts enlarge the passage and produce the frost riven appearance of ceilings and walls.

Rockfall frequencies were high during the freeze thaw cycles of late summer when the rock surfaces were moist. Rockfall was spatially concentrated at the top of the passage where tensional stresses are maximum and groundwater seeps common. Clast fallout and occasional slab failure generate the debris mantle and talus rampart. These materials are moved slowly downslope by slow mass wasting

processes. At the Bear Rock and Dodo Canyon Sites, the strata that support these features are primarily vuggy particulate cemented floatbreccias.

6.7.2 Solution Caves

The Nahanni Formation of the southern Mackenzie Mountains is host to extensive solution caves in the South Nahanni River area (Brook, 1976). The Hume Formation is the northern Mackenzie Mountain equivalent to the Nahanni Formation. Solution caves are most common in the upper massive member of the Hume at the Bonus Lake and Dodo Canyon Sites.

The caves explored and mapped were limited in their length. There were no significant finds in the area examined. Cave entrances were modified by periglacial processes. They displayed many attributes of slope caves: frost riven walls, debris ramparts, and patterned ground. The extent of frost penetration into a cave is related to the passage diameter, average wind conditions, and cave geometry (Wigley and Brown, 1976). Caves with multiple large entrances may experience seasonal frost several hundred metres within a passage. Most of the caves examined in the study had only one entrance, often of small diameter, or had a low passage close to the mouth. Frost shattered surfaces generally extended only 5 to 20 m into these caves. In the largest caves, there were marked changes in cave climate. The frost riven entrance zone experiences above freezing temperatures during the summer period; this is backed by an area of hoar frost and ice speleothem that occasionally thaw, and finally within the interior a dry permafrozen zone.

Solution caves were found in the following situations: (i) as vertical fissures adjacent to cliff edges, (ii) on the downslope wall of dolines, and (iii) as fragments of strike aligned phreatic passage. In the first case, the initial fissures may have been generated by stresses accompanying cambering at cliff edges. However, there is evidence of solutional enlargement. One example from Carcajou Canyon displayed subrounded passages and a horizontal section. This cave had no upslope catchment, suggesting the possibility of ice contact speleogenesis. At a steep exposure at Bonus

Lake, vadose passages are cut through 20 to 30 m of the Hume Formation where allogenic drainage is concentrated off the Hare Indian Formation. Similar features are reported in the Franklin Mountain Formation at the MacKay Range (Ford, personal communication, 1994).

In the second situation, small cave fragments were observed penetrating the downslope walls of dolines in the Hume Formation at Bonus Lake. These fragments were above the level of the active doline ponors. The passages were frost riven with much rockfall debris on their floors. These fragments are abandoned conduits that were last active when doline floors were at a higher level. In these dolines, vertically directed solution and subsidence exceeded lateral erosion and therefore horseshoe or breached sinks did not develop.

Most of the caves examined belong to the third class. At Bonus Lake, remnants of an extensive system of phreatic conduits are preserved in upland blocks of the Hume Formation. The system has been dissected and fragments can be extrapolated across dolines, canyons, valleys, and meltwater channels. Mapping shows a system of passages that are predominantly parallel to strike with a slight inclination down dip. Some sections are aligned with joints and fractures that are normal to strike. The cave passages examined were phreatic in their morphology, they have smooth walls that are subrounded in section with occasional solution pockets. The single longest cave explored had only 100 m of maze passage. Usually the caves became impassable due to sediment fills, breakdown or pinches. Much of the sediment fill was of glaciolacustrine and fluviglacial origin. Composite forms were present as arches. The single largest example was 20 m high and 15 m wide (Chapter VIII).

The distribution and characteristics of these caves suggest the initial development occurred on gently dipping exposures of the Hume Formation. A system of strike aligned proto-conduits was gradually enlarged as shallow solution dolines were developed and linked. Events in the Quaternary fragmented the conduit aquifer at Bonus Lake. Canyon incision and the erosion of meltwater channels locally increased the hydraulic potential, driving groundwater circulation into the

underlying Fort Norman Formation. Subsidence-collapse produced deeper dolines and troughs, and large scale foundering. Consequently, the Hume conduit aquifer was abandoned. The relict passages have been modified by glacial and periglacial processes. Many contain glacial fills and all have been modified by frost, producing the coarse ramparts at entrances.

6.8 Tufa

Tufa and travertine are the principal output landforms of the karst system. Tufa is a granular deposit of calcium carbonate that accretes to algal filaments and plant fragments at spring and shoreline locations (Ford and Williams, 1989). Typically tufa is coarse grained, earthy, and has a high porosity. Travertine is a dense, layered, crystalline carbonate deposited within conduits or at highly mineralized hot springs.

In the study area, tufa deposits were observed at spring locations at the Dodo Canyon and Bear Rock Sites. In both cases, the spring waters were oversaturated with respect to calcite. These data are presented in Chapters VII and IX.

6.9 Pseudokarst Forms

In the study area there are depressions that were not formed primarily by solution, including: (i) kettles in fluvio-glacial outwash, (ii) depressions in mass movement deposits, (iii) thermokarst forms, and (iv) hummocky moraine. Usually it was possible to differentiate between such pseudokarst forms and legitimate karst depressions.

The characteristics used to distinguish between kettles and dolines are discussed in Section 6.3.1, kettles are not plotted on Figure 6.9. Several rotational slumps were observed on canyon margins in the Mount Kindle Formation (e.g., Figure 5.8). In addition, a major rock avalanche is present on the western wall of Carcajou Canyon southeast of the Dodo Canyon Site developed in the Franklin Mountain Formation. There were also several active layer detachments and mudflows in surficial materials. Normally the mass movement deposits did not

possess closed depressions. However, on slumped blocks of the Mount Kindle Formation there are depressions that function hydrologically as dolines. Solution contributed little to their development and they are not identified on Figure 6.9. The deposit of the Carcajou Canyon rock avalanche contains several depressions. The failure surface appears to have been the contact zone between the Saline River and Franklin Mountain Formations. Solution within the former may have contributed to the failure. It is likely that solution continues in the slide mass and these depressions are therefore treated as karst.

Thermokarst forms were identified at the periphery of the Bear Rock Site, in an area of high ground ice content. Such depressions are primarily confined to the Mackenzie Plain and are not significant in the mountainous terrain where ground ice content is generally low. Similarly, hummocky moraine deposits are not common in the study region. There are small ponds and depressions in glacial sediments in some high cirques in the Canyon Ranges but these are easily recognized from aerial photography.

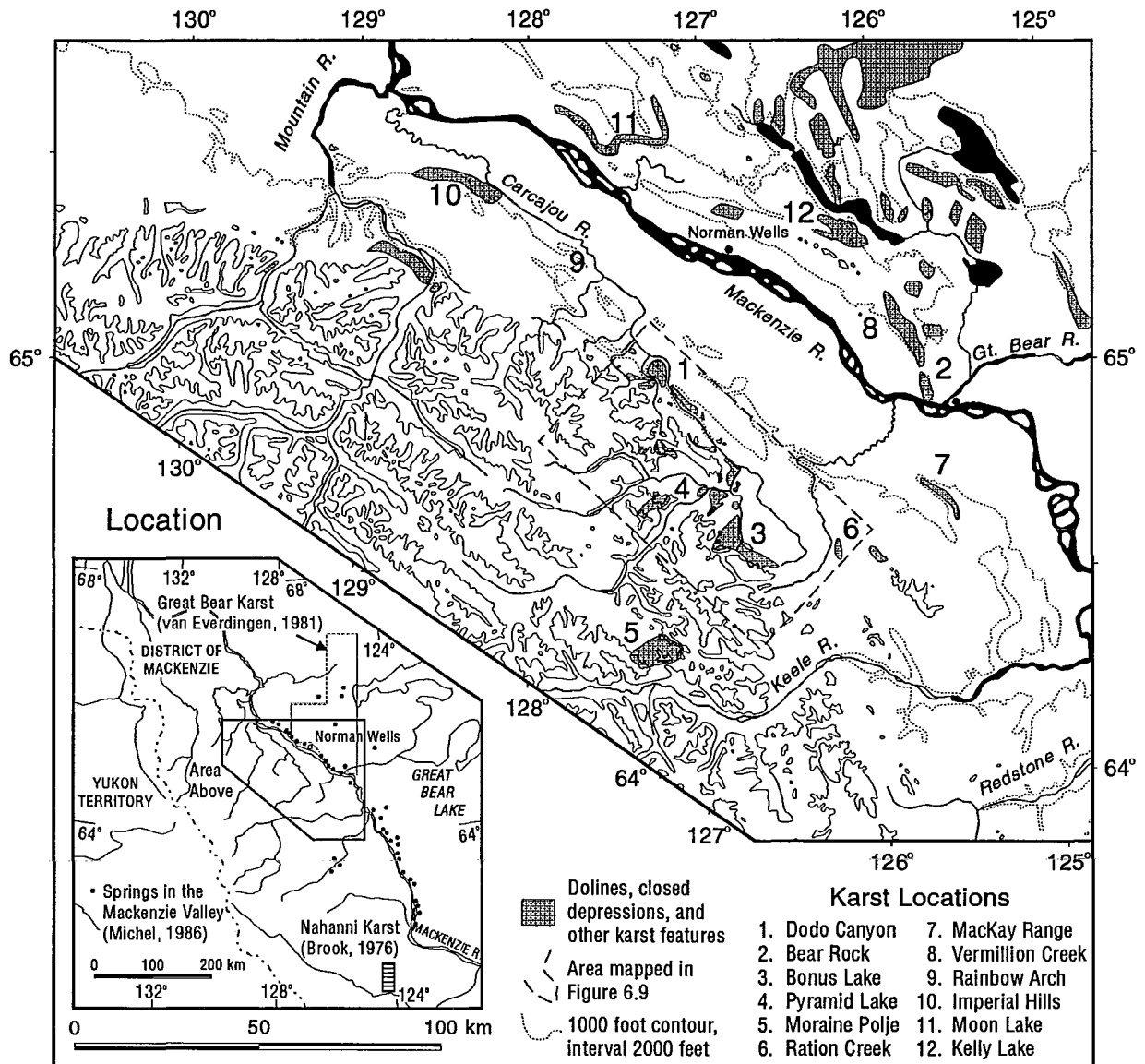


Figure 6.1: Distribution of karst in the northern Franklin and Mackenzie Mountains. The shaded regions are characterized by internal drainage and/or a frequency of dolines and closed depressions greater than 2 km^2 . Karst data are from aerial photographic interpretation, van Everdingen (1981), and Duk-Rodkin (personal communication, 1990). Also indicated are spring locations sampled by Michel (1986) in a hydrogeological study of the Mackenzie Valley, and the position of the southern Mackenzie Mountain Nahanni Karst (Brook, 1976).



Figure 6.2: Oblique aerial view of the Dodo Pavement. This schichttreppenkarst (stepped pavement) is developed on gently dipping dolomite of the Mount Kindle Formation. The pavement covers an area of approximately 2 km² and has been ice free for 12-13 ka (photograph by J.A. Lundberg).

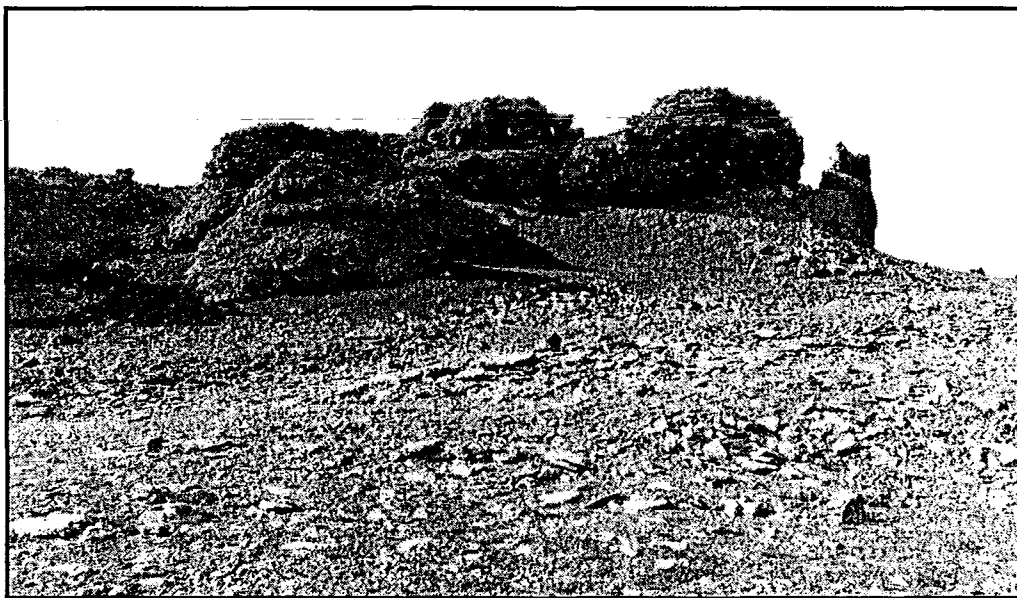


Figure 6.3: Tors on the Plains of Abraham, strata is dolomite of the Mount Kindle Formation. This area is in continuous permafrost and is unglaciated. Outcrop surfaces are mantled in shillow, karst pavements are absent. Geomorphic processes are dominated by frost shatter and slow mass wasting (photograph by D.C. Ford).



Figure 6.4: Dense pitting of the Mount Kindle Formation at the Pyramid Lake Site. This weathering morphology has some similarity to phytokarst, although the concavities are smaller and the outcrop frost shattered. This site is at 1100 m elevation, in continuous permafrost, and has been ice free for >13 ka.



Figure 6.5: Solution pan (kaminitza) on the Dodo Pavement. Pan diameter is approximately 25 cm, depth varies between 5 and 8 cm. The raised rim and flat organic covered bottom are typical of pan features on the Mount Kindle Formation and on the Landry Member of the Bear Rock Formation.



Figure 6.6: Rillenkarrren on the Landry Member of the Bear Rock Formation. The lower portion of the outcrop has been broken away to show the crackle breccia of the limestone.

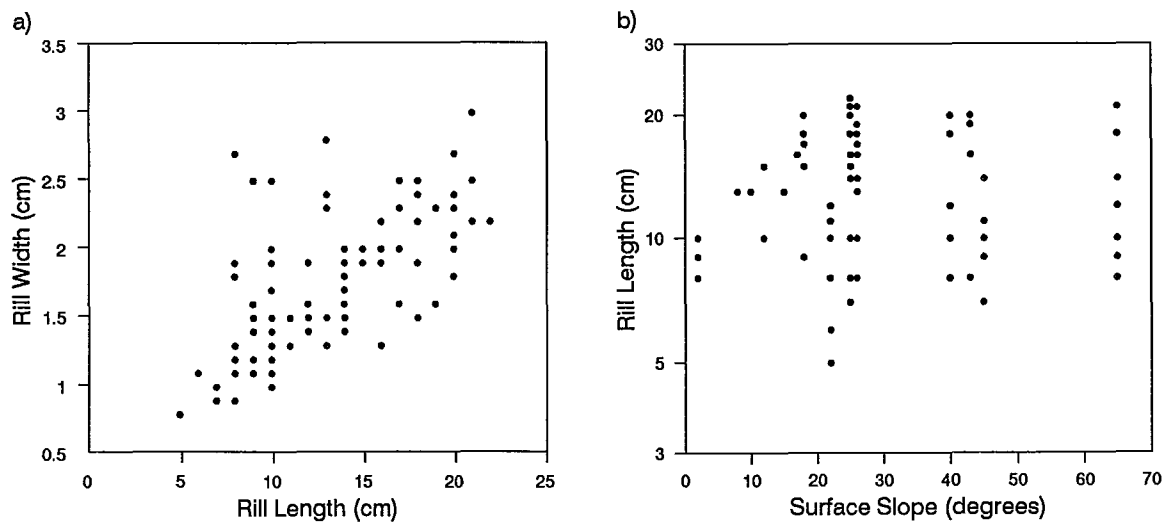


Figure 6.7: Rillenkarrren data from the Dodo Site: a) rill width vs rill length and; b) rill length vs surface slope. The latter is consistent with other field studies (Ford and Williams, 1989).

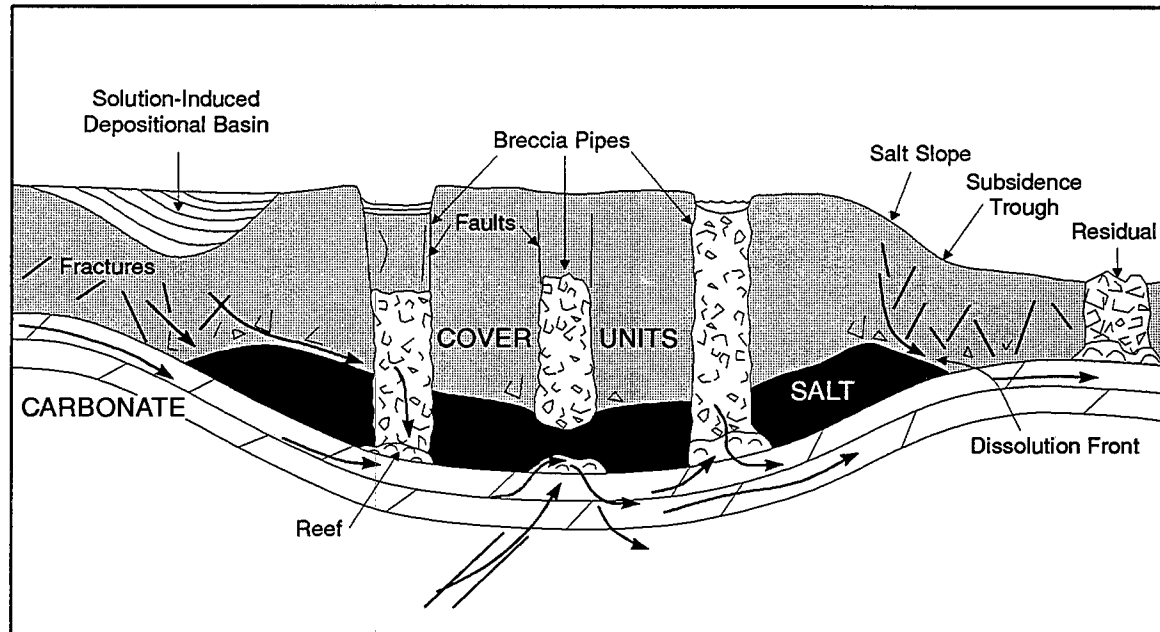


Figure 6.8: Model illustrating the occurrence of areal subsidence-collapse features in cover units above an evaporite subcrop. The evaporite may be either halite or anhydrite. Solution-induced subsidence basins, salt slopes, and subsidence troughs are generated at the evaporite margin (zero edge). Brecciation will normally accompany subsidence at the evaporite surface. Breccia pipes commonly develop where groundwater travels via carbonate mounds (reefs) or deep fractures to the evaporite surface, and solutes are removed through brine density circulation. Consequent sagging of the evaporite unit initiates an upward stopping pipe. There are several examples of such large scale subsidence features in the study region, including the Vermillion Creek Sinkhole (Figure 6.11) (Ford and Williams, 1989).



Figure 6.9: Distribution of dolines, ponors within closed depressions, dolomite pavement, major springs, and areas of internal drainage in the Carcajou Range, Mackenzie Mountains, N.W.T. In areas where doline or ponor frequency is very high the distribution depicted on this figure is a representative sample. The majority of sink features illustrated have a minimum diameter of 25 m. The areas of internal drainage may have overflow channels that are activated only during extreme events. Regions of dolines not mapped as areas of internal drainage do function as recharge zones but have overflow or surface channels that are active on a seasonal basis. Efforts were made to exclude obvious depressions in outwash, although some suffosion sinks are plotted. Several sinks in a large mass movement deposit are included because the failure occurred in the Saline River Formation and the slide mass does function as a hydrological karst (data from aerial photographs and field checking).

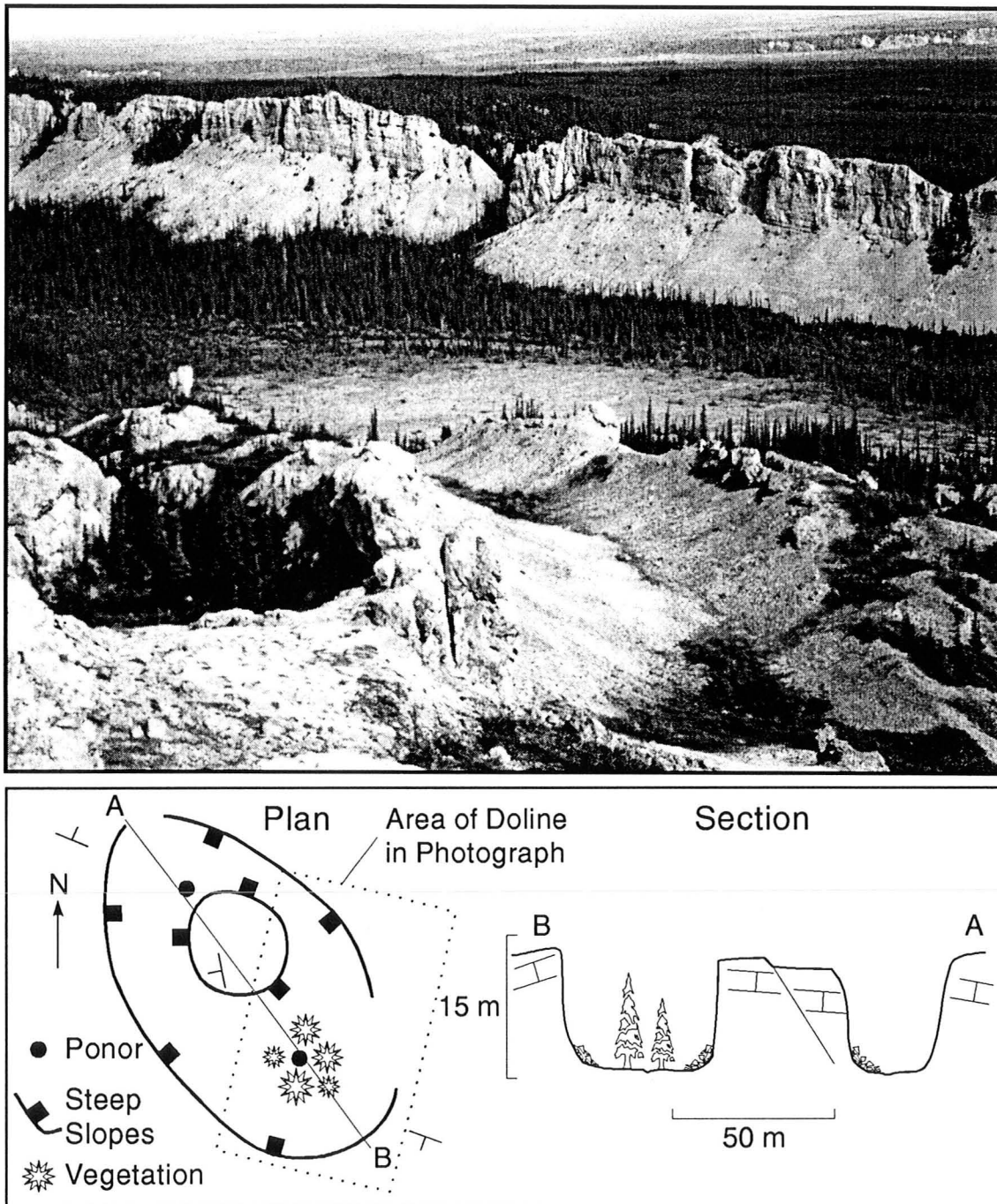


Figure 6.10: A vertical walled collapse doline at the Dodo Canyon Site (lower left of photo). It is in the resistant Landry Member of the Bear Rock Formation. Only the southern end of the feature is visible (see plan view). Variable dips indicate uneven foundering; faults on the walls and within a large interior block show vertical displacement. There are two ponors within the doline and another in a clump of vegetation in the small trough to the lower right. In the study region, a majority of dolines of this size were partially infilled by talus from local rockfall. The valley running left to right across the photograph is the principal discharge zone of the Main Karst at the Dodo Canyon Site. The Hume Formation produces the cliff. The area of low relief behind the Hume cliff is the interstratal North Karst (in clastics). The positions of sinks are shown by clusters of unusually tall spruce and aspen.

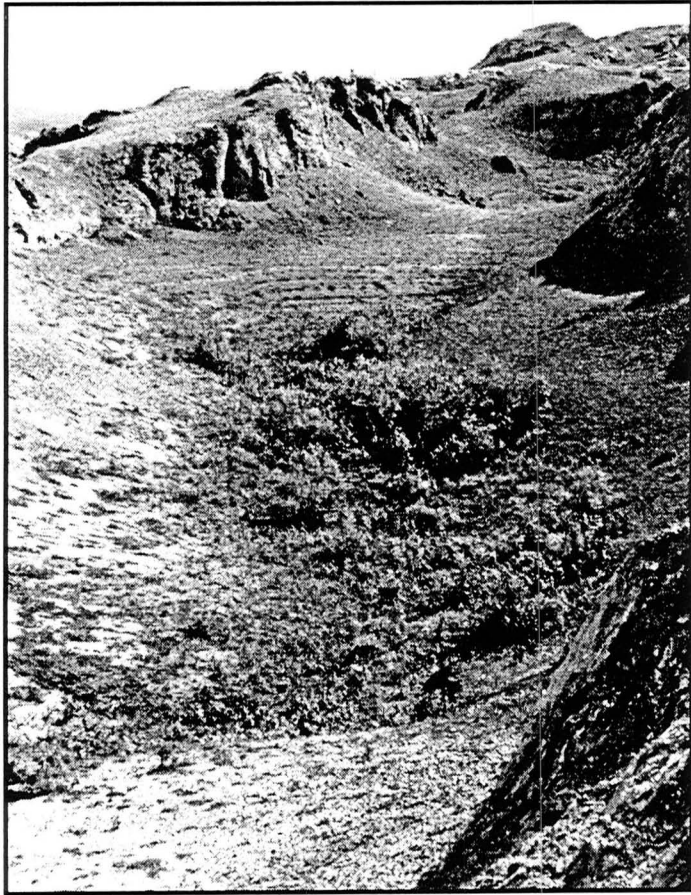


Figure 6.11: Examples of dolines from the study region. (Left) A series of solution-subsidence dolines in a linear trough and meltwater channel at the Dodo Canyon Site. (Upper right) The Vermillion Creek Sinkhole, a collapse-subsidence feature in shale of the Canol and Imperial Formations. Subrosion occurs in the underlying Fort Norman Formation. (Lower right) A shallow vegetated doline in the Bear Rock Formation.

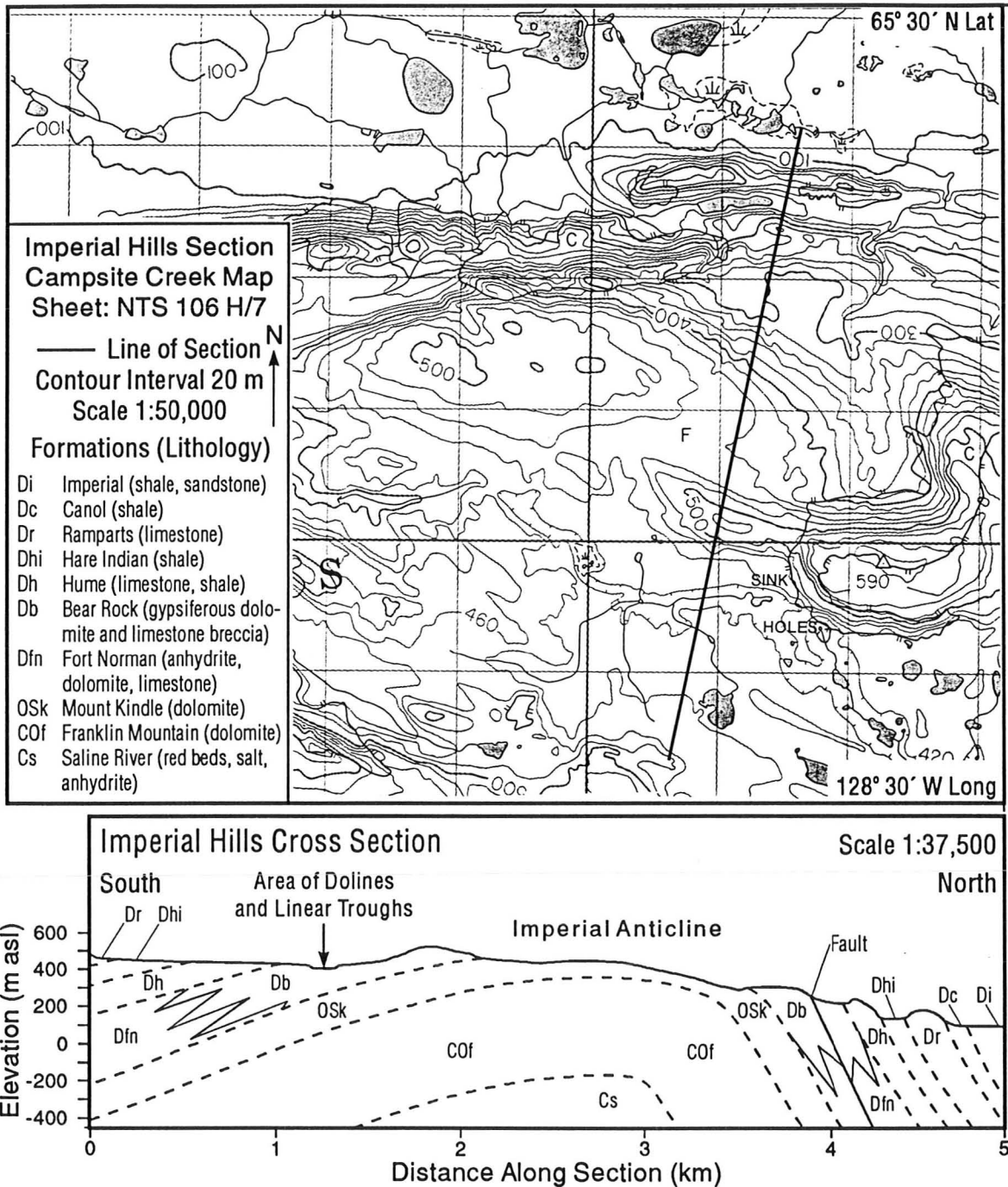


Figure 6.12: The Imperial Hills are a series of low mountains located on the Mackenzie Plain between Carcajou River and the Mackenzie Mountain front. The Hills consist of folds in Paleozoic strata. The Imperial Anticline runs the length of the western section of the Hills. Karst occurs in the Hume and Bear Rock Formations along the crests and limbs of this, and other anticlines. In the section and map above there are a number of compound dolines within a subsidence trough in the Bear Rock Formation. To the east, sharp collapse dolines are developed where the Hume Formation forms a cover unit over the Fort Norman Formation along anticline crests (geology after Aitken *et al*, 1982; Pugh, 1993).

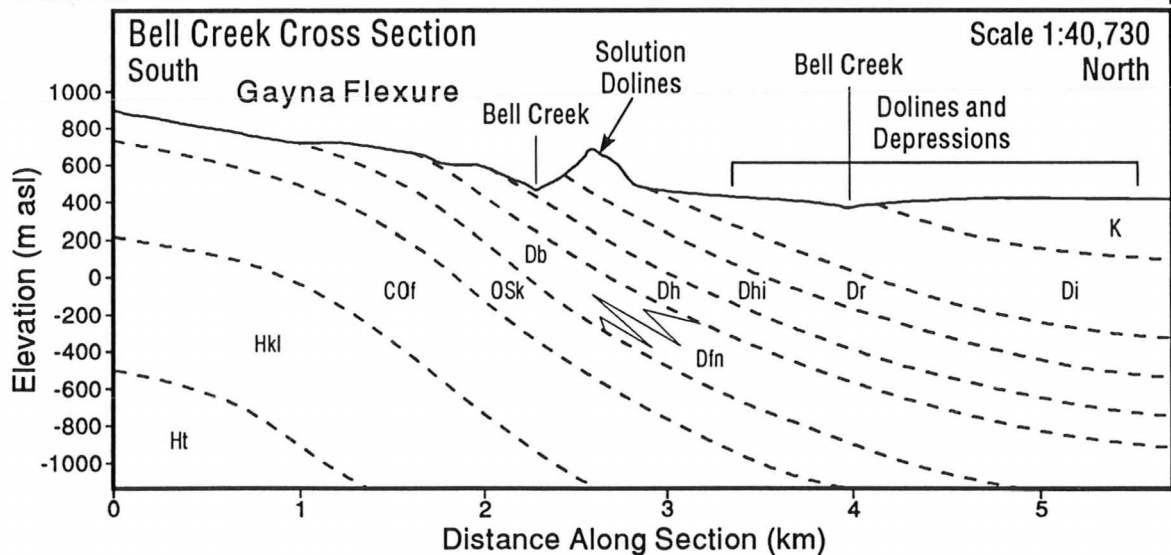
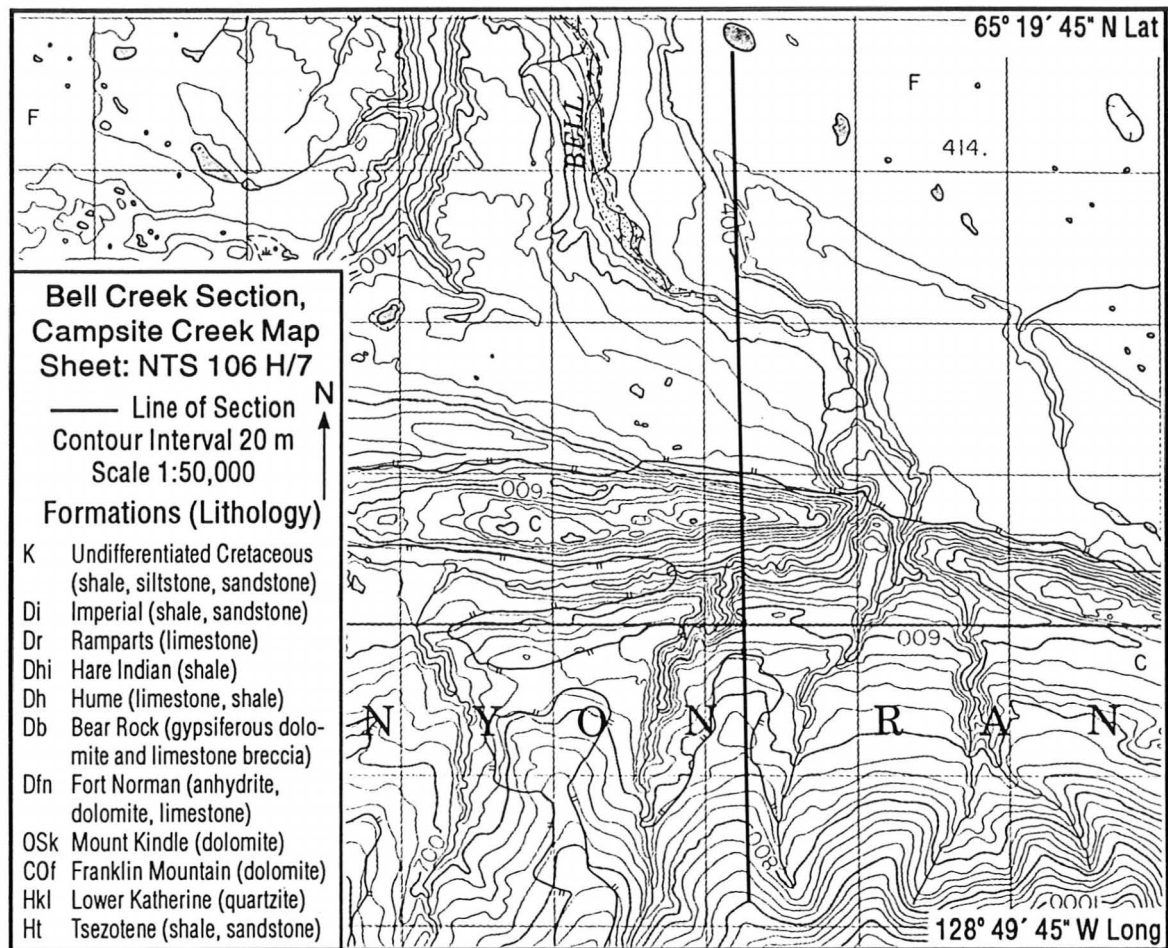
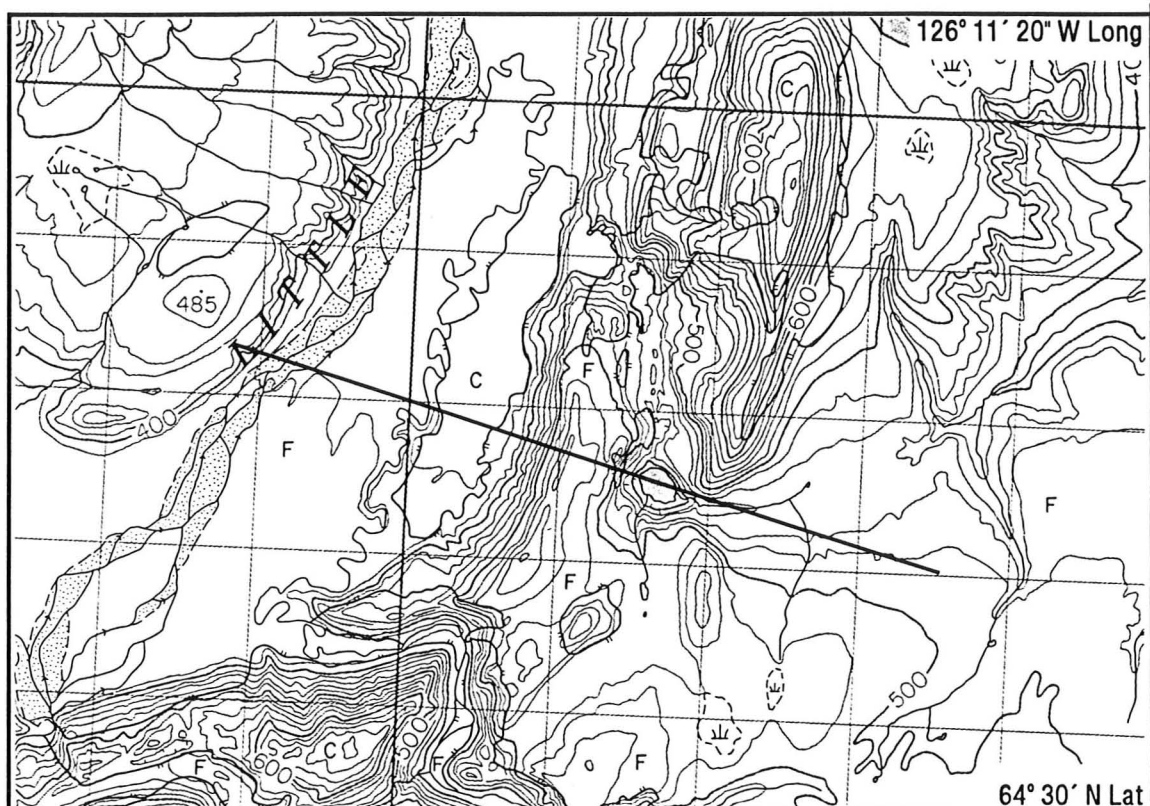


Figure 6.13: The Gayna Flexure forms the mountain front in the Mountain River area. The map shows a small tributary of Mountain River cutting through Devonian strata on the limb of the monocline. Solution dolines occur on Ramparts Formation, and collapse-subsidence features are developed on clastics of the Imperial Formation and the Cretaceous units. The latter features are the surficial expressions of breccia pipes generated by subsrosion of the Fort Norman Formation under a maximum of 1200 m of cover (after Aitken *et al*, 1982; Pugh, 1993).



Ration Creek Section, Ration Creek Map Sheet: NTS 96 D/9 — Line of Section Contour Interval 20 m Scale 1:50,000	N ↑	Formations (Lithology)	
		Kle Little Bear (sandstone, shale), East Fork (shale, sandstone) Di Imperial (shale, sandstone) Dhc Hare Indian/Canol (shale) Dh Hume (limestone, shale)	Db Bear Rock (gypsiferous dolomite and limestone breccia) Dfn Fort Norman (anhydrite, dolomite, limestone) OSk Mount Kindle (dolomite) COf Franklin Mountain (dolomite) Cs Saline River (red beds, salt, anhydrite)

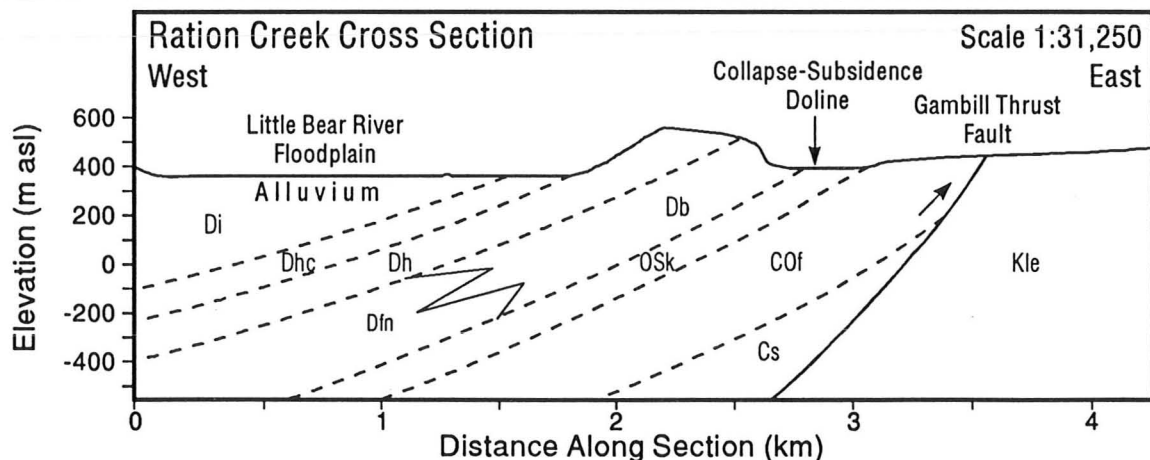


Figure 6.14: Dolines and linear depressions occur on the hanging wall of Gambill Thrust, east of Little Bear River. The largest feature, Ration Creek Doline, is an oval shaped, steep walled sink located within a linear trough. The trough is in the Bear Rock Formation, its axis is parallel to strike. The doline extends into the Mount Kindle Formation. The morphology suggests a collapse-subsidence origin. Subsidence originates in the Saline River Formation which subcrops 500 to 600 m below the feature (after Aitken and Cook, 1974; Pugh, 1993).

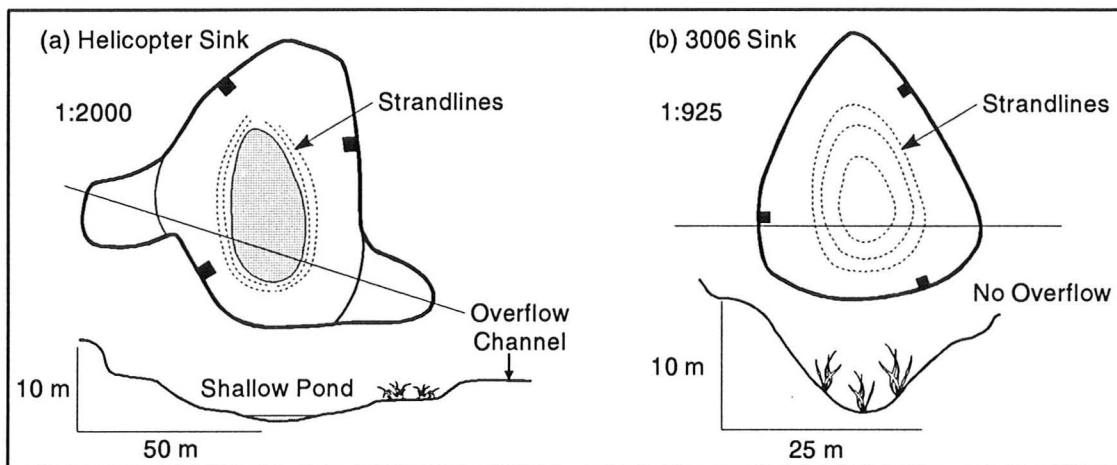


Figure 6.15: Two types of dolines in the Bear Rock Formation observed at the Dodo Canyon Site. (a) Helicopter Sink is an example of a slowly draining, flat bottomed, shallow doline developed in the Landry Member. (b) 3006 Sink has a high depth to width ratio, drains rapidly, and extends vertically into the Brecciated Member.

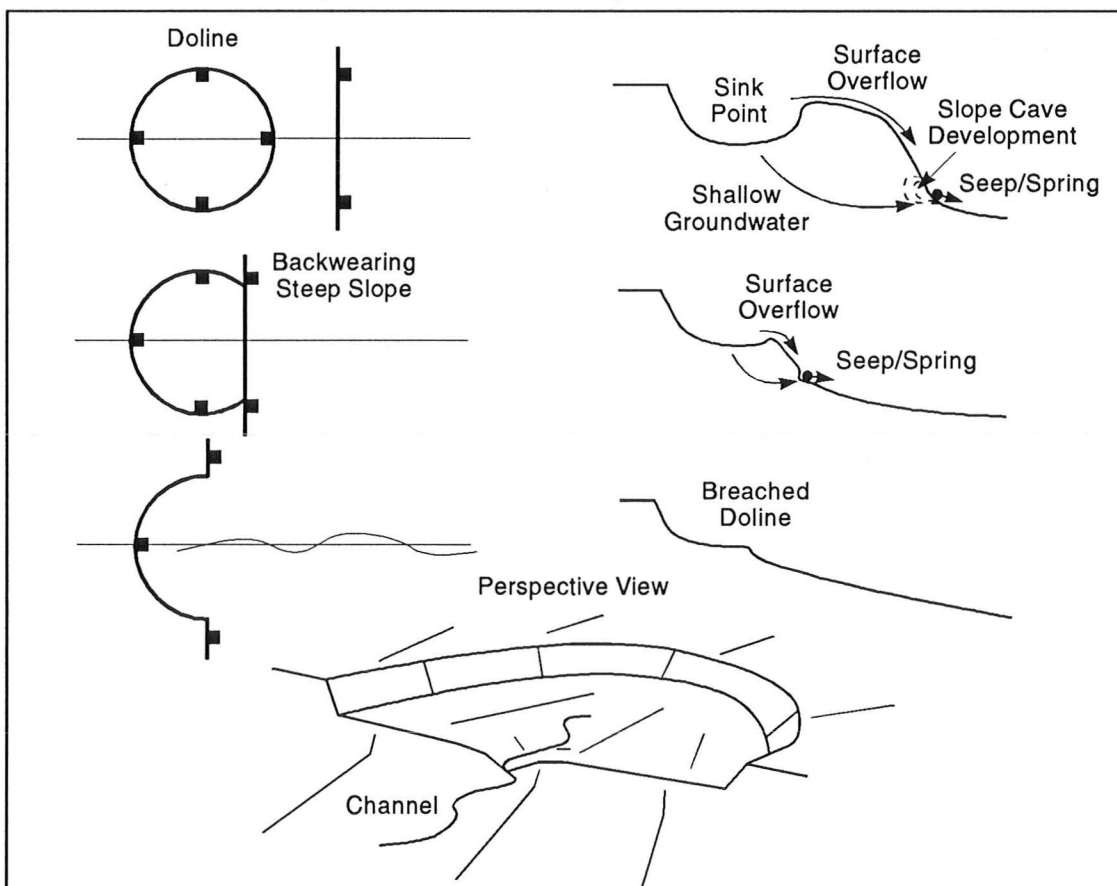


Figure 6.16: Development of a breached or horseshoe doline. The model is based on observations at the Dodo Canyon Site. The downslope wall of the doline is eroded by a combination of: solution along shallow groundwater flowpaths, breakdown in slope caves, and surface overflow. Debris is removed by slow mass wasting, solution, and surface runoff. Permafrost may inhibit a deeper circulation of sinking waters with the effect of increasing lateral erosion and the opening up of dolines.

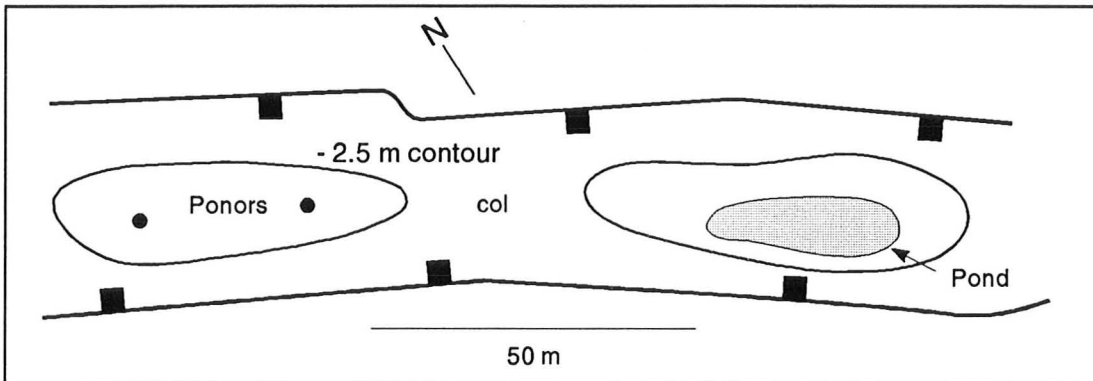


Figure 6.17: Plan view of two dolines in a linear trough at the Dodo Canyon Site. The trough cuts through the resistant Landry Member into the Brecciated Member. These dolines are similar to those depicted on Figure 6.11. These troughs functioned as meltwater channels during glaciation. Many dolines are located in such features.

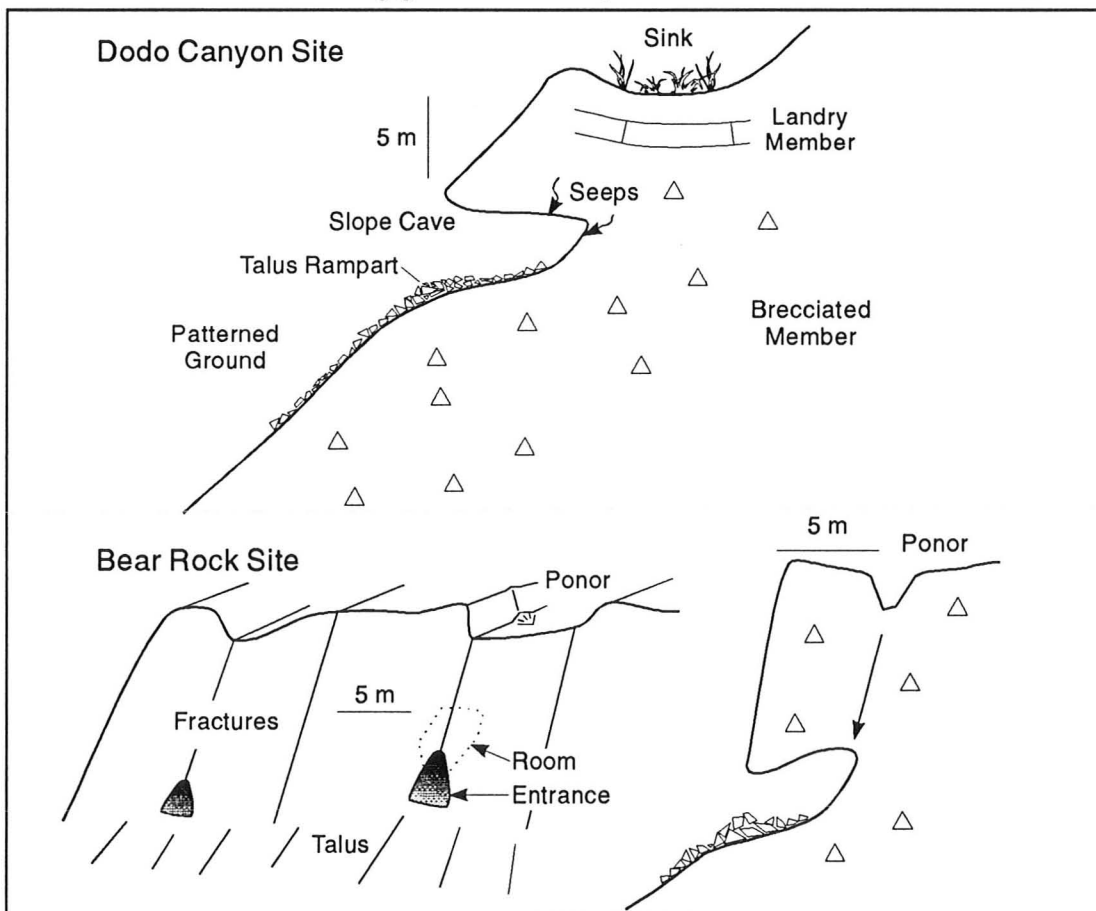


Figure 6.19: Characteristic morphology of slope caves in the study region illustrated by three examples. They are most common in the Brecciated Member of the Bear Rock Formation. In cross section the cave consists of a short, steeply inclined passage with a broad opening. A talus rampart occurs at the entrance. Patterned ground may be present on the cave floor or as stone stripes in the mobilized debris. Expansion occurs by solution and frost wedging at seep points. An upslope sink or ponor supplies groundwater to the cave seeps, fractures operate as flowpaths.

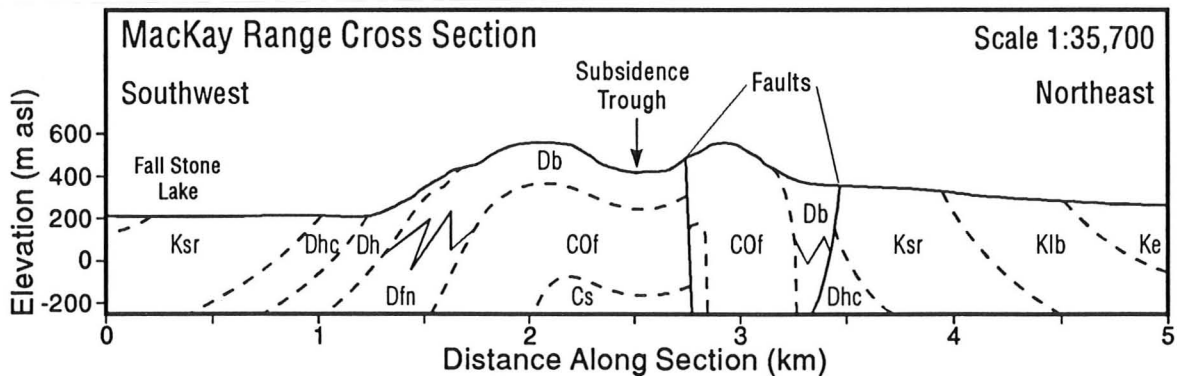
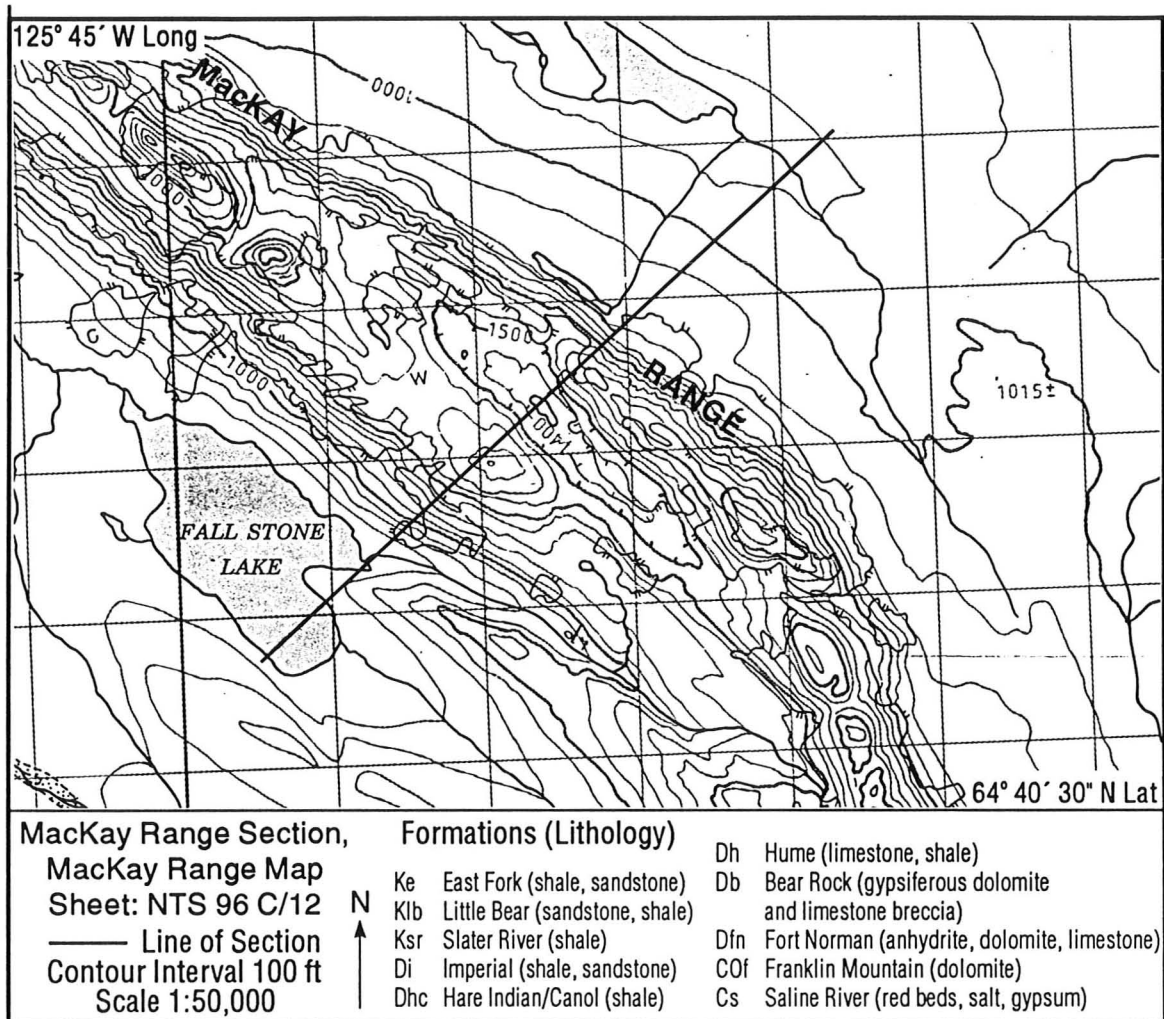


Figure 6.18: An anticline runs the length of MacKay Range. The northeastern limb is cut by a series of steep reverse faults, strata on both limbs dip sharply, locally approaching vertical. The Mount Kindle Formation is absent over this area. Along the crest of MacKay Range there are two large linear depressions interpreted as subsidence troughs. The northern trough is shown on the map above with a section below. Local well records (G-78: Table 4.3) indicate the Fort Norman Formation exceeds 300 m in thickness and the salt of the Saline River Formation is 150 m (Figure 4.8). The troughs are developed through subsrosion of these units along the anticline crest and faults. Elsewhere on the range, dolines and karren occur on the Bear Rock and Hume Formations (geology after Cook and Aitken, 1976; Pugh, 1993).

CHAPTER VII

THE DODO CANYON SITE

7.1 Introduction

The Dodo Canyon Site is situated at the Mackenzie Mountain front approximately 40 km southwest of Norman Wells (Figure 3.1). The terrain rises abruptly from the Mackenzie Plain to a sloping upland that is sharply incised by river canyons (Figure 7.1). Segments of canyon, valley, and channel features are either underfit or abandoned, such as Kindle and Dry Canyons (Figures 7.1, 7.7). This morphology is due to glacial meltwaters and diversion of mountain drainage as described in Chapter V. Karst input landforms occur on some upland blocks. Springs discharge into bordering canyons and valleys.

Fieldwork was conducted at the Dodo Canyon Site in June and July of 1987, May and July of 1988, and August of 1991. Geological and geomorphological mapping were undertaken, and water samples were collected for hydrochemical and stable isotope analyses. Figures 7.2 and 7.9 show water sampling locations. The pattern of recharge was monitored at sink points, and the discharge of springs and surface streams were measured. This chapter reviews these data, proposes a model of groundwater circulation in the local aquifer, and discusses the geomorphic role of solution at the site.

7.2 Site Description

Dodo Canyon divides the study site into western and eastern sections (Figure 7.2). Dodo West comprises the Mount Kindle pavement described in Chapter VI, and an area of dolines on the Bear Rock Formation. The Main Karst lies on the Bear Rock Formation between Dodo and Carcajou Canyons, south of a meltwater channel

developed along the Bear Rock-Hume contact (Figures 7.3, 7.4). Informally, this channel is called Carcadodo Valley (Figures 7.5, 7.6). Northward is an interstratal karst on the Hume, Canol, Hare Indian, and Imperial Formations (North Karst) (Figures 7.7, 7.8).

The Main Karst is separated into crude zones of holokarst (Sink Zone), fluviokarst (Fluvial Zone), and discharge (Carcadodo Valley). It was initially thought to represent a small autogenic karst basin (Figure 7.9). The Sink Zone is a region of dolines and dry valleys that operate as a recharge area for a series of springs in Carcadodo Valley (Figure 7.5). Most of the dolines and ponors store surface runoff during snowmelt and gradually drain through the spring and early summer (e.g., sample location D8). A few of the ponds remain perched (e.g., D19). The largest linear depressions are Straight and Dry Valleys. Both contain several ponors and lack integrated surface channel networks (Figures 7.9, 7.10). At the northern end of Straight Valley is a large doline called Big Sink (D7), where much runoff converges during snowmelt and precipitation events. Straight Valley is an example of a blind valley. It was formed by allogenic runoff from the Mount Kindle Formation and was subsequently truncated by Dodo Canyon. The Straight Valley should be considered semi-blind because some autogenic recharge is diverted away from ponors and the Big Sink to adjacent surface streams in the Glade. Dry Valley is oriented parallel to strike and located up-dip of a major break in slope. It has morphological similarities to a subsidence trough. A deep unnamed doline occurs at the western end of the valley and is the focus of recharge (Figure 7.10).

There are several dolines located along a ridge crest at the northern end of the Sink Zone. This ridge is the Scarp. The Landry Member outcrops along the full length of the Scarp and it has been dissected by glacial meltwater channels (e.g., Figures 6.11, 6.17). Most of the depressions penetrate into the underlying Brecciated Member. In places, the dolines have a sharp collapse form, though they are more appropriately classified as point solution-subsidence features (e.g., Figure 7.11). Big Depression is a compound feature at the eastern end of the Scarp. Other large

dolines include Bear Scat Sink and Strandline Sink (Figures 7.9, 7.12). In the southern portion of the Sink Zone, dolines are shallow and the depressions broad.

The Fluvial Zone is an area of ephemeral streams, small meltwater channels, and breached dolines located between the Scarp and the springs of Carcadodo Valley. Most of the precipitation that falls on this zone infiltrates into small ponors and dolines, fractured bedrock outcrops, angular surface debris, and channel beds. This zone is considered a fluviokarst. Two channels, Window and Fan Canyon Streams, carry most of the discharge. Fan Canyon Stream heads in a large breached depression called the Glade (D26, D40) and flows through a steep canyon (D14) to an alluvial fan built onto the floor of Carcadodo Valley (Figure 7.9). Under normal flow conditions, Fan Canyon Stream sinks into its bed near the apex of this fan (D38). This flow is thought to resurge at the eastern boundary of the fan as a diffuse collection of small springs. Window Stream is fed by supraperafrost springs downslope of the Big Depression (D18), and surface flow to Carcadodo Valley is recorded only during snowmelt and following summer storms (D17).

Carcadodo Valley is the principal discharge area of the Main Karst, and process investigations were focussed within and south of this channel (Figures 7.2, 7.4, 7.5, 7.6, 7.9). Several springs occur in coarse fluvio-glacial sediments west of the fan. These springs comprise the Great Spring Line. Water was sampled from the Great Spring Line in a channel east of the main springs at location D33. Additional samples were taken 400 m downstream of D33 at location D5, where discharge was also periodically gauged. This is Fan Stream. It was thought to be a resurgence of Fan Canyon Stream (D38), but data show they should be treated separately. Eastward, Fan Stream joins a series of small ponds in the valley. A second stream (Fox Spring/Stream) flows into the first pond at its southwestern end. This stream is fed by at least two groups of springs, including a low discharge flow emerging from fractures in the Bear Rock Formation (Fox Moss Spring: D4), and nearby aggraded springs supplying an area of wetland. Fox Swamp Stream (D39) drains this wetland and is tributary to the flow of Fox Moss Spring. In portions of the 1988

field season, the combined discharges of Fox Swamp Stream and Fox Moss Spring were measured at location D43 (Fox Well) and are collectively called Fox Spring. The aggregate flows of Great Spring Line/Fan Stream, Fox Spring, Window, and Fan Canyon Streams account for most of the discharge into Carcadodo Valley. Flow variations of these and other sources are reviewed in later sections.

The size of the ponds in Carcadodo Valley varied with season and stage. The discharge of Red Rock Brook, the stream that links these ponds was monitored at location D3 for much of the 1987 and 1988 field seasons (Figure 7.5). The discharge record is not available for early July of 1988 when the ponds coalesced following a major precipitation event. There are no significant inputs into Carcadodo Valley between D3 and the Terminal Sink, where Red Rock Brook drains near the contact between the Bear Rock and Hume Formations (Figure 7.6).

The floor of Carcadodo Valley is approximately 100 m above that of Carcajou Canyon. There is a series of springs at the base of the west wall of Carcajou Canyon, east of Terminal Sink. Water samples were drawn from individual spring points (D2, D42) and from a spring-fed channel (Carca-Spring Stream: D1, D35, D37). Springs discharged directly from the Bear Rock Formation or from alluvium stratigraphically below the Hume contact. At location D2, water was taken directly from a fissure in the Landry Member. Samples from other locations are discussed elsewhere in the text.

7.3 Geology of the Dodo Canyon Site

Outcrop in the Dodo Canyon area spans the Upper Proterozoic to Upper Cretaceous (Figure 7.8; Aitken and Cook, 1974). Dodo Mountain is at the northwestern plunging end of MacDougal Anticline, the axial trace of which extends to the southeast, parallel to Carcajou River. Resistant Proterozoic strata of the Katherine Group and Unit H₅ of the Little Dal Group outcrop in the anticline core. Paleozoic strata comprise the northern flank of Dodo Mountain and dip to the northeast toward Grotto Syncline of the Mackenzie Plain Synclinorium. At the field site, older strata

occur in subcrop and are exposed in Dodo Canyon at the base of Dodo Mountain. Across the Main Karst and the Dodo Pavement, the Bear Rock and Mount Kindle Formations dip gently to the north-northeast at 5° to 10° . However, at the local scale, the dip and strike of the upper Bear Rock Formation is highly variable. Towards the Scarp of the Main Karst, strata dip more sharply. At the floor of Carcadodo Valley and Carcajou Canyon, dips average 20° and are locally as great as 35° (Figure 7.8).

At the Dodo Canyon Site, the areas that function as hydrological karst are confined primarily to the Bear Rock and Hume Formations, with a small zone on Upper Devonian clastics of the North Karst. These areas are depicted as belts of enclosed drainage on Figure 7.7. Under most circumstances, precipitation onto these zones is captured by karst input landforms, though overflow can occur under extreme conditions. Much precipitation onto the Mount Kindle Formation also sinks over the area of the Dodo Pavement, but delineation of enclosed drainage on the pavement was not attempted. In the following section, field descriptions are limited to the main doline-hosting strata, the Bear Rock and Hume Formations. The Dodo Pavement was described in Chapter VI and the regional stratigraphy in Chapter IV.

7.3.1 Hume Formation

The Bear Rock and Hume Formations were examined at several locations in Dodo Canyon. Observations were consistent with the surface division of the Hume Formation into an upper resistant unit and a lower recessive unit. At three locations, the thickness of the upper member was measured between 60 and 70 m. The recessive interval is partially covered by talus and has a maximum observed thickness of 25 m. The upper unit is a thick bedded, grey weathering, cliff-forming wackestone and packstone. The lower unit consists of alternating sequences of: thin to thick bedded nodular wackestone, and thin to laminated, planar and wavy beds of argillaceous lime mudstone and shale. The nodular beds are discontinuous and are draped by the argillaceous laminae. The content of terrigenous material is highest

5 to 10 m above the base of the lower member. The lower few metres of the Hume Formation is a more resistant thin to thick bedded wackestone that passes gradually into the underlying Landry Member of the Bear Rock Formation.

7.3.2 Bear Rock Formation

In the Dodo Canyon area, the Bear Rock Formation is thinner and has a higher terrigenous content than sections described elsewhere in the Mackenzie and Franklin Mountains (e.g., Morrow, 1991). The thickness varies between 80 and 100 m in exposures from Dodo Canyon, with the Brecciated Member comprising the bulk of the outcrop. The Landry Member is locally absent in the northern part of Dodo West Karst.

7.3.2.1 Landry Member

The Landry Member is assigned to the Bear Rock Formation across the area of the Norman Wells High and is the lateral equivalent of the regionally extensive Landry Formation. At the Dodo Site, the Landry Member consists of alternating sequences of: recessive, platy weathering, laminated to thin, planar and wavy bedded lime mudstone, and resistant intervals of thin to thick planar bedded, lime mudstone and wackestone (Figure 4.13). Bands of very resistant, blue grey and smooth, massive weathering lime mudstone occur between the lower Hume Formation and the Brecciated Member of the Bear Rock Formation. This generates a ribbed appearance to some outcrop. Intervals of calcite-cemented crackle breccia are present in massive weathering units. Calcite-cemented mosaic packbreccia and floatbreccia occur in some laminated intervals.

The lithology of the member was tested in the field and laboratory. All field samples were limestone. Several hand specimens and thin sections were polished, etched, and stained with Alizarine Red S and Titan Yellow using standard procedures (Dutro *et al*, 1989). The staining confirmed the field determination of calcite. Minor staining in the veins of the crackle breccia suggested the possibility

of high magnesium calcite.

The Landry Member averages 15 m in thickness at the Dodo Canyon Site, 5 to 8 m of which consists of massive units. In most exposures, the contact between the laminated Landry and the underlying Brecciated Member is gradational over a distance of 1 to 2 m. However, there are examples of abrupt contact between the breccia and massive bands. The member is distributed across the full area of the Main Karst and is locally eroded from Carcadodo Valley. Much of the rugged topographic character of the Main Karst is attributed to the resistant cap of the Landry. Where the Landry is absent, such as over much of Dodo West Karst, the topographic expression of the Bear Rock Formation is recessive.

7.3.2.2 Brecciated Member

Exposures of the Brecciated Member of the Bear Rock Formation were examined in Dodo, Dodo West, and Fan Canyons. The member is a calcite- and particulate-cemented mosaic and rubble packbreccia, discontinuously interbedded with particulate-cemented floatbreccia (Figures 4.11, 4.12). Outcrops are vuggy, highly fissured, and locally bituminous. The terrigenous content is as high as 5%. Breccia clasts are angular to subrounded and range in size from granules to boulders. Fissures and discontinuities often act as failure planes, imparting a slaky appearance to outcrop.

Packbreccias are predominantly grey weathering and resistant. Crude, wavy, thick bedding units are recognizable when outcrops are viewed from several metres, but appear chaotic upon closer examination. Clasts in packbreccias are not sorted and are poorly oriented along strike. They are, on average, larger than those in the floatbreccia intervals. Large coherent clasts with pre-breccia laminae preserved are common.

Floatbreccias tend to be tan or orange weathering and recessive. Most of the clasts are smaller than cobble size and are primarily angular, although rounding is more common than in packbreccias. Floatbreccia segments occur between thick

beds and intervals of packbreccia, and along pipes and fractures linking them. The observations support the general model of Morrow (1991) where floatbreccias develop from interbedded dolomite and anhydrite (Figure 4.15). Highly localized collapse, breakdown, and subsidence into minor conduits accompanied evaporite subsidence, producing small, slightly rounded clasts with a preferred orientation down dip. Packbreccias represent thick intervals of dolomite overlying massive anhydrite. Solution produces areal subsidence and uniform brecciation of the overlying dolomite.

The lithology of the member was examined in the field and laboratory. Approximately 70% of the clasts tested in the field were limestone; the balance were dolomite. The particulate cement was micrite. Staining of polished hand specimens and thin sections confirmed the field data. Many clasts were completely dedolomitized while others were less altered. It is suggested that dedolomitization accompanied solution brecciation. Primary depositional structures within clasts were not always destroyed by this process.

7.4 General Hydrology, Hydrochemistry, and Isotopes

The following section reviews the hydrological and hydrochemical characteristics of recharge and discharge across the Dodo Canyon Site. Over three field seasons, 130 samples of stream, spring, and pond waters were taken from 44 locations on the Bear Rock, Mount Kindle, and Hare Indian Formations (Figures 7.2, 7.9). Temperature, pH, conductivity, and ion concentrations were determined on site or in the laboratory (Chapter III). Complete analyses were undertaken for 90 samples (Appendix I). Water samples are grouped into types on the basis of their location, temperature, conductivity, discharge, and hydrochemistry (Table 7.1). Table 7.2 describes individual sampling locations. Mean values of the above parameters for each of the water types are presented in Table 7.3.

Precipitation samples are called Type 1 waters. Springs are divided into classes that crudely reflect the depth and length of flowpaths from recharge to

discharge points. Springs are from flow systems of: (i) shallow (Type 2), (ii) intermediate (Type 3), or (iii) deep origin (Type 4). Shallow springs are characterized by low values of temperature, discharge, conductivity, and TDI (total dissolved ion). In permafrost regions, such springs normally drain the suprapermafrost aquifer (van Everdingen, 1990). Deep springs (Type 4) are either: (i) thermal, low discharge flows of high conductivity and TDI, or (ii) cold, high discharge flows of low conductivity and TDI. Groundwaters of the subpermafrost aquifer have these characteristics (van Everdingen, 1990). The physical attributes of intermediate springs show some mixing between waters of shallow and deep origin.

Streams were classified by their physical and chemical similarities with one of the above spring types (Types 5, 6, and 7). Ponds and dolines were categorized according to their rate of drainage. Perched or very slowly draining ponds were separated from those that had high rates of infiltration (Types 8 and 9). Samples taken off the Bear Rock Formation or from locations remote from the Main Karst were treated separately (Types 11 through 16: Table 7.1). These samples possessed characteristics that warranted separate classification.

7.4.1 Catchment Delineation

In studies of karst aquifers, much attention is given to defining areas of recharge for spring points. Worthington (1992) identified five potential problems involved with catchment delineation: (i) groundwater boundaries may not coincide with topographic boundaries, (ii) recharge to a given area may branch to more than one spring point, (iii) flow routes in the system may vary with stage, (iv) discharge may occur from unmonitored underflow springs, and (v) the catchments may consist of non-contiguous topographic components. A specific cold region addendum to the list that may be proposed here is: (vi) flow routes may vary with season due to the influence of frost on infiltration.

Under ideal conditions, dye tracing from sink to spring points provides data

required to accurately define the area of a recharge catchment. Many factors may complicate tracing, including situations where: (i) conduit porosity is poorly developed and flow through times are lengthy, (ii) recharge is diffuse, (iii) precipitation events are infrequent, (iv) spring points are aggraded, (v) springs rise in the bottoms of rivers or lakes, and (vi) background fluorescence is high. To varying degrees, each of these difficulties were noted at the Dodo Canyon Site and only two successful traces were completed using Rhodamine WT. The first trace was an attempt to establish a connection between the Sink Zone and Carcadodo Valley. Dye was introduced into surface flows above infiltration points in the area of Big Sink (D7) on July 2, 1987 and May 26, 1988. Charcoal detectors were placed at several locations in Carcadodo Valley. Analyses of elutant from the 1987 test showed positive results at Fox Well (D43); the 1988 test was positive at Fox Well (D43) and Fan Stream (D5). Flow through times were less than 30 days to Fox Well (July 2, 1987 test) and less than 50 days to Fan Stream (May 26, 1988 test). These data show groundwater recharge moves from the Sink Zone, down dip and subparallel to strike, discharging in Carcadodo Valley.

A second set of traces were done between Terminal Sink (D44) and Carca-Spring Stream. Dye was introduced into the eastern pond on four occasions; twice detectors along Carca-Spring Stream were lost to flooding of Carcajou River. The first dye injection was done on June 18, 1987, detectors were placed between D15 and D37, collected on June 22, replaced and collected again on July 4. Analyses indicated a positive trace to location D37 by June 22, and between D1 and D35 by July 4, 1987. The test was repeated on August 16, 1991, the detector at D37 was positive by August 17 and at D35 by August 27. The flow at Terminal Sink enters the Bear Rock Formation just below the contact with the Hume Formation. The strata dip steeply to the north. Fossil conduits were observed in the Hume Formation at the Dodo Canyon Site and elsewhere. A probable location for resurgence of Red Rock Brook is along Carca-Spring Stream, south of D37, at the contact between the Hume and overlying Hare Indian Formation. However, the apparent positive

between D35 and D1 presents some difficulties with interpretation. Springs at this location discharge at the base of the Hume Formation and possess physical and chemical properties that are much different from the sinking waters of Red Rock Brook (Section 7.4.3).

The extent of the Red Rock Brook catchment can be estimated from topography. The topographic basins of Fan Canyon and Window Streams were mapped from aerial photographic interpretation and field checking. These surface waters are a small fraction of the total discharge into Carcadodo Valley. Much of the precipitation on these watersheds infiltrates into the active layer and small sinks. The approximate catchment recharging the dolines and ponors of the Sink Zone is also known and together with the Window and Fan basins a minimum area of recharge to Carcadodo Valley is established.

It is probable that there are contributions to the system from bordering streams. Dodo Mountain Stream (D23) is at the eastern end of the Main Karst and has a topographic basin of 2 km² on the northern flank of Dodo Mountain. It was examined east of the Sink Zone during dry periods and following precipitation events of 5 to 10 mm. The channel was either dry or carrying a discharge of only a few litres per second. Flow was visibly reduced as the stream crossed from the Mount Kindle to the Bear Rock Formation. The channel was armoured with cobble and boulder sized clasts showing that high flows accompany intense precipitation events. It was not possible to estimate infiltration into the stream bed across the full range of flows, nor can it be assumed that recharge is directed to Carcadodo Valley.

Additional recharge to Carcadodo Valley may also occur from an area of dolines east of Dodo Mountain Stream, and through a smaller stream channel at the southern end of the Main Karst. There is also potential for recharge from the floor of Dodo Canyon. The contact between the Mount Kindle and Bear Rock Formations occurs on the canyon floor at 380 m elevation, approximately 2.5 km south and 60 m above the elevation of the Great Spring Line. The hydrochemical facies of Great Spring Line, Fan Stream, and Fox Spring show there is a deep chloride-rich

groundwater component to the discharge of Carcadodo Valley (Section 7.4.3). Possible contributions are from Dodo Creek or from groundwaters more distantly recharged. The Saline River and Bear Rock Formations are the major aquifers in the northern Mackenzie Mountains (Michel, 1986a). An extensive outcrop of the Saline River Formation occurs along Echo Creek several kilometres to the southwest, up dip of the Dodo Canyon Site. Flow paths from this recharge area to Carcadodo Valley are not blocked by the core of MacDougal Anticline, which does effectively function as a barrier to recharge from areas to the south (Figure 6.20). These and other potential flow paths are examined together with data on hydrochemistry, discharge, temperature, and natural isotopes in subsequent sections.

7.4.2 Variations in Recharge and Discharge

The following is a general review of flow variations in the Sink, Fluvial, and Discharge Zones recorded during field observations.

7.4.2.1 Winter-Spring: Sink (Recharge) Zone

The field area was not examined during the winter period. At Norman Wells, snowfall comprises 45% of the total annual precipitation (Figure 3.2; Table 3.1). Accumulation typically begins in early October and melting is initiated in late April and early May. Snowfall levels in the winter of 1986-87 were average, and in 1988-89 approximately 70% of normal (Figure 7.12). In the field season of 1987, snowdrifts persisted in shaded locations into late June, including a large snow dam in Fan Canyon above location D14. In 1988, fieldwork began on May 14 and at that time the snowpack was observed to be ripe. The last spring snowfalls occurred over the period May 14 to 16 and totalled 5-6 cm. The distribution of snow in the Sink Zone showed the importance of winter drifting. Exposed surfaces were largely snow-free while deeper snow was present in depression features and in the forested floor of the Carcadodo Valley. Melting accelerated in late May when daytime highs reached 15°C.

Several ponds were completely or partially frozen over in mid-May of 1988. These were shallow, flat bottomed ponds that freeze to their beds and drain very slowly through the summer period. In steep sided conical dolines, standing water was fed by melting snow and overland flow from local catchments. At several sinks, large drifts and surface seeps supplied recharge at rates greater than the infiltration capacity (Figure 7.13). Where there were highly fractured outcrops or solution conduits at doline bases, snowmelt and surface seeps infiltrated quickly. In the Big Sink (D7), much of the snow had melted by May 20 and standing water was restricted to several small depressions. In the more densely forested Straight Valley, mid-May snow depth was up to 50 cm and persisted into late May. Water marks showed ponors in that area were slowly draining.

7.4.2.2 Winter-Spring: Fluvial Zone

In the basins of Fan Canyon and Window Streams, many surface seeps and suprapermafrost springs contributed to stream flow in the spring period. In June of 1987 and May and June of 1988, the discharge of Fan Canyon Stream (location D14), varied between 2 and 15 L s⁻¹. This stream was typically sustained to the north end of Fan Canyon (location D38) where it infiltrated into the coarse surface of an alluvial fan. Over the same period, the discharge of Window Stream varied between 5 and 20 L s⁻¹. The flow seeped into angular debris below a break in slope at location D17, and entered a pond in Carcadodo Valley as a diffuse flow through an organic mat east of Fox Spring. In addition, there were several other minor streams in the Fluvial Zone, including Camp Stream (D11, D13), which discharged into the western end of Carcadodo Valley.

7.4.2.3 Winter-Spring: Discharge Zone

The main springs supplying flow to the Carcadodo Valley are not perennial. The Great Spring Line (D33) and Fox Spring (D4, D39, D43) were examined in May of 1988. Neither displayed the large icing features that characterize perennial, low

discharge spring points in the region. It is likely that flow ceases in the early winter before major icing construction. Spillway Spring (D36) comprises a series of perennial low temperature subpermafrost springs. Frost blisters and icings develop at spring outlets and persist well into late summer. The thermal springs feeding Carca-Spring Stream also flow through the winter period, though icings associated with them are removed by Carcajou River when in flood.

In the summer period, a series of shallow ponds occupies the eastern portion of Carcadodo Valley (Figure 7.5). In mid-May of 1988, there was little open water on the valley floor. Most of the pond basins were covered by a veneer of fine sediments overlying 10 to 15 cm of needle ice. Ground icings and small frost blisters were locally present. The needle ice, ground icings, and frost blisters resulted from freezing of saturated sediments and minor groundwater discharges. Some shore-fast ice was located on the pond margins. The ice distribution suggested the ponds had partially drained before freeze-up. Ice was also present in some parts of Red Rock Brook (D3), however, much was the result of snow drifting into the channel and refreezing earlier in the melt season.

During the snowmelt period, flow into Carcadodo Valley included contributions from several small suprapermafrost springs (e.g., D10), Fox Moss Spring (D4), Fan Canyon (D14, D38), Window (D17), Camp (D11) and several minor streams. Great Spring Line (D33), Fan (D5), and Fox Swamp Streams (D39) were not active. A shallow channel carried the combined discharge under the ice of Red Rock Brook to Terminal Sink. High water marks showed an earlier pulse of snowmelt had infilled that pond to near capacity, dislodging and melting the shore-fast ice.

Due to channel ice, the continuous discharge series from Red Rock Brook is not available for late May and early June of 1988. However, manual gaugings were undertaken several times and the systems response to precipitation monitored. On May 19, 1988 the discharge of Red Rock Brook was 32 L s^{-1} at the well location (D3). The level of Terminal Sink was low, the stream infiltrating as it approached

the easternmost ponor. A 20 mm rainfall event on May 23 and 24 triggered a rapid response in discharge. Flow peaked at D3 late on the 24th, at over 70 L s^{-1} . On the afternoon of May 25 the discharge had fallen to 53 L s^{-1} . Terminal Sink backed up to its characteristic summer level on May 24 but had returned to pre-storm levels by May 25 (Figure 7.14). These observations indicate that the surface streams and suprapermafrost aquifer of the Fluvial Zone translate rainfall pulses rapidly to the valley bottom. The capacity of Terminal Sink was only temporarily exceeded and the level quickly dropped. A smaller event on May 30 produced a similar response. The discharge of Fan Stream (D5) was very low through this period, 1.8 L s^{-1} on May 19 and 9.0 L s^{-1} on May 25. Much of the flow was from local snowmelt, with no contribution provided by Great Spring Line.

Gradual flooding of the ponds accompanied the precipitation events and melting of ground ice in late May. At the western end of Carcadodo Valley, a pond called Circular Swamp (D34) was dry during the snowmelt of 1988. Four ponors occur on its base. This feature gradually infilled following heavy rainfall events in late June and early July.

7.4.2.4 Summer: Sink and Fluvial Zone

Most of the recharge dolines and ponors were dry by mid to late June. Summer precipitation infiltrated into the active layer. In the Sink Zone, suprapermafrost waters were directed downslope to sink points, little surface runoff was observed. Several ponds drained slowly or remained perched through the summer period. They are flat bottomed, less than 1 m in depth, 20 to 30 m in diameter, and occur at open sites with little vegetation. These basins comprise about 5-10% of the recharge area.

Discharges of 1 to 3 L s^{-1} were sustained in Fan Canyon Stream, the upper part of Window Stream, and Dodo Mountain Stream through the summer period. Flows were increased by an order of magnitude following major precipitation events. Suprapermafrost springs at the base of the Scarp supplied Window and its tributary Winding Stream (D18). Fan Canyon Stream was fed by similar springs and seeps

in its breached headwater depression, the Glade (D26, D40).

7.4.2.5 Summer: Discharge Zone

At Red Rock Brook (D3), stage was continuously measured for six weeks in 1987, and for ten weeks in 1988. The water level at Fox Spring was monitored at location D43 for several weeks in May, June, and July of 1988. These data are plotted on Figure 7.15 as a discharge series with daily temperature and precipitation records from Norman Wells. Discharge was also manually gauged at Red Rock Brook during August of 1991 and at Fan Stream (D5) in each of the three field seasons.

Following the snowmelt period an increasing proportion of the total discharge into Carcadodo Valley was provided by Great Spring Line, Fan Stream, and Fox Spring (Figure 7.16). The shallow suprapermafrost springs and streams that were active during the melt season were dry by late June. Flows associated with snowmelt were not the dominant flood events under the period of observation. Discharge gradually increased through the summer season with low frequency, high magnitude rainfall events triggering the highest flows.

The summer of 1987 was warmer and drier than average. At Norman Wells, the combined June, July, and August precipitation was 60% of normal and the average June and July temperature was 0.8°C above. The most substantial rainfall events occurred on June 10 (13.8 mm) and June 13 (10.2 mm). A stilling well was installed at D3 (RRB) on June 14, but the record shows little evidence of the preceding precipitation. The Sink and Fluvial Zones were dry by the middle of June. Between June 14 and July 4 the discharge of Red Rock Brook varied between 115 and 128 L s⁻¹. The discharge of Fan Stream increased over that interval from 84 to 123 L s⁻¹. There was little variation in the discharge of Red Rock Brook, declining to 105 L s⁻¹ in mid July and subsequently increasing to 140 L s⁻¹ following local thunderstorm events (Figure 7.15).

The summer of 1988 was wetter than average with significant rainfall events on June 23 (25.2 mm), June 30 (26.6 mm), July 15 (10.4 mm), and July 29 (13.6

mm). The response of the system to these inputs was influenced by the magnitude and intensity of precipitation and antecedent moisture conditions in the suprapermafrost aquifer. There was a slight increase in the discharge of Red Rock Brook following the June 23 event. A survey of the upper portion of the karst on June 27 and 28 showed the Sink and Fluvial Zones to be dry despite an additional 7 mm of rain on June 26. However, rainfall on June 30 and July 1 did produce substantial responses in the Fluvial Zone, and at Great Spring Line, Fan Stream, Fox Spring, and Red Rock Brook. A reactivation of suprapermafrost springs and streams occurred during the storm peak (e.g., Camp Stream, Bubbling Spring). The discharge of Red Rock Brook was manually gauged at 117 L s^{-1} , 202 L s^{-1} , and 292 L s^{-1} on June 26, 30 and July 1, respectively. The latter discharge far exceeded the capacity of Terminal Sink and the ponds of the Carcadodo Valley coalesced, backing up for several days as far west as Fox Spring. The discharge peak of July 15 accompanied a localized thunderstorm event during which 10 mm of rain were recorded at the base camp in 30 minutes. The discharges of Red Rock Brook and Fox Spring gradually increased into late July and then declined. Discharge and solute variations associated with the June 30 event are described in Section 7.6.

There are no continuous discharge records from the summer of 1991. Many streams of the Mackenzie Mountains experienced high flows during that period, in some cases surpassing their 1988 peaks. Red Rock Brook was gauged on August 14, 20, 24, and 29 at: 212 , 166 , 163 , and 156 L s^{-1} , respectively. Pond levels in Carcadodo Valley were normal.

The capacity of Terminal Sink is not consistent through the spring and summer seasons. In late May 1988, ponding to normal summer levels was produced by an input flow of only 70 L s^{-1} . Through June and July of 1987, inputs of 105 to 140 L s^{-1} sustained the normal pond level. In mid-August 1991, inflows as high as 212 L s^{-1} were accommodated by Terminal Sink. The apparent increase in capacity through the course of the summer is attributed to activation of higher level ponors and increased permeability of the talik. At low water levels in May 1988, two ponors

were visible on the base of Terminal Sink. One was inundated only as the pond level increased in early-June. There may be other aggraded ponors that are activated at higher levels, or the increase in capacity from late June into August is due to the slow melting of seasonal ground ice at the base of Terminal Sink.

7.4.3 Hydrochemical Signatures

A Piper or trilinear diagram is a graphical representation used to identify hydrochemical facies (Fetter, 1988). For each water sample, the abundances of individual cation and anion species are plotted as percentages of the total cation and anion concentrations (e.g., Figure 7.17). Hydrochemical facies reflect a water sample's travel history, as influenced by the lithologies encountered and the kinetics of solution. The individual samples collected at the Dodo Canyon Site are plotted on Figure 7.17. These data are summarized on Figure 7.18. The data groupings of Figures 7.17 and 7.18 are organized by physical position within the karst and are not an exact match of the classification of Table 7.1. The average ion concentrations for the groups of Table 7.1 are presented as fingerprint diagrams on Figure 7.19. The general characteristics of those groups are outlined in the following sections.

7.4.3.1 Recharge Waters of the Sink Zone

Recharge in the Sink Zone was sampled from draining and perched waters in ponds and dolines on the Main Karst (Types 8 and 9: Table 7.1). Most of Type 9 waters were from shallow ponds on the Landry Member, while Type 8 samples included dolines that extend vertically into the Brecciated Member. Types 8 and 9 have low concentrations of dissolved ions (TDI = 2.74 and 3.24 meq L⁻¹; Total Hardness = 67 and 77 mg L⁻¹ CaCO₃), high pH values (8.35 and 8.46), high Ca²⁺/Mg²⁺ ratios (6.4 and 8.6), and low *p*PCO₂ (3.57) (Table 7.3). The *p*PCO₂ indicates these samples are equilibrated with atmospheric concentrations of CO₂.

These waters have a calcium bicarbonate facies (Figures 7.17, 7.18), with ion abundances Ca²⁺ > Mg²⁺ >> Na⁺ and HCO₃⁻ >> SO₄²⁻ ≥ Cl⁻ by equivalence (Figure 7.19).

The concentrations of Na^+ , Cl^- and SO_4^{2-} ion are only marginally above that of atmospheric inputs. The differences in temperature between Types 8 and 9 are due to time of sampling, most of the former were taken during snowmelt. Draining waters (Type 8) were found to be near equilibrium with respect to calcite ($\text{SI}_c = 0.03$) and strongly aggressive toward dolomite ($\text{SI}_D = -1.12$). Perched waters are less aggressive to dolomite ($\text{SI}_D = -0.31$).

7.4.3.2 Discharge Waters of the Sink and Fluvial Zones

This group includes the shallow (suprapermafrost) springs and streams of the Sink and Fluvial Zones, essentially Types 2 and 5 of Table 7.1. Complete analyses are available for only two suprapermafrost springs of discharge $>1 \text{ L s}^{-1}$, though the temperature and conductivity measurements from a larger set were similar to those from D10 (Bubbling Spring) and D24. Streams of Type 5 were usually supplied by a number of small shallow diffuse springs, and their characteristics reflect that mix.

The average temperature, total dissolved ion concentration, and total hardness of suprapermafrost springs are: $T \approx 2^\circ\text{C}$ ($n = 15$), $\text{TDI} = 4.68 \text{ meq L}^{-1}$, and $\text{TH} = 113 \text{ mg L}^{-1} \text{ CaCO}_3$. Measurements from streams are slightly higher: $T = 4.1^\circ\text{C}$, $\text{TDI} = 6.79 \text{ meq L}^{-1}$, and $\text{TH} = 171 \text{ mg L}^{-1} \text{ CaCO}_3$. The pH (8.01 and 8.18) and $p\text{PCO}_2$ values (2.96 and 3.15) indicate some CO_2 enrichment from the soil atmosphere. These waters have a calcium bicarbonate facies with average ion abundances $\text{Ca}^{2+} > \text{Mg}^{2+} \gg \text{Na}^+$ and $\text{HCO}_3^- > \text{SO}_4^{2-} \gg \text{Cl}^-$ by equivalence (Figures 7.17, 7.18, 7.19).

The low concentrations of Na^+ and Cl^- show a lack of input from dissolved halite. The average concentrations of Mg^{2+} and SO_4^{2-} indicate there are contributions from dolomite and gypsum. However, SO_4^{2-} concentrations range from 0 to $>1 \text{ meq L}^{-1}$, depending upon location. At Fan Canyon Stream (D14, D38) and its headwaters (D26, D41), SO_4^{2-} makes up approximately 25% of the anion charge (Appendix I). At Camp Stream (D11) and early in the melt season at Window Stream (D17, D18), SO_4^{2-} is either absent or occurs at low concentrations. Streams of the Fluvial Zone that run throughout the summer period maintain relatively high SO_4^{2-} concentrations.

This suggests that some component of the flow to these streams is not confined to the active layer. There is a contribution from local flow systems circulating deeply enough in the Bear Rock Formation to encounter gypsum or anhydrite. On average, these waters are slightly saturated with respect to calcite and aggressive toward dolomite (Table 7.3). Samples with high SO_4^{2-} content were saturated with respect to both minerals (Appendix I).

The $\text{Ca}^{2+}/\text{Mg}^{2+}$ ratios of 3.5 and 5.0 (Types 2 and 5) suggest dissolution is mainly of calcite. Limestone waters typically have ratios between 3 and 10, while interbedded limestone and dolomite yield values between 1.5 and 3 (White, 1988). In a study of over 400 water samples from the southern Rocky and Selkirk Mountains of Alberta and British Columbia, Ford (1971) found an average ratio value of 2.5, with most waters in the range of 1.75 to 3.5. The samples were largely drawn from limestone with minor interbedded dolomite. At the Dodo Canyon Site and at other locations in this study, the highest ratios are from water samples of shallow origin collected on the Landry Member (e.g., Type 9: $\text{Ca}^{2+}/\text{Mg}^{2+} = 8.6$) or from the Hume Formation (Chapter VIII). Both of these units are limestone. Ratios from Types 2 and 5 are considered high, given their contact with dolomite of the Bear Rock Formation. However, for Type 5 and other waters, ratio values are inflated by the Ca^{2+} contributed from gypsum dissolution. Thus, $\text{Ca}^{2+}/\text{Mg}^{2+}$ ratios may overstate the importance of limestone dissolution over dolomite.

7.4.3.3 Discharge Waters of Carcadodo Valley

Waters of this group include the springs and streams of intermediate chemistry that discharge onto the floor of Carcadodo Valley (Types 3 and 6: Table 7.1). Springs classified as Type 3 include Fox Moss Spring (D4) and the Great Spring Line (D33). Circular Swamp (D34) was included in this grouping although its hydrology is unique. Type 6 waters include Red Rock Brook (D3), Fan Stream (D5), Fox Swamp Stream (D39), and Fox Well (Spring) (D43). Additional sources of discharge to Carcadodo Valley are treated separately (e.g., D10), or incorporated into one of the

above locations.

Mean temperature, total dissolved ion, and hardness data from the intermediate springs are: $T = 4.5^{\circ}\text{C}$, $\text{TDI} = 15.21 \text{ meq L}^{-1}$, and $\text{TH} = 237 \text{ mg L}^{-1} \text{ CaCO}_3$ (Table 7.3; Figure 7.19). The same parameters for the streams are: $T = 7.4^{\circ}\text{C}$, $\text{TDI} = 16.1 \text{ meq L}^{-1}$, and $\text{TH} = 238 \text{ mg L}^{-1} \text{ CaCO}_3$. The temperature value for Type 3 springs is skewed by the one observation from site D34 ($T = 17.9^{\circ}\text{C}$), the average temperature of Fox Moss Spring was 1.6°C ($n = 4$), and for Great Spring Line 4.0°C ($n = 5$). The mean concentrations of Ca^{2+} , Na^+ , HCO_3^- , and Cl^- were approximately 3 meq L^{-1} , and for Mg^{2+} and SO_4^{2-} were 1.5 meq L^{-1} . In ion abundances these intermediate waters are characterized as $\text{Ca}^{2+} \approx \text{Na}^+ > \text{Mg}^{2+}$ and $\text{HCO}_3^- \approx \text{Cl}^- > \text{SO}_4^{2-}$, by equivalence (Table 7.3; Figure 7.19). Many of the individual samples are tightly clustered on the trilinear diagram, depicting a grouping of similar hydrochemical facies (Figures 7.17, 7.18). Samples from Fox Moss Spring plot between the bulk of the intermediate waters and the shallow waters of the Sink Zone.

The primary differences in hydrochemistry between Carcadodo Valley and the Fluvial Zone are higher concentrations of Mg^{2+} and SO_4^{2-} , and the presence of Na^+ and Cl^- . The ratio of the latter ions suggests that a component of discharge into Carcadodo Valley has encountered the Saline River Formation, several hundred metres below the valley floor ($\text{Na}^+/\text{Cl}^- \approx 1.0$). Data also show that in passing from the Fluvial Zone to Carcadodo Valley there is: (i) a drop in the $\text{Ca}^{2+}/\text{Mg}^{2+}$ ratio (Type 5 = 5.0; Type 6 = 2.2), revealing a rise in dolomite solution through the system, (ii) an increase in $p\text{PCO}_2$ values from 2.96 (Type 2) and 3.15 (Type 5) to 2.7 (Type 3) and 2.92 (Type 6), and (iii) a corresponding decrease in pH (Type 3 = 7.88; Type 6 = 8.06). Additional CO_2 may be dissolved in the soil zone or more likely supplied by redox reactions involving hydrocarbons in the Bear Rock Formation. Spring waters (Type 3) are near equilibrium towards calcite and dolomite but are more aggressive to the latter. Stream waters (Type 6) are saturated with both minerals (Table 7.3).

There are important variations in the hydrochemistry of discharge in

Carcadodo Valley. Temporal changes are reviewed in Section 7.6, spatial variations are discussed below. The mean ion concentrations for each of the sites in Carcadodo Valley are plotted on Figure 7.20 (Table 7.4). Fan Stream (D5), Circular Swamp (D34), Great Spring Line (D33), and Red Rock Brook (D5) all have ion abundances of $\text{Na}^+ > \text{Ca}^{2+} > \text{Mg}^{2+}$ and $\text{Cl}^- > \text{HCO}_3^- > \text{SO}_4^{2-}$ by equivalence. At Fox Swamp Stream (D39) and Fox Well (D43), concentrations of Na^+ and Cl^- are lower than those of Ca^{2+} and HCO_3^- . Fox Moss Spring (D4) has little Na^+ and Cl^- , although its concentrations are still an order of magnitude higher than those of Fan Canyon Stream (D14, D38). The range in Ca^{2+} , Mg^{2+} , HCO_3^- , and SO_4^{2-} concentrations between sites is $< 1 \text{ meq L}^{-1}$, the range in Na^+ and Cl^- is $> 4 \text{ meq L}^{-1}$. The sites with the highest total dissolved ion content are Fan Stream (20.36 meq L^{-1}), Great Spring Line (17.81 meq L^{-1}), and Circular Swamp (17.63 meq L^{-1}). Stream discharge increases from Great Spring Line (D33) to Fan Stream (D5) but the hydrochemistry is consistent (Table 7.4; Appendix I). The differences in the mean concentrations on Figure 7.20 are due largely to the interval sampled, most of the Great Spring Line samples date from the 1991 season, when discharges through the system were high and solute concentrations slightly lower. The hydrochemistry at Fox Well (Spring) (D43) reflects mixing between the waters of Fox Moss Spring and Fox Swamp Stream. The same is noted for Red Rock Brook, a site that reflects the mixing of all waters of Carcadodo Valley.

The data presented above allow some preliminary interpretation of the components that contribute flow to Carcadodo Valley. During the summer period, most of the discharge is supplied by Great Spring Line to Fan Stream. This is likely a subpermafrost groundwater component with high concentrations of Na^+ , Cl^- , Mg^{2+} , and SO_4^{2-} . There is also a flow component from surface and shallow suprapermafrost waters of the Fluvial Zone (e.g., Fan Canyon Stream), these waters lack Na^+ and Cl^- and sink at the edge of the valley. The flow from Fan Canyon Stream probably mixes with the groundwater supplying Fox Swamp Stream, thus diluting its concentration of Na^+ and Cl^- . Fox Moss Spring may merit unique treatment. It is a

cold, low discharge spring of calcium bicarbonate chemistry but with concentrations of Na^+ and Cl^- (0.5 meq L^{-1}) differentiating it from waters of the Fluvial Zone. It is possible that the Na^+ and Cl^- are from minor halite interbedded with gypsum and anhydrite of the Fort Norman/Bear Rock Formation, although halite is not reported in the literature. In later sections, the variations of these ions with discharge are examined more closely and the mixing model refined.

7.4.3.4 Discharge Waters into Carcajou Canyon

A series of spring points located at the base of the west wall of Carcajou Canyon were considered a possible resurgence of the sinking drainage of Carcadodo Valley. Several low discharge springs issue from bedrock and alluvium below or near the Bear Rock-Hume contact. Two of these springs were sampled for a complete analysis, Salt Spring (D2) and Colluvium Spring (D42). They are classified as Type 4 or deep springs. Samples were also drawn from three locations in Carca-Spring Stream at D1, D35, and D37. These are Type 7 or deep stream waters. A single sample was taken from an intermittent low discharge stream coming off the Bear Rock Formation at the east end of the Main Karst (D15). In addition, periodic measurements of temperature, conductivity, salinity, and discharge were made at a number of nearby locations. Certainly there are undetected aggraded spring points that contribute flow to Carca-Spring Stream and the channel of Carcajou River. The positions of the sample locations are indicated on Figure 7.21.

Mean values of temperature, total dissolved ion, and total hardness for the deep springs (Type 4) and streams (Type 7) are: $T = 9.5$ and $11.6 \text{ }^\circ\text{C}$, $\text{TDI} = 190.6$ and 142.7 meq L^{-1} , $\text{TH} = 463$ and $358 \text{ mg L}^{-1} \text{ CaCO}_3$ (Table 7.3). These waters have a sodium chloride facies (Figures 7.17, 7.18). Ion abundances for both groups are $\text{Na}^+ \gg \text{Ca}^{2+} > \text{Mg}^{2+}$ and $\text{Cl}^- \gg \text{SO}_4^{2-} \geq \text{HCO}_3^-$ by equivalence. The concentrations of Ca^{2+} , Mg^{2+} , HCO_3^- , and SO_4^{2-} are higher than other samples of the Main Karst, but are low relative to the exceptionally high concentrations of Na^+ and Cl^- . The $\text{Ca}^{2+}/\text{Mg}^{2+}$ ratios (1.8 and 1.7) are lower than other waters of the Main Karst. The

average concentrations from Salt and Colluvium Springs (86 meq L⁻¹ Na⁺ and 86.6 meq L⁻¹ Cl⁻) indicate that approximately 5.1 g of NaCl are dissolved per litre of water. Field data show that downstream of Salt Spring, discharge of Carca-Spring Stream gradually increases, but conductivity and salinity remain high (Figure 7.21). The pH of these samples are on average lower than other waters of the Main Karst (Type 4 = 7.63; Type 7 = 7.96), and the *p*PCO₂ values are the highest (Type 4 = 2.56; Type 7 = 2.91). The deep springs are near equilibrium with respect to calcite and slightly undersaturated with respect to dolomite.

In view of the hydrochemistry and physical characteristics of these deep spring waters, it is unlikely that they represent a resurgence of the sinking drainage of Carcadodo Valley. These warm highly mineralized groundwaters represent discharge from a regional flow system circulating as deeply as the Saline River Formation. These waters contrast markedly to discharge from the intermediate and shallow flow systems of the Main Karst on the Bear Rock Formation. The extent of these flow systems, depth of circulation, and linkages between them are discussed in subsequent sections in conjunction with isotopic and geological data. The positive dye trace from Terminal Sink to D37 strongly suggests the sinking waters of Carcadodo Valley resurge in alluvium on the floor of Carcajou Canyon.

7.4.3.5 Spillway Spring

North of the Main Karst is an area of dolines and depressions of solution and interstratal origin that are developed on the Hume and Hare Indian Formations. Many of these features have been altered or modified by glacial meltwaters; numerous spillway channels cut across the area of karst. An east-west trending channel incised into the Hare Indian Formation has local relief of about 50 m. At the base of a steep slope at the southern end of the channel is a series of springs. The spring area closest to the Carcajou River is Spillway Spring (D36; Type 11). It was sampled on two occasions. Shale of the Hare Indian Formation was observed on the surface, but based on outcrops on the west bank of Carcajou River it is expected that

the Hume-Hare Indian contact was in the shallow subsurface. Other springs occurred farther west in the same structural situation.

Spillway Spring consists of a series of diffuse, perennial, low discharge springs of subpermafrost origin. The discharge area is marked by extensive frost blisters. The site is similar to other subpermafrost spring points at Bear Rock in the Norman Range (van Everdingen, 1978, 1981; Chapter X) and at North Fork Pass in the Ogilvie Mountains (Pollard and French, 1983). Sampling occurred in a channel about 50 m downstream of several spring points. The discharge at the sampling point was approximately 5 L s^{-1} . It is not possible to estimate the total discharge from the area given the aggraded nature of many spring points and the presence of an extensive wetland. The average temperature at the sampling location was $3.9 \text{ }^\circ\text{C}$, the total dissolved ion content 25.9 meq L^{-1} , and total hardness $642 \text{ mg L}^{-1} \text{ CaCO}_3$. At the spring points, the temperature ranged between 1.5 and $2.1 \text{ }^\circ\text{C}$. These waters have a calcium bicarbonate and calcium sulphate hydrochemical facies (Figure 7.17, 7.18). Ion abundances are $\text{Ca}^{2+} > \text{Mg}^{2+} > \text{Na}^+$ and $\text{HCO}_3^- \approx \text{SO}_4^{2-} > \text{Cl}^-$ by equivalence (Figure 7.19). The concentrations of Ca^{2+} , HCO_3^- , and SO_4^{2-} at Spillway Spring are higher than any other location at the Dodo Canyon Site (Table 7.3; Appendix I). Ratios between the major ions indicate solution has occurred predominantly in limestone and gypsum, no halite is encountered by the groundwater feeding these springs. The pH of Spillway Spring was the lowest at the Dodo Canyon Site and $p\text{PCO}_2$ the highest. Spring waters are saturated with respect to dolomite and calcite ($\text{SI}_C = 0.7$, $\text{SI}_D = 0.74$). Tufa deposits were widespread in the frost blister area.

7.4.3.6 Mount Kindle Samples

The Mount Kindle Formation occurs in outcrop across the area of the Dodo Pavement. Water samples were collected from a pond, spring, and stream on the dolomite. They have been grouped together for analyses (Type 12: Table 7.2). Conductivity measurements from other surface waters on the pavement suggest these samples are representative. The only variable that differed substantially between

samples was temperature. The spring was coldest at 3.5°C, the pond warmest at 19.5°C. Average values for total dissolved ion and total hardness are 5.71 meq L⁻¹ and 141 mg L⁻¹ CaCO₃. These waters have a calcium-magnesium bicarbonate facies (Figures 7.17, 7.18). Ion abundances are Ca²⁺ ≥ Mg²⁺ >> Na⁺ and HCO₃⁻ >> Cl⁻ > SO₄²⁻ by equivalence (Figure 7.19). There are only trace amounts of SO₄²⁻, Na⁺, and Cl⁻. A Ca²⁺/Mg²⁺ ratio of 1.3 indicates solution of dolomite. The pH of these samples is high and the *p*PCO₂ low, all samples were highly saturated with respect to calcite and dolomite.

The fourth sample in the Dodo West area was taken from a low discharge seep emerging from talus at the base of an outcrop of the Bear Rock Formation (D31; Type 16; Table 7.2). The temperature of this sample was elevated by radiative heating of the talus at the collection location. This sample warranted separate treatment because of its location and some chemical differences to those of the Fluvial Zone. A high Mg²⁺ concentration, low SO₄²⁻ content, and low Ca²⁺/Mg²⁺ ratio indicate this water had circulated in part through the Mount Kindle Formation despite the apparent surface relationship.

7.4.3.7 Dodo West Creek, Dodo Creek, and Carcajou River

Conductivity and temperature measurements were periodically taken at Dodo West Creek, Dodo Creek, and Carcajou River. The former stream drains the Dodo West Karst and two small basins further westward, a total of approximately 15 km². The discharge of Dodo West Creek was often only 10 to 20 L s⁻¹, and during the summer some sections of the channel were dry. Channel bed materials suggest that periodic high discharge events do occur. The Mount Kindle and Bear Rock Formations are exposed through Dodo West Canyon. A series of springs at the base of the south wall of Dodo Canyon, 1.5 km west of the base camp, may be a resurgence of sinking Dodo West Creek waters (Figures 7.2, 7.7). A single chemical analysis was done on 130788 (Table 7.3: Type 13; Figures 7.17, 7.19). The hydrochemistry was most similar to waters sampled on the Mount Kindle Formation, temperature was 8.2 °C,

total dissolved ion 7.6 meq L^{-1} , total hardness $159 \text{ mg L}^{-1} \text{ CaCO}_3$, and the $\text{Ca}^{2+}/\text{Mg}^{2+}$ ratio was 1.3. Ion abundances were $\text{Ca}^{2+} > \text{Mg}^{2+} > \text{Na}^+$ and $\text{HCO}_3^- > \text{Cl}^- > \text{SO}_4^{2-}$ by equivalence. The occurrence of Na^+ , Cl^- , and SO_4^{2-} show groundwater contributions from the Bear Rock and possibly the Saline River Formations.

Upstream of the base camp, the Dodo Creek basin has an area of approximately 225 km^2 . The discharge regime is flashy, the floor of Dodo Canyon is mantled in coarse alluvium, channels are braided and shallow. Dilution gauging would be the only practical method of discharge measurement, however this was not undertaken as part of this project. Data on the hydrochemistry of Dodo Creek are few and should be interpreted with caution (Table 7.3: Type 14). Specific conductivity and salinity measurements varied between 300 and $820 \text{ } \mu\text{S cm}^{-1}$, and 0.0 and $0.6 \text{ } \%$, temperature averaged 4.6°C . The hydrochemical facies varied with stage. During flood events Na^+ , Cl^- , and SO_4^{2-} ions constituted a minor component of the dissolved load. At average discharges, the facies is similar to that of Red Rock Brook, though ion concentrations in Carcadodo Valley are higher (Figures 7.17, 7.19).

Carcajou River is gauged by the Water Survey of Canada, 20 km downstream of Carca-Spring Stream. Few hydrochemical data are available from that location (Chapter III). In the field area, a single sample was collected on the west bank at location D16, 100 m downstream of the deep springs. The data suggest a mixing with deep groundwaters at this location, and thus this sample is in no way viewed as representative of the average river chemistry (Table 7.3; Figures 7.17, 7.19).

7.4.4 Meteoric Waters

The natural isotopes of oxygen and hydrogen provide information on the origin, flowpaths, and velocities of ground and surface waters (Fritz *et al*, 1976; Sklash *et al*, 1976; Sklash and Farvolden, 1979; Fritz and Fontes, 1980; Moore, 1989; McDonnell *et al*, 1990; Payne, 1990; Mazor, 1991). Craig (1961) established the global meteoric water line using $\delta^{18}\text{O}$ and δD data from surface waters and

precipitation samples. Regional and local meteoric lines are available from precipitation data collected by the IAEA. Groundwaters of meteoric origin should lie close to the local lines. Deviations are attributed to fractionation effects. These may involve changes in state before infiltration, particularly surface evaporation, or exchanges with rock minerals, CO₂, or H₂S. Under ideal conditions natural isotopes function as conservative tracers.

7.4.4.1 Local Meteoric Line

Several $\delta^{18}\text{O}$ and δD measurements are available from precipitation samples in the study region (Table 7.5). The closest IAEA station is Fort Smith, 900 km southeast of Norman Wells. A meteoric water line is available from Fort Smith based on data collected in the 1960's. Data from the study region produce a meteoric water line that matches very closely with the Fort Smith line (Figure 7.22). The difference may be due to the temperature effect. The mean annual temperature at Norman Wells is -6.0°C , while at Fort Smith it is -3.0°C . Dansgaard (1964) has shown average global deviations attributed to the temperature effect are $0.7\text{‰}/^{\circ}\text{C}$ for $\delta^{18}\text{O}$ and $5.6\text{‰}/^{\circ}\text{C}$ for δD .

7.4.4.2 Sample Deviation from the Local Meteoric Line

Most of the samples collected in 1991 were analyzed for both $\delta^{18}\text{O}$ and δD , only $\delta^{18}\text{O}$ was measured for the 1983, 1987, and 1988 samples. The 1991 data were divided into: (i) discharge waters of Carcadodo Valley, (ii) discharge waters of Carca-Spring Stream, (iii) streams of the Fluvial Zone, and (iv) a pond of the Sink Zone. These data are plotted against the Fort Smith and local meteoric water lines (Figure 7.23). Most of the data fall below the Fort Smith and local line, but the deviation is slight. The distribution shows the sampled waters have a meteoric origin. This eliminates the possibility that waters of Carcadodo Valley or Carca-Spring Stream are fossil or connate. The positions of two samples requires further comment. One point is to the far right of the local line, this sample is from a slow

draining pond and the departure is attributed to the evaporation effect. The second point, lying above the cluster of data, was from Red Rock Brook (D3). The δD value is markedly different from other Red Rock Brook and Carcadodo Valley samples. It may be the result of sample contamination or analytical error.

The small average departure between the Dodo Canyon data and the Fort Smith line may reflect minor fractionation. The possibilities include: (i) evaporation of surface waters before infiltration, (ii) sublimation and evaporation from ice and snow, and (iii) mineral-water interactions. The latter are ruled out due to the low temperatures of the sampled groundwaters (Savin, 1980). In the summer period, surface waters in perched and slowly draining ponds are enriched by evaporation. Michel (1986a) documented a similar effect in the Franklin Mountains. However, at the Dodo Canyon Site, much snowmelt and summer rainfall infiltrates rapidly at doline locations and little recharge is held in depression storage for prolonged periods. Therefore, it is expected that the evaporative deviation of the discharge waters will be slight. Evaporation and sublimation also occur from the active layer and the snowpack. Known winter vapour fluxes from seasonal ice in the active layer to the snowpack vary between 3 and 30 mm cm⁻² a⁻¹ (Woo, 1986). The remaining pore and lense ice are enriched. The snowpack is also enriched by sublimation and evaporation to the atmosphere. Moser and Stichler (1980) recorded a linear increase in both $\delta^{18}O$ and δD with evaporative weight loss. The effect is particularly important in the surface layers. However, if the rate of mass removal is equalled or exceeded by the condensation of water vapour on the snow surface the net effect may be little change in the isotopic composition (Moser and Stichler, 1980).

A progressive depletion in $\delta^{18}O$ values is observed in passing from surface waters of the Sink and Fluvial Zones to deeply circulating springs of Carca-Spring Stream (Figure 7.23, Table 7.6). Pond and surface streams are heaviest with respect to ^{18}O , waters of Carca-Spring Stream are the most depleted, and discharge of Carcadodo Valley has an intermediate signature. Physical and hydrochemical data suggest some surface streams are fed by suprapermafrost and shallow aquifers in the

Bear Rock Formation, and Carca-Spring Stream is supplied by a subpermafrost aquifer in the Saline River Formation. Discharge into Carcadodo Valley includes a mix of groundwater components, including the above aquifers and subpermafrost waters that circulate deeper through the Bear Rock and Mount Kindle Formations. Where SO_4^{2-} ion is absent or at concentrations below 0.5 meq L^{-1} , it is assumed that there has been little mixing and the waters have a supraperafrost origin. The mean $\delta^{18}\text{O}$ of such springs and streams is -20.8 ‰ with a range from -20 to -22 ‰ (Table 7.6). Supraperafrost discharge with higher concentrations of SO_4^{2-} have a mean $\delta^{18}\text{O}$ of -21.6 ‰ . In Carcadodo Valley, the mean $\delta^{18}\text{O}$ of Type 3 and Type 6 waters is -21.7 ‰ . The data from Carca-Spring Stream yield a value of -21.9 ‰ $\delta^{18}\text{O}$, and it is -22.35 ‰ from Salt, Spillway, and Colluvium Springs. These data suggest that recharge to the subpermafrost aquifers must be lighter than recharge to supraperafrost aquifers. This may be due to a combination of the following factors: (i) the freezing effect, (ii) the area over which recharge occurs, and (iii) the timing of that recharge.

7.4.4.3 Freezing Effect

Evaporation and sublimation remove water from a hydrological system and alter the isotopic balance over an annual period. Freezing does not have the same effect but may produce isotopic stratification within active layer ice. The active layer attains its maximum thickness in late summer. In the fall and early winter, freezing proceeds downward from the surface and upward from the frost table. Fractionation occurs when the freezing front advances slowly into the soil (Michel, 1983; Mackay, 1983b). With downward freezing, ice formed deeper in the active layer is progressively isotopically depleted. Michel and Fritz (1982) report on fractionation from several cores penetrating the active layer at the Illisarvik experimental site of Mackenzie Delta. A 2 ‰ $\delta^{18}\text{O}$ fractionation is observed downward from the surface, a reverse trend upward from the base of the active layer showed two-sided freezing. The fractionation effect is strongest in closed systems such as frost blisters and

pingos. A depletion from -20 to -28 ‰ $\delta^{18}\text{O}$ is reported in frost blister ice resulting from a single phase of downward freezing in a water filled cavity at North Fork Pass (Michel, 1986b).

In spring and summer, water in the active layer originates from snowmelt, rainfall, and thawing of winter ice. Consequently, the isotopic composition of suprapermafrost groundwater reflects mixing or averaging of the above sources (Mackay, 1983b). If fractionation has occurred during freezing, then gradual thawing of the active layer will liberate progressively lighter water through the early summer. This effect may be masked by mixing with isotopically heavier rain. In the field area, the $\delta^{18}\text{O}$ of summer rainfall ranged between -16.1 and -22.1 ‰, with most measurements between -16 and -20 ‰ (Table 7.5; Figure 7.22). The difference between the $\delta^{18}\text{O}$ of suprapermafrost discharge and summer precipitation may be attributed to summer melting of isotopically light ice stored in the active layer. Therefore, it is also expected that recharge to the subpermafrost aquifers will also be isotopically lighter than the summer precipitation suggests alone. However, since subpermafrost discharge is more depleted with respect to ^{18}O than suprapermafrost flow there must be additional factors influencing recharge to the latter aquifers.

7.4.4.4 Recharge Area

Discharge from deep and intermediate flow systems should have $\delta^{18}\text{O}$ values that are close to annual average values of precipitation (Michel, 1983, 1986b; van Everdingen, 1990). There are insufficient data to calculate a precipitation average from Norman Wells. The value recorded from perennial subpermafrost springs at the Dodo Canyon Site is -22.4 ‰ (Table 7.6). Other subpermafrost springs in the region have $\delta^{18}\text{O}$ ratios as low as -23 ‰ (Chapter X). The lower values for subpermafrost springs may be partially related to the locations of their recharge areas.

Recharge areas for springs of Carcadodo Valley and Carca-Spring Stream cannot be precisely defined. It is suggested that the Sink and Fluvial Zones are areas

of recharge for Carcadodo Valley. The deeper groundwater component and the perennial subpermafrost springs of Carca-Spring Stream may be recharged at higher elevations on Dodo Mountain or possibly to the southwest along pediments bordering Dodo Canyon and its tributaries. Waters of Spillway Spring do not encounter the Saline River Formation, and thus it is most reasonable that the North Karst functions as its recharge area. In each of these cases, the recharge areas are at higher elevations than locations where precipitation and discharge have been sampled. The magnitude of the altitude effect is not constant between regions. There are insufficient data from the study area to calculate a local rate. Values from the literature typically range from -0.2 to -0.4 ‰/100 m (Mazor, 1991). Thus, the altitude effect does not account for the total variation between $\delta^{18}\text{O}$ values of supra- and subpermafrost waters in the study region. The elevation differences are too small. It is likely that the subpermafrost aquifers are recharged, in part, by snowmelt and the timing of recharge is an important factor.

7.4.4.5 Temporal Variations in $\delta^{18}\text{O}$

At the Dodo Canyon Site, $\delta^{18}\text{O}$ data were collected over portions of four summers from locations on the Main Karst. This data set has been divided into: (i) springs in Carcajou Canyon and Carca-Spring Stream, (ii) springs and streams in Carcadodo Valley, (iii) springs and streams in the Fluvial Zone, (iv) sinks and ponds in the Sink Zone, and (v) precipitation. Carcadodo Valley samples are from Great Spring Line, Fan Stream, Fox Spring, and Red Rock Brook. Fluvial Zone waters include Fan Canyon and Window Streams, and several small springs. Samples from the Sink Zone contain recharge waters collected in May 1988 from Bear Scat Sink, Straight Valley and other locations, and several samples from perched ponds collected during the summers. These data are plotted against time of collection on Figure 7.24.

The snowmelt period makes up an important pulse of recharge in the Sink and Fluvial Zones. A mid-May sample of ripe, melting snow yielded a $\delta^{18}\text{O}$ value of -25.1 ‰. Water sinking in dolines and ponors in late May had $\delta^{18}\text{O}$ values in the

range -21 to -23 ‰, while precipitation was in the range -17 to -21 ‰. Springs and streams in the Fluvial Zone and Carcadodo Valley were -19.5 to -21.5 ‰. During the melt period, water arrives at spring points in Carcadodo Valley from both suprapermafrost and subpermafrost aquifers, and the discharge of streams in the Fluvial Zone is relatively high. The isotopic values at these locations reflect the mixing of rainfall, melting snow, and melting ice in the upper part of the active layer. The signature suggests precipitation and suprapermafrost waters contribute substantially to the total discharge.

Through June and July, $\delta^{18}\text{O}$ values of springs and streams become progressively more negative, decreasing from -20 to -23 ‰. Over the same period, the $\delta^{18}\text{O}$ values of precipitation are heavier, with many samples in the range -16.5 to -18 ‰. Perched ponds have isotope values that are very close to that of precipitation. The relationship between discharge and precipitation is clearly out of phase, with a maximum difference in late July. In the summer period, the $\delta^{18}\text{O}$ values of springs and streams in the Fluvial Zone and Carcadodo Valley are similar to those of draining waters in the Sink Zone during snowmelt. The simplest interpretation is that there is a time lag between infiltration in the Sink Zone and discharge in Carcadodo Valley. Based on Figure 7.24, that lag is approximately 40 to 50 days, which is in good agreement with the dye trace between the two areas.

There are other factors that may also contribute to the light summer isotopic signature of Carcadodo Valley and Fluvial Zone discharge. It is possible that recharge may pass from Dodo Canyon to Carcadodo Valley. These waters would be isotopically lighter due to the high average elevation of Dodo Creek basin. This would influence precipitation by the altitude effect, and would delay and prolong snowmelt from cooler high elevation areas. Also, in the summer period the thickness of the active layer gradually increases. The slow melting of active layer ice should liberate water that is progressively depleted in ^{18}O due to the freezing effect. This effect may partially account for the early summer observations in the Fluvial Zone.

Data from August show a gradual increase in $\delta^{18}\text{O}$ values from discharge

samples of Carcadodo Valley and the Fluvial Zone. Precipitation becomes more depleted through August and September, and reaches levels that are typical of May and June meltwaters. In late September and October, the $\delta^{18}\text{O}$ of precipitation is typical of winter values in the region. Infiltration of this isotopically light water on the Main Karst would continue until freeze-up. The gradual late summer increases in spring and stream $\delta^{18}\text{O}$ may signify the passage of isotopically heavy summer precipitation through to spring points. These waters sink at dolines and ponors during summer storms. These data support the model of a lengthy time lag between infiltration and discharge on the Main Karst.

The few data from Carca-Spring Stream exhibit lower variance than the data sets of Carcadodo Valley and the Fluvial Zone. The springs of Carca-Spring Stream are interpreted as discharge from a regional subpermafrost aquifer in the Saline River Formation. Flow paths and travel times are long, discharge is thermal and perennial. It would be expected that under these conditions, discharge from this aquifer would have $\delta^{18}\text{O}$ values close to that of the annual average precipitation. This is in sharp contrast with data from Carcadodo Valley and the Fluvial Zone, which show a complex relationship between $\delta^{18}\text{O}$ of precipitation and discharge. The pattern may be related to a delay between Sink Zone infiltration and discharge in Carcadodo Valley, but explanation must also address mixing of shallow, intermediate, and deep groundwater components.

7.5 Hydrochemical Mixing in the Main Karst

The hydrochemical facies of shallow recharge waters reflect the local lithology of their basins. The facies of springs and streams in Carcadodo Valley are associated with mixing of groundwaters from different aquifers, the time of year, and variations in discharge. This section describes the pattern of groundwater mixing in the Main Karst, with a focus on springs of Carcadodo Valley. Section 7.6 reviews seasonal and discharge related variations in hydrochemistry.

Information on the depth and length of groundwater flowpaths may be

discerned from chemical, isotope, and temperature data. Composition diagrams consist of pairs of hydrochemical parameters plotted as scattergrams. Most commonly the concentrations of major ions are graphed as a function of total dissolved ions (TDI). When the discharge and chemistry from an aquifer are constant, these data plot in clusters. Where groundwaters of multiple aquifers discharge at common springs, data plot along mixing lines (Mazor, 1991).

In a mixing model, averaged values of ion concentration and discharge are assigned to each known surface and groundwater component (Figures 7.25, 7.26). The least complex case involves two hydrological end members of distinct chemistry. The effects of mixing are determined by applying a mass balance equation to a specific discharge condition. The following mass balance equation separates two components:

$$C_T Q_T = C_O Q_O + C_N Q_N \quad (7.1)$$

where C_T is the ion concentration in the spring water, Q_T is the total discharge, C_O , C_N , Q_O , and Q_N are the concentrations and the flow contributions of the two components. If the total discharge and the concentrations of the flow components are known, or can be estimated, it is possible to calculate the discharge of each component. If:

$$Q_T = Q_O + Q_N \quad (7.2)$$

then, at a point in time:

$$Q_O = Q_T \frac{(C_T - C_N)}{(C_O - C_N)} \quad (7.3)$$

This approach of treating aquifers as separate elements is a simple representation of reality where a continuum of transmissivity and hydrochemistry exists between rock units. This is further complicated by attempting to separate three or more flow

components. Thus, field data often vary from the model cases described below.

Three general patterns of mixing are recognized between two components: (i) data extrapolate to a value on the TDI axis, (ii) data extrapolate to point on the ion axis, and (iii) data extrapolate to the origin (Figure 7.25). In the first case, one member has a very low concentration of the ion under consideration, while the other is higher. In the second case, both waters have measurable but unequal concentrations of the ion. In the final situation, a fresh water component is progressively diluted by a water of high TDI. The mixing permutations increase when three or more flow components are involved. Two potential interactions of three-way mixing are represented on Figure 7.26. In Figures 7.25 and 7.26, relationships are depicted for only a single ion species.

7.5.1 Fluvial Zone

In the Fluvial Zone, concentrations of Ca^{2+} , HCO_3^- , SO_4^{2-} , and Mg^{2+} are positively correlated with total dissolved ions (Figure 7.27). Samples of low TDI were taken from intermittent streams thought to be supplied by the suprapermafrost aquifer (Camp Stream: D13; Winding Stream: D18). Sites where discharge occurred throughout the summer period record the presence of SO_4^{2-} , and have higher TDI values (Fan Canyon Stream: D14, D38; Streams in Glade: D26, D40; Tributary stream to Fan Canyon: D41). Data from Fan Canyon Stream display considerable variation, with the highest concentrations from the late summer.

The patterns on the composition diagram of Figure 7.27 suggest two-member mixing occurs in passing from the topographically high to low areas of the Fluvial Zone. The fresher component has a calcium bicarbonate chemistry and little Mg^{2+} and no SO_4^{2-} . The concentrated component brings in SO_4^{2-} and higher concentrations of Mg^{2+} . The levels of Na^+ and Cl^- are negligible in all waters sampled. The hydrochemistry suggests that circulation of the shallow component is limited to limestone of the Landry Member and may be largely restricted to the suprapermafrost aquifer. The deeper water has encountered the Brecciated Member

of the Bear Rock Formation as indicated by the SO_4^{2-} data. Recharge to this component must locally penetrate the permafrost. Water temperatures are consistent with relatively shallow circulation for both waters.

The hydrochemical data and the topographic positions of spring points in the Fluvial Zone support this model. Ephemeral, high elevation springs and streams are dominated by the fresher component. Its flowpaths are short, shallow, and restricted to the upper part of the Bear Rock Formation. Springs and streams within large depressions (e.g., Glade) or Fan Canyon have higher TDI's and SO_4^{2-} ion. These springs take flow from intrapermafrost and subpermafrost waters recharged at nearby dolines. They flow throughout the summer and have a hydrochemical facies that shows contact with the Brecciated Member.

7.5.2 Carcadodo Valley

In discharge waters of Carcadodo Valley, all major anions and cations are positively correlated with TDI (Figure 7.28). There are important differences from data of the Fluvial Zone, including the addition of a Na^+ and Cl^- rich groundwater component. At Red Rock Brook (D3), TDI values range from 7 to 22 meq L^{-1} . The low TDI samples were taken during the melt season prior to activation of Great Spring Line (D33), and the high TDI samples when Fan Stream (D5) accounted for most the discharge. There is clustering of data from some individual sites, showing consistent hydrochemistry, but these are superimposed on mixing trends. The range of TDI at Fox Well (D43) was 8 to 16 meq L^{-1} , samples from Fox Moss Spring (D4) were at the low end ($\approx 10 \text{ meq L}^{-1}$), and those of Fox Swamp Stream (D39) were higher ($\approx 15 \text{ meq L}^{-1}$). Sites of the highest TDI are Great Spring Line and Fan Stream (17 to 24 meq L^{-1}). The rate of change in ion concentrations with TDI is not constant between species (Figure 7.28). In samples of $\text{TDI} > 10 \text{ meq L}^{-1}$, Na^+ and Cl^- increase at the highest rate (slopes = 0.34 and 0.35). The rate is much lower for Ca^{2+} and HCO_3^- (slopes = 0.07 and 0.04) and intermediate for SO_4^{2-} and Mg^{2+} (slopes = 0.12 and 0.09).

The mixing lines suggest all components of discharge contain Ca^{2+} , HCO_3^- , and Mg^{2+} , though the latter occurs at low concentrations in a low TDI input. The ions Na^+ , Cl^- , and SO_4^{2-} are absent in the freshest input but are present in one or more other waters. At least three groundwater components contribute to discharge in Carcadodo Valley: (i) a calcium bicarbonate water of low TDI, (ii) a water of intermediate TDI with SO_4^{2-} and a low $\text{Ca}^{2+}/\text{Mg}^{2+}$ ratio, and (iii) a water of high TDI with high concentrations of Na^+ and Cl^- . Spring and stream hydrochemistry reflect mixing between these outputs. The data from the Fluvial Zone show mixing of a calcium bicarbonate water with a groundwater component of the Bear Rock Formation, the latter bringing in SO_4^{2-} . These two components also discharge into Carcadodo Valley. The SO_4^{2-} and Mg^{2+} concentrations may be higher than those recorded in Fan Canyon Stream due to deeper and longer flowpaths. Assuming a permafrost thickness of approximately 50 m, much of the recharge from the Sink Zone would travel through the Bear Rock Formation in a subpermafrost position. The $\text{Ca}^{2+}/\text{Mg}^{2+}$ ratios of the Carcadodo waters are much lower than those of the Fluvial Zone suggesting circulation through dolomites of the Mount Kindle and Franklin Mountain Formations is likely. The ion ratio between Na^+ and Cl^- suggests halite as a source of these ions in the discharge of Carcadodo Valley. The Saline River Formation is the only rock unit with the proper mineralogy. This component has therefore circulated through this formation and has come to the surface through approximately five hundred metres of overlying carbonate. This component is not uniformly discharged at the surface; the concentrations of Na^+ and Cl^- are highest at Great Spring Line and Fan Stream.

7.5.3 Carca-Spring Stream

In Carcajou Canyon, data are available from Salt and Colluvium Springs, and three locations along Carca-Spring Stream. All samples are dominated by Na^+ and Cl^- . Salt Spring has the highest TDI and its chemistry and discharge were consistent over the period of observation. Composition diagrams show mixing occurs along Carca-

Spring Stream between saline groundwater and a fresher component (Figure 7.29). The latter component is a resurgence from Carcadodo Valley or Carcajou River water seeping through alluvium. The saline component is presumed to discharge from the subpermafrost Saline River aquifer.

7.5.4 Temperature of Spring Waters

The minimum depth of groundwater circulation in an aquifer may be estimated from the temperature of discharge by:

$$D \approx \frac{T_{measured} - T_{surface}}{\Delta T/100} \quad (7.4)$$

where D is the depth of circulation in metres, $T_{measured}$ is the spring or well temperature, $T_{surface}$ is the local average ground surface temperature, and ΔT is the local geothermal gradient (Mazor, 1991). Temperature data are available from samples of the Main Karst (Appendix I). The values measured from springs and spring-fed streams may differ from those equilibrated with aquifer rocks. Subpermafrost waters may be cooled in passing through the permafrost zone. Diffuse springs may be warmed in the soil zone. However, at a few locations waters flowed directly from bedrock or from high discharge aggraded spring points. In these cases, temperature changes during ascent would be less and the spring temperatures would provide a minimum estimate of the average depth of circulation.

Temperature data from Fox Moss Spring, Great Spring Line, Colluvium Spring, and Salt Spring are presented on Figure 7.30. Temperature and TDI are positively correlated. The depth of circulation was calculated with an annual ground temperature of -2°C and a geothermal gradient of $3^{\circ}\text{C}/100\text{ m}$. The shallowest average circulation is shown for Fox Moss Spring and the deepest for Salt Spring. At Fox Moss Spring and Great Spring Line, deep and shallow groundwater components are mixed, with the deep component elevating the temperature of the discharge. It is likely that much of the flow of Fox Moss Spring does not circulate

below 100 m. The figure of 383 m from Salt Spring is probably a minimum, as these waters would experience some cooling when rising to the surface.

7.5.6 Sulphur Isotopes

The $^{34}\text{S}/^{32}\text{S}$ abundance ratios in sulphates from the Saline River Formation are higher than those from the Bear Rock (Fort Norman) Formation (Figure 7.31)(van Everdingen and Krouse, 1977; van Everdingen *et al*, 1982a). It is possible to trace groundwaters to one of these units by determining the $\delta^{34}\text{S}$ of dissolved sulphates. Four water samples from the Main Karst area were analyzed (Figure 7.31). The $\delta^{34}\text{S}$ values from Red Rock Brook and Great Spring Line are 12.3 and 15.4 ‰, these are close to the Bear Rock (Fort Norman) Formation mean of 17.8 ‰ (van Everdingen *et al*, 1982a). The value from Salt Spring is 23.0 ‰ which lies in the range of Bear Rock (Fort Norman) sulphate (Figure 7.31). However, the hydrochemistry of Salt Spring is dominated by Na^+ and Cl^- , suggesting contact with the Saline River Formation. A similar situation is described by van Everdingen *et al* (1982b) from a site in the Norman Range northwest of Norman Wells. At Paige Mountain, sulphurous springs with high concentrations of Na^+ and Cl^- discharge into a valley near the contact between the Bear Rock and Hume Formations. The $\delta^{34}\text{S}$ ratios range from 16.2 to 22.0 ‰. It is possible that only halite facies are encountered in the Saline River Formation, or that descending water becomes saturated with sulphate of the Fort Norman Formation. If the residence time in the Saline River Formation is relatively brief there would be little exchange of dissolved sulphate. Also, ascending waters would contact the Fort Norman Formation a second time before discharge. The value from Salt Spring is near the range established for sulphates of the Saline River Formation and there may be a mix of sulphates from both the Fort Norman and Saline River Formations. The final sample was from Spillway Spring, the $\delta^{34}\text{S}$ value of 2.3 ‰ is unlike other data reported from the Fort Norman Formation. It is possible the ratio value has been lowered through production of secondary SO_4^{2-} involving redox reactions in the shales of the Canol

and Hare Indian Formations. Such reactions are described by van Everdingen *et al* (1982b) from Paige Mountain.

7.5.7 Model of Circulation in the Main Karst

In the Fluvial Zone, composition diagrams show mixing between two flow components. The first is water of low TDI restricted to the surface and shallow subsurface of the Landry Member. The second is water of higher TDI that includes sulphate ion from the Brecciated Member. Discharge in Carcadodo Valley includes: (i) the combined flows of the Fluvial Zone, (ii) additional subpermafrost discharge through the Bear Rock, Mount Kindle, and possibly the Franklin Mountain Formations, and (iii) a deep saline component from the Saline River Formation (Figure 7.32). The facies of the latter is represented by the thermal Salt Spring of Carcajou Canyon. Variations in the hydrochemistry and discharge of Red Rock Brook are related to changes in the above flow contributions to Carcadodo Valley. A simple model of the system involves three way mixing between flows of the Fluvial Zone (1), the Bear Rock-Mount Kindle-Franklin Mountain aquifers (2), and the Saline River aquifer (3):

$$C_T Q_T = C_1 Q_1 + C_2 Q_2 + C_3 Q_3 \quad (7.5)$$

where C_T and Q_T are ion concentrations and discharge of Red Rock Brook (T). In equation 7.5, C_T and Q_T are known, and C_3 may be estimated from Salt Spring. Measurements are also available from the Fluvial Zone, but much of the discharge through the upper Bear Rock Formation is not visible in Window and Fan Canyon Streams.

How solution is spatially distributed within these aquifers is important to landform development of the Main Karst. If it assumed that all Na^+ and Cl^- recorded in Red Rock Brook have an origin in the Saline River aquifer, it is possible to calculate Q_3 for a particular discharge condition. In this calculation Equation 7.5 reduces to:

$$C_T Q_T = C_3 Q_3 \quad (7.6)$$

The average concentrations of Na^+ and Cl^- from Salt Spring are 92.1 and 92.7 meq L^{-1} (C_3). Concentrations from Red Rock Brook are 3.27 and 3.25 meq L^{-1} (C_T). The average summer discharge of Red Rock Brook is approximately 150 L s^{-1} (Q_T). From Equation 7.6, the flow contribution of the Saline River component is calculated at 5.3 L s^{-1} (Q_3). Data from Fan Stream can also be used. The Na^+ and Cl^- concentrations are both 4.68 meq L^{-1} and the discharge is 125 L s^{-1} (Figure 7.16). The Saline River component has a calculated discharge of 6.4 and 6.3 L s^{-1} , based on the Na^+ and Cl^- data. The two estimates of the Saline River contribution to Carcadodo Valley are in good agreement. From this approximation, it is possible to calculate the proportions of Red Rock Brook's Ca^{2+} , Mg^{2+} , and SO_4^{2-} that may be traced to the deep aquifer. The average concentrations of these ions in Salt Spring are 6.21, 3.44, and 6.03 meq L^{-1} (Q_3), while in Red Rock Brook they are 3.10, 1.44, and 1.75 meq L^{-1} (Q_T). Assuming discharges of 6 and 150 L s^{-1} for the Saline River (Q_3) and Red Rock Brook (Q_T) components, the contributions from the Saline River aquifer account for only 12.5% of the Ca^{2+} , 10.5% of the Mg^{2+} , and 7.3% of the SO_4^{2-} . The balance of the ions are contributed by the shallow (1) and intermediate flow components (2). Thus, most of the carbonate and gypsum solution occurs in the Bear Rock, Mount Kindle and Franklin Mountain Formations.

Estimating the amount of flow that travels through the shallow pathways of the upper Bear Rock Formation to Red Rock Brook is more difficult (Q_1). Section 7.6.3 describes hydrograph separation at Fox Spring. Under non-storm conditions the shallow water component is determined to comprise approximately 33% of Fox Spring discharge. This is interpreted as flow through the upper Bear Rock Formation. Hydrochemical data suggest that this component comprises a smaller percentage of the total flow at Great Spring Line and Fan Stream, and therefore at Red Rock Brook. Assuming the average ion concentrations of Fan Canyon and similar streams (Type 5: Table 7.3) are typical of the shallow component, and the

concentrations from Salt Spring represent the deep component, then it is possible to determine the average ion concentrations of the intermediate water (C_2) from Equation 7.5. This is done for the discharge conditions when Q_i is equal to 33% and 20% of Q_T (Table 7.7). In both cases the ion concentrations of the intermediate component are similar to the average values from Red Rock Brook. They differ from the shallow water in concentrations of Mg^{2+} and SO_4^{2-} , indicating deeper circulation through the Bear Rock Formation and into the underlying dolomites of the Mount Kindle and Franklin Mountain Formations.

7.6 Hydrograph Analyses

Monitoring discharge and chemistry of spring points is a basic method in karst hydrology. Spring hydrographs can provide data on the physical properties of aquifers, particularly when coupled with hydrochemical and isotopic data. The properties of aquifers that may be explored include: (i) the dynamic storage volume and effective porosity (Bonnaci, 1987), (ii) the amount of groundwater recharge (Korkmaz, 1990), and (iii) the nature of the flow system and degree of karstification (Mangin, 1975; Bakalowicz and Mangin, 1980). The standard approaches are examinations of recessional limbs and the separation of hydrographs into flow components with the aid of chemical or isotopic data. The following sections present discharge records and the associated solute variations from Carcadodo Valley.

7.6.1 Hydrograph Recession

Hydrographs of springs or spring-fed streams typically rise to maximums during periods of precipitation and aquifer recharge, and then display gradual reductions in discharge on recessional limbs. The form of a recession may be described by a variety of mathematical expressions, including simple exponential decays, double exponential, hyperbolas, or combinations of these functions (Ford and Williams, 1989). In complex aquifers, the hydrograph recession may contain multiple log-linear segments each representing the drainage of a different flow component within

the aquifer (Milanovic, 1981). In some cases, the falling limb may be subdivided into a short, steep segment that follows the discharge peak, and a gently sloping log-linear segment (Mangin, 1975; Figure 7.33). The rapidly declining, non-linear interval may correspond with the passage of a flood pulse through the system, and the linear portion a baseflow recession. The baseflow recession is described by:

$$Q_b = Q_i e^{-\alpha t} \quad (7.7)$$

where Q_b is the discharge at time t , Q_i is the discharge at t_i , and α is the recession coefficient. At time t_i , the baseflow comprises the total discharge ($Q_b = Q_i$; Figure 7.33). The recession coefficient is determined from:

$$\alpha = \frac{\log Q_{b1} - \log Q_{b2}}{0.4343 \times (t_{b2} - t_{b1})} \quad (7.8)$$

where Q_{b1} and Q_{b2} are discharges for times t_{b1} and t_{b2} . These data are taken from the log-linear portion of the hydrograph (Figure 7.33). The value of the recession coefficient varies with aquifer transmissivity, storativity, and catchment geometry (Foster, 1974). This parameter has a range from 0 to 1. Steep baseflow recessions are represented by high α values, suggesting a rapidly draining aquifer with a high effective porosity, perhaps an integrated conduit network. A gently sloping recession and low value of α , suggests an aquifer dominated by diffuse flow with a large storage volume. There may be difficulties with this basic interpretation since the coefficient has no clear physical meaning.

The dynamic volume of an aquifer is storage in the phreatic zone above the level of the spring outlet. It is calculated from:

$$V = \frac{Q_t}{\alpha} c \quad (7.9)$$

where V is the dynamic volume, Q_t is the discharge at time t , and c is a constant that

equals 86400 when discharge is expressed in $\text{m}^3 \text{s}^{-1}$ and α in day^{-1} . This volume can be calculated for any point on a recession. The discharge used to determine maximum dynamic volume should not exceed the maximum baseflow discharge (Q_{bo} on Figure 7.33).

7.6.1.1 Recession of Red Rock Brook and Fox Spring

There were several recharge events in the field season of 1988 that generated flood peaks at Fox Spring and Red Rock Brook. The single largest event produced a flood hydrograph at Fox Spring with a long recession suitable for analysis (Figures 7.34, 7.35). The discharge record of Red Rock Brook shows a gradual increase through June and July in response to a prolonged period of recharge. This is followed by a long recession initiated in late July (Figure 7.34). Superimposed on that trend are several flood peaks and recessions that correspond with individual storms. The late summer recession and two other peaks are examined (Figure 7.35).

The recession coefficients calculated for Red Rock Brook range from 0.021 to 0.028 day^{-1} , with the late summer recession having a value of 0.025 day^{-1} (Figure 7.35). The discharge of Red Rock Brook may be extrapolated into September and October based on the latter value. The coefficient from Fox Spring is 0.049 day^{-1} . These values are moderately high and may be indicative of an aquifer with a high effective porosity and transmissivity. The maximum dynamic volumes for Red Rock Brook and Fox Spring aquifers are $7.5 \times 10^5 \text{ m}^3$ and $6.5 \times 10^4 \text{ m}^3$. The order of magnitude difference is not unexpected since Fox Spring aquifer is simply a subcatchment of the larger aquifer that feeds Great Spring Line, Fan Stream, and Red Rock Brook. Mangin (1975) suggests that in karst aquifers the ratio between the dynamic volume and the total annual flow is < 0.5 . Recharge passes through highly transmissive karst aquifers more rapidly and with less storage than diffuse aquifers. Based on the 1988 data, the total discharge is estimated at $1.5 \times 10^6 \text{ m}^3$ (Section 7.6.4) and the maximum dynamic volume at $7.5 \times 10^5 \text{ m}^3$, yielding a ratio of 0.5.

7.6.2 Discharge Solute Relationships

There are sufficient data from locations in Carcadodo Valley to examine temporal variations in solute concentration and the relationship with discharge. Figure 7.36 plots Na^+ , Ca^{2+} , Mg^{2+} , Cl^- , HCO_3^- , and SO_4^{2-} concentrations recorded from Red Rock Brook (D3), Fox Spring (D43), and Fan Stream (D5) against time. These data are presented along with the discharge series from Red Rock Brook and Fox Spring.

During the snowmelt period, concentrations of Na^+ , Mg^{2+} , Cl^- , and SO_4^{2-} are lower than typical summer values. In Red Rock Brook, the late May concentrations of these ions are $<1 \text{ meq L}^{-1}$, while concentrations of Ca^{2+} and HCO_3^- are in the 1 to 2 meq L^{-1} range. In June, the values increase for all ions and remain high through the summer period. Maximums approach 5 meq L^{-1} for Na^+ and Cl^- , 3 meq L^{-1} for Ca^{2+} and HCO_3^- , and 2 to 2.5 meq L^{-1} for Mg^{2+} and SO_4^{2-} . Concentrations are slightly higher in Fan Stream, and lower at Fox Spring, particularly for Na^+ and Cl^- . The Ca^{2+} and HCO_3^- ion concentrations are most consistent between sites and years (Figure 7.36). Higher variability is exhibited by Na^+ and Cl^- ions, due to changes in discharge of the shallow and intermediate flow components.

There is a complex relationship between discharge and solute concentrations. The gradual increase in TDI that follows snowmelt is related to a shift from suprapermafrost and surface flows that dominate in May, to subpermafrost spring flow that comprises most of the summer discharge. Consequently, ion concentrations and discharge are lowest during the snowmelt period. Despite fluctuations in summer flows, the ion concentrations remain relatively stable; only the high magnitude event of June 30 - July 1, 1988 generated substantial variability. In this event, all ions experienced a decrease in concentration that corresponded with the discharge peak, although for Ca^{2+} and HCO_3^- the reduction was minor. This event is discussed in detail in Section 7.6.3.1. In the 1991 samples, ion concentrations remained consistent, despite a substantial drop in discharge over the sampling interval. The average lower concentrations of Na^+ and Cl^- in the 1991 samples may be due to greater dilution of the deep Saline River component by shallow and

intermediate discharge.

The discharge solute trends observed in Carcadodo Valley can be extrapolated to Fan Canyon and Window Streams of the Fluvial Zone. The TDI of Fan Canyon Stream (D14) on May 26 and July 3, 1988 were 5.9 and 7.4 meq L⁻¹; samples from August 1991 have TDI's of 9.3 meq L⁻¹ (Appendix I). These increases are due to higher concentrations of Ca²⁺, Mg²⁺, HCO₃⁻, and SO₄²⁻. Ion concentrations at Salt Spring did not vary substantially over the period of observation and seem to behave independently of discharge in Carcadodo Valley and other surface streams.

7.6.3 Hydrograph Separation

It is common practise in hydrology to separate storm hydrographs into genetic components. A distinction is usually made between pre-event and event waters. Pre-event waters may be groundwater, baseflow, or subsurface stormflow, and event waters are overland flow, quickflow, stormflow, or surface stormflow. Appropriate use of these terms requires the recognition of the flow components involved and their temporal contribution to the hydrograph. When a hydrograph is separated into only two components the terms 'new' and 'old' water are useful, where 'new' denotes flow derived from the precipitation and 'old' from water presently in a system store (Pilgrim *et al*, 1979; Anderson and Burt, 1982). The storm peak is usually attributed to a 'new' component which is normally shallow subsurface or surface flow. Deeper circulating components are assigned to the recession.

Separation into two components is accomplished using the mass balance equation (Equation 7.1) with discharge data and a conservative tracer. The latter include: (i) environmental isotopes (Sklash *et al*, 1976; Sklash and Farvolden, 1979; Sklash *et al*, 1986; Moore, 1989; McDonnell *et al*, 1990), (ii) electrical conductivity (Pilgrim *et al*, 1979; Kobayashi, 1986), (iii) solute concentrations (Pinder and Jones, 1969; Caine, 1989), (iv) temperature (Kobayashi, 1985), or (v) a combination of parameters (Hooper and Shoemaker, 1986; Kennedy *et al* 1986).

Hydrograph separations have been done in a range of environments from the

humid temperate to the periglacial, but not in regions influenced by permafrost. The technique requires that the total discharge be measured and the concentrations or signatures of the tracers for each flow component be known and remain constant throughout the event. The latter condition is rarely satisfied. Changes in solute load and conductance partially reflect the contact time between a flow component and the soil or aquifer materials; this contact time will vary with flow conditions.

In karst systems, the phreatic and subcutaneous zones represent stores where the solute load and conductance of old waters may be high. A hydrograph separation model proposed by Atkinson (1977) and modified by Williams (1983) for conduit aquifers divides the flood hydrograph into a series of components representing different stores and flowpaths within the aquifer (Figure 7.37). The rising limb represents the displacement of old water stored in phreatic conduits. This is followed by old waters derived from fissures of the subcutaneous and phreatic zones. The initial fluxes are marked by increases in conductivity and dissolved solids concentration. The arrival of new water at the spring point is marked by a decrease in conductance and an increase in turbidity. This model suggests that much of the peak area of the hydrograph may be composed of old waters. This contrasts sharply with models from non-karst basins where new water forms the bulk of the hydrograph peak.

7.6.3.1 Hydrograph Separation: Fox Spring

Data collected at Fox Spring in 1988 include: (i) a continuous discharge series, (ii) ion concentration and $\delta^{18}\text{O}$ measurements from ten water samples, and (iii) a record of electrical conductance. The discharge series contains three storm peaks that are potential candidates for hydrograph separation, with the largest single event lasting from June 30 to July 3 (Figure 7.15). Prior to the event, the Sink and Fluvial Zones of the Main Karst were dry, and the discharges of Fan Canyon and Window Streams low (Section 7.4.2.4). At the Dodo Canyon base camp, rainfall was recorded in two heavy pulses. The first pulse began on the evening of June 29 and lasted until 10

a.m. on the 30th, with the most intense precipitation between 4 and 8 a.m. (Figure 7.38). Following light midday rains on June 30, the precipitation intensity increased after 5 p.m. and remained high until 3 a.m. on July 1. Rainfall then declined and ceased by 12 p.m. In all, 56.6 mm of rainfall were recorded.

There were immediate responses at Fox Spring and Red Rock Brook to the first precipitation input. Both sites experienced a moderate increase in discharge and peaked around 12 p.m. on the 30th. Elsewhere in Carcadodo Valley and the Fluvial Zone, increased flows were observed at Great Spring Line, Fan, Window, and Fan Canyon Streams, and at suprapermafrost springs and streams that had previously taken flow only during snowmelt (e.g., Camp Stream (D13) and Bubbling Spring (D10)). The second precipitation pulse generated a similar but much greater response. Discharge rose rapidly through the early morning hours of July 1 peaking at 66 L s^{-1} at Fox Spring, $>290 \text{ L s}^{-1}$ at Red Rock Brook, and $>30 \text{ L s}^{-1}$ at Fan Canyon Stream. The latter flowed 70-100 m over the surface of the alluvial fan before completely infiltrating. Window Stream reached or exceeded its snowmelt discharge. Circular Swamp (D34), dry before the event, was flooded during this period. The capacity of Terminal Sink was exceeded and the eastern portion of Carcadodo Valley was flooded. The lake reached the stage recorder at Red Rock Brook at 2 p.m. on July 1 and continued to rise until 3 p.m. on July 3. At its maximum extent, the lake backed up to a position approximately 25 m east of Fox Spring. By July 3, the discharge of Window Stream had decreased to 4 L s^{-1} and Fan Canyon Stream to 15 L s^{-1} . The lake impounded in Carcadodo Valley slowly drained to pre-storm levels by July 11.

Ion concentrations at Fan Stream, Fox Spring, and Red Rock Brook were reduced across the peak of the storm event (Figure 7.36). These variations were recorded in greater detail at Fox Spring by continuous monitoring of electrical conductance (Figure 7.38). Conductivity increased from 700 to $750 \mu\text{S cm}^{-1}$ with the initial rise in discharge on June 30. There was an abrupt reduction to a minimum of $580 \mu\text{S cm}^{-1}$ on July 1 that was coincident with the flood portion of the hydrograph.

Recovery to pre-storm conductivity levels was achieved by midday of July 2. The flood pulse was also recorded by an increase in $\delta^{18}\text{O}$ from -21.9 to -21.6 ‰. While this is a small change, the enrichment was recorded at the height of the flood (Figure 7.38). The storm generated substantial increases in suspended sediment concentration in Dodo Creek and Carcajou River, but at no time did Fox Spring or any other waters in Carcadodo Valley exhibit turbidity. Sinking waters on the Main Karst were not observed at the peak of the event but it is not expected they were turbid.

There are at least three flow components contributing to Carcadodo Valley: (i) discharge from a shallow unconfined aquifer in the Bear Rock Formation, (ii) discharge from a subpermafrost aquifer in the Bear Rock, Mount Kindle, and possibly Franklin Mountain Formations, and (iii) thermal discharge from a deep aquifer in the Saline River Formation (Section 7.5). The shallow flow component is represented by supraperafrost dominated springs and streams, including Fan Canyon and Window Streams (Types 2 and 5: Tables 7.1, 7.3). These waters lack Na^+ and Cl^- and have average electrical conductivities around $250 \mu\text{S cm}^{-1}$. Waters of subpermafrost origin account for most of the discharge of Carcadodo Valley (Types 3 and 6: Tables 7.1, 7.3). Much of this flow is supplied by the Bear Rock-Mount Kindle aquifer that is recharged in the Sink Zone, but also incorporated is a Na^+ and Cl^- rich Saline River aquifer component. The latter comprises approximately 3 to 4% of the total discharge (Section 7.5). Sites that are thought to be representative of the combined intermediate and deep flow components are Great Spring Line (D33) and Fan Stream (D5); they have average electrical conductivities of 800 and $970 \mu\text{S cm}^{-1}$ (Table 7.4).

The data of Figure 7.38 were collected at the Fox Well location (D43), which is called Fox Spring through this text. The site takes flow from Fox Moss Spring (D4) and Fox Swamp Stream (D39). The latter is fed by a diffuse set of aggraded springs west of the well. Under average summer flow conditions, Fox Moss Spring is about 15-20% of the total discharge of Fox Spring. The hydrochemistry of Fox

Swamp Stream is similar to other waters of Carcadodo Valley, but with lower concentrations of Na^+ and Cl^- . Fox Moss Spring is the least mineralized of the subpermafrost springs (Figure 7.20). Its low total dissolved ion concentration suggests that, relative to Red Rock Brook, the shallow flow component comprises a higher percentage of its discharge. The presence of Na^+ and Cl^- show a deep groundwater contribution. At Fox Swamp Stream, dilution of the intermediate and deep components may be due to a resurgence of Fan Canyon Stream. At Fox Moss Spring, much of the flow is from a shallow aquifer in the Bear Rock Formation.

Variations in conductivity, hardness, and oxygen isotope ratios suggest the relative proportions of shallow, intermediate, and deep flow components that supply Fox Spring were altered through the flood event of June 30 - July 1. A series of hydrograph separations are undertaken using the mass balance equation with the conductivity data (Figures 7.39, 7.40). In these models, it is assumed that the conductivities of the flow components remain constant through the event. In the first separation, the hydrograph is divided into 'shallow' and 'deep' components using conductivities of 250 and 900 $\mu\text{S cm}^{-1}$ (Figure 7.39a). The 'deep' fraction is thought to incorporate both the intermediate and deep flow components described above. The 900 $\mu\text{S cm}^{-1}$ figure is typical of the conductivity of Fan Stream and Great Spring Line. The 'shallow' component is thought to be dominated by supraperafrost water but likely includes some intra and subpermafrost discharge; its conductivity was based on the mean value of Type 2 and 5 waters (Table 7.3). The separation shows 'deep' waters comprise most of the flood discharge. The volume of 'shallow' water is highest on the steep rising limb where it approaches that of the 'deep' component. There is a sharp decrease in 'shallow' discharge on the falling limb. The position of the 'shallow' water peak suggests that most of the waters travel to the spring point along pathways of high hydraulic conductivity.

In the second separation, a distinction is made between 'old' and 'new' waters using conductivities of 700 and 200 $\mu\text{S cm}^{-1}$ (Figure 7.39b). The 700 $\mu\text{S cm}^{-1}$ figure is the approximate pre- and post storm conductivity of Fox Spring. The 200 $\mu\text{S cm}^{-1}$

value is thought to be representative of suprapermafrost waters. The hydrograph separation shows 'new' or suprapermafrost waters are about 25% of the discharge at the flood peak. This component contributes to the total discharge during the second pulse of rainfall, reflecting a rapid movement of throughflow to the spring point. The final separation divides the hydrograph into three components interpreted as suprapermafrost, subcutaneous/shallow phreatic, and phreatic discharge (Figure 7.40). The suprapermafrost component is the 'new' water from Figure 7.39b, and the phreatic component is the 'deep' water of Figure 7.39a, the difference comprises the subcutaneous fraction. The distinction between suprapermafrost and subcutaneous waters may not apply across the whole area of the karst. In places, suprapermafrost waters will be restricted to a thin active layer. However, in areas adjacent to water bodies or near taliks, the suprapermafrost aquifer may extend several metres below the surface into the region that is considered the subcutaneous zone in karst hydrology. The phreatic flow component as depicted is large, but this interpretation is supported by chemical and isotopic data which show little dilution by storm waters during the event.

A general model based on the third separation and other data recorded at Fox Spring is presented in Figure 7.41. The initial portion of the rising limb is interpreted as phreatic water displaced from fractures and pores near the spring point, as the first pulse of precipitation infiltrates through dolines and ponors. The arrival of this water at the spring is marked by a gradual increase in electrical conductivity. This is followed by a rapid discharge increase and a corresponding decrease in conductivity. The majority of the water is probably moved from storage in the phreatic zone. Displacement from the subcutaneous or the epiphreatic zones mimics the general pattern in phreatic waters. At the height of the flood, the conductivity decrease is due to the arrival of suprapermafrost waters at the spring. The precipitation intensity exceeds the infiltration capacity of the subcutaneous aquifer over the area of the Fluvial Zone, suprapermafrost waters then move laterally as throughflow. The reactivation of suprapermafrost springs during this period is

related to this perching of new water above the permafrost and subcutaneous zone. A similar conductivity spike was observed in the storm event of July 15. The falling limb of the hydrograph is marked by a gradual recession as water is withdrawn from both phreatic and subcutaneous storage.

The lack of turbidity at the spring throughout the event indicates the Bear Rock aquifer at this site does not host a well developed conduit network. The physical properties of the formation do not favour conduit development. In outcrop, the breccia has a low strength. In subcrop, the solution of gypsum generates widespread subsidence and collapse. The steep hydrograph recessions do suggest an aquifer of high effective porosity and transmissivity but this is not due to a conduit system. A high fissure frequency related to solution brecciation is responsible.

The data from this event and general observations from other periods suggest that only locally does permafrost function as a significant barrier to infiltration. The occurrence of perched ponds show that frozen ice-rich sediments have very low hydraulic conductivities but across most of the karst precipitation infiltrates quickly. This is probably due to a low ground ice content in the active layer and a high fissure frequency at the top of the subcutaneous zone. Where permafrost is close to the surface, water may travel laterally through the active layer until it encounters a doline, ponor, or fracture. Widespread overland flow is observed only when the precipitation intensity is very high, or when unfrozen portions of the active layer are saturated. These conditions occur locally during the snowmelt period and following long intervals of heavy precipitation.

7.6.4 Water Balance

The water balance is expressed by:

$$Q = P - E \pm \Delta S \quad (7.10)$$

where Q is runoff (discharge), P is precipitation, E is evapotranspiration, and ΔS is

change in storage. Data from Red Rock Brook are limited but the parameters of the 1988 water balance can be estimated by assuming no change in storage. Discharge measurements from Red Rock Brook are available from May 15 to August 14, 1988 and over that interval there was $1.08 \times 10^6 \text{ m}^3$ of discharge recorded. This figure includes some interpolation at the beginning of the record when there was channel ice and across the discharge peak of the June 30 - July 1 storm event.

The record may be extended to August 30 by extrapolation of the late summer recession, and to May 1 by assuming a linear increase in discharge from a value of zero on May 1 to the first discharge measurement of May 15. This yields a volume of $1.32 \times 10^6 \text{ m}^3$; which likely underestimates discharge over that interval. Extending the record to October 10 along the late summer recession gives a volume of $1.5 \times 10^6 \text{ m}^3$. Storage for the 1988 discharge season begins in October with freeze-up and snowfall accumulation. From October 1987 to August 1988, there were 283.5 mm of precipitation recorded at Norman Wells. This value is adjusted to 410 mm based on the Dodo Canyon - Norman Wells rainfall relationship of Figure 3.3. The adjusted value for October 1987 to July 1988 is 378 mm. There are few evapotranspiration data in the region; Burns (1973) provides an annual estimate of 150 mm. September lake evaporation is 8.5% of the annual total (Section 3.2.1.3), the 150 mm figure is reduced by that amount to 137 mm as a measure of May to August evapotranspiration. Assuming no change in storage, the 1988 water balance yields a runoff (discharge) of 273 mm using the October to August precipitation data. The value is 241 mm if August precipitation is excluded.

The runoff values are lower than those from other basins in the northern Mackenzie Mountains, which range between 318 and 507 mm (Table 3.4). These basins have higher average elevations and corresponding levels of precipitation. Using the data from the Main Karst, it is possible to estimate the size of recharge area feeding Red Rock Brook. From the discharge volume of $1.32 \times 10^6 \text{ m}^3$ (May 1 to August 30) and runoff of 241 mm, the recharge area is calculated to be 5.5 km^2 . The area is reduced to 4.8 km^2 if the 273 mm runoff value is used. The region

mapped on Figure 7.2 as the Main Karst has an area of 5.4 km². This mapping included the Sink and Fluvial Zones, and Carcadodo Valley. It represents the maximum topographic catchment of Red Rock Brook. It is likely that some precipitation on the margins of this area are routed to Dodo and Carcajou Canyons, and not to Carcadodo Valley. Seasonal discharge volumes greater than the 1.32×10^6 m³ estimate would require larger recharge areas. Therefore, additional recharge to the Red Rock Brook aquifer must occur at other locations. Probable areas are up dip along Dodo Canyon through exposures of the Saline River, Franklin Mountain, and Mount Kindle Formations. Recharge in those positions would supply deeper circulating groundwaters discharged in Carcadodo Valley.

7.6.5 Groundwater Velocity

Temporal variations in $\delta^{18}\text{O}$ suggest there is a delay of 40 to 50 days between infiltration in the Sink Zone and discharge in Carcadodo Valley (Section 7.4.4.5). Dye tracing established a 30 day connection between the Big Sink and Fox Well (Section 7.4.1). Much of the discharge of Carcadodo Valley is recharged through the Sink Zone. It is possible to estimate the macroscopic groundwater velocity and hydraulic conductivity of the principal aquifer. The elevation of the Sink Zone is 450-550 m and that of Carcadodo Valley 300 m. These areas are separated by a distance of 1200-2500 m. This yields a hydraulic gradient (dh/dl) of approximately 0.10-0.13. Assuming an average flowpath distance of 2500 m and a travel time of 30 days, the macroscopic groundwater velocity is on the order of 10^{-4} m s⁻¹. Use of this velocity for specific discharge (u) in Darcy's Law (Equation 7.11) yields a hydraulic conductivity (K) of 10^{-3} m s⁻¹.

$$u = -K \frac{dh}{dl} \quad (7.11)$$

These values are similar to those from other fissured limestone aquifers (Ford and Williams, 1989). At such velocities, flow through small fissures and proto-conduits

would be laminar. This is consistent with the behaviour of the aquifer during and following storm inputs. There is no turbidity recorded at spring points and much of the flashy character of flood hydrographs is attributed to discharge from the suprapermafrost and subcutaneous aquifers in the Fluvial Zone. Rapid increases in phreatic outputs are not related to the transmission of recharge through conduits, but rather the style of that recharge in the Sink Zone. Surface and suprapermafrost waters are moved laterally to dolines, ponors, and large fractures. This point style of recharge results in an increase of phreatic output by a piston flow mechanism.

7.7 Summary

At the Dodo Canyon Site, karst landforms occur on dolomite, solution breccia, and limestone of the Mount Kindle, Bear Rock, and Hume Formations. Interstratal karst is found on the clastic Hare Indian Formation. The morphology of many dolines and depressions suggests an origin partially attributed to subsurface solution of evaporites and associated subsidence of cover units. Gypsum of the Bear Rock/Fort Norman Formation subcrops throughout the distribution of depression forms. Bare Karst is also present as a dolomite pavement and as depression forms on limestone. The site was glaciated in the Late Wisconsinan and lies in the zone of widespread discontinuous permafrost. The rugged terrain is characterised by low ranges and plateaux that are sharply incised by canyons of Quaternary age. Elements of the karst system are older than the Quaternary canyons.

Hydrological observations show there are zones of holokarst (Sink Zone), fluviokarst (Fluvial Zone), and discharge (Carcadodo Valley) across the core area of the site. There is active circulation of meteoric groundwaters to depths of perhaps 500 m. Recharge occurs in the Sink and Fluvial Zones from snowmelt to freeze-up. Early in the melt season, discharge is dominated by low TDI surface and near subsurface waters. The higher TDI subpermafrost springs of Carcadodo Valley are only activated following the snowmelt period. The delay may be due to frozen outlets or the functioning of Great Spring Line as overflow springs. The lack of

icings, the presence of spring hierarchy (e.g., Smart, 1983) and hydrochemical data support the overflow interpretation. Perennial thermal springs in Carcajou Canyon flow from a deep aquifer in the Saline River Formation and display little variation in discharge and chemistry. The subpermafrost springs of Carcadodo Valley discharge from the Bear Rock, Mount Kindle, and the Franklin Mountain Formations. There is also a small contribution from the Saline River Formation. These springs flow only after the Bear Rock Formation has been recharged by a snowmelt pulse. Suprapermafrost springs and streams are partially independent of discharge from the main aquifer. This is due to permafrost functioning as a leaky aquitard, locally perching water in ponds and the active layer. In the recharge area, permafrost laterally routes waters to dolines, ponors, and fractures in response to steep gradients. The combination of point style recharge in the Sink Zone and near subsurface flow in the Fluvial Zone generates rapid spring responses to summer storm inputs.

Hydrochemical data indicate much of the solute load of Carcadodo Valley is composed of ions dissolved from evaporite rocks. Accordingly, depression landforms are partially attributed to subsidence. The distribution of solution within the aquifers feeding Carcadodo Valley and the geomorphic implications are described in detail in the concluding chapter of the thesis.

Table 7.1: Grouping of water samples from the Dodo Canyon Site on the basis of their physical characteristics and location within the karst.

Type	Description
	1 Precipitation
Springs	2 Shallow (suprapermafrost) Springs: Flow is highest during snowmelt and following intense rainfall events, usually: $Q < 5 \text{ L s}^{-1}$, $T < 5 \text{ }^\circ\text{C}$, $\text{SPC} < 200 \text{ } \mu\text{S cm}^{-1}$, bicarbonate chemistry
"	3 Intermediate Springs: Intermediate between types 2 and 4, flow not perennial, Q from individual spring points, usually: $Q < 5 \text{ L s}^{-1}$, $T < 5 \text{ }^\circ\text{C}$, $200 \text{ } \mu\text{S cm}^{-1} < \text{SPC} < 2000 \text{ } \mu\text{S cm}^{-1}$, bicarbonate chemistry with some ions of evaporite origin
"	4 Deep (subpermafrost) Springs: Flow is usually perennial, two subtypes: (i) low discharge springs, Q constant and $< 10 \text{ L s}^{-1}$, may be thermal, T normally $> 5 \text{ }^\circ\text{C}$, $\text{SPC} > 1000 \text{ } \mu\text{S cm}^{-1}$, evaporite chemistry; (ii) high discharge, Q variable $> 10 \text{ L s}^{-1}$, $T < 5 \text{ }^\circ\text{C}$, bicarbonate chemistry, some ions of evaporite origin
Streams	5 Stream, predominantly fed by springs of Type 2
"	6 Stream, predominantly fed by springs of Type 3
"	7 Stream, predominantly fed by springs of Type 4
Ponds	8 Pond/Doline/Ponor: Surface water infiltrating into a ponor or doline
"	9 Pond/Doline/Ponor: Surface water impounded in a slow draining depression
Lakes	10 Lake: Intermittent spring-fed water bodies of area $> 10^5 \text{ m}^2$
Other	11 Location D36 (Spillway Spring): subpermafrost water on Hare Indian Fm
	12 Locations D28, D29, D30: Samples taken from the Mt. Kindle Formation
	13 Location D12: Dodo Creek sampled near base camp
	14 Location D16: Carcajou River sampled on west bank below canyon rim
	15 Location D32: Stream at the base of Dodo West Canyon
	16 Location D31: Seep on the Bear Rock Formation east of Pavement

Note: No springs of Type 4 (ii) were located at the Dodo Karst.

Table 7.2: Description and classification of water sampling sites at Dodo Canyon Site.

Location	Description	Type
D1	<i>Carca-Spring Stream.</i> Spring-fed stream on the floor of Carcajou Canyon.	7
D2	<i>Salt Spring.</i> Thermal spring from the Landry Member on the floor of Carcajou Canyon.	4
D3	<i>Red Rock Brook.</i> Main spring-fed stream in the Carcadodo Valley.	6,10
D4	<i>Fox Moss Spring.</i> Small spring in Bear Rock Formation in Carcadodo Valley.	3
D5	<i>Fan Stream.</i> Stream fed by Great Spring Line and other springs, northeast of Fan	6
D6	Water draining into ponor in Straight Valley.	8
D7	Surface runoff to Big Sink.	8
D8	Surface runoff to Strandline Sink.	8
D9	Surface runoff to Bearscat Sink.	8
D10	<i>Bubbling Spring.</i> Small spring on the south side of Carcadodo Valley.	2
D11	<i>Camp Stream.</i> Stream in Carcadodo Valley, downslope of D13.	5
D12	<i>Dodo Creek.</i>	13
D13	<i>Camp Stream.</i> Spring-fed stream above Carcadodo Valley.	5
D14	<i>Fan Canyon Stream.</i> Stream in upper Fan Canyon.	5
D15	Stream draining into Carcajou Canyon, off of Bear Rock Formation.	5
D16	<i>Carcajou River.</i>	14
D17	<i>Window Stream.</i> Stream south of Carcadodo Valley.	5
D18	<i>Winding Stream.</i> Intermittent stream north of Big Depression.	5
D19	Slow draining pond on scarp.	9
D20	Slow draining pond southwest of West End.	9
D21	Slow draining pond southwest of Straight Valley.	9
D22	Slow draining pond in the Sink Zone.	9
D23	<i>Dodo Mountain Stream.</i> Stream at southern boundary of Main Karst.	5
D24	Spring/seep from east wall of Dodo Canyon.	2
D25	Slow draining pond northeast of Dodo Canyon.	9
D26	Intermittent stream southwest of West End.	5
D27	Slow draining pond in Sink Zone.	9
D28	Pond at the Mt. Kindle/Bear Rock contact; Dodo West.	12
D29	Spring from Mt. Kindle Formation; Dodo West.	12
D30	Stream on Mt. Kindle Formation; Dodo West.	12
D31	Spring draining the Bear Rock Formation; Dodo West.	16
D32	Stream in the floor of Dodo West Canyon.	15
D33	<i>Great Spring Line.</i> Line of springs in Carcadodo Valley northwest of Fan Canyon.	3
D34	<i>Circular Swamp.</i> Pond with fluctuating water levels; west end of Carcadodo Valley.	3
D35	<i>Carca-Spring Stream.</i> Spring-fed stream in the floor of Carcajou Canyon, east of D1.	7
D36	<i>Spillway Spring.</i> Springs in meltwater channel near the Hume/Hare Indian contact.	11
D37	<i>Carca-Spring Stream.</i> Spring-fed stream in the floor of Carcajou Canyon, east of D35.	7
D38	<i>Fan Canyon Stream.</i> Fan Canyon Stream sampled at apex of the fan.	5
D39	<i>Fox Swamp Stream.</i> Spring-fed stream, southeast of Great Spring Line.	6
D40	Spring-fed Stream in West End.	5
D41	Stream draining into Fan Canyon.	5
D42	<i>Colluvium Spring.</i> Spring in the floor of Carcajou Canyon, near Landry/Hume contact.	4
D43	<i>Fox Well.</i> Stream fed by Fox Moss Spring and Fox Swamp Stream.	6
D44	<i>Terminal Sink.</i> Easternmost sink point in the Carcadodo Valley.	6
D45	Small stream below Scarp.	5

Table 7.3: Mean temperature, conductivity, pH, total hardness, ion concentrations, total dissolved ions, Ca²⁺/Mg²⁺ ratio, saturation indices (calcite and dolomite), and pPCO₂ for water types of Dodo Canyon Site.

Type	Temp	SPC	pH	THd	Ca ²⁺	Mg ²⁺	HCO ₃ ⁻	SO ₄ ²⁻	Na ⁺	Cl ⁻	TDI	Ca/Mg	SI _c	SI _d	pPCO ₂	n
2: Shallow Springs	1.9	237	8.01	113	1.77	0.50	2.18	0.16	0.06	0.01	4.7	3.5	0.15	-0.32	2.96	2
3: Intermediate Springs	4.5	666	7.88	237	3.25	1.50	3.25	1.74	2.79	2.68	15.2	2.2	0.13	-0.13	2.70	11
4: Deep Springs	9.5	9840	7.63	463	5.99	3.27	3.21	5.57	85.98	86.56	190.6	1.8	0.02	-0.23	2.56	6
5: Shallow Streams	4.1	288	8.18	171	2.86	0.57	2.66	0.64	0.04	0.02	6.8	5.0	0.33	-0.18	3.15	17
6: Intermediate Streams	7.4	758	8.06	238	3.30	1.48	3.10	1.76	3.24	3.22	16.1	2.2	0.37	0.34	2.92	45
7: Deep Streams	11.6	7220	7.96	358	4.52	2.64	3.19	3.84	66.46	62.02	142.7	1.7	0.28	0.36	2.91	6
8: Pond; Draining	5.8	113	8.35	67	1.16	0.18	1.32	0.01	0.05	0.02	2.7	6.4	0.03	-1.12	3.57	6
9: Pond; Perched	15.4	124	8.46	77	1.38	0.16	1.51	0.13	0.04	0.02	3.2	8.6	0.29	-0.31	3.57	6
11: Spillway Spr (D36)	3.9	845	7.70	642	10.19	2.63	6.58	6.36	0.14	0.03	25.9	3.9	0.70	0.74	2.29	2
12: Mt. Kindle Samples	10.2	234	8.58	141	1.60	1.23	2.82	0.01	0.03	0.02	5.7	1.3	0.63	1.13	3.48	3
13: Dodo W Ck (D32)	8.2	305	8.34	159	1.78	1.40	3.12	0.30	0.53	0.46	7.6	1.3	0.46	0.77	3.20	1
14: Dodo Creek (D12)	4.6	566	8.28	178	2.39	1.17	2.47	1.79	3.18	2.55	13.6	2.0	0.32	0.30	3.02	4
15: Carcajou R (D16)	8.2	1410	7.83	113	1.52	0.74	2.00	2.08	20.12	16.73	43.2	2.1	-0.29	-0.83	2.78	1
16: Sample D31	17.2	266	8.56	150	2.02	0.98	2.92	0.21	0.05	0.03	6.2	2.1	0.80	1.35	3.39	1

Temp: temperature in °C; SPC: specific electrical conductivity, expressed to 25 °C, in μS cm⁻¹; THd: Total Hardness in mg L⁻¹ CaCO₃; Ion concentrations reported in meq L⁻¹; Ca/Mg: Ca²⁺/Mg²⁺ ratio; SI_c: Saturation index for calcite; SI_d: Saturation index for dolomite; pPCO₂: -log of partial pressure of CO₂

Table 7.4: Mean temperature, conductivity, pH, total hardness, ion concentrations, total dissolved ions, Ca²⁺/Mg²⁺ ratio, saturation indices (calcite and dolomite), and pPCO₂ for water samples in Carcadodo Valley.

Type	Temp	SPC	pH	THd	Ca ²⁺	Mg ²⁺	HCO ₃ ⁻	SO ₄ ²⁻	Na ⁺	Cl ⁻	TDI	Ca/Mg	SI _c	SI _d	pPCO ₂	n
D3: Red Rock Brook	8.9	753	8.10	227	3.10	1.44	2.93	1.75	3.27	3.25	15.7	2.2	0.44	0.53	2.98	18
D4: Fox Moss Spring	1.6	440	7.88	224	3.34	1.14	3.26	1.30	0.57	0.52	10.1	2.9	0.04	-0.49	2.60	5
D5: Fan Stream	7.3	967	8.05	274	3.65	1.83	3.27	2.25	4.68	4.68	20.4	2.0	0.34	0.35	2.87	12
D33: Great Spring Line	4.0	800	7.88	248	3.22	1.74	3.27	1.96	3.86	3.76	17.8	1.9	0.16	-0.02	2.76	5
D34: Circular Swamp	17.9	905	7.88	236	3.00	1.72	3.12	1.96	4.05	3.78	17.6	1.7	0.27	0.38	2.67	1
D39: Fox Swamp Str	9.9	741	8.08	256	3.62	1.50	3.24	1.71	2.36	2.47	14.9	2.4	0.48	0.57	2.92	1
D43: Fox Well (Spr)	5.4	585	8.01	222	3.16	1.27	3.15	1.42	2.24	2.21	13.5	2.5	0.31	0.14	2.89	14

Temp: temperature in °C; SPC: specific electrical conductivity, expressed to 25 °C, in μS cm⁻¹; THd: Total Hardness in mg L⁻¹ CaCO₃;
 Ion concentrations reported in meq L⁻¹; Ca/Mg: Ca²⁺/Mg²⁺ ratio; SI_c: Saturation index for calcite; SI_d: Saturation index for dolomite; pPCO₂: -log of partial pressure of CO₂

Table 7.5: $\delta^{18}\text{O}$ and δD data from precipitation in the study region.

Date	Location	Type	$\delta^{18}\text{O}$ ‰	δD ‰
220977	N.W. Airport*	Rain	-24.5	-186.5
230977	N.W. Airport*	Snow	-20.3	-155.6
230977	N.W. Airport*	Snow	-20.2	-157.7
011078	N.W. Airport*	Snow	-20.0	
071078	N.W. Airport*	Snow	-24.2	-190.4
071078	N.W. Airport*	Snow	-22.8	-180.5
101078	N.W. Airport*	Snow	-31.5	-244.5
101078	N.W. Airport*	Snow	-31.9	-250.0
180787	Bear Rock Site	Rain	-16.8	
250787	Bear Rock Site	Rain	-16.1	
150588	Dodo Canyon Site	Snow	-17.2	
160588	Dodo Canyon Site	Snow	-19.5	
240588	Dodo Canyon Site	Rain	-18.0	
310588	Dodo Canyon Site	Rain	-20.9	
240688	Bonus Lake Site	Rain	-17.1	
300688	Dodo Canyon Site	Rain	-17.5	
010788	Dodo Canyon Site	Rain	-16.9	
150788	Dodo Canyon Site	Rain	-16.2	
220788	Bear Rock Site	Rain	-19.4	
120888	Bear Rock Site	Rain	-18.1	
130791	Pyramid Lake Site	Rain	-20.4	-161.6
190891	Dodo Canyon Site	Rain	-22.1	-172.9
230891	Dodo Canyon Site	Rain	-15.9	-132.0
240891	Dodo Canyon Site	Snow	-28.7	-224.4

* Data from van Everdingen (1981)

Table 7.7: Discharge and hydrochemistry of shallow, intermediate, and deep flow components in the Dodo Canyon Karst.

Case #1: Discharge of shallow component (Q_1) is 33% of the total discharge of Red Rock Brook (Q_T)

Flow Component	Discharge	Ca ²⁺	Mg ²⁺	HCO ₃ ⁻	SO ₄ ²⁻	Na ⁺	Cl ⁻
1. Shallow: Upper Bear Rock Fm (Q_1)	50	2.86	0.57	2.66	0.64	0.04	0.02
2. Intermediate: Bear Rock-Franklin Mtn Fms (Q_2)	94	3.03	1.78	3.06	2.07	-	-
3. Deep: Saline River Fm (Q_3)	6	6.21	3.44	3.19	6.03	92.12	92.66
Total Discharge of Red Rock Brook (Q_T)	150	3.10	1.44	2.93	1.75	3.27	3.25

Case #2: Discharge of shallow component (Q_1) is 20% of the total discharge of Red Rock Brook (Q_T)

Flow Component	Discharge	Ca ²⁺	Mg ²⁺	HCO ₃ ⁻	SO ₄ ²⁻	Na ⁺	Cl ⁻
1. Shallow: Upper Bear Rock Fm (Q_1)	25	2.86	0.57	2.66	0.64	0.04	0.02
2. Intermediate: Bear Rock-Franklin Mtn Fms (Q_2)	119	2.99	1.52	2.97	1.77	-	-
3. Deep: Saline River Fm (Q_3)	6	6.21	3.44	3.19	6.03	92.12	92.66
Total Discharge of Red Rock Brook (Q_T)	150	3.10	1.44	2.93	1.75	3.27	3.25

Discharge is in $L s^{-1}$, ion concentrations are in $meq L^{-1}$.

The ion concentrations of the shallow component (C1) are the average of Type 5 waters (Shallow Streams: Table 7.3). The concentrations of the deep component (C3) are the averages from Salt Spring (D2). The ion concentrations of the intermediate component (C2) are calculated from Equation 7.5 using the above discharges.

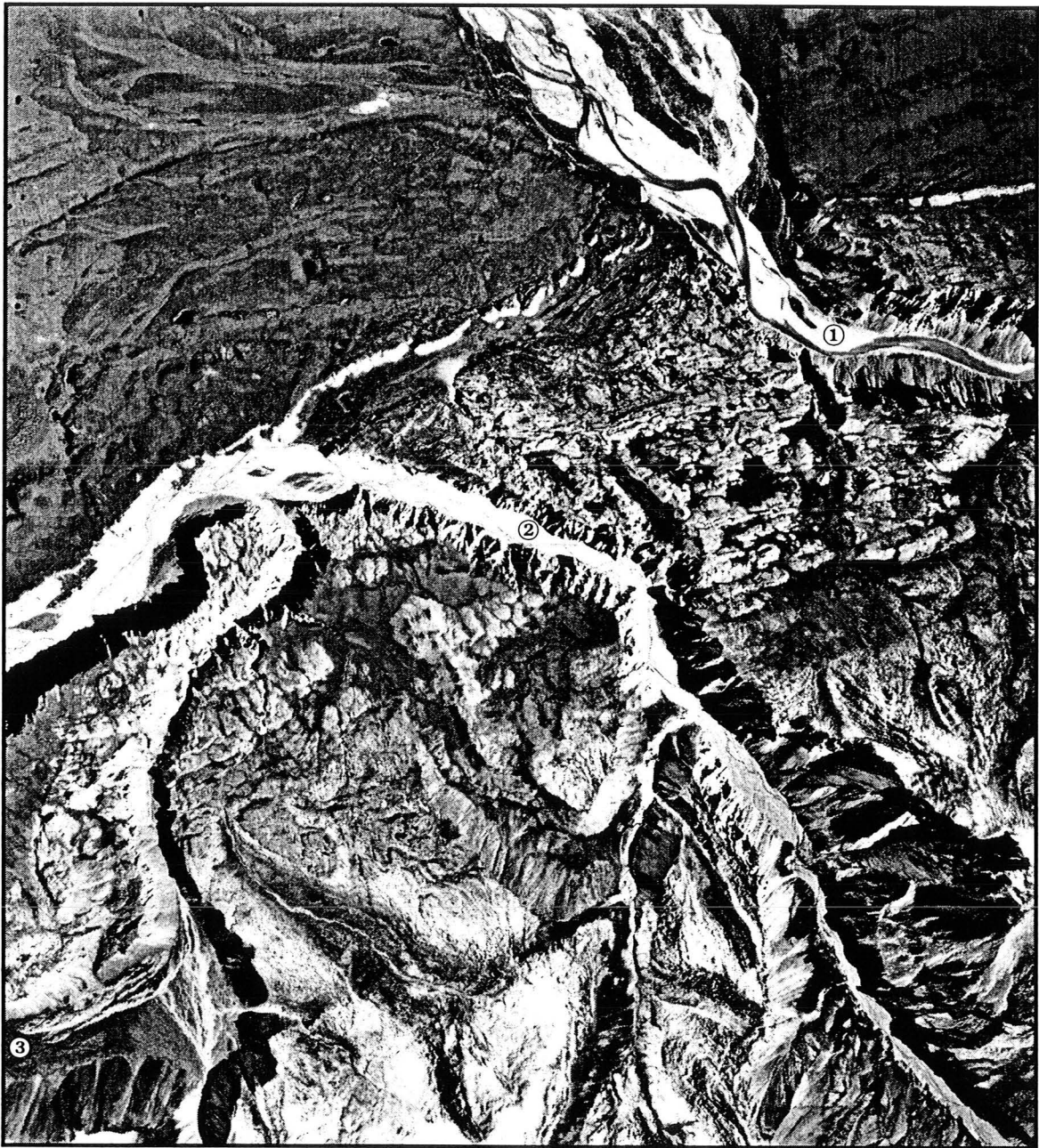


Figure 7.1: Vertical aerial photograph of the Dodo Canyon Site. The average scale is 1:47,000, the top of the photograph is northeast. The site is at the mountain front. Rolling terrain of the Mackenzie Valley is to the north and east, rugged canyon topography of the Carcajou Range extends to the south and west. The primary study area is the Main Karst, on the Bear Rock Formation between Carcajou and Dodo Canyons (① and ②). Northward, dolines occur on the Hume, Canol, and Hare Indian Formations (North Karst). The Dodo West Karst is west of Dodo Canyon and includes dolines on the Bear Rock Formation and a pavement on the Mount Kindle Formation. The largest area of pavement is east of the steep, narrow canyon running north of the marker ③. Dry Canyon (③) is typical of the abandoned, misfit, or anomalous drainage channels of the Canyon Ranges (Figure 5.8). Dodo Canyon cuts through the flank of Dodo Mountain in the lower right (NAPL A23932-60).

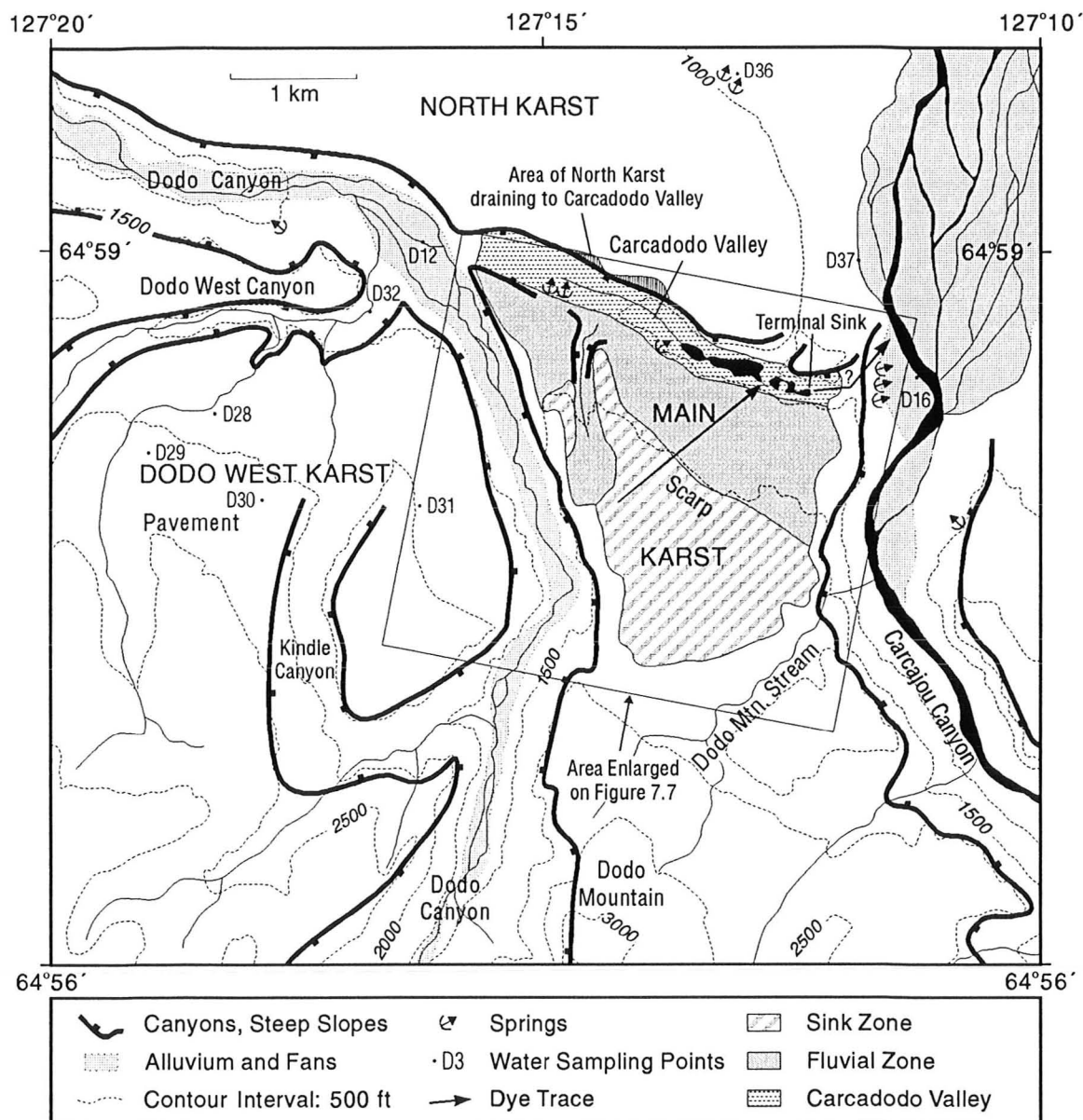


Figure 7.2: The Dodo Canyon Site is divided into the Dodo West, Main, and North Karsts. The former is dominated by the Mount Kindle Pavement (or Dodo Pavement) located west of Kindle Canyon. The North Karst is an interstratal doline karst on the Hume, Hare Indian, Canol, and Imperial Formations, north of Carcadodo Valley. The Main Karst is partitioned into zones of holokarst (Sink Zone), fluviokarst (Fluvial Zone), and discharge (Carcadodo Valley). The shaded areas denote the maximum topographic catchment of Red Rock Brook (Carcadodo Valley), this includes a small area of the North Karst. All discharge into Carcadodo Valley sinks at Terminal Sink. Dye traces established linkages between the Sink Zone and Carcadodo Valley, and from Terminal Sink to Carcajou Canyon. Water sampling locations within the Main Karst are indicated on Figure 7.7.

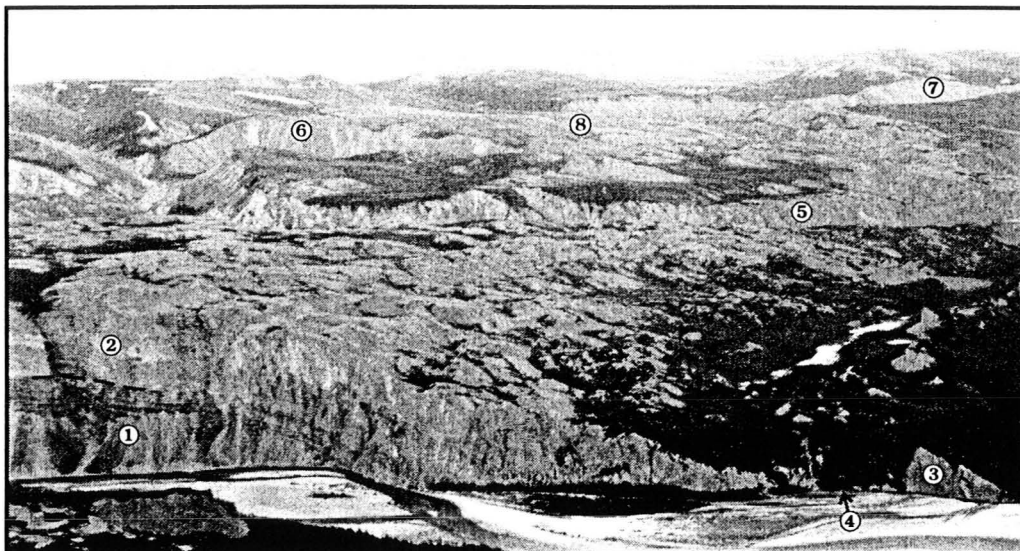


Figure 7.3: Oblique aerial photograph looking west over Carcajou Canyon to the Main Karst and Dodo Canyon(⑤). Exposed on the wall of Carcajou Canyon are the Mount Kindle (①), Bear Rock (②), and Hume Formations (③). A spring-fed stream (④:Carca-Spring Stream) runs at the base of Carcajou Canyon, east of Terminal Sink in Carcadodo Valley. The pavement of Dodo West Karst (⑧) lies between Kindle (⑥) and Dry Canyons (⑦).



Figure 7.4: Oblique aerial photograph looking northwestward over the Main Karst. Dodo Canyon is in the upper left (⑤). Large depression features along the Scarp and within the Sink Zone include: Big Depression(①), Dry Valley (②), and Big Sink (③). Fan Canyon Stream (④) cuts through the Scarp to Carcadodo Valley (⑥). Dolines of interstratal origin are located across the area of the North Karst (⑦).

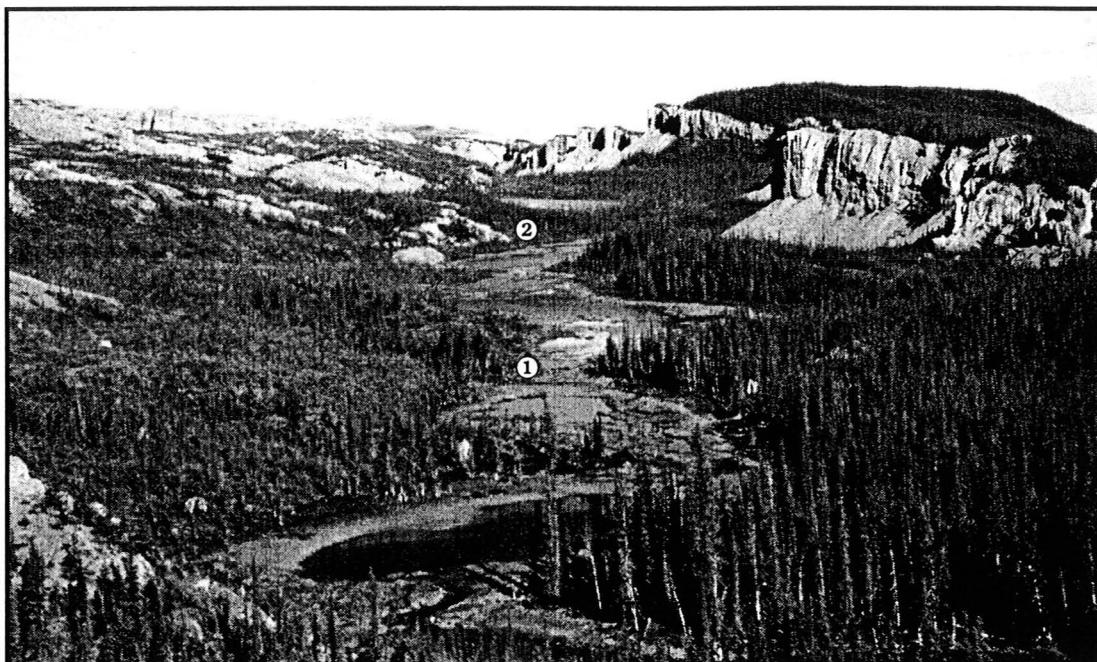


Figure 7.5: A view of Carcadodo Valley looking west to Dodo Canyon. This is the discharge area of the Main Karst. The flow direction through the spring-fed ponds is eastward to Terminal Sink. The springs are aggraded or are observed to discharge from the upper Bear Rock Formation. Stage was recorded at Red Rock Brook (①) and at Fox Spring (②). West of Fox Spring is a small fan and the Great Spring Line. The Hume Formation forms the prominent cliff.



Figure 7.6: The eastern end of Carcadodo Valley. The Terminal Sink is the pond on the right of the photograph. Most of the discharge of Red Rock Brook sinks into a ponor at the northern end of the pond, near the contact between the Hume and Bear Rock Formations. The Carcadodo Valley has its origin as a meltwater channel but functions hydrologically as a border polje. Sinking waters resurge in the floor of Carcajou Canyon located to the ENE.



Figure 7.7: General geomorphology of the Dodo Canyon Site. Several canyon features have orientations that are parallel to the mountain front, others occupy anomalous positions that cut across older drainage. This distribution is related to the diversion of mountain streams and the routing of meltwaters by Laurentide Ice near the mountain front. Streamlined features indicate an ESE-WNW movement of Laurentide Ice. In the high range west of Dodo Mountain both montane and Laurentide moraines are recognized. Preliminary interpretation favours a minor montane advance following the Laurentide Katherine Creek maximum. The karst features shown are springs, dolines, pavement, and areas of enclosed drainage (shaded). The pavement is located on the Mount Kindle Formation, the majority of the doline karst is on the Bear Rock and Hume Formations. The size of the doline markers represents the approximate minimum dimension of their immediate catchment, divided into: small (<10 m), intermediate (25 m), or large basins (>50 m). At this scale not all karst input or output features are depicted.

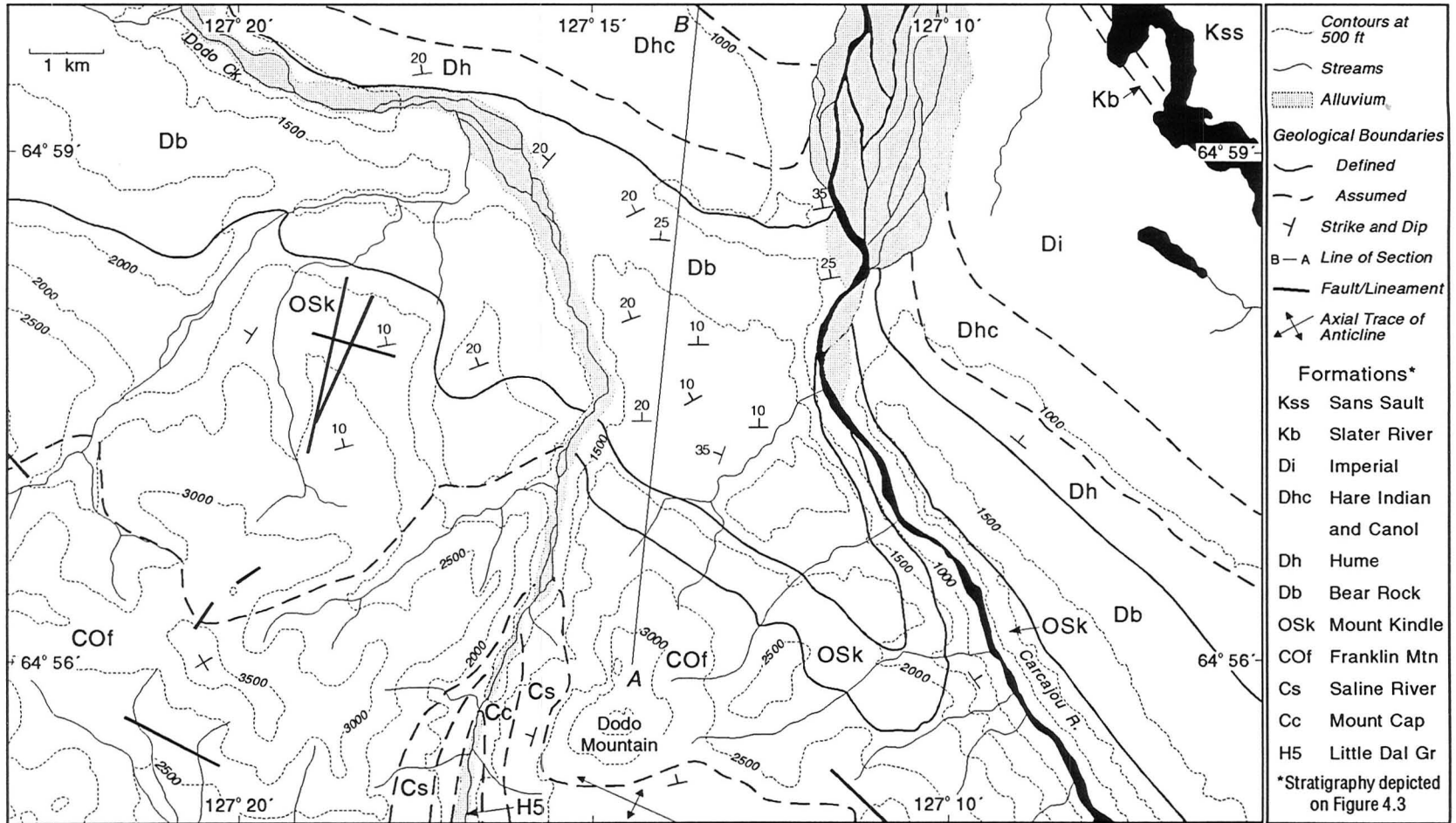
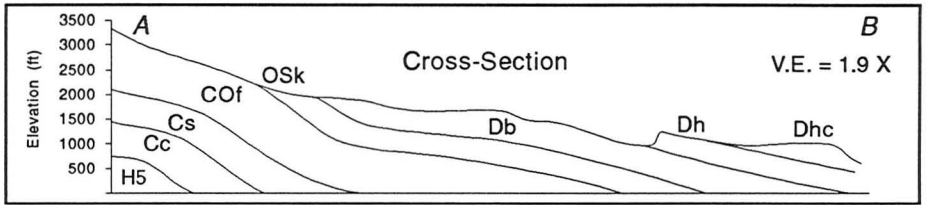


Figure 7.8: Bedrock geology of the Dodo Canyon Site. Dodo Mountain sits at the northwestern plunging end of MacDougal Anticline. Paleozoic strata outcrop on the northern and western flanks of Dodo Mountain and dip toward the Mackenzie Plain Synclinorium. Cross section is through the Main Karst. Data are from field observations, aerial photographic interpretation and published work by Aitken and Cook (1974).



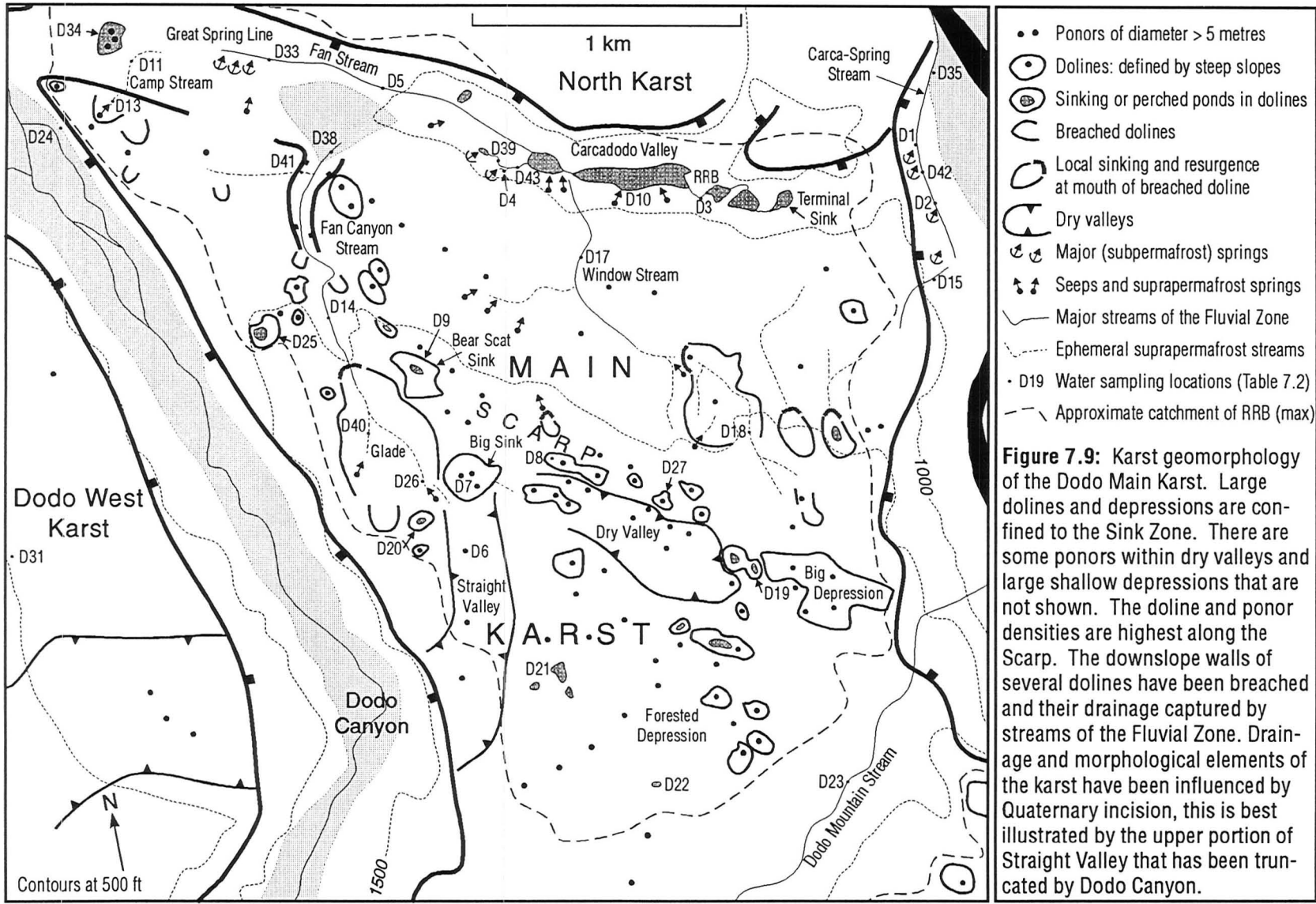




Figure 7.10: A view looking east through "Dry Valley", a linear depression in the Sink Zone of the Main Karst (Figure 7.9). The Landry Member forms a resistant cap on the surrounding slopes. Landry strata on both the north and south rims dip toward the central axis of the depression, yielding a draped topography indicative of a subsidence trough. Precipitation and snowmelt are captured by several ponors and a deep doline marked by trees at the western end of the valley.



Figure 7.11: A solution-subsidence doline east of Fan Canyon near D14 (Figure 7.9). The upper steep walls are in the Landry Member, the base extends into the Brecciated Member. The overall profile is conical and the long axis is elongated with strike. The doline origin was likely as the surficial expression of breccia pipe, but it has been deepened by solution within the catchment.

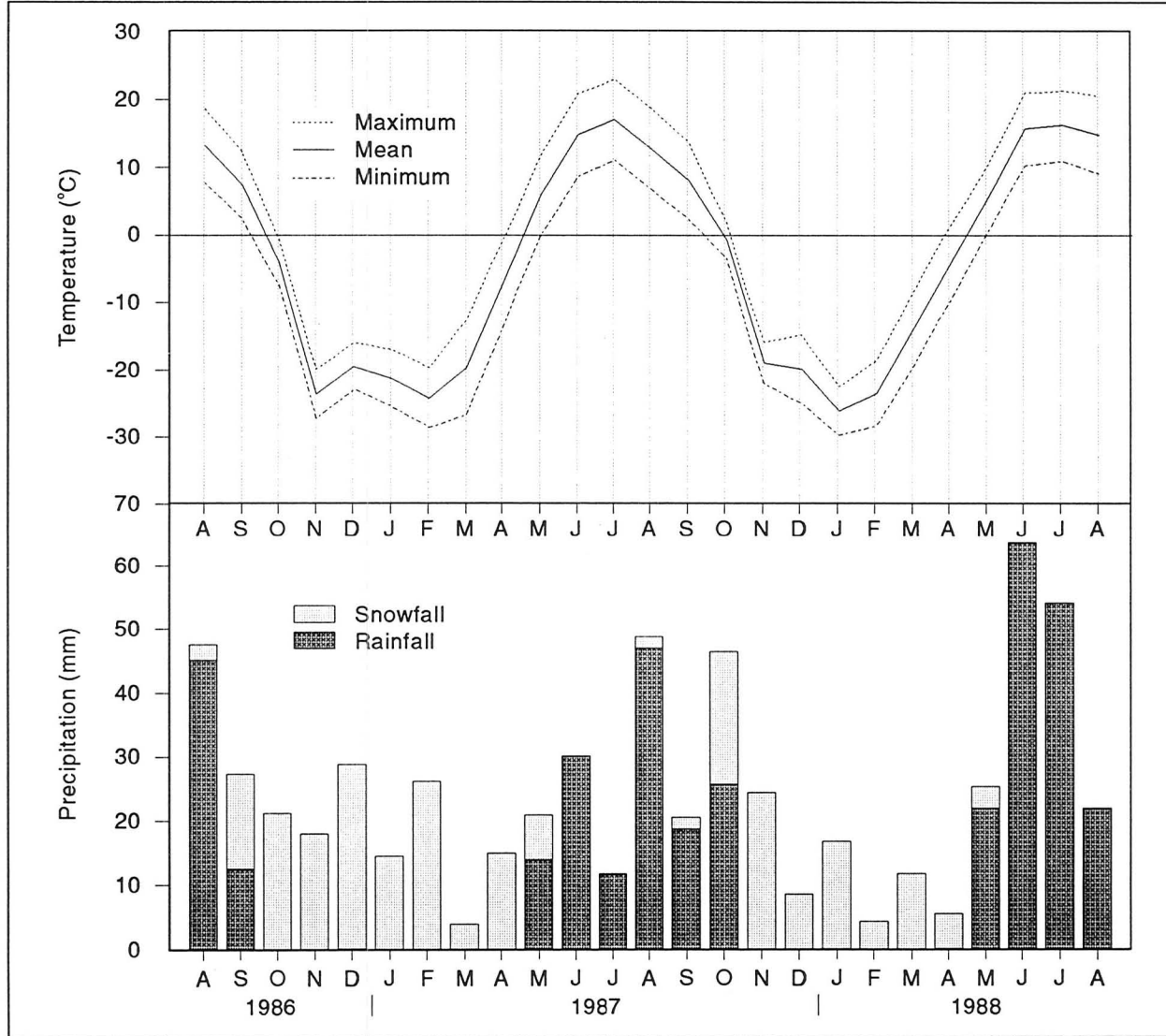


Figure 7.12: Monthly temperature and precipitation at Norman Wells, August 1986 to 1988.



Figure 7.13: A view of the base of Bear Scat Sink looking west along the Scarp (location on Figure 7.9). The upper photograph was taken on May 18, 1988. Runoff to the doline was from surface flows and suprapermafrost seeps generated by snowmelt and rainfall. The water level was observed to drop slowly over the next week. The lower photograph was taken in mid-July and represents the typical summer condition of the doline. Following major rainfall events there is a short period of ponding when the infiltration capacity is exceeded.



Figure 7.14: Two views of Terminal Sink, the easternmost pond in Carcadodo Valley (Figures 7.5, 7.6). The upper photograph was taken on May 25, 1988 when the discharge of Red Rock Brook was 53 L s^{-1} . This flow infiltrated immediately into the pond base. The level on the 24th had been higher following a precipitation event on May 23, but that pulse passed quickly through the system. The lower photograph was taken in mid-July and represents the summer level when the input discharge is typically 150 L s^{-1} . At this higher level additional ponors on the margin are activated.

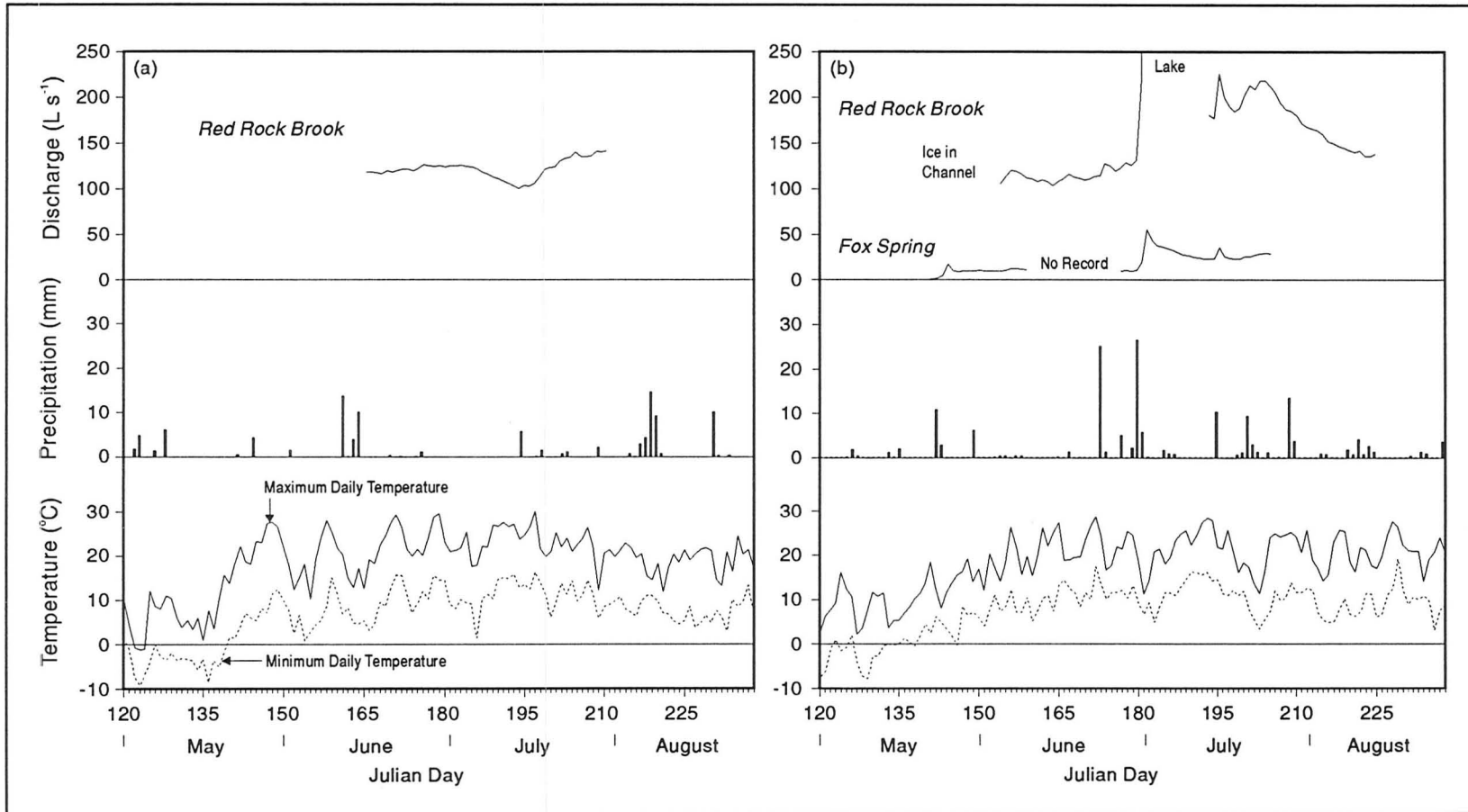


Figure 7.15: (a) Average daily discharge of Red Rock Brook in the 1987 field season. (b) Average daily discharges of Red Rock Brook and Fox Spring in the 1988 field season. Daily precipitation and maximum and minimum temperature data are from Norman Wells. The 1987 discharge record shows little variation. A dry late June and early July produced a decrease in discharge to mid-July. Subsequent precipitation returned Red Rock Brook to June levels. The records of 1988 show much variability related to high precipitation events, particularly in late June. The second June storm generated a flashy response in both Fox Spring and Red Rock Brook. A ponding event in eastern Carcadodo Valley interrupted the Red Rock Brook series. Overall both records show a gradual increase in discharge from early June to late July, with peaks superimposed on that trend.

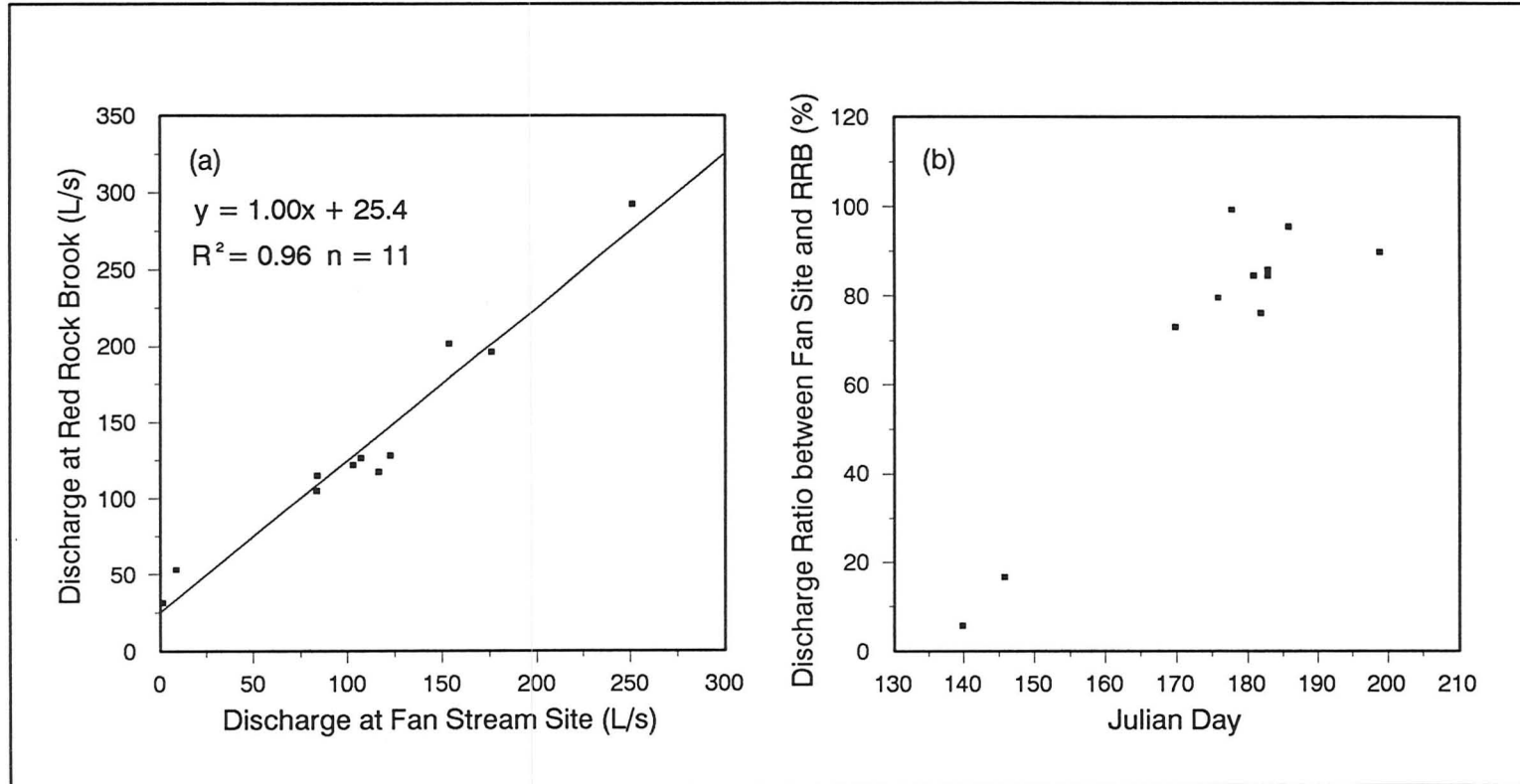


Figure 7.16: (a) Discharge of Red Rock Brook (D3) versus discharge of Fan Stream (D5). Data are from 1987 and 1988, the two points closest to the origin are from May, the balance are from June and July. (b) Discharge ratio between Fan Stream and Red Rock Brook versus time. These graphs show that with exception of the snowmelt period, the majority of flow in Red Rock Brook is provided by Fan Stream. The latter is supplied by springs of Great Spring Line. In the melt season these springs are inactive and Fan Stream contributes little to the total flow of Carcadodo Valley. Important inputs at that time include Fox Spring, Fan Canyon and Window Streams. These sources experience decreased flows through the summer.

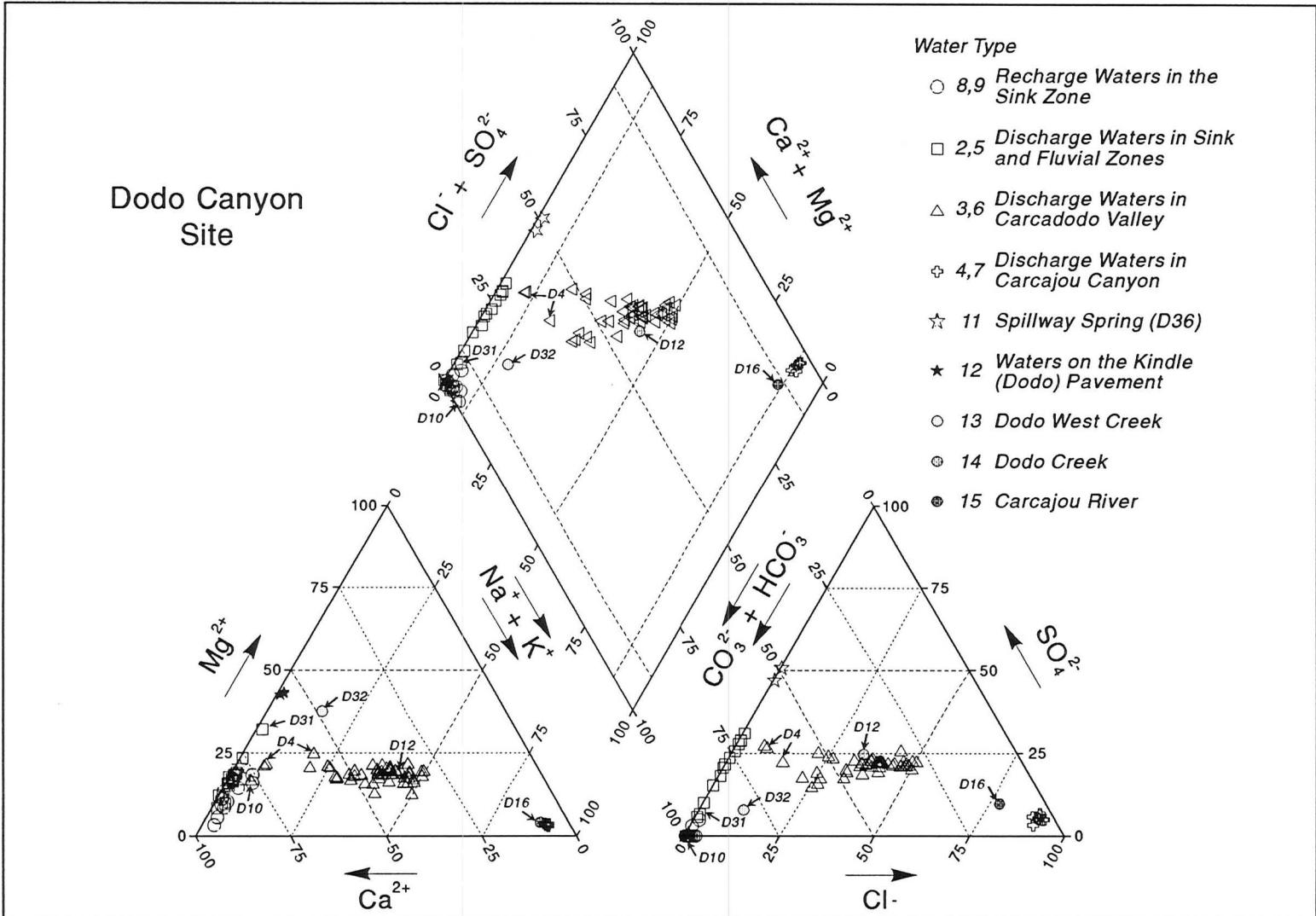


Figure 7.17: Trilinear diagram of waters from the Dodo Canyon Site. Sample D31 (Type 16) is plotted with discharge waters of the Sink and Fluvial Zones (Types 2 and 5). Sample D10, a suprapermafrost spring, is plotted with Types 3 and 6.

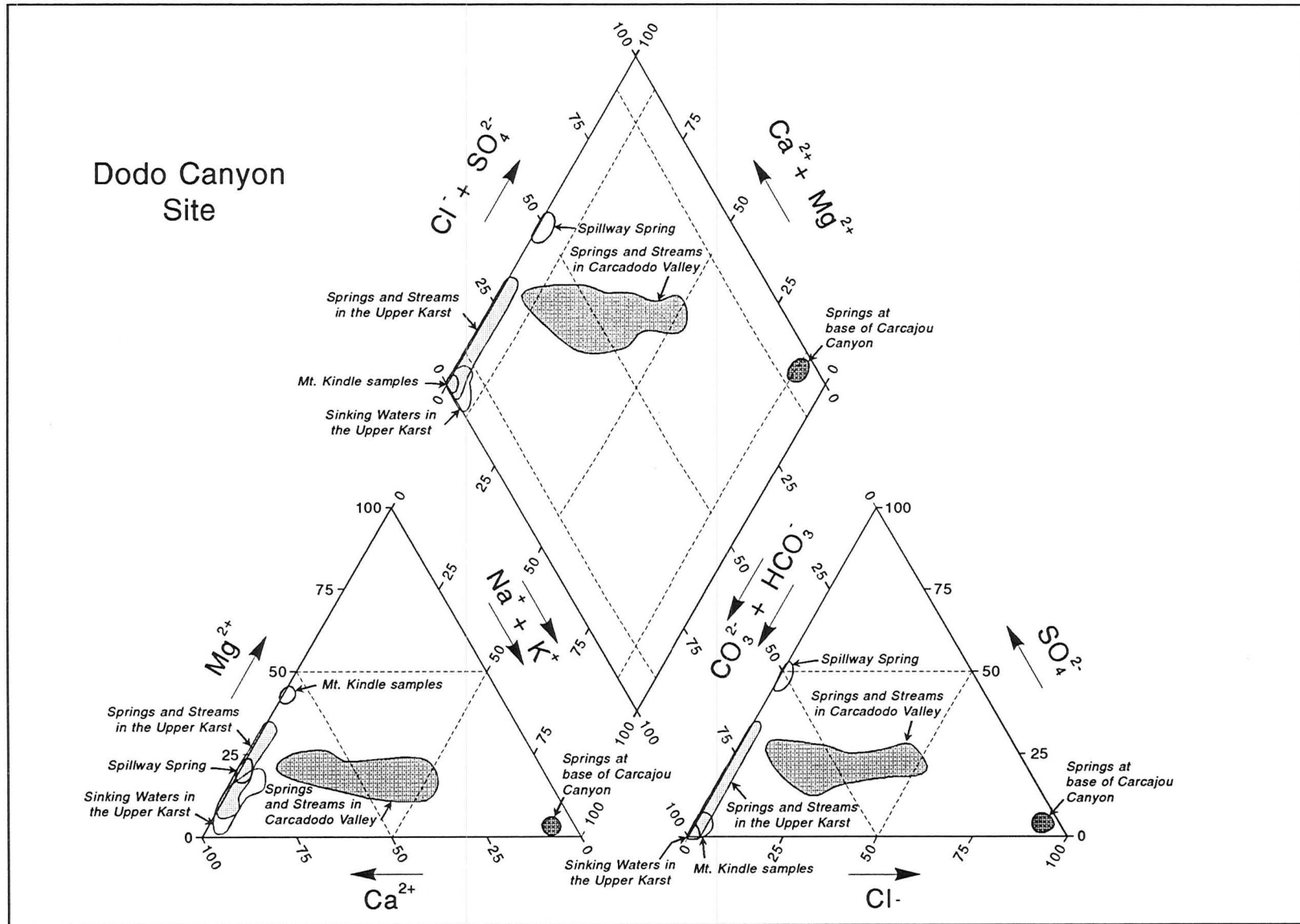


Figure 7.18: Summary diagram of data presented in the trilinear diagram from the Dodo Canyon Site (Figure 7.17).

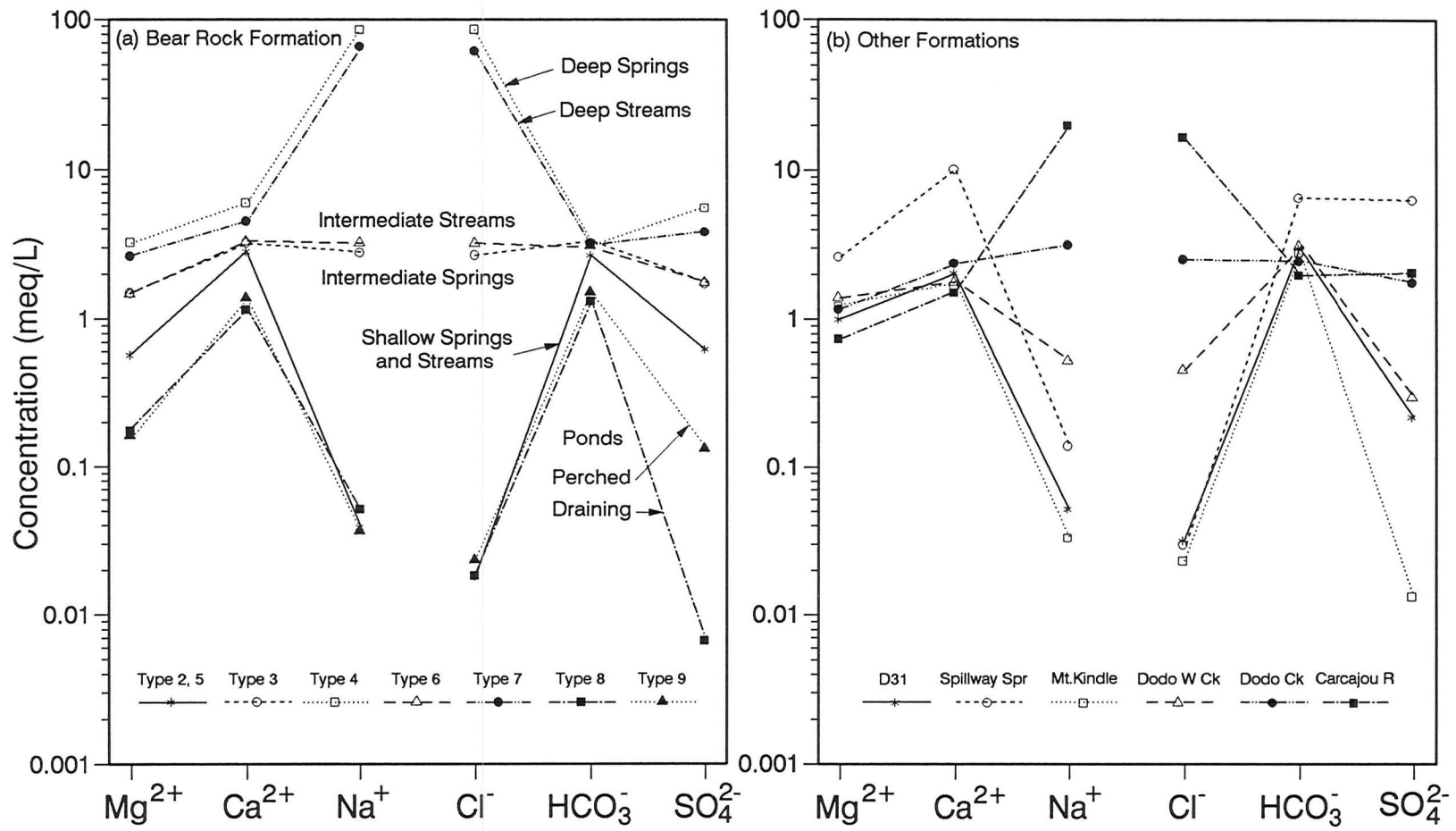


Figure 7.19: Mean concentrations of major anion and cation species in meq L⁻¹ for water types in the Dodo Canyon Karst. (a) Samples drawn from the Bear Rock Formation or the Main Karst, water types are shown. (b) Samples from Dodo West (D31, Mt. Kindle Formation), North Karst (Spillway Spring), and from Dodo West Creek, Dodo Creek, and Carcajou River.

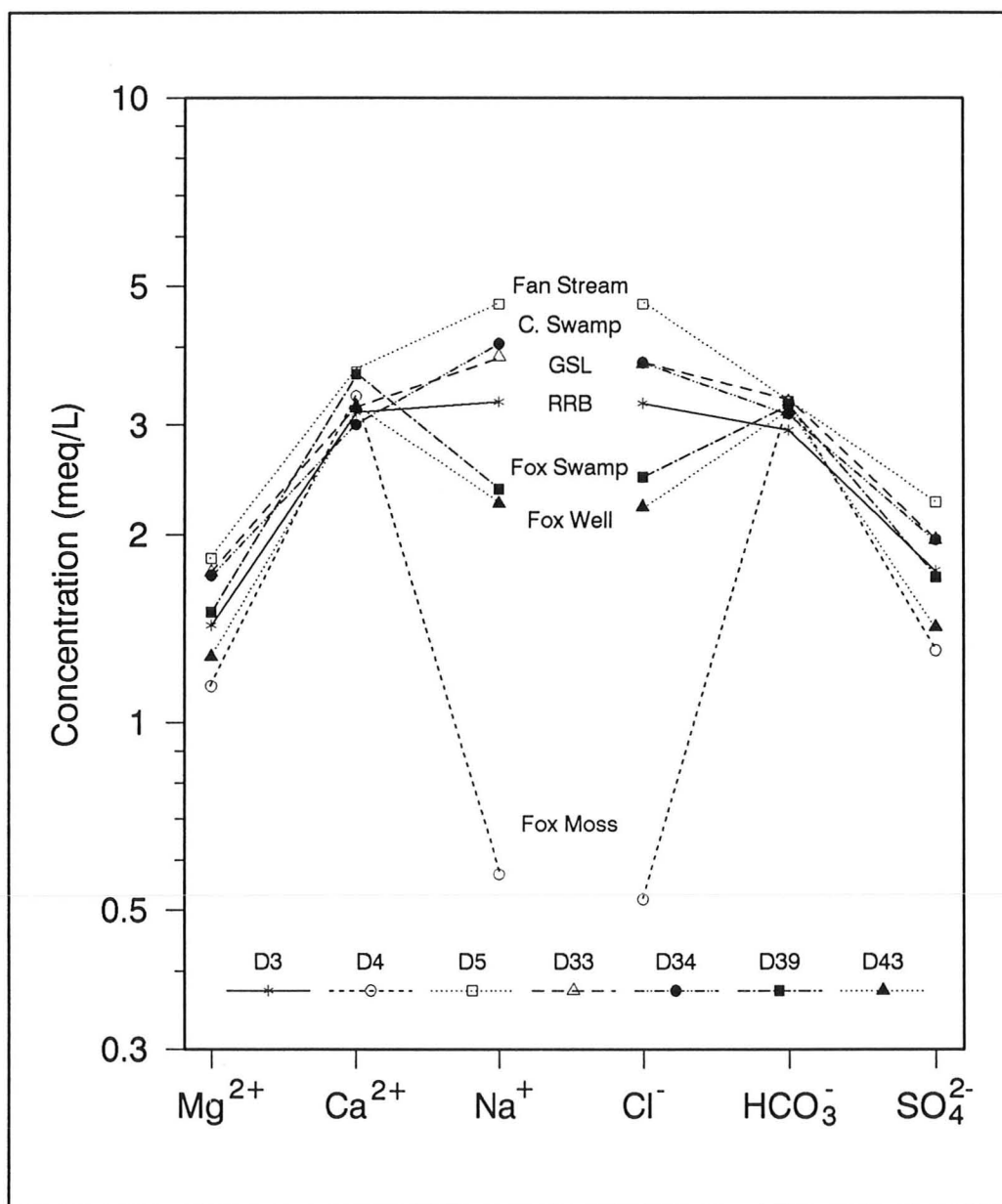


Figure 7.20: Mean concentrations of major anion and cation species in meq L⁻¹ for discharge waters of Carcadado Valley (Types 3 and 6 in Table 7.1).

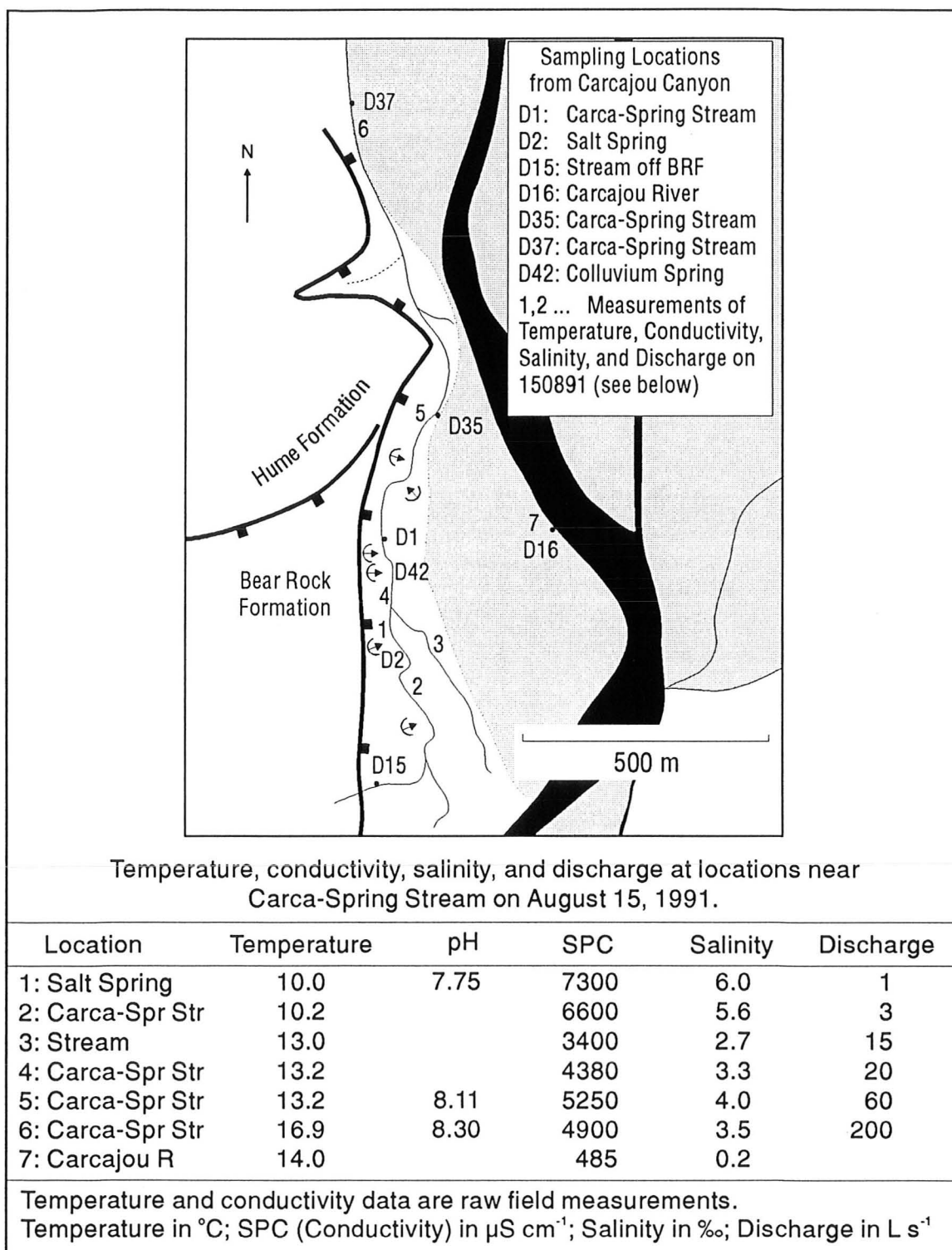


Figure 7.21: Sketch map of sample locations at the base of Carcajou Canyon. Salt Spring (D2) discharges from fractures in the Landry Member. Carca-Spring Stream was sampled at several locations. Raw data from 150891 are presented above.

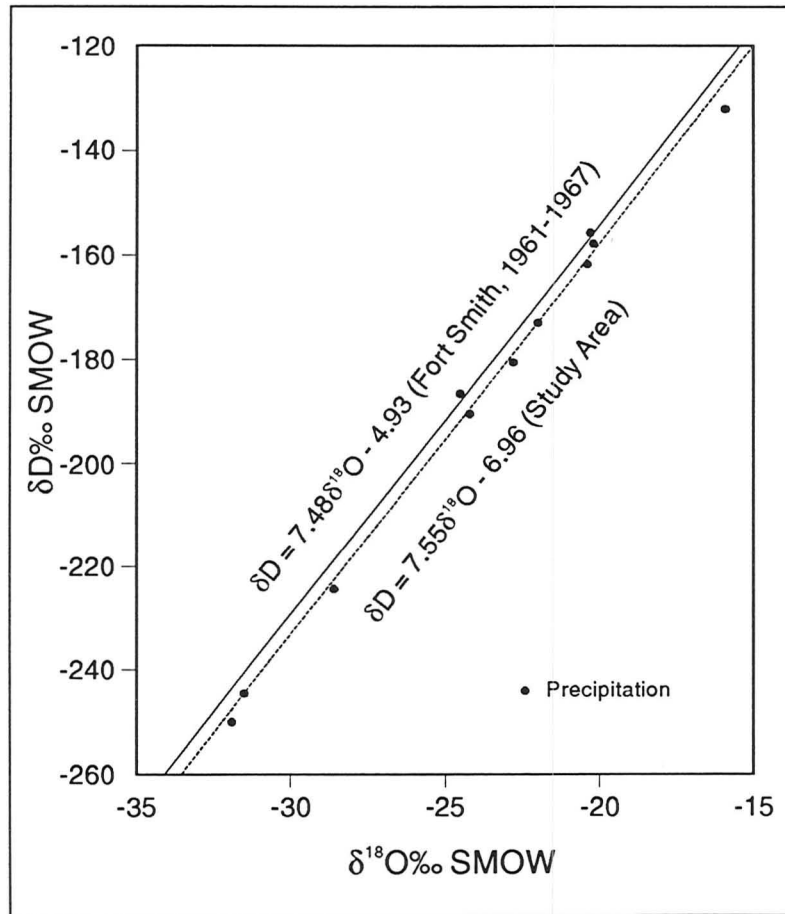


Figure 7.22: Meteoric water lines from Fort Smith and the study area. Data used in construction of the local line are from this study and van Everdingen (1981).

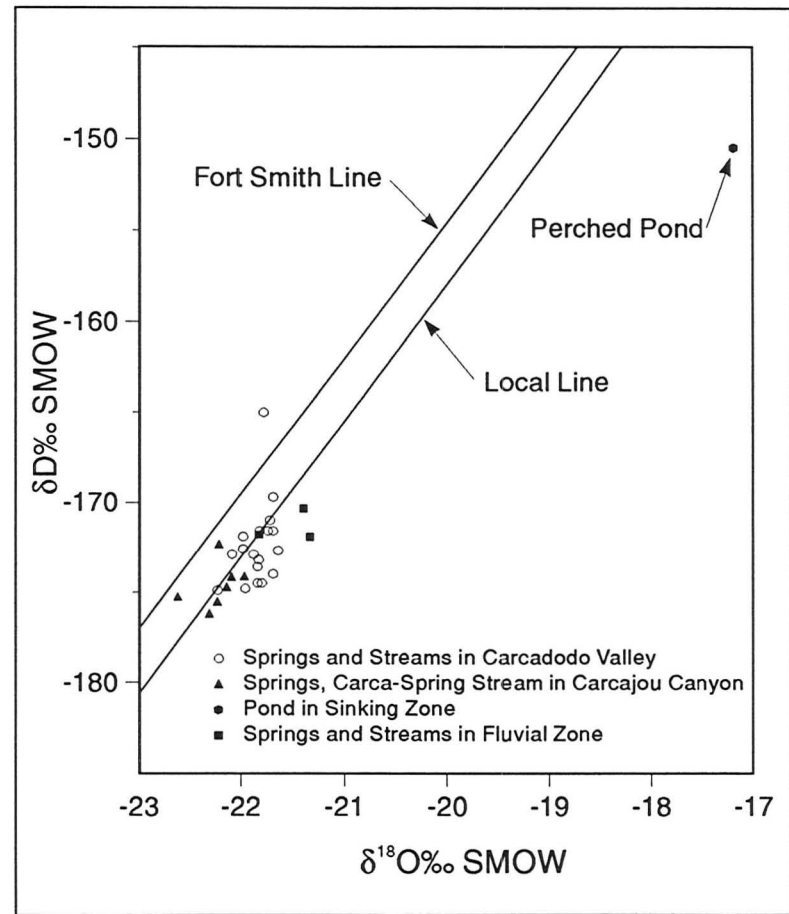


Figure 7.23: Isotope samples from the Dodo Canyon Site plotted with the local and Fort Smith meteoric water lines. Springs at the site discharge meteoric water. The deepest circulated samples (Carca-Spring Stream) are the lightest, and the surface samples the heaviest.

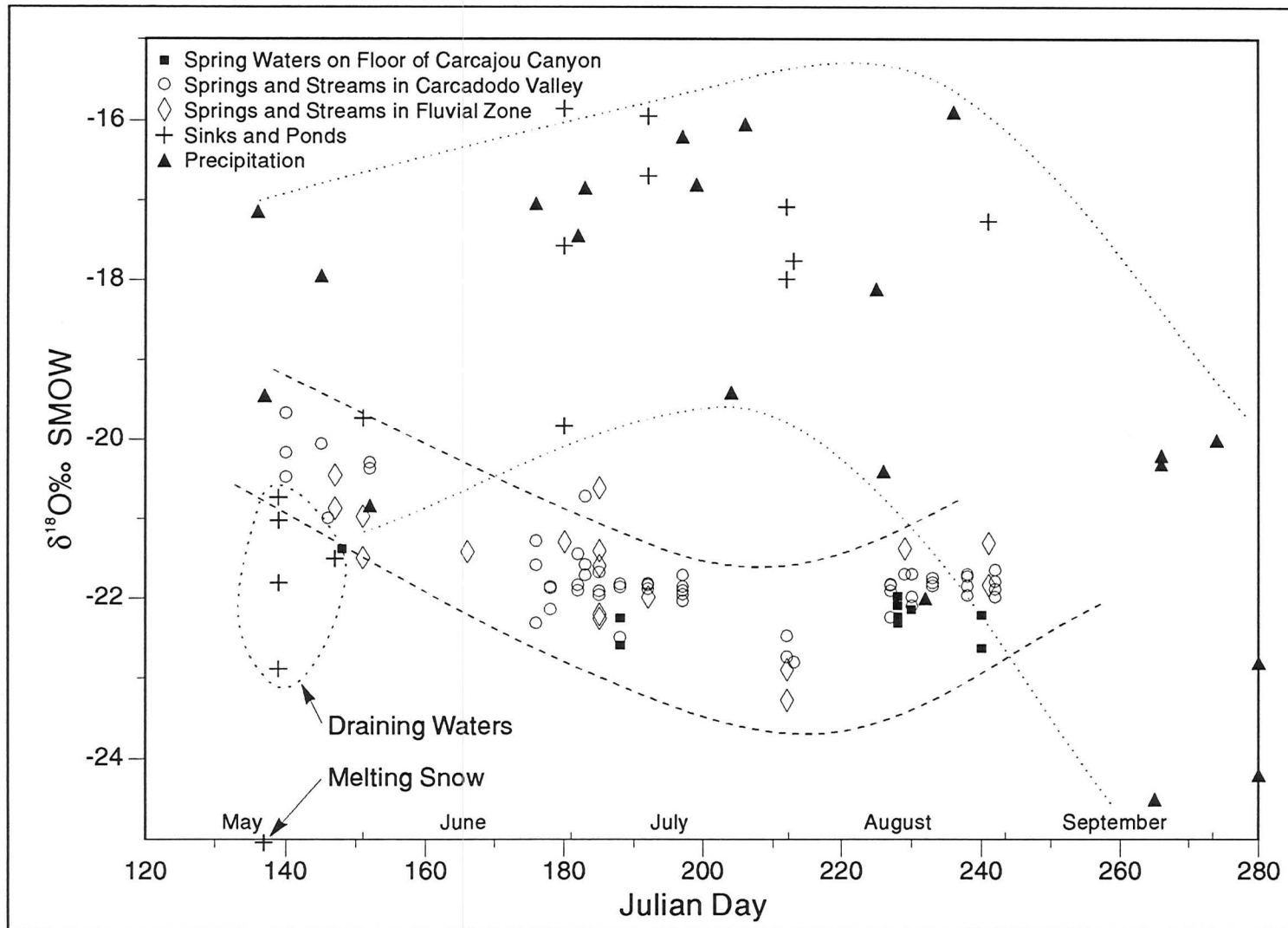


Figure 7.24: $\delta^{18}\text{O}$ of water samples at the Dodo Canyon Site versus time. The pattern shows the isotopic signature of springs and streams is out of phase with precipitation. This suggests there is time lag of at least 40 days between infiltration in the Sink Zone and resurgence in Carcadodo Valley.

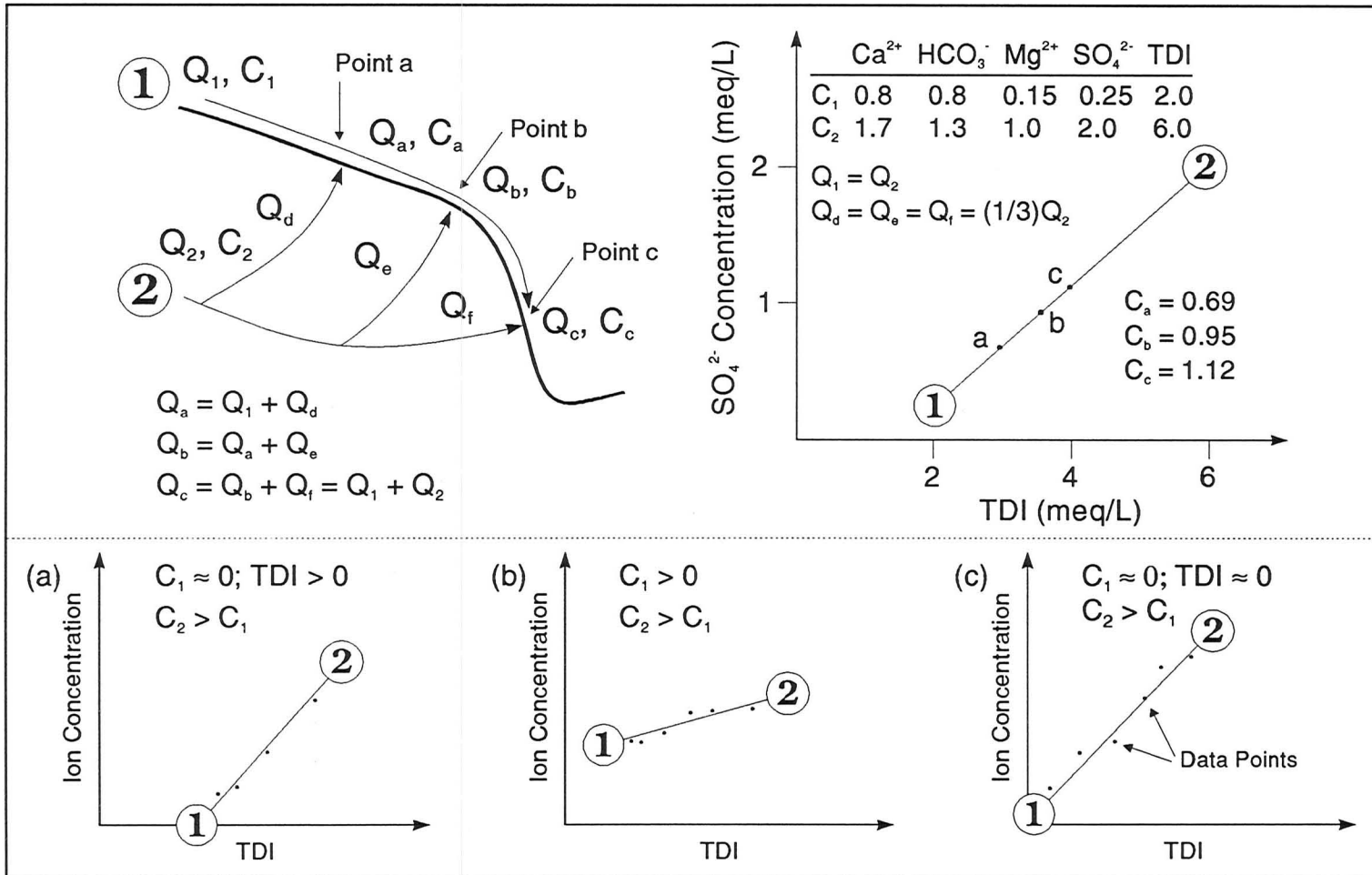


Figure 7.25: Model depicting the mixing of two flow components of equal magnitude ($Q_1 = Q_2$) (upper). In the example shown, a surface stream mixes with equal amounts of groundwater ($Q_d = Q_e = Q_f$) at three points (Q_a , Q_b , Q_c). The TDI of the surface water is 2.0 meq L^{-1} , and the groundwater 6.0 meq L^{-1} . A composition diagram is shown using SO_4^{2-} as the ion. A mixing line that passes through points a, b, and c is drawn between the end members ① and ②. The resulting SO_4^{2-} concentrations are also given. The mixing line extrapolates back to the TDI axis since the SO_4^{2-} concentration in the surface water is very low (a). Other two-way mixing situations and the conditions in which they occur are shown in (b) and (c).

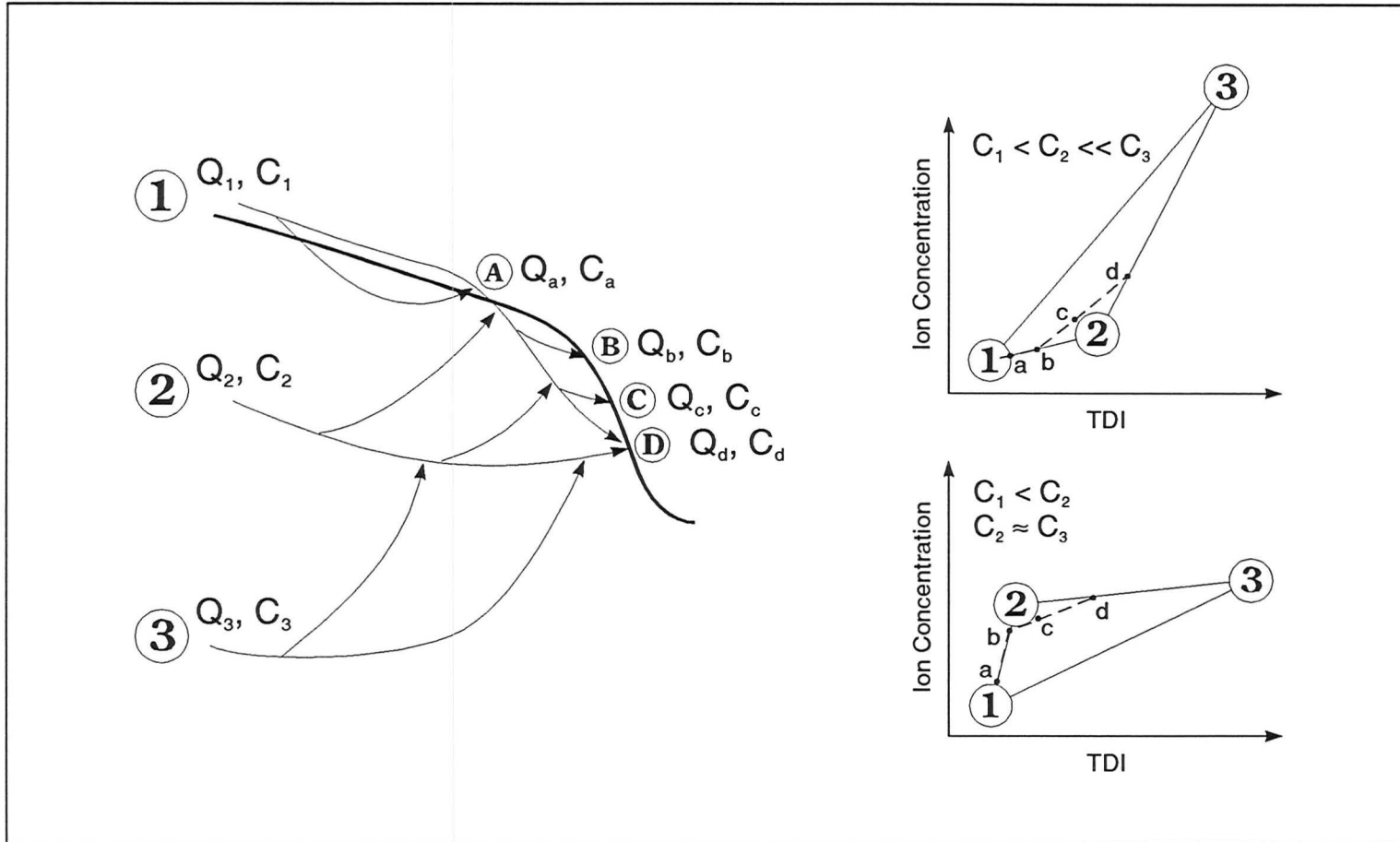


Figure 7.26: Model of three-way mixing. A surface water is shown mixing with two groundwater components along a hierarchy of springs at points A to D. Waters at point A have a facies dominated by component 1, point B takes flow from 1 and the aquifer 2, points C and D take flow from all three members. Two possible mixing situations are illustrated. The positions of each end member are plotted and mixing lines joined between them. Points A and B lie on the line between 1 and 2, points C and D on a mixing line directed toward 3.

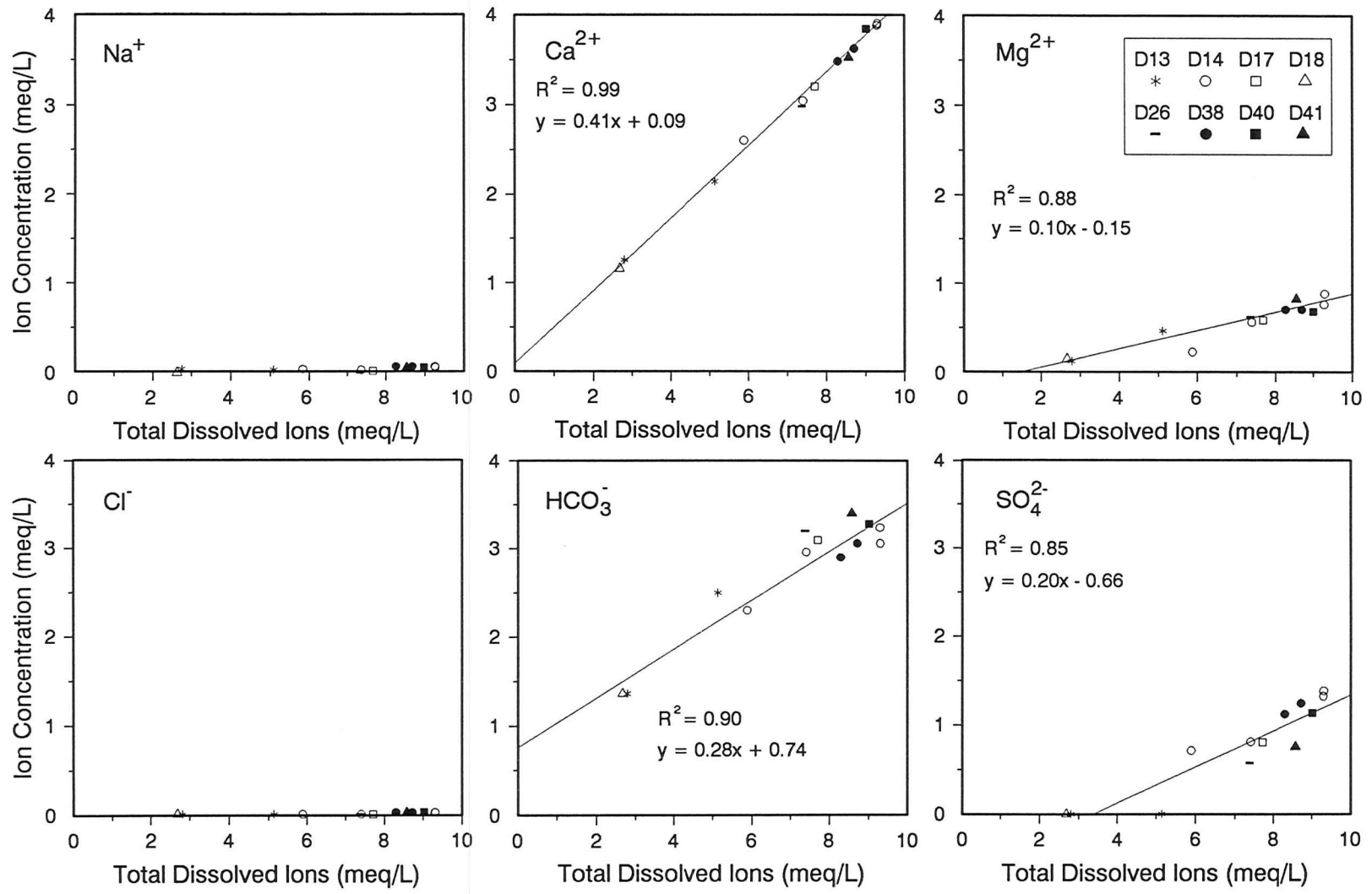


Figure 7.27: Concentrations of major anions and cations versus total dissolved ions for samples of the Fluvial Zone. Data show two-way mixing between low TDI discharge of the Landry Member and SO₄²⁻ rich water of the Brecciated Member.

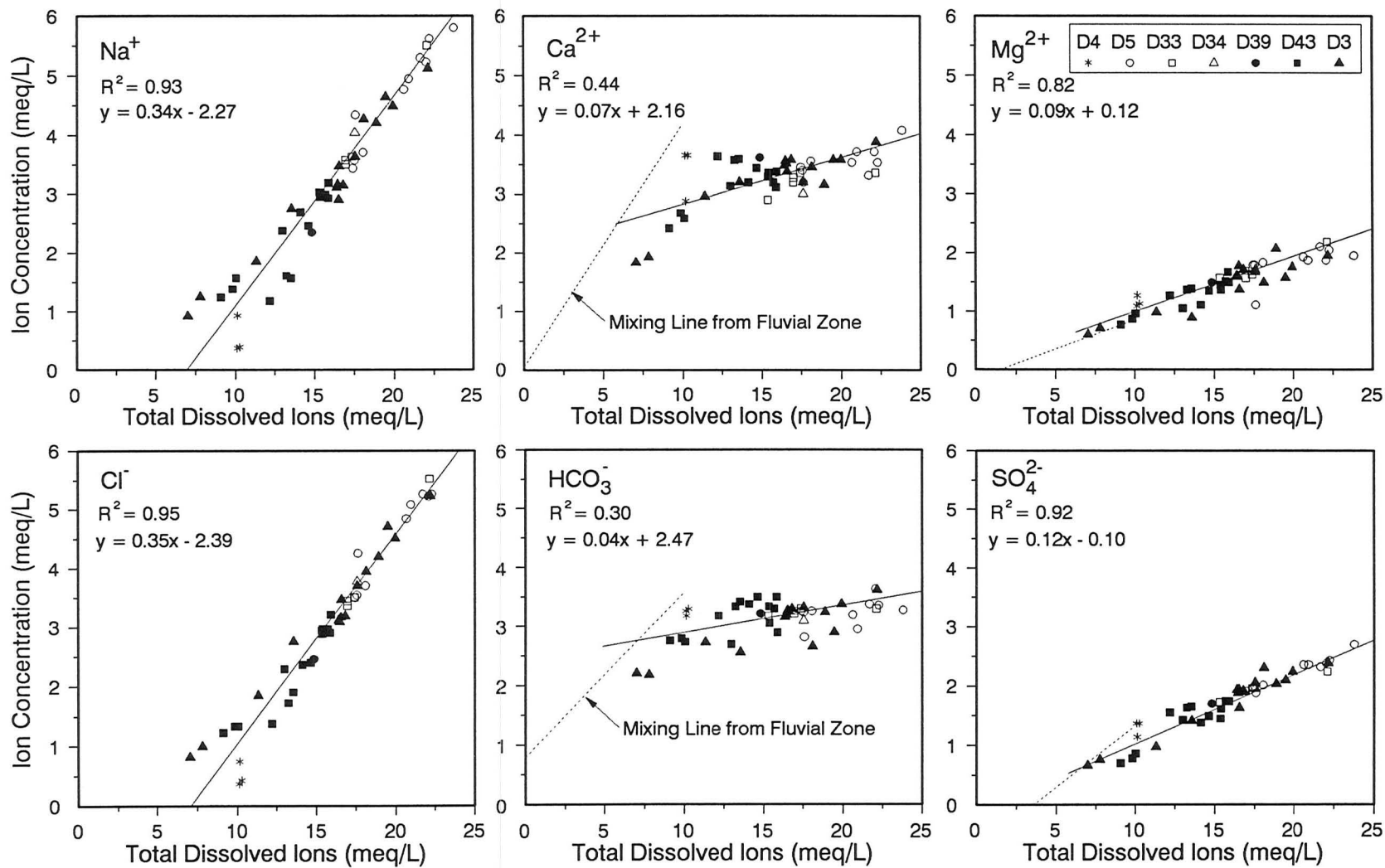


Figure 7.28: Concentrations of major anions and cations versus total dissolved ions for samples of Carcadado Valley. Data show the addition of a Na^+ and Cl^- rich groundwater to discharge from the Landry and Brecciated Members.

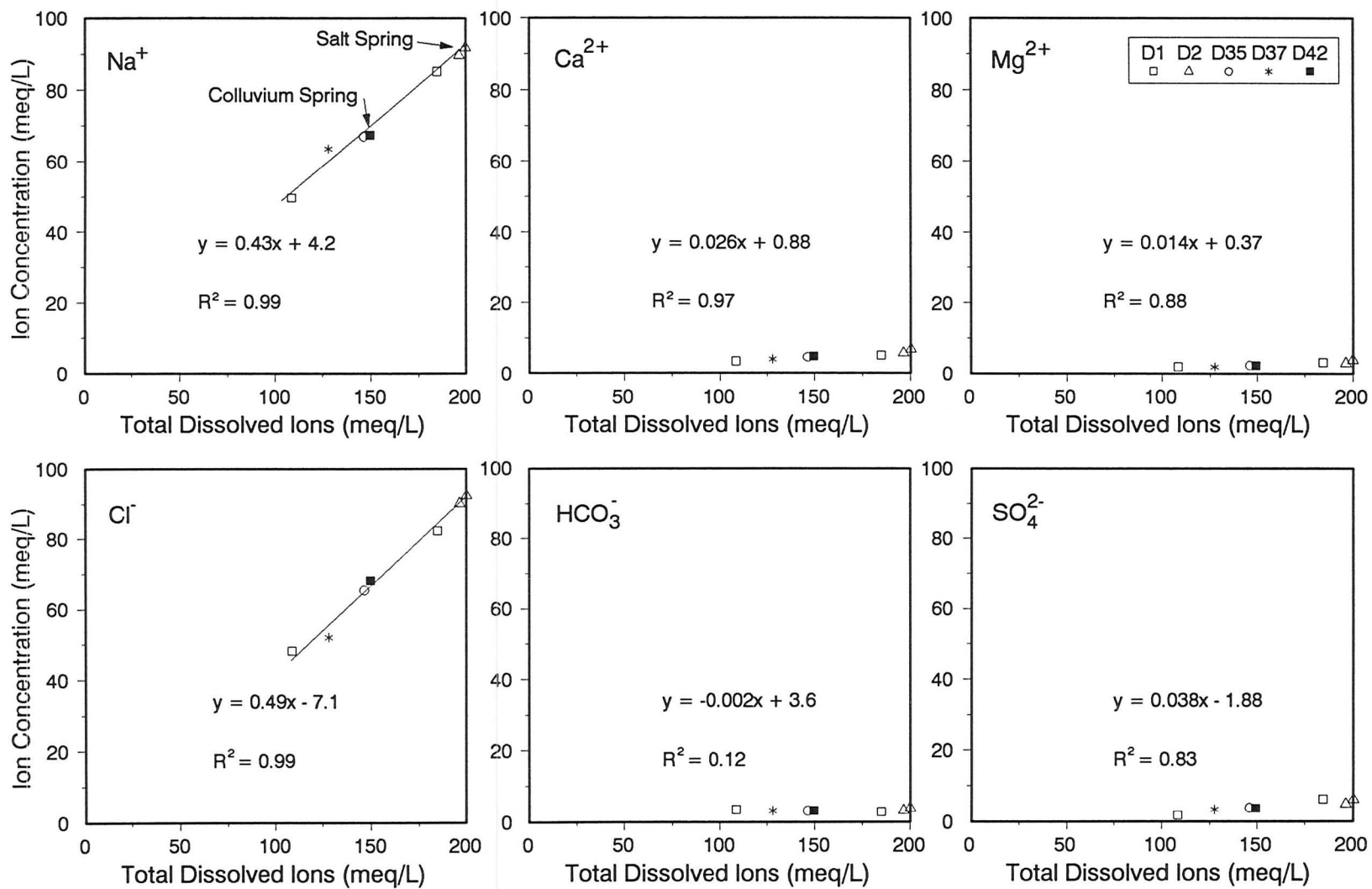


Figure 7.29: Concentrations of major anions and cations versus total dissolved ions for samples from Salt and Colluvium Springs, and Carca-Spring Stream. One sample from Salt Spring is beyond the range of the x-axis (TDI = 210 meq L⁻¹).

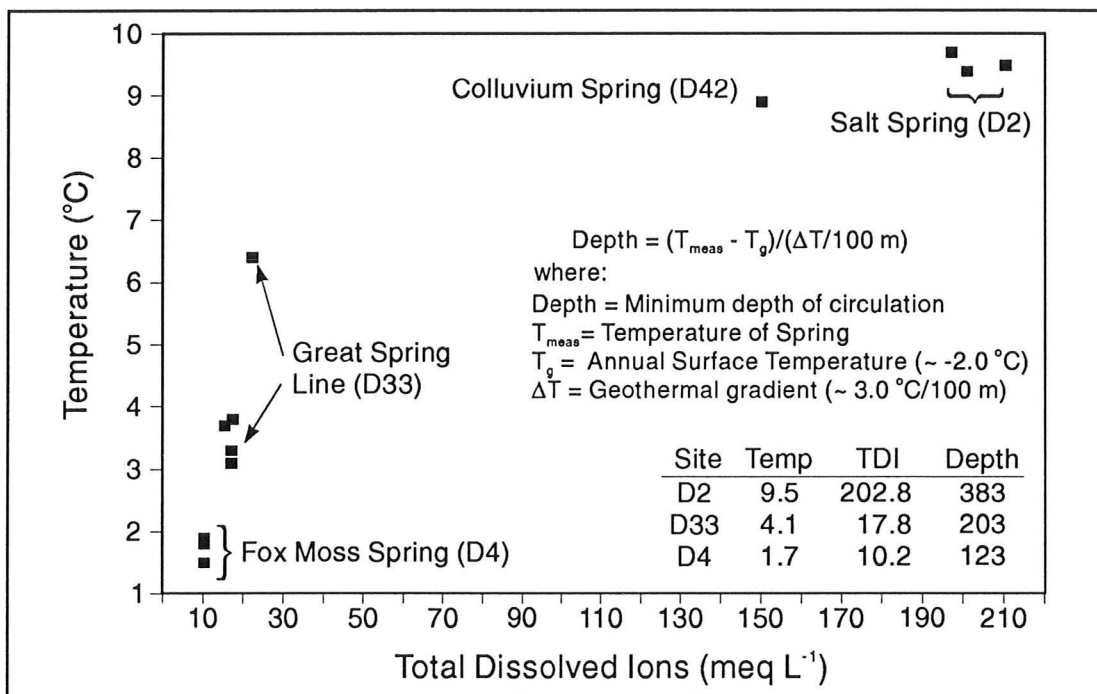


Figure 7.30: Temperature versus total dissolved ions for selected springs in the Main Karst. Water temperatures were taken from the springs in July and August of 1988 and 1991. The temperature data are used to approximate the minimum depth of circulation.

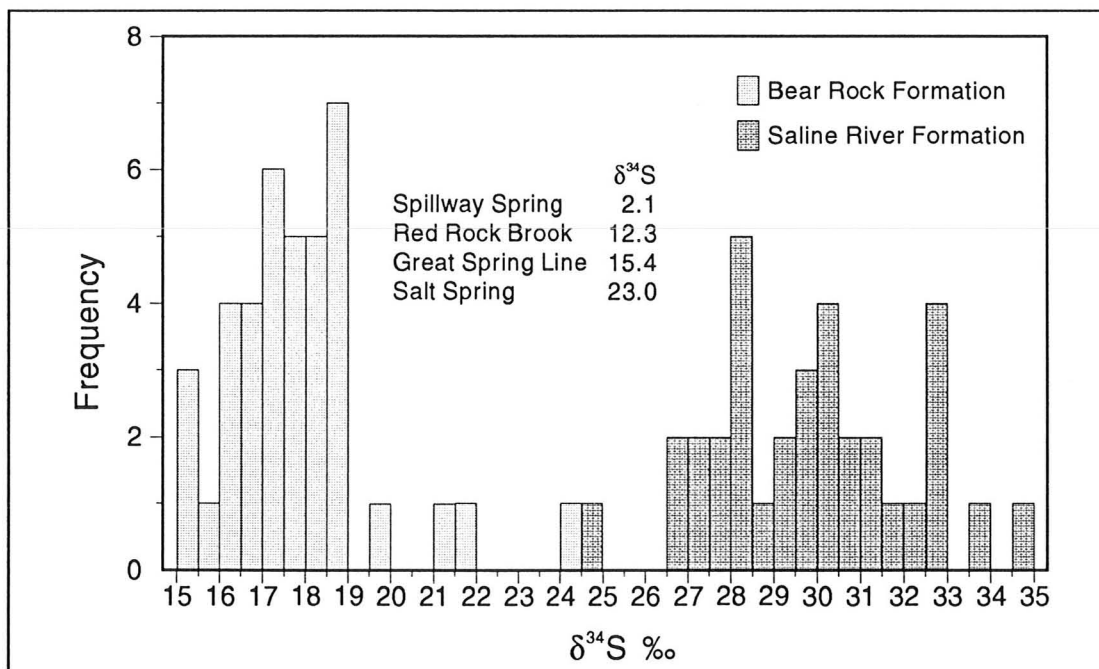


Figure 7.31: Histogram of $\delta^{34}\text{S}$ values in ‰ for SO_4^{2-} from gypsum and anhydrite samples of the Bear Rock and Saline River Formations. Data are from van Everdingen *et al* (1982a). $\delta^{34}\text{S}$ values for SO_4^{2-} from four waters samples of the Dodo Canyon Karst are shown. The values from Red Rock Brook, Great Spring Line, and Salt Spring correlate with the range of $\delta^{34}\text{S}$ for sulphate from the Bear Rock Formation.

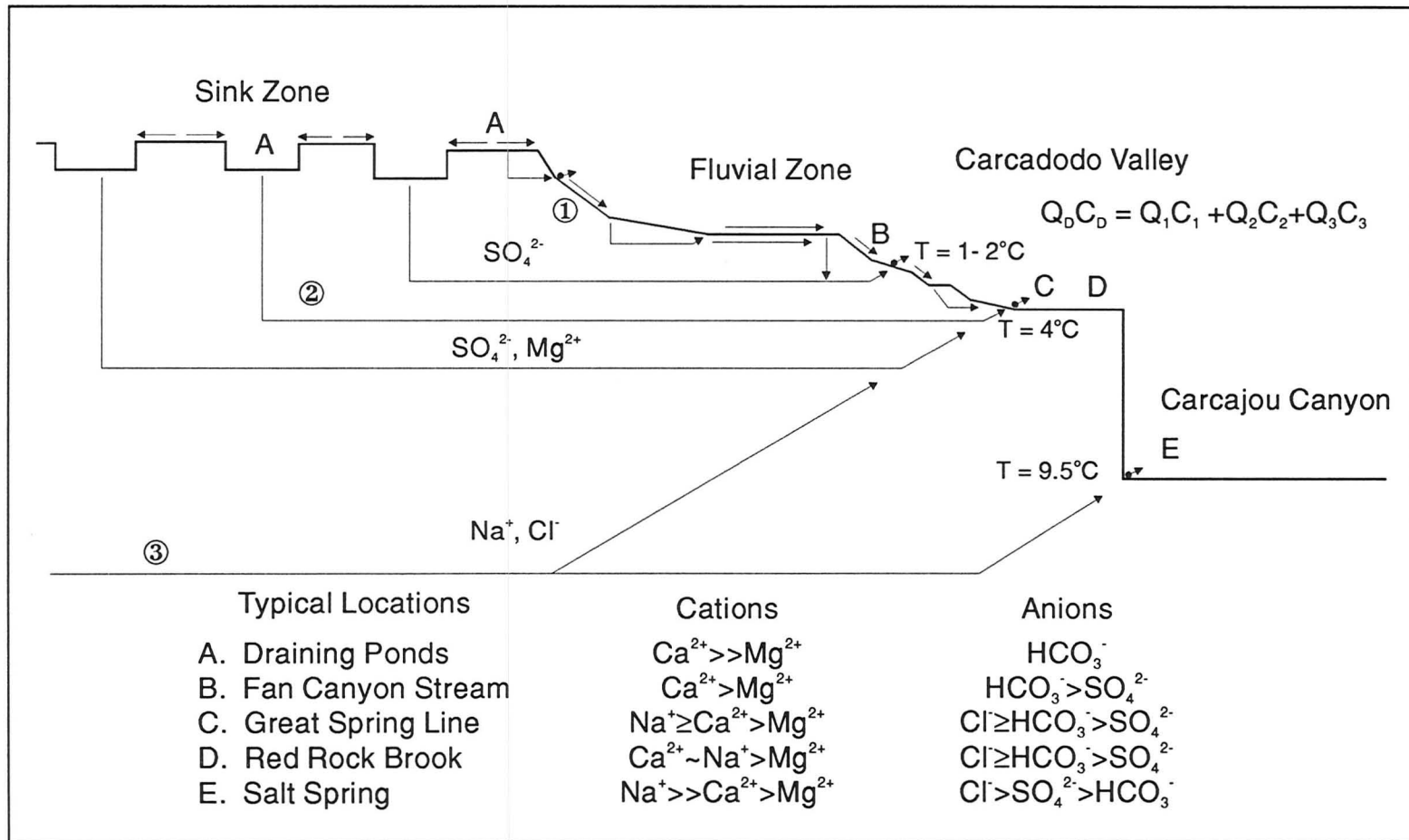


Figure 7.32: Schematic diagram of groundwater circulation in the Dodo Canyon Karst. The figure is not to scale. Changes in ion abundance are indicated for five locations that are typical of the data set. Spring temperatures are shown for the Fluvial Zone, Carcadodo Valley, and along Carca-Spring Stream. Red Rock Brook takes flow from shallow, intermediate, and deep groundwater components. The latter has high concentrations of Na^+ and Cl^- . Much of the SO_4^{2-} and Mg^{2+} is from the intermediate Bear Rock and Mount Kindle Formations aquifer.

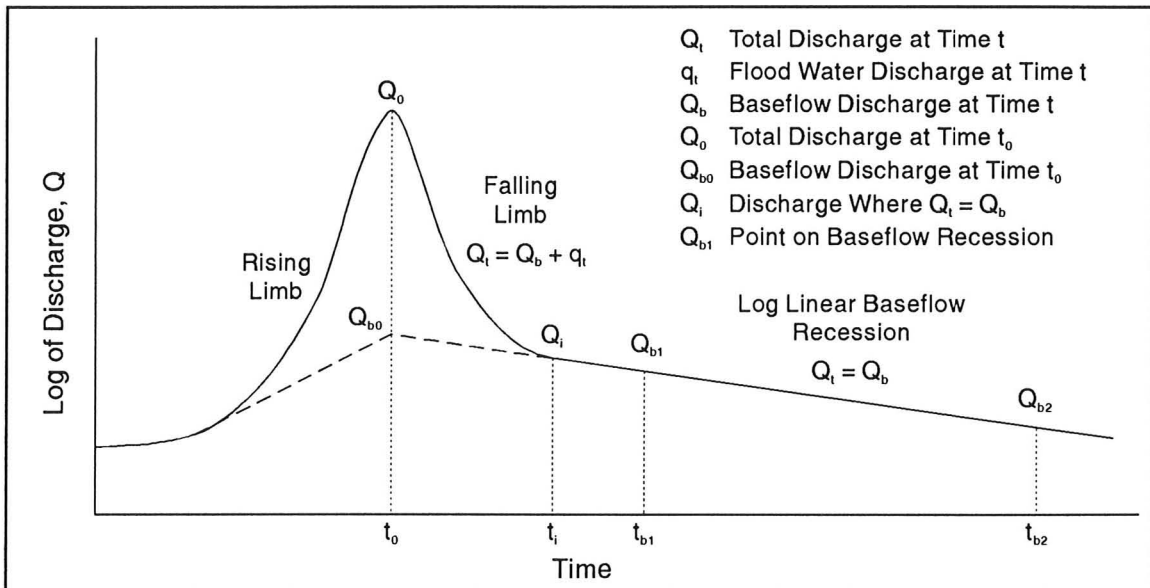


Figure 7.33: Terms used in karst spring recession. The falling limb is often typified by a log-linear recession, or a series of log-linear segments where each represents withdrawal from different aquifer storage. In the case illustrated, the falling limb is divided into two sections: (i) a steep non-linear portion showing a decline in flood waters, and (ii) a log-linear portion representing the baseflow recession (modified after Mangin, 1975).

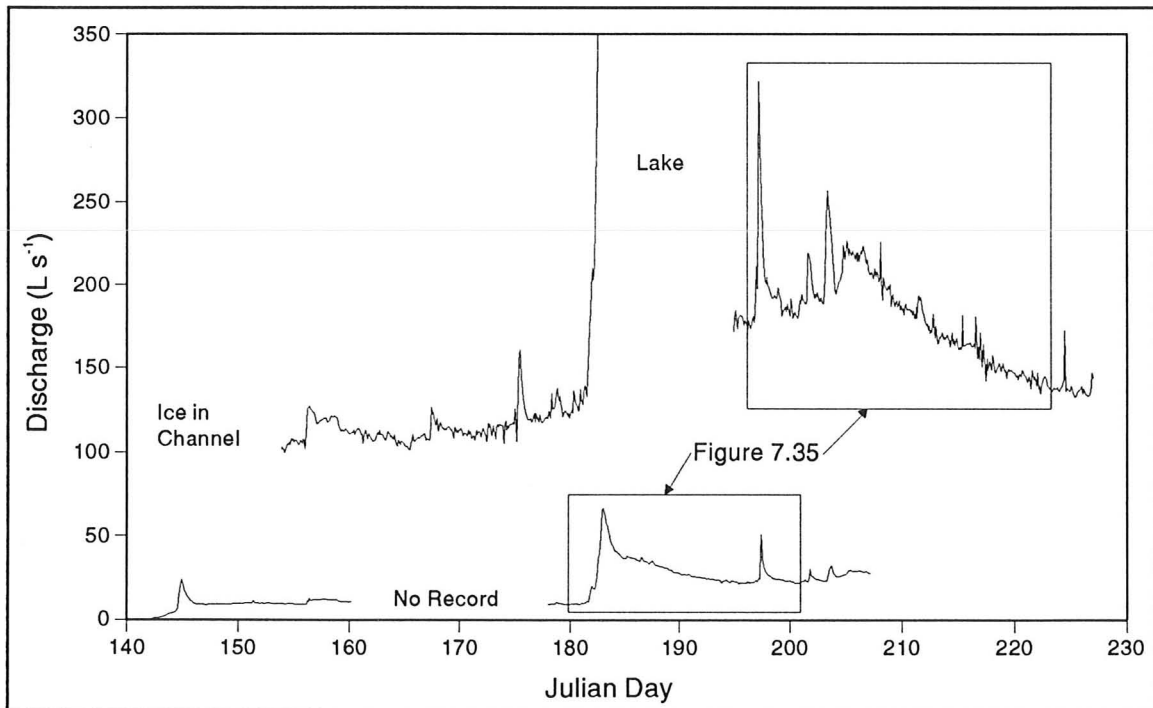


Figure 7.34: Instantaneous discharge of Red Rock Brook and Fox Spring in the field season of 1988. Data are digitized at 1 to 2 hour intervals. The records display greater short term variability than the averaged daily data (Figure 7.15). The areas enclosed in boxes are presented in detail on Figure 7.35.

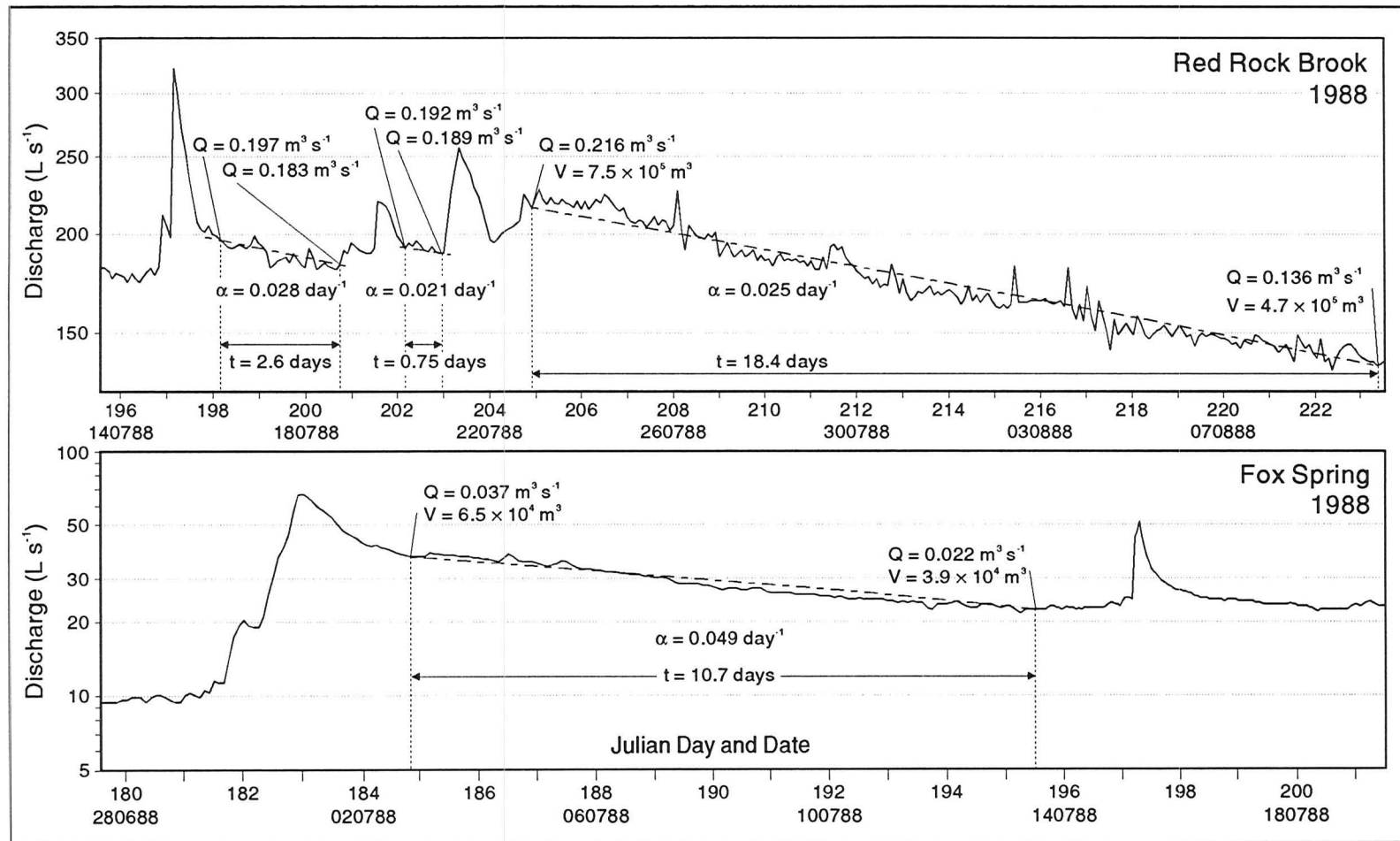


Figure 7.35: Discharge of Red Rock Brook and Fox Spring over portions of the 1988 field season. The discharge data are plotted on a logarithmic scale. Linear sections represent periods of baseflow recession that follow major precipitation events. Three recessions are depicted for Red Rock Brook, and one for Fox Spring. The bounding discharges and the lengths of each recession interval are given. The values of the recession coefficients (α), are calculated from Equation 7.7. Dynamic volumes are calculated for the longest recessions using Equation 7.8. The α values are high and indicate rapid drainage of the aquifer feeding Red Rock Brook and Fox Spring. Extrapolation of the late July and early August recession of Red Rock Brook yields discharges of $0.038 \text{ m}^3 \text{ s}^{-1}$ and $0.019 \text{ m}^3 \text{ s}^{-1}$ for September 30 and October 30, respectively. These low discharges are consistent with evidence that suggests Red Rock Brook does not sustain flow following freeze-up in mid-October.

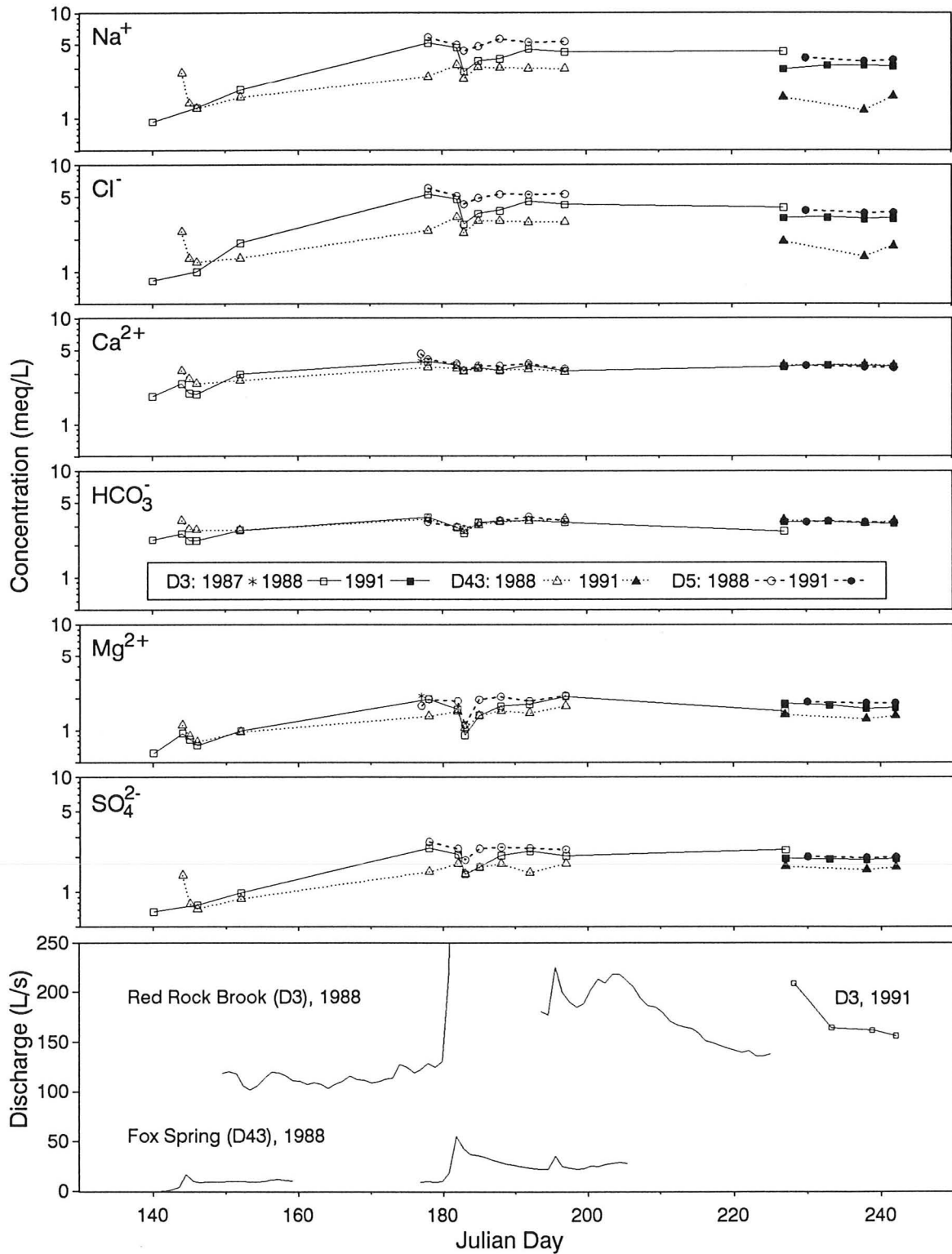


Figure 7.36: Concentrations of major anion and cation species in Red Rock Brook (D3), Fox Spring (D43), and Fan Stream (D5) verses time. Data are from 1987, 1988, and 1991.

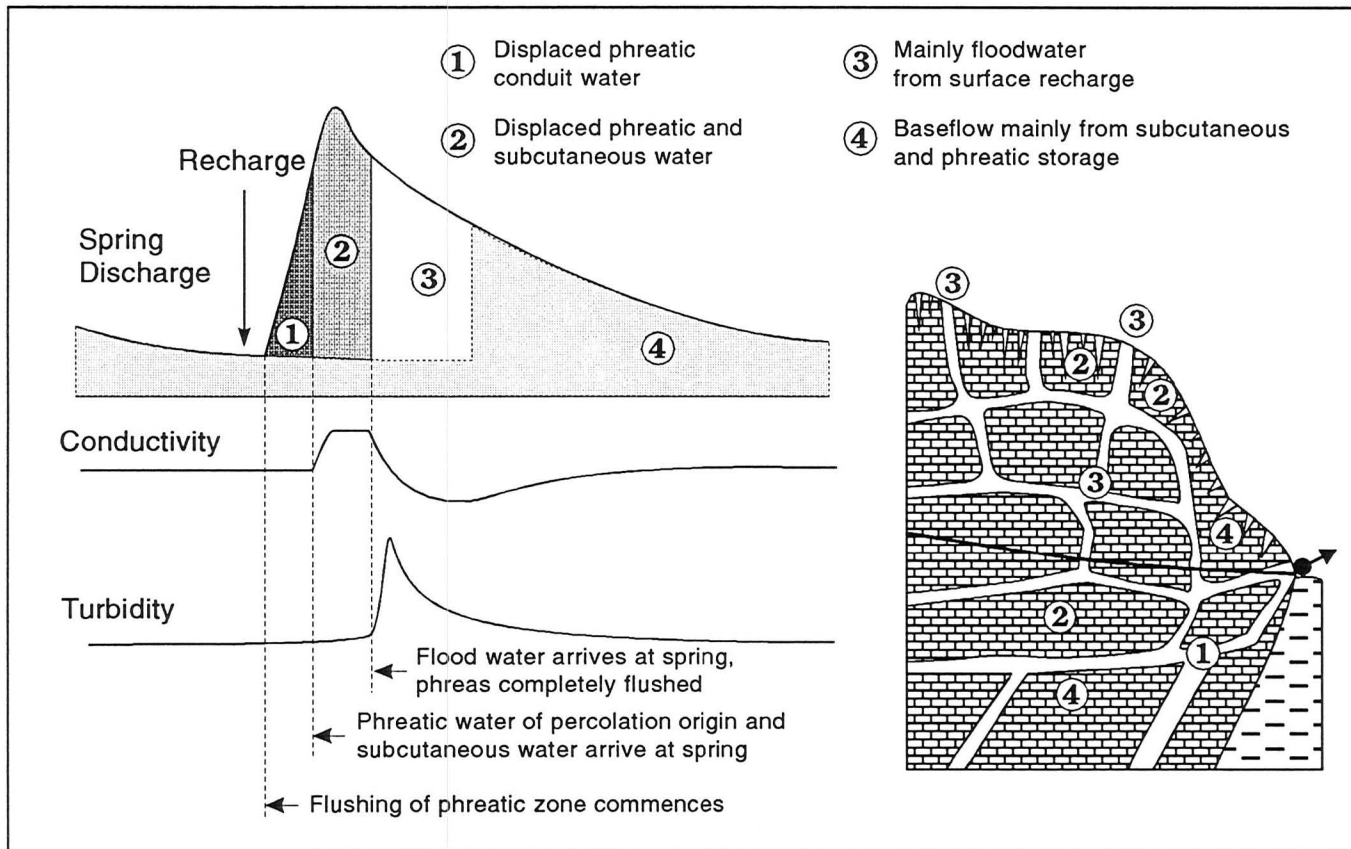


Figure 7.37: Separation of a karst spring hydrograph. Allogenic and autogenic recharge enter and travel through karst aquifers by several pathways (Chapter II). The soil, subcutaneous, and phreatic zones constitute important stores. Water travels through conduits, fissures, and pores to the spring point. The diagram above depicts the separation of a hydrograph into a variety of flow components. Conductivity and turbidity data aid in this separation. Throughout the flood event, discharge at the spring will be a mixture of the flow components, although a particular component may dominate a section of the hydrograph. The timing and positions of these components will vary depending upon the characteristics of a given karst (after Atkinson, 1977; Williams, 1983; Bonnaci, 1987; Ford and Williams, 1989).

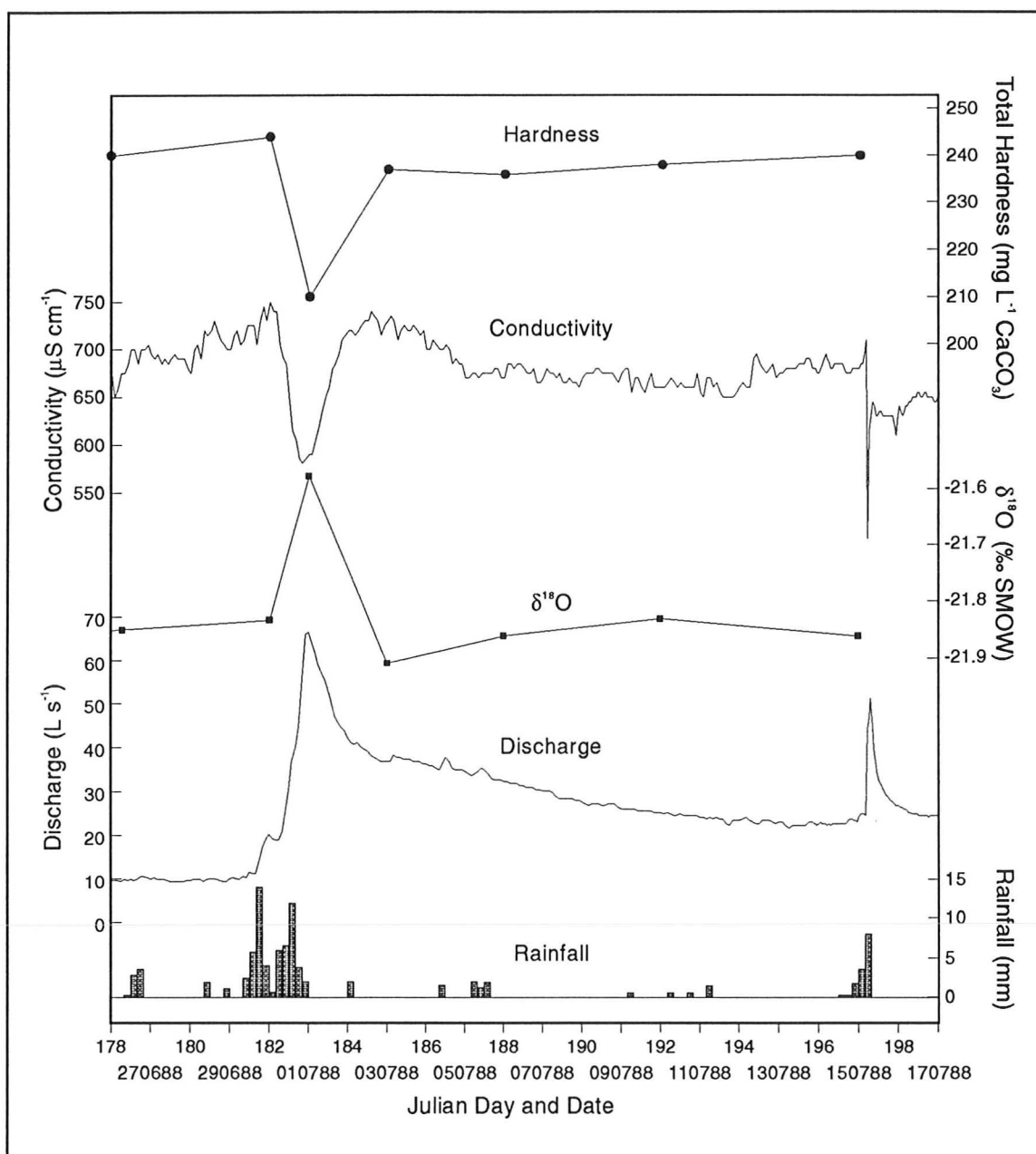


Figure 7.38: Total hardness, conductivity, $\delta^{18}\text{O}$, and discharge of Fox Spring from June 26 to July 17, 1988. Rainfall recorded at the Dodo Canyon base camp is presented in four hour intervals along the base of the diagram. The time markers are centred on 12 noon of each day. Variations in hardness, conductivity, and $\delta^{18}\text{O}$ all show the effect of the major storm of June 30 and July 1. Reductions in hardness and conductivity, and the small change $\delta^{18}\text{O}$ show the passage of a shallow, rainfall diluted flow component across the peak area of the hydrograph. Sampling on July 15 occurred before the heavy late afternoon precipitation triggered the sharp increase in discharge, and therefore is not represented in the conductivity and isotope data.

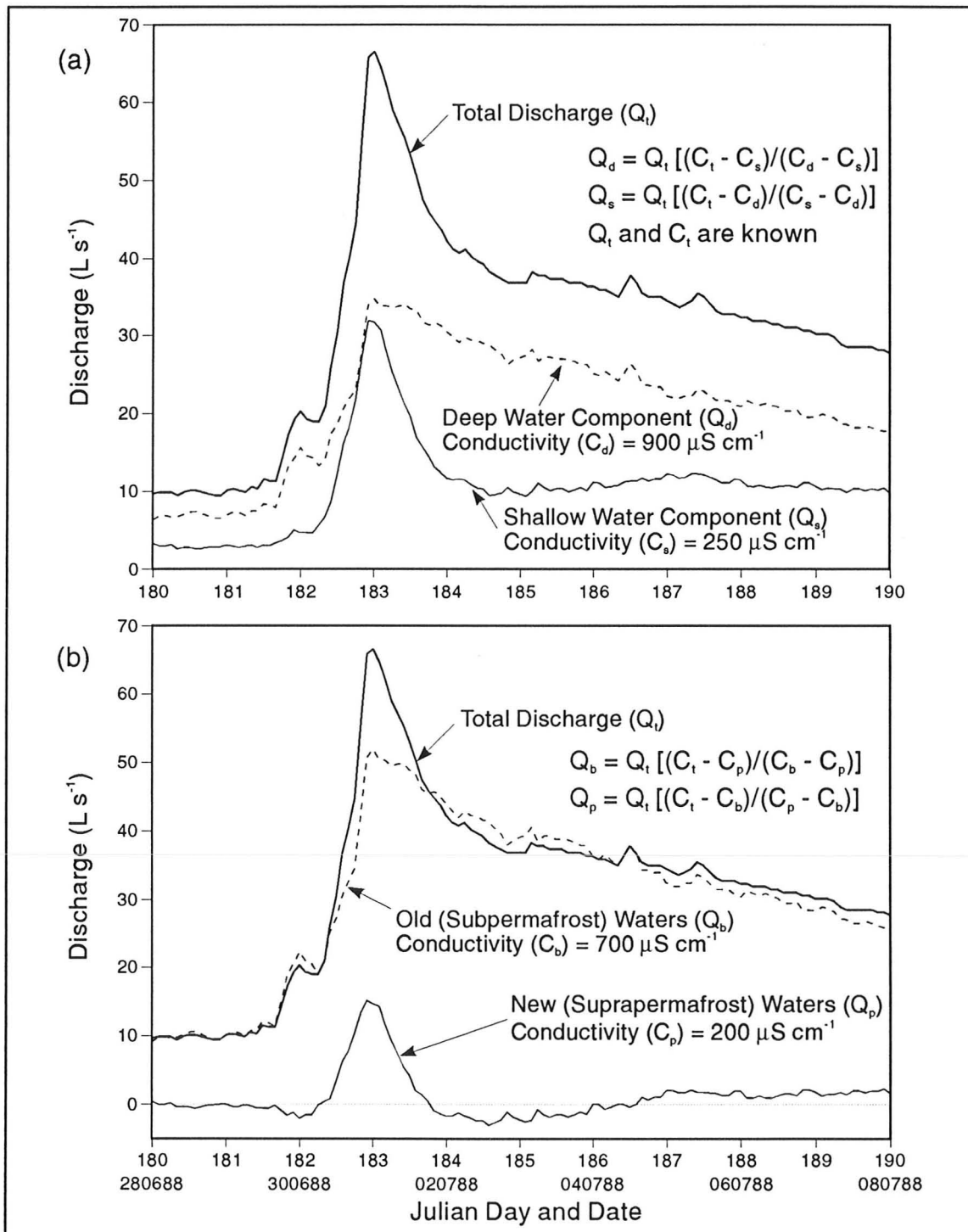


Figure 7.39: Hydrograph separation at Fox Spring. In diagram (a) the hydrograph is divided into shallow and deep water components. The deep component is assigned a conductivity of $900 \mu S cm^{-1}$, the shallow water $250 \mu S cm^{-1}$. In diagram (b) the hydrograph is divided into new and old waters using assigned conductivities of $700 \mu S cm^{-1}$ and $200 \mu S cm^{-1}$. The new waters are interpreted as suprapermafrost discharge.

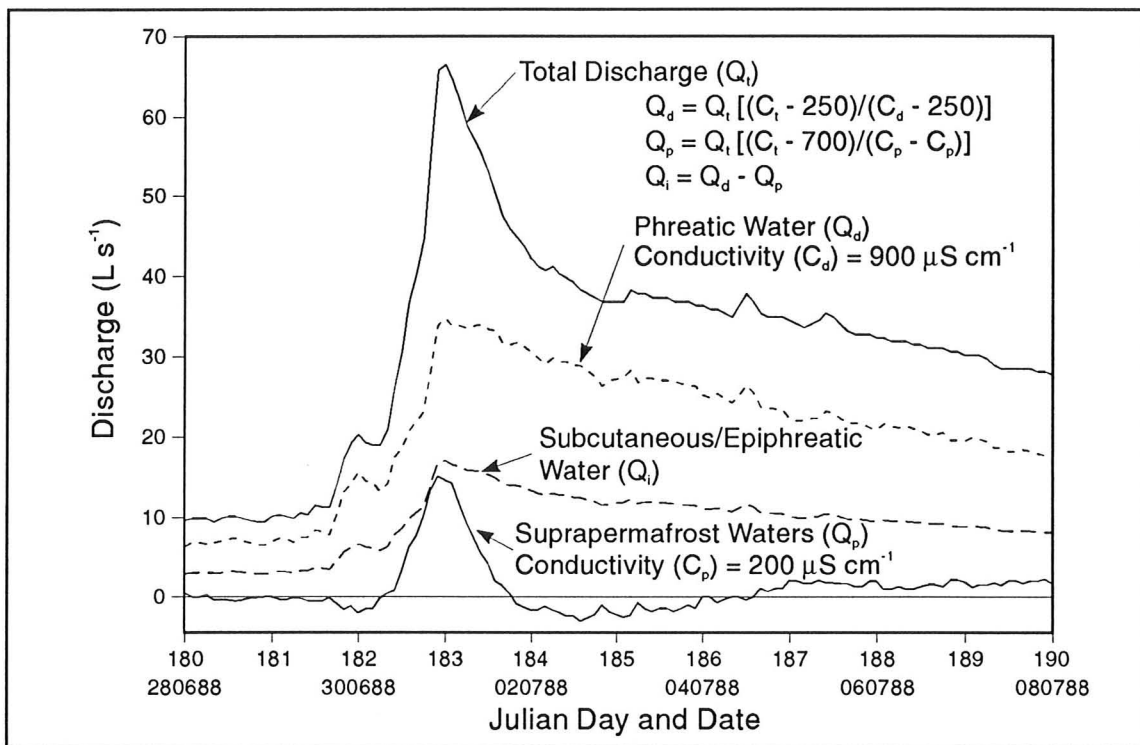


Figure 7.40: Separation of Fox Spring hydrograph into three components. Flow through the upper Bear Rock Formation is divided into suprapermafrost and subcutaneous waters. The phreatic water includes discharge from the main Bear Rock-Mount Kindle aquifer and the deep Saline River aquifer. Phreatic water comprises a larger proportion of the discharge from Great Spring Line and therefore also Red Rock Brook.

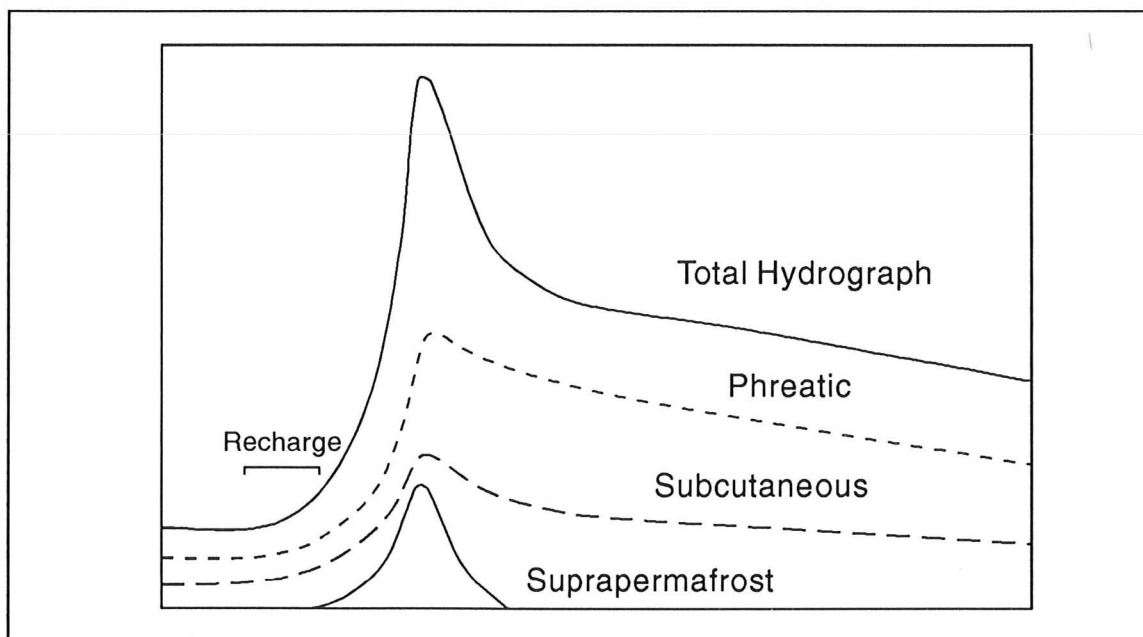


Figure 7.41: General model of hydrograph separation in Carcadodo Valley. The hydrograph is divided into suprapermafrost, subcutaneous, and phreatic contributions.

CHAPTER VIII

THE BONUS LAKE SITE

8.1 Introduction

Karst is widely distributed on the Bear Rock and Hume Formations in the Carcajou Range (Chapter VI). Besides the Dodo Canyon Site, karst on these formations was also examined at Bonus Lake (Figures 3.1, 8.1). Bonus Lake was first visited by D.C. Ford and party in the summer of 1983. The author worked the site on the dates June 12 - 24, 1988, and August 2 - 11, 1991. Fieldwork involved mapping and describing karst landforms, observing the hydrology of the system, and spot sampling for hydrochemistry and isotopes.

Unlike the Dodo Canyon example, the Bonus Lake Site is primarily developed on the Hume Formation. Groundwater circulation is comparatively shallow and the system responds rapidly to recharge events. As with the Dodo Canyon Site, the karst has been strongly influenced by glaciation. This chapter describes the physical, hydrological, and hydrochemical characteristics of the Bonus Lake Karst.

8.2 Site Description

Bonus Lake occupies the floor of a spillway approximately 20 km southeast of Carcajou Canyon (Figures 3.1, 8.1). The spillway is called Bonus Valley and it is locally developed along the contact between resistant limestones of the Hume Formation and recessive shales of the Hare Indian Formation. Karst occurs in the Hume limestones and in the Bear Rock Formation on the southwestern flank of the valley.

The site is divided into three zones of recharge, each displaying a

characteristic morphology: (i) Upper Sink Zone, (ii) Grikeland, and (iii) Lower Sink Zone (Figure 8.2). The first is an area of shallow depressions and small ridges located on gently sloping terrain in the upper portion of the karst. Downslope is the Grikeland, a narrow zone of residual towers and corridors (streets) that are developed along the crest of the slope above Bonus Valley. The Lower Sink Zone is an area of dolines and corridors that extends from steeply dipping strata on the valley side to gentler terrain on the valley floor.

The karst is cross-cut by several small, narrow, and deeply incised canyons that are oriented normal to Bonus Valley. Twin Bridges, Central, and North Canyons occur in the main area investigated (Figure 8.2). Streams from each of these canyons have produced large fans on the floor of Bonus Valley, impounding Bonus Lake, and Trout Lake to the northwest. Valley floor deposition and lake impoundment have infilled and drowned several dolines of the Lower Sink Zone that extend onto the floor of Bonus Valley. The infilling sediments are not restricted to alluvium but there are also glaciofluvial and lacustrine materials.

The floor of Bonus Valley functions as the discharge area. Several diffuse springs are located on the northern margin of Twin Bridges Fan (Sampling Point B1: Table 8.1). Much larger springs discharge from alluvium of Central Fan (B17, B18) and from bedrock and talus near Trout Lake (B15, B16). Additional springs discharge from alluvium and talus near North Fan. The total discharge of the system is represented by Bonus Stream (B26) above the confluence with Rouge Mountain River. The Bonus Stream basin has an area of approximately 60 km². Most of this area is in non-karst rock above the elevation of the Hume Formation, and is drained by the three canyons. Under average discharge conditions, the canyon streams sink into their channels as they cross the Hume outcrop. Only under heavy precipitation are surface flows maintained through the canyons and across the fans. Precipitation onto the karst proper is routed to dolines and ponors.

In the region, there is a gradual rise in elevation from the Mackenzie Plain to the Mackenzie Mountains. The topography surrounding the karst is of low relief.

Broad, gently sloping terrain stretches to the northeast and southwest (Figure 8.1). These areas are incised by other meltwater channels and their tributaries. Adjacent to the karst are two flat, higher elevation surfaces labelled as North and South Upland on Figure 8.2. These features are laterally extensive along Bonus Valley and are interpreted as kame terraces (Section 8.2.3.1). Some drainages from these surfaces are focussed to sink points on the Hume Formation.

8.2.1 Geology

The general geology of the Bonus Lake Site is shown on Figure 8.3. Karst is hosted on the Hume and Bear Rock Formations. The Hume Formation is well exposed in the Grikeland, Lower Sink Zone, and in the canyons. The Bear Rock Formation outcrops in the canyons and in Bear Rock Valley of the Upper Sink Zone (Figure 8.3). Reverse faults, tight folds, and subsided blocks are common in the Bear Rock Formation. The larger features extend vertically into the Hume Formation.

8.2.1.1 Hume Formation

The subsurface Hume Formation is divided into Upper, Middle, and Headless Members (Pugh, 1983, 1993; Chapter IV). In outcrop, the latter two are often grouped into a recessive lower member (Morrow, 1991). At the Bonus Lake Site, the Upper Member is exposed over the Sink Zones and Grikeland. It is massively bedded, grey to orange weathering, fine-grained, fossiliferous wackestone and lime mudstone. Exposures in Central Canyon range from 60 to 80 m in thickness. Strata across the Grikeland and Upper Sink Zone dip gently to the northeast. Dips steepen toward Bonus Valley approaching 30° in the Lower Sink Zone and then flatten out on the valley floor. The general structure is that of a monocline (Figure 8.3). The Upper Member is very resistant and cliff forming. Many exposures display cavernous porosity, particularly in the upper 20 m. Crackle breccia fabrics were observed in both the Upper Member and the underlying units. The incidence of breccia was highest in large foundered blocks near Trout Lake. All field samples

tested were limestones.

The lower recessive members are not easily discerned in the field. Canyon sections show 30 to 40 m of poorly exposed fossiliferous, thin bedded, argillaceous wackestone with interbedded calcareous shale. Much of the interval is talus covered. These units outcrop in the canyons, in Bear Rock Valley, and in Bonus Valley near sampling point B26. Intervals of black shale occur at the latter two locations. Springs at B30 are perched above the argillaceous lower member.

8.2.1.2 Bear Rock Formation

The Bear Rock Formation outcrops in the canyons and Bear Rock Valley (Figure 8.3). Its characteristics differ from exposures at the Dodo Canyon Site. Overall, the formation is less brecciated, contains less terrigenous material, and is easily separated into its subsurface components. The Landry Member is buff coloured, thick to thin bedded, fossiliferous wackestone and lime mudstone. In the canyon exposures, thicker beds form resistant cliff units, thinly bedded intervals are recessive. All field samples tested as limestone. The unit shows some brecciation, fabrics vary from crackle to floatbreccias. Breccias are frequent where strata are displaced by faults, tight folds, and subsidence. Elsewhere the Landry beds are largely undisturbed.

At the Bonus Lake Site, the transition from the Landry to Brecciated Member is gradual. There is a change over 20 - 30 m from well bedded limestones of the Landry Member to dolomitic pack and floatbreccias of the Brecciated Member. The intervening section is equivalent to the subsurface Arnica Formation. It is lightly brecciated with calcite cemented crackle and packbreccia fabrics most common. Bedding is well preserved in some exposures but the degree of disturbance is much higher than in the overlying Landry. There are several tight folds and small faults developed in the unit. The larger reverse faults pass upward through the Landry and into the Hume Formation. The reverse faults indicate some deformation may be attributed to tectonic compression. However, the high frequency of tight folds,

convoluted and slumped blocks in the Arnica portion suggest much of the disturbance may be related to underlying volumetric expansion that accompanied hydration of anhydrite to gypsum. There is also evidence of multi-stage brecciation and deformation. Some beds were brecciated and then folded; others folded and then brecciated and faulted. The incidence of floatbreccias and gypsiferous outcrops increase lower in the section. In these intervals, many clasts are subrounded, although crude bedding is preserved throughout. A white precipitate assumed to be gypsum was found around some groundwater seeps.

8.2.2 Geomorphology

The distribution of karst, glacial, and fluvial features in the area between Twin Bridges and North Canyons is shown on Figure 8.4. This area is considered to be the core of the Bonus Lake Karst. The following text describes the karst zones of this area, from the non-karst upland to the Lower Sink Zone. Karst does extend to the northwest on the western flank of Rouge Mountain River, but it was not examined.

8.2.2.1 Upland

The Uplands are broad, gently sloping areas that border the karst. They lie above treeline, with vegetation dominated by a heath tundra community, and scattered tree islands of white and black spruce. Bedrock of the South Upland includes the Bear Rock and Mount Kindle Formations. The Franklin Mountain Formation underlies the higher ground denoted on Figure 8.1 by ponds. Outcrops on the South Upland are few as the area is mantled by an extensive red-weathering glacial deposit. The drainage density is high with the numerous channels marked by lines of dense vegetation (Figure 8.1). Precipitation onto this zone is rapidly translated as overland flow or throughflow to these channels. This is due to the texture of the glacial sediments and the probable continuous distribution of permafrost across the area.

The upland is not an unbroken plain; it exists as a series of discontinuous terraces. South Upland is a prominent terrace between 780 and 810 m that occurs

southwest of the Upper Sink Zone (Figure 8.2). Drainage from this upland sinks in ponors on the floor of Bear Rock Valley. The same terrace level is labelled North Upland southwest of Trout Lake. It extends to the northwest beyond the confluence of Rouge Mountain River and Bonus Stream. In the latter area, there is a karst on the Bear Rock Formation with a single large draining lake and many suffosion dolines. A second well-developed terrace occurs between 690 and 710 m. This surface is northeast of Bonus Valley and below the 790 m surface west of Rouge Mountain River. A fragmentary surface is also seen above Rouge Mountain River at 850 m.

The origin of these features is determined through inspection of their distribution, surficial sediments, and association with surrounding landforms. These surfaces are not structural terraces because dipping bedrock is bevelled across them. Morphologically, they do have the characteristics of cyropediments, cyroplanation surfaces, or any other type of erosion surface, since over short distances they occur at three distinct elevations. In plan view, they are oriented parallel to glacial meltwater channels, and are mantled in glacial deposits. These deposits are found elsewhere at the site, but over the karst their distribution is sporadic. The deposit is a red weathering, massive, sandy silt with a coarse gravel fraction that comprises about 30% of surface exposures. It is composed of local materials. Many coarse clasts are rounded quartzites of the Katherine Group and range in size from granules to cobbles. There are occasional boulders across the full area of the karst. Striae are rare on clasts in the deposit. The red matrix also incorporates fine grained clastics and carbonates from the Little Dal Group. The deposit is poorly consolidated and is not associated with subglacial or supraglacial landforms. It is therefore not considered a till. Based on its general distribution and characteristics it is interpreted as a fluvio-glacial deposit, and the uplands as kame terraces. Deposition occurred in channels and shallow water bodies at the margin of the Laurentide Ice Sheet. Mountain drainage was diverted to the northwest along this margin and the local materials were deposited by the rerouted Little Keele River. Both the Little Dal and

Katherine Groups outcrop extensively in the headwaters of Little Keele River on the flank of Foran Anticline, only 10 to 15 km southwest of the study site.

8.2.2.2 Upper Sink Zone

This recharge zone is characterized by a terrain of small ridges and shallow depressions and a single large linear trough. The latter feature is a strike-aligned depression called Bear Rock Valley. It meanders from the upper part of North Canyon, south of the North Upland, across Central Canyon and ends in a large sink (Figures 8.2, 8.4). Along most of its length, Bear Rock Valley is developed along or near the contact between the Bear Rock and Hume Formations (Figure 8.3). The average relief is 20 to 30 m and locally approaches 40 m. The northern portion of the valley receives large allogenic inputs from the Uplands and has shallow alluviated sinks linked by overflow channels. Closer to Central Canyon and at its southern end, several sinks and ponors on the floor and southwestern flank of the valley accommodate recharge from the South Upland (Figure 8.4). The morphology at the southern end is similar to that of a blind valley.

Where Central Canyon Stream cuts through Bear Rock Valley, over 30 m of Bear Rock strata are exposed. In that area, the valley bottom is mantled by 1 to 2 m of the fluvioglacial sediment. On the north wall, a 10 m deep tapering fissure is displayed; it is infilled with the deposit. Similar fissures are observed in the Grikeland and Lower Sink Zone. These solutionally enlarged fissures show the presence of a preglacial karst surface of substantial relief. On the south wall of Central Canyon Stream, the Hume Formation pinches out at the northeastern scarp of Bear Rock Valley. Strata below the valley floor are Landry Member, they are deformed and in places subsided in synclinal structures by up to 10 m. The deformation has been propagated upward from the underlying breccia along what appear to be reverse faults. The glacial sediment partially infills the resulting depressions. On the surface, strata exposed on the valley sides show a general cambering toward the valley axis. Dips and strikes are highly variable at the local

scale.

Given the morphology and structure of the feature, it is most probable that Bear Rock Valley developed as a subsidence trough or as a string of subsidence dolines in the contact zone between the Bear Rock and Hume Formations. Alternatively, the feature could have evolved as a blind valley taking allogenic drainage off the Mount Kindle Formation to the west. The orientation of the upper part of the current North Canyon Stream suggests it could have drained into Bear Rock Valley before the postglacial expansion of canyons and disruption of the preglacial karst drainage. Duk-Rodkin (personal communication, 1991) interprets the feature as a subglacial meltwater channel. However, while the presence of sediments indicate it has clearly been utilized by glacial meltwaters, the author argues for a karst origin.

A single large depression with a total relief of 25 m is located north of Bear Rock Valley (Figure 8.4). Within this depression, shallow surface channels direct precipitation to a large ponor near sample point B8. The ponor is a 2 m deep vertical fissure floored by angular debris. There are no overflow channels leading from this depression. Strata within the feature primarily dip to the northeast but there are areas on the perimeter where bedding is cambered toward the ponor and the depression centre. The morphology suggests a solution subsidence origin, with warm based glacial ice scouring the bounding ridges. Elsewhere in the Upper Sink Zone, there are several small dolines and ridges on gently dipping and horizontal strata of the upper Hume Formation. The frequency of small troughs or corridors increases towards Bonus Valley.

8.2.2.3 Grikeland

The lateral expansion of grikes by solution and frost action can generate a topography of intersecting linear depressions and valleys separated by residual bedrock masses. The term corridor or street is applied to mesoscale grikes, box valley is applied to squared valley forms, and platea to large closed depressions. The

resulting landform assemblage is a giant grikeland, corridor karst, or labyrinth karst (Ford and Williams, 1989). The Nahanni Karst described by Brook (1976) and Brook and Ford (1978) is the best example of such terrain developed in cold climates, with individual streets (corridors) exceeding several hundred metres in length and 50 m in depth. That karst is in massive limestones of the Nahanni Formation, which is the southern Mackenzie Mountain equivalent of the Hume Formation. Labyrinth formation is favoured by massive strata, a deep water table, and a long period of erosion.

The Grikeland of the Bonus Lake Karst is a narrow belt of strike-aligned linear corridors, platea, and residual towers found along the crest and upper flanks of the slope above Bonus Valley (Figures 8.2, 8.4). It is developed in massive strata of the upper Hume Formation. The Grikeland straddles a broad monoclinial fold across which there is a change in dip from horizontal and gently dipping strata to values in excess of 20° in the northeast. Tension across the area fractured the Hume Formation and a prominent joint set is developed approximately parallel to strike. Solution and frost action have opened joints. These are gradually enlarged into corridors and platea by solution and rockfall (e.g., Brook and Ford, 1978). Slow mass wasting at the base of slopes preserve the vertical wall form. Scouring by glacial ice and meltwaters have also enlarged the features and removed debris from their bases. In some areas, vertical fissures are infilled with glacial sediments. The lateral continuity of these features and the subsurface relief show they have a preglacial origin.

The largest platea straddles Central Canyon between the Upper and Lower Sink Zones (B7 area: Figure 8.4). The feature is several hundred metres in length and has a maximum depth of 50 m. Sections of its flat bottom are covered by glacial sediments. It is dissected by Central Canyon which has captured much of its drainage. Similar depressions and isolated towers extend to the northwest. In general, the rock walls of these features are steep to vertical with broad talus foots stretching onto platea floors. Frost-solution pinnacles are common on rock walls.

Cave fragments are preserved in the blocks at several locations. The strata that comprise many of the tower blocks are flat lying or dip with the regional trend. However, several coherent blocks show some signs of rotation, dipping at relatively steep and varying angles. This foundering is common in the Lower Sink Zone near Trout Lake (Figure 8.8). It is likely this subsidence is due to the solution of underlying evaporites.

8.2.2.4 Lower Sink Zone

The Lower Sink Zone is an area of corridors, dolines, breached and inundated sinks that occupy the steep slopes above Bonus and Trout Lakes, and a portion of the valley floor (Figures 8.4, 8.5, 8.7, 8.8). Strata dip sharply on the valley flank approaching a maximum of 30°. Downslope and on the floor of Bonus Valley, strata dip more gently. The general morphology of the zone is that of a scabland. The area appears to have been swept by rerouted drainage at the margin of the Laurentide Ice Sheet. A series of corridors or meltwater channels run northward from the area of Twin Bridges Canyon to Bonus Lake. The single largest corridor heads in a breach of Twin Bridges Canyon downstream of B2 (Figure 8.4). Along its course are dolines which give it an undulating long profile (e.g., B3, B4, B25). At its widest point, the corridor includes several dolines that have coalesced. This pattern of dolines or compound depressions occurring within or cutting across corridors is seen elsewhere. The undulating profile along corridor bases contrasts with the flat or gently sloping bottoms of the Grikeland. This is attributed to postglacial deepening of dolines by solution and subsidence within the area. Foundered blocks near Trout Lake are evidence of subsidence accompanying evaporite subsidence (Figure 8.8).

There are several breached and inundated dolines in the area adjacent to Bonus and Trout Lakes (Figures 8.4, 8.7). The lower walls of breached sinks have been eroded by either slope cave development and mass wasting, or by diverted drainage routed through corridors. Some of the breached sinks have been flooded by Bonus and Trout Lakes, and form lobate inlets. Others have been partially

infilled by sediments. Excavations revealed a combination of fluvial and lacustrine materials. Much of the sediment is from aggrading alluvial fans. There are other dolines that probably lie buried beneath this cover. Despite the burial of this portion of the karst, it continues its hydrological function. A sink point was located at the northern end of Bonus Lake and others probably occur in deeper water. This drainage may resurge at the major springs north of Central Fan.

8.2.2.5 Caves

The general characteristics of caves in the study area were discussed in Chapter VI. At the Bonus Lake Site, the Hume Formation supports the best developed solution caves in the region. Cave fragments are found in the Grikeland and Lower Sink Zone. In general, they have a phreatic morphology and are oriented parallel to strike. The longest example has only 80-100 m of passage. Caves occur as fragments in tower, corridor or doline walls, and as composite forms such as archways (Figure 8.5). The positions of many caves are well above the current level of groundwater circulation. However, sediments within them show a period of activity during Late Wisconsinan glaciation. The reddish fluvioglacial deposits seen on the terraces and across the karst are observed to fill several passages. In the largest caves, exploration was limited by these fills. Other caves that cut through small tower blocks or doline walls are sediment-free and may have been developed or enlarged during glaciation.

The caves also provided some insight into the distribution of permafrost at the site. In two caves, hoar frost was encountered within 10-15 m of the entrance where air circulation was restricted by a tight passage. In August of 1991, ice stalactites were located 15 m into a maze cave. There were drips observed at that time. Inner passages tended to be dry and subfreezing.

8.3 Hydrology and Hydrochemistry

A range of hydrological conditions occurred during the periods of fieldwork. Dry

weather in late May and June of 1988 produced low water levels and discharges. Conversely, heavy rains in July of 1991 generated high flows and lake levels in early August of that year. Discharge and conductivity were not continuously monitored at springs and streams. However, spot discharge and hydrochemical measurements were obtained at a variety of locations.

The location of sampling sites are shown on Figures 8.2 and 8.4, and the site characteristics are described in Table 8.1. Physical and chemical data from the study area are presented in Appendix II. For analytical purposes, these data have been organized by sample locations within the karst (Table 8.2). Where data warrant, a water type is defined for each area (Upper and Lower Sink Zones, Grikeland, and Bonus Valley) and flow category (recharge, springs, and streams). The physical characteristics of each water type are outlined in the following sections.

8.3.1 Recharge

Recharge to the karst occurs in the Upper and Lower Sink Zones and Grikeland. During both field seasons, precipitation over these areas was observed to infiltrate readily into soil, regolith, or karst input landforms. At some valley floor locations and doline bases, water collected in shallow channels and depressions before infiltration. At no time were sheetflow or overbank channel flows noted, though the site was not visited during snowmelt.

In both June of 1988 and August of 1991, the Upper Sink Zone was observed to be well drained with little standing water. The exception was a broad level area in Bear Rock Valley just north of Central Canyon that contained small wetlands. Allogenic inputs from the South Upland (e.g., B10, B28) fed sinking streams in Bear Rock Valley (e.g., B9, B11). These streams sustained their flow during the dry period of June 1988 and increased their discharge following rainfall events. The discharge of Upland streams, B10 and B28, were estimated between 4 and 8 L s⁻¹ in early August of 1991. Draining waters in the Upper Sink Zone are referred to as Type 1 waters (Table 8.2).

The Lower Sink Zone and Grikeland have much exposed bedrock and talus, but shallow ponds still persist on the floors of some depressions and corridors. These ponds are usually located against the downslope walls of depressions (e.g., B3, B4, B6, B25). Several are supplied by low discharge springs that issue from talus at the base of the upslope walls (e.g., B5, B12). Other ponds are presumably supplied by the melting of drifted snow and supplemented by summer precipitation (e.g., B6). The latter ponds lost volume over the period of fieldwork in 1988. Across the Lower Sink Zone and Grikeland, all draining ponds are called Type 2 waters (Table 8.2). The elevated temperatures of some ponds suggest that infiltration can occur at a slow rate. The water levels in some dolines fluctuated substantially. The doline at B31 is circular in plan, with a steep conical section. The floor is mantled in regolith. Its lowest wall is 60 m from the southern end of Trout Lake and its floor about 10 m higher. In 1988, water inundated about one third of the doline floor, in 1991 the floor was completely covered. In aerial photographs from the summer of 1974 the doline was drained.

Discharge waters in the Grikeland and Lower Sink Zone consist of small springs (e.g., B22, B5) and spring-fed streams (e.g., B7, B24, B29) (Type 3: Table 8.2). Most of the springs are located in talus beneath steep slopes. Their temperature and hydrochemistry suggest many derive their flow from the suprapermafrost aquifer. Spring discharges are typically $<1 \text{ L s}^{-1}$, and that of the largest stream (B29) only 3 L s^{-1} . Most of these flows are directed to draining ponds located in corridors and dolines. However, some spring-fed streams discharge into canyons (e.g., B7) or to the floor of Bonus Valley (e.g., B24).

8.3.2 Discharge

The canyon streams (Type 4: Table 8.2) drain the non-karst areas southwest of the exposed Hume and Bear Rock Formations. The discharge response to precipitation inputs is rapid and flow variations are flashy. The highest observed discharge was estimated at 500 L s^{-1} in Central Canyon Stream on June 24, 1988. This followed 21

mm of precipitation on the 23rd and 24th. Aerial reconnaissance of the karst on July 28, 1991 showed the canyon streams at a higher flood stage. This occurred after 59 mm of rain over the period July 26 to 28. In the latter event, the streams were highly turbid and traversed the full length of their fans, flowing directly into Bonus Lake, Trout Lake, or Bonus Stream. By August 2, the discharge of Twin Bridges Stream was 30 L s^{-1} , and by August 3, North Canyon Stream was 80 L s^{-1} . The steep discharge decline was accompanied by a concurrent decrease in sediment concentration. Twin Bridges Stream infiltrated into its channel about 50 m below sample point B2, and North Canyon Stream into alluvium in the upper part of its fan. Under average conditions, the canyon streams are characterized by a gradual loss of discharge where they flow through the area of Hume outcrop and infiltrate into their channel beds.

A series of springs are located on the floor of Bonus Valley. Low discharge, cold springs occur on the perimeters of the fans and below steep slopes (e.g., B1, B16, B30; Type 5: Table 8.2). The maximum discharge of this type of spring was 4 L s^{-1} at point B16. At B1 and at B30, there are a series of diffuse springs discharging from alluvium. They are located down gradient of the sinking canyon streams and some of their flow may resurge from those sources. However, their hydrochemistry and slow response to precipitation suggest they are largely independent of those waters.

High discharge springs are also located in Bonus Valley; three such springs and spring-fed streams occur south of Trout Lake. Spring B15 issues from a highly fractured outcrop of the Hume Formation below the Lower Sink Zone. Two discharge estimates from B15 were 100 and 200 L s^{-1} (Table 8.1). It is treated separately in some portions of the data analysis (Type 8: Table 8.2). Two large aggraded springs flow from alluvium of Central Fan. These springs supply the stream channels at points B17 and B18 (Type 6: Table 8.2). They and other springs coalesce to form Bonus Stream which was sampled at B13 and again downstream of North Fan at B26. The spring-fed streams, B17 and B18, varied in discharge

between 50 and 350 L s⁻¹ and together account for much of the flow of Bonus Stream (Table 8.1). On June 21, 1988 the discharge at B13 was estimated at 600 L s⁻¹. The discharge of B15, B17, and B18 were 100, 80, and 50 L s⁻¹ respectively. The total flow of small springs in the area of B16 was approximately 20 L s⁻¹. Thus, between points B17 and B13, Bonus Stream must gain additional flow from unseen springs discharging through the channel bed. The position of the aggraded springs and their hydrochemistry suggest B17 and B18 are a resurgence of Central Canyon Stream and the sinking waters of Bonus Lake.

The water level of Bonus Lake fluctuated about 2 m over the periods of observation. Levels in 1988 were 1.5 m below a prominent trimline on the lake perimeter. Heavy rains in July of 1991 expanded the lake to the full area enclosed by the 520 m depression contour on Figure 8.2, inundating areas of trees on its margin. The level depicted in Figure 8.2 is lower than that recorded in 1988. In that season, Bonus Lake was observed to drain into a drowned sink at its northern end (Figure 8.7). Lake waters flowed into the base of a bedrock wall in a partially buried doline. At lower levels, other sink points must also be active. There were no major springs located on the lake perimeter, though some must issue through either the drowned portion of the Lower Sink Zone or from the margin of Twin Bridges Fan. The level of Trout Lake was consistent through the fieldwork. During periods of high flow at B15, B17, and B18 there were corresponding increases in the downstream discharge of Bonus Stream. In early August of 1991, the discharge of Bonus Stream (B26) was between 900 and 1100 L s⁻¹. The gain indicates further inputs to Bonus Stream from a resurgence of North Canyon Stream and other aggraded springs.

8.3.3 Stable Isotopes

Measurements of $\delta^{18}\text{O}$ were done for most of the samples collected in June of 1988. In addition, $\delta^{18}\text{O}$ and δD were determined for seven samples collected in August, 1991. There is little variance in $\delta^{18}\text{O}$ between water types. Averages show several

water types have similar values, only canyon flows and low discharge valley springs differ from the overall mean (Table 8.3). Recharge waters (sinking streams and ponds) of the Upper and Lower Sink Zones and Grikeland (Types 1 and 2) have an average $\delta^{18}\text{O}$ value of -21.09‰ . The figure for springs and streams of the Lower Sink Zone and Grikeland (Type 3) is -21.33‰ . High discharge springs and streams in Bonus Valley (Types 6 and 8) have a value of -21.41‰ , and Bonus and Trout Lakes -21.15‰ (Type 7). The canyon streams (Type 4) are the heaviest at -20.57‰ and the low discharge valley bottom springs (Type 5) the lightest at -22.11‰ .

Most of these samples date from June, when isotopically light meltwaters from snow and ground ice would comprise a significant portion of the recharge and discharge. August samples are approximately 0.5 to 1 ‰ heavier than their June counterparts, suggesting a dominance of summer precipitation at that time. The general pattern shows Bonus and Trout Lakes, and the major springs (e.g., B15) and spring-fed streams (e.g., B17, B18) have signatures very similar to that of the recharge waters (Types 1, 2, and 3). The lower value from the canyon streams (Type 4) may reflect the characteristics of those basins. These streams respond quickly to inputs and thus more closely resemble the isotopic value of summer precipitation. The low discharge springs (Type 5) flow from alluvium or talus and may receive meltwaters from the active layer for much of the summer period.

The $\delta^{18}\text{O}$ and δD data from the 1991 samples plot very closely to the local and Fort Smith meteoric water lines (Figure 8.9). Most of these samples were collected between August 2 and 4 on the recessional limb of a major discharge peak. Recharge waters (B11 and B25) from the Sink Zones and discharge from the canyon streams (B2 and B27) plot in a cluster. Two readings from Bonus Stream (B17 and B26) are slightly heavier, indicating inputs of isotopically heavier spring and lake water.

Stable isotope values from Bonus Lake water differ substantially from Dodo Canyon discharge samples, they are heavier and more closely resemble that of summer precipitation. At the Dodo Canyon Site, there is a substantial delay between

recharge and discharge. The heavier Bonus Lake values and the concordance between recharge and discharge suggest circulation through the Bonus Lake aquifer is rapid. Outcrops of the Hume Formation show well developed cavernous porosity, supporting the view of a conduit aquifer.

8.3.4 Hydrochemical Facies

All sampled waters at the Bonus Lake Site have a calcium bicarbonate facies but there is some diversity in composition (Figure 8.10). Samples from the Upper and Lower Sink Zones, and Grikeland (Types 1, 2, and 3) are dominated by Ca^{2+} and HCO_3^- , and have low amounts of Mg^{2+} . Canyon streams (Type 4) have more Mg^{2+} and SO_4^{2-} , and the spring, stream, and lake waters of Bonus Valley have some Cl^- and Na^+ . While the facies vary little through the system, there are changes in concentration. Magnesium, calcium, and total hardness all increase between the Sink Zones and Bonus Valley (Figure 8.11). This increase is most marked with magnesium hardness. The modal concentration for Sink Zone and Grikeland waters (Types 1, 2, and 3) lies in the range 0 to 6 mg L^{-1} CaCO_3 (Figure 8.11). The same figure for Canyon and Bonus Valley waters (Types 4 to 8) is 24 to 30 mg L^{-1} CaCO_3 . Calcium hardness increases from a mean of 85 mg L^{-1} CaCO_3 in the Sink Zones to 99 mg L^{-1} CaCO_3 in Bonus Valley.

Mean values of temperature, conductivity, pH, ion concentrations, $p\text{PCO}_2$, $\text{Ca}^{2+}/\text{Mg}^{2+}$, and saturation indices of calcite and dolomite are presented for each water type in Table 8.4. The ion concentration data are plotted in Figure 8.12. The relationships between $p\text{PCO}_2$ and calcite saturation index and total hardness are shown in Figures 8.13 and 8.14. The sections that follow describe these data for each water type.

8.3.4.1 Sink Zones and Grikeland

Samples from the Upper Sink Zone (Type 1) include allogenic streams off the South Upland, and sinking waters in Bear Rock Valley and the depression at B8. This

water type has the lowest mean total hardness ($89 \text{ mg L}^{-1} \text{ CaCO}_3$) and TDI values (3.46 meq L^{-1}) across the karst. Ion abundances are $\text{Ca}^{2+} > \text{Mg}^{2+} \gg \text{Na}^+$ and $\text{HCO}_3^- \gg \text{SO}_4^{2-} > \text{Cl}^-$ by equivalence. The concentrations of Na^+ , Cl^- , and SO_4^{2-} are low, with Ca^{2+} and HCO_3^- comprising 91% of the ion load (Table 8.4, Figure 8.12). Samples off the Upland have higher concentrations of Mg^{2+} (e.g., B9, B10) reflecting contact with the Bear Rock Formation. Two Upland samples (Table A2: BL88-10 and BL88-11) had high ion balance errors and were excluded from the calculations (Table 8.4, Figure 8.12). Upper Sink Zone waters are aggressive to calcite and dolomite ($\text{SI}_C = -0.40$; $\text{SI}_D = -1.79$) and the $p\text{PCO}_2$ value of 3.07 shows CO_2 enrichment in the soil zone. The temperature (3.9°C), hydrochemistry, and flow behaviour indicates these are suprapermafrost waters that are restricted in their circulation to the glacial cover and the fractured uppermost portions the Bear Rock and Hume Formations. Recharge in this zone mainly occurs at dolines in the Hume Formation and represents significant solvent potential due to the undersaturated state of these waters.

Water samples of the Lower Sink Zone and Grikeland were collected from draining ponds (Type 2) and from springs and spring-fed streams (Type 3). The total hardness and TDI values of the pond waters ($97 \text{ mg L}^{-1} \text{ CaCO}_3$ and 3.88 meq L^{-1}) are similar to the Upper Sink Zone. Ion abundances are $\text{Ca}^{2+} > \text{Mg}^{2+} \gg \text{Na}^+$ and $\text{HCO}_3^- \gg \text{Cl}^-$ by equivalence. The pond temperatures were high (average = 14.5°C) and saturated with respect to calcite ($\text{SI}_C = 0.5$), $p\text{PCO}_2$ values are close to atmospheric (3.31).

Springs and spring-fed streams have an average total hardness of $113 \text{ mg L}^{-1} \text{ CaCO}_3$ and TDI of 4.42 meq L^{-1} . Ion abundances are $\text{Ca}^{2+} \gg \text{Mg}^{2+} > \text{Na}^+$ and $\text{HCO}_3^- \gg \text{SO}_4^{2-}$ by equivalence, with 94% total dissolved ions composed of Ca^{2+} and HCO_3^- . Concentrations of the latter ions are higher than those in recharge samples or canyon streams (Figure 8.12). The hydrochemical facies, low temperature (2.9°C), high $\text{Ca}^{2+}/\text{Mg}^{2+}$ ratio (13.9), and near equilibrium value of the calcite saturation index ($\text{SI}_C = 0.05$) suggests these waters are discharge from a suprapermafrost aquifer in the

upper Hume Formation.

8.3.4.2 Canyon Streams

Canyon streams (Type 4) have an average total hardness of 110 mg L⁻¹ CaCO₃ and a TDI of 4.43 meq L⁻¹. Ion abundances are Ca²⁺>Mg²⁺>>Na⁺ and HCO₃⁻>SO₄²⁻>Cl⁻ by equivalence. While the hardness and TDI values are similar to those of discharge waters of the Lower Sink Zone, the concentrations of Ca²⁺ and HCO₃⁻ are lower (Table 8.4; Figure 8.12). The higher concentrations of Mg²⁺ and SO₄²⁻ and a Ca²⁺/Mg²⁺ ratio of 3.1 indicate contact with dolomite and gypsum. The canyon stream basins are in the Mount Kindle and Franklin Mountain Formations, with intervals of the Brecciated Member of the Bear Rock Formation exposed in the canyons. Runoff from these units has produced a facies that differs from that of the Sink Zones (Figure 8.10). These streams are thought to be largely suprapermafrost waters but additional intra- and subpermafrost flows must circulate through the Bear Rock Formation and discharge into the canyons.

8.3.4.3 Bonus Valley

Recharge to the Sink Zones is thought to discharge on the floor of Bonus Valley. Four water types were sampled in Bonus Valley. Each of these have ion abundances of Ca²⁺>Mg²⁺>Na⁺ and HCO₃⁻>SO₄²⁻>Cl⁻ by equivalence. The recorded Na⁺ and Cl⁻ concentrations are above the trace levels seen in the Sink Zones and Canyons (Table 8.4; Figure 8.10, 8.12). The presence of Na⁺ and Cl⁻ suggests that a deep flow component mixes with the groundwaters circulating through the Hume and Bear Rock Formations.

The low discharge, cold springs (Type 5) have the highest total hardness and TDI values across the karst, 159 mg L⁻¹ CaCO₃ and 6.45 meq L⁻¹. These waters are aggressive to both calcite and dolomite (SI_C = -0.22, SI_D = -1.19), were the most enriched in CO₂ (pPCO₂ = 2.58), and have the lowest δ¹⁸O values (-22.1 ‰). They were sampled at fan margins and the valley floor. These springs were less

responsive to precipitation inputs than the high discharge springs and streams. Their characteristics suggest they represent discharge from a mix of flow components including possible resurgence from canyon or Lower Sink Zone streams, local supra- and intrapermafrost discharge, and a diffuse deeper circulating groundwater.

A single high discharge, cold spring flows from an outcrop of the Hume Formation (B15: Type 8). The spring has a total hardness of $120 \text{ mg L}^{-1} \text{ CaCO}_3$ and a TDI of 5.43 meq L^{-1} . It has the highest concentrations of Mg^{2+} , Na^+ , and Cl^- (0.76 , 0.43 , 0.33 meq L^{-1} , respectively) and the lowest $\text{Ca}^{2+}/\text{Mg}^{2+}$ ratio (2.1). B15 is near equilibrium with respect to calcite ($\text{SI}_C = -0.14$) and aggressive towards dolomite ($\text{SI}_D = -0.71$). Its discharge fluctuated markedly with precipitation. These characteristics suggest B15 is a subpermafrost spring, discharging groundwaters that are likely recharged in the Upper Sink Zone through dolines in the Hume and Bear Rock Formations. The high concentration of Mg^{2+} indicate circulation through the Bear Rock and into the dolomites of the Mount Kindle Formation. The Na^+ and Cl^- may have an origin in the underlying Saline River Formation but the cold temperature (2.6°C) suggests little of the flow is contributed by deep thermal groundwaters. It is likely that similar aggraded or drowned springs discharge into Bonus or Trout Lakes and alluvium of the canyon fans.

Bonus Lake (Type 7) takes flow from Twin Bridges Canyon (Type 4), low discharge cold springs (Type 5), aggraded springs (Type 8?), and direct precipitation. Bonus Stream (Type 6) takes flow from water Types 4, 5, and 8 and the resurgence from Bonus Lake. The lake samples have a mean total hardness of $112 \text{ mg L}^{-1} \text{ CaCO}_3$ and TDI of 5.02 meq L^{-1} . The same data from Bonus Stream (Type 6) are $127 \text{ mg L}^{-1} \text{ CaCO}_3$ and 5.50 meq L^{-1} . The main differences between these waters are their temperatures, $p\text{PCO}_2$, and saturation indices. Bonus Streams' temperature is similar to that of the canyon streams (8.3°C) and it was also undersaturated with respect to dolomite ($\text{SI}_D = -0.55$). Lake waters have higher temperatures (18.1°C), are saturated with respect to both calcite and dolomite ($\text{SI}_C = 0.38$, $\text{SI}_D = 0.22$), and have near atmospheric $p\text{PCO}_2$ (3.33).

8.4 Summary

At the Bonus Lake Site, karst landforms occur on solution breccia and limestone of the Bear Rock and Hume Formations. Depression forms include linear troughs, corridors, plateaus, and single and compound dolines. The linear depressions are cross cut by sharply incised river canyons and meltwater channels. Glacial sediments infill karst features including relict caves and subsoil grikes. These relationships show elements of the karst predate glaciation and fluvial incision. However, modern karstification proceeds despite the presence of permafrost. Recent subsidence is marked by deep conical dolines in corridor floors and foundered blocks.

The hydrochemistry and flow behaviour of recharge, canyon, and discharge waters vary across the karst. Recharge waters are of low hardness and TDI. Many samples were aggressive to calcite and dolomite (Type 1). Before infiltration through input landforms, circulation is limited to the suprapermafrost aquifer. The canyon streams drain the higher elevation areas and react rapidly to precipitation. Most of their flow has a suprapermafrost origin but there is also a subpermafrost contribution that contains SO_4^{2-} from the Bear Rock Formation. At high stage, they are aggressive but do not completely infiltrate into the karst. Most of the discharge samples of Bonus Valley are close to equilibrium with respect to calcite and aggressive towards dolomite. Bonus Stream and the subpermafrost springs have a calcium bicarbonate hydrochemistry with minor amounts of SO_4^{2-} , Na^+ , and Cl^- ions. This indicates solution at the site occurs primarily in limestone and the deep groundwater contributions from subjacent anhydrite and halite is minimal in comparison to the Dodo Canyon Site.

Aggressiveness and total hardness are strongly influenced by $p\text{PCO}_2$ (Figures 8.13, 8.14). Discharge waters of Bonus Valley (Types 5, 6, 7, 8), and waters of the Lower Sink Zone (Types 2, 3) show decreases in the calcite saturation index with higher partial pressures of CO_2 (Figure 8.13). Canyon streams (Type 4) were aggressive when in flood stage, while recharge waters of the Upper Sink Zone (Type 1) were aggressive despite low $p\text{PCO}_2$ values. All water types show increased

hardness with higher partial pressures of CO₂ (Figure 8.14).

The physical properties of the aquifer feeding the springs and streams of Bonus Valley differ from those described from the Dodo Canyon Site. Several lines of evidence suggest that conduit porosity characterizes the aquifer at the Bonus Lake Site. Relict conduits are common in exposures of the Hume Formation. Conduits could also extend into the Bear Rock Formation. At Bonus Lake, this formation is less brecciated and contains little terrigenous material. Point recharge landforms occur across the Sink Zones. At low stage, the canyon streams infiltrate into alluvium above the Hume Formation. Bonus Lake sinks into a drowned doline. High discharge springs flow from alluvium and bedrock. Precipitation inputs are translated quickly to spring points. Hydrochemical data show minor contributions from evaporites, and $\delta^{18}\text{O}$ values are similar to those of summer precipitation. These data support a model of rapid, shallow circulation through a conduit aquifer in the Hume and Bear Rock Formations.

Table 8.1: Description of water sampling locations at the Bonus Lake Site.

Location	Description	Sample Dates
B1	Spring from gravels of Twin Bridges Fan. $Q_1 = 0.5 \text{ L s}^{-1}$, $Q_2 = 0.5 \text{ L s}^{-1}$.	150688 230688
B2	<i>Twin Bridges Stream</i> . Sampled above Arch. $Q_1 < 1 \text{ L s}^{-1}$, $Q_2 \approx 30 \text{ L s}^{-1}$.	150688 020891
B3	Slow draining pond in doline.	150688
B4	Slow draining pond in large doline.	150688
B5	Springs from base of talus slope. $Q < 1 \text{ L s}^{-1}$.	150688
B6	Slow draining pond in gravel.	150688
B7	Small spring-fed stream draining to Central Canyon. $Q \approx 1 \text{ L s}^{-1}$.	180688
B8	Sinking stream sampled in large depression above ponor. $Q < 1 \text{ L s}^{-1}$.	180688
B9	Sinking stream in Bear Rock Valley above ponor. $Q_1 \approx 0.5 \text{ L s}^{-1}$, $Q_2 \approx 3 \text{ L s}^{-1}$.	180688 070891
B10	Stream coming off South Upland. $Q \approx 8 \text{ L s}^{-1}$.	180688
B11	Sinking stream in Bear Rock Valley, just below Hume Scarp. $Q_1 \approx 8 \text{ L s}^{-1}$, $Q_2 \approx 2 \text{ L s}^{-1}$, $Q_3 \approx 5 \text{ L s}^{-1}$.	180688 040891 070891
B12	Small springs at foot of talus below cliff. $Q \approx 2 \text{ L s}^{-1}$.	180688
B13	<i>Bonus Stream</i> . Sampled above Trout Lake. $Q \approx 600 \text{ L s}^{-1}$.	210688
B14	<i>Trout Lake</i> .	210688
B15	Large cold spring from the Hume Formation. $Q_1 \approx 100 \text{ L s}^{-1}$, $Q_2 \approx 200 \text{ L s}^{-1}$.	210688 030891
B16	Small spring north of B15. $Q \approx 4 \text{ L s}^{-1}$.	210688
B17	<i>Bonus Stream</i> . Sampled below main resurgence point. $Q_1 \approx 80 \text{ L s}^{-1}$, $Q_2 \approx 350 \text{ L s}^{-1}$, $Q_3 \approx 300 \text{ L s}^{-1}$.	210688 030891 090891
B18	<i>Bonus Stream</i> . Sampled north resurgence. $Q_1 \approx 50 \text{ L s}^{-1}$, $Q_2 \approx 250 \text{ L s}^{-1}$.	210688 090891
B19	<i>Bonus Lake</i> . Sampled at Sink Inlet.	230688
B20	<i>Bonus Lake</i> . Sampled at Oil Drum Inlet.	230688
B21	<i>Bonus Lake</i> . Sampled at Bear Beach.	230688
B22	Small springs feeding B7. Flow is from talus foot. $Q_1 \approx 1 \text{ L s}^{-1}$, $Q_2 \approx 2 \text{ L s}^{-1}$.	240688 070891
B23	<i>Central Canyon Stream</i> . Sampled above Central Fan. $Q \approx 500 \text{ L s}^{-1}$.	240688
B24	Small spring-fed stream from Horseshoe Sink near base camp. $Q \approx 1 \text{ L s}^{-1}$.	240688
B25	Sinking water in pond below spring B5.	020891
B26	<i>Bonus Stream</i> . $Q_1 \approx 1.1 \text{ m}^3 \text{ s}^{-1}$, $Q_2 \approx 0.9 \text{ m}^3 \text{ s}^{-1}$.	030891 090891
B27	<i>North Canyon Stream</i> . Sampled at fan apex. $Q \approx 80 \text{ L s}^{-1}$.	030891
B28	Small stream off South Upland. $Q \approx 4 \text{ L s}^{-1}$.	070891
B29	Small surface stream draining to Trout Lake. $Q \approx 3 \text{ L s}^{-1}$.	090891
B30	Spring at the margin of North Fan. $Q \approx 3 \text{ L s}^{-1}$.	090891
B31	Fluctuating pond in large doline, draining at time of sampling.	090891

Table 8.2: Grouping of water samples from the Bonus Lake Site on the basis of their location.

Type	Description	Locations
1	Recharge waters in Upper Sink Zone	B8, B9, B10, B11, B28
2	Recharge waters in Lower Sink Zone and Grikeland	B3, B4, B6, B25, B31
3	Springs and streams in Lower Sink Zone and Grikeland	B5, B7, B12, B22, B24, B29
4	Streams in Canyons	B2, B23, B27
5	Low discharge springs in valley bottom	B1, B16, B30
6	High discharge streams in valley bottom	B13, B17, B18, B26
7	Bonus and Trout Lakes	B14, B19, B20, B21
8	Location B15: High discharge spring in valley bottom	B15

Table 8.3: $\delta^{18}\text{O}$ of water samples from the Bonus Lake Site (in ‰).

Location	Date	$\delta^{18}\text{O}$	Location	Date	$\delta^{18}\text{O}$
Recharge waters: Upper and Lower Sink Zones			Low discharge springs in valley bottom		
B3	150688	-21.93	B1	150688	-22.55
B4	150688	-21.57	B16	210688	-22.05
B6	150688	-20.81	B1	230688	-22.26
B8	180688	-20.91	B30	090891	-21.57
B9	180688	-21.22		AVG	-22.11
B10	180688	-21.15	High discharge springs and streams in valley bottom		
B11	180688	-21.18	B13	210688	-21.67
B25	020891	-20.75	B15	210688	-21.96
B11	040891	-20.33	B17	210688	-21.53
	AVG	-21.09	B18	210688	-21.68
Springs and streams in Lower Sink Zone and Grikeland			B17	030891	-20.93
B5	150688	-22.16	B26	030891	-20.69
B7	180688	-21.14		AVG	-21.41
B12	180688	-21.73	Streams in Canyons		
B22	240688	-20.88	B2	150688	-21.09
B24	240688	-20.75	B23	240688	-20.24
	AVG	-21.33	B2	020891	-20.49
Streams in Canyons			B27	030891	-20.48
B2	150688	-21.09		AVG	-20.57
B23	240688	-20.24	Lakes		
B2	020891	-20.49	B14	210688	-21.37
B27	030891	-20.48	B19	230688	-20.95
	AVG	-20.57	B21	230688	-21.13
				AVG	-21.15

Table 8.4: Mean temperature, conductivity, pH, total hardness, ion concentrations, total dissolved ions, Ca²⁺/Mg²⁺ ratio, saturation indices (calcite and dolomite), and pPCO₂ for water samples at the Bonus Lake Site.

Type	Temp	SPC	pH	THd	Ca ²⁺	Mg ²⁺	HCO ₃ ⁻	SO ₄ ²⁻	Na ⁺	Cl ⁻	TDI	C/M	SI _c	SI _d	pPCO ₂	n
1: Recharge, Upper Sink Zone	3.9	168	7.85	89	1.57	0.20	1.57	0.06	0.03	0.03	3.46	7.9	-0.40	-1.79	3.07	6 (4)
2: Recharge, Lower Sink Zone	14.5	166	8.29	97	1.68	0.25	1.88	0.00	0.04	0.03	3.88	6.7	0.50	-0.51	3.31	5 (3)
3: Springs and Streams, LSZ	2.9	174	8.14	113	2.08	0.15	2.09	0.09	0.01	0.00	4.42	13.9	0.05	-1.53	3.21	7 (5)
4: Streams in Canyons	9.9	186	8.08	110	1.66	0.54	1.67	0.50	0.03	0.03	4.43	3.1	-0.08	-0.71	3.21	4 (4)
5: Low Q Springs, Bonus Valley	3.9	252	7.75	159	2.60	0.58	2.72	0.27	0.15	0.13	6.45	4.5	-0.22	-1.19	2.58	4 (3)
6: High Q Streams, Bonus Valley	8.3	231	7.95	127	1.99	0.54	2.16	0.38	0.23	0.20	5.50	3.7	0.03	-0.55	2.98	8 (4)
7: Bonus and Trout Lakes	18.1	241	8.33	112	1.81	0.43	1.87	0.41	0.29	0.21	5.02	4.2	0.38	0.22	3.33	4 (4)
8: High Q Spring: Location B15	2.6	183	8.05	120	1.63	0.76	2.03	0.25	0.43	0.33	5.43	2.1	-0.14	-0.71	3.07	2 (1)

Temp: temperature in °C; SPC: specific electrical conductivity, expressed to 25 °C, in μS cm⁻¹; THd: Total Hardness in mg L⁻¹ CaCO₃; Ion concentrations reported in meq L⁻¹; C/M: Ca²⁺/Mg²⁺ ratio; SI_c: Saturation index for calcite; SI_d: Saturation index for dolomite; pPCO₂: -log of partial pressure of CO₂; n: number of cases, figure in brackets is number of cases for which Na⁺, Cl⁻, and SO₄²⁻ were measured.

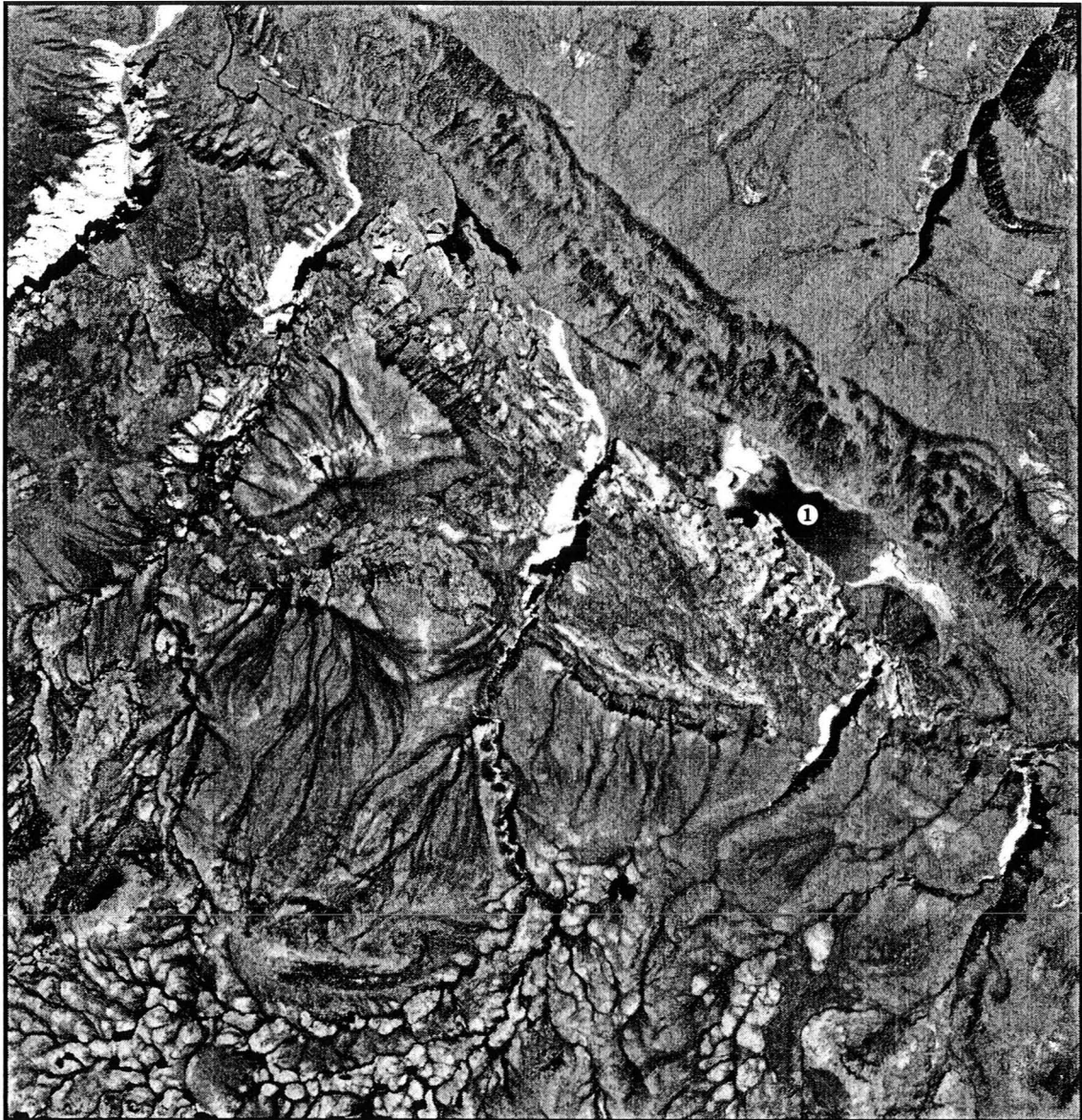


Figure 8.1: Vertical aerial photograph of the Bonus Lake Site. The average scale is 1:60,000. The top of the photograph is north. The terrain is dominated by a broad, gently sloping upland dissected by river canyons and glacial meltwater channels. Bonus Lake (①) lies in a spillway that extends from Little Bear River to Carcajou Canyon (Figure 5.6). This spillway is called Bonus Valley. Strata dip to the northeast in a monocline. Clastics of the Hare Indian, Canol, and Imperial Formations lie on the northeastern flank of Bonus Valley. A belt of dolines and depressions occurs on the southwestern flank. These karst features are in the Hume Formation. The Bear Rock Formation outcrops in the southern portions of the sharp canyons that cut across the doline karst. Much of the outcrop of the Bear Rock and Mount Kindle Formations are mantled by a veneer of lacustrine and fluvial deposits of glacial origin. These deposits locally form terraces (NAPL A24224-105).

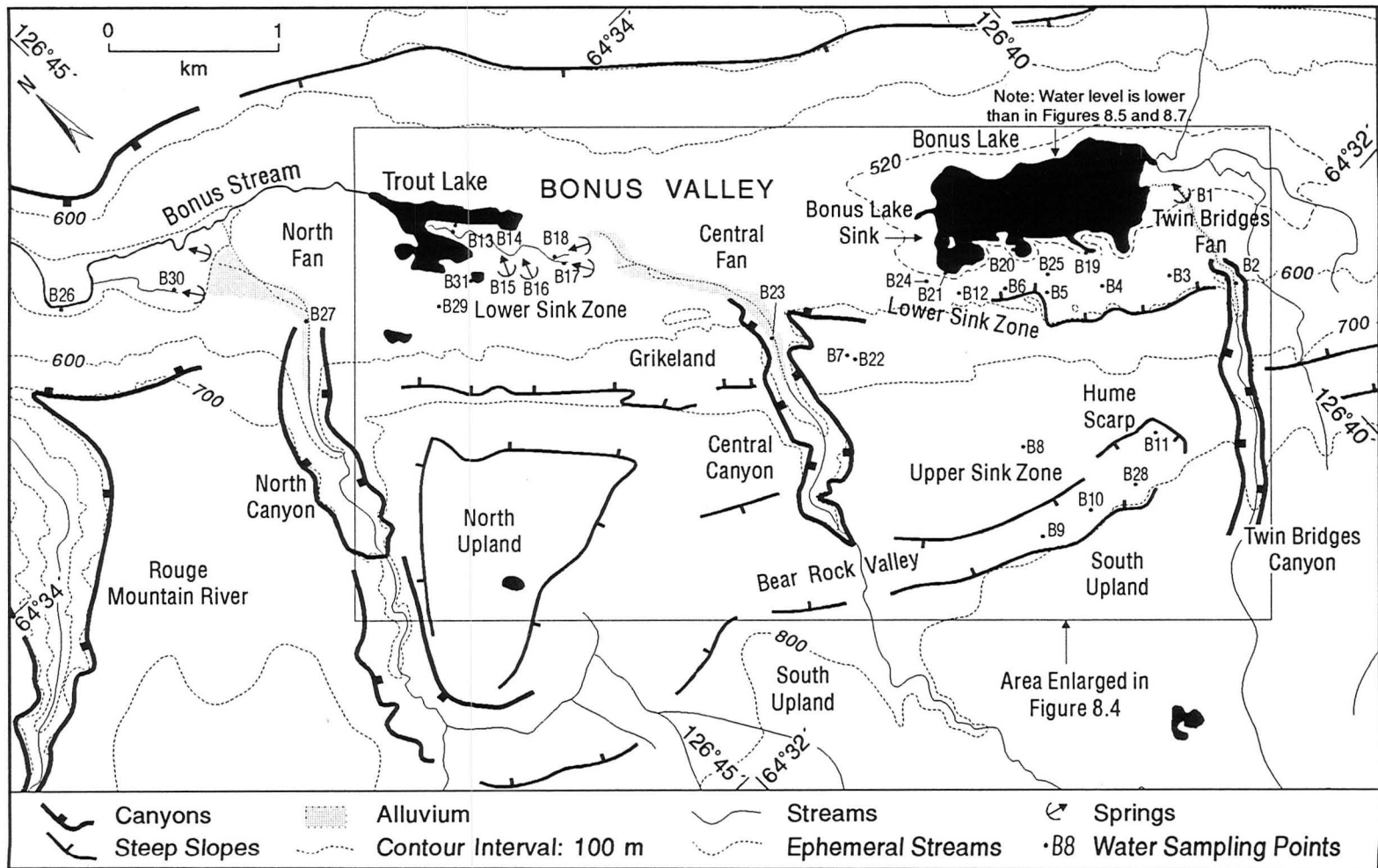


Figure 8.2: Map of the Bonus Lake Site. The main area of karst is southwest of Bonus and Trout Lakes between North and Twin Bridges Canyons. That region is divided into Upland, Upper and Lower Sink Zones, Grikeland, and discharge. The Uplands are high elevation areas mantled by glacial deposits. The Upper Sink Zone is an area of large depressions in the Hume and Bear Rock Formations. The Lower Sink Zone has deep dolines in steep, rugged terrain. The Grikeland is a zone of large, strike-aligned towers that are separated by corridors. The floor of Bonus Valley is a discharge area. Bonus Lake is largely fed by subaqueous springs and drains into a drowned doline at its northern end. Major springs located north of Central Fan discharge from alluvium (B17, B18) and bedrock (B15). Additional springs flow from North Fan (B30).

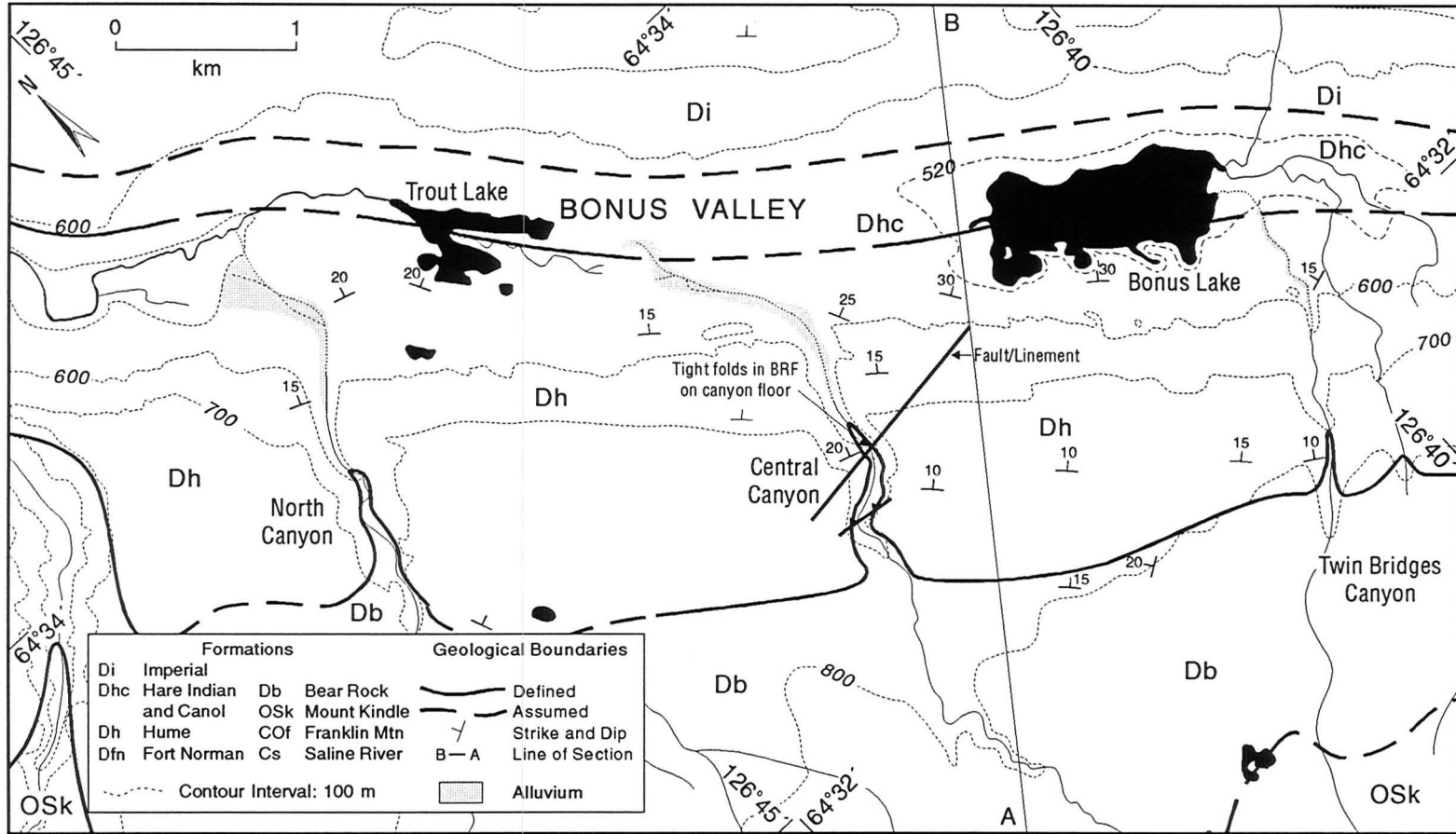
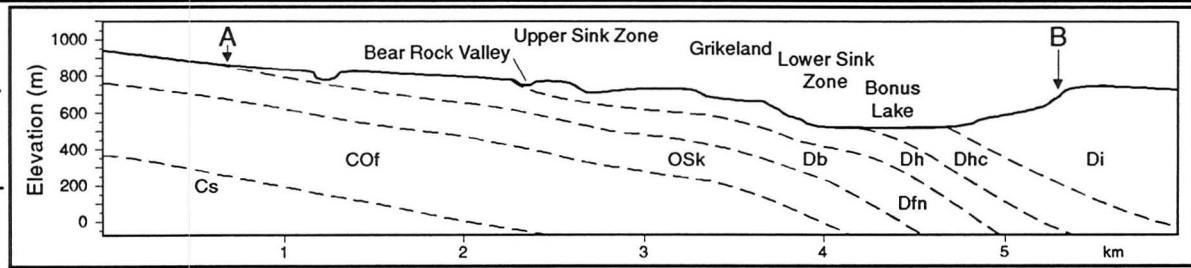


Figure 8.3: Geology of the Bonus Lake Site. Karst occurs on the Hume Formation on the northeastern dipping limb of a monocline (geology from field observations and after Aitken and Cook, 1974).



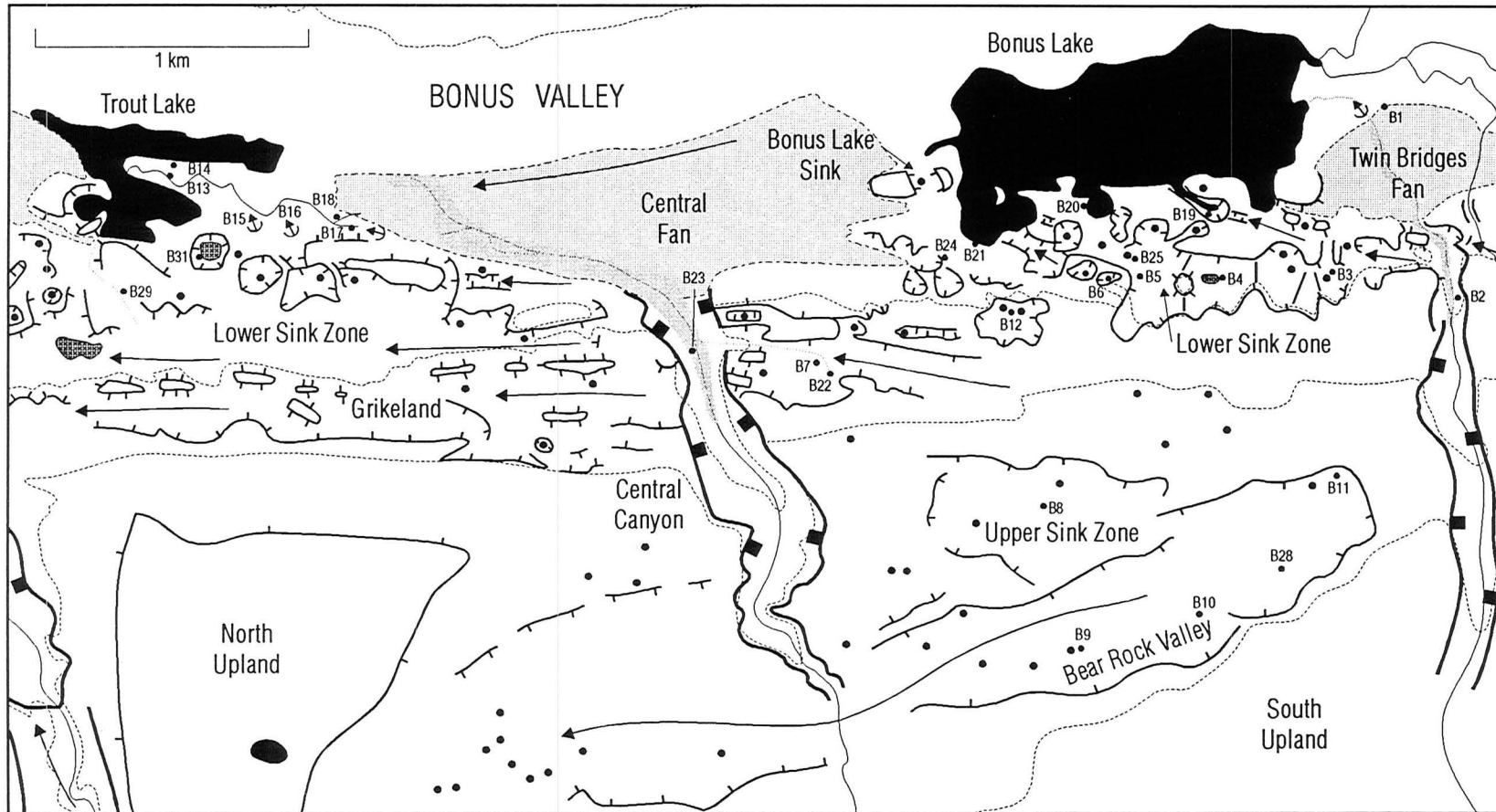
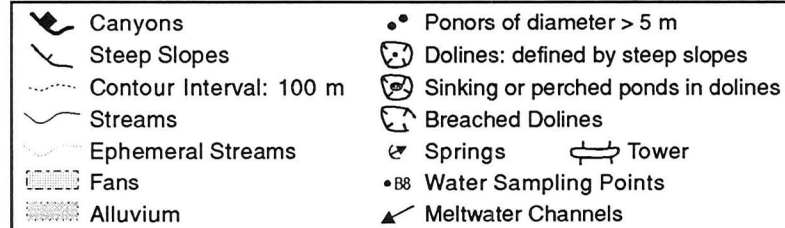


Figure 8.4: Karst geomorphology of the core area of the Bonus Lake Site. The Upper Sink Zone is a recharge area of shallow dolines and depressions. The Grikeland is an area of corridors and tower forms. The Lower Sink Zone has corridors, compound depressions and breached sinks. Infilled and drowned dolines extend onto the floor of Bonus Valley. Springs discharge from the alluvium of the fans and at the base of the Lower Sink Zone.



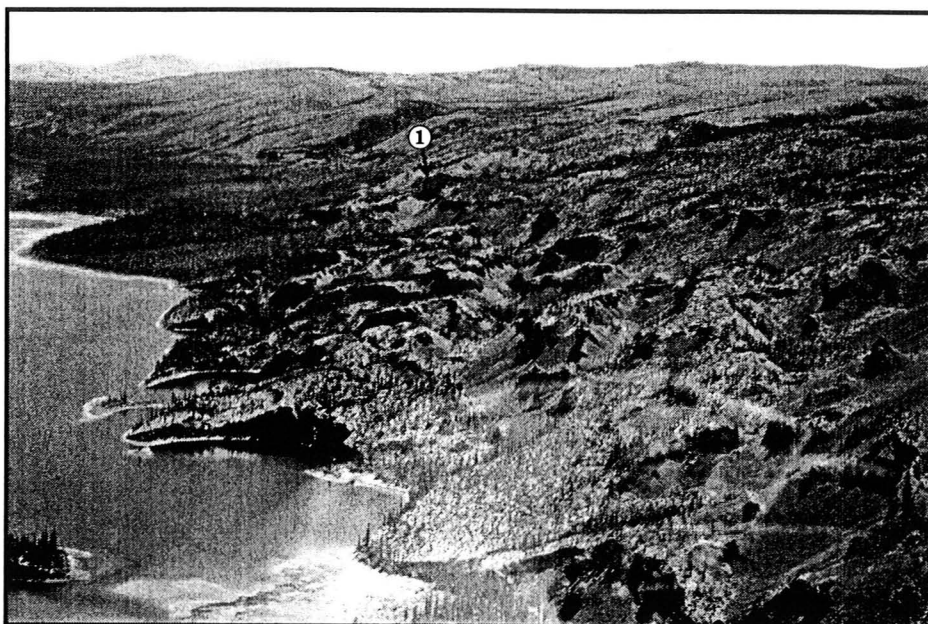


Figure 8.5: View of the Lower Sink Zone southwest of Bonus Lake. The photograph runs the full length of the lake. The Hume Formation is exposed throughout the area and dips sharply to the northeast. Partially drowned and buried dolines occur along the lake margin. Deep collapse dolines and linear rock walled depressions are on the sloping ground. The marker ① is the Arch.

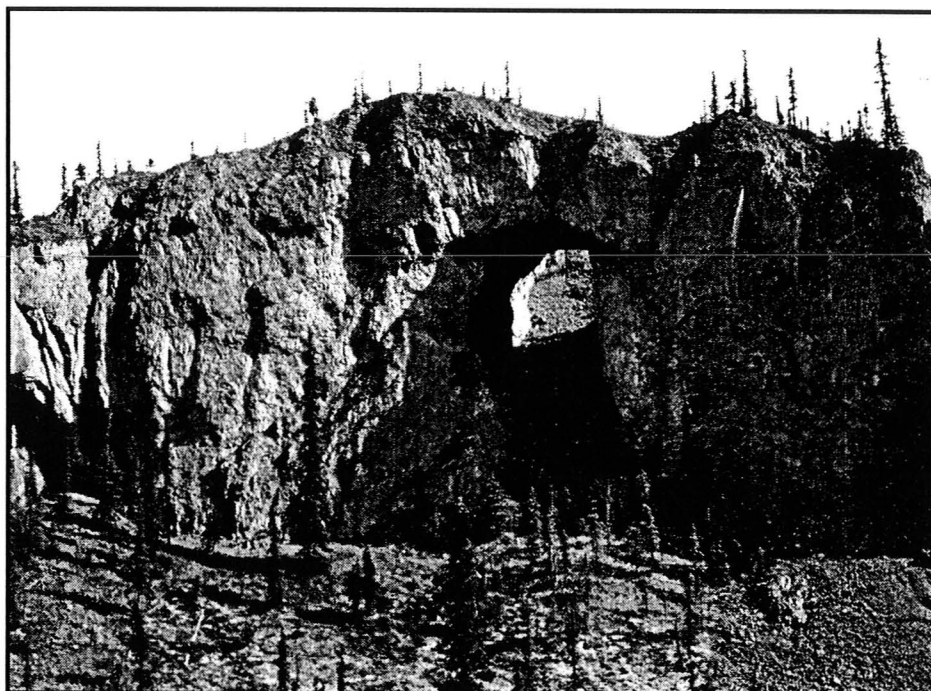


Figure 8.6: Natural bridge exposed on the southern wall of Twin Bridges Canyon, the feature is called the Arch. It is the largest of several natural arches at the site. The rock wall has a height of approximately 20 m. This and other features are fragments of a dissected strike-aligned conduit system.



Figure 8.7: View of the northwestern end of Bonus Lake. In the foreground is a large doline infilled with alluvial and lacustrine sediments. A second doline at the top of the photograph is drowned by Bonus Lake. At the water level shown, the lake drains into the rock wall of the drowned doline at the marker ①.



Figure 8.8: View of the western end of Trout Lake showing three blocks of the upper Hume Formation. Each block represents the same interval of strata. From left to right, the strata dip to the NE, E, and NNW. This variation is due to subsidence and collapse in the underlying Bear Rock Formation.

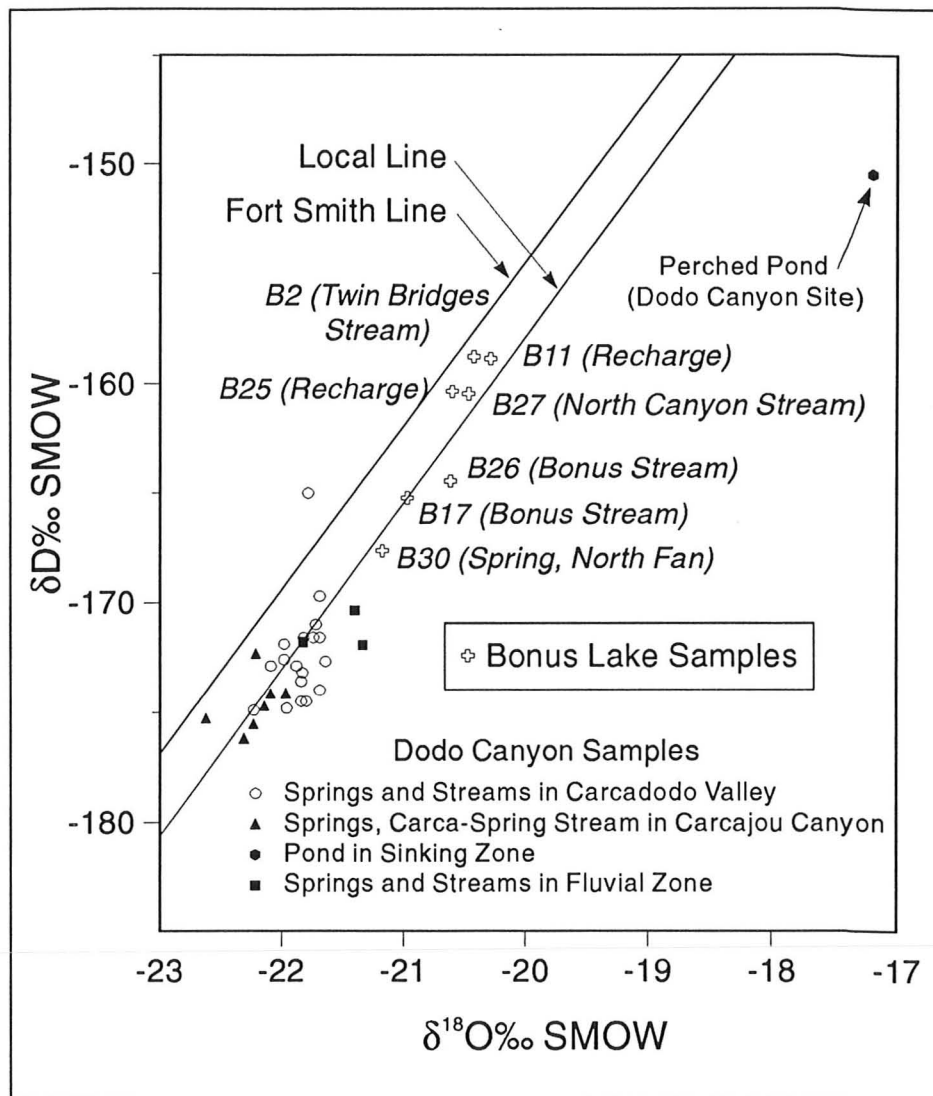


Figure 8.9: Isotope samples from the Bonus Lake Site plotted with the local and Fort Smith meteoric water lines. Data from the Dodo Canyon Site are also shown. All but one of the Bonus Lake samples were collected between August 2nd and 4th, 1991; B30 was sampled on August 9, 1991. The Dodo Canyon samples are from mid to late August of 1991. The graph shows waters of the Bonus Lake Site are meteoric in origin and are isotopically heavier than discharge waters of the Dodo Canyon Site. Recharge (B25, B11) and canyon stream (B2, B27) samples have the highest $\delta^{18}\text{O}$ and δD values, Bonus Stream values are lower. This pattern is consistent with data from 1988 (Table 8.3).

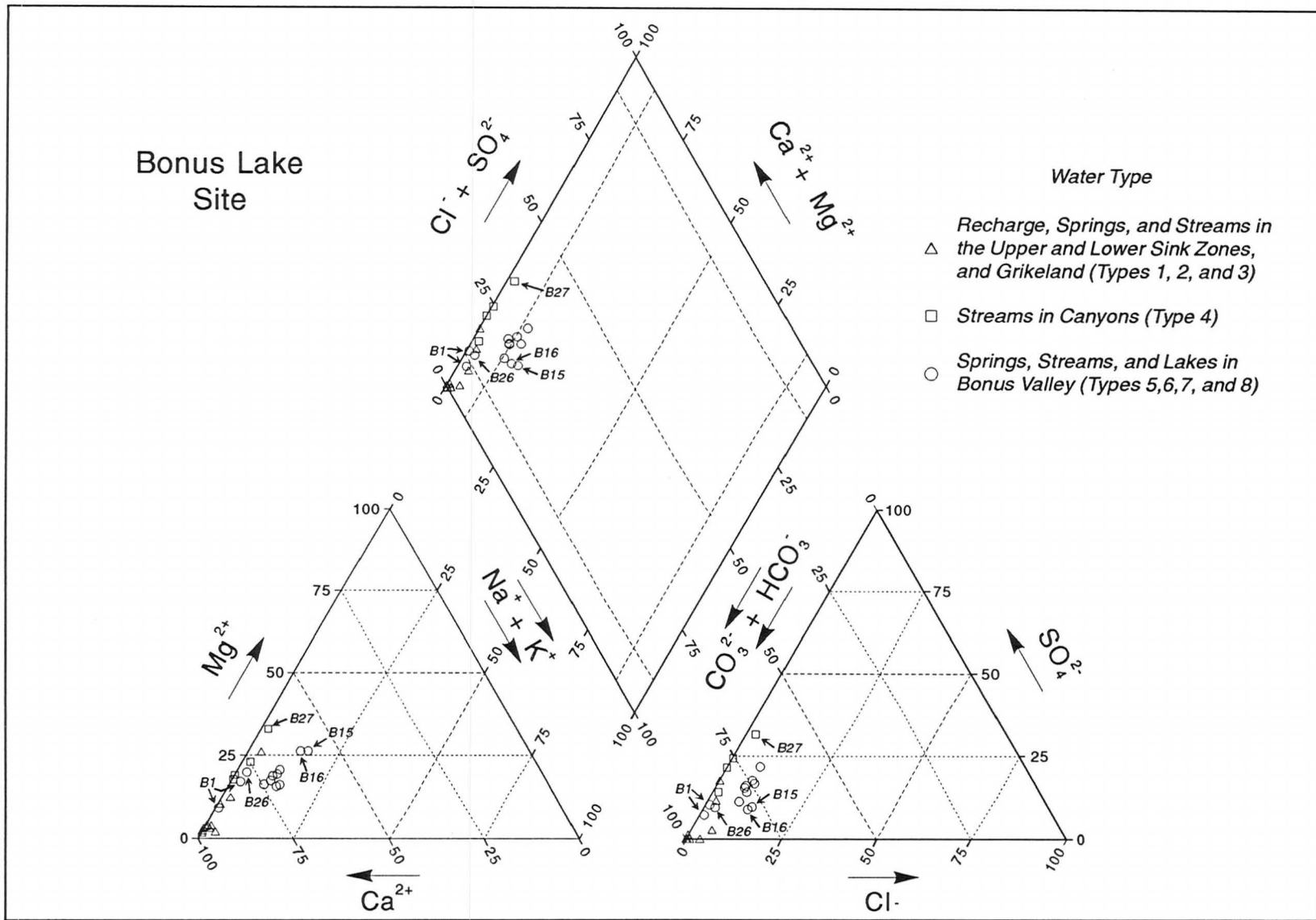


Figure 8.10: Trilinear diagram of waters from the Bonus Lake Site. All samples have a calcium bicarbonate facies. Discharge waters of Bonus Valley have the highest abundance of evaporite ions.

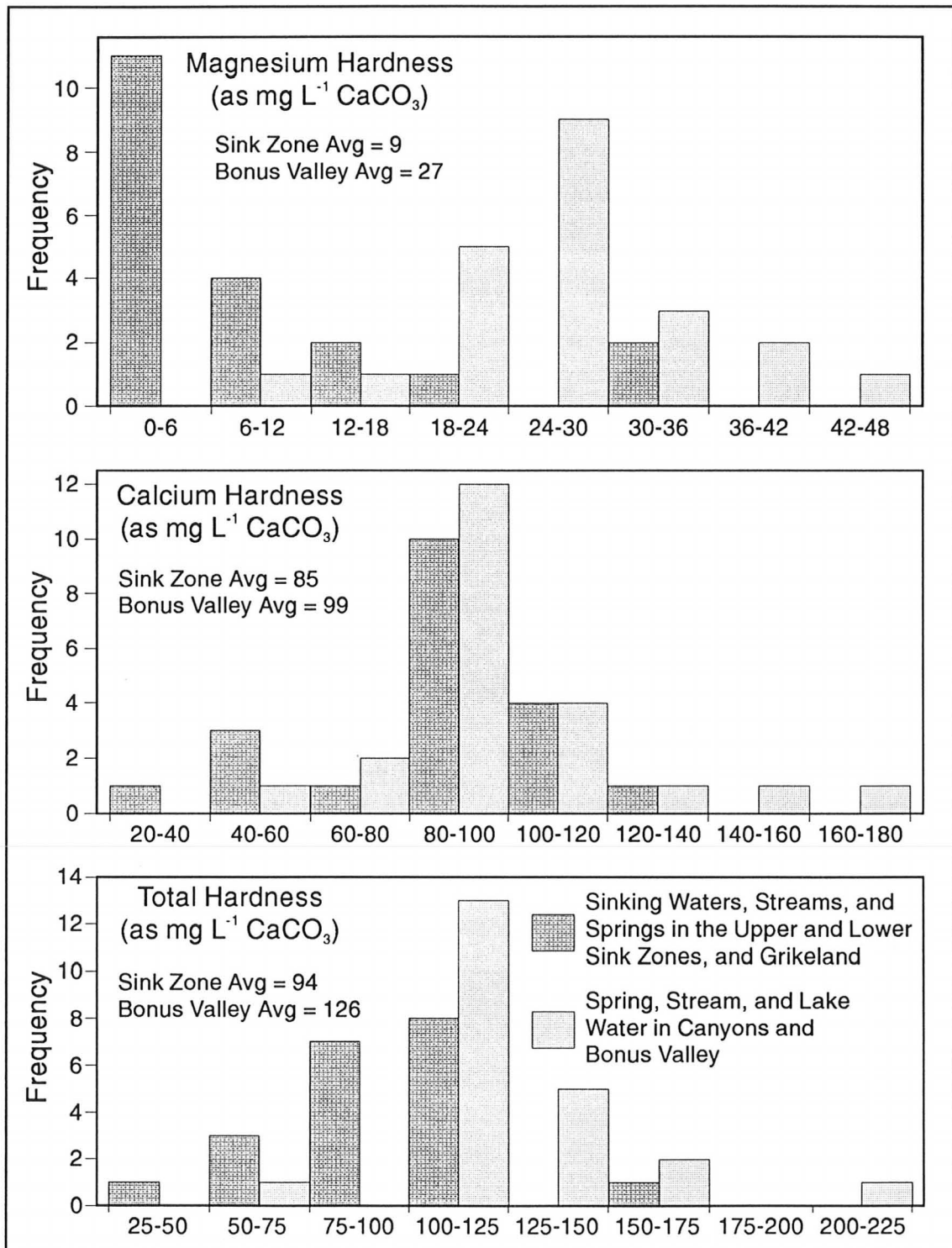


Figure 8.11: Frequency of magnesium, calcium, and total hardness values in samples across the Bonus Lake Site. Samples are divided into two classes based on position within the karst. The increase in total hardness that is observed in discharge waters of the canyons and Bonus Valley are due mainly to higher concentrations of magnesium.

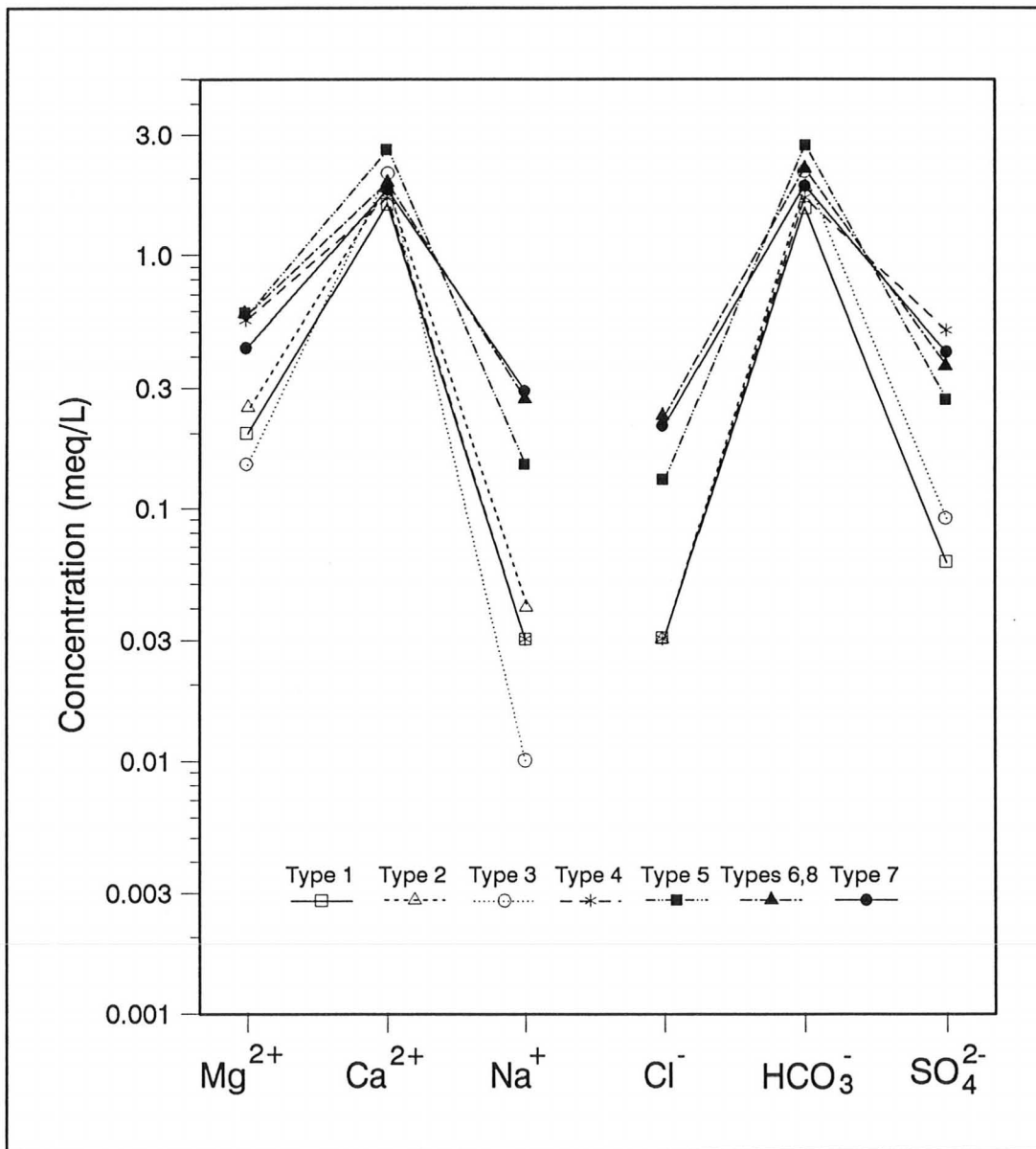


Figure 8.12: Mean concentrations of major anion and cation species in meq L⁻¹ for water types of the Bonus Lake Karst (types defined in Table 8.2).

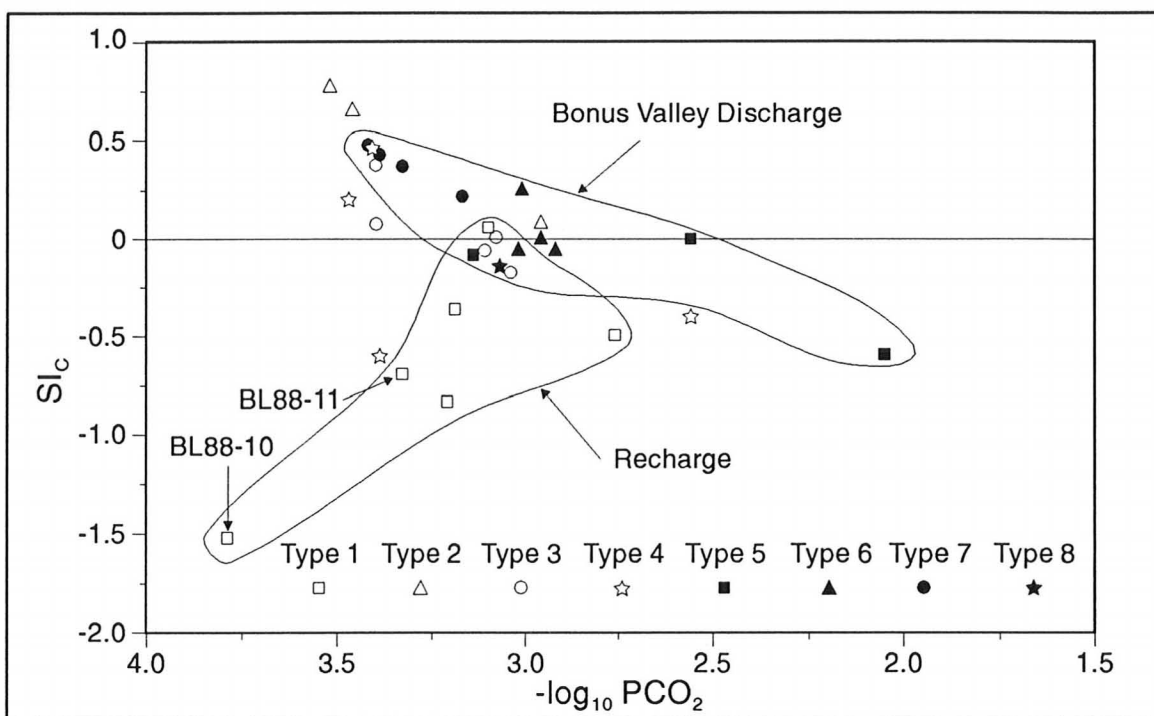


Figure 8.13: Saturation index of calcite versus $-\log_{10}$ of the partial pressure of CO_2 for water samples at the Bonus Lake Karst. The water types are defined in Table 8.2. Envelopes are placed around Recharge (Type 1) and Discharge waters (Types, 5-8).

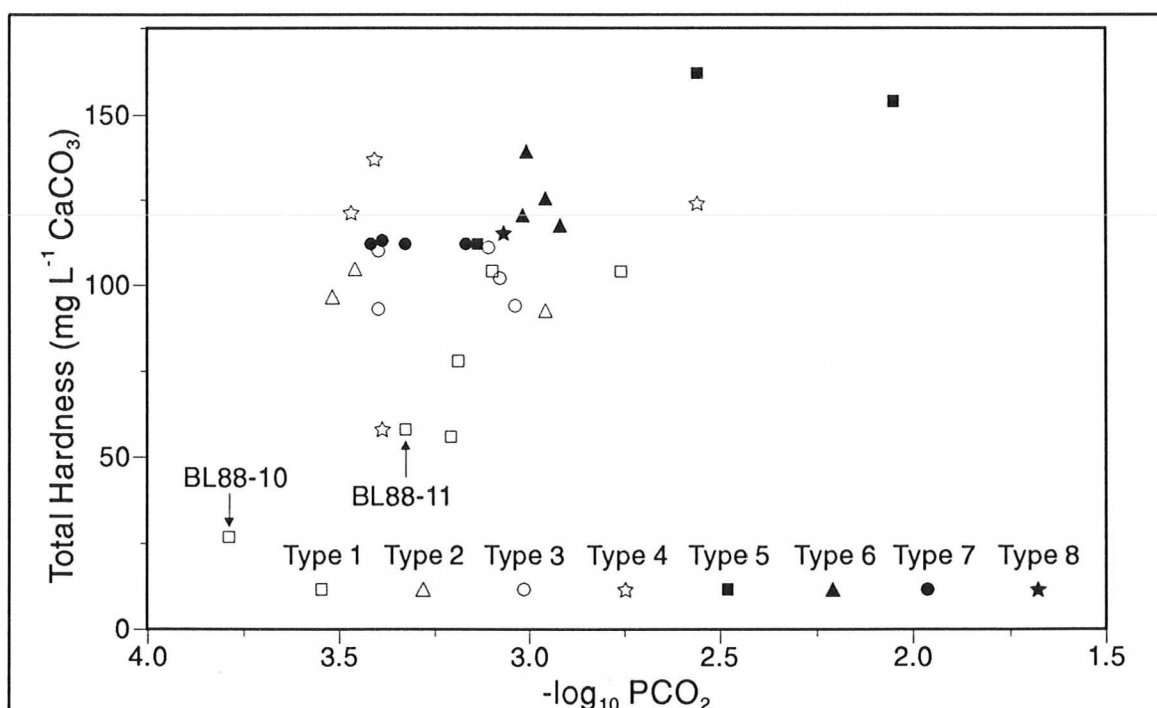


Figure 8.14: Total hardness versus $-\log_{10}$ of the partial pressure of CO_2 for water samples of the Bonus Lake Karst. The positions of BL88-10 and 11 are shown on Figures 8.13 and 8.14 despite high ion balance errors.

CHAPTER IX

THE PYRAMID LAKE SITE

9.1 Introduction

The Pyramid Lake Site is located in the Carcajou Range of the Mackenzie Mountains, 75 km south-southwest of Norman Wells (Figure 3.1). The main feature of the site is the karstically draining Pyramid Lake. Surficial karst landforms are limited to karren. This site provides an opportunity to examine karst hydrology in an area of continuous permafrost. Field work was undertaken between July 13 and 28, 1991. The field objectives were: (i) to supplement the regional hydrochemical data base, (ii) to attempt to locate spring points for the sinking waters of Pyramid Lake, and (iii) to observe variations in the level of Pyramid Lake and its springs. While on site, adverse weather presented some challenges. Consequently, water sampling was undertaken at only 17 points and several samples were not fully analyzed. However, hydrochemical trends across the site are identified.

9.2 Site Description

The Pyramid Lake Site lies between Little Keele and Carcajou Rivers, northeast of a range called the Blue Mountains (Figures 9.1, 9.2). The Canol Road and pipeline traverse the site. Pyramid Lake occupies a shallow depression and is flanked to the west and south by local hills that rise 300 to 400 m above the lake level. To the north and east, a broad cryopediment extends to Little Keele River. The latter area is shown by a series of dark lines on Figure 9.1 which mark zones of dense vegetation next to channels. Pyramid Lake is fed by several small streams draining the surrounding slopes (e.g., sample sites P12, P13, P15, P16: Figure 9.2) and by two streams from the Blue Mountains. The largest channel is Blue Creek; it was sampled

below steep terrain (P14) and again just upstream of Pyramid Lake (P10). In all, the topographic catchment of Pyramid Lake has an area of 34.4 km² and an elevation range from 786 m at lake level to 1780 m along Blue Mountain ridge.

West of the Pyramid Lake basin is a broad topographic swale developed along the axis of a tight syncline. This area is called Misery Valley. The trend of this structural valley is east to west, but it has been dissected and its drainage captured by a series of northward flowing streams (P1, P2, P3, P8, P9). Drainage from the western portion of Blue Mountains is routed south of Misery Valley to Little Keele River (P4). The largest stream, Boulder Creek, was sampled at point P17 (Figure 9.2). The channels of Boulder and Blue Creek are coarse and shallow. Where these streams traverse carbonate rocks, they lose flow (Figure 9.2). At the western end of Misery Valley there are a series of low discharge, diffuse springs in alluvial deposits (P5, P6). There is also a high discharge, cold spring flowing from the base of a bedrock knoll (P7). This is Horseshoe Spring. It has no topographic catchment and is identified as a possible resurgence for sinking waters of the Pyramid Lake basin.

9.2.1 Geology

The geology of the Pyramid Lake Site is shown on Figure 9.3. The exposed succession spans the Upper Proterozoic (Helikian) to Lower Devonian. The following sections review structure and lithology.

9.2.1.1 Structure

Major structural features include Stony Anticline and Canyon Fault (Figure 4.6). Stony Anticline forms a series of ranges that stretch as an arc of high ground from Carcajou to Mountain Rivers. Strata of the Upper Proterozoic Katherine Group outcrop along the crest and flanks of this anticline. Canyon Fault is a major thrust in the Mackenzie Mountains. Along most of its length the fault plane passes through and displaces only Proterozoic strata. In the study area, Canyon Fault brings the

Lower Katherine Group to rest upon units ranging from the Upper Proterozoic Little Dal Group to the Franklin Mountain Formation. Canyon Fault extends into the Franklin Mountain Formation west of Pyramid Lake at its northern end. The fault trace is marked by a small bluff and the fault plane dips westward at 5° to 10°. In addition to these major structural elements there are tight folds in Paleozoic strata. Misery Syncline runs from Pyramid Lake to Little Keele River (Figure 9.3). Sharply dipping strata of the Franklin Mountain and Mount Kindle Formations form the limbs of the syncline. The Bear Rock Formation outcrops in the syncline core. A series of folds splay from Misery Syncline west of Little Keele River.

9.2.1.2 Lithology and Distribution

Strata of the Lower Katherine Group outcrop along the crest and flank of Stony Anticline (Figure 9.3). This unit consists of more than 1000 m of resistant, orthoquartzite with minor shale and dolomite (Section 4.4.1.3). Exposures along Blue and Boulder Creeks consist of very fine and fine grained, pale yellow and pink, well sorted, cross-bedded quartzite. No outcrops of shale or dolomite were observed. North of Blue Mountains, the Lower Katherine Group is unconformably overlain by the Saline River or Franklin Mountain Formations. To the east, Canyon Fault brings the Lower Katherine Group into contact with these same units.

The Saline River Formation occurs south of Misery Syncline and east of Canyon Fault (Figure 9.3). In the former area, there are few good exposures but the trace of the formation is marked by its recessive weathering, which contrasts well with the bordering resistant units. However, the positions of the geological contact are not well controlled. On the west bank of Little Keele River there are exposures of shale. In this region, the formation is near its zero edge and is represented by a redbed facies. Little or no evaporite is expected in the subsurface.

There are outcrops of the Franklin Mountain Formation around Pyramid Lake and on the flanks of Misery Syncline. Horseshoe Spring discharges from the Franklin Mountain Formation near the syncline axis. Exposures west of Pyramid

Lake are tan coloured, thinly to thickly bedded, micro to finely crystalline dolomite. Some intervals are finely laminated, others display vug porosity. East of sample point P14, the contact between the Franklin Mountain Formation and overlying Mount Kindle Formation descends to the level of Blue Creek. Along a steep exposure, vertically tapering breccia pipes extend downward 3 to 5 metres from the Mount Kindle into an interval of massively bedded Franklin Mountain dolomite. Nearby, there are other intervals of breccia at that contact. These breccia pipes are interpreted as paleokarst features.

The Mount Kindle Formation occurs on high ground in Misery Syncline and east of Pyramid Lake. Outcrops are primarily light to dark grey, medium bedded, fine to medium grained, fossiliferous, vuggy, dolomite. Most of the outcrops are frost riven but there are small areas of karren on the ridge west of Pyramid Lake and along Blue Creek (e.g., Figure 6.4).

The Bear Rock Formation is mapped along the core of Misery Syncline (Figure 9.3). Much of that area is mantled in frost shattered debris, and peat rich soils. There are few good exposures. Outcrops observed are finely crystalline dolomite with no extensive breccia. The area was free of surficial karst landforms. The mapped boundary of the Bear Rock Formation is approximate, corresponding to a slight rise in topography.

9.2.2 Geomorphology

The geomorphology of the Pyramid Lake area is characterised by structural and periglacial features. Resistant strata on the crests and limbs of folds, form prominent ridges and mountain plateaux. The uplands are incised by valleys and spillways, but their morphology differs from those of the Dodo Canyon area. West of the Pyramid Lake Site, the channels of Carcajou, Little Keele, and other major rivers are braided and occupy relatively wide, flat floored valleys with moderately steep longitudinal profiles. Rectilinear valley and mountain sides commonly approach slopes of 30°. There are isolated conical and pyramidal shaped mountains. Above treeline, bedrock

weathering and sediment transfer are dominated by frost processes. Downslope sediment transport is achieved by slow mass wasting and rillwash. Steep mountain slopes are bordered by gently inclined, broad cryopediments. Most of the pediments are vegetated and solifluction across them is limited (Section 5.4.1). In the main, the morphology of the mountains and pediments reflect parallel slope retreat and pedimentation attributable to long periods of frost action associated with periglacial climates.

Carcajou and Little Keele Rivers pass through knick points adjacent to the site. The channels incise sharply into their braidplains and change in pattern from braided to meandering. In the latter sections, the streams are confined to narrow, 100 to 200 m deep canyons that feature abandoned meander loops. Below the confluence of Carcajou and Little Keele Rivers, Carcajou Canyon deepens, widens and the channel re-establishes a braided pattern. The meandering reach coincides with a broad area of low relief and pediments. The incision is related to Quaternary uplift and glaciation across the area. Two small waterfalls mark the post-glacial headward progression up Carcajou River. Downstream of these falls is 3 km of abandoned braidplain attributed to the last glaciation. This provides a minimum estimate of post-glacial incision along this channel.

Erratics are distributed to elevations as high as 1150 m at the site. There are no well-defined moraine or ice marginal meltwater features. Drift cover is thin and sporadic. Laurentide ice advanced to the flanks of the Blue Mountains during the Hungry Creek Glaciation, covering the full area of Misery Valley, Pyramid Lake, and the surrounding hills (Figure 5.6). The glacial limit is based on the erratic distribution and extrapolation from adjacent areas. During the Katherine Creek Phase it is suggested that there was Laurentide ice in Misery Valley and over Pyramid Lake but the uplands existed as nunataks. The area has been ice-free since retreat from the Katherine Creek maximum.

Permafrost mapping does not extend into the area but the site has attributes of the zone of continuous permafrost. There is active felsenmeer on unvegetated

pediments northeast of the Blue Mountains. Earth hummocks and stone stripes are common. Lowland areas are boggy with much peat. The site includes forest-tundra and tundra vegetation communities.

9.3 Hydrology and Hydrochemistry

Although the duration of fieldwork at the Pyramid Lake Site was limited, there was a range of hydrological conditions observed. Following a relatively dry period there was 20 mm of rainfall on July 14 and 15. On July 19 there was an additional major rainfall event estimated at 30 mm, a further 20 mm was estimated for July 20. During the July 19-20 event there was a 50 cm rise in the level of Pyramid Lake, flooding the base camp and climate station. The hydrological response in the Pyramid Lake area was typical of basins in continuous permafrost. Small seeps and springs draining the suprapermafrost aquifer were activated. The discharge of surface streams increased rapidly. Over the period of July 25-27, there was an additional 58 mm of rain that triggered the maximum response observed.

Water samples were collected from a number of streams, springs and from Pyramid Lake (Table 9.1; Figure 9.2). All waters are meteoric in origin and similar in their isotopic composition to those from the Bonus Lake Site (Figure 9.4). Detailed analyses were done for only nine samples from six locations (Table 9.2). The sampled waters display a calcium bicarbonate chemistry, with only trace amounts of SO_4^{2-} and Cl^- ions. Conductivity data are available from a larger set of sampling sites. Based on data listed in Table 9.2, relationships were generated to estimate total hardness and total dissolved ions for the larger data set (Figure 9.5). Overall, there is a strong relationship between $p\text{PCO}_2$ and total hardness of the sampled waters (Figure 9.6).

The data have been organized into six groups to identify spatial patterns across the site. They are: (1) streams in Misery Valley, (2) low discharge springs (along Little Keele River), (3) Blue Mountain streams, (4) Pyramid Lake streams, (5) Pyramid Lake, and (6) Horseshoe Spring. The following sections review the

hydrology and chemistry of each type.

9.3.1 Streams in Misery Valley

Three northward flowing streams dissect Misery Valley. They are in the Franklin Mountain, Mount Kindle, and Bear Rock Formations. The temperatures and conductivities of streams P1, P2, and P3 varied between 9.7 and 10.7°C, and 191 and 231 $\mu\text{S cm}^{-1}$ (Table 9.3). The estimated values for total hardness and total dissolved ions range from 127 to 155 mg L^{-1} as CaCO_3 , and 5.0 to 6.1 meq L^{-1} . Streams P1 and P2 were also sampled north of the valley at points P8 and P9. There were increases in temperature, conductivity, and discharge at these downstream locations. On July 15, discharges were 20 and 30 L s^{-1} at the upper sites, rising to between 35 and 50 L s^{-1} downstream (Table 9.1). These measures followed 20 mm of rainfall on the previous day.

Based on the topographic setting and physical characteristics of these waters, they are interpreted as flow from local suprapermafrost aquifers. Samples P1, P2, and P3 were taken below steeply sloping terrain. The channels were fed by seeps discharging from talus and moss covered colluvium, and from lightly forested peat-rich soils. Across Misery Valley temperature and conductivity were consistent. The high hardness values reflect the local carbonates and the slow rate of percolation through the organic soils. These waters are perched above the permafrost and are not associated with springs to the west.

9.3.2 Low Discharge Springs (Little Keele River)

At the west end of Misery Valley there are several small springs flowing from alluvium located on terraces and on the bank of Little Keele River. The temperature and conductivity of springs P5 and P6 were measured at 11.7 and 13.7°C, and 238 and 244 $\mu\text{S cm}^{-1}$ (Table 9.3). The conductivity values yield total hardness and TDI estimates of approximately 163 mg L^{-1} as CaCO_3 and 6.4 meq L^{-1} . East of the spring points the terrain slopes gently towards Little Keele River. The physical measures

are similar to those from streams of Misery Valley, suggesting these springs discharge local suprapermafrost waters.

9.3.3 Blue Mountain Streams

A series of steep, braided streams drain the northern flank of the Blue Mountains. Sample sites included Boulder Creek (P17), Blue Creek (P14), and a small tributary of the latter (P15). These basins are in quartzites of the Katherine Group and are largely above treeline.

Boulder Creek was examined at point P17. The sample location lies below a cliff in the Franklin Mountain Formation. The strata dip sharply to the north-northwest. The discharge at the site was variable. The channel was dry on July 15. The total flow was infiltrating upstream into a cobble and boulder bed. Following the heavy rains of July 25 to 27, the discharge increased to approximately 350 L s^{-1} at P17. Downstream there was a gradual loss in flow through infiltration. An icing at the confluence of Boulder Creek and Little Keele River persisted into mid-July, indicating some winter flow through the channel bed.

The morphology of the upper and middle reaches of Blue Creek are similar to Boulder Creek. Near Pyramid Lake, channel bed sediments gradually fine and the stream adopts a meandering pattern. The flow of Blue Creek is diminished where it crosses the Franklin Mountain Formation. At low stage, the total discharge infiltrated near point P14. Moderate flows occupied the channel to approximately point P16. Only during the high flows associated with the July 19 to 20 and 25 to 27 events was the channel occupied to Pyramid Lake. Between July 22 and 27, flows observed at P14 ranged from 150 to 400 L s^{-1} , although the maximum discharge associated with the July 25 to 27 event was not estimated. The channel at P15 is also coarse grained and in quartzites, but it is partially below treeline. Flows were observed only following rainfall events.

Stream temperatures varied between 3.1 and 8.7°C . Conductivity values ranged from 21 to $61 \mu\text{S cm}^{-1}$ (Table 9.3). On average, this group has the lowest

total hardness and TDI values of the water types: 16 mg L⁻¹ as CaCO₃, and 0.6 meq L⁻¹. At site P14, TDI was measured at 0.24 and 0.25 meq L⁻¹ and total hardness at 6 mg L⁻¹ as CaCO₃ (Table 9.2). These waters are aggressive towards calcite and dolomite (P14: SI_C = -3.1; SI_D = -6.4) with *p*PCO₂ values equilibrated to atmospheric concentrations of CO₂ (*p*PCO₂ ≈ 3.7). The data indicate that Blue and Boulder Creeks are supplied by suprapermafrost waters. This is consistent with their temperature and flashy discharge response to precipitation. The low hardness is a function of the basin materials.

On July 23, the discharge of Blue Creek at P14 was 150 L s⁻¹. Rhodamine WT dye was introduced into the stream at that point. The flow infiltrated into the bed across the next 100 m of channel. Charcoal detectors were placed at Horseshoe Spring to the northwest and were collected on July 27. Laboratory analysis of the effluent established a positive trace to Horseshoe Spring.

At point P10, Blue Creek flows through a small sand and gravel channel within a wide floodplain. Downstream, the floodplain gradually narrows and the stream passes through several meanders where a prominent levee of fine textured sands encloses a high capacity channel. A small bird-foot delta extends into the lake. At P10, the level of the July 19 to 20 flood event was marked by overbank deposits and organic detritus. Measurement of the local floodplain geometry, down valley slope, and surface roughness allowed calculation of the flood velocity using the Manning Equation:

$$V = \frac{R^{2/3} S^{1/2}}{n} \quad (9.1)$$

where *V* = mean channel velocity (m s⁻¹), *R* = hydraulic radius (m) which equals the cross-sectional area of the channel divided by the wetted perimeter, *S* = water surface gradient (m m⁻¹), and *n* = Manning's resistance coefficient. A mean channel velocity of 0.6 m s⁻¹ was calculated from a hydraulic radius of 0.28 m, a gradient of 0.015 m

m^{-1} , and a Manning's n of 0.09. The latter value was estimated from standard tables that conform to a floodplain of grasses and willows (Gardiner and Dackombe, 1983). The area of the flood channel is 3 m^2 , which yields a flood peak of 1.8 m s^{-1} . This is a minimum estimate of the peak flow since the selected value of roughness coefficient is thought conservative.

9.3.4 Pyramid Lake Streams

These streams drain the wetlands and slopes around Pyramid Lake and the small basins in carbonate rocks to the south. The water type includes the lower portion of Blue Creek (P10), as well as Cache Creek (P13) and the streams P12 and P16.

Blue Creek at P10 was gauged on July 16 at 20 L s^{-1} and on July 23 at 40 L s^{-1} . Analysis of the July 16 sample yielded: total hardness of 192 mg L^{-1} as CaCO_3 , TDI of 7.51 meq L^{-1} , $\text{Ca}^{2+}/\text{Mg}^{2+}$ ratio of 1.2, $p\text{PCO}_2$ of 2.94, and positive saturation indices ($\text{SI}_C = 0.49$, $\text{SI}_D = 0.89$) (Table 9.2). At low stage, Blue Creek (P10) takes flow from Stream P16 and nearby wetlands. Stream P16 is developed along the trace of Plateau Fault. One half of the basin is in quartzite and the balance in dolomite. The elevated $p\text{PCO}_2$ reflects CO_2 enrichment in organic soils. This sample may be typical of the low discharge diffuse flows that drain into Pyramid Lake. However, it does not capture the bulk character of the Blue Creek input that is cold, aggressive, and of low hardness.

Cache Creek (P13) was sampled following the July 19 to 20 event. The July 22 discharge was 45 L s^{-1} . Its chemistry is similar to P10 though more diluted by stormflow. Total hardness was 139 mg L^{-1} as CaCO_3 and TDI was 5.48 meq L^{-1} . The $p\text{PCO}_2$ of 3.35 suggests only marginal CO_2 enrichment in the soil zone. The sample is saturated with respect to calcite and dolomite ($\text{SI}_C = 0.52$, $\text{SI}_D = 0.90$). The differences with P10 reflect, in part, basin parameters; much of the Cache Creek basin lies above treeline in talus and exposed dolomite.

The flow of Stream P12 greatly increases following precipitation events. It was sampled on July 22 with a discharge of 25 L s^{-1} . The sample temperature was

4.2°C, total hardness 93 mg L⁻¹ as CaCO₃, TDI 3.7 meq L⁻¹, *p*PCO₂ 3.64, and the saturation indices near equilibrium (SI_C = 0.21, SI_D = 0.15). The stream drains a small, steeply sloping basin in dolomite above treeline. Flows to the channel emerge from talus as suprapermafrost seeps.

On average, waters of this grouping are similar in temperature, conductivity and hardness to the suprapermafrost streams of Misery Valley (Table 9.3). Their chemistry reflects the dolomite bedrock and colluvium that dominate the basins.

9.3.5 Pyramid Lake

Pyramid Lake is fed by Blue and Cache Creeks and by streams and seeps draining the local slopes and wetlands. The total area of the watershed is 34.4 km², of which 16 km² occurs upslope of location P15. Pyramid Lake has no surface outlet, its elevation is 785 m. A survey on July 16 showed total inflow at 50 to 75 L s⁻¹. The contributions from diffuse inputs were difficult to estimate. At the western end of the lake, there is a steep bluff in the Franklin Mountain Formation. The shoreline outcrop hosts fractures and frost shattered solution pockets that approach 20 cm in diameter and extend 0.5 m into the bedrock. The strata dip to the west (Figure 9.3). The water depth next to this bluff was 5 m. This site is the only location where a bedrock bluff forms the shoreline and it is identified as a sink point. While the lake bathymetry is unknown, it is probable there are other swallets.

During and following heavy precipitation events, flows into Pyramid Lake increase by an order of magnitude. Most of the input originates from the Blue Creek watershed. The minimum estimate of the July 19 to 20 Blue Creek peak is 1.8 m³ s⁻¹. By July 21, a plume of suspended sediment had spread across the full area of the lake in the upper part of the water column (e.g., Figure 9.1). The process was repeated during and following the July 25 to 27 event. On such occasions, a pulse of cold, aggressive, sediment laden, low hardness water enters Pyramid Lake. Presumably such flows also occur during the snowmelt period. There is a substantial difference in the temperature and turbidity of the summer storm and fair weather flows. The

cold, turbid waters may generate density currents that deliver a mass of bedload to the lake bottom and spread a plume of suspended materials laterally.

Pyramid Lake was sampled at the shoreline just below the Franklin bluff at point P11. Conductivity and temperature were recorded at the surface and at 1.5 m depth (Table 9.3). Analysis of the latter sample showed: temperature of 11.2°C, total hardness of 77 mg L⁻¹ as CaCO₃, TDI of 3.1 meq L⁻¹, Ca²⁺/Mg²⁺ ratio of 1.3, *p*PCO₂ of 3.51, and near equilibrium saturation indices (SI_C = -0.04, SI_D = -0.17) (Table 9.2). The surface sample had a temperature of 12.7°C and a conductivity of 302 μS cm⁻¹, yielding a total hardness estimate of 207 mg L⁻¹ as CaCO₃. The two samples suggest the lake is stratified. Waters at depth are assumed to have low temperatures and low hardness. It is not known if the 1.5 m sample is representative of the lake body. It may characterize a mixing zone between the cold, dense, aggressive flood waters (e.g., P14) and the fair weather, warm, high hardness flows of Cache Creek (P13) and lower Blue Creek (P10). A sample was also retained from 1.5 m depth for isotope analysis (Figure 9.4).

9.3.6 Horseshoe Spring

Horseshoe Spring is located 10 m above the level of Little Keele River at the west end of Misery Valley (Figure 9.2). The spring elevation is 720 m. No surface streams or gullies drain towards the site. The majority of the flow issues from alluvium on a terrace of Little Keele River adjacent to an outcrop of the Franklin Mountain Formation. A 5 m diameter pool marks the position of the principal outflow. Upwelling of spring waters is sufficiently vigorous to suspend sands. The alluvium in the pool area has been reworked. Gravels line the pool bed while fine sands border its margin and comprise the channel draining to Little Keele River.

A hierarchy of springs is present. The discharge increased below the pool due to further aggraded inputs into the channel. Also, several small capacity conduits occur in the adjacent outcrop. At high stage, the upper bedrock conduits were activated. Discharge measurements varied between 1.2 and 1.7 m³ s⁻¹ (Table

9.1). Deposits from the spring area provided evidence of higher flows. At the time of the July 27 measurement ($Q \approx 1.7 \text{ m}^3 \text{ s}^{-1}$) the highest spring points were not flowing. However, within and below these conduits were recent deposits of fine sands. Extensive overbank deposits and flattened vegetation fringed the channel below the pool. The charcoal detectors placed on the channel bed on July 23 were buried by 5 to 15 cm of fine and very fine sand.

Horseshoe Springs' temperature and conductivity averaged 3.0°C and $86 \mu\text{S cm}^{-1}$ (Table 9.3). The two samples analysed displayed consistent chemistry (Table 9.2). Data from July 27 show: a total hardness of 74 mg L^{-1} as CaCO_3 , TDI of 2.81 meq L^{-1} , $\text{Ca}^{2+}/\text{Mg}^{2+}$ ratio of 1.5, $p\text{PCO}_2$ of 3.42, and aggressive saturation indices ($\text{SI}_C = -0.49$, $\text{SI}_D = -1.25$). This chemistry is similar to that of Pyramid Lake (P11) and intermediate between that of the Blue Mountain Streams (Type 3) and streams of the carbonate basins (Type 4).

9.4 Pyramid Lake Aquifer

The character of the Pyramid Lake aquifer can be deduced from Horseshoe Spring data. The low $\text{Ca}^{2+}/\text{Mg}^{2+}$ ratio shows circulation has been through dolomite. Discharge is high and variable and the waters are aggressive. The temperature and conductivity are low compared with nearby suprapermafrost springs (Type 2). Clastic sediments are flushed through the outlet during storm events. The sediments have a texture similar to that of the Lower Katherine Group quartzites. A dye trace established a less than 4 day connection between Blue Creek and Horseshoe Spring. In total, these data support a model of high groundwater velocity and a short residence time in the aquifer. Circulation is not sufficiently deep to produce thermal discharge. These observations indicate that Horseshoe Spring drains a subpermafrost conduit aquifer.

There is ample evidence supporting the interpretation of a conduit aquifer but few data are available regarding the style of its recharge and the extent of its recharge area. The dye trace shows a connection between the middle reaches of Blue

Creek and Horseshoe Spring. Through that section, the stream loses flow under all discharge conditions where it crosses the Franklin Mountain Formation. The strata are on the flank of Misery Syncline and dip sharply to the northwest. Infiltration also occurs into the channel of Boulder Creek in a similar structural situation. It is possible that Boulder Creek waters are also discharged at Horseshoe Spring. The isotopic signature of Horseshoe Spring is most similar to the water sampled from Pyramid Lake (Figure 9.4). The chemistry and isotope ratios of the spring indicate that Blue Mountain waters do not constitute the sum of the recharge. There are other inputs to the aquifer. It is suggested that waters of Pyramid Lake sink at the eastern end of Misery Syncline into western dipping strata and discharge at Horseshoe Spring. There is a possibility that Pyramid Lake waters are routed to unknown springs on the Little Keele or Carcajou Rivers. However, the chemistry of Horseshoe Spring requires the input of a high hardness water. There are insufficient data to evaluate if inputs and outputs to the system balance. However, there is room for speculation.

There were several rainfall events during the period of fieldwork. Each successive storm generated a greater discharge response. The level of Pyramid Lake rose by 1.3 m between July 13 and 28. In the event of July 25 to 27, there was 59 mm of precipitation recorded at the Pyramid Lake base camp. At the flood peak, most of the flow of Boulder Creek infiltrated into its bed and a pulse of cold, sediment laden water entered Pyramid Lake from Blue Creek. The peak discharge at Horseshoe Spring was missed but it was likely near $2 \text{ m}^3 \text{ s}^{-1}$. In this event, the volume of recharge to the Pyramid Lake basin was at least $2.0 \times 10^6 \text{ m}^3$. With Horseshoe Spring discharging at $1.5 \text{ m}^3 \text{ s}^{-1}$, this rainfall pulse would pass through the system in 15.4 days. The volume of recharge (discharge) and the time estimate are increased if Boulder Creek waters also contribute to Horseshoe Spring, as is suspected. These figures seem reasonable given the storage capacity of Pyramid Lake. As the lake level increased some of the small conduits on its western shoreline were inundated. On an annual basis, runoff in the area may be as high as 500 mm

(Table 3.4: Tsichu River). Over the whole basin that represents $17.2 \times 10^6 \text{ m}^3$ of recharge. At $1.5 \text{ m}^3 \text{ s}^{-1}$, Horseshoe Spring could discharge such a volume in a season of 132.7 days. Again the volumes and time estimates would be higher if the sinking waters of Boulder Creek contribute to Horseshoe Spring. There are few data that can be used to validate these estimates. However, they do suggest that Horseshoe Spring is capable of accomodating recharge across the full area of Pyramid Lake basin and some flow from Boulder Creek.

The final difficulty are the sediments that are flushed through the aquifer during storm events. Waters draining off the quartzites of the Katherine Group represent allogenic waters in this system. When flood waters from Blue Creek enter Pyramid Lake they may behave as turbidity currents with cool, dense water moving below the surface. Fine grained sediments are suspended but the sands move along the lake floor, perhaps to a conduit where they enter the aquifer. Alternatively, sands enter the system through aggraded conduits along Blue or Boulder Creeks.

9.5 Summary: Pyramid Lake Site

The significance of the Pyramid Lake Site is not in the range or distribution of surficial landforms but rather the presence of a large conduit aquifer developed in dolomite bedrock in a previously glaciated and continuous permafrost environment.

Recharge passes through north and westward dipping strata of Misery Syncline. It is focussed to the axis of the syncline, and discharges just above local base level at Horseshoe Spring. Water samples have a calcium bicarbonate chemistry. Total hardness is strongly correlated with $p\text{PCO}_2$ (Figure 9.6). Hardness and ion concentrations are lower than samples from other sites in this study. The latter reflect the cold climate and the dolomite geology. Under the current environmental conditions, the development of a high capacity, integrated conduit aquifer in dolomite would be improbable. Surficial processes are dominated by frost action. Permafrost is continuous. There is a possibility that the Pyramid Lake aquifer is a reactivated paleokarst.

Table 9.1: Description of water sampling locations at the Pyramid Lake Site.

Map Location	Site Description	Sample Date(s)
P1	Small stream in Misery Valley draining northward. $Q \approx 30 \text{ L s}^{-1}$.	150791
P2	Small stream in Misery Valley draining northward. $Q \approx 30 \text{ L s}^{-1}$.	150791
P3	Small stream in Misery Valley draining northward. $Q \approx 20 \text{ L s}^{-1}$.	150791
P4	<i>Little Keele River</i> . Braided stream, $Q > 10 \text{ m}^3 \text{ s}^{-1}$.	150791
P5	Springs discharging from alluvium. $Q \approx 10 - 15 \text{ L s}^{-1}$.	150791
P6	Springs discharging from alluvium. $Q \approx 10 \text{ L s}^{-1}$.	150791
P7	<i>Horseshoe Spring</i> . Large spring discharging from an outcrop of the Franklin Mountain Formation. Discharge is high and variable. $Q_1 \approx 1.2 - 1.3 \text{ m}^3 \text{ s}^{-1}$, $Q_2 \approx 1.2 - 1.3 \text{ m}^3 \text{ s}^{-1}$, $Q_3 \approx 1.6 - 1.8 \text{ m}^3 \text{ s}^{-1}$.	150791 180791 270791
P8	Stream channel downstream of location P2. $Q \approx 50 \text{ L s}^{-1}$.	150791
P9	Stream channel downstream of location P1. $Q \approx 35 - 40 \text{ L s}^{-1}$.	150791
P10	<i>Blue Creek</i> . Sampled in channel above Pyramid Lake. Discharge variable. $Q_1 \approx 20 \text{ L s}^{-1}$, $Q_2 \approx 40 \text{ L s}^{-1}$, $Q_{\text{max}} > 1.8 \text{ m}^3 \text{ s}^{-1}$ (based on Manning Equation).	160791 230791
P11	<i>Pyramid Lake</i> . Sampled at the surface and at a depth of 1.5 m.	210791
P12	Small stream in steep channel above treeline. Flow sampled after heavy precipitation. $Q \approx 20 - 30 \text{ L s}^{-1}$.	220791
P13	<i>Cache Creek</i> . Stream draining a forested basin. $Q \approx 40 - 50 \text{ L s}^{-1}$.	220791
P14	<i>Blue Creek</i> . Braided channel with a boulder and cobble bed. At this site, flow was observed throughout the period of field observations. Discharge decreased below the sampling point. $Q_1 \approx 200 \text{ L s}^{-1}$, $Q_2 \approx 150 \text{ L s}^{-1}$, $Q_3 \approx 300 - 400 \text{ L s}^{-1}$.	220791 230791 270791
P15	Stream with a coarse channel. Basin is partially below treeline. $Q \approx 30 \text{ L s}^{-1}$.	220791
P16	Stream along the contact between quartzite of the Katherine Group and dolomite of the Franklin Mountain Formation. Basin partially below treeline. $Q \approx 25 \text{ L s}^{-1}$.	220791
P17	<i>Boulder Creek</i> . Braided channel with a boulder and cobble bed. Flow at the sampling site occurs only after rainfall events. Flow is reduced downstream. $Q \approx 300 - 400 \text{ L s}^{-1}$.	270791

Table 9.2: Temperature, conductivity, pH, total hardness, ion concentrations, total dissolved ions, Ca²⁺/Mg²⁺ ratio, saturation indices (calcite and dolomite), and pPCO₂ of water samples at the Pyramid Lake Site.

Location	Site	Date	Temp	SPC	pH	THd	Ca ²⁺	Mg ²⁺	HCO ₃ ⁻	SO ₄ ²⁻	Cl ⁻	TDI	C/M	SI _c	SI _d	pPCO ₂	IBE
Horseshoe Spr	P7	180791	2.7	79	8.34	53	0.60	0.46	1.02	0.08	0.02	2.18	1.3	-0.48	-1.17	3.71	-2.8
Horseshoe Spr	P7	270791	2.5	102	8.11	74	0.88	0.60	1.18	0.13	0.02	2.81	1.5	-0.49	-1.25	3.42	5.4
Blue Creek	P14	220791	7.1	21	7.45	6	0.08	0.04	0.12	0.00	0.00	0.24	2.0	-3.05	-6.44	3.69	0.1
Blue Creek	P14	270791	3.6	33	7.38	6	0.12	0.00	0.08	0.05	0.00	0.25		-3.16	99.00	3.83	-4.1
Blue Creek	P10	160791	11.5	284	8.18	192	2.12	1.72	3.68	0.00	0.00	7.51	1.2	0.49	0.89	2.94	2.0
Pyramid Lake	P11	210791	11.2	139	8.38	77	0.86	0.68	1.52	0.00	0.04	3.10	1.3	-0.04	-0.17	3.51	-2.3
Stream	P12	220791	4.2	135	8.52	93	1.12	0.74	1.84	0.00	0.00	3.70	1.5	0.21	0.15	3.64	0.6
Cache Creek	P13	220791	11.7	215	8.45	139	1.60	1.18	2.70	0.00	0.00	5.48	1.4	0.52	0.90	3.35	1.5
Boulder Creek	P17	270791	3.1	61	7.71	25	0.36	0.14	0.30	0.05	0.05	0.90	2.6	-1.82	-4.13	3.59	11.5

Temp: temperature in °C; SPC: electrical conductivity, expressed to 25°C, in µS cm⁻¹; THd: Total Hardness in mg L⁻¹ CaCO₃; Ion Concentrations reported in meq L⁻¹, analyses for Na⁺ were not done; TDI: Total Dissolved Ions in meq L⁻¹; C/M: Ca²⁺/Mg²⁺ ratio; SI_c: Saturation Index of Calcite; SI_d: Saturation Index of Dolomite; pPCO₂: -log of partial pressure of CO₂; IBE: Ion balance error in %. 99.00 indicates no computation.

Table 9.3: Temperature, conductivity, total hardness, and total dissolved ions for Pyramid Lake Site sample groups.

Water Type	Date	Site	Temp	SPC	THd	TDI
1 Stream waters in Misery Valley (stream basins are in carbonates of the Franklin Mountain, Mount Kindle, and Bear Rock Formations)	150791	P1	9.7	191	127	5.0
	150791	P2	10.5	221	148	5.8
	150791	P3	10.7	231	155	6.1
	150791	P8	15.7	228	153	6.0
	150791	P9	13.6	262	178	7.0
	Average		12.0	227	152	6.0
2 Low discharge springs east of Little Keele River	150791	P5	11.7	238	161	6.3
	150791	P6	13.7	244	164	6.5
	Average		12.7	241	163	6.4
3 Blue Mountain streams (basins are largely in quartzites of Katherine Group, the flow of Blue Creek (P14) is directed to Pyramid Lake)	220791	P14*	7.1	21	6	0.2
	230791	P14	7.2	35	13	0.5
	270791	P14*	3.6	33	6	0.3
	220791	P15	8.7	59	30	1.2
	270791	P17*	3.1	61	25	0.9
	Average		5.9	42	16	0.6
4 Pyramid Lake streams (stream basins in Franklin Mountain and Mount Kindle Formations southeast of Pyramid Lake)	160791	P10*	11.5	284	192	7.5
	230791	P10	7.8	246	166	6.5
	220791	P12	4.2	135	93	3.7
	220791	P13*	11.7	215	139	5.5
	220791	P16	9.9	181	119	4.7
	Average		9.0	212	142	5.6
5 Pyramid Lake (samples taken at two depths; ** at the surface; * taken at 1.5 m depth)	210791	P11**	12.7	302	207	8.1
	210791	P11*	11.2	139	77	3.1
	Average		12.0	221	142	5.6
6 Horseshoe Spring (flows from Franklin Mountain Formation)	150791	P7	3.7	78	44	1.7
	180791	P7*	2.7	79	53	2.2
	270791	P7*	2.5	102	74	2.8
	Average		3.0	86	57	2.2
Little Keele River	150791	P4	9.9	183	120	4.7

* Data used to generate regression relationships to estimate THd and TDI for the full data set; Temp: Temperature in °C; SPC: specific electrical conductivity, expressed to 25 °C, in $\mu\text{S cm}^{-1}$; THd: Total Hardness is expressed in mg L^{-1} as CaCO_3 ; TDI: Total Dissolved Ions in meq L^{-1} .



Figure 9.1: Vertical aerial photograph of the Pyramid Lake Site (top). North is at the top. The scale is 1:69500 in the Pyramid Lake (①) area. Horseshoe Spring is located near Little Keele River at ②. The channel of Blue Creek (③) is shown below. The Canol Road is seen to the lower right.

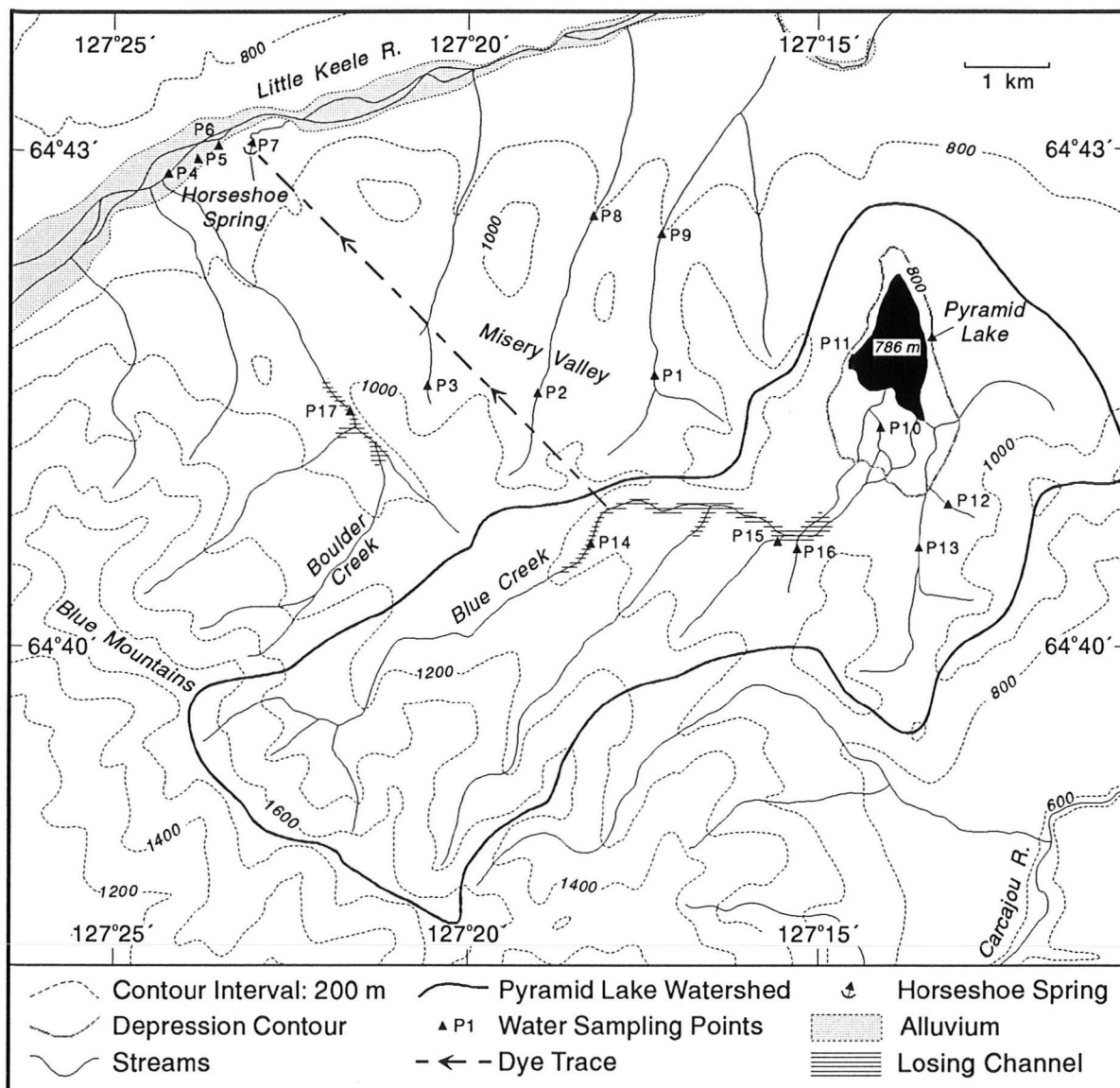


Figure 9.2: Map of the Pyramid Lake Site illustrating topography, drainage, and water sampling locations. Pyramid Lake is supplied by several small streams draining the local hills and by Blue Creek. The watershed has an area of 34 km². Blue Creek drains a portion of the Blue Mountains which rise to 1780 m elevation and possess an alpine topography. The Laurentide glacial limit occurs below 1300 m. A broad pediment extends north of Pyramid Lake towards Little Keele River. Undulating terrain occurs through Misery Valley to the west. Karst input landforms are restricted to a small area of karren along Blue Creek and the hills west of Pyramid Lake. Horseshoe Spring is east of Little Keele River and flows from the Franklin Mountain Formation. Blue Creek and the neighbouring Boulder Creek have coarse braided channels that lose discharge where they flow over carbonates. A dye trace shows a connection between Blue Creek and Horseshoe Spring.

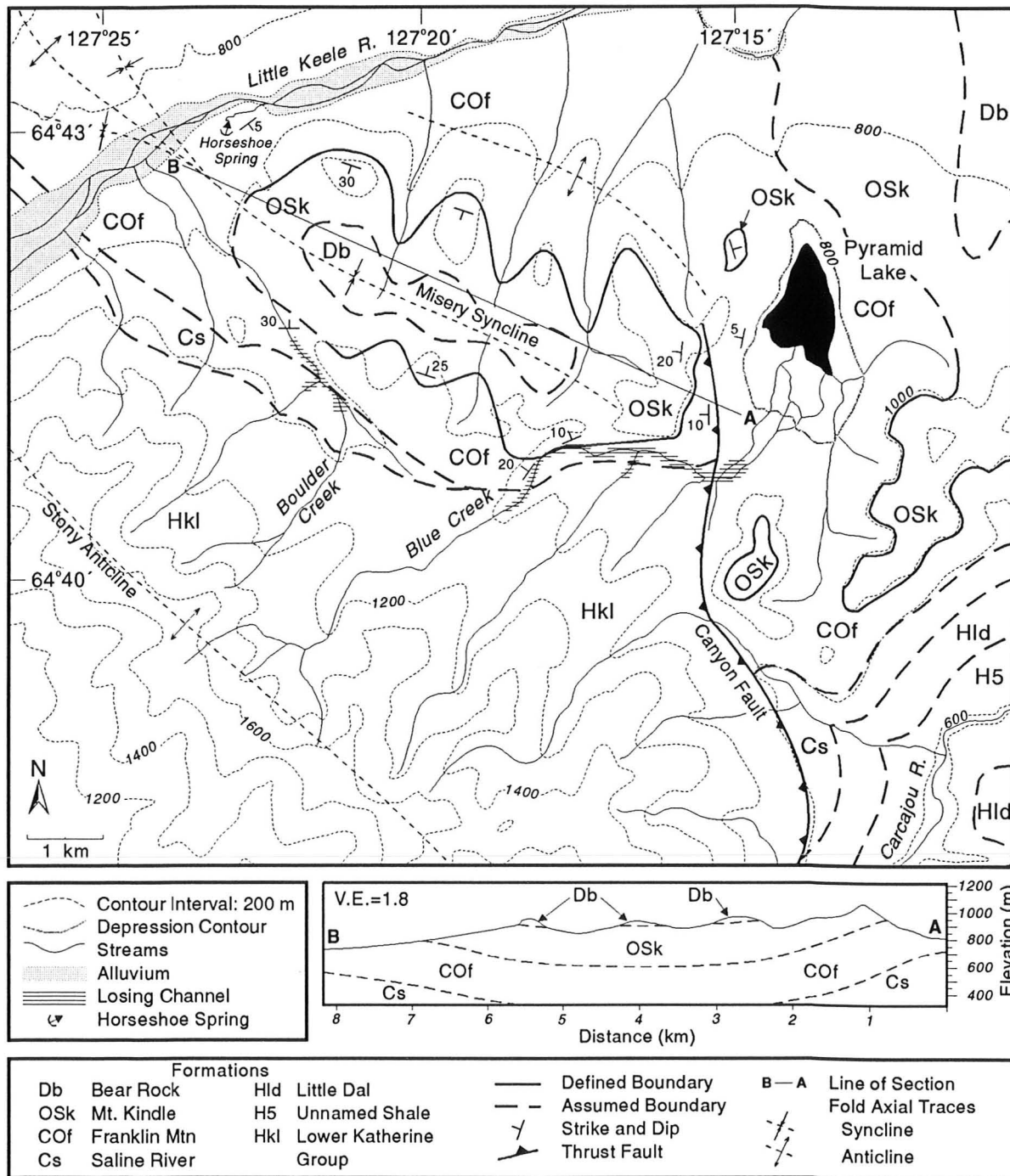


Figure 9.3: Geology of the Pyramid Lake Site. Pyramid Lake sits at the eastern end of a doubly plunging syncline (Misery Syncline) developed in the Franklin Mountain, Mount Kindle, and Bear Rock Formations. To the south, Proterozoic strata of the Lower Katherine Group outcrop along the crest and flanks of Stony Anticline. West of Canyon Fault, the Saline River and Franklin Mountain Formations unconformably overlie quartzites of the Lower Katherine Group. Canyon Fault also brings the latter units into contact with a variety of younger strata in the eastern section of the map (after Aitken and Cook, 1974).

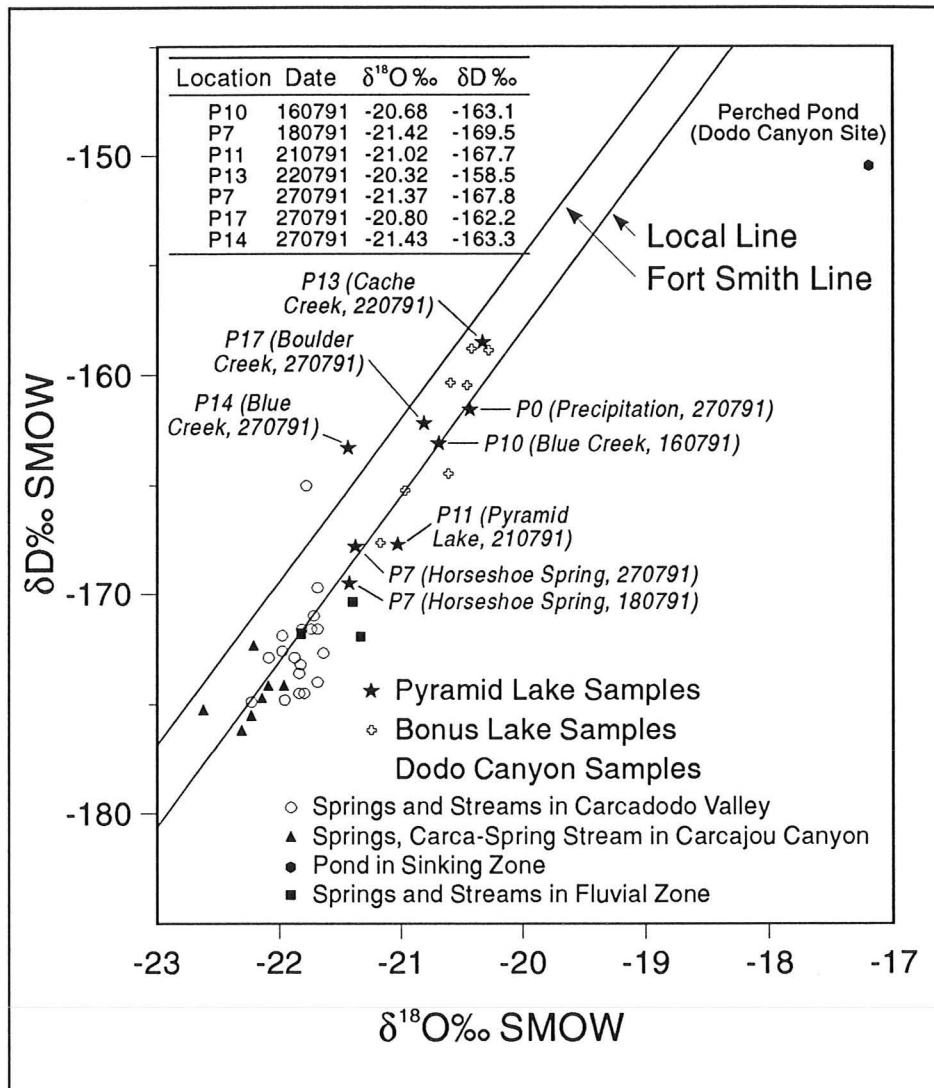


Figure 9.4: Isotope samples from the Pyramid Lake Site plotted with the local and Fort Smith meteoric water lines. Data from the Dodo Canyon and Bonus Lake Sites are also shown. The Pyramid Lake samples were collected between July 16th and 27th, 1991. The Bonus Lake samples are from early August, 1991 and the Dodo Canyon samples from mid to late August of 1991. The graph shows waters of the Pyramid Lake Site are meteoric in origin and are isotopically heavier than discharge waters of the Dodo Canyon Site. The isotopic signature of Pyramid Lake (P11) is most similar to that of Horseshoe Spring (P7). Stream waters (P10, P13, P14, P17) are heavier and more closely reflect summer precipitation (P0).

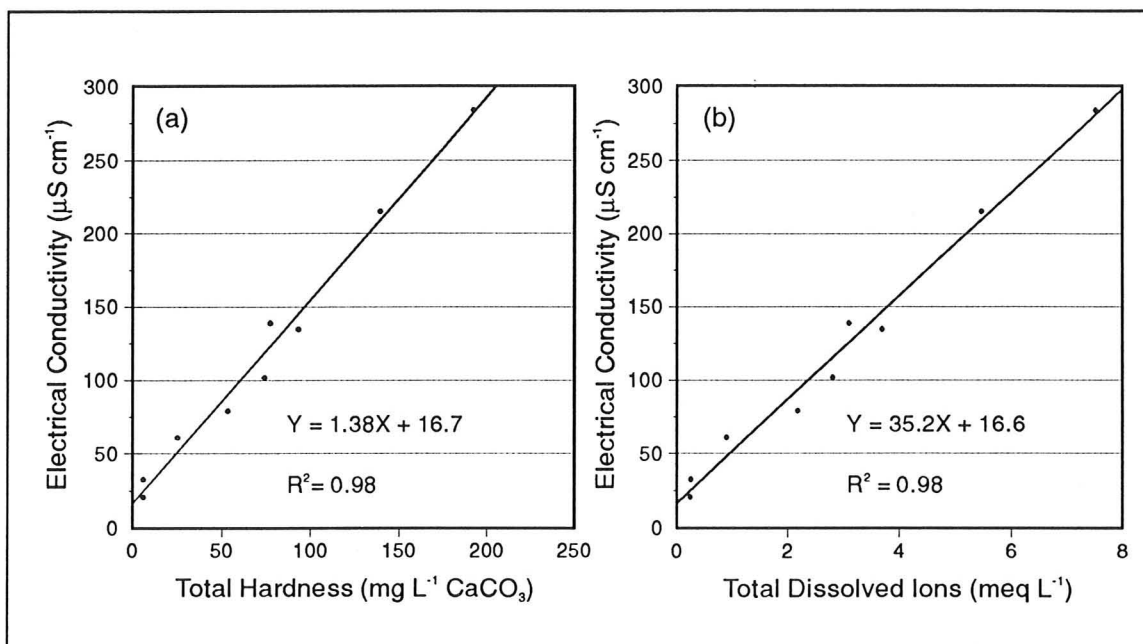


Figure 9.5: Electrical conductivity versus total hardness (a) and total dissolved ions (b) for water samples at the Pyramid Lake Site. These relationships are used to estimate total hardness and total dissolved ions for samples that lack a full chemical analyses (Table 9.3).

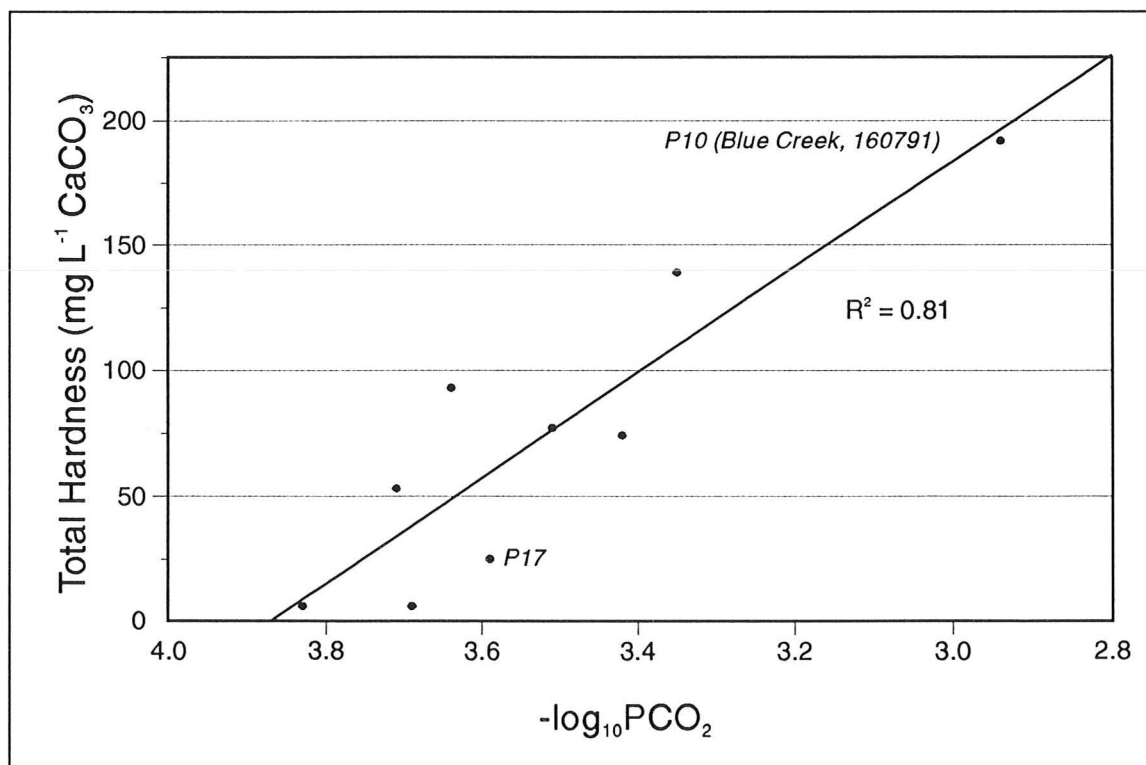


Figure 9.6: Total hardness versus $-\log_{10}$ of partial pressure of CO_2 for water samples from the Pyramid Lake Site. Sample P17 is shown despite the high ion balance error. The relationship is consistent with data from the Bonus Lake Site.

CHAPTER X

THE BEAR ROCK SITE

10.1 Introduction

The Bear Rock Site is located 4 km west of the confluence of the Mackenzie and Great Bear Rivers (Figure 3.1). The term "Bear Rock" was applied by Franklin (1828) and Hume (1954) to an upland at the southern end of the Norman Range between 64°54' and 64°59' north latitude. In current cartographic usage the name is reserved for single peak at the northeastern end of the range (e.g., NTS 96 C/13). However, in this work "Bear Rock" is employed in accordance with the original intent.

At its southern end, Bear Rock rises abruptly from the level of the Mackenzie River and runs northward. The range is 4 km in width and 8 km in length. Steep slopes occur at the margin of Bear Rock along the Mackenzie River and above the lowland to the east (Figure 10.1). There are prominent cliffs at the north and south ends of the range. To the west, sheer slopes mark the trace of the Hume Formation and a series of faults. Local relief approaches 400 metres.

Across the central portion of the upland there are a variety of karst depressions that are developed primarily on the Bear Rock Formation. Several larger features contain ponds and lakes. In the northern portion of the range, the density of dolines is high, many are circular in plan, and there are large compound and linear depressions. This area is the North Karst (Figure 10.2). The single largest feature of the North Karst is Camp Depression. It is a compound doline or uvala centred on two small ponds (Figures 10.2, 10.4). A ridge separates the North Karst from the bordering South Karst (Figure 10.3). The southern area is dominated by a compound linear depression that is developed parallel to the axis of a small anticline. Two large

lakes are found within this zone: Round and Long Lakes. Both the Bear Rock and Franklin Mountain Formations outcrop in their basins.

Hydrogeologically, Bear Rock may be divided into recharge and discharge zones. The recharge zone runs the full length of the range through the central portion of the upland. This zone includes the area of karst depressions and those regions where surface drainage is routed towards sink points or infiltrates into channel beds. Recharge occurs in the Bear Rock and Franklin Mountain Formations. The discharge zone includes the marginal and sloping areas of the upland and the low ground that borders Bear Rock. Drainage elements of the latter area include ephemeral streams and a series of springs at the periphery of the range (Figure 10.1). At the southeastern end of Bear Rock, several low discharge, perennial springs flow into a grass and sedge clearing at the base of a steep slope (Figure 10.5). This spring line and glade is called the Bear Rock Spring Area. The perennial discharge generates frost blisters at that location. The hydrochemistry of these springs has been described by Michel (1977) and van Everdingen (1978, 1982). Similar springs also flow from talus and outcrops along the north bank of the Mackenzie River. A second set of important springs occurs at the base of a gully near the contact of the Bear Rock and Hume Formations at the southwest edge of the range. These springs feed Forest and Blood Streams (Figure 10.1). They have a high discharge and differ in their chemistry from those of the Bear Rock Spring Area. Another major spring is located 2.5 km north of Forest Stream and supplies West Stream. Its point of discharge is also near the Bear Rock-Hume contact. In the area of the North Karst, there were few springs located. A single low discharge spring flows from a bench of the Franklin Mountain Formation southwest of Trout Lake, and small springs contribute to the flow of Vale Stream in the northwestern portion of the range. The bulk of the recharge through the North Karst must discharge through unseen flooded or aggraded springs.

The specific objectives of fieldwork at the Bear Rock Site were: (i) to map the geomorphology with a focus given to the distribution and range of karst

depressions, (ii) to describe the hydrology of the site, (iii) to collect surface and spring waters for chemical analyses, and (iv) to identify flow paths from the zone of recharge to discharge.

Fieldwork was conducted from three base camps. Camp One was occupied between July 6 and August 2, 1987. During that season the field effort was concentrated in mapping the South Karst area. In 1988, fieldwork was done from Camps Two and Three. Camp Two provided easy access to the Bear Rock Spring Area. In 1988, it was used between June 1 and June 10, July 28 and July 31, and August 8 and August 11. Camp Three occupies the largest depression in the North Karst. It was used between July 19 and 27, August 1 to 7, and August 12 to 14, 1988. While at the latter site, water samples were collected and mapping was conducted over the area of the North Karst.

10.2 Geology

The geology of the Bear Rock area was mapped by Stelck (1944) during the Canol Project. The work is reviewed by Hume and Link (1945) and Hume (1954). During Operation Norman, sections on and near Bear Rock were examined by Aitken *et al* (1973) and a geological map of the Fort Norman map area (96E) was prepared by Cook and Aitken (1976). There is broad agreement on lithological boundaries between the geological maps. However, structural features are modified in the Cook and Aitken version. Morrow and Meijer-Drees (1981) remeasured Stelck's type section of the Bear Rock Formation and revised some formational boundaries of the Cook and Aitken map. Savigny (1989) subsequently reinterpreted regional structural features.

During fieldwork, the author traversed most of Bear Rock noting the distribution and lithology of the formations present. Emphasis was placed on: (i) describing the lithology of the karst hosting strata (Bear Rock and Franklin Mountain Formations), (ii) establishing the distribution and orientation of these units, and (iii) interpreting the broad structure of Bear Rock. These objectives have been largely

achieved. The Bear Rock and Franklin Mountain Formations were examined at many locations, and the contact between them and adjacent units have been well established. However, there is uncertainty regarding the aerial extent and the displacement of faults in the western and southern portions of the range. Access to some locations was limited by steep slopes and interpretation hindered by covered intervals. The geological map presented in Figure 10.6 incorporates field observations and data from previous work. The following sections describe the lithology and structure of Bear Rock.

10.2.1 Lithology and Distribution

Strata exposed at Bear Rock span the Cambrian to Tertiary. Outcrop on the upland includes the Saline River, Franklin Mountain, Bear Rock, and Hume Formations. Younger strata are distributed to the east and west.

10.2.1.1 Saline River Formation

The Saline River Formation outcrops on the eastern margin of Bear Rock where it occurs in the hanging wall of a major thrust. In this area, the formation rests upon strata of Tertiary age (Section 10.2.2). Owing to its recessive character it is generally poorly exposed. A section in a steep gully at the southeastern end of Bear Rock shows 34 m of the upper beds along a reverse fault (Section MQ-3: Aitken *et al*, 1973). This section was described by Aitken *et al* (1973) and examined by the author. It mainly consists of red to reddish brown gypsiferous mudstone with minor interbedded dolomite. Thin bands of gypsum (selenite) and green mudstone were present. Beds were highly contorted and there were many small faults and folds. The contact with the overlying Franklin Mountain Formation is covered.

A complete section was described by Aitken *et al* (1973) from a valley side location northwest of Bear Rock (Section MQ-2: 65°17' N Lat., 126°16' W Long.). The upper portion is recessive, red mudstone with some interbedded dolomite and other clastics. Lower in the section the mudstone becomes progressively more

contorted and folded, brecciated intervals of dolomite occur and the content of gypsum increases. The latter is noted as selenite crystals, nodular gypsum, and massive gypsum beds. There is evidence of gypsum solution and reprecipitation at some surfaces. The total exposure is 162 m in thickness and may represent a complete section. The subsurface thickness of the Saline River Formation is highly variable in the area. At Vermillion Ridge No. 1 Well the thickness exceeds 885 m with 796 m occurring as evaporite (Salt Member: Pugh, 1993).

10.2.1.2 Franklin Mountain Formation

The Franklin Mountain Formation forms the bold cliffs at the northern and eastern flanks of Bear Rock. It is also exposed in the Long Lake area of the South Karst. The formation is divided into the Cyclic, Rhythmic, and Cherty Members. In the lower Keele River area, it has an average thickness of 400 to 450 m (Pugh, 1993). In the southern Norman Range, the formation thins markedly. The Cherty Member was eroded during pre-Devonian activity across Keele Arch (Figure 4.4). Only the Cyclic and Rhythmic Members of the formation are present in the Bear Rock area.

The basal Cyclic Member conformably overlies the Saline River Formation. In the main, it is a yellowish orange, recessive unit that has an average thickness of about 40 m in the region. At the MQ-3 section, the Cyclic Member consists of alternating sequences of: (i) recessive, argillaceous dolomite and dolomitic shale, (ii) yellowish orange, very finely crystalline dolomite, (iii) flat pebble conglomeritic dolomite, and (iv) stromatolitic dolomite. There are brecciated intervals. The measured thickness is 44 m. The pattern of lithic cycles is repeated elsewhere in the Norman Range (Aitken and Cook, 1974). The Cyclic Member forms a prominent structural bench along the eastern flank of Bear Rock. The strata dip to the southwest and the bench elevation decreases southward.

The Rhythmic Member is characterized by a colour banding due to recurring couplets of light brownish grey and brownish grey dolomite. At the Bear Rock Site, this member comprises the bulk of the Franklin outcrop. The upland at the

northeastern end of the range is a dip slope in this member. Elsewhere, it is represented as a second topographic bench sitting above that of the Cyclic Member. The best exposures of the Rhythmic Member are on the steep southern flank of Bear Rock. The member consists of intervals of buff or light greyish brown, thin bedded, micro and very finely crystalline dolomite that alternate with darker brown, fine to medium crystalline, thin to medium bedded dolomite (Morrow and Meijer Drees, 1981).

In the Bear Rock area, the Rhythmic Member forms the upper unit of the Franklin Mountain Formation. It is unconformably overlain by the Bear Rock Formation. The Cherty Member of the Franklin Mountain Formation and the Mount Kindle Formation are absent across the area of Keele Arch due to pre-Kindle and pre-Devonian erosion. At Bear Rock, this erosion was sufficient to partially remove the Rhythmic Member. Consequently, its thickness is variable due to differential erosion. At the nearest borehole the unit has a thickness of 210 m (Candel Police Island: 64°45'38" N Lat. 125°12'57" W Long.: Pugh, 1993), and it averages 200 m in the Norman Range to the north. Exposures on the east side of Bear Rock show a stratigraphic thickness estimated at 270 m for the Rhythmic Member. The total thickness for the Franklin Mountain Formation is 320 m. In southern Bear Rock, this thickness may be inflated due to fault repeats. The possibility also exists that the lower beds of the Cherty Member are locally preserved, though they were not observed on site. The Cherty Member is coarsely crystalline dolomite, pale in colour, with abundant light coloured chert and minor amounts of quartz sand.

The contact with the Bear Rock Formation is typically poorly exposed. However, at several locations the unconformity is seen to be irregular. A large mass of breccia, 20 m in width, extends 5 to 10 m into a depression in the Rhythmic Member at a site 4.5 km north of the Mackenzie River. Elsewhere, tabular and columnar masses of Bear Rock Formation breccia reach several metres into well-bedded sequences of the Rhythmic Member (Morrow and Meijer Drees, 1981). Breccia pipes taper downward and often include chert nodules that were likely

eroded from the Cherty Member. The nature of the contact shows the pre-Devonian erosion surface on the Franklin Mountain Formation displayed considerable relief and likely possessed karst landforms. Currently, surficial karst features are restricted to the Rhythmic Member of the formation.

10.2.1.3 Bear Rock Formation

Much of the upland surface at Bear Rock is composed of the Bear Rock Formation (Figure 10.6). Exposures on the steep slopes overlooking the Mackenzie River comprise the type section (Hume, 1954; Morrow and Meijer Drees, 1981). The formation was examined at the type section and across the karst area. It is divided into a lower Brecciated Member and an upper bedded limestone unit called the Landry Member. At the type section, the Brecciated Member is primarily a massive weathering, particulate rubble packbreccia and floatbreccia. Clasts are angular, very poorly sorted, finely crystalline dolomite and calcite. The matrix is predominantly reprecipitated micrite and is locally silty (Morrow and Meijer-Drees, 1981). The clast size increases upward through the section with the upper portion of the exposure containing clasts that exceed 1 m in diameter. In outcrop, many clasts appear rounded due to solution in rainwater following exposure. The Brecciated Member weathers a pale grey colour and contains little terrigenous material relative to exposures in the area of the Norman Wells High (e.g., Dodo Canyon area). It does have thin irregular intervals of calcite cemented crackle breccia and zones where the interfragmentary spaces are open. Cavernous and vug porosity are conspicuous, fissure frequencies are high. Stelck (1944) described the outcrop as gypsiferous dolomite and limestone. No massive or nodular beds of gypsum were located. Field testing of hand samples with dilute HCl acid revealed the character of the unit is calcareous with most clasts testing as limestone. The thickness of this unit at the type section is 154 m, which exceeds that of exposures in the Canyon Ranges.

The brecciated interval passes through a thin unit of calcite cemented mosaic packbreccia into the overlying Landry Member. The base of the Landry is

characterized by a thinly bedded recessive unit of silty lime mudstone. This is overlain by a thick interval of resistant medium bedded, pelletal lime mudstone. The Landry has a thickness of 65 m at the type section, making a total thickness of 219 m for the Bear Rock Formation. The formation is conformably overlain by the Hume Formation. The Landry Member is present at the type section and along the southern and western flanks of the Bear Rock upland. Where present, it is a resistant weathering unit. Across most of the North and South Karsts the Landry is absent which has a strong influence on the topographic expression of the karst.

10.2.1.4 Hume Formation

The Hume Formation outcrops on the southwestern and western edges of Bear Rock. It is lithologically similar to exposures described from the Canyon Ranges. The upper portion forms a prominent cliff that runs along the western margin of Bear Rock (Figure 10.1). It was examined where it is cut by Forest Stream. It consists of thickly bedded, resistant, fossiliferous limestone. The lower recessive portion was examined along the banks of the Mackenzie River. It is thinly bedded, argillaceous limestone and minor shale. In the nearest borehole to the site, the Hume Formation has a total thickness of 114 m (Imperial Bluefish Canol I-A: 64°56'1" N Lat., 125°50'54" W Long.: Pugh, 1993). The upper resistant interval comprises 52 m of that total.

10.2.1.5 Other Units

The Hare Indian and Canol Formations outcrop to the west of the Hume Formation. The positions of these units are not well defined. These formations are lithologically dominated by shale. The easternmost position of the Hare Indian as mapped on the northern bank of the Mackenzie River corresponds with the first thick interval of exposed shale. On the east side of Bear Rock, the Saline River Formation rests on coarse clastics of Tertiary age (Paleocene and Eocene) (Cook and Aitken, 1976). The cover of glacial sediments on Bear Rock is thin. The low elevation areas to the

east and west are covered in a veneer of ground moraine (till) and glaciolacustrine sediments (Savigny, 1989). Much of the lowland was flooded by proglacial Lake Mackenzie following the Late Wisconsinan retreat (Smith, 1992).

10.2.2 Structure

East of Norman Wells, the Norman Range trends to the southeast. Approaching Bear Rock, the orientation of the range gradually turns southward. Paleozoic strata are exposed on the flanks and crest of the range. Strata on the western flank dip moderately to the southwest. The northeastern slope is far more rugged and is characterized by a series of sharp fault scarps. Thrust faults occur at the base of scarp slopes above Kelly Lake and east of Discovery Ridge. This fault system extends along the east slope of the Norman Range south to the Mackenzie River (Figure 4.2). In the Bear Rock area, the associated thrust brings the Saline River Formation into contact with Tertiary clastics (Figure 10.6). The position of the fault trace is obscured by glacial sediments. As mapped, it is thought to lie below the elevation of the Bear Rock Spring Area and follows a path approximately parallel to Congo River. Bear Rock is located near the eastern limit of deformation in the Mackenzie Fold Belt. Its general structure is that of a westward dipping upthrust block. Steep scarp slopes mark its eastern margin. Strata dip moderately to the west and southwest. While the range as a whole is not a large anticlinal feature, there is a tight anticline in the South Karst. In addition, there are several poorly mapped minor faults and folds.

In the South Karst, there are two minor thrust faults exposed on the slopes adjacent to the Mackenzie River (Figure 10.6). Both faults pass up gullies from the base of Bear Rock onto the upland. The eastern fault has a vertical throw of less than 30 m. On the upland surface, the Franklin Mountain Formation is exposed above the Bear Rock Formation on a steep bluff. The contact is covered. In the hanging wall, Franklin strata dip to the west at 30°. Just above the contact, strata are shattered with many fractures, some are infilled with calcite. Bear Rock Formation strata below the

fault plane are brecciated and the bedding is upturned to an almost vertical position.

The second fault appears very steep. Strata in the hanging wall dip at angles greater than 60° to the west and northwest. The vertical throw is unknown but the fault exposes over 40 m of the Saline River Formation where it rests on the Franklin Mountain Formation in the footwall. On the upland surface, the fault can be traced to a position within 500-600 m of Long Lake. Northward there is a gap in surface linear features but Cook and Aitken (1976) extend the fault trace along the eastern shore of Long and Round Lakes to the area west of Franklin Lake. They show the Franklin Mountain Formation on the west side of the fault in the hanging wall, and Bear Rock Formation in the footwall. The topography of the South Karst is consistent with this interpretation. A steep slope marks the eastern shore of Long and Round Lakes. Stelck, as reported in Hume (1954), also noted that the two faults at the south end of Bear Rock show thrusting from the southwest to northeast. However, the fault traces are not extended into the Long Lake area by Stelck, instead an anticline is shown parallel to the depression. The axis of the anticline runs along Long Lake. The Franklin Mountain Formation is mapped on both shorelines. Fieldwork by this author has validated Stelck's interpretation. Long Lake lies in an anticline in the Franklin Mountain Formation (Figure 10.6). On the west slopes, strata dip sharply to the southwest at angles between 35° and 55° . Strata of the overlying Bear Rock Formation have a similar orientation. West of Camp One on the eastern slope above Long Lake, the Franklin Mountain Formation was located below the slope crest. Strata dip to the east and northeast at 30° to 45° . Overlying exposures of the Bear Rock Formation breccia also dip eastward and contain some chert. The presence of chert is indicative of the basal beds of the Bear Rock Formation in the area. Thus, the Franklin Mountain Formation has not been thrust over the Bear Rock Formation at the contact. The Long Lake anticline was traced to the area northeast of Round Lake where it plunged. The western shoreline of Round Lake is in the Bear Rock Formation. At the Round Lake Sink Point (R17) strata appear to dip to the southwest at 20° . Franklin Lake is entirely in the Franklin

Mountain Formation. The Franklin Mountain and surrounding Bear Rock strata dip to the west and northwest at 10° to 25° . There is the possibility that the fault mapped by Cook and Aitken (1976) does outcrop on the floor of Long Lake or it simply does not propagate to the surface. The thrust and the Long Lake anticline are clearly related and were probably generated by the same compressive forces that influenced the South Karst area during uplift.

On the southwest flank of Bear Rock there is a series of minor folds. A tight syncline occurs in the Bear Rock Formation west of the Franklin contact. The section passes through westward, near vertical, and eastward dipping strata. West of this steeply dipping zone, there is a covered interval that was mapped by Stelck (cited in Hume, 1954) and Cook and Aitken (1976) as Hume Formation. The area is considered Bear Rock Formation by Morrow and Meijer Drees (1981) and is depicted as such in Figure 10.6. The Landry Member is clearly visible at a prominent headland just east of the mapped boundary with the Hume Formation (Figure 10.6). Strata are folded and faulted at the river level. Cook and Aitken (1976) show another synclinal feature at that location. Farther west in the Hume Formation there is a small anticline. Strata on the east side of the feature dip at 25° to the southeast. West of the axis, the Hume Formation is partially brecciated and dips at 45° to the southwest. Shales of the Hare Indian Formation are exposed 100 m east of Blood Stream where they are observed to dip sharply to the southwest. The controls on these folds are few and their positions should be considered approximate.

The south flank of Bear Rock has several steep cliffs in the Bear Rock and Hume Formations. Stelck mapped faults at the bases of these cliffs but did not comment on their nature. One exposure below Forest Spring has the appearance of a fault scarp. Savigny (1989) shows a normal fault extending from this area to the northwest. The fault is parallel to the contact of the Hume and Bear Rock Formations, with the Hume in the footwall. This feature is not shown on Figure 10.6 as the author has not thoroughly inspected that site. The other cliffs facing the Mackenzie River are erosional features. Late Wisconsinan ice of the Mackenzie

Lobe advanced from east to west across the region. The steep slopes were probably accented by plucking and block entrainment along joints, fractures, and other fissures in the strata.

In the eastern section of the North Karst, strata of the Franklin Mountain Formation dip to the west and southwest at 15° to 20° (Figure 10.6). The Bear Rock Formation forms most of the outcrops in the recharge area. Recognition of bedding in the brecciated interval requires large, clean exposures. Where outcrops are weathered, frost shattered, and partially vegetated, the measurement of strike and dip proved difficult. The most credible estimates are taken from the base of the Brecciated Member or from the Landry Member. Over most of the North Karst, the Landry Member is absent and the Bear Rock strata are mainly float and packbreccias. Consequently, many dip readings are estimated. In the central area of the North Karst, the Bear Rock Formation dips between 20° and 30° to the south and southwest. On the northwest flank of the upland several outcrops dip to the northwest. There is much variability at the scale of individual depressions. Bedding often appears draped towards sink points or the central axes of linear depressions and valleys. In the largest example, strata bordering the upper Vale Stream valley dip into the valley axis.

A few lineaments are shown on Figure 10.6. These were located from aerial photographs as aligned drainage courses, steep slopes or breaks in slope, and linear patterns in vegetation. A major lineament runs from Round Lake to Vale Stream, another from Long Lake anticline to the eastern margin of Camp Depression. These and other lineaments may represent minor faults or fracture zones that do not involve substantial displacement of rock units. If so, they should represent pathways of high hydraulic conductivity for circulating groundwaters and possibly areas of increased bedrock and surface subsidence.

There are a series of faults in the northwest part of Bear Rock. The high ground west of Vale Stream is bounded by faults on its west side. A fault runs southward from the northern boundary of Figure 10.6 through the Bear Rock

Formation. This is mapped as a normal fault by Cook and Aitken (1976) with the downthrown block on the west. They extend this fault past the topographic high towards the headwaters of West Stream. Stelck (reported in Hume 1954) also noted the presence of this fault and that the upthrown block was on the east. Where the fault forms the boundary between the Hume and the Bear Rock Formations, it appears that Bear Rock strata are thrust against the Hume and the inclination of the fault plane is very steep. Field examinations of that area were limited but it was apparent there is a thrust between the Bear Rock and Hume Formations. The morphology and displacement of the units do not correspond with that of an extension fault. Given the discrepancy with the interpretation of Cook and Aitken (1976) the sense of displacement is not shown for that fault on Figure 10.6.

10.3 Geomorphology

The general topographic features of Bear Rock are related to the structure and lithology of the bedrock units that comprise the range. The bold cliffs that border the upland are fault generated or the product of differential erosion between formations of varying resistance. Superimposed on the structural features are karst, glacial, fluvio-glacial, and periglacial landforms. The terrain reflects this variety of processes and the properties of the bedrock. On the upland surface, distinctive topographies are associated with the Franklin Mountain and Bear Rock Formations. The former is expressed as gently sloping ground and benches at the northeastern and eastern portions of the range, while the latter is an undulating surface of karst depressions. In the following sections, the characteristics of karst landforms at the site are reviewed. A map of karst features is presented in Figure 10.7. Aerial photographs of the North and South Karst areas are shown in Figures 10.2 and 10.3. Due to the impact of glaciation on the geomorphology the glacial record is briefly reviewed.

10.3.1 Glacial

Glacial sediments occur across the full range of elevations at Bear Rock. In the

Pleistocene, Bear Rock was repeatedly glaciated by the Laurentide Ice Sheet. The Late Wisconsinan glacial maximum occurred during the Hungry Creek Glaciation, when Laurentide ice advanced into the Canyon Ranges of the Mackenzie Mountains. The retreat was broken by three stadials: Katherine Creek, Tutsieta Lake, and Kelly Lake Phases (Chapter V). After the Tutsieta Lake Phase, it is possible that Laurentide ice retreated to a position below the Bear Rock upland. The subsequent readvance of the Kelly Lake Phase is marked by a sharp moraine on an upland 55 km north of Bear Rock (Hughes, 1987). The moraine rises to an elevation of 490 m. During this stadial, Laurentide ice is thought to have occupied the floor of the Mackenzie Valley almost as far north as Mountain River (Figure 5.4). High ground in the Franklin Mountains stood above the level of the glaciation, but it is likely the whole of Bear Rock was ice covered. Dating control on the Kelly Lake Phase is provided by plant materials recovered from deltaic sediments associated with Glacial Lake Mackenzie near Fort Norman. The minimum deglaciation date on the lowland is $10,600 \pm 260$ BP (GSC-2328). The Tutsieta Lake Phase has a minimum date of $12,900 \pm 150$ BP (GSC-1784-2). Thus, the final retreat of ice from the Bear Rock upland occurred some time before 10,600 BP (12 ka?). Pedestals beneath erratics reach a maximum height of 80 mm at Bear Rock.

A range of glacial landforms are present on the upland surface. The most striking are a series of streamlined bedrock forms developed on the Brecciated Member at several areas of the range. They are less frequent and poorly developed on the Franklin Mountain Formation. The streamlined landforms are primarily whaleback ridges and rock drumlin features (Figures 10.8, 10.9). The long axes of the ridges have an east to west orientation. These landforms impart a ribbed appearance to the North Karst where they cover much of the surface area (Figures 10.2, 10.9). Ridge heights vary from less than one metre to tens of metres. Many extend laterally for distances of hundreds of metres. In cross-section, some features are symmetrical with smooth bedrock or debris mantled surfaces on their flanks and crests. Others have sharp pinnacles developed along the ridge line. Many have

smooth south facing slopes and steep north facing slopes. The northern faces often appear quarried, producing a roche moutonnée appearance. In addition, there are several small examples of crag and tail depositional landforms or flutes. In long profile, these features taper from east to west.

The bedrock landforms were produced by subglacial abrasion and plucking. Their presence and morphology suggests the last ice over Bear Rock was warm based and moved in an east to west direction. This is consistent with ice direction indicators from adjacent areas. The possibility that the aligned ridges are purely structural in origin has been rejected. In the areas of the range where they occur, the Bear Rock Formation does not display uniform properties. Dips vary from south to northwest. Strata along individual ridges range from particulate cemented floatbreccia to calcite cemented packbreccia. In places, smooth gently sloping surfaces may approximate dip slopes and the steep faces may be small scarp features but no consistent pattern was observed. The less prominent nature of these features on the Franklin Mountain Formation is probably due to the resistant nature of that unit. The high fissure frequency of the Bear Rock breccia makes it susceptible to glacial plucking. Abrasion rates would be high due to the low hardness of the breccia relative to the shield erratics functioning as tools in the basal ice. These processes would be favoured by the undulating karst of Bear Rock. The karst presents a bed of high surface roughness which would be expected to increase the rate of enhanced creep and the formation of regelation ice (Drewry, 1986). While the aligned ridges are attributed to glaciation and can be observed in the Franklin Mountains to the north, the controls on the spacing of the streamlined features are unknown.

Glaciation also produced steep walled troughs and may have contributed to scouring of depressions. There are a series of meltwater channels northwest of Bear Rock and small drainage features on the upland surface. Channels occupy positions between aligned ridges, and can be continuous across depressions. The cover of glacial sediments across Bear Rock is sporadic. At the higher elevations and ridges,

there is a lag of winnowed erratic materials ranging in size from sands to boulders. The floors of some depressions are flat, due in part to infilling with glacial drift. Excavations from the Camp Depression area show a widespread distribution of fluvioglacial sediments in doline bottoms. Finally, at several outcrops of the breccia, small solution conduits were infilled with silts.

10.3.2 Karst

Chapter VI described the characteristics of karst landforms occurring in the region. The following sections provide additional information on major features present at the Bear Rock Site. The suite of karst landforms includes a variety of closed depressions and dolines forms and an area of spring deposits. No karren were observed.

10.3.2.1 Mapping

The boundary of the recharge zone and the locations of ponors and springs are shown on Figure 10.7. These features were identified from field surveys and aerial photography. Mapping was done with low level photographs of 1:10,625 scale. The recharge zone is defined based on surface topography. It includes some areas that slope away from the central portion of the upland but where the drainage is still captured by dolines. Regions external to the mapped boundary may also function as areas of recharge but lack surface karst. The recharge zone is divided into many small basins. Occasionally it was possible to delimit basins on the order of a single doline or ponor. Where there is little local relief or dense vegetation, the local basin boundaries are not well defined.

Ponors are sink points on the floors of dolines or compound depressions. Many are seasonally flooded and appear as ponds or pools of standing water following snowmelt. When drained, the larger sink points are usually marked by open grassy areas bordered by deciduous vegetation. Other sink points are in bedrock. These types of ponors were easily seen on the photographs. However,

ground surveys showed many ponors of radius less than 2 m. Where they occur in areas of thick coniferous cover, they were often not visible on the photography. The distribution depicted on Figure 10.7 cannot be considered a census of the total population but it is thought to be representative. Previous mapping of karst at Bear Rock involved the shading of areas enclosed in 50 foot depression contours (van Everdingen, 1981). This only identified deep depressions and not individual sink points.

The Bear Rock Site is not characterized by dolines and depressions that are easily mapped as discrete features (e.g., Figure 10.4). On the upland surface, steep slopes and ridges partially or fully enclose some circular and linear depressions (Figure 10.7). More common are dolines that are irregular in plan and are bordered by variable slopes and rolling hills. Illustration of the latter features was difficult. As mapped, it appears many dolines are breached or open sinks. The presence or absence of ponors indicates if drainage is karstic. Subdivisions within the recharge zone mark the local depression basins.

10.3.2.2 Dolines and Depressions

Most of the karst landforms are developed on the breccia of the Bear Rock Formation. Doline density is highest through the central part of the North Karst and western portion of the South Karst. There are a few shallow dolines on dolomite of the Franklin Mountain Formation at the northeastern end of the range. Where the slope of the upland is steep there are few ponors. In the central part of the range, sink points on the breccia are located on gentle terrain, often between streamlined ridges and on the bases of lobate or circular dolines (Figure 10.7). Relief surrounding the sinks may be high.

Swales between many of the parallel ridges are flat to gently sloping. In places, there are small depressions in these valleys. Some are linked by shallow channels. The capacities of some of these sinks are low and surface waters were often observed to be routed towards larger dolines. In some valleys, bedrock spurs

extend from ridge crests into the central valley axis dividing the swale into sub-basins. Ponors may occur within these basins (e.g., R20 and R21). Most of the spurs are preserved as fragments on the margins of the valleys. The ponors may mark the positions of dolines that have been removed or greatly modified by subglacial erosion and the bedrock spurs are remnants of bordering hills or walls. Much of the eastern and northern portions of the recharge zone have a topography of linear ridges and swales. This is well expressed east of sample point R34, where there are several ponors within a series of parallel valleys. Despite glacial erosion across the recharge zone, the hydrological functions of the ponors are preserved. In the swales where sink points are absent, they are presumably infilled with glacial sediments or were completely removed by erosion. Between the North and South Karst, there is a low elevation area in the Bear Rock Formation that lies outside the recharge zone. The region lacks depressions and sink points due to the impact of glaciation. The area is characterized by many small whaleback ridges, crag and tail features, and glacial meltwater channels. A similar situation occurs at the north end of Bear Rock. Outcrops of the breccia are mantled in a thick glacial cover and drainage is nonkarstic.

The very sharp collapse-subsidence dolines seen at Dodo Canyon, Bonus Lake, and at sites elsewhere in the Canyon Ranges and Franklin Mountains are rare at the Bear Rock Site. The explanation is the lack of a resistant cover over an evaporite-rich unit. At Dodo Canyon, the Landry Member and Hume Formations function as cover to the Bear Rock breccia. To the northeast, very sharp collapse dolines in the Mount Kindle and Franklin Mountain Formations occur above evaporites of the Saline River Formation. Vermillion Creek sinkhole is a collapse feature in shales and limestone above gypsum of the Fort Norman (Bear Rock) Formation. There are steep sided dolines located in the western portion of the recharge zone along a lineament that extends southeast from upper Vale Stream. These dolines are at the western end of the steep ridge that separates the North and South Karsts and are developed entirely within the breccia.

The typical doline of Bear Rock is a solution-subsidence landform developed in the Brecciated Member. They are circular to lobate in plan and bound by irregular hills and slopes of moderate steepness. Doline floors are gently sloping to flat. Diameters range from several to hundreds of metres. Local relief is variable but is commonly between 10 and 20 m. In places, the morphology is not unlike that of the tropical doline or cockpit.

Ponors are located at the low points of doline floors adjacent to or close to bedrock outcrops. Many ponors have the attributes of small suffosion sinks. The bases are in sediment and the sink points appear as gently sloping cones or shallow vegetated hollows. Ponors in sediment are seasonally flooded. Typical dimensions of the flooded areas are 10 m in diameter. Other ponors are developed in bedrock and are steep walled. Shafts of 2 m depth and width are typical of this group. Infiltration into these sinks is rapid. Despite the high density of ponors, standing pools of water remain perched on doline bases through the summer period, often only metres away from sink points.

Compound dolines occur at several locations on Bear Rock. The largest is Camp Depression. In plan it has an irregular outline (Figure 10.7). It is bound by a linear ridge to the north and a steep rise to the east. The latter boundary is aligned to a lineament (Figure 10.6). The margin to the south and west is lobate. In section the floor of Camp Depression is flat with small residual knolls of bedrock. The morphology suggests the depression has expanded by lateral corrosion and captured the basins of adjacent dolines. The depth of the Franklin Mountain Formation below the sink point (R37) is unknown, but it may function as an inlier of low permeability strata at the depression base. This would encourage lateral corrosion over vertical. Periglacial processes also favour slope erosion in this environment.

Elsewhere on the upland, there are compound depressions of varying dimensions and stages of development. South of Camp Depression, there are a series of interconnected lobate and circular dolines (Figure 10.7). Within these are a hierarchy of sink points. The lowest ponor is in bedrock and is well-drained. At

higher elevations, there are suffosion sinks and eroded doline walls. These dolines appear to have coalesced by the breaching of downslope walls. East of Franklin Lake is a broad depression with three, widely spaced, well-drained ponors. The depression is partially enclosed by steep bedrock walls. Two glacial troughs cut into the feature from the east. In the centre of the depression is a conical bedrock knoll from which fragmented ridges extend to the depression margins. The feature is developed from the merging of at least three dolines. Locally, the floors are flat due to infilling by glacial sediments.

There are few depressions on the Franklin Mountain Formation. East of sample point R29 there is a linear depression developed along the contact of the Bear Rock and Franklin Mountain Formations. The breccia is exposed on the west wall and the dolomite on the east. Within it two sink points accept drainage from a large area north of point R20 (Figure 10.7). The deepest ponor is enclosed in dolomite. Northward is another doline developed almost entirely in the Franklin Mountain Formation. As mapped, there are two ponors and a closed basin. However, following rainfall an overflow channel that drains westward onto the Bear Rock Formation was activated. There are similar ponors near the contact of the two units to the south.

The largest karst feature at Bear Rock is the deep, linear depression that runs through Long, Round, and Franklin Lakes of the South Karst. The southern and central portions of this depression are aligned with the axial trace of an anticline in the Bear Rock and Franklin Mountain Formations. Only one ponor was located on the southern shoreline of Round Lake at sample point R17, but all three water bodies drain karstically. This depression is a linear subsidence trough. Folding and faulting in the South Karst would open pathways of high permeability to infiltrating groundwaters. A series of subsidence-solutions dolines would be expected to develop in the Bear Rock Formation along the anticline crest. Expansion of the features and increased depth of circulation would bring meteoric groundwaters into contact with evaporite of the underlying Saline River Formation. Deep groundwaters

may also have travelled along fault traces to the subface of the formation. Subrosion of the thick Salt Member would produce subsidence and expansion of the surface dolines into a single linear depression. Hydrochemical data from Blood and Forest Streams show the process continues (Section 10.4).

10.4 Hydrology and Hydrochemistry

Most of the observations at the Bear Rock Site occurred in mid-summer. In June of 1987, there was a brief reconnaissance of the Bear Rock Spring Area, and a survey of southern Bear Rock was done in early June of 1988. However, the snowmelt period was not observed nor were water samples collected during that time. Due to these limitations no attempt is made to characterize the hydrology of the site across the seasons. Hydrological data are reviewed in subsequent sections alongside hydrochemical data. The hydrochemical data are organized into groups reflecting the type of water body and the sampling location within the karst (Table 10.1). Eight water types are defined; three are classified as recharge waters and five as discharge. Recharge waters were sampled on the upland and are divided into: (i) surface waters infiltrating through dolines, ponors, or ponds (Type 1), (ii) perched or slowly infiltrating waters in ponds, lakes, and wetlands (Type 2), and (iii) springs, seeps, and surface streams in the recharge area (Type 3). Discharge water types include: (i) Forest and Blood Streams (Type 4), (ii) streams draining the upland margins (Type 5), (iii) springs and streams in the Bear Rock Spring Area (Type 6), (iv) Congo River (Type 7), and (v) other springs on the margin of Bear Rock (Type 8). Individual sample sites are listed and described in Table 10.2. Sample positions are shown on Figure 10.7. Raw data are presented in Appendix III.

Ion abundances for each water sample are plotted on a trilinear diagram (Figure 10.10). In all samples, Ca^{2+} comprises the dominant cation. Most recharge waters have a calcium bicarbonate chemistry while many discharge samples are calcium sulphate waters. Average ion concentrations for each water type are graphed in Figure 10.11. Additional physical and chemical data for the water types are

presented in Table 10.3. These data are discussed in the following sections.

10.4.1 Recharge Zone

The topographic limit of the recharge zone is shown on Figures 10.1 and 10.7. Over most of that area, surface waters are routed to the large depressions and dolines that occur through the central portion of the range (e.g., Camp Depression, Round and Long Lakes). Recharge also occurs through several dolines and channels that are in the peripheral areas of the zone and several that lie outside (e.g., R34). Near the margins of the recharge zone, there are some shallow ponds and dolines that have overflow channels. An example is along the upper part of Vale Stream below streams R25 and R28 (Figure 10.7). These streams flow to a shallow pond that functions as a sink. Downslope there are two additional ponors. It is possible that the capacities of these sinks may be exceeded during periods of intense precipitation or snowmelt and their overflow channels activated. Under these conditions surface waters can flow directly from the linear pond at R32 to lower Vale River (R27). A similar situation exists above the headwaters of West Stream where a doline occurs near the margin of the recharge zone. When observed in the field, all of these sink points were dry or draining. Aerial photographs from the snowmelt period of early June 1972 show them in a similar hydrological status.

10.4.1.1 Water Type 1: Draining Ponds and Dolines

This type includes waters sinking in ponds, dolines, or ponors where the infiltration rate is high (Tables 10.1, 10.2). Samples were taken from dolines on the Bear Rock Formation in the Camp Depression area (R20, R21, R23) and from the sink points from Round Lake (R17) and the west pond at Camp Depression (R37). Sample R29 was excluded from calculations due to a high ion balance error (8.8%).

The average temperature, total hardness, and total dissolved ions for this water type are 9.0°C, 167 mg L⁻¹ CaCO₃, and 6.51 meq L⁻¹ (Table 10.3). Ion abundances are Ca²⁺>Mg²⁺ and HCO₃⁻>SO₄²⁻ by equivalence, Cl⁻ and Na⁺ occur only

in trace amounts. These waters are aggressive towards calcite ($SI_C = -0.42$) and dolomite ($SI_D = -1.51$) and show enrichment in CO_2 ($pPCO_2 = 2.36$). The Ca^{2+} , SO_4^{2-} , and TDI concentrations are inflated by the one sample from location R20. This sample was drawn from a doline located between two sharp pinnacled ridges east of Camp Depression. Discharge into the sink was about $1 L s^{-1}$. The high Ca^{2+} and SO_4^{2-} values show this water had encountered gypsum. This may indicate there is gypsum close to the surface of the Brecciated Member or that local groundwater circulation within the recharge area is driven below the permafrost. The high relief near the sample point would favour the latter. It is also likely that the distribution of permafrost on south facing slopes is sporadic. Other recharge samples of this type (R21, R37) and Types 2 and 3 also have high concentrations of SO_4^{2-} . This contrasts with the Dodo Canyon Site where circulation in the recharge area is confined to the suprapermafrost aquifer.

There are many small dolines and ponors where surface waters infiltrated rapidly. They are located in the swales between the parallel ridges and in the depressions through the central portion of the range. Following summer rainfall events, surface flows were observed in small channels within depressions (e.g., Water Type 3). Between storm events most of the channels are dry. The basins in which these sinks are located are vegetated and have soils with thick organic surface horizons. The high $pPCO_2$ values suggest the waters are equilibrated with high CO_2 concentrations from the soil atmosphere.

On the southwestern shoreline of Round Lake, a small channel flows into a cave at the base of a bluff in the Bear Rock Formation. This is Round Lake Sink (R17) and was the only ponor located on the margins of Long, Round, and Franklin Lakes. The cave is 5 m in length and pinches into breakdown. The flow from the lake infiltrates through the channel bed and the cave floor. An aerial survey in early June of 1987 showed a high discharge to the sink point. In a ground check on July 12, 1987 the flow was only $2 L s^{-1}$. Presumably the lake level had fallen, following passage of the snowmelt pulse into the system. The flow was sampled on June 9,

1988 when the discharge into the cave was 10 - 15 L s⁻¹. The water has a calcium bicarbonate chemistry and is strongly aggressive to calcite and dolomite ($SI_C = -0.65$, $SI_D = -2.01$). It is very likely there are other unseen sink points below the water line in Round Lake.

Rhodamine WT was introduced into the Round Lake Sink on July 14, 1987 and again on June 9, 1988. Detectors had been placed at Forest and Blood Streams to the southwest. The 1987 detectors were poorly secured and were lost to a storm event. The 1988 detectors were recovered on August 9. The elutant tested as positive in the laboratory. This trace established a less than 60 day connection between Round Lake Sink and Blood and Forest Streams. Detectors had also been placed at the Bear Rock Spring Area, though a positive result was not expected. Elutant extracted from these detectors showed a high background fluorescence but was negative.

10.4.1.2 Water Type 2: Perched Lakes and Ponds

Samples of this water type are perched or slowly draining surface waters (Tables 10.1, 10.2). Included are samples drawn from the shorelines of Round and Long Lakes (R6, R7), samples from wetlands (R30, R35), and doline and pond waters from the upper Vale Stream area (R31, R32, R33). A complete analysis is not available for location R34.

The average temperature, total hardness, and total dissolved ions for this water type are 14.0°C, 128 mg L⁻¹ CaCO₃, and 5.43 meq L⁻¹ (Table 10.3). Ion abundances are Ca²⁺ > Mg²⁺ >> Na⁺ and HCO₃⁻ > SO₄²⁻ >> Cl⁻ by equivalence. Samples are near equilibrium with respect to calcite ($SI_C = 0.17$) and dolomite ($SI_D = -0.13$) and are little enriched in CO₂ ($pPCO_2 = 3.02$). The high temperature and the equilibrium saturation indices are expected for perched and slowly draining waters. The high concentration of SO₄²⁻ (0.45 meq L⁻¹) shows that a variety of waters circulating within the recharge zone encounter gypsum.

There is much variability within this data grouping that is not captured by the

average values above. Sample R31 was drawn from a pond at the base of a doline. It has a low total hardness ($64 \text{ mg L}^{-1} \text{ CaCO}_3$) and SO_4^{2-} concentration (0.1 meq L^{-1}). The water is aggressive to calcite and dolomite ($\text{SI}_C = -0.81$, $\text{SI}_D = -1.87$) and the $\delta^{18}\text{O}$ value shows a dominance of summer precipitation (-17.7 ‰). Sample R33 was taken from a nearby shallow pond. It has a higher total hardness ($173 \text{ mg L}^{-1} \text{ CaCO}_3$) and SO_4^{2-} concentration (0.88 meq L^{-1}), and has near equilibrium saturation indices ($\text{SI}_C = 0.18$, $\text{SI}_D = -0.02$). The $\delta^{18}\text{O}$ value of -21.3 ‰ show melting ground ice and snow contribute to its flow. The basin of R33 is larger and includes several small seeps that discharge from the surrounding slopes towards the sample point. A sub or intrapermafrost circulation of this water is suggested by the isotope ratio and water chemistry.

There is a high density of ponors in the recharge zone, but there were many locations where water was observed perched on the surface in shallow ponds and wetlands. In some instances these perched waters were within several metres of drained sink points but were not connected hydrologically. This was most common where there were thick organic-rich soils or surface deposits of fine grained materials. Late July excavations into peaty soils that were dry on the surface showed the thickness of the active layer varied between 50 and 80 cm on the floor on Camp Depression. Where relief was gentle, the suprapermafrost water table was generally within 40 cm of the surface.

Samples R30 and R35 were drawn from wetlands at the base of large depressions. Both samples are aggressive towards calcite and dolomite ($\text{SI}_C = -0.27$ and -0.43 , $\text{SI}_D = -1.11$ and -1.58), have high total hardness and total dissolved ion values ($\text{Thd} = 188$ and $229 \text{ mg L}^{-1} \text{ CaCO}_3$, $\text{TDI} = 7.46$ and 9.09 meq L^{-1}) and are equilibrated with high concentrations of CO_2 ($p\text{PCO}_2 = 2.09$ and 1.82). The high hardness suggests flowpaths to these points involve long travel times through the suprapermafrost aquifer. These waters were observed to be draining very slowly to channels or sink points. Such waters represent significant solvent potential due to their aggressive nature.

The four samples from Round and Long Lakes (R6 and R7) contrast with the wetland locations. Total hardness and total dissolved ion values are low ($\approx 105 \text{ mg L}^{-1} \text{ CaCO}_3$ and 4.1 meq L^{-1}), the samples are saturated with respect to calcite and dolomite ($SI_C \approx 0.65$, $SI_D \approx 0.8$) and are equilibrated to atmospheric concentrations of CO_2 ($p\text{PCO}_2 = 3.65$). These samples were collected from shallow water at the shoreline in late July. The Round Lake Sink sample (R17) collected in early June is aggressive. There may be a seasonal pattern in the aggressiveness of these lake waters.

10.4.1.3 Water Type 3: Springs and Streams

This water type includes springs, seeps, and streams within the recharge zone (Tables 10.1, 10.2). Four samples were drawn from the catchment of Camp Depression (R18, R19, R24, R36) and two from the upper Vale Stream area (R25, R28). In the recharge zone, there are many small channels located between ridges and on the floors of dolines. Seeps and springs are found below steep slopes, often discharging from talus. Spring flows either contribute directly to stream channels, to other surface waters, or infiltrate into the active layer. While flows increased following rainfall events the magnitudes of those responses were small. There was much surface detention, storage in the active layer, and discharge from small groundwater seeps. Consequently, the discharge of streams flowing to ponors was sustained at low levels for much of the summer period.

The average temperature, total hardness, and total dissolved ions for this water type are 10.6°C , $197 \text{ mg L}^{-1} \text{ CaCO}_3$, and 7.82 meq L^{-1} (Table 10.3). Ion abundances are $\text{Ca}^{2+} > \text{Mg}^{2+} > \text{Na}^+$ and $\text{HCO}_3^- > \text{SO}_4^{2-} > \text{Cl}^-$ by equivalence. Samples are aggressive towards calcite ($SI_C = -0.31$) and dolomite ($SI_D = -1.29$) and are enriched in CO_2 ($p\text{PCO}_2 = 2.04$). While the hardness and dissolved ion values are higher than the other recharge groups, the pattern is similar (Figures 10.10, 10.11). Once again, the relatively high SO_4^{2-} concentration (0.44 meq L^{-1}) shows samples contain dissolved gypsum.

In this grouping, water samples R25 and R36 have the highest total hardness and dissolved ion values ($T_{hd} = 188$ and $229 \text{ mg L}^{-1} \text{ CaCO}_3$, $TDI = 7.46$ and 9.09 meq L^{-1}). They are also strongly aggressive to calcite and dolomite ($SI_C = -0.63$ and -0.56 , $SI_D = -1.88$ and -1.81). Stream R36 drains low ground in Camp Depression and has a chemistry similar to wetland sample R35. Stream R25 is fed by diffuse seeps below a steep bluff in the Bear Rock Formation in the upper Vale Stream area. R25 has the highest SO_4^{2-} concentration (1.23 meq L^{-1}) and the lowest $\delta^{18}\text{O}$ value (-22.54) in the grouping. This sample suggests groundwater circulation to the seep points, and ultimately the stream, is not confined to a thin active layer. Also notable about samples R25 and R36 are a low pH of 6.91 and $p\text{PCO}_2$ values of 1.71 and 1.66. Such values suggest the partial pressure of CO_2 in the soil should approach 0.02 atmospheres (2% by volume). Measurements of soil CO_2 were taken from an organic soil at a site adjacent to the wetland in Camp Depression (Chapter II). However, the highest concentrations were 0.13% by volume. This discrepancy may be a function of poor sampling technique of the soil atmosphere or CO_2 enters the system by other means.

10.4.1.4 Recharge Zone Summary

Recharge in the North Karst is accomplished through small ponors and channels in dolines that are widely scattered on the Bear Rock and Franklin Mountain Formations (Figure 10.7). The single largest point recharge occurs in the west pond of Camp Depression (R37). In the South Karst, the same diffuse autogenic style of recharge is accomplished in over 40% of the area. The basins of Franklin, Round, and Long Lakes comprise 60% of the South Karst. Surface flows to the lakes were few and often infiltrated into the active layer or small ponors on the basin slopes. There was little fluctuation observed in lake levels. Only a single ponor was located on a lake margin that functioned as a site of point recharge, and it was largely inactive in the late summer. While there are no data on lake bathymetry and likely positions of sink points below the water line, the style of recharge through the South

Karst lakes may not differ from elsewhere on the range.

There is uniformity in hydrochemical facies and ion concentrations between groups of samples in the recharge zone (Figures 10.10, 10.11). Waters have a calcium bicarbonate facies; most are aggressive to calcite and all to dolomite. The total hardness and total dissolved ion concentrations are high, compared with values from the recharge zones of the Dodo Canyon and Bonus Lake Sites (Chapters VII, VIII). Much of the difference is due to the presence of Ca^{2+} and SO_4^{2-} from the dissolution of gypsum. The $\text{Ca}^{2+}/\text{Mg}^{2+}$ ratios of the recharge water types are 3.8, 3.4, and 4.4. These values suggest limestone solution is favoured over dolomite. However, these ratios are inflated by the Ca^{2+} contributed from gypsum solution.

Individual sampling points highlight differences across the area. There are a series of high hardness and SO_4^{2-} rich samples that indicate local circulation within the recharge zone is not confined to the active layer but is sufficiently deep to encounter gypsum. These samples are springs and spring-fed streams in areas of high local relief. Other perched and draining samples have low hardness values and low SO_4^{2-} concentrations. These waters are thought to have a short residence time in a supraperafrost aquifer. At other sites in this study, a relationship has been noted between $\delta^{18}\text{O}$ and the inferred flowpath. Subpermafrost groundwaters are most depleted in ^{18}O (e.g., Figure 7.23). The SO_4^{2-} ion concentration may be used to deduce flowpath history at the Bear Rock Site. Waters that are restricted to shallow circulation in the Franklin Mountain or Bear Rock Formations should contain little or no SO_4^{2-} ion. Sampling such waters in July and August should yield an isotopic signature dominated by summer rainfall (e.g., $\delta^{18}\text{O} \approx -17\text{‰}$). Waters circulating to intermediate depths in the Bear Rock Formation would encounter more gypsum and have moderately high SO_4^{2-} concentrations. Recharge will include snowmelt and the isotopic signature of summer discharge is more negative (e.g., $\delta^{18}\text{O} \approx -20\text{‰}$). Waters that fully penetrate the Bear Rock Formation and pass through the Franklin Mountain into the underlying Saline River Formation will have high SO_4^{2-} concentrations and an isotopic signature that reflects the weighted mean

of annual recharge (e.g., $\delta^{18}\text{O} \approx -23\text{‰}$). This model is supported by $\delta^{18}\text{O}$ data from samples across the Bear Rock Site. These data are plotted as a function of SO_4^{2-} concentration for all water types (Figure 10.12). All but one of the recharge samples were collected in the period mid-July to early August. There is an inverse relationship between $\delta^{18}\text{O}$ and SO_4^{2-} concentration (Figure 10.12). This is observed within samples of a given water type and between groups of samples. In the recharge zone, the high SO_4^{2-} waters have low $\delta^{18}\text{O}$ values. Circulation within the recharge zone is not confined to the active layer but is locally subpermafrost.

$\delta^{18}\text{O}$ data are also plotted as a function of time for all water types (Figure 10.13). The values from the recharge samples range from -17.7 to -22.5‰. Perched samples are the most positive (Type 2), likely due to the evaporation effect. There is much less variance in $\delta^{18}\text{O}$ of discharge samples. Early June waters from the Bear Rock Spring Area and Forest Stream fall in the range -21.9 to -23.6‰. These ratios are virtually unchanged in July and August. This consistency suggests discharge waters are supplied by deep subpermafrost aquifers. The isotopic signature of recharge waters reflects the local site conditions.

10.4.2 Discharge Zone

Samples of the discharge zone include a series of ephemeral low discharge streams draining the flanks of the upland (Type 5) and several springs or spring areas on the margin of Bear Rock. Sampling of the springs and spring-fed streams focussed on Forest and Blood Streams (Type 4) and the Bear Rock Spring Area (Type 6).

10.4.2.1 Water Type 4: Forest and Blood Streams

A steep gully southwest of Round Lake is the largest drainage course in the southern area of Bear Rock. Several small breached depressions and troughs are tributary to this main valley. Forest Spring (R5) is located in the lower reach of the valley near the contact of the Bear Rock and Hume Formations. The flow is diffuse and emerges at several points from bare and moss covered limestone fragments. It was sampled

at the spring point on July 12, 1987 when the discharge was estimated at 3 to 5 L s⁻¹. The channel upslope was observed to be dry in July of 1987 and 1988. The distribution of vegetation and sediment in the channel suggests it takes flow following heavy precipitation and rainfall events. The closest outcrop to the spring is the Landry Member of the Bear Rock Formation, strata dip sharply to the west and northwest.

Initially it was thought the spring was fed exclusively by interflow and local seepage from the surrounding slopes and catchment of the gully area. However, the relatively high conductivity indicated these were not simply active layer waters. The flow was followed downstream to the head of a short, narrow gorge where it cuts through the Hume Formation just north of the Mackenzie River. The discharge increases through and below this stretch. Aerial photographs from June 1972 show an icing at the head of this gorge just above a small waterfall. This may suggest that the discharge is perennial. Forest Stream (R9) was sampled above its confluence with the Mackenzie River. The discharge was estimated on two occasions at 16 and 25 L s⁻¹ (300787 and 090888). Blood Stream (R10) is located to the east (Figure 10.7). It takes flow from springs discharging from the lower portion of the Hume Formation, at the base of a steep bluff. There may be a connection between the Forest Spring gully and Blood Stream. However, such a feature was not located on the ground. Discharge estimates of Blood Stream are 55 and 60 L s⁻¹ (300787 and 090888).

Average temperature, total hardness, and total dissolved ions for Forest and Blood Streams are 5.1°C, 361 mg L⁻¹ CaCO₃, and 17.62 meq L⁻¹ (Table 10.3). Ion abundances are Ca²⁺>Mg²⁺>Na⁺ and HCO₃⁻>SO₄²⁻>Cl⁻ by equivalence. Samples are saturated with respect to calcite (SI_C = 0.37) and at equilibrium with dolomite (SI_D = 0.04). These samples are the only waters at the Bear Rock Site that were found to contain more than trace amounts of Na⁺ (1.42 meq L⁻¹) and Cl⁻ (1.20 meq L⁻¹) (Figures 7.10, 7.11). The presence of these ions shows a deep groundwater contribution from the Saline River Formation. The low average δ¹⁸O value of -

23.3‰ is also consistent with deep subpermafrost flowpaths to the spring points. It is concluded that Forest and Blood Streams discharge from the same aquifer based on their chemical similarity and the dye trace between Round Lake Sink (R17) to both streams.

10.4.2.2 Water Type 5: Streams

There are several small streams that drain marginal areas of the Bear Rock upland. The discharge of these surface waters was observed to be high in early June following the snowmelt period. In July and August, channels were dry or carried declining flows. Few of these waters were tested. A single early June sample is available from Gully Stream (R14). This stream drains a small portion of the upland east of Long Lake. It flows to the south end of the Bear Rock Spring Area with a discharge of 5 to 10 L s⁻¹. Its basin is in the Bear Rock and Franklin Mountain Formations. This water has a low total hardness and SO₄²⁻ ion concentration (107 mg L⁻¹ CaCO₃ and 0.31 meq L⁻¹) and is thought to represent mainly suprapermafrost flow.

A second stream was sampled on the upland at location R22 in late July. The discharge was 2 L s⁻¹. The stream was fed by small seeps discharging from the base of a steep slope and by seepage from an area of low relief on the Franklin Mountain Formation. Total hardness and SO₄²⁻ ion concentration are high (238 mg L⁻¹ CaCO₃ and 1.46 meq L⁻¹). The SO₄²⁻ levels suggest some contribution from subpermafrost waters. Two other samples complete this grouping. They are from lower Vale Stream, taken downslope of the recharge zone boundary. Sample R26 was collected at the top of a small canyon, sample R27 at the base. Discharge was 0.5 L s⁻¹ throughout the section. Total hardness is 211 and 206 mg L⁻¹ CaCO₃ for R26 and R27, and SO₄²⁻ ion concentrations 0.73 and 0.83 meq L⁻¹. Three of the four samples of this grouping are aggressive to calcite and all to dolomite. Overall there is little difference in the physical characteristics of Water Type 5 and Water Type 3.

10.4.2.3 Water Type 6: Bear Rock Spring Area

The Bear Rock Spring Area is located below a steep grade at the southeastern margin of Bear Rock (Figure 10.1). A series of perennial, low temperature, low discharge springs flow from angular frost shattered colluvium and moss covered gravels at the base of the slope. There are no clean outcrops at the spring elevations but strata of the Franklin Mountain Formation are exposed on the bluffs above. The spring points are thought to be close to the contact between the Franklin Mountain and Saline River Formations. A map of the Bear Rock Spring Area is shown on Figure 10.14. Springs labelled as R1 and R2 are indexed to Table 10.2. Locations R1 and R15 are the same water course. R1 is called Spring S1 and R15 is Stream S1. In the discussion they are collectively called Spring S1. A second set of labels (V1, V2, etc.) are the spring locations sampled by van Everdingen (1978, 1982). In some cases, locations of the two sample sets coincide.

An opening in the forest canopy occurs below the spring line. Some of the northern portion of this spring area is mantled in tufa and travertine precipitates (Figures 10.5, 10.14). The southern part of the spring area is characterized by a cover of grass, sedge, and moss on thick organic soils. The perennial discharge of groundwater is responsible for the winter development of frost blisters and icings at the site. Frost blisters form in the southern and central part of the spring area with most collapsing in the summer. Individual mounds rise to 4.9 m with diameters approaching 65 m (van Everdingen, 1978, 1982). Icings and icing blisters blanket most of the spring area during the winter and decay in the early spring period. The presence of frost blisters, icings, and active layer ground ice greatly influences the site hydrology.

The spring area was observed in early June, and from early July to mid-August. In 1988, icing mounds had completely melted by June 6. Frost blisters were more persistent, gradually decaying through the summer period. During the slow collapse of the frost blisters layers of segregated ground ice beneath the soil cover are exposed. Much of the summer runoff from the spring area is released from the

melting of ground ice in the spring area.

Steep gullies cut the slopes west of the spring line. These channels accommodate surface runoff from the upland during snowmelt and following heavy precipitation. The basins are small and the flows are ephemeral. In early June of 1988 the discharge of Gully Stream (R14) was between 5 and 10 L s⁻¹. Most of that flow was directed towards Spring S1 (R1, V6, R15) and a small fraction to Spring S2 (R2, V4, V5). A similar channel supplied Spring S0 (R16, V7). There did not appear to be any significant surface inputs to Springs S3a (R12, V3), S3 (R3, V2), and S4 (R39, V1) during the same period. By early July, the discharges of these gully streams were much reduced, the channels taking flow only during precipitation events. It is likely that interflow of soil moisture from these basins occurs through the summer and that suprapermafrost waters continue to comprise part of the total flow observed at Springs S0, S1, and possibly S2.

A series of shallow channels cut across the surface of the spring area below the spring points (Figure 10.14). The channel flows sink below the soil cover at many locations or branch into a series of diffuse distributaries. The local sinking is related to the melt of ground ice and the erosion of conduits through ice-rich soils and sediments. The stream below Spring S1 displays the most impressive thermokarst features. It incised a channel as deep as 1.5 m into ice-rich sediments. In places, a cover of vegetated soil spans the underlying conduit. However, much of the spring discharge seemed to travel on the surface or through the upper part of the active layer. The amount of moisture visible on the surface of the open area increased through the middle part of the day. Discharge from the spring area flows eastward to a narrow southward flowing channel called Congo River.

A variety of data are available from the Bear Rock Spring Area. Conductivity and stage of Congo River were monitored below of the spring inputs in 1987 (Section 10.4.2.4). Similar data were also collected from Springs S2 (R2 and V4) and S3 (R3) in 1988. Discharge was measured at several locations across the spring area and samples collected from spring points for chemical and oxygen

isotope analyses. In addition, chemical, isotope, and precipitate data are available from van Everdingen (1978, 1981, 1982).

Water samples from the spring area have a meteoric origin (Figure 10.15, Table 10.5). Samples plot closely to the Fort Smith water line and are more negative than those of the Canyon Ranges. The low $\delta^{18}\text{O}$ values suggest snowmelt comprises a high proportion of the recharge to these springs and that circulation is subpermafrost. There is little variance in $\delta^{18}\text{O}$ over the course of the summer (Figure 10.13).

Most of the samples from the Bear Rock Spring Area have a calcium sulphate facies (Figure 10.10, 10.11). Ion abundances are $\text{Ca}^{2+} > \text{Mg}^{2+} \gg \text{Na}^+$ and $\text{SO}_4^{2-} > \text{HCO}_3^- \gg \text{Cl}^-$ by equivalence. The average temperature, total hardness, and total dissolved ions are 3.7°C , $946 \text{ mg L}^{-1} \text{ CaCO}_3$, and 39.57 meq L^{-1} (Table 10.3). Samples are saturated with respect to calcite ($\text{SI}_c = 0.53$) and dolomite ($\text{SI}_d = 0.22$). These average figures do not capture the spatial and temporal variability that is present on site. Ion concentrations increase from the southern to northern portions of the spring area. Also, the southern springs experience an increase in ion concentration through the course of the summer period. Table 10.4 contains physical data from the site. The data are arranged along a north to south transect. There are multiple sampling dates for each spring. The spatial trend can be observed by comparing locations for the same date. For example, TDI from June 6 or 7, 1988 for Springs S0, S1, S2, S3a, S3, and S5 (south to north) are 8.43, 15.16, 40.56, 27.77, 37.26, and 51.60 meq L^{-1} . The SO_4^{2-} ion concentrations along the same transect are 1.38, 4.48, 15.20, 9.58, 13.64, and 22.28 meq L^{-1} . Spring S2 is the only sampling point that does not fit the general pattern. This spatial trend persists through the summer period but is less pronounced in August and September. Data from September 9, 1975 (van Everdingen, 1978) for Springs S0, S1, S2, S3a, S3, and S4 show TDI's of 21.48, 35.06, 56.89, 41.61, 46.52, and 60.54 meq L^{-1} . While the TDIs of Springs S0 and S1 remain lower than sample sites to the north they do increase over the summer period. The June 6 TDIs for Springs S0 and S7 are 8.43 and 15.16. The July 30 data are

19.86 and 37.60 meq L⁻¹. In contrast, Spring S2 and the northern springs experience little temporal variation between the spring and summer periods (Table 10.4).

Ion concentrations are plotted against TDI on Figure 10.16. The relationships depict mixing between at least two waters. The regression line of the SO₄²⁻ graph extrapolates to a point on the TDI axis. This indicates one input is a low TDI water with measurable concentrations of ions other than SO₄²⁻. The HCO₃⁻ and Mg²⁺ data extrapolate to the ion axes, suggesting all input waters have significant concentrations of these ions. At first inspection it appears the Ca²⁺ graph is identical to that for SO₄²⁻. However, two linear segments are depicted. This pattern suggests the possibility of a three-way mixing (Figure 7.26). The three components may be represented by high, moderate, and low TDI waters, each representing flow from a separate aquifer. Springs S4 and S5 most closely represent the deepest subpermafrost component. These springs have high concentrations of Ca²⁺ and SO₄²⁻ (≈27 and 23 meq L⁻¹) and a summer temperature of 4 to 7°C. Based on their chemistry it is probable this flow component discharges from either the Bear Rock (Fort Norman) or Saline River Formations. The structure at the site favours the latter unit. δ³⁴S analyses of dissolved SO₄²⁻ vary between 25.1 and 32.7‰ for the spring samples (Table 10.6). These values fall within the range for sulphates of the Saline River Formation (Figure 7.31).

The shallow component is suprapermafrost water that originates from either surface streams that drain onto the spring area or from the local melt of segregated ice in the active layer. Gully Stream (R14) typifies this input, with a low TDI (4.3 meq L⁻¹) and a facies dominated by Ca²⁺ and HCO₃⁻ ions (1.96 and 1.84 meq L⁻¹). The Ca²⁺ and SO₄²⁻ graphs do not show a linear mixing between Gully Stream and Spring S5 (Figure 10.16). Thus, a third component is inferred. This intermediate component would have higher concentrations of all ions compared to Gully Stream but would have substantially lower concentrations of Ca²⁺ and SO₄²⁻ compared with the deep water represented by Spring S5 (e.g., Figure 7.26). This input is likely subpermafrost water circulating through the Franklin Mountain Formation.

Spatial and temporal trends in ion concentrations observed across the spring area vary with the mixing of the flow components. During and immediately following the snowmelt period, the southern springs (S0, S1) receive direct flow from suprapermafrost streams. Through the summer months the suprapermafrost inputs are reduced and the ion concentrations increase. There is less variation in the northern springs because they are thought to receive minimal shallow inputs.

All but one sample collected from the spring area was saturated with respect to calcite. The degree of saturation was highest in mid summer. Data from July 29 or 30, 1988 show SI_C values at Springs S5, S2, S3, and S0 of 1.01, 0.96, 0.84, and 0.65. The SI_D values for the same dates and sites are 0.91, 0.93, 0.94, and 0.89, and the SI_G (saturation index of gypsum) values are -0.01, -0.16, -0.39, and -0.90. The highest SI_C value is from the central portion of the travertine deposit. The mineralogy of precipitates in the spring area was examined by van Everdingen (1982). Deposits from the large area of travertine were composed of calcite (92%), quartz (5%), and dolomite (2%). Tufa deposits on vegetative cover were gypsum (95%) and calcite (5%), as was a powdery precipitate attributed to freezing of mineralized water during icing formation. The $\delta^{34}S$ values of sulphate from these three precipitates were 28.9, 27.9, and 28.4‰ (Table 10.6). These values are typical of the Saline River Formation (Figure 7.31).

A stilling well was placed in gravel 30 m below the discharge point of Spring S2 (R2) in early June of 1988. This well was operational until mid-August, with some missing intervals in the record (Figure 10.17). Spring S2 corresponds with van Everdingen's Spring 5 (V5). Below the spring point, it is joined by flow from Spring V4. The well was located to record the combined discharge. Spring S2 (R2) comprised 60-70% of that total. The record shows an increase in stage from June 2 to 9, and then a gradual decrease into August. The initial rise was accompanied by an increase in discharge from 1.2 to 1.7 L s⁻¹. At that time, part of the flow of Gully Stream (R14) appeared directed towards Spring S2. The increase in discharge followed light rain on June 3 and 4, and a trace on June 8. The stage record is

notable for its lack of variability. A small peak on July 20 was in response to a 10 mm rainfall (Norman Wells). At the end of the record the discharge was 1.1 L s^{-1} , virtually unchanged from the first June measurement.

A second well monitored the water level of a small pool into which Spring S3 (R3) discharged. This pool is drained by a channel that flows eastward along the boundary of the travertine deposits and the vegetated area. Discharge was gauged in this channel. The well record shows a gradual decline in the pool water level over the measurement interval (Figure 10.17). However, discharge varied little, decreasing from 3.5 L s^{-1} on June 9 to 2.8 L s^{-1} on August 10. The substantial decrease in stage was due to the lowering of the channel outlet through the summer period by melting of ground ice in the active layer. The record of Spring S3 shows negligible response to precipitation events. A 32 mm rainfall on June 30 - July 1 generated only a small spike in the stage record. It was likely the result of direct precipitation onto the pool and throughflow from the slopes above. The stage records show the Bear Rock springs do not respond to storm inputs. Springs of this character flow from deep regional aquifers where flowpaths and residence times are long. This is supported by the highly mineralized discharge and the consistency in chemical and isotopic data.

10.4.2.4 Water Type 7: Congo River

Waters of the spring area drain eastward to Congo River (Figure 10.14: R4, R8). The stream channel in the area of R4 is composed of fine grained sediments and the banks are heavily vegetated with willow and herbaceous ground cover. The flow is turbid. Upstream at point R8 there is a sandy channel with no suspended sediment. The stage of Congo River was monitored at point R4 during July of 1987. A stilling well was dug into the channel bank on July 8 and operated until July 31. The stream was gauged at the well site six times and the stage record transformed into a discharge series using a rating curve. Discharge shows a gradual increase in the early part of the record and then plateaus at around 50 L s^{-1} (Figure 10.18).

Superimposed on this trend is a pronounced diurnal pattern. Daily discharge maximums are attained at midday and minimums in the early morning. Rainfall events on July 14 (3 mm), 15 (5 mm), 18 (5 mm) and 24 (2 mm) disrupt the cycle. Temperature and conductivity were also recorded in the first 11 days of the record. The temperature series displays a daily cycle reaching maximums in the late afternoon hours. Conductivity also shows a cycle but it is not synchronized with discharge. The discharge pattern is attributed to variations in solar radiation at the site. The spring area faces east and is direct sunlight through the morning and early afternoon hours. Solar noon occurs at 2:00 p.m. local time. The area is gradually shaded following solar noon by high ground to the west. The daily peaks are due to the melting of segregated ice in the active layer and frost blister ice in the spring area. Rainfall onto this surface generates rapid responses because of the high moisture content of spring area soils. The daily peaks do not reflect variations in flow from the spring points.

Congo River takes flow from the spring area and from Trout Lake at the northeastern end of Bear Rock. On July 23, 1987 discharge measurements were done at several locations in the spring area (Figure 10.14). The discharge of Congo River at R4, above the spring inputs, was 32 L s^{-1} . At the well site, the discharge increased to 50 L s^{-1} . The difference is contribution from the Bear Rock Spring Area. It is unlikely that all of the flow from the spring area is recorded at the well (R4). The stream at R40 in the northern part of the spring area was measured at almost 7 L s^{-1} and the southern springs had a total discharge between 5 and 6 L s^{-1} . The balance is attributed to the melting of ground ice and possible aggraded spring inputs. On July 27, Congo River had a discharge of 26 L s^{-1} at R8 and was unchanged at R4. From these data, the total summer discharge of the springs is approximately $10\text{-}15 \text{ L s}^{-1}$. Some winter discharge is stored as ground ice and melted through the summer period.

There are few chemical data from Congo River, and no samples for which SO_4^{2-} was determined (Table 10.3). On July 27, the total hardness of Congo River

at points R8 and R4 were 413 and 593 mg L⁻¹ CaCO₃ and the conductivities were 716 and 900 μS cm⁻¹. The increase in hardness and conductivity from R8 to R4 is due the spring inputs between the two points. The change in δ¹⁸O from -18.65 to -19.85 across the same distance reflects the same input.

10.4.2.5 Water Type 8: Other Springs

Several other springs discharge on the margin of Bear Rock. A spring was sampled below a talus slope south of the Bear Rock Spring Area at site R38. The spring point was close to the trace of the small thrust exposed on the cliffs above. This sample has a total hardness and total dissolved ions concentration of 752 mg L⁻¹ CaCO₃ and 31.98 meq L⁻¹ (Table 10.3). In ion abundance, it is similar to waters of the spring area though with higher concentrations of Mg²⁺. This may be due to a proportionally higher contribution of water discharging from dolomite of the Franklin Mountain Formation.

On the south flank of Bear Rock, below a steep gully, there is a vegetated fan. At the fan margin, there are a series of diffuse springs with a combined discharge of 3 to 5 L s⁻¹. Low conductivity suggests local seepage through the fan surface. Westward, near the axis of the small anticline exposed on the slopes above the Mackenzie River, there is a set of sulphurous springs with a conspicuous odour of H₂S and yellowish precipitates. The total discharge of this set was estimated at 10 L s⁻¹. No samples were taken of these springs. Other springs on the west flank of Bear Rock (e.g., West Spring) were not investigated and their chemistry and discharge behaviour are unknown.

10.4.2.6 Discharge Zone Summary

Streams draining the gullies and valleys of the Bear Rock upland have a chemistry that is similar to waters of the recharge zone (Figure 10.10, 10.11; Table 10.3). These waters are suprapermafrost in origin with some local contributions from subpermafrost groundwater. Springs that discharge from several areas at the base of

the upland differ markedly to waters of the recharge zone. They are predominantly calcium sulphate waters with high hardness and ion concentrations. They are supplied by subpermafrost aquifers in the Bear Rock, Franklin Mountain, and Saline River Formations.

The majority of infiltrating waters (Types 1 and 3) and streams draining the upland flanks (Type 5) are aggressive towards calcite and dolomite. Forest and Blood Streams (Type 4), and discharge of the Bear Rock Spring Area are saturated, as are some perched samples of the recharge zone (Type 2). For each water type, there is an inverse relationship between the calcite saturation index and $p\text{PCO}_2$ (Figure 10.19). The same relationship is observed for dolomite. Consistently aggressive waters were sampled in the recharge zone from boggy environments. Highly saturated spring waters are associated with tufa and travertine deposits, including deposits of gypsum. The spring waters discharging from the base of Bear Rock are thought to be recharged on the upland. The substantial changes in chemistry are due largely to the subsolution of gypsum in the Bear Rock and Saline River Formations. The increase in Ca^{2+} activity associated with the evaporite solution generates the positive saturation indices. As waters move through the system and dissolve gypsum, they become progressively saturated, first with respect to calcite and then to dolomite. Total hardness is also related to contact with gypsum. The Bear Rock Springs have the highest total hardness values. In samples where SO_4^{2-} concentrations are low, total hardness is strongly correlated with $p\text{PCO}_2$ (Figure 10.20).

10.5 Groundwater Circulation at Bear Rock

There are few data available that may be used to resolve groundwater flowpaths at Bear Rock. No major springs were located on the margins of the North Karst. It was expected that groundwater circulation would be east to west in accordance with the dip of the Franklin Mountain Formation. The recharge zone of the North Karst covers an area of approximately 4.5 km². Outside that zone, there are additional

areas where surface waters seasonally infiltrate. On an annual basis, recharge may be $1.4 \times 10^6 \text{ m}^3$. Future work may determine if there are spring points farther west along Vale Stream or other drainage courses. In the South Karst, there are sufficient data to attempt a summary.

10.5.1 South Karst

The primary discharge points on the southern margin of Bear Rock are Forest and Blood Streams and the Bear Rock Spring Area. Interpretation of groundwater flow in the South Karst is complicated by few data and a difficult geology. Ultimately, it may be possible to subdivide the South Karst into zones of recharge for each of the major spring areas. At this preliminary stage, models are speculative.

10.5.1.1 Forest and Blood Streams

The combined discharges of Forest and Blood Streams were measured at 71 and 85 L s^{-1} . It is not known if these values are typical of summer conditions or if the streams are perennial. The streams are fed by subpermafrost springs and by local drainage from the upslope gully (Forest Valley) and its tributaries. The subpermafrost waters are recharged in part, or in full, within the Round Lake basin. It is expected that winter discharge will be reduced due to freezing of the active layer in the gully area. Icings at Forest Spring suggest some groundwater flow occurs in the winter months. The gully watershed has an area of approximately 1.4 km^2 . This figure includes a small portion of the recharge area located downslope of the height of land, west of Long Lake (Figure 10.7). The basin of Round Lake has an area of 1.7 km^2 . This estimate includes the doline basins that are west of Round Lake. Long and Franklin Lakes have basin areas of 0.6 and 0.55 km^2 . Round Lake sits 15 m below the level of Long Lake and 5 m below that of Franklin Lake. Conduits between Round and Long Lakes are possible but their presence has not been established. The geological structure at Round Lake favours groundwater flow through the Bear Rock Formation to the southwest. A dye trace confirmed this

connection in under 60 days. However, the chemistry of Forest and Blood Streams show contributions from units as deep as the Saline River Formation. Travel times in the Bear Rock Formation do not represent the deeper, longer flowpaths through Franklin Mountain and Saline River strata.

If the Round Lake and gully basins function as the source area for Forest and Blood Streams, there should be concordance between stream discharge and basin recharge. Data from nearby Jungle Ridge Creek suggest runoff in the Bear Rock area may approach 300 mm a^{-1} (Table 3.4). Applying this value as a recharge estimate across the 3.1 km^2 area of the Round Lake and gully watersheds yields an annual recharge volume of $9.3 \times 10^5 \text{ m}^3 \text{ a}^{-1}$. Assuming perennial flow at Forest and Blood Streams, the mean daily discharge would be approximately 30 L s^{-1} . Summer discharges would be higher than those of winter. While there are few data to support this model it does show an order of magnitude agreement between the measured discharge and what might be expected based on structure and regional runoff data.

10.5.1.2. Bear Rock Spring Area

The Bear Rock Spring Area is characterized by highly mineralized, perennial groundwater discharge. Flow contributions from three aquifers are suspect. Suprapermafrost waters flow onto the southern portion of the spring area from surface gullies. Subpermafrost springs discharge both an intermediate component that has circulated through the Bear Rock and Franklin Mountain Formations, and a deep water component from the Saline River Formation. Mixing between these components accounts for spatial and temporal variability across the site. Hydrological, chemical, and isotopic data justify a model of circulation through diffuse, subpermafrost aquifers. Spring discharges are consistent and do not respond to storm inputs on the recharge area. Conductivity and ion concentrations are high and, at a given spring, show little variance. Low $\delta^{18}\text{O}$ values suggest spring discharge must incorporate winter precipitation. Sulphur isotopes show dissolved sulphate from the Saline River Formation.

There are tritium data available from the Bear Rock Spring Area (van Everdingen, 1982). In 1975, springs sampled had an average of 211 tritium (^3H) units. Data from 1978 show an average of 123 tritium units. Comparisons with tritium in precipitation from Fort Smith and Ottawa lead van Everdingen (1982) to conclude that water discharging at the Bear Rock Spring Area fell as precipitation 5 or 6 years earlier. This age may be overestimated if there are large surface water bodies in the recharge area. Fractionation during evaporation can affect the apparent tritium age of water. A single sample from Round Lake in 1976 had 210 tritium units (van Everdingen, 1982). This is the same as the spring discharge in 1975. If lake waters comprise a significant portion of the recharge, then tritium concentrations in the spring waters will be inflated and their age overestimated.

The obvious source area for the Bear Rock Springs is the Long Lake basin and the eastern portion of the recharge zone and upland. Long Lake occupies the core of an anticline and recharge through its flanks may infiltrate into strata that dip to the southeast. However, it is also possible that drainage is to the southwest. The combined summer discharges of the springs are a minimum 10 L s^{-1} . Assuming a 300 mm annual recharge across the South Karst and a constant spring discharge, the recharge area supplying the springs is 1.05 km^2 . The topographic area of the Long Lake basin is 0.6 km^2 . The 1.05 km^2 estimate would be lower if some of the spring discharge is from a deep regional flow, perhaps exploiting the thrust fault at the eastern margin of Bear Rock. While there is certainly such a deep water component, its flow contribution is probably minor, though it may supply much dissolved material. The tritium data suggest a short average residence time and thus a short flow system from recharge to discharge. It is proposed that Long Lake and the eastern upland function as the recharge area for the Bear Rock Springs. Circulation is subpermafrost and encounters the Saline River Formation. The aquifers cannot be characterized as having a conduit or fissure porosity, based on the consistency in discharge and chemistry at the spring area.

10.6 Summary: Bear Rock Site

At the Bear Rock Site, there are a variety of dolines attributed to solution and subsidence in the Bear Rock Formation. Ponor density is high and a large continuous area of internal drainage occurs on the rugged upland. Depressions are not limited to the breccia; a large subsidence trough is developed along the breached core of a tight anticline. The subsidence is due to subrosion in the underlying Saline River Formation. Shallow dolines also occur on the Franklin Mountain dolomites. Karst features on Bear Rock are thought to predate glaciation in the region. Glaciers have locally eroded karst input landforms and infilled elements of the karst drainage system with subglacial and fluvio-glacial sediments. However, despite repeated glaciation most of the upland area continues to be drained karstically.

Bear Rock is located in the zone of widespread discontinuous permafrost. The site spans treeline and patterned ground is common on exposed ridges and slopes. Precipitation and surface waters infiltrate through a widely distributed network of ponors and water bodies on the upland that function as open taliks. Recharge to subpermafrost aquifers in the Bear Rock, Franklin Mountain, and Saline River Formations supplies mineralized springs on the margin of Bear Rock. Flow-through times from recharge to discharge vary with the depth of circulation and porosity of the individual rock units. The hydrochemistry of spring and stream waters show the process of gypsum subrosion continues across the site. While much occurs at depth in the Saline River Formation, gypsum solution is locally important in near surface strata of the recharge area. The development of dolines and depressions continues at the site.

Table 10.1: Grouping of water samples from the Bear Rock Site on the basis of location in the karst. Waters are divided into recharge and discharge categories. Recharge occurs in the upper portion of the range largely through the Bear Rock Formation. The discharge area consists of the low ground on the perimeter of the range.

	Type	Description
Recharge	1	Pond/Doline/Ponor: Surface waters in the recharge zone infiltrating into a ponor or doline. Includes ponds at the base of dolines that drain.
	2	Pond/Lake/Wetland: Surface waters in the recharge zone impounded in a slowly draining or perched pond, lake, or wetland. Some water bodies are within dolines and large closed depressions.
	3	Springs/Seeps/Streams: Surface waters in the recharge zone directed towards dolines, ponors, ponds, and lakes.
Discharge	4	Forest Spring, Forest Stream, and Blood Stream: Discharge near the Bear Rock-Hume contact at the southwestern end of the range.
	5	Streams and Springs: Surface waters from the upper portion of the range directed towards the discharge zone. Some on the Franklin Mountain Formation.
	6	Springs and Streams in the Bear Rock Spring Area.
	7	Congo River: Stream draining Trout Lake and the Bear Rock Spring Area.
	8	Other Springs on the margin of the range.

Table 10.2: Description and classification of water sampling locations at the Bear Rock Site.

Location	Description	Type
R1	<i>Spring S1.</i> Spring in Bear Rock Spring Area (BRSA). Takes flow from R14 at high stage.	6
R2	<i>Spring S2.</i> Spring in BRSA. One of a several located below a gully. Gauged in 1988.	6
R3	<i>Spring S3.</i> Spring in BRSA. Located at margin of travertine deposits. Gauged in 1988.	6
R4	<i>Congo River.</i> Stream draining Trout Lake and BRSA. Gauged in 1987.	7
R5	<i>Forest Spring.</i> Spring discharging from moss covered gravels in a gully, winter icings.	4
R6	<i>Round Lake.</i> Lake located in the southern portion of Bear Rock.	2
R7	<i>Long Lake.</i> Lake located southeast of Round Lake.	2
R8	<i>Congo River.</i> Congo River sampled above contributions from BRSA.	7
R9	<i>Forest Stream.</i> Spring-fed stream sampled above its confluence with the Mackenzie River.	4
R10	<i>Blood Stream.</i> Spring-fed stream sampled above its confluence with the Mackenzie River.	4
R11	<i>Spring S5.</i> Spring in BRSA located in the central portion of the travertine deposit.	6
R12	<i>Spring S3a.</i> Spring in BRSA. Spring discharges from moss covered gravels.	6
R13	<i>Stream S3a.</i> Spring-fed stream in BRSA, sampled downstream of Spring S3a (R12).	6
R14	<i>Gully Stream.</i> Stream draining steep ravine west of BRSA.	5
R15	<i>Stream S1.</i> Spring-fed stream in BRSA, sampled downstream of Spring S1 (R1).	6
R16	<i>Spring S0.</i> Spring in BRSA. Takes flow from gully at high stage.	6
R17	<i>Round Lake Sink.</i> Sinking point for waters of Round Lake.	1
R18	Surface seep draining a wetland near Camp Three. $Q < 0.5 \text{ L s}^{-1}$ (210788).	3
R19	Stream between the two ponds at Camp Three. $Q \approx 1.0 \text{ L s}^{-1}$ (210788).	3
R20	Pond/Sink. Draining waters in a doline. Flow into doline $\approx 1.0 \text{ L s}^{-1}$ (230788).	1
R21	Pond/Sink. Draining waters in a doline. Flow into doline $\approx 0.5 \text{ L s}^{-1}$ (230788).	1
R22	Stream near the Bear Rock-Franklin contact. $Q \approx 2.0 \text{ L s}^{-1}$ (230788).	5
R23	Pond. Draining pond in a shallow doline.	1
R24	Seeps emerging from talus. Drain to wetland near Camp Three. $Q < 0.5 \text{ L s}^{-1}$ (230788).	3
R25	Stream draining to the NW and sinking at a swamp/pond. $Q \approx 0.5 \text{ L s}^{-1}$ (260788).	3
R26	<i>Vale Stream.</i> Stream above small canyon below an area of seeps. $Q \approx 0.5 \text{ L s}^{-1}$ (260788).	5
R27	<i>Vale Stream.</i> Stream at the foot of the canyon, sinks into its bed. $Q \approx 0.5 \text{ L s}^{-1}$ (260788).	5
R28	Stream draining pond R32. Drains to sink below R25. $Q \approx 1.0 \text{ L s}^{-1}$ (260788).	3
R29	Small perched pond draining into adjacent ponor.	1
R30	Small perched pond in a wetland area.	2
R31	Pond at the base of large doline, water level below that of overflow channel.	2
R32	Pond with overflow channel at its western shoreline. Channel is stream R28.	2
R33	Pond/Wetland with overflow channel draining toward R28.	2
R34	Perched pond within circular doline with an overflow channel.	2
R35	Standing water in the wetland south of Camp Three.	2
R36	Stream draining wetland south of Camp Three. $Q < 0.5 \text{ L s}^{-1}$ (060888).	3
R37	<i>Camp Three Sink.</i> Ponor of west pond at Camp Three. Q into ponor $\approx 0.5 \text{ L s}^{-1}$ (060888).	1
R38	Spring below steep talus slope in Franklin Mountain Formation. $Q \approx 2.0 \text{ L s}^{-1}$ (090888).	8
R39	<i>Spring S4.</i> Spring in BRSA, low discharge, flows intermittently.	6
R40	<i>Stream S5.</i> Spring-fed stream in BRSA below Spring S5.	6

Table 10.3: Mean temperature, conductivity, pH, total hardness, ion concentrations, total dissolved ions, Ca²⁺/Mg²⁺ ratio, saturation indices (calcite and dolomite), and pPCO₂ for water types of the Bear Rock Site.

Type	Temp	SPC	pH	THd	Ca ²⁺	Mg ²⁺	HCO ₃ ⁻	SO ₄ ²⁻	Na ⁺	Cl ⁻	TDI	C/M	SI _c	SI _d	pPCO ₂	n
1: Dolines and Ponors	9.0	309	7.41	167	2.61	0.68	2.43	0.77	0.00	0.01	6.51	3.8	-0.42	-1.51	2.36	6 (5)
2: Lakes and Ponds	14.0	228	8.07	128	1.98	0.59	2.38	0.45	0.02	0.02	5.43	3.4	0.17	-0.13	3.02	10 (5)
3: Springs and Streams	10.6	328	7.25	197	3.21	0.73	3.43	0.44	0.01	0.01	7.82	4.4	-0.31	-1.29	2.04	7 (5)
4: Forest, Blood Streams	5.1	621	8.02	361	4.96	2.25	4.40	3.39	1.42	1.20	17.62	2.2	0.37	0.04	2.49	6 (3)
5: Streams off Upland	4.0	298	7.06	191	3.05	0.75	3.06	0.83	0.00	0.01	7.71	4.0	-0.66	-2.08	1.97	4 (4)
6: Bear Rock Springs	3.7	1336	7.68	946	16.64	2.35	4.84	15.65	0.06	0.01	39.57	7.1	0.53	0.22	2.36	35 (15)
7: Congo River	13.5	871	8.39	561	8.65	2.55	3.32					3.5				4 (0)
8: Other Springs				752	11.51	4.00	4.74	11.45	0.27	0.02	31.98	2.9				1 (0)

Temp: temperature in °C; SPC: specific electrical conductivity, expressed to 25°C, in μS cm⁻¹; THd: Total Hardness in mg L⁻¹ CaCO₃; Ion concentrations reported in meq L⁻¹; C/M: Ca²⁺/Mg²⁺ ratio; SI_c: Saturation index for calcite; SI_d: Saturation index for dolomite; pPCO₂: -log of partial pressure of CO₂; n: number of cases for each type, value in brackets represents the number of cases for which there is a complete data set.

Table 10.4: Mean temperature, conductivity, pH, total hardness, ion concentrations, total dissolved ions, saturation indices (calcite and dolomite), and ion balance errors for Bear Rock Springs.

Date	Location	Map	Temp	SPC	pH	Ca ²⁺	Mg ²⁺	HCO ₃ ⁻	SO ₄ ²⁻	Na ⁺	Cl ⁻	TDI	SI _c	SI _d	SI _g	IBE
100888	Spring S4	R39	4.2	1838	7.1	27.97	2.40	5.53	24.94	0.17	0.02	61.04	0.34	-0.43	-0.03	0.1
090975	Spring S4	V1	1.6	2210	7.5	29.64	3.33	5.44	21.86	0.24	0.03	60.54	0.71	0.39	-0.04	9.7
070688	Spring S5	R11	6.1	1660	7.7	22.30	2.48	4.40	22.28	0.13	0.02	51.60	0.75	0.51	-0.13	-3.5
290788	Spring S5	R11	5.4	1850	7.8	28.05	2.36	5.75	26.96	0.06	0.01	63.20	1.01	0.91	-0.01	-3.6
100888	Stream S5	R40	7.4	1890	7.4	26.38	2.08	3.70	25.71	0.13	0.02	58.01	0.41	-0.29	-0.04	-1.5
070688	Spring S3	R3	1.7	1340	7.5	15.83	2.48	5.24	13.64	0.08	0.01	37.26	0.45	0.02	-0.37	-1.3
290788	Spring S3	R3	4.9	1480	7.8	15.07	3.04	5.51	14.37	0.05	0.01	38.05	0.84	0.94	-0.39	-4.6
090975	Spring S3	V2	2.6	1650	7.5	20.61	3.23	5.24	17.28	0.11	0.05	46.52	0.58	0.28	-0.22	3.0
130978	Spring S3	V2	4.8	1536	7.6	15.47	3.14	5.24	13.74	0.09	0.01	37.47	0.61	0.48	-0.39	-0.8
070688	Spring S3a	R12	1.7	824	7.4	11.59	2.08	4.48	9.58	0.05	0.01	27.77	0.29	-0.26	-0.57	-1.3
290788	Spring S3a	R12	2.3	1050	7.7	16.86	1.62	5.18	15.09	0.06	0.02	38.83	0.67	0.24	-0.31	-4.5
110576	Spring S3a	V3	0.1	1638	7.5	18.51	3.32	5.20	15.32	0.09	0.03	42.47	0.52	0.20	-0.28	3.2
090975	Spring S3a	V3	1.9	1500	7.5	17.86	3.07	5.11	15.41	0.10	0.06	41.61	0.52	0.19	-0.30	1.1
130978	Spring S3a	V3	4.9	1529	7.5	16.32	2.72	5.00	14.16	0.08	0.01	38.29	0.51	0.20	-0.36	-0.1
300788	Stream S3a	R13	6.7	1303	7.5	15.89	2.82	5.04	14.57	0.06	0.01	38.38	0.53	0.28	-0.37	-2.2
070688	Spring S2	R2	3.7	1289	7.7	17.66	2.84	4.80	15.20	0.06	0.01	40.56	0.67	0.49	-0.31	1.4
290788	Spring S2	R2	6.5	1597	7.9	21.42	2.36	4.88	21.13	0.04	0.01	49.84	0.96	0.93	-0.16	-4.4
090975	Spring S2	V5	2.8	2025	7.5	26.35	2.83	4.83	22.69	0.13	0.06	56.89	0.62	0.20	-0.07	3.0
130978	Spring S2	V5	4.3	2110	7.6	23.60	2.65	4.93	20.82	0.13	0.02	52.15	0.70	0.41	-0.13	1.2
110675	Spring S2	V4	1.7	1620	7.6	19.56	2.25	4.44	18.32	0.08	0.02	44.67	0.57	0.12	-0.21	-2.0
130978	Spring S2	V4	5.0	1989	7.5	21.76	2.81	4.80	19.57	0.09	0.01	49.04	0.58	0.22	-0.18	0.6
060688	Stream S1	R15	2.7	537	7.6	5.44	2.04	3.16	4.48	0.05	0.01	15.16	0.09	-0.32	-1.08	-0.8
300788	Stream S1	R15	4.9	1261	7.5	14.85	3.22	5.12	14.37	0.04	0.01	37.60	0.50	0.29	-0.39	-3.7
090975	Spring S1	V6	3.1	1500	7.5	17.56	3.65	4.96	15.61	0.11	0.06	41.95	0.51	0.26	-0.31	1.6
130978	Spring S1	V6	4.0	1434	7.5	14.42	3.22	4.83	12.49	0.08	0.02	35.06	0.45	0.19	-0.44	1.1
060688	Spring S0	R16	1.6	287	7.6	2.76	1.28	2.96	1.38	0.04	0.02	8.43	-0.20	-0.83	-1.74	-3.4
300788	Spring S0	R16	3.6	685	8.0	6.69	3.08	4.66	5.41	0.00	0.02	19.86	0.65	0.89	-0.97	-1.6
090975	Spring S0	V7	3.5	890	7.6	7.68	3.44	4.47	5.81	0.06	0.02	21.48	0.32	0.22	-0.90	4.1

Temp: temperature in °C; SPC: specific electrical conductivity, expressed to 25 °C, in $\mu\text{S cm}^{-1}$; Ion concentrations reported in meq L^{-1} ; SI_c: Saturation index for calcite; SI_d: Saturation index for dolomite; SI_g: Saturation Index for gypsum; IBE: Ion balance error in %.

Table 10.5: $\delta^{18}\text{O}$ and δD values in ‰ SMOW from the Bear Rock Spring Area. Data are from van Everdingen (1981, 1982).

Site	Date	$\delta^{18}\text{O}$	δD
Spring V1 (S4)	090975	-22.9	-177.1
Spring V2 (S3)	090975	-22.9	-176.6
Spring V2 (S3)	130978	-23.1	-175.0
Spring V3 (S3a)	090975	-22.8	-175.3
Spring V3 (S3a)	130978	-23.1	-176.0
Spring V4	130978	-23.6	-178.0
Spring V5 (S2)	110675	-23.6	-179.2
Spring V5 (S2)	090975	-23.2	-178.4
Spring V5 (S2)	130978	-23.4	-181.0
Spring V6 (S1)	090975	-22.4	-176.3
Spring V6 (S1)	130978	-22.9	-178.8

Table 10.6: $\delta^{34}\text{S}$ values in ‰ for aqueous and precipitated sulphates from the Bear Rock Spring Area. Data are from van Everdingen (1978).

Site	SO_4^{2-} aqueous	SO_4^{2-} precipitate
Spring V1 (S4)	32.7	27.9*
Spring V2 (S3)	25.1	
Spring V2 (S3)	25.3	
Spring V3 (S3a)	26.0	
Spring V5 (S2)	30.1	28.9**
Spring V5 (S2)	29.5	28.4***
Spring V6 (S1)	27.8	
Spring V6 (S1)	27.8	

* Precipitate on moss

** Travertine deposit

*** Precipitate from icing

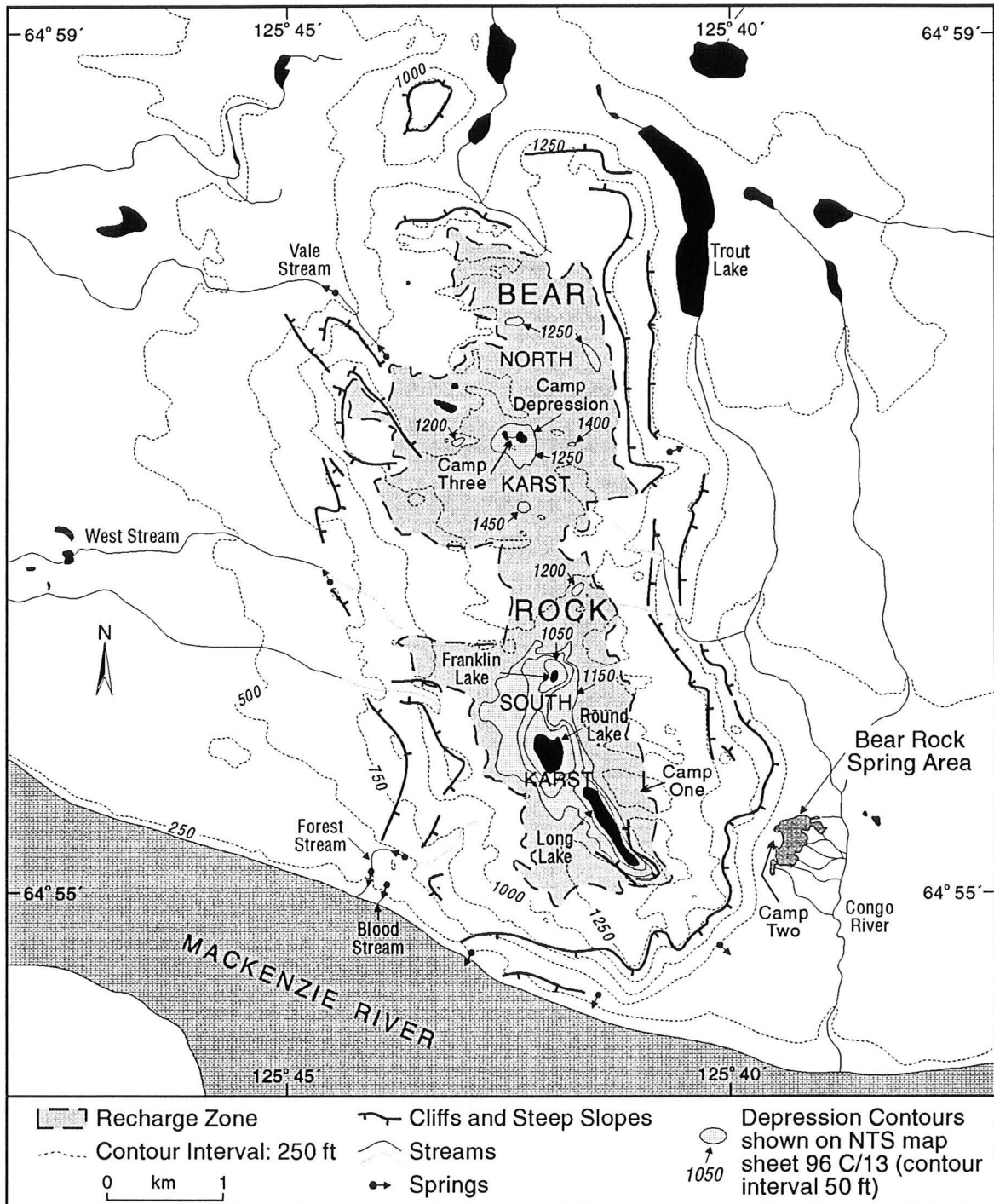


Figure 10.1: Map of the Bear Rock Site showing topography and drainage. Bear Rock is located west of the confluence of the Mackenzie and Great Bear Rivers. Karst depressions occur through the central portion of the range (e.g., Figure 10.2). Several are shown by depression contours at 50 foot intervals. Areas within these contours are lightly shaded. The recharge zone is more extensive than what is indicated by the depression contours. Discharge occurs from a series of springs and streams draining the flanks of the range. The Bear Rock Spring Area is a region of perennial low discharge springs (Figure 10.3). Other important springs discharge at the southwest and western sides of the range (e.g., Forest Spring).

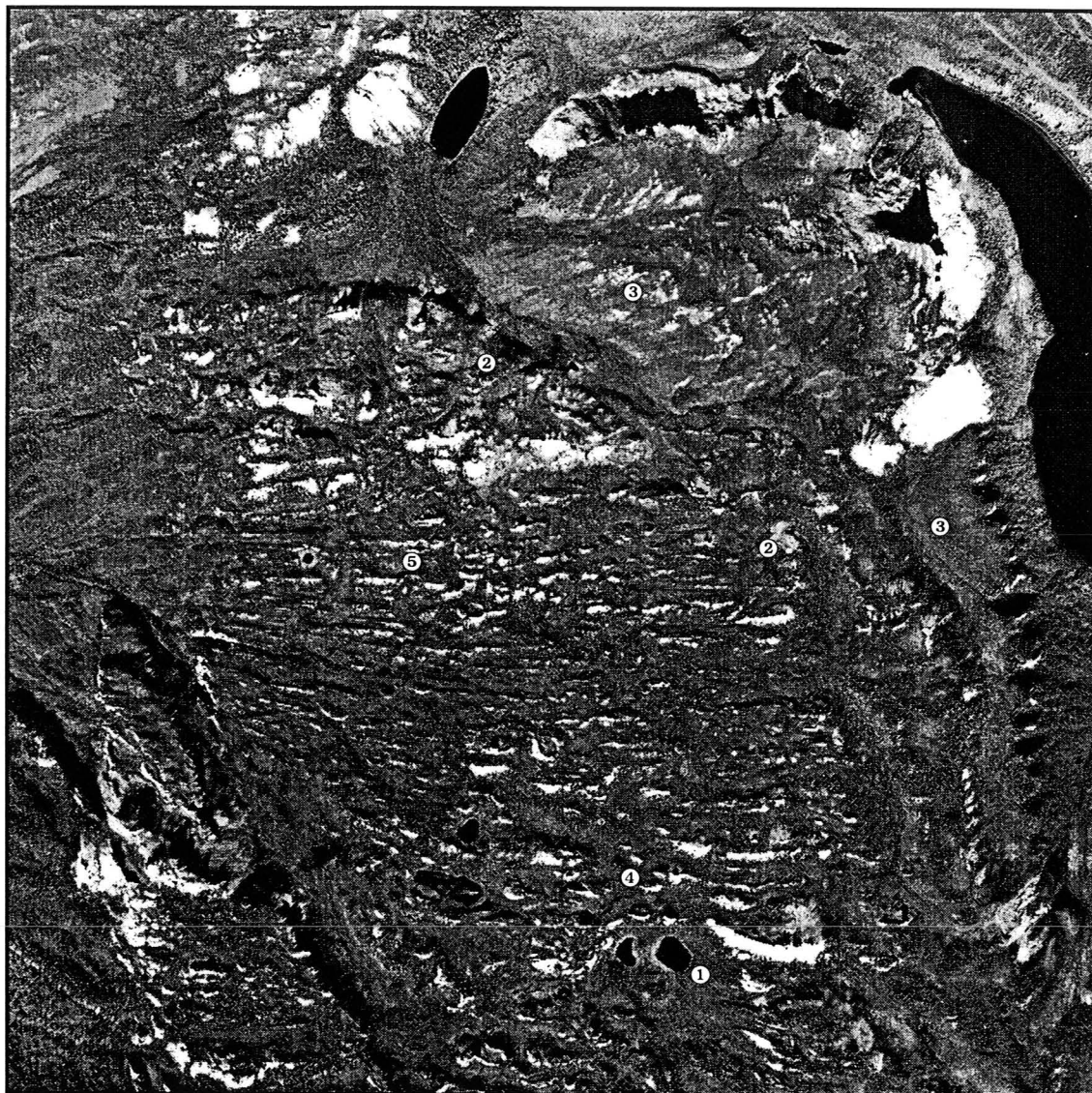


Figure 10.2: Aerial photograph of the North Karst, Bear Rock Site. North is at the top of the photo. The scale is approximately 1:24,500. The large depression centred on the two ponds at ① is Camp Depression (Figure 10.4). There is a marked topographic contrast between terrain on the Bear Rock (②) and Franklin Mountain Formations (③). The Bear Rock Formation supports an undulating surface of dolines, depressions (e.g., ④) and ridges and swales (e.g., ⑤). The latter features are attributed to subglacial erosion and are parallel to the direction of ice flow across the region. The Franklin Mountain Formation forms a westward sloping bench on the upland, and bold cliffs along the eastern margin of Bear Rock (NAPL A26416-78).



Figure 10.3: Aerial photograph of the South Karst, Bear Rock Site. The top of the photo is northeast. The scale is approximately 1:30,500. Camp Depression is in the upper left. The South Karst is dominated by a large linear depression developed along the core of an anticline in the Bear Rock and Franklin Mountain Formations. The anticline axis runs through Long Lake (①) and along the eastern margin of Round Lake (②). A ponor located on the shoreline of Round Lake (③) is the deepest point in the depression. Sinking waters were traced from that location to the spring-fed Forest and Blood Streams to the southwest (④). A major group of perennial springs discharge east of Long Lake at the Bear Rock Spring Area (⑤, and Figure 10.5) (NAPL A22889-147).



Figure 10.4: Camp Depression of the North Karst. The view is from the south rim of the depression looking north. This rolling terrain is typical of the North Karst. The forested area in the central portion of the photo drains to the sinking ponds on the depression base. The eastern pond is visible in the centre.



Figure 10.5: Photograph of the Bear Rock Spring Area. The springs are perennial, low temperature, low discharge, and highly mineralized. The very light tone on the left is an area of tufa and travertine deposits. At the extreme right, a channel is seen incised into the ice-rich sediments that comprise the spring area.

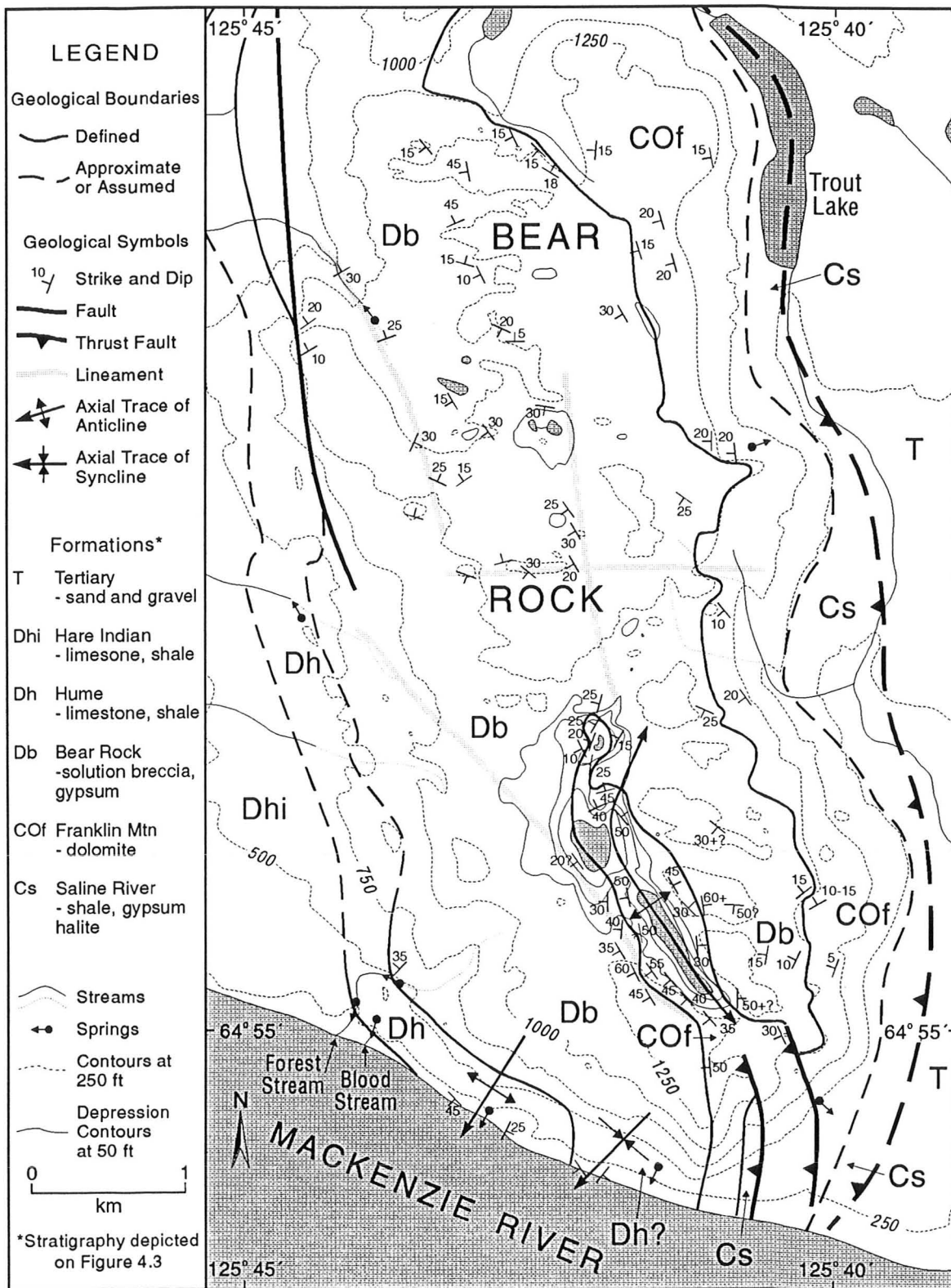


Figure 10.6: Geology of the Bear Rock Site (after Stelck in Hume (1954), Cook and Aitken (1976), Morrow and Meijer Drees (1981) and fieldwork conducted on site).



Figure 10.7: Karst geomorphology of the Bear Rock Site. The shading denotes the recharge zone. Dashed lines mark drainage basins within that zone. These boundaries are defined from surface topography and may not coincide with groundwater basins. In areas of low relief or dense vegetation the subdivision into drainage units is not complete. Ponors and sink points are shown as solid circles. Ticks on solid lines depict the directions of steep bedrock slopes. At some locations they define circular dolines and linear depressions. Spring locations are shown as are water sampling points.

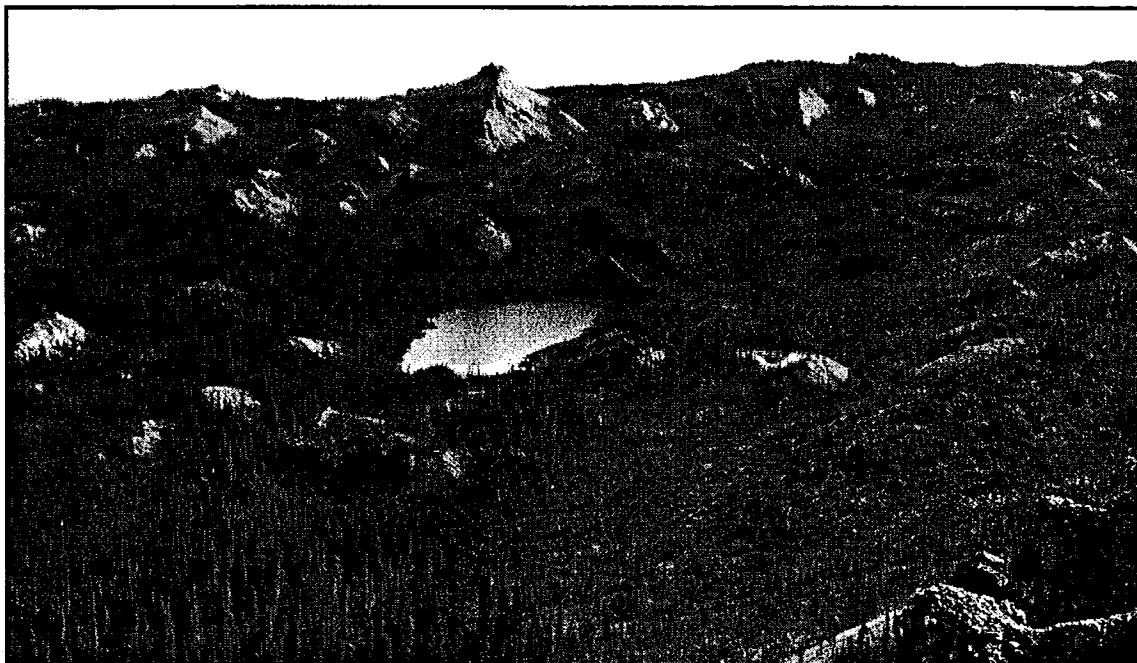


Figure 10.8: A view of the North Karst looking east from a position west of sample point R25. Camp Depression is obscured from view. The hill in the background is oriented east to west. It is an example of a large streamlined whaleback ridge. Similar ridges occur to the north. The pond in the foreground drains towards two ponors in the trees in the lower left.

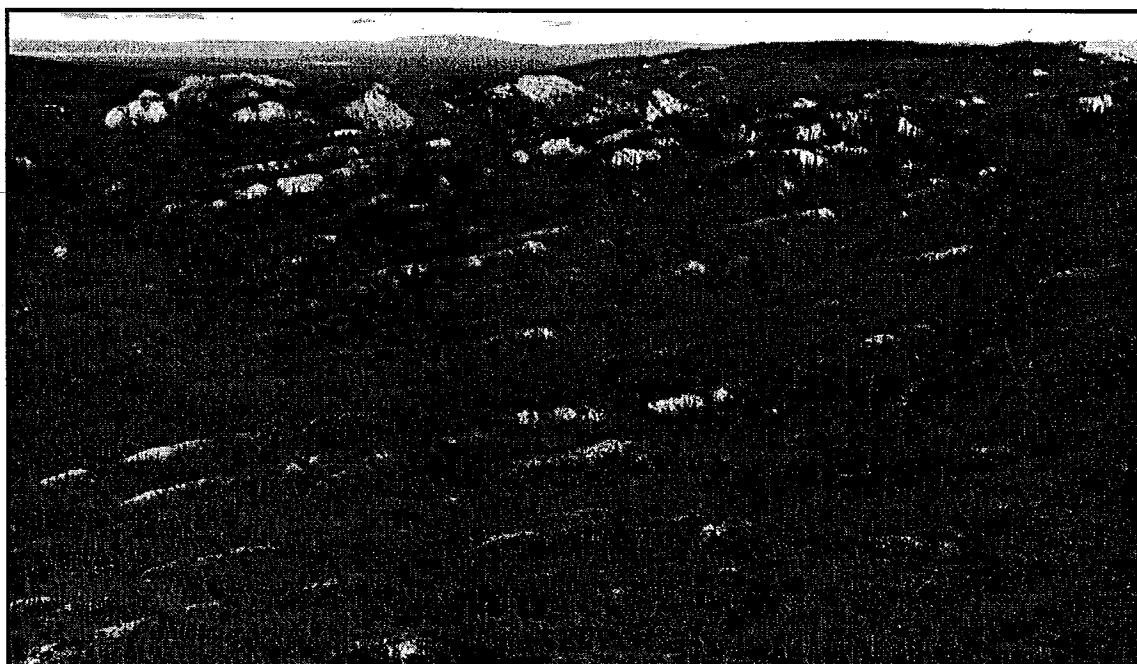


Figure 10.9: Small streamlined ridges and crag and tail features developed on the Bear Rock Formation in the area around point R34. The photo looks northeast. The landforms show glacial ice moved east to west across the range. The treeless smooth surface in the background in the upland above Trout Lake in the Franklin Mountain Formation.

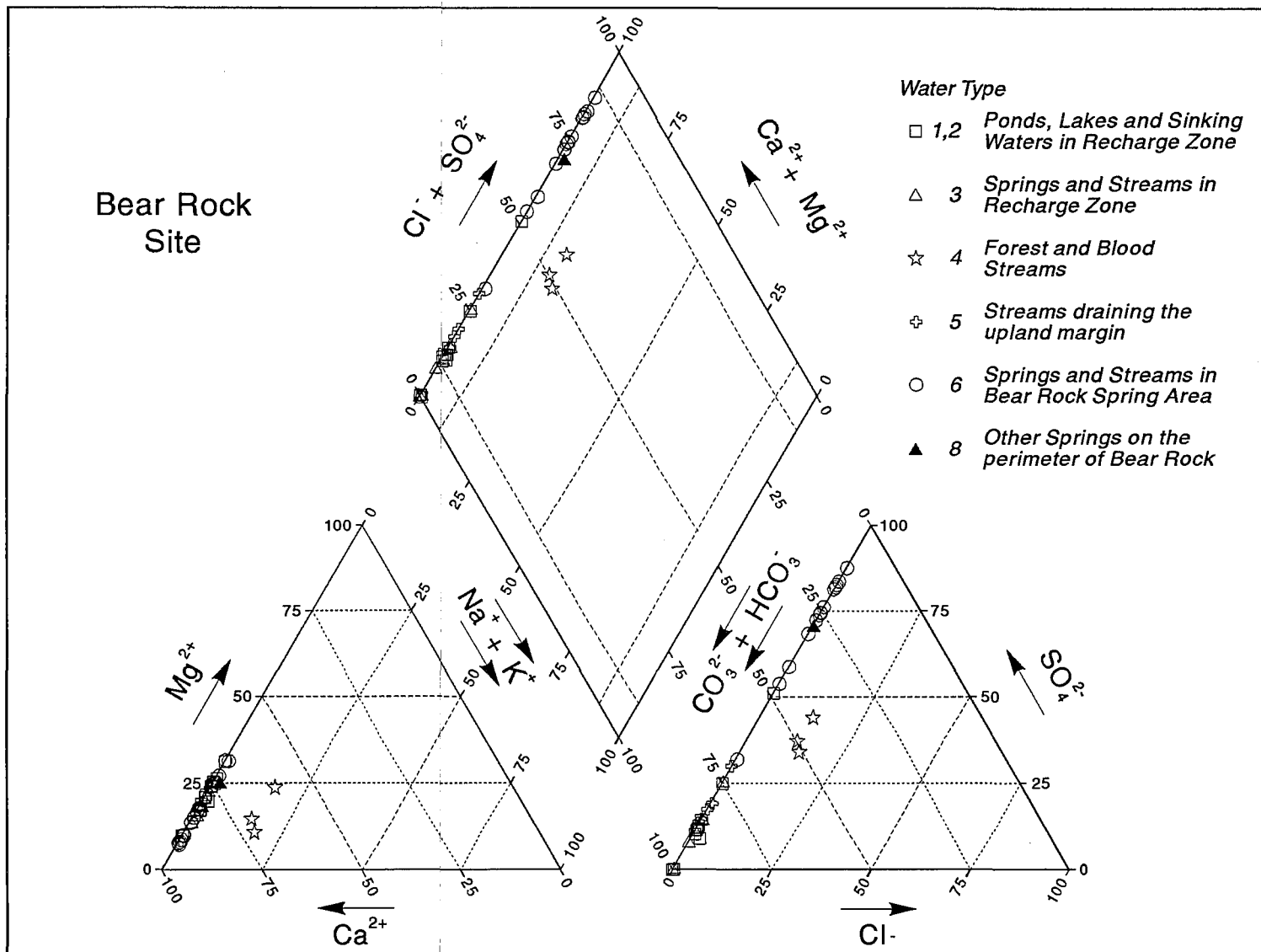


Figure 10.10: Trilinear diagram of waters from the Bear Rock Site. No samples from Congo River (Type 7) are plotted, nor are van Everdingen's (1981, 1982) samples from the Bear Rock Spring Area.

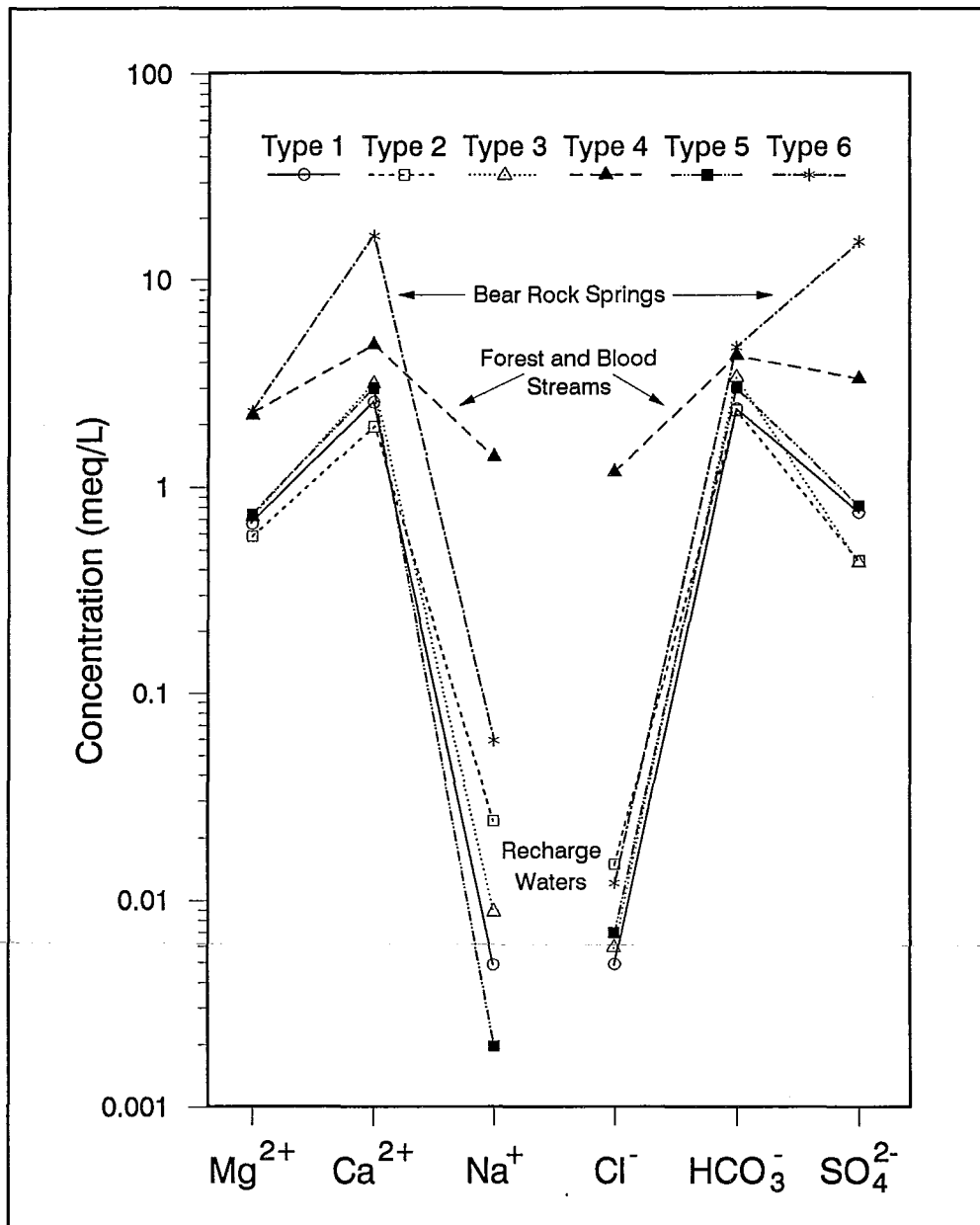


Figure 10.11: Mean concentrations of major anion and cation species in meq L⁻¹ for water types at the Bear Rock Site. Water types 7 and 8 are not plotted due to insufficient data.

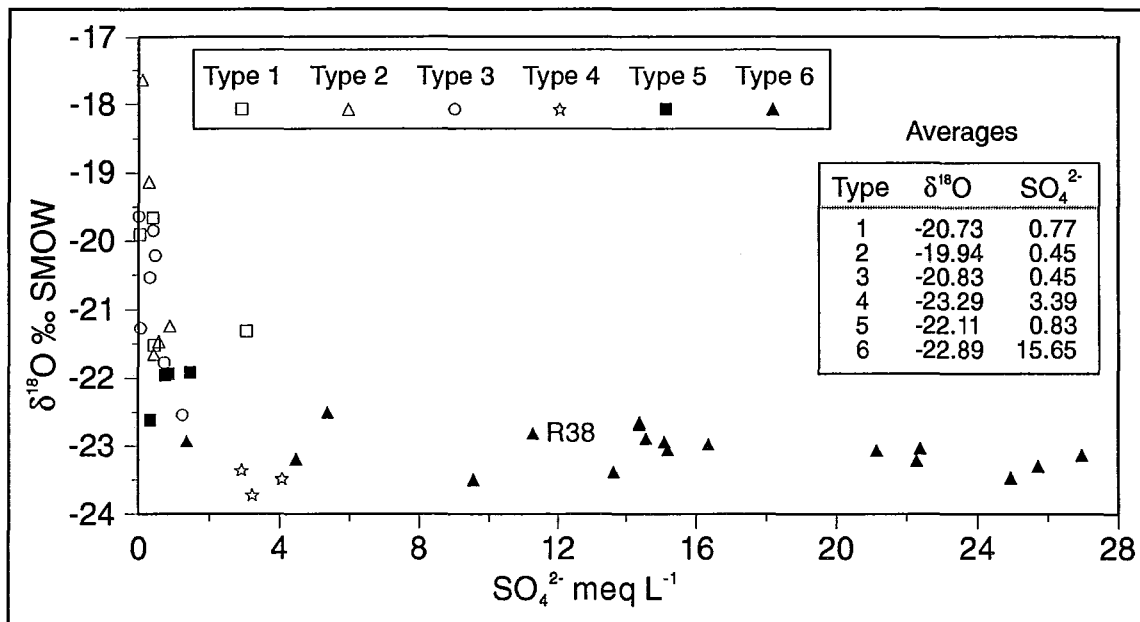


Figure 10.12: $\delta^{18}\text{O}$ of water samples at the Bear Rock Site versus SO_4^{2-} concentration. An inverse relationship exists between $\delta^{18}\text{O}$ and SO_4^{2-} . The long residence times and flowpaths of deeply circulating groundwaters yield high SO_4^{2-} concentrations (e.g., Type 6 waters). Their low $\delta^{18}\text{O}$ values suggest recharge to these systems includes winter precipitation. In contrast, shallow circulating waters (e.g., Types 1 and 2) have low SO_4^{2-} concentrations and an isotopic signature strongly influenced by summer rainfall.

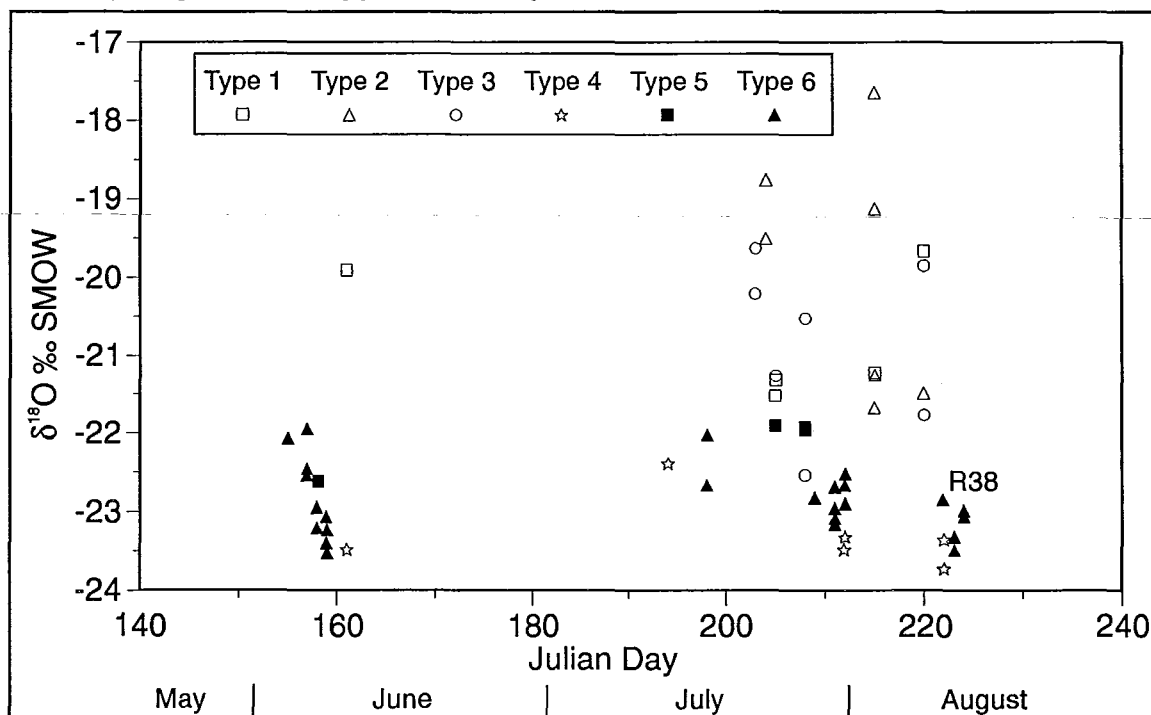


Figure 10.13: $\delta^{18}\text{O}$ of water samples at the Bear Rock Site versus time. The data show Types 4 and 6 experience little change in $\delta^{18}\text{O}$ through the summer period. There is much variance in the isotopic values of recharge waters (Types 1, 2, and 3). Samples drawn from perched or slowly draining ponds may have been affected by evaporation.

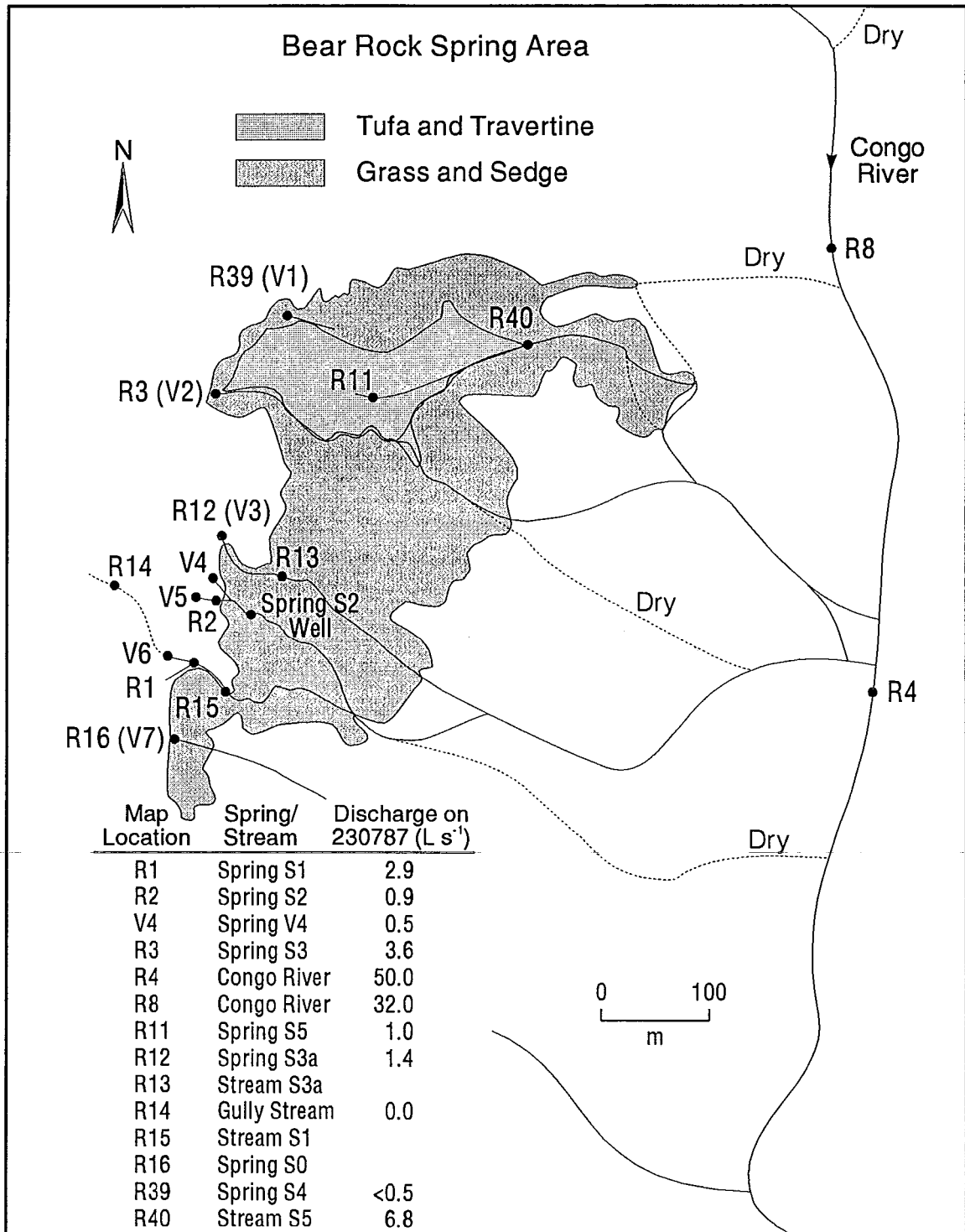


Figure 10.14: Sketch map of the Bear Rock Spring Area showing the positions of the spring points and streams. The numbered labels prefaced with "R" are indexed to Tables 10.2 and 10.4. Sites denoted by "V" are from van Everdingen (1978, 1982). The table presents discharge measurements from a variety of locations at the spring area on July 23, 1987.

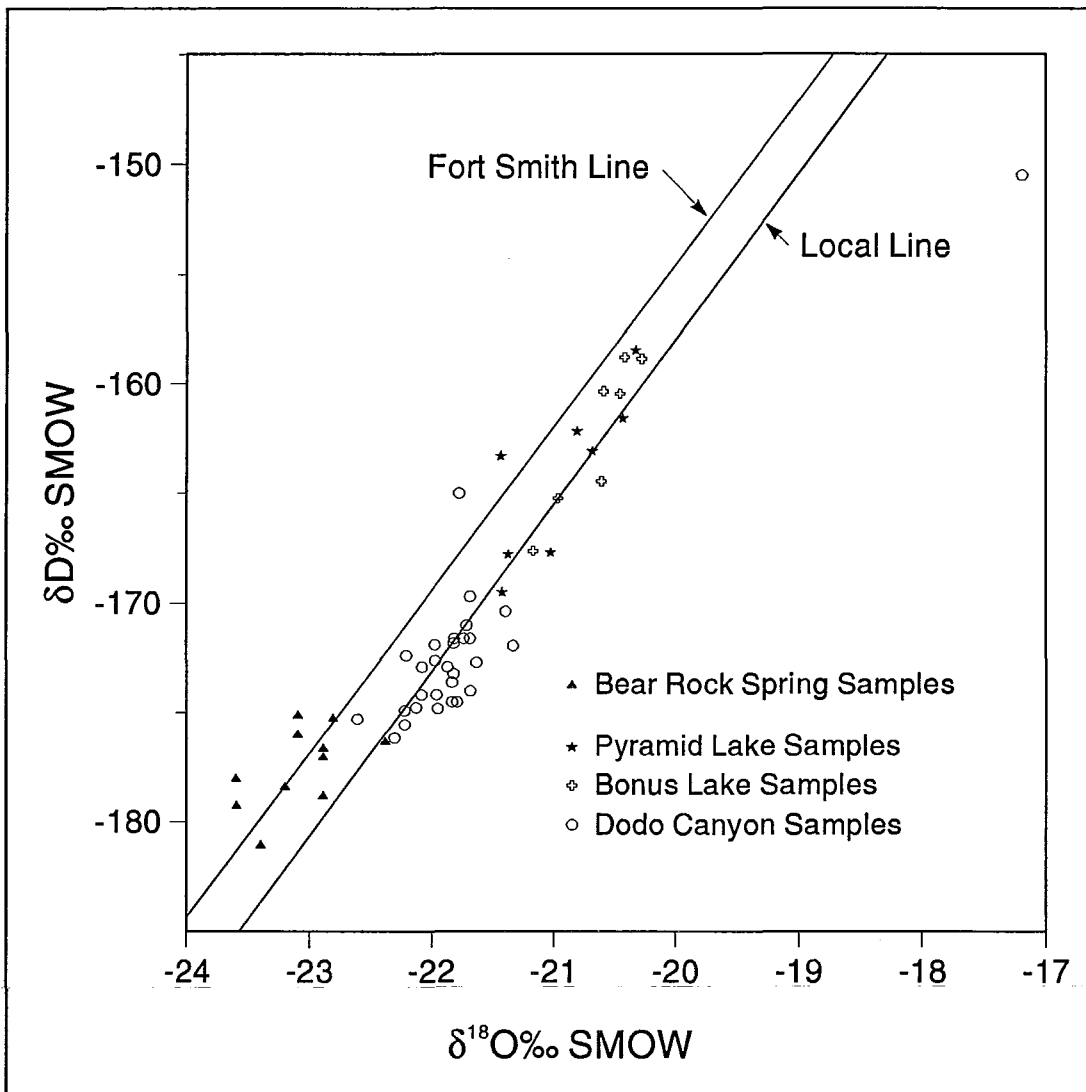


Figure 10.15: Isotope samples from the Bear Rock Spring Area plotted with the local and Fort Smith meteoric water lines. Data from the Dodo Canyon, Bonus Lake, and Pyramid Lake Sites are also shown. The data from Bear Rock are listed in Table 10.5. Samples were collected in June and September of 1975 and 1978 by van Everdingen (1982). The graph shows the spring waters are meteoric in origin, plot closely to the Fort Smith line, and have lower values relative to samples from the Canyon Ranges.

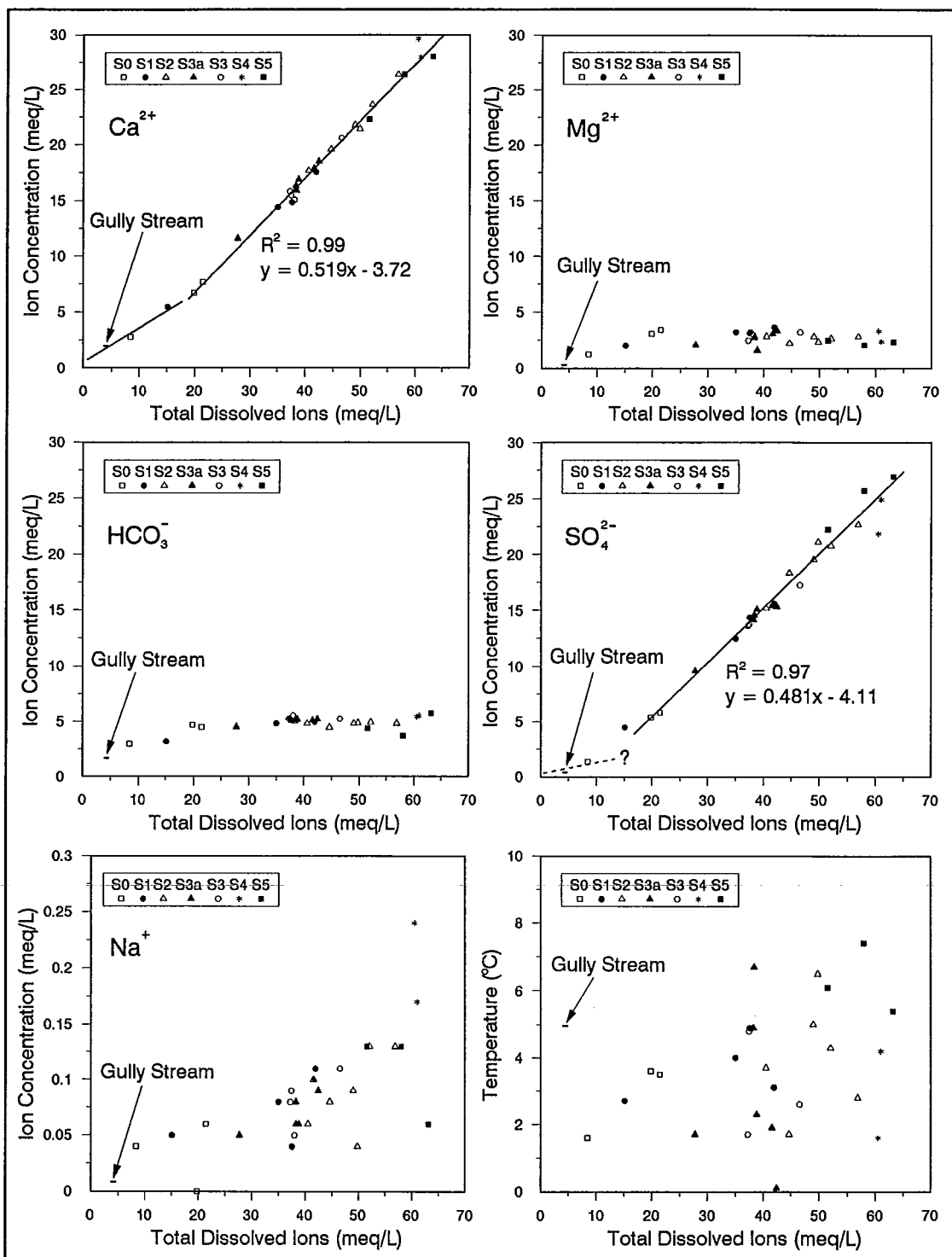


Figure 10.16: Concentrations of major anions and cations versus total dissolved ions for samples of the Bear Rock Spring Area. Data show a possible three-way mixing between deep, intermediate, and shallow flow components.

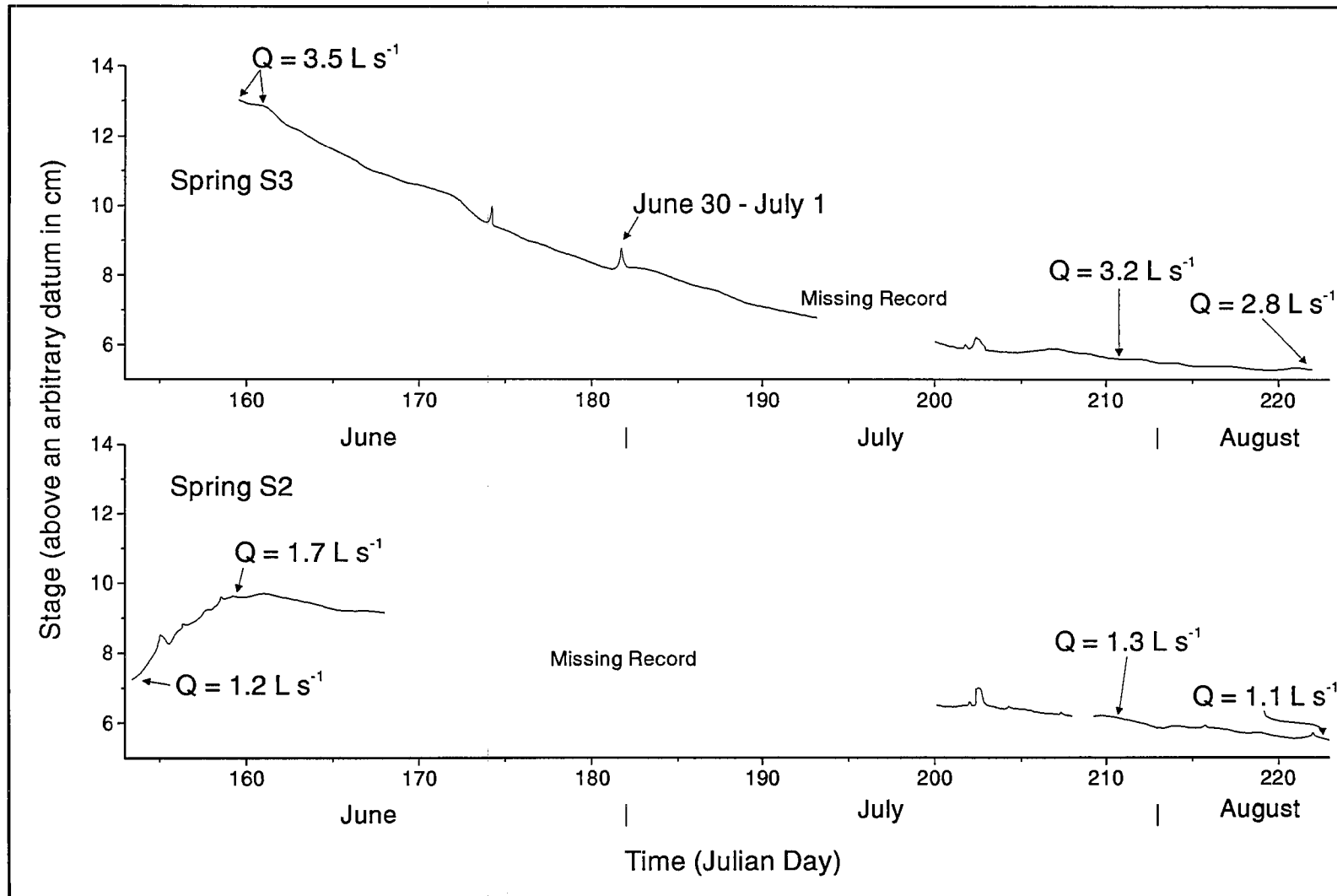


Figure 10.17: Stage recorded at Springs S2 (Location S2 Well) and S3 (Location R3) in June, July, and August of 1988.

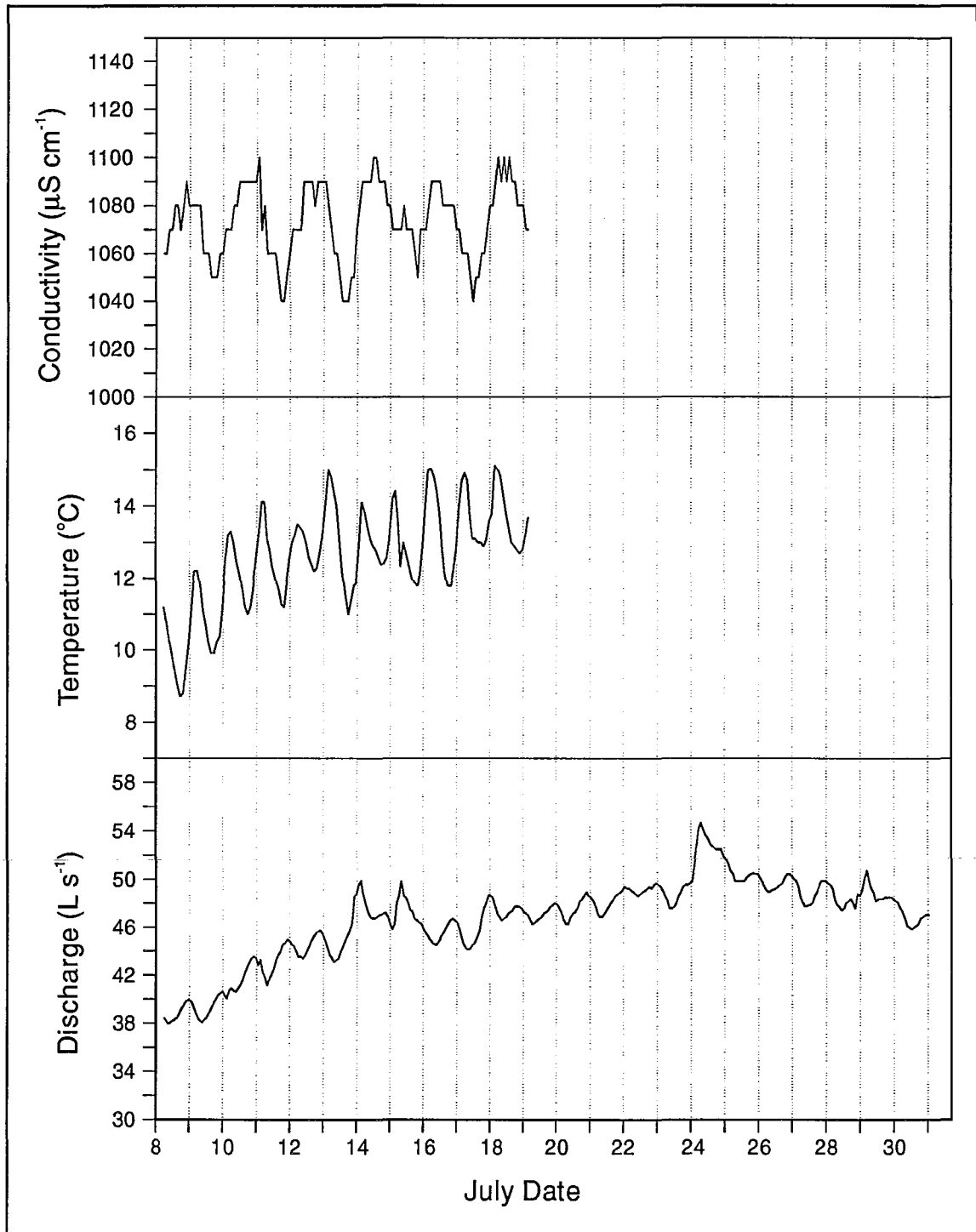


Figure 10.18: Discharge, temperature, and conductivity of Congo River. The date ticks are aligned to 12 noon. Discharge and temperature show a diurnal pattern and reach their maximums at midday. The variation in conductivity is not synchronized with discharge.

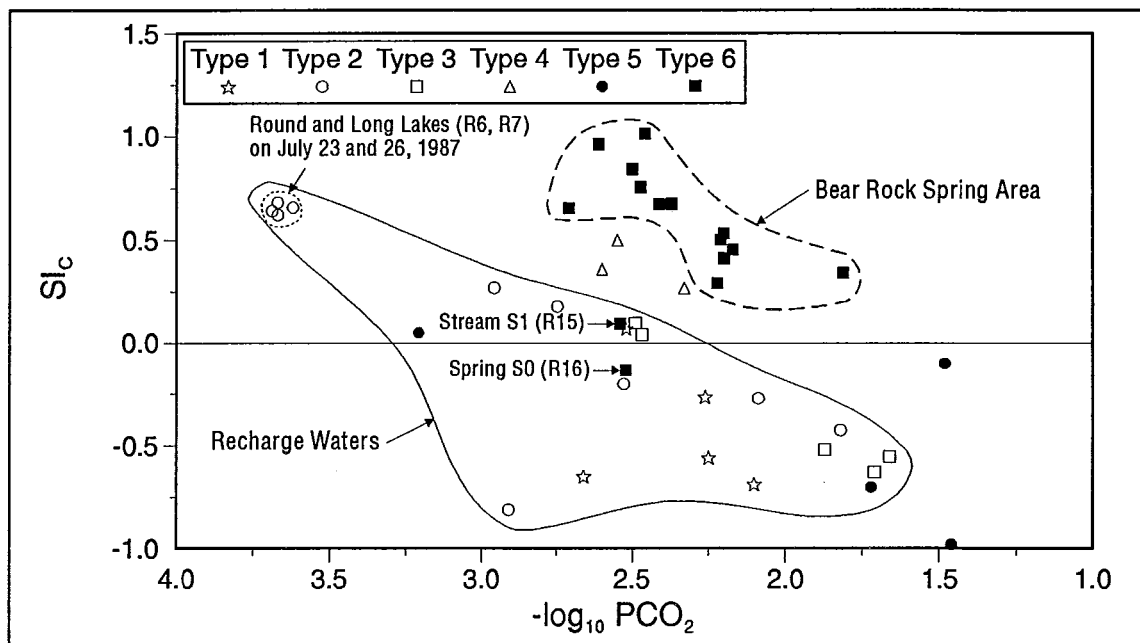


Figure 10.19: Saturation index of calcite versus the negative logarithm of the partial pressure of CO₂ for water samples of the Bear Rock Site. Most recharge waters are aggressive. Springs of the discharge area are saturated. Samples R15 and R16 are from the southern part of the Bear Rock Spring Area. They were sampled on June 6, 1988 when much of their flow consisted of surface runoff from Type 5 streams.

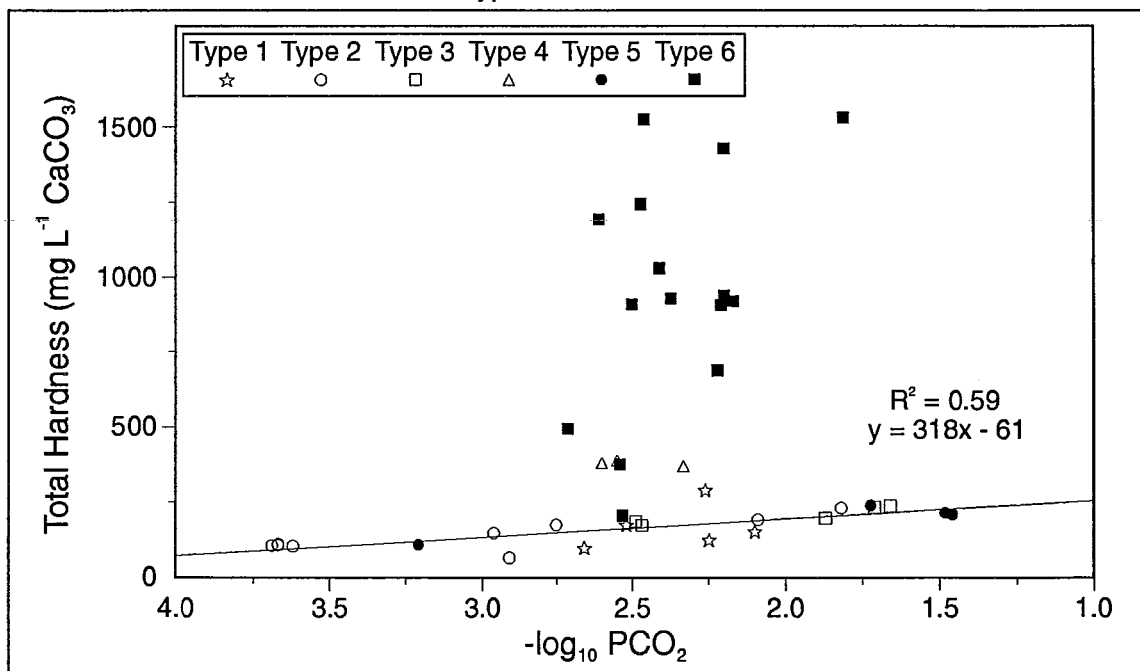


Figure 10.20: Total hardness versus the negative logarithm of the partial pressure of CO₂ for water samples of the Bear Rock Site. Recharge (Types 1, 2, and 3) and suprapermafrost streams of the discharge area (Type 5) have relatively low concentrations of SO₄²⁻. For these waters there is a good correlation between total hardness and CO₂. The plotted regression line is for these water types. The hardness of the subpermafrost springs is inflated by the dissolution of gypsum at depth.

CHAPTER XI

DISCUSSION AND CONCLUSION

11.1 Introduction

The principal objectives of this thesis were to describe the distribution, morphology, and development of karst landforms and drainage systems in the northern Mackenzie Mountain region (Chapter I). The preceding chapters have: (i) outlined the framework and methods of the study (Chapters I and III), (ii) provided a review of karst and permafrost literature (Chapter II), (iii) examined the regional hydrology, geology, and geomorphology (Chapters III, IV, and V), (iv) described the distribution and range of karst landforms (Chapter VI), and (v) presented a variety of data from individual study sites with a focus on detailed mapping, surface and groundwater hydrology, and hydrochemistry (Chapters VII, VIII, IX, and X). In many of these chapters, discussion has accompanied the presentation of data. This chapter will not reiterate each of the points of discussion from the individual sites. The intent of this chapter is to summarize the main findings.

The discussion is organized in accordance with the primary themes of the opening chapters. Specific topics include examination of: (i) the relationships between lithology, structure and the characteristics of karst landforms and drainage systems, (ii) the impact of glaciation on karst systems in the region, (iii) the role of permafrost in karst processes, and (iv) the spatial and temporal characteristics of dissolution. Finally, by coupling the regional observations with the process data, the conclusion will summarize the development of karst in the northern Mackenzie Mountains.

11.2 Distribution of Karst Landforms

Karst features have been mapped across the Carcajou Range of the Mackenzie Mountains, and the southern portion of the Norman Range, Franklin Mountains. Intermediate-scale landforms were easily identifiable on aerial photography. The distribution of these landforms is controlled by bedrock lithology and structure, topography, glaciation, and permafrost.

11.2.1 Morphology, Lithology, and Structure

Major depression landforms include dolines, dry valleys, subsidence troughs, and poljes. A variety of solution, subsidence, and collapse depressions occur. The distribution of dolines, springs, pavement, and areas of internal drainage in the Carcajou Range are mapped with bedrock geology on Figure 11.1. The density of sink points is highest on the Bear Rock and Hume Formations. They also occur on the Franklin Mountain and Mount Kindle dolomites, the Saline River Formation, and on some of the clastic units overlying the Hume Formation. The main genetic types of depressions are summarized below.

Shallow, flat bottomed dolines occur as bare karst on limestones of the Hume and Ramparts Formation, and on the Landry Member of the Bear Rock Formation. These dolines have a solution origin and their frequency of occurrence is low. At the Bear Rock Site, there are also a few solution dolines in dolomite of the Franklin Mountain Formation. Karren forms occur on exposed limestone and dolomite, with the best developed karst pavements on the dolomites of the Mount Kindle Formation.

More common are dolines of subsidence and collapse origin. Most intermediate-scale subsidence features occur where evaporite bedrock, usually gypsum, is found in the shallow subsurface. Solution of carbonates in the soil and subcutaneous zones may also contribute to their development. Most of these dolines evolve where meteoric waters infiltrate through surface fissures and fractures and come into contact with the upper beds of underlying evaporites. Dissolution is accompanied by brecciation and subsidence. Alternatively, some may result from

upward stoping of breccia pipes. Through subsidence, surface catchments are enlarged, focussing drainage as point recharge. These dolines are usually conical in section and are most often found on outcrops of the Brecciated Member of the Bear Rock Formation, and occasionally on outcrops of the Saline River Formation. They are the predominant type of doline at the Dodo Canyon and Bear Rock Sites. In areas of high doline density, adjacent features may coalesce to form large lobate compound depressions. Where allogenic drainage is routed onto these karst surfaces, blind or dry valleys may develop. Linear depressions or troughs occur above zero edges of underlying evaporites or where dissolution is focussed along major lineaments, fractures, or faults. Poljes are rare in the region, though examples of border (Moraine Polje) and overflow poljes (Carcadodo Valley) are noted.

Many dolines also display a sharp, steep sided morphology. These depressions have an origin attributed to a combination of collapse and subsidence into cavities of underlying evaporites. Collapse depressions are located where cover rocks provide a resistant cap above gypsum and salt rich units. The cover rocks are carbonate or clastic formations. Subrosion may occur in the shallow subsurface or at depths as great as several hundred metres. The evaporite units are Bear Rock/Fort Norman and Saline River Formations. Collapse dolines formed by dissolution of gypsum in the Bear Rock/Fort Norman Formation are seen on the Landry Member, and on the Hume, Hare Indian, and Canol Formations. In the Landry Member and Hume Formation, surficial dissolution of limestone expands doline catchments. Collapse-subsidence dolines also occur in dolomite of the Mount Kindle and Franklin Mountain Formations in response to subrosion of halite and gypsum of the Saline River Formation. They are most frequent on the Great Bear Plain to the east of the study area. Many collapse-subsidence dolines are thought to occupy positions where breccia pipes have propagated to the surface, particularly where subrosion is deep seated (e.g., Figure 6.8).

Subsidence and collapse dolines, depressions and troughs occur where karst and cover rocks overlie evaporitic strata. They are most common in the following

structural situations: (i) on crests or flanks of anticlines (e.g., Imperial Hills, MacKay Range, Bear Rock), (ii) on flanks of monoclinal folds (e.g., Dodo Canyon, Bonus Lake, Mountain River/Bell Creek), (iii) on gently dipping strata along or near lineaments or faults (e.g., Bear Rock), and (iv) above the zero edge of evaporite subcrops (e.g., Ration Creek, Dodo Canyon). In most of these situations, meteoric groundwaters circulate through local or intermediate flow systems from topographically high recharge areas to bordering discharge areas. Much dissolution occurs at depth where fresh groundwaters encounter highly soluble evaporites. Meteoric waters percolate to the suprafacial surface of evaporite beds through fractured or highly porous strata or may be delivered to the subface by artesian flow through underlying strata. The Bear Rock/Fort Norman evaporite is underlain by dolomites. Below the Saline River Formation are fractured quartzites and sandstones of the Little Dal and Katherine Groups. The dolomite and clastic units function as aquifers. Topography exercises control by influencing the local hydraulic gradients. Where gradients are gentle, or where circulation is impeded by aquicludes or aquitards, there are fewer karst landforms. Depression density is highest where the gradients are steepest, that is on uplands immediately adjacent to river valleys, canyons, and glacial meltwater channels. In studying covered karst, Quinlan (1978) describes similar relationships between structure and landform characteristics. Where carbonates are draped over gypsum, steep subsidence features may develop by vertical percolation of meteoric waters and artesian flow. Linear subsidence troughs occur above the zero edge of evaporite subcrops. Breccia pipes and collapse dolines are commonplace where gypsum is in subcrop. The association between depression location and major lineaments and anticlines is noted in other studies (e.g., Jassim *et al*, 1995).

Examples of each of the genetic depression types occur at the Dodo Canyon Site. There are solution and subsidence dolines, and linear troughs on the Bear Rock Formation. Collapse-subsidence depressions extend to the Hume and overlying clastic formations. Subrosion occurs in gypsum of the Bear Rock Formation. The

local undisturbed thickness of the subsurface evaporite is not known. From nearby boreholes and the breccia thickness, it is estimated that at least 100 m of anhydrite and gypsum are interbedded with the dolomite where it is unaffected by meteoric groundwaters. Karst depressions at the Dodo Canyon Site exhibit local relief up to 30 m. From boreholes near the Bear Rock Site, there are 200 m of undisturbed evaporite underlying the dolomite (Figure 4.10). At this site, depressions on the Bear Rock Formation differ only slightly from those at Dodo Canyon. Solution-subsidence dolines and large compound features are more common at the Bear Rock Site, due mainly to the local absence of the resistant Landry Member. The difference in the subsurface evaporite thickness is not reflected in topography. Priesnitz (1974; cited in Quinlan, 1978) notes that while a very small proportion of the total evaporite removed is expressed through overlying topographic relief, the proportion is greater above the feather or zero edges of evaporite subcrops. At Dodo Canyon, Bonus Lake, and at other locations on monoclines or anticlines a substantial karst relief is developed where carbonates straddle the feather edge of evaporite subcrops.

11.2.2 Influence of Glaciation and Permafrost

Each of the study sites investigated were glaciated in the Late Wisconsinan by the Laurentide Ice Sheet. In the region, there is evidence of several Pleistocene montane and Laurentide advances (Chapter V). During the last glaciation, Laurentide ice spread westward from Great Bear Plain over the Franklin Mountains and Mackenzie Valley into the Canyon Ranges. The valleys, plateaus, and low ridges of the front ranges were ice covered. To the west, ice of the Cordilleran Ice Sheet advanced into the main valleys of the Backbone Ranges. Cirque and small valley glaciers also spread from high elevations of the Canyon Ranges, in places forming piedmont glaciers. In the Canyon Ranges, the main geomorphic impact of glaciation was the formation of canyons through diversion of mountain drainage by the Laurentide Ice Sheet into ice marginal channels. The cover of glacial sediments in the region is thin.

West of the main study area, high plateaus and ridges of the Canyon Ranges have been unglaciated for at least several hundred thousand years (Hughes, 1972). The rock formations that support the karst of the Carcajou and Norman Ranges also outcrop in that area. Aerial photographs of portions of the unglaciated terrain were examined. There were no meso-scale karst depressions or drainage features identified outside the limits of Wisconsinan glacial ice or meltwater channels. The unglaciated areas are at higher elevations than the study sites. The permafrost distribution is continuous and of greater thickness. There are geological structures that are similar to those hosting karst in the front ranges but the geology of the unglaciated area has not been examined in detail. However, solution breccias are reported in the Bear Rock Formation (Aitken and Cook, 1974; Morrow, 1991). The landscape has the geomorphic characteristics associated with long periods of cryogenic (periglacial) weathering: cryoplanation landforms, flat floored valleys with braided channels, and evidence of parallel slope retreat (Preisnitz and Schunke, 1983; Preisnitz, 1988). This area provides a model of landform development in mountains under the climatic conditions that generate continuous permafrost. It is highly significant that the incidence of karst on the Bear Rock Formation and other rocks differs so greatly between the glaciated and non-glaciated terrain. Given the absence of karst in areas beyond the ice limit, it must be concluded that glaciation has had an overall positive role on karstification.

Specific glacial impacts were identified at the study sites. Destructive and deranging effects on the karst include: (i) erosion of karren, dolines, and other input landforms, (ii) dissection of conduits and drainage systems by meltwater channels, and (iii) infilling of conduits and input landforms with glacial sediments. Dolines and depressions were eroded across the region. Despite the partial removal of surface karst, the hydrological role of many input landforms were either preserved or re-established following deglaciation. Portions of drainage systems were fragmented by canyon and valley incision. The best example is from Bonus Lake, where an abandoned conduit aquifer is preserved as fragments of cave passage in

widely scattered upland blocks. The aquifer was cut by meltwater channels and by collapse and subsidence following deglaciation. At the same site, input landforms and caves are infilled with glacio-lacustrine and fluvial sediments. Some dolines at the Dodo Canyon Site that are partially infilled with sediment have lost their hydrological function.

Evidence from the Carcajou Range and the Bear Rock Site suggests that the last Laurentide ice was warm based. The stimulative or positive impacts of glaciation include: (i) focusing meltwaters to input landforms in subglacial or ice marginal environments, (ii) lowering spring point elevations through canyon and valley incision, (iii) scouring, deepening, or expanding depressions by abrasion, plucking, or meltwater erosion, and (iv) degradation of permafrost under warm ice. In the Carcajou Range, meltwaters and impounded mountain drainage were routed through ice marginal or subglacial channels. Some channels developed along or cut across subsidence troughs and dolines. The importance of meltwater focusing to input landforms is seen by the close association between the distribution of meltwater channels and sink points at the study sites. The topographic and hydrologic characteristics of the karst are strongly related to the interstratal dissolution of gypsum. Unlike carbonate minerals, the dissolution rate of gypsum is transport controlled and it is independent of the PCO_2 of infiltrating waters. Subglacial karstification would continue beneath a warm ice cover if meltwaters recharged underlying strata. However, the superimposition of glacial ice would not have steepened the hydraulic gradient substantially, and thereby generated an increased flux of meltwater from the glacial aquifer into the bedrock aquifer. At most of the karst sites, recharge zones sit on upland surfaces. Discharge from local groundwater flow systems is accomplished into bordering valleys and canyons. The hydraulic gradients are steep. During the Laurentide glacial advance, the discharge zones were ice covered before the recharge zones. At the height of glaciation, hydraulic gradients are reduced due to the gently sloping potentiometric surfaces in the overlying glacial aquifer. This 'Canadian Type' of mountain glaciation does not

favour subglacial karstification (Ford, 1993).

In the Pleistocene, the Laurentide Ice Sheet advanced repeatedly into the Mackenzie Valley. The pre-glacial Mackenzie River followed a course east of the Franklin Mountains (Duk-Rodkin and Hughes, 1993). Formations of Cretaceous and Tertiary age had originally extended as a clastic wedge from the Canyon Ranges across to the western slopes of the Franklin Mountains. These were largely removed by the Laurentide Ice Sheet (Hughes, personal communication, 1991). The course of the Mackenzie River shifted to its current position. The erosion of the clastic wedge and re-orientation of the Mackenzie River had the effect of lowering base level and increasing gradients in the front ranges of the Mackenzie Mountains. Combined with diversions of mountain drainage at the ice margin, a series of deep canyons were incised in the front ranges. This expanding network of canyons continues to dissect an older drainage network in the mountains. The effect on karst systems has been to lower the elevation of spring points, steepen hydraulic gradients, and increase hydraulic potential. The elevations of recharge and discharge areas are primary boundary controls on the development and behaviour of karst aquifers (Figure 2.4). A lowering of spring points favours deeper circulation in local flow systems. The post-glacial flux of fresh meteoric waters along deeper flowpaths would increase, as would subsidence of evaporites, subsidence, brecciation, and development of interstratal karst.

In the unglaciated areas, geomorphic processes have been dominated by frost and slow mass wasting processes for the whole of the Pleistocene. Outcrops of carbonate and clastic rocks are frost shattered. Debris moves downslope by creep, solifluction, and rillwash. Groundwater circulation is impeded by permafrost. Small undulations or depressions in the topography are infilled by the slow mass wasting of surface debris. In the mountain areas that have been glaciated, these periglacial processes operate under current conditions. Slow mass wasting has partially infilled some dolines. Where the removal of solutes has kept pace, the landform has been preserved. However, there are dolines where ice plugs or fine-grained sediments

have perched them above the main aquifer. Some have been breached by surface overflow others partially infilled. Glaciation of these terrains may restore the hydrologic function of some dolines by removing materials and scouring depressions.

In Chapter II, a simple thermal model of glacial superimposition on permafrost was presented (Section 2.7.4, Figures 2.11, 2.12). Assuming typical values for ground heat flux, ice surface temperature, and thermal conductivities of ice and bedrock, it was calculated that over a long period of time permafrost would degrade under 400 to 600 metres of glacial ice. In the Carcajou Range, the main belt of karst runs along the monocline that forms the mountain front (Figure 11.1). The Laurentide ice limit was west of this belt during the Hungry Creek and Katherine Creek phases of the last glaciation, a period of at least several thousand years. At the glacial maximum, ice thicknesses over most of the karst areas were over 800 metres. Given these conditions, it is suggested that permafrost degraded during glaciation. The same conclusion is applied to the Bear Rock Site. Permafrost degradation increases the permeability of near surface materials. This has a minor stimulative effect on subglacial groundwater circulation. The greater influence on karstification occurs during and following deglaciation. Meltwater recharge through deglaciated surfaces that lack permafrost may experience rapid generation of karst landforms due to unimpeded infiltration of high volumes of recharge (Lauritzen, 1984b, 1986a; Ford, 1993). As spring points are deglaciated, local groundwater circulation is driven deeper and interstratal karst expanded. Subsequent aggradation of permafrost strongly influences hydrology but does not necessarily alter the function of input landforms.

The model of Ford (1993; Figure 2.13) depicts the relationship between permafrost and groundwater circulation in carbonate and evaporite rocks. In widespread discontinuous permafrost, circulation through carbonates is locally impeded. Permafrost becomes more of an aquitard in the continuous zone where circulation between the suprapermafrost and subpermafrost aquifers is normally

absent. A similar pattern is shown for gypsum and halite although their higher solubilities permit an easier exchange between aquifers. Brook (1976) describes the same relationship for rugged terrain (Figure 2.14). The model illustrates the variable nature of permafrost distribution in mountains and its effects on circulation. These models are based on, or describe well, several karst terrains from northern Canada, including: Nahanni (Brook, 1976, 1983; Brook and Ford, 1980), Great Bear Plain (van Everdingen, 1981), north Yukon (Tsi-It-Toh-Choh: Cinq-Mars and Lauriol, 1985; Roberge *et al*, 1986; Thibaudeau *et al*, 1988), Horton and Anderson Rivers (Ford, 1993), Akpatok Island (Lauriol and Gray, 1990) and King William and Somerset Islands (Bird, 1967).

In portions of the study region, permafrost has acted to restrict the development of karst landforms and drainage systems. Where permafrost has a continuous distribution, surficial karst and groundwater circulation in carbonates is absent, or is poorly developed. However, a full range of landforms occur in the discontinuous zone. Groundwater circulation is least impeded where there are evaporites in the near subsurface. Such areas are identified by interstratal karst. Many of the dolines and ponors of the study region that survived glaciation, or were formed post-glacially, function as open taliks. Depressions trap drifting snow and many experience periodic ponding. Snow cover, surface detention, and aspect influence the local ground thermal regime resulting in an uneven permafrost distribution.

The study sites span the widespread discontinuous and continuous permafrost zones. At the Bear Rock Site, permafrost on the upland locally perches surface waters in small ponds, but overall it functions as a leaky aquiclude with many sink points operating as taliks. The recharge areas of the Dodo Canyon and Bonus Lake Sites are similar. The observations support Brook's (1976) model of variable permafrost distribution in rugged terrain. An addendum to the model is a lithological consideration. Several flat bottomed dolines at Dodo Canyon, that are developed in limestone of Landry Member, hold water through the summer period. However,

nearby dolines that penetrate the gypsiferous Brecciated Member drain readily. Solution breccias of the Bear Rock Formation appear to have a much higher permeability than bedded limestones of the Landry Member or Hume Formation. This may be attributed to a higher fissure frequency in the breccia and not a permafrost effect.

Permafrost strongly influences seasonal changes in hydrological pathways (Figure 11.2). This was best seen at the Dodo Canyon Site where there was a hierarchy of springs. The model of Figure 11.2 is based on that site. During winter, the suprapermafrost aquifer is inactive. Precipitation is stored as snow and is redistributed in depressions. Soil moisture freezes as pore and lense ice in the active layer. Perennial springs discharging from deep aquifers of regional flow systems are marked by icings. Most of these springs have high concentrations of dissolved ions, some are thermal. They exhibit little variation in flow or chemistry. Exceptions are springs that drain conduit aquifers (e.g., Horseshoe Spring at Pyramid Lake). In the spring period, snowmelt and precipitation are stored in depressions. Rates of infiltration into underlying strata vary considerably. During this time, the streams and springs draining the karst are fed primarily by waters of suprapermafrost origin. This is reflected in their low conductivity, hardness, and temperature, and by their flashy discharge response to rainfall. In the late spring and through the summer, infiltration to subpermafrost aquifers continues through sink points across recharge areas. Springs draining the local karst systems are marked by increases in concentrations of dissolved materials, particularly ions from evaporite minerals, indicating subpermafrost contributions. Springs may also continue to discharge suprapermafrost waters. The discharge response to rainfall events remains flashy. Storm flow moves through the supra and subpermafrost aquifers to spring points. The style of recharge in the sink zones contributes to rapid discharge responses. Precipitation in these areas is routed as throughflow to surface depressions due to the permafrost aquitard in the near subsurface. The end result is aggressive recharge, focussed through discrete input points in a short interval of time. Thus permafrost,

when widely distributed may contribute to the karstification of an aquifer as a result of these focussed inputs. It seems unlikely that these systems would develop independently where permafrost is continuous. The elements of the flow system may be inherited from warmer climates or paraglacial conditions. However, once established the systems continue to function as long as taliks persist.

The Pyramid Lake Site is unlike the other sites in the study. It features a conduit aquifer in dolomite in the zone of continuous permafrost. The site lies just within the ice limit of the Hungry Creek Glaciation and has been ice free for 14 ka. There are no evaporites in the subsurface. Under current conditions, it would not be possible to develop such an aquifer in dolomite. The possibilities include subglacial or paraglacial karstification and inheritance. Conduits associated with subglacial karstification are usually short fragments that occupy anomalous drainage positions. The Pyramid Lake aquifer is an extensive integrated network. The karst must be inherited from a period of warmer climate and is possibly a reactivated paleokarst. Inheritance is thought to play a role across the whole of the region. At Dodo Canyon, a large dry valley is truncated by canyon incision. Many karst features have been modified or removed by glaciation and other processes in the Quaternary, but the original karst in the study region probably dates to the Tertiary. These ideas are reviewed at the conclusion of this chapter.

11.3 Karst Hydrogeology

The primary aquifers of the study region are the Bear Rock and Saline River Formations, important secondary aquifers include the Franklin Mountain, Mount Kindle, and Hume Formations (Brandon, 1965; Michel, 1986a). The geology of these strata were reviewed in Chapter IV. The characteristics of karst drainage systems have been described in Chapters VII through X. From each field site, data have been presented on: hydrochemistry, surface hydrology, and the flow routes and flow through times of groundwater systems. Each of the principal aquifers is associated with a distinctive hydrochemical facies.

Broad differences between sites and aquifers can be illustrated with the full data set. Conductivity is plotted as a function of total dissolved ions concentration for all samples for which there is a complete analysis and low ion balance error (Figure 11.3). Samples with the highest conductivity and TDI are thermal discharge from a deep aquifer in the Saline River Formation. These waters have a sodium chloride facies and were collected at the Dodo Canyon Site at the base of Carcajou Canyon where it emerges at the mountain front. A second group of samples also lies away from the main trend. These samples have a calcium sulphate facies and moderately high conductivities and TDI's. They are perennial discharge waters from an intermediate flow system at the Bear Rock Site. The dissolved gypsum is from the Fort Norman/Bear Rock Formation.

Most of the samples in the study area have TDI values below 30 meq L⁻¹. They may be divided into two groups. At TDI levels below 10 meq L⁻¹, water samples have a calcium bicarbonate facies (sum of Ca²⁺, Mg²⁺, and HCO₃⁻ concentrations ≥ 75% of TDI). There is a linear relationship between TDI and conductivity over this range (Figure 11.3). These waters were sampled from the Bear Rock, Hume, Mount Kindle, and Franklin Mountain Formations. Those from the Bear Rock Formation were either recharge or shallow circulating discharge waters. At higher TDI concentrations, the proportions of evaporite ions increase and samples have a mixed chemistry. These samples are from springs and spring-fed streams that have a groundwater component which has contacted the subsurface Bear Rock or Saline River Formations. Samples aligned along the sulphate trend of Figure 11.3 have travelled mainly through the Bear Rock Formation. Those aligned with the chloride trend have a component of discharge from the Saline River Formation. Due to the variable response of conductivity with the different hydrochemical facies, field conductivity measurements as a surrogate for TDI are best restricted to bicarbonate waters.

There is substantial variability in the structural characteristics of the flow systems studied. At the Pyramid Lake Site, allogenic inputs supply recharge to a

conduit aquifer developed in dolomite of the Franklin Mountain Formation. The basin area is 34 km². It is drained by a single known high discharge, low hardness, subpermafrost spring. Recharge occurs on the flanks of the syncline. Flowpaths are down dip and subparallel to the long axis of the fold. The maximum distance between sinking waters and the spring exceeds 8 km. Flow velocities and travel times are rapid and the spring responses are typical of a conduit aquifer. A similar system is seen at Moraine Polje (Section 6.6). The latter site was visited by D.C. Ford and party. Runoff from an area of 92 km² drains to a polje, north of Keele River. Sink points are in bedrock near the contact of the Bear Rock and Hume Formations. A hierarchy of subpermafrost springs drain the system (Ford, 1993). Again, groundwater flow is routed along a fold axis. A conduit aquifer is suspected.

At the Bonus Lake Site, groundwaters circulate from recharge to discharge zones through the Hume Formation and the upper part of the Bear Rock Formation in a monoclinial structure. Many outcrops of the Hume Formation show relict conduits. The chemistry and hydrology of the main springs support a model of rapid, conduit flow through the portions of the system in the Hume Formation. There are also groundwater contributions from the subsurface Bear Rock Formation and underlying strata as indicated by SO₄²⁻ and Cl⁻ ions.

A monocline also forms the structure at the Dodo Canyon Site. Over the main karst, recharge is accomplished through the Bear Rock Formation. Groundwater flow is down dip to bordering topographic lows. Most of the spring discharge is water from the local flow system. Groundwater circulates through supra and subpermafrost aquifers in the Bear Rock Formation, and subpermafrost aquifers in underlying strata. Local boreholes show Bear Rock breccias to depths as great as several hundred metres (Chapter IV). In the subsurface, reports of cavernous porosity and lost circulation are common (e.g., Hume, 1954). Outcrops have a very high fissure frequency but do not have relict conduits. Groundwater flow through the Bear Rock aquifer is probably of a mixed flow regime (e.g., Figure 2.5). Rapid responses in the discharge of springs is related to the style of recharge. Permafrost

in recharge areas functions as an aquitard. Suprapermafrost water moves as throughflow to sink points. Infiltration displaces subcutaneous and phreatic storage by a piston mechanism.

At the Bear Rock Site, the main aquifers are the Bear Rock, Franklin Mountain, and Saline River Formations. Recharge across an extensive upland in the Bear Rock Formation discharges through bordering springs. There is evidence of slow diffuse flow and a more rapid mixed flow through different areas of the South Karst. The perennial, highly mineralized Bear Rock Springs discharge waters from an intermediate flow system. Recharge is presumed to occur in Long Lake basin. Travel times through the system are several years based on isotope analyses. Circulation is driven to the depth of the Saline River Formation and may be guided by a thrust fault in that unit. Also in the South Karst, there is a system of similar size from Round Lake to Forest and Blood Streams. Discharge is from the Bear Rock and Hume Formations. Travel times along shallow flowpaths are measured in weeks, as shown by dye tracing. However, there are also contributions from underlying deeper flowpaths.

11.4 Rate and Distribution of Solution

The most common hydrochemical measure from karst areas is that of total hardness. When coupled with discharge, total hardness measures can be used to calculate rates of solutional denudation in carbonate basins. In the study region, the range in total hardness values are from 6 to $>1500 \text{ mg L}^{-1}$ as CaCO_3 . Across the full data set, there is a linear relationship between conductivity and total hardness for non-chloride samples (Figure 11.4). Chloride samples are defined here as waters where the sum of Na^+ and Cl^- concentrations is greater than 15% of TDI. Chloride waters are present at Carca-Spring Stream and Carcadodo Valley of the Dodo Canyon Site. Non-chloride waters of very high hardness contain abundant Ca^{2+} from subsurface dissolution of gypsum (e.g., Bear Rock Spring Area). For bicarbonate waters, the range in total hardness is 6 to 240 mg L^{-1} as CaCO_3 . Conductivity measures provide

a good estimate of total hardness over this range (Figure 11.4).

There are several factors that influence the rate of dissolution of carbonate minerals and these are reflected in the average hardness values from a variety of karst environments. Of particular importance are PCO_2 and water temperature. Corbel (1959) suggested from several field studies that water hardness and rates of limestone denudation were highest in mountain and arctic regions. The high rates were partially attributed to increased solubility of carbon dioxide in cold water. This was not affirmed in subsequent studies (e.g., Smith, 1972). In a broad survey, Smith and Atkinson (1976) found average water hardness to be lowest in arctic and alpine regions and highest in tropical environments. The key variable is the addition of biogenic CO_2 in the soil zone. On theoretical grounds, White (1984, 1988) supports the field data summarized by Smith and Atkinson (1976). Repeated work in the Canadian arctic and subarctic shows average water hardness values that are in the range of the bicarbonate waters of the study region (e.g., McCann and Cogley, 1971; Cogley, 1972; Smith, 1972; Wilkinson and Bunting, 1975; Brook, 1976, 1980; Woo and Marsh, 1977; Thibaudeau *et al*, 1988; Lauriol and Gray, 1990). A frequency distribution of total hardness, organized by site, is shown on Figure 11.5. Most of the samples were drawn from below treeline. Many of the low hardness waters are from recharge areas above treeline. Between the study sites, average hardness is lowest at Pyramid Lake and highest at Bear Rock. This distribution is influenced by geology and by vegetation. Allogenic inputs at Pyramid Lake drain areas in quartzite and have very low hardness values. Some of the bicarbonate samples from the Bear Rock and Dodo Canyon Sites contain Ca^{2+} from gypsum dissolution and their hardness values are inflated by the evaporite contribution. Most of the Bear Rock Site is below treeline and organic soils are common. At the Dodo Canyon and Bear Rock Sites, soil PCO_2 concentrations were higher in protected areas below treeline than on exposed ridges and slopes in tundra vegetation. Woo and Marsh (1977) show hardness of surface and active layer waters is directly related to biogenic carbon dioxide. In the study area, there is a positive correlation between total

hardness and the partial pressure of carbon dioxide for the bicarbonate water samples (Figure 11.6).

11.4.1 Denudation

Denudation is a measure of the rate of mass transfer from a system. Most karst studies consider only the transfer of solutes and not clastics. Such treatment is normally adequate to describe landform development in karst areas. Denudation rates on carbonate rocks are directly correlated with runoff and PCO_2 , and inversely related to water temperature (White, 1984, 1988). Due to the high solubilities of gypsum and halite, evaporite dissolution is a function of the volume of water contacting the rock mass. Ford and Williams (1989) suggest that for a given runoff, gypsum denudation per unit area is approximately one order of magnitude higher than that of limestone.

Denudation is usually expressed as a thickness of rock eroded across a uniform surface per thousand years ($mm\ ka^{-1}$); this is equivalent to a volume per unit area per unit time (e.g., $m^3\ km^{-2}\ a^{-1}$). Alternatives are to state denudation in units of volume per volume per unit time ($m^3\ km^{-3}\ a^{-1}$) or as a mass per unit area per unit time ($t\ km^{-2}\ a^{-1}$) (Beckinsale, 1972; Goudie, 1990). Solutional denudation is commonly estimated from: (i) weight loss of bedrock tablets, (ii) micro-erosion measures, (iii) heights of bedrock pedestals, and (iv) discharge and solute data. Bedrock tablets often yield rates that are orders of magnitude lower than those suggested by solute data (Crowther, 1983) and errors associated with micro-erosion meters can produce unreliable results (Spate *et al*, 1985). In the study area, estimates of solutional denudation are based on the latter two methods.

On the Mount Kindle Formation at the Dodo Canyon Site, bedrock pedestals are 70 mm in height, yielding a post-glacial surface lowering rate of 5 to 6 $mm\ ka^{-1}$ (Section 6.2.1). Pedestals of 80 mm height are on the Bear Rock Formation at the Bear Rock Site, producing a surface denudation rate of 7 $mm\ ka^{-1}$. These rates are low compared to the temperate zone but are similar to values from other Arctic and

alpine sites (e.g., 2.5 mm ka⁻¹ at Spitzbergen: Akerman, 1983). While these data provide estimates of surface lowering they say nothing about subsurface dissolution. Data from many field studies in limestone areas suggest that most dissolution occurs in the soil and epikarst zone, with relatively little occurring in conduits and fissures (e.g., Gunn, 1981). However, the morphology of the Mackenzie Mountain karst is strongly controlled by subsurface dissolution. Groundwaters percolating through the epikarst may be near saturation with respect to calcite but still be very aggressive towards evaporite minerals and contribute to the formation of interstratal karst. Discharge and solute data from springs and spring-fed streams can illustrate spatial variations in solution with an aquifer.

Solutional denudation rates are calculated from averages of solute concentration and discharge, or through the use of continuous time series of discharge and concentration data. The time series approach accounts for variations in the discharge-solute relationship and provides high quality estimates when there are several years of data. The use of annual or seasonal averages of discharge and solute concentration typically overestimate denudation rates (Gunn, 1981; Ford and Williams, 1989). A major concern in denudation calculations are solute contributions from allogenic inputs. Solute and discharge data recorded at basin outlets often include allogenic components. Isolation and removal of these inputs requires that the discharge and solute concentrations of allogenic streams be measured (Lauritzen, 1990). Allogenic groundwaters may also contribute to the solute load. Another problem is measuring the basin area, which is exacting in karst areas.

In the simplest case, where basin boundaries are well defined and there are no allogenic inputs to a system, denudation can be evaluated from:

$$D = K \frac{Q_t C_a}{NA\rho} \quad (11.1)$$

where D is denudation in mm ka⁻¹, Q_t is total annual discharge in m³ a⁻¹, C_a is the

average solute concentration in g m^{-3} , ρ is mineral density in g cm^{-3} , A is the basin area in km^2 , N is the fraction of the basin underlain by the soluble rock, and K is a constant of conversion that equals 10^{-6} if the units above are used. Variants of this expression are used when continuous time series are available.

11.4.1.1 Denudation Rates

There are few data from rivers of the Mackenzie Mountains upon which to base estimates of regional denudation (e.g., Tables 3.5, 3.6). However, variations in the spatial distribution of dissolution are seen with the existing data. Water quality data from Keele, Redstone, and Mountain Rivers and from some recharge and discharge waters of the Dodo Canyon, Bonus Lake, and Bear Rock Sites are presented in Table 11.1. The major rivers integrate solute inputs over a variety of geological environments. The field data are specific to regions that contain karst landforms. The average total dissolved ions concentrations of river waters are similar to those of the recharge and shallow discharge waters of the karst sites. A higher proportion of the ion content of the karst waters are composed of Ca^{2+} and HCO_3^- . Some karst discharge waters have high average TDI values, owing largely to contributions of Ca^{2+} , SO_4^{2-} , Na^+ , and Cl^- from evaporites in the Bear Rock and Saline River Formations. These are predominantly discharge waters of local and intermediate flow systems where subsurface dissolution is linked to the local generation of subsidence and collapse landforms. From the limited water quality data from the Mackenzie Mountain Rivers, estimates are made of the solutional denudation rates (Table 11.2). The estimates were derived from Equation 11.1 using average total annual discharge (Q), average total dissolved solids concentration (C), basin area (A), a rock density of 2.65 gm cm^{-3} (ρ), and assuming a uniform distribution of soluble rock across the river basins ($N=1$). Solutional denudation rates for the Carcajou, Redstone, and Mountain River basins are 34, 29, and $33 \text{ m}^3 \text{ km}^{-2} \text{ a}^{-1}$. These rates should obviously be viewed with considerable caution. Rates of denudation associated with the transfer of clastic sediments range between 50 and $75 \text{ m}^3 \text{ km}^{-2} \text{ a}^{-1}$.

Discharge and solute data are available from Red Rock Brook of the Dodo Canyon Site. The average concentrations of the major ion species reflect a mix of three groundwater components (Table 7.7). The load of each ion in Red Rock Brook is calculated in t a^{-1} from average concentration data (C) and an estimated annual discharge of $1.5 \times 10^6 \text{ m}^3 \text{ a}^{-1}$ (Q) (Table 11.3). The objective is to use these data to determine the volumes of rock that are represented by the solute load of Red Rock Brook and if possible to translate those data into measures of denudation. The aquifers that contribute to the flow are the Bear Rock, Mount Kindle, Franklin Mountain, and Saline River Formations. The subsurface mineralogy of these aquifers is dominated by dolomite, anhydrite, and halite. Outcrops of the Bear Rock Formation are calcareous due to the subsurface generation of dedolomite.

The Na^+ and Cl^- loads (112.8 and 172.8 t a^{-1}) are expressed as halite (NaCl) and divided by the mineral density to derive the rock volume eroded (Table 11.4). The volume estimates based on the Na^+ and Cl^- concentrations are 130.4 m^3 and 129.5 m^3 . This analysis assumes all Na^+ and Cl^- originate from halite dissolution and ignores atmospheric inputs. The SO_4^{2-} load in Red Rock Brook is 126.2 t a^{-1} . Assuming all SO_4^{2-} originates from anhydrite (CaSO_4) the volume of rock eroded is 61.9 m^3 (Table 11.4). Anhydrite is used in the calculation and not gypsum ($\text{CaSO}_4 \cdot 2\text{H}_2\text{O}$). The latter has an atmospheric component and the anhydrite represents the true subsurface rock volume. There are difficulties in calculating the volume of carbonate rock eroded due to dedolomite in the Bear Rock Formation. Since dolomite is prevalent in the subsurface it is used to represent carbonates. The Mg^{2+} , HCO_3^- , and Ca^{2+} ion loads provide estimates of dolomite erosion. The Mg^{2+} load of 26.3 t a^{-1} is equivalent to 199.4 t a^{-1} of dolomite, which yields an eroded rock volume of 71.2 m^3 (Table 11.4). The HCO_3^- ion load (268.2 t a^{-1}) is adjusted in two steps. One half of the HCO_3^- load has an origin wholly from atmospheric water and carbon dioxide, it is removed from consideration. The balance of the bicarbonate is stated as CO_3^{2-} ion to remove the remaining atmospheric hydrogen and then expressed as dolomite. In this calculation, 72.4 m^3 of dolomite are eroded. There is good

agreement between the Mg^{2+} and HCO_3^- estimates. The remaining Ca^{2+} load is 40.5 t a^{-1} , this is equivalent to 186.4 t a^{-1} of dolomite which represents 66.6 m^3 of rock eroded. The lower Ca^{2+} estimate is due to the replacement of Mg^{2+} by Ca^{2+} within the Bear Rock Formation.

These calculations show the eroded volumes of halite, anhydrite, and dolomite in the Red Rock Brook catchment are approximately 130, 60, and 70 m^3 . The halite has an origin in the subsurface Saline River Formation. This unit is over 500 m below the topographic surface of the Main Karst. Recharge to the Saline River Formation probably occurs on the flank of MacDougal Anticline and in valleys tributary to Dodo Canyon several kilometres to the south and southwest of Carcadodo Valley. The extent of the recharge zone and the area that is influenced by subsrosion in the Saline River Formation are unknown. For these reasons, it is difficult to translate the rock volume estimate into a denudation rate. The recharge area of the Main Karst is 5.5 km^2 . If it is assumed that all of the halite discharged at Red Rock Brook was dissolved beneath the Main Karst, then from Equation 11.1 the halite denudation rate is $23.6 \text{ m}^3 \text{ km}^{-2} \text{ a}^{-1}$ (mm ka^{-1}). At Salt Spring and along Carca-Spring Stream, concentrations of Na^+ and Cl^- approach 30 times that of Red Rock Brook. While discharges are lower, the volume of eroded rock is at least an order of magnitude higher than the Red Rock Brook estimate. These data indicate much dissolution occurs at depth in the Saline River Formation.

The anhydrite/gypsum components can originate from the Bear Rock or Saline River Formations. Sulphur isotopes show the SO_4^{2-} ion is derived from the Bear Rock Formation and the mixing model of Chapter VII suggests the deep Saline River aquifer contributes only 14% of the SO_4^{2-} load to Red Rock Brook (Table 7.7). It can be assumed that the balance of anhydrite dissolution occurs within the Bear Rock Formation ($\approx 52 \text{ m}^3$). From Equation 11.1, these data yield a denudation rate attributed to anhydrite subsrosion of $9.4 \text{ m}^3 \text{ km}^{-2} \text{ a}^{-1}$ (mm ka^{-1}). For dolomite, the deep groundwater component supplies 9% of the Mg^{2+} load, and $<5\%$ of the HCO_3^- (Table 7.7). The dolomite volume eroded by intermediate and shallow groundwaters is

adjusted to 67 m^3 assuming the deep aquifer contributes only 5% of the carbonate rock dissolution. From Equation 11.1 this yields a denudation rate of $12.1 \text{ m}^3 \text{ km}^{-2} \text{ a}^{-1}$ (mm ka^{-1}) attributed to dolomite dissolution. Bedrock pedestals on the Mount Kindle Formation show a surface lowering rate of 5 to 6 mm ka^{-1} . The total solutional denudation rate from the Main Karst is $\approx 45 \text{ m}^3 \text{ km}^{-2} \text{ a}^{-1}$ (mm ka^{-1}). This calculation ignores allogenic groundwater contributions which are expected to be substantial for halite, and thus is an overestimate of autogenic denudation. Compared with karst regions of similar morpho-climatic regimes, the total rates are high (Smith and Atkinson, 1976; Bogli, 1980). The denudation estimate from Red Rock Brook does not differ greatly from what is suggested by the few regional data available. They do indicate much of the dissolution occurs below the soil and subcutaneous zones and within the body of evaporite-rich aquifers. The predominance of subsidence and collapse landforms is related to this distribution of solution.

11.5 Development of the Northern Mackenzie Mountain Karst

There is evidence of paleokarst in dolomite of the Franklin Mountain and Mount Kindle Formations. Erosion in the Ordovician and Silurian is marked by unconformities (Figure 4.3). It is likely that collapse and subsidence features are present in the Franklin Mountain Formation, resulting from Ordovician or Silurian subsidence of the underlying Saline River evaporites. However, the main karst rock of the region is the Lower Devonian Bear Rock Formation. The unit is a massive breccia in outcrop. A small fraction of the brecciation is attributed to early diagenetic dissolution and subsidence. The majority is late diagenetic solution brecciation by meteoric groundwaters. Important periods of erosion are marked by regional unconformities at the base and top of the Cretaceous. The Tertiary and Quaternary are also characterized by lengthy intervals of erosion (Figure 4.3). Boreholes show evidence that, at some locations, brecciation of the Bear Rock/Fort Norman Formation accompanied the hiatus between the Upper Devonian and

Cretaceous (Tables 4.3, 4.5). The mid to Upper Cretaceous was a time of orogeny in the northern Cordillera, with uplift continuing into the Tertiary (Section 4.8). During this time, an erosion surface developed in the mountain areas and clastic deposits accumulated in the foredeep to the east. Presumably, where the Bear Rock Formation was exposed to meteoric groundwaters, solution brecciation occurred and interstratal karst developed. The Bear Rock Formation was exposed or was in shallow subcrop along positive structural features of the foldbelt such as anticlines, monoclines, and on the hanging walls of thrust faults. Remnants of the late Tertiary drainage network suggest gradients from the Canyon Ranges to the Mackenzie Plain were gentle. Many of the regions larger karst landforms (dry valleys and subsidence troughs) and drainage systems date to the Tertiary and developed under the conditions of a warm and wet climate. Gradual cooling and aggradation of permafrost in the Mackenzie Mountains occurred by the Upper Pliocene. Where permafrost was continuous, karst drainage and landform development were inhibited. The karst landscape may have been degraded through this period. In the Pleistocene, there were several glaciations. The foredeep clastics of the Mackenzie Plain were eroded and the Canyon Ranges were directly influenced by glacial ice and drainage diversions. A resulting steepening of gradients, coupled with minor uplift and glacial drainage diversions, triggered incision of the canyons. Some karst features and the Tertiary drainage network are older than this young expanding network of canyons. They are cross-cut and dissected by the latter. In some areas, glaciation has removed karst landforms but the net effect was positive. This was due to permafrost degradation beneath warm based ice, scouring and removal of surface debris from input landforms, and the post-glacial increase in hydraulic gradients and potentials through the effect on topography.

Under the current conditions, karst drainage systems operate in several formations and karst landforms continue to develop. In the global context, the landform assemblage of the northern Mackenzie Mountain Karst is not typical of that associated with carbonate rocks in arctic climates (Table 1.2). The persistence of the

karst is in part related to the shallow subcrops of evaporite rocks. Drainage is less inhibited by permafrost due to the solubility of evaporite rocks. However, components of the karst systems are inherited from previous warmer climates or have been influenced by past conditions that favoured infiltration and circulation of groundwater. The development of these systems occurred over a long period in the Tertiary. Cooling to a permafrost climate created a new set of conditions. Erosional systems respond slowly to climate change and the hydrological function of portions of the system continued. Pleistocene glaciation revitalized areas by steepening gradients and degrading permafrost. The landscape now has features that are attributed to a variety of processes and its geomorphology must be viewed in that context.

11.6 Future Directions

To date, work on the northern Mackenzie Mountain Karst has been of a reconnaissance nature. Future investigations should focus on areas that have been only briefly considered by this thesis or have yet to be explored. Mapping the distribution and range of karst landforms and drainage should continue to the south and northwest of the study region. Currently, there is information available on the Nahanni Karst of the southern Mackenzie Mountains and from the Old Crow region of Northern Yukon. Mapping intervening areas would provide a regional perspective from which the influence of glaciation, permafrost, and lithology on karst development could be more fully evaluated. Additional mapping should involve morphometric measurements of the main landform types to facilitate comparison with other karst regions. Within the study region, there is much detailed work to be done on the hydrology and hydrochemistry of karst at the scale of small basins and sub-basins. The individual field sites offer much in continued study. The Bear Rock Site represents a true autogenic system and is suited to the long term examination of discharge solute relationships with an aim to calculate some meaningful denudation rates. The Pyramid Lake Site features a conduit dolomite aquifer in a continuous

permafrost environment. The limited field work has suggested a responsive system that is unlike other karst drainage in the region. Moraine Polje may be similar but that has yet to be established by fieldwork. The Dodo Canyon and Bonus Lake Sites have a full range of landforms, hydrological, and permafrost conditions and may serve as type areas for this karst assemblage. At each of these sites and at others, there is a requirement for additional geological mapping. This will permit the development of models describing the structural situations in which these systems operate. Ultimately, the formation of subsidence and collapse landforms will be better understood.

END

Table 11.1: Mean ion concentrations for rivers of the Mackenzie Mountains and selected water types from Dodo Canyon, Bonus Lake, and Bear Rock field sites. River samples are from the months May to September (raw data in Table 3.6). All data are in meq L^{-1} .

River	Ca^{2+}	Mg^{2+}	HCO_3^-	SO_4^{2-}	Na^+	Cl^-	TDI
Keele	1.89	0.92	1.78	1.06	0.22	0.19	6.06
Redstone	1.74	0.92	1.96	0.85	0.25	0.17	5.89
Mountain	1.96	0.94	1.94	1.02	0.13	0.06	6.05
Dodo Canyon Site							
Shallow Streams	2.86	0.57	2.66	0.64	0.04	0.02	6.79
Carcadodo Valley	3.30	1.48	3.10	1.76	3.24	3.22	16.10
Carca-Spring Str	4.52	2.64	3.19	3.84	66.46	62.02	142.67
Bonus Lake Site							
Sink Zone Recharge	1.57	0.20	1.57	0.06	0.03	0.03	3.46
Bonus Valley Str	1.99	0.54	2.16	0.38	0.23	0.20	5.50
Bear Rock Site							
Dolines and Ponors	2.61	0.68	2.43	0.77	0.00	0.01	6.51
Bear Rock Springs	16.64	2.35	4.84	15.65	0.06	0.01	39.57

Table 11.2: Solutional denudation in Carcajou, Redstone, and Mountain River basins.

River	Basin Area (km^2)	Annual Average Discharge ($10^3 \text{ m}^3 \text{ a}^{-1}$)	Average Total Dissolved Solids Concentration (mg L^{-1})	Solutional Denudation Rate ($\text{m}^3 \text{ km}^{-2} \text{ a}^{-1}$ or mm ka^{-1})
Carcajou	7,400	2,360,000	279	34
Redstone	15,400	5,590,000	208	29
Mountain	11,100	3,860,000	252	33

Table 11.3: Average ion concentrations for Red Rock Brook, Dodo Canyon Site and solute load, by ion, as tonnes over the hydrological season (data from 1988).

Average Ion Concentrations	Ca ²⁺	Mg ²⁺	HCO ₃ ⁻	SO ₄ ²⁻	Na ⁺	Cl ⁻
meq L ⁻¹	3.10	1.44	2.93	1.75	3.27	3.25
mg L ⁻¹	62.1	17.5	178.8	84.1	75.2	115.2
Solute Load = Ion Concentrations in mg L ⁻¹ (C) multiplied by Q of 1.5 × 10 ⁶ m ³ a ⁻¹						
Ion	Ca ²⁺	Mg ²⁺	HCO ₃ ⁻	SO ₄ ²⁻	Na ⁺	Cl ⁻
Load in tonnes a ⁻¹	93.2	26.3	268.2	126.2	112.8	172.8

Table 11.4: Volume of halite, anhydrite, and dolomite discharged from the Red Rock Brook aquifer, Dodo Canyon Site. Calculations are based on data from 1988.

Mineral/Rock	Mineral Load (t a ⁻¹)	Mineral Density (t m ³)	Volume Eroded (m ³)
Halite (NaCl)			
112.8 t of Na ⁺ as NaCl	286.8	2.2	130.4
172.8 t of Cl ⁻ as NaCl	284.8	2.2	129.5
Anhydrite (CaSO₄)			
126.2 t of SO ₄ ²⁻ as CaSO ₄	179.4	2.9	61.9
179.4 t of anhydrite requires 52.7 t of Ca ²⁺ , leaving a balance of 40.5 t of Ca ²⁺ in RRB			
Dolomite (CaMg(CO₃)₂)			
26.3 t of Mg ²⁺ as (CaMg(CO ₃) ₂)	199.4	2.8	71.2
40.5 t of Ca ²⁺ as (CaMg(CO ₃) ₂)	186.4	2.8	66.6
263.8 t of CO ₃ ²⁻ as (CaMg(CO ₃) ₂)	202.7	2.8	72.4

Note: The HCO₃⁻ ion load is converted to CO₃²⁻ to remove the mass from atmospheric hydrogen.

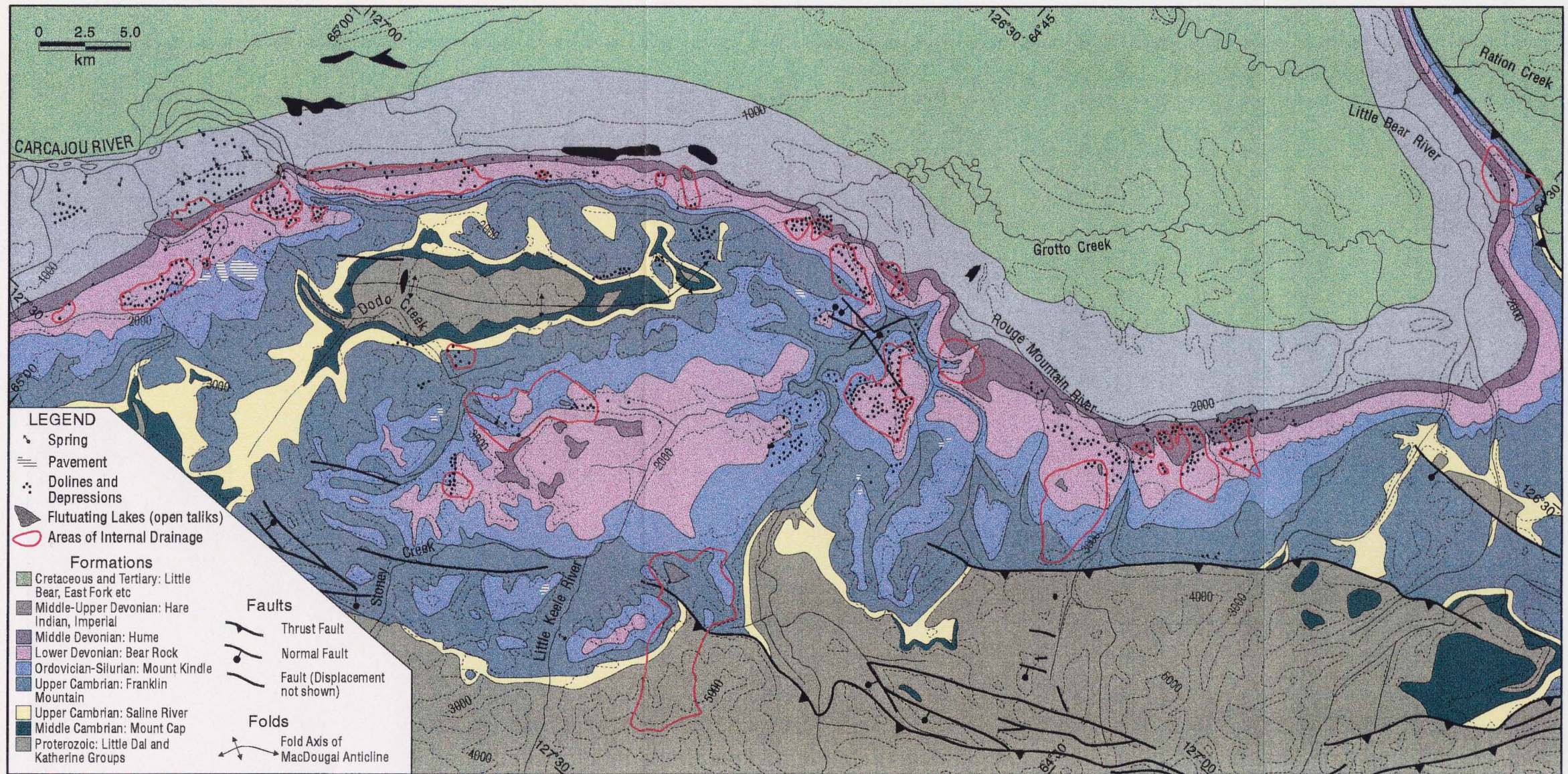


Figure 11.1: Bedrock geology, distribution of dolines, ponors within closed depressions, dolomite pavement, major springs, and areas of internal drainage, Carcajou Range, Mackenzie Mountains, N.W.T. The karst distribution is the same as that of Figure 6.9. Doline and ponor frequency is highest on the Bear Rock and Hume Formations. Other groups of depressions occur on the Mount Kindle, Franklin Mountain, and Saline River Formations. Collapse dolines on Middle and Upper Devonian clastics are in the upper left of the map. Major faults and the trace of MacDougal Anticline are shown. Many fold features are not depicted (geology after Aitken and Cook, 1974).

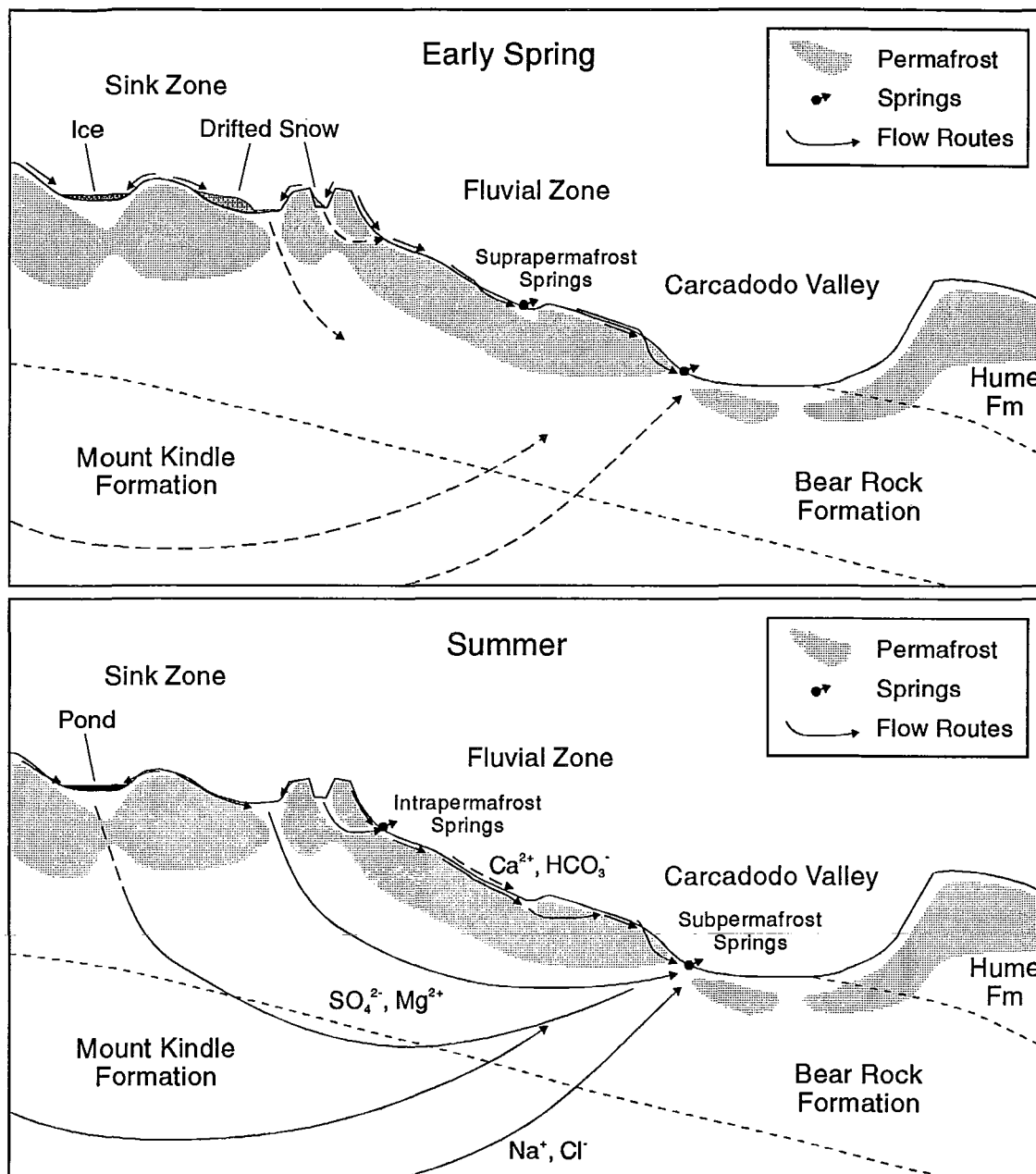


Figure 11.2: Influence of permafrost on hydrological pathways in karst of the northern Mackenzie Mountains. This schematic diagram is based on the Dodo Canyon Site and is not to scale. The distribution of permafrost is in accordance with observations of surface infiltration. It is thought absent beneath large dolines or water bodies. During the early spring (upper) melting snow and precipitation travel as surface runoff or as shallow suprapermafrost water. Much of this runoff is stored in depressions of the Sink (Recharge) Zone. Discharge in the Fluvial Zone and Carcadodo Valley are dominated by surface or suprapermafrost waters. By mid-summer, precipitation infiltrates rapidly through input landforms of the Sink Zone. There is little surface runoff. Groundwaters circulating through the Bear Rock Formation and underlying strata discharge at subpermafrost springs of Carcadodo Valley.

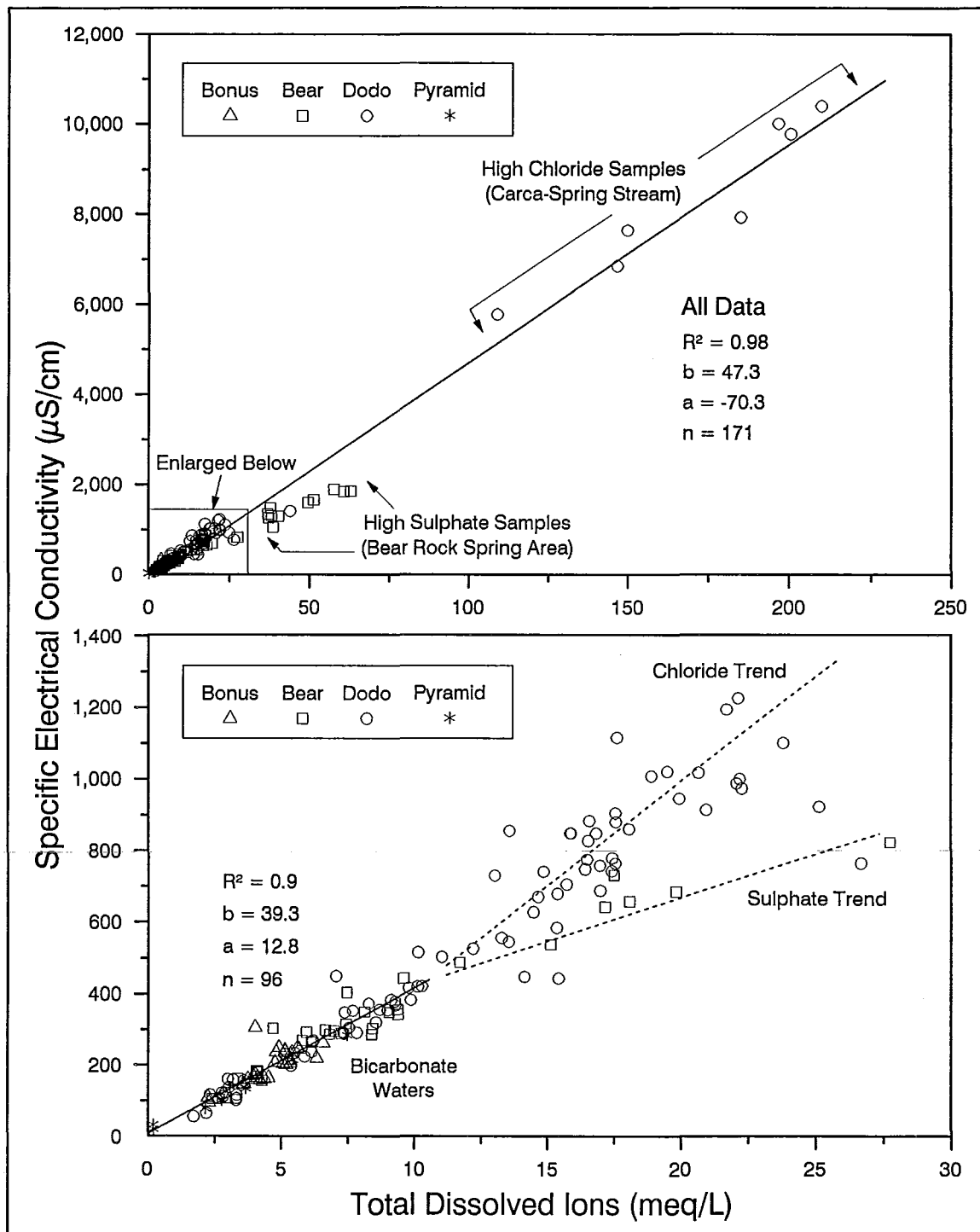


Figure 11.3: Specific electrical conductivity vs total dissolved ions concentration for samples from the field sites. The regression line in the upper figure is based on all data. The lower figure shows data near the origin. In the latter, a regression line is plotted using samples with a bicarbonate chemistry. There is a linear relationship between conductivity and TDI for bicarbonate waters. Addition of evaporite ions increases conductivity, but at different rates for SO_4^{2-} and Cl^- .

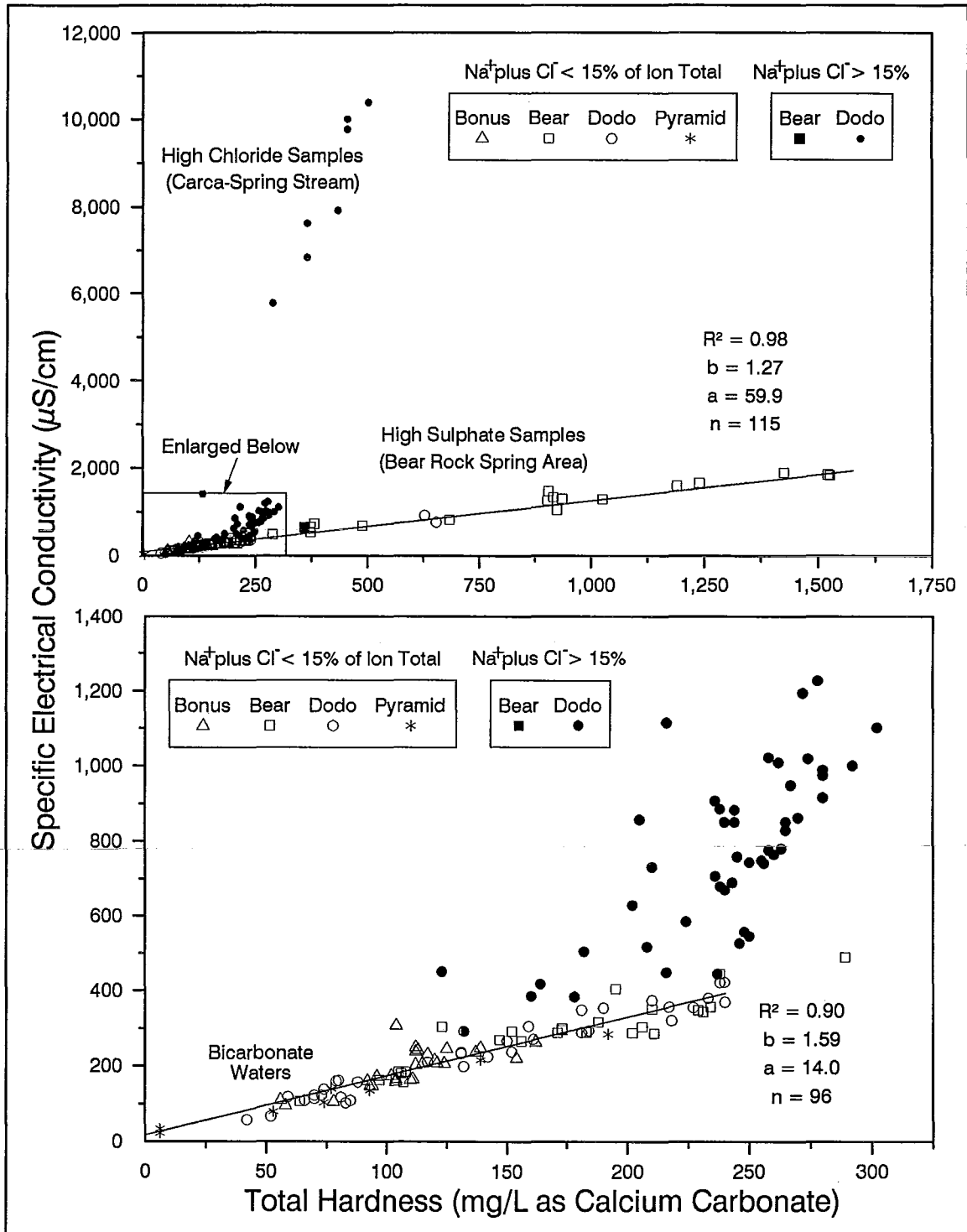


Figure 11.4: Specific electrical conductivity vs total hardness for samples from the field sites. Waters with high concentrations of Cl^- lie above the main trend (solid markers). The regression line in the upper figure is based on all samples where the sum of Na^+ and Cl^- is $\leq 15\%$ of TDI. The regression line in the lower figure is plotted using samples with a bicarbonate chemistry. There is a linear relationship between conductivity and total hardness for bicarbonate waters.

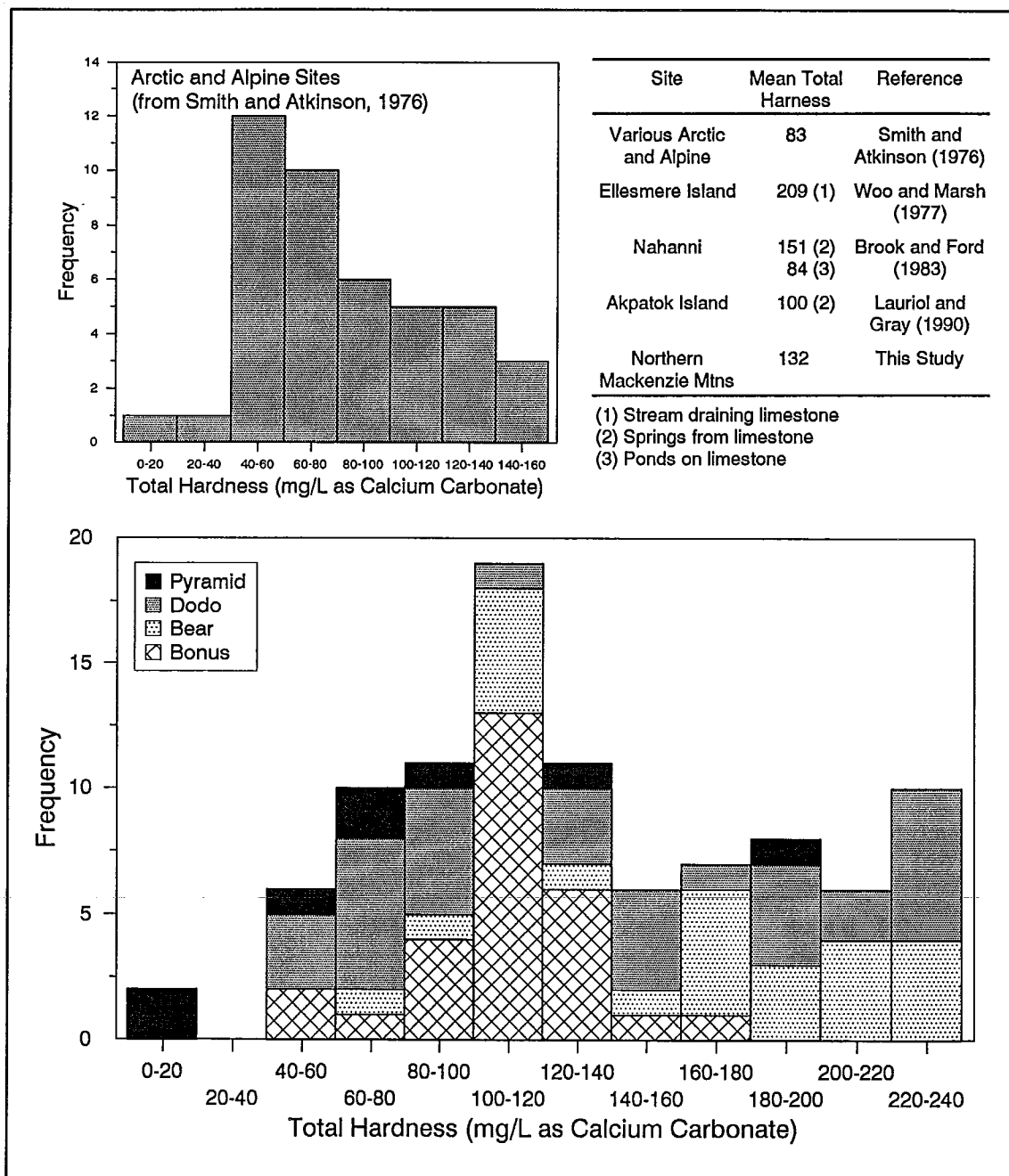


Figure 11.5: Frequency distribution of total hardness from the study region. Only water samples with a bicarbonate facies are shown. Total hardness is lowest at the Pyramid Lake Site and higher at the Dodo Canyon and Bear Rock Sites. At the latter locations, many bicarbonate samples have Ca^{2+} from gypsum dissolution. The mean hardness of all samples is 132 mg L^{-1} as CaCO_3 . This mean is similar to those of the Nahanni Karst (Brook and Ford, 1982) and Akpatok Island (Lauriol and Gray, 1990). The high value from Woo and Marsh (1977) is due to biogenic CO_2 production by tundra vegetation and is not thought typical of high arctic locations. The distribution of Arctic and Alpine Sites from Smith and Atkinson is shown in the upper left.

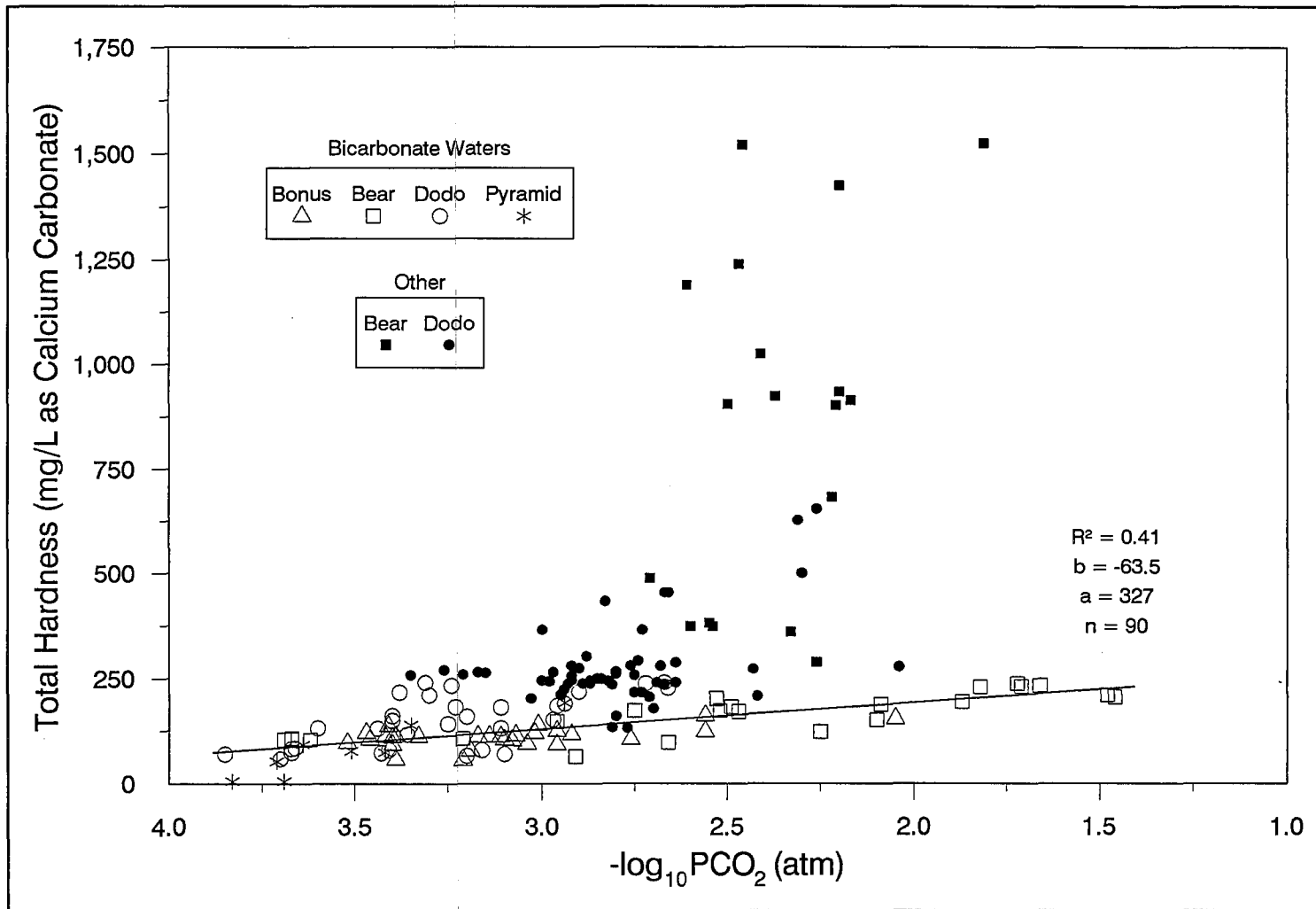


Figure 11.6: Total hardness vs $-\log_{10}$ of PCO_2 for water samples of the study region. Samples of a bicarbonate facies are shown with open markers. A linear regression shows a positive correlation between the variables for these data points.

REFERENCES

- Abbott, J.G. (1982) Structure and stratigraphy of the Macmillan Fold Belt: evidence for Devonian faulting. Exploration and Geological Services Division, Department of Indian and Northern Affairs, Whitehorse, Yukon, Open File.
- Abbott, J.G. (1983) Geology of the Macmillan Fold Belt. Exploration and Geological Services Division, Department of Indian and Northern Affairs, Whitehorse, Yukon, Open File.
- Adams, J.E. (1940) Structural development, Yates area, Texas. *American Association of Petroleum Geologists Bulletin*, 24, 134-142.
- Adams, J.E. (1944) Upper Permian Ochoa series of the Delaware Basin, west Texas and southeastern New Mexico. *American Association of Petroleum Geologists Bulletin*, 28, 1596-1625.
- Agriculture Canada Expert Committee on Soil Survey (1987) *The Canadian System of Soil Classification*. 2nd edition, Agriculture Canada Publication 1646. Ottawa, Canada.
- Aitken, J.D. (1981) Generalizations about Grand Cycles. *In. Short Papers for the Second International Symposium on the Cambrian System*, M.E. Taylor (ed.), 8-14. United States Geological Survey, Open File Report 81-743.
- Aitken, J.D. and D.G. Cook (1974) Carcajou Canyon map area, District of Mackenzie, Northwest Territories. Geological Survey of Canada, Paper 74-13.
- Aitken, J.D., D.G. Cook and C.J. Yorath (1982) Upper Ramparts River (106G) and Sans Sault Rapids (106H) map areas, District of Mackenzie. Geological Survey of Canada, Memoir 388.
- Aitken, J.D. and D.G.F. Long (1978) Mackenzie tectonic arc - reflection of early basin configuration? *Geology*, 6, 626-629.
- Aitken, J.D., D.G.F. Long and M.A. Semikhatov (1978) Progress in Helikian stratigraphy, Mackenzie Mountains. *In. Current Research, Part A*, 481-484. Geological Survey of Canada, Paper 78-1A.
- Aitken, J.D., R.W. Macqueen and J.L. Usher (1973) Reconnaissance studies of Proterozoic and Cambrian stratigraphy, Lower Mackenzie River Area (Operation Norman), District of Mackenzie. Geological Survey of Canada, Paper 73-9.
- Aitken, J.D. and M.E. McMechan (1991) Middle Proterozoic assemblages. *In. Geology of the Cordilleran Orogen in Canada*, H. Gabrielse and C.J. Yorath (eds.), 97-124. Geological Survey of Canada, Geology of Canada, No. 4.
- Akerman, J.H. (1983) Notes on chemical weathering, Kapp Linne, Spitzbergen. *In Proceedings Fourth International Conference on Permafrost*, National Academy of Sciences, Washington, D.C., 1-15.
- American Public Health Association (APHA) (1985) *Standard Methods for the Examination of Water and Wastewater. Sixteenth Edition*. Water Works Association and Water Pollution Control Federation.

- Anderson, D.M. and N.R. Morgenstern (1973) Physics, chemistry, and mechanics of frozen ground: a review. *North American Contribution, Second Permafrost International Conference*, U.S. National Academy of Sciences, Washington, D.C., 257-288.
- Anderson, M.G. and T.P. Burt (1982) The contribution of throughflow to storm runoff: An evaluation of a chemical mixing model. *Earth Surface Processes and Landforms*, 7, 565-574.
- Atkinson, T.C. (1977) Diffuse flow and conduit flow in limestone terrain in the Mendip Hills, Somerset (Great Britain). *Journal of Hydrology*, 35, 93-110.
- Atkinson, T.C. (1985) Present and future directions in karst hydrogeology. *Ann. Soc. Geol. Belgique*, 108, 293-296
- Back, W. and J. Zotl (1975) Application of geochemical principles, isotopic methodology, and artificial tracers to karst hydrology. *In. Hydrogeology of Karstic Terrains*, A. Burger and L. Dubertet (eds.), 105-121. International Union of Geological Sciences, Series B, 3.
- Bakalowicz, M. (1976) Geochimie des eaux karstiques. Une methode d'etude de l'organisation des ecoulements souterrains. *Ann. Sci. Univ. Besancon*, 25, 49-58.
- Bakalowicz, M. and A. Mangin (1980) L'aquifere karstique. Sa definition, ses caracteristiques et son identification. *M. L. sr. Soc. geol. France*, 11, 71-79.
- Bassett, H.G. (1961) Devonian stratigraphy, central Mackenzie River region, Northwest Territories, Canada. *In. Geology of the Arctic, V. 1*, G.O. Raasch (ed.), 481-495. Alberta Society of Petroleum Geologists and University of Toronto Press.
- Bassett, H.C. and J.G. Stout (1966) Devonian of western Canada. *In. International Symposium on the Devonian System, V. 1*, D.H. Oswald (ed.), 717-752. Alberta Society of Petroleum Geologists.
- Berger, G.W. (1987) Thermoluminescence dating of the Pleistocene Old Crow tephra and adjacent loess, near Fairbanks, Alaska. *Canadian Journal of Earth Sciences*, 24, 1975-1984.
- Berner, R.A. (1978) Rate control of mineral dissolution under earth surface conditions. *American Journal of Science*, 278, 1235-1252.
- Bird, J.B. (1967) *The Physiography Of the Arctic Canada With Special Reference to the Area South of Parry Channel*. Baltimore: Johns Hopkins University Press.
- Blake, W., Jr. (1983) Geological Survey of Canada radiocarbon dates XXIII. Geological Survey of Canada, Paper 83-7.
- Blake, W., Jr. (1987) Geological Survey of Canada radiocarbon dates XXVI. Geological Survey of Canada, Paper 86-7.
- Blatt, H., G.V. Middleton and R. Murray (1980) *Origin of the Sedimentary Rocks*. New Jersey: Prentice-Hall.
- Blount, C.W. and F.W. Dickson (1973) Gypsum-anhydrite equilibria in systems $\text{CaSO}_4\text{-H}_2\text{O}$ and $\text{CaSO}_4\text{-NaCl-H}_2\text{O}$. *American Mineralogist*, 58, 323-331.
- Blount D.N. and C.H. Moore (1969) Depositional and non-depositional carbonate breccias, Chiantla quadrangle, Guatemala. *Geological Society of America, Bulletin*, 80, 429-442.
- Blusson, S.L. (1971) Sekwi Mountain map area, Yukon Territory and District of Mackenzie. Geological Survey of Canada, Paper 71-22.

- Bogli, A. (1961) Karrentische, ein Beitrag sur Karstmorphologie. *Zeit. Geomorph*, 5, 185-193.
- Bogli, A. (1980) *Karst Hydrology and Physical Speleology*. Berlin: Springer-Verlag.
- Bonacci, O. (1987) *Karst Hydrology*. Berlin: Springer-Verlag.
- Bosak, P., D.C. Ford, and J. Glazek (1992) *Paleokarst - A World Review*. Amsterdam: Elsevier.
- Bostock, H.S. (1948) Physiography of the Canadian Cordillera, with special reference to the area north of the fifty-fifth parallel. Geological Survey of Canada, Memoir 247.
- Bostock, H.S. (1966) Notes on glaciation in central Yukon Territory. Geological Survey of Canada, Paper 65-36.
- Bostock, H.S. (1970) Physiographic subdivisions of Canada. In *Geology and Economic Minerals of Canada*, R.J.W. Douglas (ed.), 10-30. Ottawa: Geological Survey of Canada.
- Brandon, L.V. (1965) Groundwater hydrology and water supply in the District of Mackenzie, Yukon Territory, and adjoining parts of British Columbia. Geological Survey of Canada, Paper 64-39.
- Brook, G.A. (1976) *Geomorphology of the North Karst, South Nahanni River Region, Northwest Territories, Canada*. Unpublished Ph.D. Thesis, McMaster University, Department of Geography.
- Brook, G.A. (1983) Hydrology of the Nahanni, a highly karsted carbonate terrain with discontinuous permafrost. In *Proceedings Fourth International Conference on Permafrost*, 86-90. Washington D.C.: National Academy Press.
- Brook, G.A., M.A. Folkoff and E.O. Box (1983) A world model of soil carbon dioxide. *Earth Surface Processes and Landforms*, 8, 79-88.
- Brook, G.A. and D.C. Ford (1978) The origin of labyrinth and tower karst and the climatic conditions necessary for their development. *Nature*, 275, 493-496.
- Brook, G.A. and D.C. Ford (1980) Hydrology of the Nahanni karst and the importance of extreme summer storms. *Journal of Hydrology*, 46, 103-121.
- Brook, G.A. and D.C. Ford (1982) Hydrologic and geologic controls of carbonate water chemistry in the sub-Arctic Nahanni Karst, Canada. *Earth Surface Processes and Landforms*, 7, 1-16.
- Brown, R.J.E. (1970) *Permafrost in Canada: Its Influence on Northern Development*. Toronto: University of Toronto Press.
- Budel, J. (1982) *Climatic Geomorphology*. New Jersey: Princeton University Press.
- Burns, B.M. (1973) *The Climate of the Mackenzie Valley - Beaufort Sea Volumes I and II*. Climatological studies number 24, Atmospheric Environment Service, Environment Canada, Toronto, Ontario.
- Burt, T.P. and P.J. Williams (1976) Hydraulic conductivity in frozen soils. *Earth Surface Processes*, 1(4), 349-360.
- Caine, N. (1989) Hydrograph separation in a small alpine basin based on inorganic solute concentrations. *Journal of Hydrology*, 112, 89-101.
- Camsel, C. and W. Malcolm (1921) *The Mackenzie River basin (Revised Edition)*. Geological Survey of Canada, Memoirs 108.

- Cary, J.W. and H.F. Mayland (1972) Salt and water movement in unsaturated frozen soil. *Soil Science Society of America, Proceedings*, 36(4), 549-555.
- Catto, N.R. (1986) *Quaternary sedimentology and stratigraphy, Peel Plateau and Richardson Mountains, Yukon and N.W.T.* Unpublished PhD thesis, University of Alberta.
- Cecile, M.P. (1982) The Lower Paleozoic Misty Creek embaymeny, Selwyn Basin, Yukon and Northwest Territories. Geological Survey of Canada, Bulletin 335.
- Cecile, M.P., D.G. Cook and L.R. Snowdon (1982) Plateau overthrust and its hydrocarbon potential, Mackenzie Mountains, Northwest Territories. *In* Current Research, Part A, Geological Survey of Canada, Paper 82-1A, 89-94.
- Cecile, M.P. and B.S. Norfold (1991) Ordovician and Silurian assemblages. *In* *Geology of the Cordilleran Orogen in Canada*, H. Gabrielse and C.J. Yorath (eds.) 184-196. Geological Survey of Canada, Geology of Canada, No. 4.
- Cederstrom, D.J., P.M. Johnston and S. Subitzky (1953) Occurrence and development of ground water in permafrost regions. United States Geological Survey, Circular 275.
- Chatterton, B.D.E. (1978) Aspects of late Early and Middle Devonian conodont biostratigraphy of western and northwestern Canada. *In* *Western and Arctic Canadian Biostratigraphy*, C.R. Stelck and B.D.E. Chatterton (eds.), 161-232. Geological Association of Canada, Special Paper 18.
- Chorley, R.J. (1962) *Geomorphology and general systems theory*. United States Geological Survey Professional Paper No. 500B.
- Chorley, R.J. (1966) The application of statistical methods to geomorphology. *In* *Essays in Geomorphology*, G.H. Dury (ed.), 275-387. London: Heinemann.
- Chorley, R.J. and B.A. Kennedy (1971) *Physical Geography: A Systems Approach*. London: Prentice-Hall.
- Christiansen, E.A. (1971a) Geology and groundwater resources of the Melville area (62K, L). Saskatchewan Research Council Geology Division Map No. 12.
- Christiansen, E.A. (1971b) Geology of the Crater Lake collapse structure in southeastern Saskatchewan. *Canadian Journal of Earth Sciences*, 8, 1505-1513.
- Christiansen, E.A., D.J. Gendzwill, and D.R. Derry (1973) Pipe-shaped structures. *Economic Geology*, 68, 1334-1336.
- Church, M. (1974) Hydrology and permafrost with reference to northern North America. *In* *Proceedings Workshop Seminar on Permafrost Hydrology*, 7-20. Ottawa: Can. Nat. Comm.
- Church, M. and J.M. Ryder (1972) Paraglacial sedimentation. *Geological Society of America Bulletin*, 83, 3059-3072.
- Ciry, R. (1962) Le Role du Foid dans la Speleogenese. *In* *Spelunca* (4th Serie) Memoires #2, 29-34.
- Cinq-Mars, J. and B. Lauriol (1985) Le karst de Tsi-It-Toh-Choh: notes preliminaire sur quelques phenomenes karstique du Yukon septentrional, Canada. *Comptes Rendus du Colloque International de Karstique Applique*, Universite de Liege, 185-196.
- Cogley, J.G. (1972) Process of solution in an Arctic limestone terrain. Institute of British Geographers, Special Publication No. 4, 201-211.

- Cook D.G. (1975) The Keele Arch - a pre-Devonian and pre-Late Cretaceous paleo-upland in the northern Franklin Mountains and Colville Hills. Ottawa: Geological Survey of Canada.
- Cook, D.G. and J.D. Aitken (1972) Tectonics of northern Franklin Mountains, Colville Hills of Canada. *The Oil and Gas Journal*, 70 (10), 150-160.
- Cook, D.G. and J.D. Aitken (1973) Tectonics of the northern Franklin Mountains and Colville Hills, District of Mackenzie, Canada. In: *Arctic Geology*, M.G. Pitcher (ed.), 13-22. American Association of Petroleum Geologists, Memoir 19.
- Cook, D.G. and J.D. Aitken (1975) Geology, Norman Wells (96E) and Mahony Lake (96F), District of Mackenzie. Geological Survey of Canada, Open File 304.
- Cook, D.G. and J.D. Aitken (1976) Geology, Blackwater Lake (96B) and Fort Norman (96C), District of Mackenzie. Geological Survey of Canada, Open File 402.
- Cook, F.A. (1992) Racklan orogen. *Canadian Journal of Earth Sciences*, 29(11), 2490-2496.
- Corbel, J. (1957) Les Karsts du nord-ouest de l'Europe. *Mem Inst. Etudes Rhodaniennes*, 12, 1-544.
- Corbel, J. (1959) Erosion en Terrain Calcaire. *Annales de Geographie*, 68, 7-120.
- Corbel, J. (1964) Les karsts des regions polaires. *Rev. Belge. Geogr.*, 88, 83-103.
- Craig, B.G. (1960) Surficial geology of north-central District of Mackenzie, Northwest Territories. Geological Survey of Canada, Paper 60-18.
- Craig, B.G. (1965) Glacial Lake McConnell and the surficial geology of parts of Slave River and Redstone River map-areas, District of Mackenzie. Geological Survey of Canada, Bulletin 122.
- Craig, H. (1961) Isotopic variations in meteoric waters. *Science*, 133, 1702-1703.
- Craig, P.C. and P.J. McCart (1975) Classification of stream types in Beaufort Sea drainages between Prudhoe Bay, Alaska, and the Mackenzie delta, N.W.T., Canada. *Arctic and Alpine Research*, 7, 183-198.
- Crowther, J. (1983) A comparison of the rock tablet and water hardness methods for determining chemical erosion rates on karst surfaces. *Zeit. Geomorph.*, 27(1), 55-64.
- Cryer, R. and S.T. Trudgill (1990) Solutes. In: *Geomorphological Techniques, Second Edition*, A.Goudie, M. Anderson, T.Burt, J. Lewin, K. Richards, B. Whalley, and P. Worsley (eds.), 260-279. London: Unwin Hyman.
- Dansgaard, W. (1964) Stable isotopes in precipitation. *Tellus*, 16, 436-468.
- Davis, W.M. (1899) The geographical cycle. *Geographical Journal*, 14, 481-503.
- De Mille, G.D., J.R. Shouldice and H.W. Nelson (1964) Collapse structures related to evaporites of the Prairie Formation, Saskatchewan. *Geological Society of America Bulletin*, 75, 307-316.
- Denton, G.H. and T.J. Hughes (1983) Milankovitch theory of ice ages: hypothesis of ice-sheet linkage between regional insolation and global climate. *Quaternary Research*, 20, 125-144.

- Dingman, S.L. (1973) Effects of permafrost on streamflow characteristics in the discontinuous permafrost zone of Central Alaska. *In* Proceedings *Permafrost: The North American Contribution to the Second International Conference, Yakutsk, USSR*, 447-453. Washington, D.C.: National Academy of Sciences.
- Domenico, P.A. and F.W. Schwartz (1990) *Physical and Chemical Hydrogeology*. Toronto: Wiley.
- Dostal, J. and C. Elson (1980) General principles of neutron activation analysis. *In* *Neutron Activation Analysis in the Geosciences*, G.K. Mueke (ed.), 21-42. Short Course Handbook, V.5, Mineralogical Association of Canada.
- Douglas, R.J.W. (1980) Proposals for time classification and correlation of Precambrian rocks and events in Canada and adjacent areas of the Canadian Shield, Part 2: a provisional standard for correlating Precambrian rocks. Geological Survey of Canada, Paper 80-24.
- Douglas, R.J.W., H. Gabrielse, J.O. Wheeler, D.F. Stott and H.R. Belyea (1970) Geology of western Canada. *In* *Geology and Economic Minerals of Canada, Report No. 1*, R.J.W. Douglas (ed.), 367-546. Ottawa: Geological Survey of Canada.
- Douglas, R.J.W. and D.K. Norris (1961) Camsell Bend and Root River map areas, District of Mackenzie, Northwest Territories. Geological Survey of Canada, Paper 61-13.
- Douglas, R.J.W. and D.K. Norris (1963) Dehadinni and Wrigley map areas, District of Mackenzie, Northwest Territories. Geological Survey of Canada, Paper 62-33.
- Dowling, D.B. (1922) Geological structure of the Mackenzie River region. *In* *Summary Report 1921, Part B*, 79-90. Ottawa: Geological Survey of Canada.
- Drake, J.J. (1980) The effect of soil activity on the chemistry of carbonate groundwaters. *Water Resources Research*, 16, 381-386.
- Drake, J.J. (1984) Theory and model for global carbonate solution by groundwater. *In* *Groundwater as a Geomorphic Agent*, R.J. LaFleur (ed.), 210-226. Boston: Allen & Unwin.
- Drake, J.J. and T.M.L. Wigley (1975) The effect of climate on the chemistry of carbonate groundwater. *Water Resources Research*, 11, 958-962.
- Drew, D.P. and D.I. Smith (1969) Techniques for the tracing of subterranean drainage. *BGRG Technical Bulletin*, 2.
- Drewry, D.J. (1986) *Glacial Geologic Processes*. London: Edward Arnold.
- Dreybrodt, W. (1988) *Processes in Karst Systems: Physics, Chemistry, and Geology*. Berlin: Springer.
- Duk-Rodkin, A. and O.L. Hughes (1991) Age relationships of Laurentide and montane glaciations, Mackenzie Mountains, Northwest Territories. *Geographie physique et Quaternaire*, 45, 79-90.
- Duk-Rodkin, A. and O.L. Hughes (1993) Mackenzie River, an integrated drainage system of Late Pleistocene age. Paper presented at Geological Association of Canada Meeting, Edmonton, 1993.
- Dunkerley, D.L. (1979) The morphology and development of rillenkarren. *Zeit. Geomorph*, 23, 332-348.

- Dutro, Jr., J.T., R.V. Dietrich and R.M. Foote (1989) AGI Data Sheets for Geology in the Field, Laboratory, and Office. Third Edition. American Geological Institute. United Book Press.
- Dyck, W., J.A. Lowdon, J.G. Fyles and W. Blake Jr. (1966) Geological Survey of Canada radiocarbon dates V. *Radiocarbon*, 8, 96-127.
- Dyke, A.S. (1987) A reinterpretation of glacial and marine limits around the northwestern Laurentide Ice Sheet. *Canadian Journal of Earth Sciences*, 24, 591-601.
- Ecoregions Working Group (1989) *Ecoclimatic Regions of Canada, First Approximation*. Ecoregions Working Group of the Canada Committee on Ecological Land Classification. Ecological Land Classification Series, No. 23, Sustainable Development Branch, Canadian Wildlife Service, Conservation and Protection, Environment Canada, Ottawa, Ontario.
- Eisbacher, G.H. (1981) Sedimentary tectonics and glacial record in the Windermere Supergroup, Mackenzie Mountains, northwestern Canada. Geological Survey of Canada, Paper 80-27.
- Environment Canada (1980) *Detailed Surface Water Quality Data, Northwest Territories, 1974-76*. Inland Waters Directorate, Western and Northern Region, Water Quality Branch, Calgary, Alberta.
- Environment Canada (1982) *Canadian Climate Normals*. Volume 2: Temperature 1951-1980. Volume 3: Precipitation 1951-1980. Atmospheric Environment Service, Environment Canada, Toronto, Ontario.
- Environment Canada (1984) *Canadian Climate Normals*. Volume 9: Soil temperature, lake evaporation, days with blowing snow, hail, fog, smoke or haze, frost, 1951-1980. Atmospheric Environment Service, Environment Canada, Toronto, Ontario.
- Environment Canada (1986) *Sediment Data, Yukon and Northwest Territories, 1984*. Inland Waters Directorate, Water Resources Branch, Water Survey of Canada, Ottawa, Canada.
- Environment Canada (1988a) *Miscellaneous Sediment Data, Canada, 1966-1983*. Inland Waters Directorate, Water Resources Branch, Water Survey of Canada, Ottawa, Canada.
- Environment Canada (1988b) *Surface Water Data, Yukon and Northwest Territories, 1987*. Inland Waters Directorate, Water Resources Branch, Water Survey of Canada, Ottawa, Canada.
- Environment Canada (1989a) *Sediment Data, Yukon and Northwest Territories, 1987*. Inland Waters Directorate, Water Resources Branch, Water Survey of Canada, Ottawa, Canada.
- Environment Canada (1989b) *Surface Water Data, Yukon and Northwest Territories, 1988*. Inland Waters Directorate, Water Resources Branch, Water Survey of Canada, Ottawa, Canada.
- Environment Canada (1990a) *Sediment Data, Yukon and Northwest Territories, 1988*. Inland Waters Directorate, Water Resources Branch, Water Survey of Canada, Ottawa, Canada.
- Environment Canada (1990b) *Surface Water Data, Yukon and Northwest Territories, 1989*. Inland Waters Directorate, Water Resources Branch, Water Survey of Canada, Ottawa, Canada.
- Environment Canada (1991) *Historical Streamflow Summary, Yukon and Northwest Territories, To 1990*. Inland Waters Directorate, Water Resources Branch, Water Survey of Canada, Environment Canada, Ottawa, Canada.
- Environment Canada (1992) *Sediment Data, Yukon and Northwest Territories, 1990*. Inland Waters Directorate, Water Resources Branch, Water Survey of Canada, Ottawa, Canada.

- Environment Canada (1993) *Canadian Climate Normals, 1961-90, Yukon and Northwest Territories*. Canadian Climate Program, Atmospheric Environment Service, Environment Canada.
- Faure, G. (1991) *Principles and Applications of Inorganic Chemistry*. Toronto: Collier MacMillan.
- Fetter, C.W. (1988) *Applied Hydrogeology*. Columbus: Merrill.
- Filippov, A. (1989) Cryokarst of the Vilujan Plateau. *Tenth International Congress of Speleology*, Budapest.
- Folk, R.L., H.H. Roberts, and C.M. Moore (1973) Black phytokarst from Hell, Cayman Islands, West Indies. *Geological Society of America Bulletin*, 84, 2351-2360.
- Ford, D.C. (1971) Characteristics of limestone solution in the Southern Rocky Mountains and Selkirk Mountains, Alberta and British Columbia. *Canadian Journal of Earth Sciences*, 8, 585-609.
- Ford, D.C. (1973) Development of the Canyons of the South Nahanni River, N.W.T. *Canadian Journal of Earth Sciences*, 10, 366-378.
- Ford, D.C. (1976) Evidences of multiple glaciations in South Nahanni National Park, Mackenzie Mountains, Northwest Territories. *Canadian Journal of Earth Sciences*, 13, 1433-1445.
- Ford, D.C. (1979) A review of alpine karst in the southern Rocky Mountains of Canada. *NSS Bulletin*, 41, 53-65.
- Ford, D.C. (1980) Threshold and limit effects in karst geomorphology. *In Thresholds in Geomorphology*, D.R. Coates and J.D. Vilek (eds.), 345-362. London: Allen & Unwin.
- Ford, D.C. (1983) Effects of glaciations upon karst aquifers in Canada. *Journal of Hydrology*, 61, 149-158.
- Ford, D.C. (1984) Karst groundwater activity and landform genesis in modern permafrost regions of Canada. *In Groundwater as a Geomorphic Agent*, R.J. LaFleur (ed.), 340-350. Boston: Allen & Unwin.
- Ford, D.C. (1987) Effects of glaciations and permafrost upon the development of karst in Canada. *Earth Surface Processes and Landforms*, 12, 507-522.
- Ford, D.C. (1993) Karst in cold environments. *In Canada's Cold Environments*, H.M. French and O. Slaymaker (eds.), 199-222. McGill Queen's University Press.
- Ford, D.C. and J.J. Drake (1982) Spatial and temporal variations in karst solution rates: The structure of variability. *In Space and Time in Geomorphology*, C.E. Thorn (ed.), 147-170. London: Allen & Unwin.
- Ford, D.C. and J.A. Lundberg (1987) A review of dissolutional rills in limestone and other soluble rocks. *Cantena, Suppl.*, 8, 119-140.
- Ford, D.C., A.N. Palmer and W.B. White (1988) Landform development: Karst. *In Hydrogeology*, W. Back, J.S. Rosenshein, and P.R. Seaber (eds.), 401-412, *The Geology of North America*, O-2. Boulder: Geological Society of America.
- Ford, D.C. and P.W. Williams (1989) *Karst Geomorphology and Hydrology*. London: Unwin Hyman.

- Foster, S.S.D. (1974) Groundwater storage-river flow relations in a chalk catchments. *Journal of Hydrology*, 23, 299-311.
- Franklin, Sir John (1828) Narrative of a second expedition to the shores of the Polar Sea in the years, 1825, 1826 and 1827. London.
- Freeze, R.A. and J.A. Cherry (1979) *Groundwater*. New Jersey: Prentice-Hall.
- French, H.M. (1976) *The Periglacial Environment*. New York: Longman.
- French, H.M. and D.G. Harry (1992) Pediments and cold-climate conditions, Barn Mountains, unglaciated northern Yukon, Canada. *Geografiska Annaler*, 74A, 145-157.
- Fried, G., J. Heinrich, G. Nagel and A. Semmel (1993) Periglacial denudation in formerly unglaciated areas of the Richardson Mountains (NW Canada). *Zeit. Geomorph. Suppl.-Bd.* 92, 55-69
- Fritz, P., J.A. Cherry, K.V. Weyer, and M.G. Sklash (1976) Runoff analyses using environmental isotopes and major ions. *In Interpretation of Environmental Isotope and Hydrochemical Data in Groundwater Hydrology*, 111-130. Vienna: I.A.E.A.
- Fritz, P. and J.C. Fontes (1980) Introduction. *In Handbook of Environmental Isotope Geochemistry, Volume 1, The Terrestrial Environment*, A, P. Fritz and J.C. Fontes (eds.), 1-19. Amsterdam: Elsevier.
- Fulton, R.J. (1984) Quaternary glaciation, Canadian Cordillera. *In Quaternary Stratigraphy of Canada - A Canadian Contribution to IGCP Project 24, GSC Paper 84-10*, R.J. Fulton (ed.), 39-47. Ottawa: Energy Mines and Resources.
- Fulton, R.J., M.M. Fenton and N.W. Rutter (1984) Summary of Quaternary stratigraphy and history, Western Canada. *In Quaternary Stratigraphy of Canada - A Canadian Contribution to IGCP Project 24, GSC Paper 84-10*, R.J. Fulton (ed.), 69-83. Ottawa: Energy Mines and Resources.
- Gabrielse, H. (1967) Tectonic evolution of the northern Canadian Cordillera. *Canadian Journal of Earth Sciences*, 4, 271-298.
- Gabrielse, H., S.L. Blusson and J.A. Roddick (1973) Geology of the Flat River, Glacier Lake and Wrigley Lake map areas, District of Mackenzie and Yukon Territory. Geological Survey of Canada, Memoir 366, Part 1 and 2.
- Gabrielse, H. and A.J. Brookfield (1992) Correlation chart for the Canadian Cordillera. *In Geology of the Cordilleran Orogen in Canada*, H. Gabrielse and C.J. Yorath (eds.). Geological Survey of Canada, Geology of Canada, No. 4.
- Gabrielse, H. and R.B. Campbell (1991) Upper Proterozoic assemblages. *In Geology of the Cordilleran Orogen in Canada*, H. Gabrielse and C.J. Yorath (eds.), 196-210. Geological Survey of Canada, Geology of Canada, No. 4.
- Gabrielse, H., J.W.H. Monger, J.O. Wheeler and C.J. Yorath (1991) Part A. Morphological belts, tectonic assemblages and terranes. *In Geology of the Cordilleran Orogen in Canada*, H. Gabrielse and C.J. Yorath (eds.), 15-28. Geological Survey of Canada, Geology of Canada, No.4.
- Gams, I. (1978) The polje: The problem of definition. *Zeit. Geomorph.*, 22, 170-181.
- Gardiner, V. and R. Dackombe (1983) *Geomorphological Field Manual*. London: Allen & Unwin.

- Garrels, R.M. and C.L. Christ (1965) *Solutions, Minerals and Equilibria*. New York: Harper & Row.
- Gendzwill, D.J. and Z. Hajnal (1971) Seismic investigation of the Crater Lake structure in southeastern Saskatchewan. *Canadian Journal of Earth Sciences*, 8, 1514-1524.
- Gilbert, D.L.F. (1973) Anderson, Horton, northern Great Bear and Mackenzie Plains, Northwest Territories. *In. Future Petroleum Provinces of Canada*, R.G. McCrossan (ed.), 213-244. Canadian Society of Petroleum Geologists, Memoir 1.
- Gilbert, G.K. (1877) Report on the geology of the Henry Mountains, Washington. United States Geological Survey.
- Glew, J.R. and D.C. Ford (1980) A simulation study of the development of rillenkarren. *Earth Surface Processes*, 5, 25-36.
- Gold, L.W. and A.H. Lachenbruch (1973) Thermal conditions in permafrost: a review. *Proceedings of the Second International Conference on Permafrost, Yakutsk, U.S.S.R., North American Contribution*, 3-25. Washington, D.C.: National Academy of Sciences.
- Goldie, H.S. (1981) Morphometry of the limestone pavements of Farleton Knott, Cumbria, England. *Trans. Brit. Cave Res. Assoc.*, 8, 207-224.
- Gordey, S.P. (1978) Stratigraphy and structure of the Summit Lake area, Yukon and Northwest Territories. *In. Current Research, Part A*, 43-48, Geological Survey of Canada, Paper 78-1A.
- Gordey, S.P. (1991) Devonian-Mississippian clastics of the Foreland and Omineca Belts. *In. Geology of the Cordilleran Orogen in Canada*, H. Gabrielse and C.J. Yorath (eds.), 230-242. Geological Survey of Canada, Geology of Canada, No. 4.
- Gordey, S.P., J.C. Abbott and M.J. Orchard (1982) Devonian-Mississippian (Earn Group) and younger strata in east-central Yukon. *In. Current Research, Part B*, 93-100. Geol Survey of Canada, Paper 82-1B.
- Goudie, A.S. (1990) Denudation and weathering. *In. Geomorphological Techniques*, A. Goudie, M. Anderson, T. Burt, J. Lewin, K. Richards, B. Whalley, and P. Worsley (eds.), 195-224. London: Unwin Hyman.
- Gray, J.T. and J. Pilon (1976) Permafrost distribution at Tasiujaq (Leaf Basin) on the south west coast of Ungava Bay, New Quebec. *Revue de Geographie de Montreal*, 30, 367-373.
- Gray, J., J.A. Pilon, and J. Poitevin (1979) Le pergélisol et la couche active dans la toundra forestière au sud de la Baie aux Feuilles, Nouveau Québec. *Geographie physique et Quartenaire*, 33, 253-264.
- Gunn, J. (1981) Limestone solution rates and processes in the Waitomo district, New Zealand. *Earth Surface Processes and Landforms*, 6, 427-445.
- Gunn, J. (1982) Magnitude and frequency properties of dissolved solids transport. *Zeit. Geomorph.*, 26, 505-511.
- Gustavson, T.C., W.W. Simpkins, A. Alhades and A. Hoadley (1982) Evaporite dissolution and development of karst features in the rolling plains of the Texas Panhandle. *Earth Surface Processes and Landforms*, 7, 545-563.
- Hack, J.T. (1960) Interpretation of erosional topography in humid temperate regions. *American Journal of Science*, 258A, 80-97.

- Hallet, B. (1976) Deposits formed by subglacial precipitation of calcium carbonate. *Geological Society of America Bulletin*, 87(7), 1003-1015.
- Hallet, B. (1981) Glacial abrasion and sliding: their dependence on the debris concentration in basal ice. *Annals of Glaciology*, 2, 23-28.
- Hamilton, S.M., F.A. Michel and C.W. Jefferson (1988) Groundwater geochemistry, South Nahanni resource assessment area, District of Mackenzie. *In* Current Research, Part E, Geological Survey of Canada, Paper 88-1E, 127-136.
- Hanley, P.T. and O.L. Hughes (1973a) Surficial geology of 96C, D, E and 106H, District of Mackenzie, N.W.T. (preliminary drafts). Scale 1:125,000. Geological Survey of Canada, Open File 294.
- Hanley, P.T. and O.L. Hughes (1973b) Surficial geology and geomorphology of Carcajou Canyon, District of Mackenzie. Scale 1:125,000. Geological Survey of Canada, Open File 96/D.
- Hanley, P.T. and O.L. Hughes (1973c) Surficial geology and geomorphology of Fort Norman, District of Mackenzie. Scale 1:125,000. Geological Survey of Canada, Open File 96/C.
- Hanley, P.T., S.C. Chatwin and O.L. Hughes (1975) Surficial geology and geomorphology of Norman Wells, District of Mackenzie. Scale 1:125,000. Geological Survey of Canada, Open File 96/E.
- Harrington, C.R. (1977) *Pleistocene mammals of the Yukon Territory*. Unpublished PhD thesis, University of Alberta, Edmonton, Alberta.
- Harlan, R.L. (1974) Dynamics of water movement in permafrost: a review. *In* *Permafrost Hydrology*, 69-77, Ottawa.
- Harmon, R.S., D.C. Ford and H.P. Schwartz (1977) Interglacial-chronology of the Rocky and Mackenzie Mountains based upon ^{230}Th - ^{234}U dating of calcite speleothems. *Canadian Journal of Earth Sciences*, 14, 2543-2552.
- Harmon, R.S., P. Thompson, H.P. Schwartz and D.C. Ford (1978) Late Pleistocene paleoclimates of North America as inferred from stable isotope studies of speleothems. *Quaternary Research*, 9, 205-218.
- Harris, S.A. (1982) Identification of permafrost zones using selected permafrost landforms. *In* Proceedings *Fourth Canadian Permafrost Conference*, 49-58. Washington, D.C.: National Academy of Sciences.
- Harris, S.A., H.M. French, J.A. Heginbottom, G.H. Johnston, B. Ladanyi, D.C. Sego, and R.O. van Everdingen. (1988) *Glossary of Permafrost and Related Ground-Ice Terms*. Technical Memorandum No. 142, Ottawa: National Research Council of Canada.
- Haskin, L.A. (1980) An overview of neutron activation analysis in geochemistry. *In* *Neutron Activation Analysis on the Geosciences*, G.K. Mueke (ed.), 1-20. Mineralogical Association of Canada, Short Course Handbook, V. 5.
- Heginbottom, J.A., P.J. Kurfurst, and J.S.O. Lau (1978) Regional occurrence of permafrost, Mackenzie Valley, Canada. *In* Proceedings *Third International Conference on Permafrost*, 399-405.
- Heginbottom, J.A. and L.K. Radburn (1992) Permafrost and ground ice conditions of northwestern Canada. Geological Survey of Canada, Map 1691A, scale 1:1,000,000.

- Hem, J.D. (1985) Study and interpretation of the chemical characteristics of natural water. United States Geological Survey, Water Supply Paper 254.
- Hills, L.V. (1975) Late Tertiary floras of Arctic Canada: an interpretation. *In* Proceedings, *Circumpolar Conference on Northern Ecology*, 161-171. Ottawa, Canada.
- Hitchon, B. and H.R. Krouse (1972) Hydrogeochemistry of the surface waters of the Mackenzie River Drainage Basin, Canada - III. Stable isotopes of oxygen, carbon and sulfur. *Geochim. Cosmochim. Acta.*, 36, 1337-1357.
- Hodgson, D.A., J.S. Vincent and J.G. Fyles (1984) Quaternary geology of central Melville Island, Northwest Territories. Geological Survey of Canada, Paper 83-16.
- Hooper, R.P. and C.A. Shoemaker (1986) A comparison of chemical and isotopic hydrograph separation. *Water Resources Research*, 22, 1444-1454.
- Hughes, O.L. (1970) Surficial geology of parts of 96C, D, E, 106G (part) and 106H, District of Mackenzie, N.W.T. (preliminary drafts). Scale 1:125,000. Geological Survey of Canada, Open File 26.
- Hughes, O.L. (1972) Surficial geology of northern Yukon Territory and northwestern District of Mackenzie, Northwest Territories. Geological Survey of Canada, Paper 69-36.
- Hughes, O.L. (1987) Late Wisconsinan Laurentide glacial limits of northwestern Canada: the Tutsieta Lake and Kelly Lake phases. Geological Survey of Canada, Paper 85-25.
- Hughes, O.L. (1989) Quaternary chronology, Yukon and northwestern District of Mackenzie, N.W.T. *In* *Late Cenozoic history of the interior basins of Alaska and Yukon*, L.D. Carter, T.D. Hamilton and J.P. Galloway (eds.), 25-29. United States Geological Survey, Circular 1026.
- Hughes, O.L., R.B. Campbell, J.E. Muller and J.O. Wheeler (1969) Glacial limits and flow patterns, Yukon Territory, south of 65 degrees north latitude. Geological Survey of Canada, Paper 68-34.
- Hughes, O.L., C.R. Harington, J.A. Janssens, J.V. Matthews Jr., R.E. Morlan, N.W. Rutter and C.E. Schweger (1981) Upper Pleistocene stratigraphy, paleoecology and archeology of northern Yukon interior, eastern Beringia 1. Bonnet Plume Basin. *Arctic*, 34, 329-365.
- Hughes, O.L., D.A. Hodgson and J. Pilon (1972a) Surficial geology of 106I, M, N, District of Mackenzie, N.W.T. (preliminary drafts). Scale 1:125,000. Geological Survey of Canada, Open File 97.
- Hughes, O.L., D.A. Hodgson and J. Pilon (1972b) Surficial geology of 106J, K, O, District of Mackenzie, N.W.T. and Yukon Territory (preliminary drafts). Scale 1:125,000. Geological Survey of Canada, Open File 108.
- Hughes, O.L., V.N. Rampton and N.W. Rutter (1972c) Quaternary geology and geomorphology, southern and central Yukon (northern Canada). 24th International Geological Congress (Montreal, Quebec), Guidebook, Field Excursion A11.
- Hughes, O.L. and J. Pilon (1973) Surficial geology of 106L, 116N (E 1/2) and O, P, District of Mackenzie, N.W.T. and Yukon Territory (preliminary drafts). Geological Survey of Canada, Open File 167.
- Hughes, O.L., R.O. van Everdingen and C. Tarnocai (1983) Regional setting - physiography and geology. *In* *Guidebook to Permafrost and Related Features of the Northern Yukon Territory and Mackenzie Delta, Canada*, H.M. French and J.A. Heginbottom (eds.), 5-34. Alaska Division of Geological and Geophysical Surveys, Fairbanks, Alaska.

- Hughes, O.L., N.W. Rutter and J.J. Clague (1989a) Yukon Territory (Quaternary stratigraphy and history, Cordilleran Ice Sheet). *In Quaternary Geology of Canada and Greenland*, R.J. Fulton (ed.), Chapter 1. Geological Survey of Canada, Geology of Canada, No. 1.
- Hughes, O.L., N.W. Rutter, J.V. Matthews Jr. and J.J. Clague (1989b) Unglaciaded areas (Quaternary stratigraphy and history, Canadian Cordillera). *In Quaternary Geology of Canada and Greenland*, R.J. Fulton (ed), Chapter 1. Geological Survey of Canada, Geology of Canada, No. 1.
- Hughes, O.L., C. Tarnocai and C.E. Schweger (in preparation) Testing interglacial climates: Pleistocene stratigraphy, paleopedology and paleoecology, Little Bear River section, western District of Mackenzie.
- Hume, G.S. (1921) Great Slave Lake area. *In Summary Report 1920, Part B*, 30-36. Ottawa: Geological Survey of Canada.
- Hume, G.S. (1923) Geology of the Norman oil Fields and a reconnaissance of part of Liard River. *In Summary Report 1922, Part B*, 47-64. Ottawa, Geological Survey of Canada.
- Hume, G.S. (1954) The lower Mackenzie River area, Northwest Territories and Yukon. Geological Survey of Canada, Memoir 273.
- Hume, G.S. and T.A. Link (1945) Canol geological investigations in the Mackenzie River area, Northwest Territories and Yukon. Geological Survey of Canada, Paper 45-16.
- Jackson Jr., L.E., N.W. Rutter, O.L. Hughes and J.J. Clague (1989) Glaciated fringe (Quaternary stratigraphy and history, Canadian Cordillera). *In Quaternary Geology of Canada and Greenland*, R.J. Fulton (ed), Chapter 1. Geological Survey of Canada, Geology of Canada, No. 1.
- Jakucs, L. (1959) Neue Methoden der Hohlenforschung in Ungarn and ihre Ergebnisse. *Die Hohle*, 10(4), 88-98.
- James, N.P. (1984) Shallowing-upward sequences in carbonates. *In Facies Models, Second Edition*, R.G. Walker (ed.), 213-228. Geosciences Canada Reprint Series 1, Geological Association of Canada, Kitchener, Ontario: Ainsworth Press Limited.
- James, N.P. and P.W. Choquette (eds.) (1988) *Paleokarst*. New York: Springer.
- Jassim, S.Z., A.S. Jibril, and N.M.S. Numan. (in review) Gypsum karstification in the Middle Miocene Fatha Formation, Mosul area, Northern Iraq.
- Jefferson, C.W. and J.C.L. Ruelle (1986) The Late Proterozoic Redstone Copper Belt, Mackenzie Mountains, Northwest Territories. *In Mineral Deposits of the Northern Cordillera*, J.A. Morin (ed.), 154-168. Canadian Institute of Mining and Metallurgy, Special Volume 37.
- Jennings, J.N. (1971) *Karst*. London: MIT Press.
- Jennings, J.N. (1985) *Karst Geomorphology*. Oxford: Basil Blackwell.
- Jones, B. (1989) The role of microorganisms in phytokarst development on dolostones and limestones, Grand Cayman, British West Indies. *Canadian Journal of Earth Sciences*, 26(11), 2204-2213.
- Kane, D.L. and J. Stein (1983a) Field evidence of groundwater recharge in interior Alaska. *In Proceedings Fourth International Conference on Permafrost*, 572-577. Washington, D.C.: National Academy of Sciences.

- Kane, D.L. and J. Stein (1983b) Water movement into seasonally frozen soils. *Water Resources Research*, 19, 1547-1557.
- Kay, A.E., A.M. Allison, W.J. Botha and W.J. Scott (1983) Continuous geophysical investigations for mapping permafrost distribution, Mackenzie Valley, N.W.T., Canada. In Proceedings *Fourth International Conference on Permafrost*, 578-583. Washington, D.C.: National Academy of Sciences.
- Kennedy, V.C., C. Kendall, G.W. Zellweger, T.A. Wyerman and R.J. Avanzino (1986) Determination of the components of stormflow using water chemistry and environmental isotopes, Mattole River basin, California. *Journal of Hydrology*, 84, 107-140.
- Kindle, E.M. and T.O. Bosworth (1921) Oil-bearing rocks of Lower Mackenzie River valley, N.W.T. In. *Summary Report 1920, Part B*, 37-63. Ottawa: Geological Survey of Canada.
- Kinsman, D.J.J. (1974) Calcium sulphate minerals of evaporite deposits: their primary mineralogy. *Proceedings of the Fourth International Symposium on Salt, Northern Ohio Geological Society*, 1, 343-348.
- Klassen, R.W. (1978) A unique stratigraphic record of Late Tertiary-Quaternary events in southeastern Yukon. *Canadian Journal of Earth Sciences*, 15, 1884-1886.
- Klassen, R.W. (1987) The Tertiary-Pleistocene stratigraphy of the Liard Plain, southeastern Yukon Territory. Geological Survey of Canada, Paper 86-17.
- Kobayashi, D. (1985) Separation of the snowmelt hydrograph by stream temperatures. *Journal of Hydrology*, 76, 155-162.
- Kobayashi, D. (1986) Separation of a snowmelt hydrograph by stream conductance. *Journal of Hydrology*, 84, 157-165.
- Korkmaz, N. (1990) The estimation of groundwater recharge from spring hydrographs. *Hydrological Sciences Journal*, 35, 209-217.
- Kuc, M. (1974) The interglacial flora of Worth Point, western Banks Island. In. *Report of Activities, Part B*, 227-231. Geological Survey of Canada, Paper 74-1B.
- Lauriol, B and J.T. Gray (1990) Drainage karstique en milieu de pergélisol: le cas de l'île d'Akpatok, T.N.N Canada. *Permafrost and Periglacial Processes*, 1, 129-144.
- Lauriol, B., L. Carrier and P. Thibaudeau (1988) Topoclimatic zones and ice dynamics in the caves of the Northern Yukon, Canada. *Arctic*, 41, 215-220.
- Lauritzen, S.-E. (1984a) A symposium: arctic and alpine karst. *Norsk Geogr. Tidsskr.*, 38, 139-144.
- Lauritzen, S.-E. (1984b) Evidence of subglacial karstification in Glomdal, Svartisen, Norway. *Norsk Geogr. Tidsskr.*, 38, 169-170.
- Lauritzen, S.-E. (1986a) Kvithola at Fauske, northern Norway: an example of ice-contact speleogenesis. *Norsk Geol. Tidsskr.*, 66, 154-161.
- Lauritzen, S.-E. (1986b) CO₂ content of glacial environments and the likelihood for subglacial karstification. In Proceedings *9th International Speleological Congress*, 127-129.
- Lauritzen, S.-E. (1990) Autogenic and allogenic denudation in carbonate karst by the multiple basin method: An example from Svartisen, north Norway. *Earth Surface Processes and Landforms*, 15, 157-167.

- Law, J. (1971) Regional Devonian geology and oil and gas possibilities, upper Mackenzie River area. *Bulletin of Canadian Petroleum Geology*, 19, 437-486.
- Lehmann, H. (ed.) (1954) Das Karstphänomen in den verschiedenen Klimazonen. *Erdkunde*, 8, 112-139.
- Lenz, A.C. and A.E.H. Pedder (1972) Lower and Middle Paleozoic sediments and Paleontology of Royal Creek and Peel River, Yukon and Powell Creek, N.W.T. International Geological Congress 24th Session, Guidebook Field Excursion A14.
- Lewin, J. (1990) River channels. In *Geomorphological techniques, Second Edition*, A. Goudie, M. Anderson, T. Burt, J. Lewin, K. Richards, B. Whalley and P. Worsley (eds.), 280-301. London: Unwin Hyman.
- Lewkowicz, A.G. and H.M. French (1982a) Downslope water movement and solute concentration within the active layer, Banks Island, N.W.T.. In *Proceedings Fourth Canadian Permafrost Conference*, 163-172. Calgary: National Research Council of Canada.
- Lewkowicz, A.G. and H.M. French (1982b) The hydrology of small runoff plots in an area of continuous permafrost, Banks Island, N.W.T.. In *Proceedings Fourth Canadian Permafrost Conference*, 151-162. Calgary: National Research Council of Canada.
- Longman, M.W. (1980) Carbonate diagenetic textures from near surface diagenetic environments. *American Association of Petroleum Geologists, Bulletin*, 64, 461-487.
- Lowdon, J.A. and W. Blake Jr. (1968) Geological Survey of Canada radiocarbon dates VII. *Radiocarbon*, 10, 207-245.
- Lowdon, J.A. and W. Blake Jr. (1970) Geological Survey of Canada radiocarbon dates IX. *Radiocarbon*, 12, 46-86.
- Lowdon, J.A. and W. Blake Jr. (1973) Geological Survey of Canada radiocarbon dates XIII. Geological Survey of Canada, Paper 73-7.
- Lowdon, J.A. and W. Blake Jr. (1976) Geological Survey of Canada radiocarbon dates XVI. Geological Survey of Canada, Paper 76-7.
- Lowdon, J.A. and W. Blake Jr. (1979) Geological Survey of Canada radiocarbon dates XIX. Geological Survey of Canada, Paper 79-7.
- Lowdon, J.A. and W. Blake Jr. (1981) Geological Survey of Canada radiocarbon dates XXI. Geological Survey of Canada, Paper 81-7.
- Lowdon, J.A., I.M. Robertson and W. Blake Jr. (1971) Geological Survey of Canada radiocarbon dates XI. *Radiocarbon*, 13, 255-324.
- Ludvigsen, R. (1975) Ordovician formations and faunas, southern Mackenzie Mountains. *Canadian Journal of Earth Sciences*, 12, 663-697.
- Lunardini, V. (1981) *Heat Transfer in Cold Climates*. New York: Van Nostrand Reinhold.
- Lundberg, J. (1977) An analysis of the form of Rillenkarren from the tower karst of Chillagoe, North Queensland, Australia. *Proceedings of the Seventh International Speleology Congress*, Sheffield, 294-296.
- Lundberg, J. and D.C. Ford (1994) Dissolutional pavements. *The Canadian Geographer*, 38, 271-275.

- MacKay, D.K. and O.H. Loken (1974) Arctic hydrology. *In* J.D. Ives and R.G. Barry (Eds.), *Arctic and Alpine Environments*, 111-132, London: Methuen.
- Mackay, J.R. (1958) The Anderson River map-area, N.W.T. Geographical Branch, Bulletin, No. 13.
- Mackay, J.R. (1963) The Mackenzie delta area, N.W.T. Geographical Branch, Memoir, no. 8.
- Mackay, J.R. (1983a) Downward water movement into frozen ground, western arctic coast, Canada. *Canadian Journal of Earth Sciences*, 20, 120-134.
- Mackay, J.R. (1983b) Oxygen isotope variations in permafrost, Tuktoyaktuk Peninsula area, Northwest Territories. *In* Current Research, Part B, Geological Survey of Canada, Paper 83-1B, 67-74.
- Mackay, J.R. and W.H. Mathews (1973) Geomorphology and Quaternary history of the Mackenzie River valley near Fort Good Hope, N.W.T., Canada. *Canadian Journal of Earth Science*, 10, 26-41.
- MacKenzie, W.S. (1974) Lower Paleozoic carbonates CDR Tenlen Lake A-73 well, Northwest Territories. *In* Report of Activities, Part B, 265-270. Geological Survey of Canada, Paper 74-1, Part B.
- Mackenzie Valley Transportation Corridor Study (1973) Report on 1973 water quality studies in the Mackenzie drainage basin. Report No. 74-19, Ottawa: Department of the Environment.
- Macqueen, R.W. (1970) Lower Paleozoic stratigraphy and sedimentology, eastern Mackenzie Mountains, northern Franklin Mountains (96C, D, E, F; 106G, H). *In* Report of Activities, Part A, 225-230. Geological Survey of Canada, Paper 70-1A.
- Macqueen, R.W. and W.S. MacKenzie (1973) Lower Paleozoic and Proterozoic stratigraphy, Mobil Colville Hills E-15 well and environs, Interior Platform, District of Mackenzie. *In* Report of Activities, Part B, 183-187. Geological Survey of Canada, Paper 73-1B.
- Mangin, A. (1975) Contribution à l'étude hydrodynamique des aquifères karstiques. DES Thesis, Université Dijon, France.
- Mathews, J.V., Jr., R.J. Mott and J-S. Vincent (1986) Preglacial and interglacial environments of Banks Island: pollen and macrofossils from Duck Hawk Bluffs and related sites. *Géographie physique et Quaternaire*, 40, 279-298.
- Mathews, J.V., Jr., C.E. Schweger and O.L. Hughes (1990) Plant and insect fossils from the Mayo Indian Village section (central Yukon): New data on middle Wisconsinan environments and glaciation. *Geographie physique et Quaternaire*, 44, 15-26.
- Mazor, E. (1991) *Applied Chemical and Isotopic Groundwater Hydrology*. Toronto: John Wiley & Sons.
- McCann, S.B. and J.G. Cogley (1972) Hydrological observations on a small arctic catchment, Devon Island, N.W.T. *Canadian Journal of Earth Sciences*, 9, 361-365.
- McClay, K.R. (1984) Tom barite-lead-zinc deposit, Yukon, Canada. *In* Structural Geology of Stratiform Lead-Zinc Deposits: Case Histories, K.R. McClay (ed.), 60-96. Cordilleran Section, Geological Association of Canada, Short Course No.2 (Part II).
- McDonnell, J.J., M. Bonell, M.K. Stewart and A.J. Pearce (1990) Deuterium variations in storm rainfall: Implications for stream hydrograph separation. *Water Resources Research*, 26, 455-458.

- Meijer Drees, N.C. (1975) Geology of the Lower Paleozoic formations in the subsurface of the Fort Simpson area, District of Mackenzie. Geological Survey of Canada, Paper 74-40.
- Meijer Drees, N.C. (1980) Description of the Hume, Funeral and Bear Rock Formations in the Candex *et al* Dahadini M-43A well, District of Mackenzie. Geological Survey of Canada, Paper 78-17.
- Meijer Drees, N.C. (1986) Evaporitic deposits of Western Canada. Geological Survey of Canada, Paper 85-20.
- Meijer Drees, N.C. (1989) *Sedimentology and Facies Analysis of Devonian Rocks, Southern District of Mackenzie, Northwest Territories, Canada*. Geologica Ultraiectina, No. 63. Utrecht: Instituut voor Aardwetenschappen der Rijksuniversiteit Utrecht.
- Meijer Drees, N.C. (1993) The Devonian succession in the subsurface of the Great Slave and Great Bear Plains, Northwest Territories. Geological Survey of Canada, Bulletin 393.
- Michel, F.A. (1977) *Hydrogeologic Studies of Springs in the Central Mackenzie Valley, North-West Territories, Canada*. Unpublished MS Thesis, University of Waterloo, Waterloo, Ontario.
- Michel, F.A. (1983) Isotope variations in permafrost waters along the Dempster highway pipeline corridor. *In* Proceedings *Fourth International Conference on Permafrost*, 843-848. Washington, D.C.: National Academy of Sciences.
- Michel, F.A. (1986a) Hydrogeology of the Central Mackenzie Valley. *Journal of Hydrology*, 85, 379-405.
- Michel, F.A. (1986b) Isotope geochemistry of frost-blister ice, North Fork Pass, Yukon, Canada. *Canadian Journal of Earth Sciences*, 23, 543-549.
- Michel, F.A. and P. Fritz (1978) Environmental isotopes in permafrost related waters along the Mackenzie valley corridor. *In* Proceedings *Third International Conference on Permafrost*, 207-211.
- Michel, F.A. and P. Fritz (1982) Significance of isotope variations in permafrost waters at Illisarvik, N.W.T. *In* Proceedings *Fourth Canadian Permafrost Conference*, 173-181. Calgary: National Research Council of Canada.
- Michel, F.A. and H.C. Wilson (1988) Groundwater Flow in Permafrost Regions of Canada. International Association of Hydrogeologists, C. N. Chapter, in 2nd International Groundwater Symposium on Hydrogeology of Cold and Temperate Climates, Halifax, Nova Scotia, May 1-5 1988.
- Middleton, G.V. (1961) Evaporite solution breccias from the Mississippian of southwest Montana. *Journal of Sedimentary Petrology*, 31, 189-195.
- Milanovic, P.T. (1981) *Karst Hydrogeology*. Colorado: Water Resources Publication.
- Miotke, F.-D. (1974) Carbon dioxide and the soil atmosphere. *Abh. Karst-und-Hohlenk A* 9.
- Mitter, P. (1983) Frost features of the karst regions of the West Carpathian Mountains. *In* Proceedings *Fourth International Conference on Permafrost*, 861-865. Washington, D.C.: National Academy of Sciences.
- Moore, R.D. (1989) Tracing runoff sources with deuterium and oxygen-18 during spring melt in a headwater catchment, southern Laurentians, Quebec. *Journal of Hydrology*, 112, 135-148.

- Morlan, R.E. (1980) Taphonomy and archaeology in the Upper Pleistocene of the northern Yukon Territory: a glimpse of the peopling of the New World. National Museum of Canada, National Museum of Man, Mercury Series, Archaeological Survey of Canada, Paper 94.
- Morlan, R.E. (1986) Pleistocene archaeology in Old Crow Basin: a critical reappraisal. *In New Evidence for the Pleistocene Peopling of the Americas*, A.L. Bryan (ed.), 27-48. Center for Study of Early Man, University of Maine.
- Morris, W.A. and J.D. Aitken (1982) Paleomagnetism of the Little Dal lavas, Mackenzie Mountains, Northwest Territories, Canada. *Canadian Journal of Earth Sciences*, 19(10), 2020-2027.
- Morrow, D.W. (1991) The Silurian-Devonian sequence in the northern part of the Mackenzie Shelf, Northwest Territories. Geological Survey of Canada, Bulletin 413.
- Morrow, D.W. and D.G. Cook (1987) The Prairie Creek Embayment and Lower Paleozoic stratigraphy of the southern Mackenzie Mountains. Geological Survey of Canada, Memoir 412.
- Morrow, D.W. and H.H.J. Geldsetzer (1991) Lower and Middle Devonian assemblages. *In Geology of the Cordilleran Orogen in Canada*, H. Gabrielse and C.J. Yorath (eds.), 196-210. Geological Survey of Canada, Geology of Canada, No.4.
- Morrow, D.W. and N.C. Meijer-Drees (1981) The Early to Middle Devonian Bear. Rock Formation in the type section and in other surface sections, District of Mackenzie. *In Current Research, Part A*, Geological Survey of Canada, Paper 81-1A. 107-114.
- Morse, J.W. and F.T. Mackenzie (1990) *Geochemistry of Sedimentary Carbonates. Developments in Sedimentology* 48. Amsterdam: Elsevier.
- Moser, H.S. (1980) Environmental isotopes in ice and snow. *In Handbook of Environmental Isotope Geochemistry, Volume 1, The Terrestrial Environment*, A.P. Fritz and J.C. Fontes (eds.), 141-178. Amsterdam: Elsevier.
- Moser, H. and W. Stichler (1980) Environmental isotopes in ice and snow. *In Handbook of Environmental Isotope Geochemistry, Volume 1, The Terrestrial Environment*, A.P. Fritz and J.C. Fontes (eds.), 141-163. Amsterdam: Elsevier.
- Mountjoy, E.W. and T.P. Chamney (1969) Lower Cretaceous (Albian) of the Yukon: Stratigraphy and foraminiferal subdivisions, Snake and Peel Rivers. Geological Survey of Canada, Paper 68-26.
- Naeser, N.D., J.A. Westgate, O.L. Hughes, and T.L. Péwé (1982) Fission-track ages of late Cenozoic distal tephra beds in the Yukon Territory and Alaska. *Canadian Journal of Earth Sciences*, 19, 2167-2178.
- Navas, A. (1990) The effect of hydrochemical factors on the dissolution rate of gypsiferous rocks in flowing water. *Earth Surface Processes and Landforms*, 15, 709-715.
- Newbury, R.W. (1974) River hydrology in permafrost areas. *In Proceedings Workshop Seminar on Permafrost Hydrology*, 31-37. Ottawa: Can. Nat. Comm. IHD.
- Norford, B.S. and R.W. Macqueen (1975) Lower Paleozoic Franklin Mountain and Mount Kindle Formations, District of Mackenzie: Their type sections and regional development. Geological Survey of Canada, Paper 74-34.
- Norris, A.W. (1985b) Stratigraphy of Devonian outcrop belts in northern Yukon Territory and northwestern District of Mackenzie (Operation Porcupine Area). Geological Survey of Canada, Memoir 410.

- Norris, D.K. (1972) En echelon folding in the northern Cordillera of Canada. *Bulletin of Canadian Petroleum Geology*, 20, 634-642.
- Norris, D.K. (1985a) Eastern Cordilleran Foldbelt of Northern Canada: Its structural geometry and hydrocarbon potential. *Bulletin of the American Association of Petroleum Geologists*, 69, 788-808.
- Norris, D.K. and C.J. Yorath (1981) The North American plate from the Arctic Archipelago to the Romanzof Mountains. *In: The Ocean Basins and Margins, V. 5, The Arctic Ocean*, A.E.M. Nairn, M. Churkin, Jr. and F.G. Stehli (eds.), 37-104. New York: Plenum.
- Olive, W.W. (1957) Solution-subsidence troughs, Castile Formation of Gypsum Plain, Texas and New Mexico. *Geological Society of America Bulletin*, 68, 351-358.
- Olovin, B.A. (1988) Filtration properties of frozen ground. *In Proceedings Fifth International Conference on Permafrost*, 418-423.
- Palmer, A.N. (1981) Hydrochemical factors in the origin of limestone caves. *In B.F. Beck (ed.), Proceedings of the Eighth International Speleological Congress*, 120-122, Bowling Green, Kentucky.
- Palmer, A.N. (1984) Objectives and current research status of alpine and arctic karst research. *Norsk Geogr. Tidsskr*, 38, 145-150.
- Park, J.K., D.K. Norris and A. Larochelle (1989) Paleomagnetism and the origin of the Mackenzie Arc of northwestern Canada. *Canadian Journal of Earth Sciences*, 26, 2194-2203.
- Payne, B.R. (1988) The status of isotope hydrology today. *Journal of Hydrology*, 100, 207-237.
- Payne, B.R. (1990) The use of stable isotope tracers for the estimation of the direction of groundwater flow. *Journal of Hydrology*, 112, 395-401.
- Pengfei, G. (1988) Classification of ground water in permafrost areas on the Qinghai-Xizang Plateau, China. *In Proceedings Fifth International Conference on Permafrost*, 583-589.
- Perez, F.L. (1988) Geocryogenic slope caves in the Southern Cascades. *In Proceedings Fifth International Conference on Permafrost*, 834-839.
- Pilgrim, D.H., D.D. Huff and T.D. Steele (1979) Use of specific conductance and contact time relations for separating flow components in storm runoff. *Water Resources Research*, 15, 329-339.
- Pinder, G.F. and J.F. Jones (1969) Determination of the ground-water component of peak discharge from the chemistry of total runoff. *Water Resources Research*, 5, 438-445.
- Plummer, L.N. and E. Busenberg (1982) The solubilities of calcite, aragonite and vaterite in CO₂-H₂O solutions between 0 and 90°C, and an evaluation of the aqueous model for the system CaCO₃-CO₂-H₂O. *Geochim. Cosmochim. Acta*, 46, 1011-1040.
- Pollard, W.H. and H.M. French (1983) Seasonal frost mound occurrence, North Fork Pass, Olgilvie Mountains, northern Yukon, Canada. *In Proceedings Permafrost: Fourth International Conference*, 1000-1004. Washington, D.C.: National Academy of Sciences.
- Pollard, W.H. and H.M. French (1984) The groundwater hydraulics of seasonal frost mounds, North Fork Pass, Yukon Territory. *Canadian Journal of Earth Sciences*, 21, 1073-1081.
- Popov, I.V., N.A. Gvozdetskiy, A.G. Chikishev and B.I. Kudelin (1972) Karst of the U.S.S.R. *In Karst: Important Karst Regions of the Northern Hemisphere*, M. Herak and V. Stringfield (eds.), 355-416. Amsterdam: Elsevier.

- Prest, V.K. (1984) The Late Wisconsinan glacier complex. *In Quaternary Stratigraphy of Canada - A Canadian Contribution to IGCP Project 24*, R.J. Fulton (ed.), 21-36. Geological Survey of Canada, Paper 84-10.
- Price, A.J., T. Dunne, and S.C. Colbeck (1976) Energy balance and runoff from a subarctic snowpack. CRREL Report No. 76-27, Cold Regions Research and Engineering Laboratory, U.S. Army Corps of Engineers, Hanover, New Hampshire.
- Priesnitz, K. (1969) Das Karstrelief des sudlichen Harzvorlandes im Lichte neuerer Arbeiten zum System CaSO₄-NaCl-H₂O. *Proceedings of the Fifth International Speleology Congress*, Stuttgart, Germany.
- Priesnitz, K. (1972) Methods of isolating and quantifying solution factors in the laboratory. *Cave Research Group, Great Britain Transactions*, 14(2), 153-158.
- Priesnitz, K. (1988) Cryoplanation. *In Advances in Periglacial Geomorphology*, M.J. Clark (ed.), 49-68. Chichester: Wiley & Sons.
- Priesnitz, K. and E. Schunke (1983) Pedimentation and fluvial dissection in permafrost regions with special reference to NW-Canada. *In Proceedings Fourth International Conference on Permafrost*, 1015-1019. Washington, D.C.: National Academy of Sciences.
- Prowse, T.D. (1990) Northern hydrology: an overview. *In Northern Hydrology: Canadian Perspectives*, T.D. Prowse and C.S.L. Ommanney (eds.) Ottawa: National Hydrology Research Institute, Environment Canada.
- Pugh, D.C. (1983) Pre-Mesozoic geology in the subsurface of Peel River map area, Yukon Territory and District of Mackenzie. Geological Survey of Canada, Memoir 401.
- Pugh, D.C. (1993) Subsurface geology of Pre-Mesozoic strata, Great Bear River map area, District of Mackenzie. Geological Survey of Canada, Memoir 430.
- Quinlan, J.F. (1978) *Types of karst, with emphasis on cover beds in their classification and development*. Unpublished PhD Thesis, The University of Texas at Austin.
- Quinlan, J.F. (1986) Discussion of 'Ground Water Tracers'. *Ground Water*, 24(2), 253-259.
- Quinlan, J.F. and D.C. Ford (1973) Karst map of Canada. *In Theme and Resource Inventory Study of the Karst Regions of Canada*, D.C. Ford and J.F. Quinlan (eds.), Contract 72-32, Ottawa: National and Historic Parks Branch.
- Quinlan, J.F. and R.O. Ewers (1985) Ground water flow in limestone terranes: Strategy, rationale and procedure for reliable, efficient monitoring of ground water quality in Karst areas. *Proceedings of the Fifth National Symposium and Exposition on Aquifer Restoration and Ground Water Monitoring*, Dublin, Ohio, 197-234.
- Quinlan, J.F., A.R. Smith, and K.S. Johnson (1986) Gypsum karst and salt karst of the United States of America. *Le Grotte d'Italia*, 4(13), 73-92.
- Raiswell, R. (1984) Chemical models of solute acquisition in glacial meltwaters. *Journal of Glaciology*, 30, 49-57.
- Rampton, V.N. (1971) Late Pleistocene glaciations of the Snag-Klutan area, Yukon Territory. *Arctic*, 24, 277-300.
- Rampton, V.N. (1980) Surficial geology, Aklavik, District of Mackenzie. Geological Survey of Canada, Map 31-1979, scale 1:250,000.

- Rampton, V.N. (1982) Quaternary geology of the Yukon Coastal Plain. Geological Survey of Canada, Bulletin 317.
- Rampton, V.N. (1988) Quaternary geology of the Tuktoyaktuk Coastlands, Northwest Territories. Geological Survey of Canada, Memoir 423.
- Reeder, S.W., B. Hitchon and A.A. Levinson (1972) Hydrogeochemistry of the surface waters of the Mackenzie River drainage basin, Canada - I. Factors controlling inorganic composition. *Geochimica et Cosmochimica Acta*, 36, 825-865.
- Ritchie, J.C. (1982) The modern and late Quaternary vegetation of the Doll Creek area, north Yukon, Canada. *New Phytologist*, 90, 563-603.
- Ritchie, J.C. (1984) *Past and Present Vegetation of the Far Northwest of Canada*. Toronto: University of Toronto Press.
- Ritchie, J.C., L.C. Cwynar and R.W. Spear (1983) Evidence from north-west Canada for an early Holocene Milankovitch thermal maximum. *Nature*, 305, 126-128.
- Ritter, D.F. (1988) *Process Geomorphology*. Iowa: W.C. Brown
- Roberge, J., B. Lauriol, and J. Cinq-Mars (1986) Caractere des karsts arctiques du Yukon septentrional. *International Speleology Congress*, Barcelona, Spain, 164-167.
- Roglic, J. (1965) The delimitations and morphological types of the Dinaric Karst. *Nase Jama*, 7, 12-20.
- Rouse, W.R. (1984) Microclimate of Arctic treeline. 2: Soil microclimate of tundra and forest. *Water Resources Research*, 20(1), 67-73.
- Rutter, N.W. (1974) Surficial geology and land classification, Mackenzie Valley transportation corridor (85D, E, 95A, B, G, H, I, J, K, N, O). *In* Report of Activities, Part A, Geological Survey of Canada, Paper 73-1A, 239-240.
- Rutter, N.W. (1984) Pleistocene history of the western Canadian ice-free corridor. *In* *Quaternary Stratigraphy of Canada - A Canadian Contribution to IGCP Project 24*, GSC Paper 84-10, R.J. Fulton (ed.), 49-56. Ottawa: Energy Mines and Resources.
- Rutter, N.W. and G.V. Minning (1972) Surficial geology and land classification, Mackenzie Valley transportation corridor (85E, 95A, B (south half), H, J). *In* Report of Activities, Part A, Geological Survey of Canada, Paper 72-1A, 178.
- Rutter, N.W. and A.N. Boydell (1973) Surficial geology and land classification, Mackenzie Valley transportation corridor (85D, 95B (north half), 95G, I, K (east half), N, O). *In* Report of Activities, Part A, Geological Survey of Canada, Paper 73-1A, 239-240.
- Salvigsen, O., O. Lauritzen and Mangerud (1983) Karst and karstification in gypsiferous beds in Mathiesondalen, Central Spitsbergen, Svalbard. *Polar Research*, 1, 83-88.
- Salvigsen, O. and A. Elgersma (1985) Large-scale karst features and open taliks at Vardeborgsletta, outer Isfjorden, Svalbard. *Polar Research*, 3, 145-153.
- Sanders, E.M. (1921) The cycle of erosion in a karst region (after Cvijic, 1918). *Geographical Review*, 11, 593-604.
- Savigny, K.W. (1989) Engineering geology of the Great Bear River area, Northwest Territories. Geological Survey of Canada, Paper 88-23.

- Savin, S.M. (1980) Oxygen and hydrogen isotope effects in low-temperature mineral-water interactions. *In Handbook of Environmental Isotope Geochemistry, Volume 1, The Terrestrial Environment*, A, P. Fritz and J.C. Fontes (eds.), 283-328. Amsterdam: Elsevier.
- Schroeder, J. (1979) Developement de cavities d'origine mecanique dans un karst froid (Nahanni, T.N.O., Canada). *Annales de la Societe Geologique de Belgique*, 102, 59-67.
- Schumm, S.A. (1977) *The Fluvial System*. New York: Wiley.
- Schumm, S.A. and R.W. Lichty (1965) Time, space and causality in geomorphology. *American Journal of Science*, 263, 110-119.
- Schweger, C.E. (1989) The Old Crow and Bluefish basins, northern Yukon; Development of the Quaternary history. *In Late Cenozoic history of the interior basins of Alaska and Yukon*, L.D. Carter, T.D. Hamilton and J.P. Galloway (eds.), 30-33. United States Geological Survey, Circular 1026.
- Schweger, C.E. and J.V. Matthews Jr (1985) Early and Middle Wisconsinan environments of eastern Beringia: stratigraphic and paleoecological implications of the Old Crow tephra. *Géographie physique et Quaternaire*, 39, 275-290.
- Selby, M.J. (1980) A rock mass strength classification for geomorphic purposes: with tests from Antarctica and New Zealand. *Zeit. Geomorph*, 24, 31-51.
- Shaw, J., G.M. Ashley, and N.D. Smith (1985) *Glacial Sedimentary Environments*. Tulsa, OK: Society of Paleontologists and Mineralogists.
- Shepelev, V.V. (1983) A classification of ground water in the cryolithozone. *In Proceedings Fourth International Conference on Permafrost*, 1139-1142. Washington, D.C.: National Academy of Sciences.
- Simpson, F. (1987) Solution-generated collapse (SGC) structures associated with bedded evaporites: importance to migration and trapping of hydrocarbons. *Ontario Petroleum Institute, Proceedings*, v. 26, Paper 7.
- Simpson, F. (1988) Solution-generated collapse (SGC) structures associated with bedded evaporites: significance to base-metal and hydrocarbon localization. *Geoscience Canada*, 15, 89- 93.
- Sklash, M.G. and R.N. Farvolden (1979) The role of groundwater in storm runoff. *Journal of Hydrology*, 43, 45-65.
- Sklash, M.G., R.N. Farvolden and P. Fritz (1976) A conceptual model of watershed response to rainfall, developed through the use of oxygen-18 as a natural tracer. *Canadian Journal of Earth Sciences*, 13, 271-283.
- Sklash, M.G., M.K. Stewart and A.J. Pearce (1986) Storm runoff generation in humid catchments 2. A case study of hillslope and low-order stream response. *Water Resources Reseach*, 22, 1273-1282.
- Slaughter, C.W., J.W. Hilgert and E.H. Culp (1983) Summer streamflow and sediment yield from discontinuous permafrost headwater catchments. *In Proceedings Fourth International Conference on Permafrost*, 1172-1177. Washington, D.C.: National Academy of Sciences.
- Slaughter, C.W. and D.L. Kane (1979) Hydrologic role of shallow organic soils in cold climate. *In Proceedings Canadian Hydrology Symposium 79, Cold Climate Hydrology*, 380-389.
- Smart, C.C. (1983a) The hydrology of the Castleguard Karst, Columbia Icefields, Alberta, Canada. *Arctic and Alpine Research*, 15, 471-486.

- Smart, C.C. (1983b) *The hydrology of the Castleguard Karst, Columbia Icefields, Alberta, Canada*. Unpublished PhD Thesis, Department of Geography, McMaster University, Hamilton.
- Smart, C.C. (1984) Glacier hydrology and potential for subglacial karstification. *Norsk Geografisk Tidsskrift*, 38, 157-162.
- Smart, C.C. (1988) A deductive model of karst evolution based on hydrological probability. *Earth Surface Processes and Landforms*, 13, 271-288.
- Smart, C.C. and D.C. Ford (1986) Structure and function of a conduit aquifer. *Canadian Journal of Earth Sciences*, 23, 919-929.
- Smart, P.L. (1986) Origin and development of glacio-karst closed depressions in the Picos de Europa, Spain. *Zeit. Geomorph. N.F.*, 30(4), 423-443.
- Smart, P.L. and M.C. Brown (1973) The use of activated carbon for the detection of the tracer dye Rhodamine WT. Proceedings *Sixth International Speleological Congress Olomouc CSSR*, 4, 285-292.
- Smart, P.L. and I.M.S. Laidlaw (1977) An evaluation of some fluorescent dyes for water tracing. *Water Resources Research*, 13, 15-33.
- Smith, D.G. (1992) Glacial Lake Mackenzie, Mackenzie Valley, Northwest Territories, Canada. *Canadian Journal of Earth Sciences*, 29, 1756-1766.
- Smith, D.I. (1969) The solutional erosion of limestone in an Arctic morphogenetic region. *In Problems of the Karst Denudation*, O. Stelci (ed.), p99-109.
- Smith, D.I. (1972) The solution of limestone in an Arctic environment. *In Polar Geomorphology*. Institute of British Geographers Special Publication. No. 4. London.
- Smith, D.I. and T.C. Atkinson (1976) Process, landforms and climate in limestone regions. *In Geomorphology and Climate*, E. Derbyshire (ed.), 369-409. London: Wiley.
- Smith, M.W. (1975) Microclimatic influences on ground temperatures and permafrost distribution, Mackenzie Delta, Northwest Territories. *Canadian Journal of Earth Sciences*, 12, 1421-1438.
- Spate, A.P., J.N. Jennings, D.I. Smith, and M.A. Greenway (1985) The micro-erosion meter: use and limitations. *Earth Surface Processes and Landforms*, 10, 427-440.
- Stanton, R.J. (1966) The solution brecciation process. *Geological Society of America Bulletin*, 77, 843-848.
- Stednick, J.D. (1991) *Wildland Water Quality Sampling and Analysis*. New York: Academic Press, Inc.
- Steer, P. and M.-K. Woo (1983) Measurement of slope runoff in a permafrost region. *Canadian Geotechnical Journal*, 20, 361-365.
- Stenner, R.D. (1969) The measurement of the aggressiveness of water towards calcium carbonate. *Transactions of the Cave Research Group of Great Britain*, 11, 175-200.
- St-Onge, D.A. (1987) Morphosedimentary zones and Wisconsinan glacial limit, Bluenose Lake Region, Northwest Territories. Geological Association of Canada, Program with Abstracts.

- Stott, D.F., C.J. Yorath and J. Dixon (1991) The Foreland Belt. *In*. *Geology of the Cordilleran Orogen in Canada*, H. Gabrielse and C.J. Yorath (eds.), 335-345. Geological Survey of Canada, Geology of Canada, No.4.
- Stumm, W. and J.J. Morgan (1980) *Aquatic Chemistry: Introduction Emphasizing Equilibria in Natural Waters*. New York: Wiley.
- Sugden, D.E. and B.S. John (1976) *Glaciers and Landscape. A Geomorphological Approach*. London: Edward Arnold.
- Summerfield, C. (1991) *Global Geomorphology*. London: Wiley.
- Sweeting, M.M. (1972) *Karst Landforms*. London: Macmillan.
- Tarnocai, C. and C.E. Schweger (1991) Late Tertiary and Early Pleistocene paleosols in northwestern Canada. *Arctic*, 44, 1-11.
- Tarnocai, C., S. Smith and O.L. Hughes (1985) Soil development on Quaternary deposits of various ages in the central Yukon Territory. *In* Current Research, Part A. Geological Survey of Canada, Paper 85-1A, 229-238.
- Tassonyi, E.J. (1969) Subsurface geology, Lower Mackenzie River and Anderson River area, District of Mackenzie. Geological Survey of Canada, Paper 68-25.
- Thibaudeau, P., J. Roberge and B. Lauriol (1988) Agressivite chimique des eaux dans less massifs calcaires du Nord du Yukon, Canada. *Revue de Géomorphologie Dynamique*, 37, 62-71.
- Thorson, R.M. and E.J. Dixon Jr. (1983) Alluvial history of the Porcupine River: role of glacial-lake overflow from northwest Canada. *Geological Society of America, Bulletin*, 94, 576-589.
- Tolstikhin, N.I. and O.N. Tolstikhin (1976) Groundwater and surface water in the permafrost region. IWD Technical Bulletin No.97, Ottawa: Environment Canada.
- Tricart, J. and A. Cailleux (1972) *Introduction to Climatic Geomorphology*. London: Longman.
- Trombe, F. (1952) *Traite de Speleologie*. Paris: Payot.
- Tsui, P.C. and D.M. Cruden (1984) Deformation associated with gypsum karst in the Salt River Escarpment, northeastern Alberta. *Canadian Journal of Earth Sciences*, 21, 949-959.
- Turc, L. (1954) Le bilan d'eau des sols: relations entre les précipitations, l'évaporation et l'écoulement. *Ann. Agron., Sér. A*, 5, 491-595.
- van Everdingen, R.O. (1974) Groundwater in permafrost regions of Canada. *In* Proceedings *Workshop Seminar on Permafrost Hydrology*, 83-93. Ottawa: Can. Nat. Comm. IHD.
- van Everdingen, R.O. (1978) Frost mounds at Bear Rock, near Fort Norman, Northwest Territories, 1975-1976. *Canadian Journal of Earth Sciences*, 15, 263-276.
- van Everdingen, R.O. (1981) Morphology, hydrology and hydrochemistry of karst in permafrost terrain near Great Bear Lake, Northwest Territories. National Hydrological Research Institute Paper No. 11. Calgary: National Hydrology Research Institute.
- van Everdingen, R.O. (1982) Frost blisters of the Bear Rock spring area near Fort Norman, N.W.T. *Arctic*, 35, 243-265.

- van Everdingen, R.O. (1987) The importance of permafrost in the hydrological regime. *In Canadian Aquatic Resources*, Healey and Wallace (eds.), 243-276. Ottawa: Can Bull. Fisheries and Aquatic Sciences.
- van Everdingen, R.O. (1988) Perennial discharge of subpermafrost groundwater in two small drainage basins, Yukon, Canada. *In Proceedings Fifth International Conference on Permafrost*, 639-643.
- van Everdingen, R.O. (1990) Ground-water hydrology. *In Northern Hydrology: Canadian Perspectives*, T.D. Prowse and C.S.L. Ommanney (eds.), 77-101. Saskatoon: Nat Hydrology Research Institute.
- van Everdingen, R.O. and H.R. Krouse (1977) Sulfur-isotope geochemistry of springs in the Franklin Mountains, N.W.T., Canada. *In Proceedings Second International Symposium on Water-Rock Interaction*, H.Pacquet and Y. Tardy (eds.), I, 134-145.
- van Everdingen, R.O., F.A. Michel, H.R. Krouse, and P. Fritz (1979) Hydrochemical and isotope analysis of groundwater flow systems, Franklin Mountains, District of Mackenzie, N.W.T., Canada. *Proceedings, National Hydrogeological Conference, Canadian National Chapter, International Association of Hydrogeologists*, 165-178.
- van Everdingen, R.O., M.A. Shakur and H.R. Krouse (1982a) 34-S and 18-O abundances differentiate Upper Cambrian and Lower Devonian gypsum-bearing units, District of Mackenzie, N.W.T. - an update. *Canadian Journal of Earth Sciences*, 19, 1246-1254.
- van Everdingen, R.O., M.A. Shakur and H.R. Krouse (1982b) Isotope geochemistry of dissolved, precipitated, airborne, and fallout sulfur species associated with springs near Paige Mountain, Norman Range, N.W.T.. *Canadian Journal of Earth Sciences*, 19, 1395-1407.
- Vernon, P. and O.L. Hughes (1966) Surficial geology, Dawson, Larsen Creek, and Nash Creek map-areas, Yukon Territory (116B and 116C E1/2, 116A and 106D). Geological Survey of Canada, Bulletin 136.
- Viles, H.A. (1987) Blue-green algae and terrestrial limestone weathering on Aldabra Atoll: an S.E.M. and light microscopic study. *Earth Surface Processes and Landforms*, 12, 319-330.
- Vincent, J.S. (1978) Limits of ice advance, glacial lakes, and marine transgressions on Banks Island, District of Franklin: a preliminary interpretation. *In Current Research, Part C*, Geological Survey of Canada, Paper 78-1C, 53-62.
- Vincent, J.S. (1982) The Quaternary history of Banks Island, N.W.T., Canada. *Géographie physique et Quaternaire*, 36, 209-232.
- Vincent, J.S. (1983) La géologie du Quaternaire et la géomorphologie de l'île Banks, Arctique canadien. Commission géologique du Canada, Mémoire 405.
- Vincent, J.S. (1984) Quaternary stratigraphy of the western Canadian Arctic Archipelago. *In Quaternary Stratigraphy of Canada - A Canadian Contribution to IGCP Project 24*, R.J. Fulton (ed.), 87-100. Geological Survey of Canada, Paper 84-10.
- Vincent, J.S. (1989) Quaternary geology of the northern Canadian Interior Plains. *In Quaternary Geology of Canada and Greenland, Geology of Canada, No. 1*, R.J. Fulton (ed.), 100-137. Ottawa: Geological Survey of Canada.
- Vincent, J.S. (1990) Late Tertiary and Early Pleistocene deposits and history of Banks Island, southwestern Canadian Arctic Archipelago. *Arctic*, 43(4), 339-363.
- Vincent, J.S. and R.W. Barendregt (1987) Late Cenozoic paleomagnetic record of the Duck Hawk Bluffs, Banks Island, Canadian Arctic Archipelago (abstract). 12th INQUA Congress, National Research Council of Canada, Ottawa, Programme with Abstracts, 282.

- Vincent, J.S., S. Occhietti, N.W. Rutter, G. Lortie, J.P. Guilbault and B. de Boutray (1983) The late-Tertiary-Quaternary stratigraphic record of the Duck Hawk Bluffs, Banks Island, Canadian Arctic Archipelago. *Canadian Journal of Earth Sciences*, 20, 1694-1712.
- Vincent, J.S. and V.K. Prest (1987) The Early Wisconsinan history of the Laurentide Ice Sheet. *Géographie physique et Quaternaire*, 41, 199-213.
- Wahl, H.E., Fraser, D.B., Harvey, R.C. and J.B. Maxwell (1987) *Climate of Yukon*. Climatological Studies Number 40. Atmospheric Environment Service, Environment Canada, Ottawa, Ontario.
- Washburn, A.L. (1979) *Geocryology, A survey of periglacial processes and environments*. New York: Wiley.
- Weertman, J. (1972) General theory of water flow at the base of a glacier or ice sheet. *Review of Geophysics and Space Physics*, 10, 287-333.
- Wheeler, J.O. and P. McFeely (1991) Tectonic assemblage map of the Canadian Cordillera and Adjacent parts of the United States of America. Geological Survey of Canada, Map 1712A.
- White, W.B. (1984) Rate process: chemical kinetics and karst landform development. *In* *Groundwater as a Geomorphic Agent*, R.J. LaFleur (ed.), 227-248. Boston: Allen & Unwin.
- White, W.B. (1988) *Geomorphology and Hydrology of Karst Terrains*. New York: Oxford.
- Wigley, T.M.L. and M.C. Brown (1976) The physics of caves. *In* *The Science of Speleology*, T.D. Ford and C.H.D. Cullingford (eds.), 329-358, London: Academic Press.
- Wilkinson, T.J. and T.B. Bunting (1975) Overland transport of sediment by rill water in a periglacial environment in the Canadian High Arctic. *Geografiska Annaler*, 57A, 105-116.
- Williams G.K. (1975) Arnica platform dolomite (NTS 85, 95, 96, 105, 106). Geological Survey of Canada, Ottawa.
- Williams, J.R. (1965) Ground water in permafrost regions - an annotated bibliography. U.S.G.S. Water Supply Paper No. 1792, U.S. Geological Survey, Washington, D.C.
- Williams, J.R. (1970) Ground water in the permafrost regions of Alaska. United States Geological Survey, Professional Paper 696.
- Williams, J.R. and R.O. van Everdingen (1973) Groundwater investigations in permafrost regions of North America: a review. *Second International Permafrost Conference, North American Contribution*, U.S. National Academy of Sciences, Washington, D.C., 435-446.
- Williams, M.Y. (1922) Exploration east of Mackenzie River between Fort Simpson and Wrigley. *In* *Summary Report 1921, Part B*, 56-66. Ottawa: Geological Survey of Canada.
- Williams, M.Y. (1923) Reconnaissance across northeastern British Columbia and the geology of the northern extension of Franklin Mountains, N.W.T. *In* *Summary Report 1922, Part B*, 65-87. Ottawa: Geological Survey of Canada.
- Williams, P.J. and M.W. Smith (1989) *The Frozen Earth. Fundamentals of Geocryology*. Cambridge: Cambridge University Press.
- Williams, P.W. (1966) Limestone pavements: with special reference to western Ireland. *Trans. Inst. Br. Geog.*, 40, 155-172.
- Williams, P.W. (1983) The role of the subcutaneous zone in karst hydrology. *Journal of Hydrology*, 61, 45-67.

- Williams, P.W. (1985) Subcutaneous hydrology and the development of doline and cockpit karst. *Zeit. fur Geomorph.*, 29, 463-482.
- Wintle, A.G. and J.A. Westgate (1986) Thermoluminescence age of Old Crow tephra in Alaska. *Geology*, 14, 594-597.
- Woo, M.-K. (1976) Hydrology of a small Canadian high Arctic basin during the snowmelt period. *Catena*, 3, 155-168.
- Woo, M.-K. (1986) Permafrost hydrology in North America. *Atmosphere Ocean*, 24, 201-234.
- Woo, M.-K. (1990) Permafrost hydrology. *In Northern Hydrology: Canadian Perspectives*, T.D. Prowse and C.S.L. Ommanney (eds.), 63-76. Saskatoon: National Hydrology Research Institute.
- Woo, M.-K. (1993) Northern hydrology. *In Canada's Cold Environments*, H.M. French and O. Slaymaker (eds). 117-142. McGill Queens University Press.
- Woo, M.-K., R. Heron and P. Steer (1981) Catchment hydrology of a high Arctic lake. *Cold Regions Science and Technology*, 5, 29-41.
- Woo, M.-K. and P. Marsh (1977) Effect of vegetation on limestone solution in a small high arctic basin. *Canadian Journal of Earth Science*, 14, 571-581.
- Woo, M.-K. and P. Steer (1983) Slope hydrology as influenced by thawing of the active layer, Resolute, N.W.T. *Canadian Journal of Earth Science*, 20, 978-986.
- Worthington, S.R.H. (1992) Karst Hydrogeology of the Canadian Rocky Mountains. Unpublished Ph.D. Thesis, McMaster University, Hamilton, Ontario.
- Wright, R. K. (1983) Relationships between runoff generation and active layer development near Schefferville, Quebec. *In Proceedings Fourth International Conference on Permafrost*, 1412-1417. Washington, D.C.: National Academy of Sciences.
- Yorath, C.J. (1991) Upper Jurassic to Paleogene assemblages. *In Geology of the Cordilleran Orogen in Canada*, H. Gabrielse and C.J. Yorath (eds.), 329-371. Geological Survey of Canada, Geology of Canada, No.4.
- Yorath, C.J. and D.G. Cook (1981) Cretaceous and Tertiary stratigraphy and paleogeography, northern Interior Plains, District of Mackenzie. Geological Survey of Canada, Memoir 398.
- Yorath, C.J. and D.G. Cook (1984) Mesozoic and Cenozoic depositional history of the northern Interior Plains of Canada. *In The Mesozoic of Middle North America*, D.F. Scott and D.J. Glass (eds.), 69-83. Canadian Society of Petroleum Geologists, Memoir 9.
- Young, G.M., C.W. Jefferson, G.D. Delaney and G.M. Yeo (1979) Middle and Late Proterozoic evolution of the northern Canadian Cordillera and Shield. *Geology*, 7, 125-128.
- Zhang, J., F. Wang, and L. Shengfeng (1993) On wind-oriented solutional microkarren on limestone surfaces in alpine and semi-desert regions in Tibet and Xingjiang, China. Abstract *In Third International Geomorphology Conference*, Programme with Abstracts, Hamilton, Canada.
- Zoltai, S.C. and C. Tarnocai (1975) Perennially frozen peatlands in the western Arctic and subarctic of Canada. *Canadian Journal of Earth Sciences*, 12, 28-43.

APPENDIX

Table A.1: Raw physical and hydrochemical data from the Dodo Canyon Site.

Table A.2: Raw physical and hydrochemical data from the Bonus Lake Site.

Table A.3: Raw physical and hydrochemical data from the Bear Rock Site.

Table A.1: Raw physical and hydrochemical data from the Dodo Canyon Site.

Field	Date	Map	Temp	SPC	pH	$\delta^{18}\text{O}$	Ca^{2+}	Mg^{2+}	HCO_3^-	SO_4^{2-}	Na^+	Cl^-	TDI	Ca/Mg	SIC	SID	pPCO ₂	Error
D87-1	230687	D1	9.7	9200	7.61	-99.00	4.70	3.18	-9.00	-9.00	-9.00	-9.00	-9.00	1.5	-9.00	-9.00	-9.00	-99.0
D87-2	230687	D2	9.6	10650	7.50	-99.00	6.05	4.06	-9.00	-9.00	-9.00	-9.00	-9.00	1.5	-9.00	-9.00	-9.00	-99.0
D87-3	250687	D3	10.8	1150	8.42	-21.31	3.92	2.10	-9.00	-9.00	-9.00	-9.00	-9.00	1.9	-9.00	-9.00	-9.00	-99.0
D87-4	250687	D4	1.3	401	8.38	-22.31	3.16	1.04	-9.00	-9.00	-9.00	-9.00	-9.00	3.0	-9.00	-9.00	-9.00	-99.0
D87-5	250687	D5	12.6	1040	8.34	-21.55	4.60	1.70	-9.00	-9.00	-9.00	-9.00	-9.00	2.7	-9.00	-9.00	-9.00	-99.0
D88-1	180588	D6	6.0	57	-9.00	-22.89	0.68	0.17	0.82	0.00	0.05	0.03	1.75	4.0	-9.00	-9.00	-9.00	3.3
D88-2	180588	D7	2.0	66	-9.00	-21.81	0.86	0.18	1.10	0.00	0.08	0.01	2.22	4.8	-9.00	-9.00	-9.00	0.2
D88-3	180588	D8	0.9	117	-9.00	-20.73	1.43	0.17	1.68	0.00	0.05	0.02	3.36	8.4	-9.00	-9.00	-9.00	-1.5
D88-4	180588	D9	3.0	157	-9.00	-21.03	1.43	0.31	1.79	0.00	0.07	0.02	3.63	4.6	-9.00	-9.00	-9.00	0.1
D88-5	190588	D3	2.9	450	-9.00	-19.66	1.83	0.61	2.23	0.67	0.93	0.82	7.09	3.0	-9.00	-9.00	-9.00	-4.9
D88-6	190588	D10	-9.0	-9	-9.00	-20.47	1.22	0.27	1.56	0.00	0.10	0.01	3.15	4.5	-9.00	-9.00	-9.00	0.4
D88-7	190588	D4	-9.0	-9	-9.00	-20.16	-9.00	-9.00	-9.00	-9.00	-9.00	-9.00	-9.00	-9.0	-9.00	-9.00	-9.00	-99.0
D88-9	210588	D12	3.9	685	8.34	-99.00	2.52	1.32	2.46	-9.00	-9.00	-9.00	-9.00	1.9	-9.00	-9.00	-9.00	-99.0
D88-10	220588	D12	6.1	650	8.38	-99.00	2.60	1.24	2.62	-9.00	-9.00	-9.00	-9.00	2.1	-9.00	-9.00	-9.00	-99.0
D88-11	230588	D43	3.0	448	7.87	-99.00	3.20	1.12	3.40	1.39	2.70	2.37	14.17	2.9	0.18	-0.19	2.73	-1.0
D88-12	230588	D3	5.7	345	7.78	-99.00	2.42	0.94	2.56	-9.00	-9.00	-9.00	-9.00	2.6	-9.00	-9.00	-9.00	-99.0
D88-13	240588	D3	3.0	260	7.88	-99.00	1.96	0.82	2.20	-9.00	-9.00	-9.00	-9.00	2.4	-9.00	-9.00	-9.00	-99.0
D88-14	240588	D43	1.5	383	7.75	-20.05	2.68	0.88	2.82	0.79	1.39	1.34	9.90	3.0	-0.08	-0.75	2.70	0.0
D88-15	240588	D12	1.2	299	8.29	-99.00	1.76	0.76	1.82	-9.00	-9.00	-9.00	-9.00	2.3	-9.00	-9.00	-9.00	-99.0
D88-16	250588	D43	2.7	384	7.85	-99.00	2.42	0.78	2.78	0.71	1.25	1.23	9.16	3.1	-0.01	-0.61	2.80	-2.9
D88-17	250588	D3	8.7	291	7.84	-20.99	1.92	0.72	2.20	0.77	1.26	1.00	7.87	2.7	-0.07	-0.60	2.77	-0.9
D88-18	260588	D13	3.2	122	7.91	-20.87	1.26	0.14	1.36	0.00	0.04	0.01	2.81	9.0	-0.40	-2.00	3.10	2.7
D88-19	260588	D14	0.6	224	8.20	-20.45	2.60	0.24	2.30	0.71	0.04	0.01	5.90	10.8	0.28	-0.59	3.25	-2.3
D88-20	260588	D9	8.2	161	8.23	-21.50	1.42	0.18	1.36	0.04	0.02	0.01	3.03	7.9	-0.02	-0.97	3.41	7.0
D88-21	270588	D2	9.7	10620	7.61	-99.00	6.47	3.52	3.10	7.70	-9.00	-9.00	-9.00	1.8	-0.16	-0.54	2.58	-99.0
D88-22	270588	D15	6.7	205	8.21	-20.48	1.48	0.20	1.42	0.00	0.02	0.01	3.13	7.4	-0.05	-1.06	3.40	8.5
D88-23	270588	D1	8.2	7920	7.86	-21.38	5.30	3.36	2.90	6.25	85.25	82.35	185.40	1.6	0.06	-0.06	2.83	1.3
D88-24	270588	D16	-9.0	-9	-9.00	-99.00	1.34	0.52	1.36	-9.00	-9.00	-9.00	-9.00	2.6	-9.00	-9.00	-9.00	-99.0
D88-25	300588	D17	4.6	210	8.23	-20.97	1.92	0.42	1.76	0.27	0.27	0.23	4.88	4.6	0.13	-0.48	3.36	7.2
D88-26	300588	D18	2.7	108	7.97	-21.49	1.16	0.16	1.36	0.00	0.00	0.01	2.69	7.3	-0.43	-1.81	3.20	-1.8
D88-27	300588	D19	14.7	118	8.46	-19.73	1.14	0.04	1.12	0.00	0.04	0.02	2.36	28.5	0.09	-1.22	3.70	3.4

Field	Date	Map	Temp	SPC	pH	$\delta^{18}\text{O}$	Ca^{2+}	Mg^{2+}	HCO_3^-	SO_4^{2-}	Na^+	Cl^-	TDI	Ca/Mg	SIC	SID	pPCO_2	Error
D88-28	310588	D3	10.7	503	-9.00	-20.30	2.58	1.06	2.75	0.98	1.86	1.85	11.07	2.4	-9.00	-9.00	-9.00	-0.7
D88-29	310588	D43	5.7	417	-9.00	-20.36	2.24	1.03	2.76	0.87	1.58	1.34	9.82	2.2	-9.00	-9.00	-9.00	-1.2
D88-50	260688	D3	13.5	1000	7.96	-22.14	3.88	1.96	3.64	2.39	5.13	5.23	22.23	2.0	0.43	0.60	2.74	-1.3
D88-51	260688	D43	9.5	670	7.82	-21.85	3.44	1.36	3.52	1.50	2.47	2.41	14.69	2.5	0.22	0.02	2.64	-1.1
D88-52	260688	D5	10.5	1101	8.00	-21.87	4.08	1.96	3.30	2.71	5.81	6.01	23.85	2.1	0.38	0.43	2.88	-0.7
D88-53	280688	D20	17.6	122	8.31	-17.57	1.24	0.22	1.38	0.00	0.06	0.04	2.93	5.6	0.10	-0.48	3.43	3.5
D88-54	280688	D21	17.7	138	8.57	-19.83	1.28	0.20	1.56	0.00	0.01	0.02	3.06	6.4	0.38	0.04	3.67	-2.9
D88-55	280688	D22	16.5	159	8.07	-15.86	1.44	0.14	1.56	0.00	0.05	0.03	3.22	10.3	-0.06	-1.06	3.16	1.3
D88-56	280688	D23	4.8	293	8.12	-21.29	3.04	0.64	3.42	0.21	0.03	0.02	7.36	4.8	0.48	0.21	2.96	0.9
D88-58	300688	D5	4.9	915	7.76	-21.90	3.72	1.88	2.98	2.37	4.96	5.09	20.99	2.0	-0.03	-0.42	2.76	0.5
D88-59	300688	D43	5.7	849	7.87	-21.83	3.38	1.50	2.92	1.75	3.20	3.22	15.95	2.3	0.06	-0.29	2.87	1.2
D88-60	300688	D3	8.1	1021	7.81	-21.44	3.58	1.58	2.92	2.10	4.65	4.71	19.54	2.3	0.08	-0.22	2.75	0.4
D88-61	010788	D3	6.2	856	7.71	-20.72	3.20	0.90	2.58	1.42	2.76	2.76	13.62	3.6	-0.11	-0.81	2.71	0.7
D88-62	010788	D43	3.7	730	7.95	-21.58	3.14	1.06	2.72	1.44	2.39	2.30	13.05	3.0	0.12	-0.31	2.95	1.0
D88-63	010788	D5	4.7	1115	7.77	-21.71	3.20	1.12	2.84	1.89	4.35	4.26	17.66	2.9	-0.05	-0.61	2.75	-1.8
D88-64	030788	D13	1.6	232	8.08	-20.61	2.14	0.48	2.50	0.00	0.03	0.01	5.15	4.5	0.11	-0.53	3.11	2.8
D88-65	030788	D14	4.2	348	8.29	-22.26	3.04	0.58	2.96	0.81	0.03	0.01	7.42	5.2	0.54	0.28	3.23	-1.7
D88-66	030788	D17	4.7	353	8.04	-21.59	3.20	0.60	3.10	0.80	0.02	0.01	7.72	5.3	0.35	-0.10	2.94	-1.1
D88-67	030788	D3	10.2	884	8.04	-21.67	3.38	1.38	3.28	1.64	3.48	3.47	16.63	2.4	0.41	0.43	2.87	-0.9
D88-68	030788	D43	8.5	444	8.04	-21.91	3.36	1.38	3.08	1.62	3.04	2.98	15.46	2.4	0.35	0.29	2.93	0.7
D88-69	030788	D5	11.6	1018	8.05	-21.96	3.54	1.94	3.22	2.37	4.78	4.85	20.70	1.8	0.41	0.57	2.90	-0.9
D88-70	050788	D24	1.9	237	8.01	-19.10	2.32	0.72	2.80	0.31	0.02	0.01	6.17	3.2	0.13	-0.34	2.97	-0.9
D88-71	050788	D12	7.0	628	8.12	-20.78	2.68	1.36	2.96	1.79	3.18	2.55	14.51	2.0	0.31	0.28	3.03	-0.6
D88-72	060788	D5	5.7	974	7.82	-22.49	3.54	2.06	3.38	2.44	5.63	5.27	22.31	1.7	0.14	0.00	2.68	0.6
D88-73	060788	D43	6.1	705	7.95	-21.86	3.20	1.52	3.32	1.75	3.00	2.98	15.76	2.1	0.26	0.14	2.81	-2.1
D88-74	060788	D16	8.2	1408	7.83	-21.71	1.70	0.96	2.64	2.08	20.12	16.72	44.22	1.8	-0.31	-0.89	2.81	3.0
D88-75	060788	D1	12.2	5775	7.80	-22.25	3.66	2.10	3.56	1.79	49.80	48.23	109.13	1.7	0.07	-0.06	2.64	1.8
D88-76	060788	D2	9.5	10392	7.41	-22.59	6.51	3.50	3.56	6.56	94.82	95.47	210.41	1.9	-0.22	-0.68	2.30	-0.4
D88-77	060788	D3	13.2	881	8.02	-21.82	3.20	1.68	3.34	2.06	3.65	3.69	17.62	1.9	0.40	0.55	2.82	-3.2
D88-78	100788	D25	16.2	113	8.72	-15.95	1.24	0.16	1.44	0.00	0.02	0.01	2.86	7.8	0.48	0.14	3.85	-0.8
D88-79	100788	D26	5.6	288	8.24	-21.99	2.98	0.64	3.20	0.57	0.00	0.01	7.39	4.7	0.55	0.37	3.11	-2.1
D88-80	100788	D27	17.7	102	8.61	-16.69	1.50	0.16	1.64	0.00	0.03	0.01	3.34	9.4	0.53	0.16	3.67	1.5
D88-81	100788	D3	12.9	947	8.00	-21.81	3.58	1.76	3.40	2.25	4.50	4.51	19.99	2.0	0.42	0.57	2.80	-1.6

Field	Date	Map	Temp	SPC	pH	$\delta^{18}\text{O}$	Ca^{2+}	Mg^{2+}	HCO_3^-	SO_4^{2-}	Na^+	Cl^-	TDI	Ca/Mg	SIC	SID	pPCO_2	Error
D88-82	100788	D43	8.7	679	8.06	-21.83	3.30	1.46	3.36	1.46	2.96	2.89	15.42	2.3	0.43	0.47	2.89	0.1
D88-83	100788	D5	9.4	988	8.12	-21.88	3.72	1.88	3.66	2.39	5.24	5.23	22.12	2.0	0.54	0.77	2.92	-2.0
D88-84	130788	D28	19.5	235	8.61	-17.81	1.48	1.14	2.84	0.00	0.04	0.04	5.53	1.3	0.74	1.46	3.44	-3.9
D88-85	130788	D29	3.5	198	8.63	-21.02	1.48	1.16	2.70	0.00	0.03	0.02	5.39	1.3	0.56	0.92	3.60	-0.8
D88-86	130788	D30	7.7	270	8.50	-20.77	1.84	1.38	2.92	0.04	0.03	0.01	6.22	1.3	0.60	1.02	3.40	4.3
D88-87	130788	D31	17.2	266	8.56	-21.85	2.02	0.98	2.92	0.21	0.05	0.03	6.20	2.1	0.79	1.34	3.40	-1.8
D88-88	130788	D32	8.2	305	8.34	-21.88	1.78	1.40	3.12	0.30	0.53	0.46	7.58	1.3	0.45	0.77	3.20	-2.3
D88-89	150788	D3	10.6	1008	7.97	-21.71	3.16	2.08	3.26	2.04	4.22	4.20	18.95	1.5	0.30	0.43	2.80	-0.2
D88-90	150788	D43	5.7	849	7.86	-21.86	3.12	1.68	3.52	1.75	2.94	2.90	15.90	1.9	0.19	0.05	2.69	-2.8
D88-91	150788	D4	1.5	516	7.52	-22.03	2.88	1.28	3.20	1.15	0.94	0.75	10.18	2.3	-0.23	-0.92	2.42	0.0
D88-92	150788	D5	8.2	1194	7.61	-21.90	3.32	2.12	3.40	2.33	5.31	5.27	21.74	1.6	-0.05	-0.31	2.43	-1.2
D88-93	150788	D33	6.4	1226	7.20	-21.95	3.36	2.20	3.32	2.25	5.52	5.53	22.17	1.5	-0.48	-1.18	2.04	-0.1
D88-94	150788	D34	17.9	905	7.88	-20.56	3.00	1.72	3.12	1.96	4.05	3.78	17.61	1.7	0.27	0.38	2.67	-0.5
D88-99	140888	D3	-9.0	-9	-9.00	-21.90	3.02	1.57	2.50	2.31	4.28	3.95	17.63	1.9	-9.00	-9.00	-9.00	0.6
D91-1	140891	D33	3.7	584	8.05	-22.23	2.90	1.58	3.20	1.73	3.04	2.95	15.39	1.8	0.28	0.22	2.94	-2.4
D91-2	140891	D43	8.8	545	8.02	-21.83	3.60	1.40	3.44	1.66	1.58	1.91	13.58	2.6	0.44	0.45	2.84	-3.2
D91-3	140891	D3	14.5	828	8.17	-21.82	3.52	1.78	3.28	1.94	2.91	3.17	16.59	2.0	0.60	0.95	2.97	-1.1
D91-4	150891	D2	9.7	10001	7.75	-22.23	5.93	3.14	3.20	4.86	89.78	90.25	197.16	1.9	0.06	-0.12	2.67	0.3
D91-5	150891	D35	12.9	6840	8.11	-22.08	4.80	2.50	3.20	3.91	67.14	65.43	146.97	1.9	0.41	0.59	3.00	1.3
D91-6	150891	D36	5.9	765	7.69	-22.31	10.29	2.80	6.59	6.84	0.14	0.03	26.69	3.7	0.74	0.87	2.26	-0.9
D91-7	150891	D37	16.6	6002	8.30	-21.97	4.16	2.04	3.24	3.39	63.62	52.03	128.48	2.0	0.59	0.97	3.16	8.7
D91-8	160891	D14	6.7	379	8.37	-21.37	3.88	0.78	3.24	1.32	0.07	0.03	9.31	5.0	0.78	0.82	3.24	1.6
D91-9	160891	D38	9.7	373	8.41	-21.69	3.48	0.72	2.90	1.12	0.07	0.03	8.31	4.8	0.77	0.84	3.30	2.7
D91-10	170891	D5	6.9	861	8.39	-22.09	3.56	1.84	3.28	2.02	3.72	3.71	18.12	1.9	0.72	1.11	3.26	0.6
D91-11	170891	D39	9.9	741	8.08	-21.98	3.62	1.50	3.24	1.71	2.36	2.47	14.89	2.4	0.48	0.57	2.92	0.4
D91-12	170891	D4	1.9	421	7.83	-21.69	3.66	1.10	3.28	1.38	0.38	0.37	10.16	3.3	0.19	-0.25	2.72	1.1
D91-13	170891	D42	8.9	7629	7.83	-22.14	4.92	2.38	3.26	3.75	67.57	68.25	150.12	2.1	0.11	-0.08	2.73	-0.3
D91-14	200891	D33	3.8	743	7.97	-21.84	3.36	1.64	3.32	1.97	3.65	3.51	17.45	2.0	0.27	0.16	2.85	-0.9
D91-15	200891	D5	5.8	860	8.20	-99.00	-9.00	-9.00	3.36	-9.00	-9.00	-9.00	-9.00	-9.00	-9.00	-9.00	-9.00	-99.0
D91-16	200891	D4	1.8	422	7.79	-21.74	3.66	1.14	3.32	1.38	0.40	0.43	10.32	3.2	0.15	-0.31	2.67	0.7
D91-17	200891	D3	10.0	849	8.33	-21.80	3.58	1.72	3.32	1.92	3.16	3.19	16.88	2.1	0.71	1.10	3.17	0.2
D91-18	200891	D38	5.9	359	8.36	-99.00	3.50	0.86	2.96	-9.00	-9.00	-9.00	-9.00	4.1	-9.00	-9.00	-9.00	-99.0
D91-19	250891	D33	3.3	688	8.09	-21.84	3.28	1.58	3.28	1.92	3.52	3.45	17.02	2.1	0.37	0.34	2.98	-1.6

Field	Date	Map	Temp	SPC	pH	$\delta^{18}\text{O}$	Ca^{2+}	Mg^{2+}	HCO_3^-	SO_4^{2-}	Na^+	Cl^-	TDI	Ca/Mg	SIC	SID	$p\text{PCO}_2$	Error
D91-20	250891	D5	3.9	779	8.26	-21.96	3.46	1.80	3.28	1.98	3.45	3.51	17.47	1.9	0.56	0.75	3.15	-0.4
D91-21	250891	D43	2.9	526	8.03	-21.72	3.64	1.28	3.20	1.56	1.19	1.38	12.24	2.8	0.36	0.19	2.92	-0.2
D91-22	250891	D3	5.0	775	8.45	-21.69	3.56	1.60	3.22	1.89	3.17	3.09	16.53	2.2	0.73	1.04	3.35	0.8
D91-23	270891	D36	1.9	924	7.71	-22.21	10.09	2.46	6.57	5.88	0.14	0.03	25.17	4.1	0.69	0.67	2.31	0.8
D91-24	270891	D37	9.8	7593	8.07	-99.00	-9.00	-9.00	3.04	-9.00	-9.00	-9.00	-9.00	-9.0	-9.00	-9.00	-9.00	-99.0
D91-25	270891	D2	9.4	9772	7.70	-22.62	6.07	3.00	2.92	5.00	91.75	92.22	200.96	2.0	-0.02	-0.33	2.66	0.3
D91-26	280891	D25	6.5	108	8.47	-17.26	1.60	0.10	1.50	0.08	0.05	0.03	3.35	16.0	0.25	-0.75	3.66	4.4
D91-27	280891	D40	2.3	355	7.78	-21.30	3.84	0.70	3.28	1.13	0.06	0.03	9.03	5.5	0.17	-0.49	2.66	1.8
D91-28	280891	D14	1.6	369	8.38	-21.83	3.90	0.90	3.06	1.38	0.06	0.03	9.32	4.3	0.72	0.69	3.31	4.2
D91-29	280891	D41	0.5	320	8.02	-99.00	3.52	0.84	3.40	0.75	0.06	0.03	8.59	4.2	0.38	0.01	2.90	2.8
D91-30	280891	D38	3.5	356	8.46	-99.00	3.62	0.72	3.06	1.24	0.07	0.03	8.73	5.0	0.79	0.79	3.38	1.0
D91-31	290891	D33	3.1	758	8.11	-21.64	3.20	1.70	3.24	1.92	3.59	3.37	17.01	1.9	0.37	0.38	3.00	-0.3
D91-32	290891	D5	3.9	764	8.32	-21.98	3.40	1.80	3.26	2.00	3.59	3.55	17.59	1.9	0.60	0.85	3.21	-0.2
D91-33	290891	D43	3.5	556	9.01	-21.88	3.58	1.38	3.36	1.64	1.62	1.73	13.31	2.6	1.27	2.02	3.95	-1.1
D91-34	290891	D3	5.4	748	9.10	-21.78	3.48	1.62	3.18	1.94	3.12	3.12	16.45	2.1	1.30	2.18	4.08	-0.1

Missing Data: -9, -9.0, -9.00 and -99.0

Map: Locations indexed on Figures 7.2 and 7.9

Temp: Temperature in °C

SPC: Specific electrical conductivity in $\mu\text{S cm}^{-1}$

Ion concentrations in meq L^{-1}

SIC: Saturation index for calcite

SID: Saturation index for dolomite

$p\text{PCO}_2$: -log of the partial pressure of CO_2

Table A.2: Raw physical and hydrochemical data from the Bonus Lake Site.

Field ID	Date	Map	Temp	SPC	pH	$\delta^{18}\text{O}$	Ca^{2+}	Mg^{2+}	HCO_3^-	SO_4^{2-}	Na^+	Cl^-	TDI	Ca/Mg	SIC	SID	$p\text{PCO}_2$	Error
BL88-1	150688	B1	5.5	220	7.16	-22.55	2.54	0.54	2.94	0.23	0.08	0.04	6.37	4.7	-0.59	-1.92	2.05	-0.8
BL88-2	150688	B2	11.2	205	7.55	-21.09	2.04	0.44	1.98	0.63	0.01	0.01	5.11	4.6	-0.40	-1.46	2.56	-2.7
BL88-3	150688	B3	18.7	158	8.50	-21.93	2.04	0.04	2.02	0.00	0.08	0.08	4.26	51.0	0.65	-0.32	3.46	1.5
BL88-4	150688	B4	17.2	160	7.99	-21.57	1.80	0.04	1.94	0.00	0.00	0.01	3.79	45.0	0.08	-1.42	2.96	-2.8
BL88-5	150688	B5	4.2	173	8.02	-22.16	1.98	0.06	2.02	0.00	0.00	0.01	4.07	33.0	0.01	-1.58	3.08	0.4
BL88-6	150688	B6	24.7	171	8.60	-20.81	1.86	0.06	2.02	0.00	0.03	0.02	3.99	31.0	0.77	0.22	3.52	-2.4
BL88-7	180688	B7	2.7	162	8.36	-21.14	2.12	0.08	2.20	0.00	0.01	0.00	4.41	26.5	0.38	-0.75	3.40	0.2
BL88-8	180688	B8	5.7	164	8.05	-20.91	2.00	0.08	2.02	0.00	0.03	0.02	4.15	25.0	0.06	-1.34	3.10	1.8
BL88-9	180688	B9	2.2	105	7.96	-21.22	1.40	0.16	1.42	0.00	0.01	0.00	2.99	8.8	-0.36	-1.76	3.19	5.0
BL88-10	180688	B10	0.7	29	7.94	-21.15	0.40	0.14	0.34	0.00	0.01	0.00	0.89	2.9	-1.52	-3.60	3.79	23.5
BL88-11	180688	B11	4.5	84	7.91	-21.18	1.10	0.06	0.86	0.00	0.00	0.00	2.02	18.3	-0.69	-2.71	3.33	14.9
BL88-12	180688	B12	5.2	147	7.92	-21.73	1.82	0.06	1.74	0.02	0.01	0.00	3.65	30.3	-0.17	-1.90	3.04	3.6
BL88-13	210688	B13	8.2	214	7.97	-21.67	1.88	0.52	1.96	0.44	0.30	0.26	5.36	3.6	-0.06	-0.70	3.02	0.8
BL88-14	210688	B14	16.5	249	8.19	-21.37	1.72	0.52	1.96	0.27	0.28	0.20	4.95	3.3	0.22	0.00	3.17	1.8
BL88-15	210688	B15	2.7	206	8.00	-21.96	1.58	0.72	2.06	0.25	0.43	0.33	5.37	2.2	-0.14	-0.71	3.07	1.8
BL88-16	210688	B16	1.9	202	8.07	-22.05	1.56	0.68	2.08	0.23	0.36	0.31	5.22	2.3	-0.08	-0.62	3.14	-0.4
BL88-17	210688	B17	8.7	230	7.92	-21.53	1.89	0.45	2.14	0.39	0.27	0.25	5.39	4.2	-0.06	-0.76	2.92	-3.2
BL88-18	210688	B18	6.7	245	7.96	-21.68	1.98	0.52	2.26	0.45	0.28	0.23	5.72	3.8	0.00	-0.64	2.96	-2.8
BL88-19	230688	B1	6.7	262	7.68	-22.26	2.92	0.30	2.98	0.34	0.02	0.04	6.60	9.7	0.00	-1.04	2.56	-1.9
BL88-20	230688	B19	17.2	241	8.39	-20.95	1.84	0.42	1.90	0.45	0.35	0.22	5.18	4.4	0.43	0.30	3.39	0.8
BL88-21	230688	B20	18.7	237	8.33	-9.00	1.84	0.40	1.82	0.56	0.33	0.22	5.17	4.6	0.37	0.18	3.33	-0.8
BL88-22	230688	B21	19.9	237	8.42	-21.13	1.84	0.40	1.82	0.37	0.22	0.19	4.84	4.6	0.48	0.40	3.42	1.8
BL88-23	240688	B22	0.0	164	7.99	-20.88	2.18	0.04	1.92	0.41	0.00	0.00	4.55	54.5	-0.06	-1.98	3.11	-2.4
BL88-24	240688	B23	7.2	95	8.02	-20.24	0.94	0.22	0.92	0.25	0.00	0.00	2.33	4.3	-0.60	-1.87	3.39	-0.5
BL88-25	240688	B24	0.7	146	8.24	-20.75	1.80	0.06	1.72	0.00	0.01	0.00	3.59	30.0	0.08	-1.43	3.40	4.3
BL91-1	020891	B25	4.9	110	8.34	-20.64	0.94	0.41	1.15	-9.00	-9.00	-9.00	-9.00	2.3	-9.00	-9.00	-9.00	-9.0

Field ID	Date	Map	Temp	SPC	pH	$\delta^{18}\text{O}$	Ca^{2+}	Mg^{2+}	HCO_3^-	SO_4^{2-}	Na^+	Cl^-	TDI	Ca/Mg	SIC	SID	$p\text{PCO}_2$	Error
BL91-2	020891	B2	10.2	207	8.33	-20.49	1.85	0.57	1.54	0.73	0.05	0.06	4.80	3.2	0.20	-0.11	3.47	3.3
BL91-3	030891	B17	6.2	208	8.05	-20.93	1.87	0.53	1.80	-9.00	-9.00	-9.00	-9.00	3.5	-9.00	-9.00	-9.00	-9.0
BL91-4	030891	B15	2.6	160	8.10	-9.00	1.68	0.80	2.01	-9.00	-9.00	-9.00	-9.00	2.1	-9.00	-9.00	-9.00	-9.0
BL91-5	030891	B26	10.8	247	8.08	-20.69	2.21	0.57	2.44	0.26	0.08	0.08	5.64	3.9	0.25	-0.10	3.01	1.7
BL91-6	030891	B27	11.2	236	8.43	-20.48	1.82	0.92	2.23	0.37	0.05	0.04	5.43	2.0	0.46	0.62	3.41	2.6
BL91-7	040891	B11	5.6	306	7.63	-20.33	1.82	0.26	1.66	0.22	0.05	0.04	4.05	7.0	-0.49	-1.88	2.76	5.3
BL91-8	070891	B22	0.6	168	8.36	-9.00	2.21	0.11	1.99	-9.00	-9.00	-9.00	-9.00	20.1	-9.00	-9.00	-9.00	-9.0
BL91-9	070891	B28	2.6	157	7.99	-9.00	1.68	0.20	1.62	-9.00	-9.00	-9.00	-9.00	8.4	-9.00	-9.00	-9.00	-9.0
BL91-10	070891	B11	4.9	168	7.61	-9.00	1.70	0.19	1.66	-9.00	-9.00	-9.00	-9.00	8.9	-9.00	-9.00	-9.00	-9.0
BL91-11	070891	B9	2.6	109	7.85	-9.00	0.82	0.30	1.03	0.03	0.04	0.06	2.28	2.7	-0.83	-2.19	3.21	2.2
BL91-12	090891	B17	7.6	216	7.74	-9.00	1.98	0.53	2.11	-9.00	-9.00	-9.00	-9.00	3.7	-9.00	-9.00	-9.00	-9.0
BL91-13	090891	B18	7.7	234	7.77	-9.00	2.02	0.54	2.17	-9.00	-9.00	-9.00	-9.00	3.7	-9.00	-9.00	-9.00	-9.0
BL91-14	090891	B29	6.8	257	8.10	-9.00	2.49	0.64	3.05	-9.00	-9.00	-9.00	-9.00	3.9	-9.00	-9.00	-9.00	-9.0
BL91-15	090891	B30	1.6	324	8.09	-21.17	3.37	0.78	2.89	-9.00	-9.00	-9.00	-9.00	4.3	-9.00	-9.00	-9.00	-9.0
BL91-16	090891	B26	10.9	256	8.11	-9.00	2.08	0.65	2.44	-9.00	-9.00	-9.00	-9.00	3.2	-9.00	-9.00	-9.00	-9.0
BL91-17	090891	B31	6.9	232	8.01	-9.00	1.78	0.70	2.27	-9.00	-9.00	-9.00	-9.00	2.5	-9.00	-9.00	-9.00	-9.0

Missing Data: -9.00 and -99.00

Map: Locations indexed on Figures 8.2 and 8.4

Temp: Temperature in °C

SPC: Specific electrical conductivity in $\mu\text{S cm}^{-1}$

Ion concentrations in meq L^{-1}

SIC: Saturation index for calcite

SID: Saturation index for dolomite

$p\text{PCO}_2$: -log of the partial pressure of CO_2

Error: Ion balance error in percent (samples BL88-10 and BL88-11 were excluded from analyses)

Table A.3: Raw physical and hydrochemical data from the Bear Rock Site.

Field ID	Date	Map	Temp	SPC	pH	$\delta^{18}\text{O}$	Ca^{2+}	Mg^{2+}	HCO_3^-	SO_4^{2-}	Na^+	Cl^-	TDI	Ca/Mg	SIC	SID	ρPCO_2	Error
BR87-1	100787	R1	4.2	1223	8.19	-99.00	-9.00	-9.00	5.10	-9.00	-9.00	-9.00	-9.00	-9.0	-9.00	-9.00	-9.00	-99.0
BR87-2	100787	R2	6.6	1470	7.96	-99.00	-9.00	-9.00	5.02	-9.00	-9.00	-9.00	-9.00	-9.0	-9.00	-9.00	-9.00	-99.0
BR87-3	100787	R3	3.7	1575	7.89	-99.00	-9.00	-9.00	5.49	-9.00	-9.00	-9.00	-9.00	-9.0	-9.00	-9.00	-9.00	-99.0
BR87-4	100787	R4	13.3	1015	8.38	-99.00	8.77	3.28	3.22	-9.00	-9.00	-9.00	15.27	2.7	-9.00	-9.00	-9.00	-99.0
BR87-5	120787	R5	4.4	468	8.26	-22.39	3.60	2.32	4.46	-9.00	-9.00	-9.00	10.37	1.6	-9.00	-9.00	-9.00	-99.0
BR87-6	160787	R1	4.7	1285	8.20	-22.05	14.63	3.40	5.14	-9.00	-9.00	-9.00	23.16	4.3	-9.00	-9.00	-9.00	-99.0
BR87-7	160787	R2	8.6	1560	8.18	-22.69	19.74	2.04	4.94	-9.00	-9.00	-9.00	26.72	9.7	-9.00	-9.00	-9.00	-99.0
BR87-8	160787	R3	6.9	1668	8.00	-99.00	14.23	2.68	5.51	-9.00	-9.00	-9.00	22.42	5.3	-9.00	-9.00	-9.00	-99.0
BR87-9	160787	R4	14.3	853	8.34	-99.00	10.43	2.22	3.42	-9.00	-9.00	-9.00	16.07	4.7	-9.00	-9.00	-9.00	-99.0
BR87-10	220787	R6	13.5	184	8.67	-18.78	1.66	0.46	1.98	-9.00	-9.00	-9.00	4.10	3.6	0.64	0.75	3.69	3.4
BR87-11	220787	R7	13.6	184	8.65	-19.53	1.64	0.52	1.98	-9.00	-9.00	-9.00	4.14	3.2	0.62	0.77	3.67	4.3
BR87-12	250787	R6	17.4	168	8.64	-99.00	1.64	0.44	2.02	-9.00	-9.00	-9.00	4.10	3.7	0.66	0.83	3.62	1.5
BR87-13	250787	R7	16.7	180	8.68	-99.00	1.58	0.54	2.04	-9.00	-9.00	-9.00	4.16	2.9	0.68	0.95	3.67	1.9
BR87-14	270787	R3	3.3	1728	8.12	-22.85	16.56	1.32	5.59	-9.00	-9.00	-9.00	23.48	12.6	-9.00	-9.00	-9.00	-99.0
BR87-15	270787	R4	12.7	900	8.46	-19.85	9.71	2.14	3.78	-9.00	-9.00	-9.00	15.63	4.5	-9.00	-9.00	-9.00	-99.0
BR87-16	270787	R8	13.5	716	8.36	-18.65	5.69	2.56	2.86	-9.00	-9.00	-9.00	11.11	2.2	-9.00	-9.00	-9.00	-99.0
BR87-17	300787	R9	7.7	559	8.34	-23.32	4.28	3.40	4.80	-9.00	-9.00	-9.00	12.47	1.3	-9.00	-9.00	-9.00	-99.0
BR87-18	300787	R10	4.2	667	8.34	-23.48	4.00	3.38	4.62	-9.00	-9.00	-9.00	11.99	1.2	-9.00	-9.00	-9.00	-99.0
BR88-1	030688	R11	2.8	1407	7.93	-99.00	22.62	2.64	4.08	-9.00	-9.00	-9.00	29.33	8.6	-9.00	-9.00	-9.00	-99.0
BR88-2	030688	R3	0.9	1339	7.56	-22.09	17.78	2.68	5.36	-9.00	-9.00	-9.00	25.82	6.6	-9.00	-9.00	-9.00	-99.0
BR88-3	040688	R3	0.7	1283	7.43	-99.00	-9.00	-9.00	5.48	-9.00	-9.00	-9.00	-9.00	-9.0	-9.00	-9.00	-9.00	-99.0
BR88-4	040688	R11	2.8	1595	7.58	-99.00	-9.00	-9.00	4.14	-9.00	-9.00	-9.00	-9.00	-9.0	-9.00	-9.00	-9.00	-99.0
BR88-5	050688	R12	1.7	1413	7.22	-21.97	13.23	1.84	4.76	-9.00	-9.00	-9.00	19.82	7.2	-9.00	-9.00	-9.00	-99.0
BR88-6	050688	R2	3.7	1403	7.63	-22.56	18.54	1.80	4.76	-9.00	-9.00	-9.00	25.10	10.3	-9.00	-9.00	-9.00	-99.0
BR88-7	050688	R13	3.4	1006	7.79	-22.48	13.39	1.92	4.70	-9.00	-9.00	-9.00	20.00	7.0	-9.00	-9.00	-9.00	-99.0
BR88-8	060688	R14	4.9	157	8.11	-22.62	1.96	0.18	1.84	0.31	0.01	0.00	4.30	10.9	0.05	-1.01	3.21	-0.2
BR88-9	060688	R15	2.7	537	7.64	-23.23	5.44	2.04	3.16	4.48	0.05	0.01	15.16	2.7	0.09	-0.32	2.54	-0.8

Field ID	Date	Map	Temp	SPC	pH	$\delta^{18}\text{O}$	Ca^{2+}	Mg^{2+}	HCO_3^-	SO_4^{2-}	Na^+	Cl^-	TDI	Ca/Mg	SIC	SID	pPCO ₂	Error
BR88-10	060688	R16	1.6	287	7.60	-22.97	2.76	1.28	2.96	1.38	0.04	0.02	8.43	2.2	-0.20	-0.83	2.53	-3.4
BR88-11	070688	R12	1.7	824	7.45	-23.54	11.59	2.08	4.48	9.58	0.05	0.01	27.77	5.6	0.29	-0.26	2.22	-1.3
BR88-12	070688	R2	3.7	1289	7.67	-23.09	17.66	2.84	4.80	15.20	0.06	0.01	40.56	6.2	0.67	0.49	2.41	1.4
BR88-13	070688	R3	1.7	1340	7.46	-23.42	15.83	2.48	5.24	13.64	0.08	0.01	37.26	6.4	0.45	0.02	2.17	-1.3
BR88-14	070688	R11	6.1	1660	7.71	-23.26	22.30	2.48	4.40	22.28	0.13	0.02	51.60	9.0	0.75	0.51	2.47	-3.5
BR88-15	080688	R12	1.4	902	7.22	-99.00	-9.00	-9.00	-9.00	8.74	-9.00	-9.00	-9.00	-9.00	-9.00	-9.00	-9.00	-99.0
BR88-16	080688	R2	1.6	1342	7.43	-99.00	-9.00	-9.00	-9.00	14.05	-9.00	-9.00	-9.00	-9.00	-9.00	-9.00	-9.00	-99.0
BR88-17	080688	R3	0.8	1341	7.23	-99.00	-9.00	-9.00	-9.00	-9.00	-9.00	-9.00	-9.00	-9.00	-9.00	-9.00	-9.00	-99.0
BR88-18	080688	R11	1.2	1668	7.63	-99.00	-9.00	-9.00	-9.00	22.38	-9.00	-9.00	-9.00	-9.00	-9.00	-9.00	-9.00	-99.0
BR88-19	090688	R17	7.7	162	7.54	-19.91	1.44	0.30	1.64	0.00	0.01	0.00	3.40	4.8	-0.65	-2.01	2.66	3.2
BR88-19	090688	R9	4.2	657	7.80	-23.49	5.34	2.14	3.92	4.06	1.43	1.23	18.12	2.5	0.35	0.23	2.60	-1.7
BR88-20	210788	R18	15.9	350	-9.00	-19.64	3.42	0.78	3.96	0.00	0.00	0.01	8.16	4.4	-9.00	-9.00	-9.00	2.9
BR88-21	210788	R19	16.2	265	-9.00	-20.21	2.62	0.50	2.56	0.45	0.02	0.00	6.15	5.2	-9.00	-9.00	-9.00	2.1
BR88-22	230788	R20	5.0	488	7.35	-21.31	4.32	1.46	2.92	3.04	0.00	0.00	11.74	3.0	-0.27	-1.07	2.26	-1.6
BR88-23	230788	R21	6.9	292	7.16	-21.52	2.30	0.74	2.52	0.42	0.01	0.00	5.98	3.1	-0.69	-1.91	2.10	1.8
BR88-24	230788	R22	3.3	444	6.87	-21.91	3.90	0.86	3.42	1.46	0.00	0.00	9.63	4.5	-0.70	-2.15	1.72	-1.2
BR88-25	230788	R23	9.9	303	7.29	-99.00	2.22	0.24	2.26	0.00	0.00	0.01	4.72	9.3	-0.56	-2.10	2.25	4.1
BR88-26	230788	R24	4.1	404	7.05	-21.27	3.36	0.54	3.56	0.02	0.02	0.01	7.50	6.2	-0.52	-1.91	1.87	4.4
BR88-27	260788	R25	6.9	343	6.91	-22.54	3.66	0.96	3.58	1.23	0.00	0.00	9.42	3.8	-0.63	-1.88	1.71	-2.0
BR88-28	260788	R26	2.4	286	6.63	-21.96	3.22	1.00	3.48	0.73	0.00	0.00	8.43	3.2	-1.01	-2.62	1.48	0.1
BR88-29	260788	R27	5.2	303	6.64	-21.93	3.14	0.98	3.50	0.83	0.00	0.02	8.47	3.2	-0.98	-2.52	1.46	-2.8
BR88-30	260788	R28	11.3	289	7.70	-20.53	2.82	0.84	3.32	0.29	0.00	0.00	7.27	3.4	0.10	-0.33	2.49	0.7
BR88-31	290788	R12	2.3	1050	7.66	-22.98	16.86	1.62	5.18	15.09	0.06	0.02	38.83	10.4	0.67	0.24	2.37	-4.5
BR88-32	290788	R2	6.5	1597	7.89	-23.11	21.42	2.36	4.88	21.13	0.04	0.01	49.84	9.1	0.96	0.93	2.61	-4.4
BR88-33	290788	R3	4.9	1480	7.83	-22.71	15.07	3.04	5.51	14.37	0.05	0.01	38.05	5.0	0.84	0.94	2.50	-4.6
BR88-34	290788	R11	5.4	1850	7.80	-23.18	28.05	2.36	5.75	26.96	0.06	0.01	63.20	11.9	1.01	0.91	2.46	-3.6
BR88-35	300788	R13	6.7	1303	7.51	-22.93	15.89	2.82	5.04	14.57	0.06	0.01	38.38	5.6	0.53	0.28	2.20	-2.2
BR88-36	300788	R15	4.9	1261	7.52	-22.69	14.85	3.22	5.12	14.37	0.04	0.01	37.60	4.6	0.50	0.29	2.21	-3.7
BR88-37	300788	R16	3.6	685	7.97	-22.55	6.69	3.08	4.66	5.41	0.00	0.02	19.86	2.2	0.65	0.89	2.71	-1.6

Field ID	Date	Map	Temp	SPC	pH	$\delta^{18}\text{O}$	Ca^{2+}	Mg^{2+}	HCO_3^-	SO_4^{2-}	Na^+	Cl^-	TDI	Ca/Mg	SIC	SID	pPCO_2	Error
BR88-38	020888	R29	11.4	236	7.31	-21.24	2.30	0.54	2.40	0.00	0.03	0.01	5.28	4.3	-0.49	-1.60	2.24	8.8
BR88-39	020888	R30	12.9	316	7.30	-21.70	3.00	0.76	3.22	0.42	0.05	0.02	7.46	3.9	-0.27	-1.11	2.09	2.1
BR88-40	020888	R31	17.0	106	7.67	-17.67	0.88	0.40	1.04	0.10	0.00	0.03	2.45	2.2	-0.81	-1.87	2.91	4.4
BR88-41	020888	R32	13.0	269	8.06	-19.15	2.20	0.74	2.56	0.29	0.02	0.02	5.82	3.0	0.27	0.08	2.96	1.5
BR88-42	020888	R33	15.4	295	7.89	-21.27	2.54	0.92	2.66	0.88	0.01	0.01	7.02	2.8	0.18	-0.02	2.75	-1.2
BR88-43	060888	R34	-9.0	-9	-9.00	-99.00	0.88	0.30	-9.00	-9.00	-9.00	-9.00	-9.00	2.9	-9.00	-9.00	-9.00	-99.0
BR88-44	070888	R35	6.3	348	7.05	-21.51	3.78	0.80	3.90	0.56	0.04	0.01	9.09	4.7	-0.43	-1.58	1.82	1.6
BR88-45	070888	R36	6.1	356	6.91	-21.77	3.80	0.88	4.02	0.69	0.00	0.02	9.40	4.3	-0.56	-1.81	1.66	-0.5
BR88-46	070888	R19	13.9	287	7.66	-19.85	2.78	0.64	3.02	0.39	0.02	0.00	6.84	4.3	0.04	-0.51	2.47	0.4
BR88-47	070888	R37	15.3	298	7.69	-19.67	2.80	0.66	2.84	0.39	0.00	0.01	6.69	4.2	0.07	-0.44	2.52	3.4
BR88-48	090888	R10	4.1	642	7.58	-23.36	6.23	0.96	4.34	2.89	1.52	1.26	17.20	6.5	0.26	-0.37	2.33	1.3
BR88-49	090888	R9	6.0	731	7.80	-23.73	6.29	1.34	4.28	3.21	1.32	1.11	17.54	4.7	0.49	0.25	2.55	2.1
BR88-50	090888	R38	-9.0	-9	-9.00	-22.84	11.51	4.00	4.74	11.45	0.27	0.02	31.98	2.9	-9.00	-9.00	-9.00	-1.4
BR88-51	100888	R39	4.2	1838	7.14	-23.51	27.97	2.40	5.53	24.94	0.17	0.02	61.04	11.7	0.34	-0.43	1.81	0.1
BR88-52	100888	R40	7.4	1890	7.38	-23.34	26.38	2.08	3.70	25.71	0.13	0.02	58.01	12.7	0.41	-0.29	2.20	-1.4
BR88-53	110888	R3	-9.0	-9	-9.00	-23.01	-9.00	-9.00	-9.00	16.34	0.03	0.01	16.39	-9.0	-9.00	-9.00	-9.00	-99.0
BR88-54	110888	R2	-9.0	-9	-9.00	-23.08	-9.00	-9.00	-9.00	22.38	0.07	0.01	22.46	-9.0	-9.00	-9.00	-9.00	-99.0

Missing Data: -9.00 and -99.00

Map: Locations indexed on Figures 8.2 and 8.4

Temp: Temperature in °C

SPC: Specific electrical conductivity in $\mu\text{S cm}^{-1}$

Ion concentrations in meq L^{-1}

SIC: Saturation index for calcite

SID: Saturation index for dolomite

pPCO_2 : -log of the partial pressure of CO_2